UNIVERSITY OF CAMBRIDGE

Synthesis of a Diverse and Three-Dimensional Fragment Collection

and

The Development of a Novel Platform for Antibody Dual Functionalisation

Abigail R. Hanby

Gonville and Caius College

University of Cambridge

September 2021

Supervised by Professor David R. Spring

This thesis is submitted for the degree of **Doctor of Philosophy**

Preface

This thesis is the result of my own work and includes nothing which is the outcome of work done in collaboration except as specified in the text. It is not substantially the same as any work that has already been submitted before for any degree or other qualification and does not exceed the prescribed word limit for the Physics and Chemistry Degree Committee.

In this thesis, bold and hashed wedges are used to depict absolute configuration, whilst unwedged bold and unwedged hashed lines represent relative configuration.

Synthesis of a Diverse and Three-Dimensional Fragment Collection and The Development of a Novel Platform for Antibody Dual Functionalisation

Abigail R. Hanby

This report describes two projects. The first focuses on the synthesis of a library of small molecules suitable for fragment-based screening. Over the past two decades, fragment-based drug discovery (FBDD) has emerged as a powerful strategy for early-stage drug discovery. However, despite its many successes, FBDD often suffers from the lack of synthetic tractability, three-dimensionality, and structural diversity (and hence biological diversity) within traditional fragment collections. As such, there is a need for the generation of novel fragment collections with these features to augment existing collections.

This work documents the diversity-oriented synthesis of a library of 38 diverse and sp^3-rich fragments, each bearing a key all-carbon quaternary centre. These motifs are currently underrepresented in screening collections; thus, it was expected that the incorporation of such a moiety would enable access to new areas of fragment space, whilst enhancing three-dimensionality. Each fragment was prepared from building blocks with general structure **I** in no more than four steps, providing a facile route by which fragments containing an all-carbon quaternary centre and multiple fragment growth positions could be generated (Figure i). Importantly, the resulting library adheres to recognised guidelines within the field of FBDD, thereby demonstrating its suitability as a screening collection.

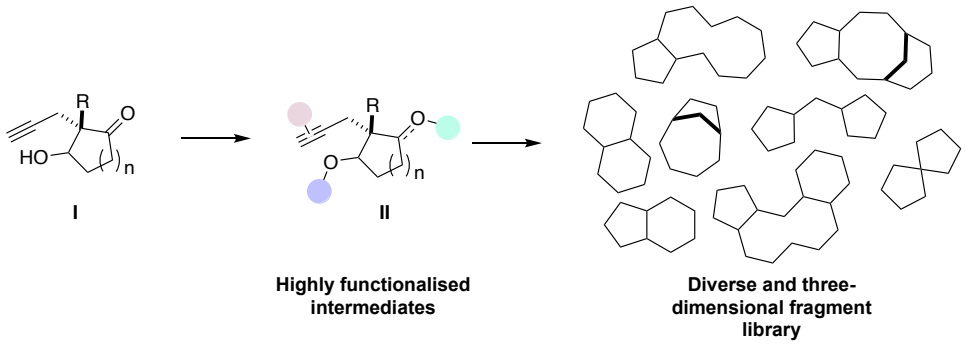

Figure i. Synthesis of a diverse and three-dimensional fragment collection.

The second project details the development of a platform for the site-selective dual modification of antibodies *via* a cysteine rebridging strategy. The site-selective modification of antibodies for use in both drug delivery and immunodetection has gained widespread interest in recent years, particularly in the field of oncology. Although many strategies have been developed to enable such modifications,

the majority only enable the incorporation of a single type of payload, thus limiting their scope. Furthermore, of the methods for the dual modification of antibodies that have been developed, many suffer from several drawbacks, including lack of efficient conjugation methods, problems with stability and solubility, incomplete conversions, low yields, and/or the use of toxic metal catalysts.

To tackle these issues, the disulfide rebridging reagent divinylpyrimidine (DVP) was modified to incorporate two orthogonal 'clickable' handles (Figure ii). By the introduction of the DVP linker into the native disulfide bonds of an antibody, subsequent one-pot dual functionalisation was successfully demonstrated to attach both cytotoxins and fluorophores. Notably, this strategy enabled the generation of theranostic antibody conjugates that exhibited selective *in vitro* cytotoxicity.

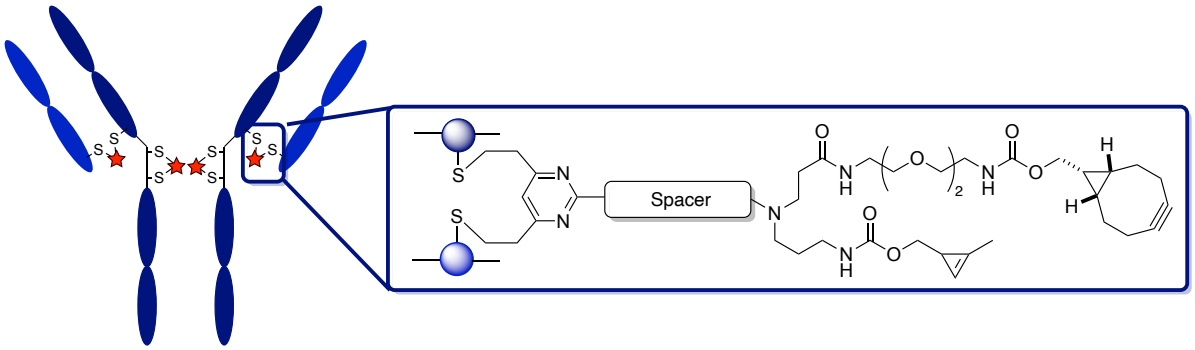

Figure ii. A novel platform based on DVP was developed to enable site-selective antibody modification with dual modalities.

Acknowledgements

Firstly, I would like to thank Professor Spring for his advice and support over the past four years, and for giving me the opportunity to work in such a friendly group. I am also extremely grateful to Steve Walsh, Kim Mortensen, and Thomas Osberger for their day-to-day supervision, as well as Sarah Kidd for her help and advice. Thank you also to those who have helped with the projects described in this thesis: Nikolaj for his input on the fragment work, and Steve Walsh for his cell-work, and to the EPSRC and the Cambridge Trust for their financial support throughout.

I am incredibly thankful for all those who have contributed to proof-reading this thesis, including Raoul Walther, Steve Walsh, Tom King, Sarah Kidd, Golf Charoenpattarapreeda, Kim Mortensen, Josie Gaynord, Tomas Deingruber, Jonny Bargh, Andrew Hanby, and Beth Cooper.

I am also grateful to the NMR team: Duncan and Andrew who went above and beyond to help me in my pursuit of the perfect NMR spectra.

I'd also like to thank the rest of the Spring group, past and present, who have contributed to a wonderful experience. I'm so grateful for all the fantastic memories I've made from Friday pub trips, teatime chats, pub lunches, away days, and Christmas dinners. A special thank you to my cohort: Sam, Rike, and Edward for your advice, support, and friendship throughout, and to my Bay 3 buddies Beth, Tomas, and Josie for keeping me going through the highs and lows of lab work.

Immense gratitude also goes to my parents for their endless support. I can never thank you enough for always being there for me, I could not have done this without you.

Finally, I will be forever grateful to Dulan for his love, patience, and understanding.

Abbreviations

3D	3-Dimensional
Ac	Acetyl
ADC	Antibody-drug conjugate
ADMET	Absorption, distribution, metabolism, elimination, and toxicity
AFC	Antibody-fluorophore conjugate
AIBN	Azobisisobutyronitrile
Alloc	Allyloxycarbonyl
Aq	Aqueous
Ar	Aromatic
AzK	Azido-lysine
BCN	(1R,8S,9S)-Bicyclo[6.1.0]nonyne
B/C/P	Build/Couple/Pair
Boc	*tert*-Butyloxycarbonyl
Bu	Butyl
br	Broad
CBS	Corey-Bakshi-Shibata
clogP	Calculated partition coefficient
COD	1,5-Cyclooctadiene
Cp*	Pentamethylcyclopentadiene
Cp	Cyclopentadiene
CuAAC	Copper-catalysed azide alkyne cycloaddition
Criz	Crizotinib
cyp	Cyclopropene
d	Doublet
da	Dalton
DAR	Drug-to-antibody ratio
DBCO	Dibenzoazacyclooctyne
DCC	*N*,*N*'-Dicyclohexylcarbodiimide
DCHA	Dicyclohexylamine
Df	Dual functional
DHP	Dihydropyran
DIBO	Dibenzocyclooctyne

DIPEA	*N*,*N*-Diisopropylethylamine
DMF	Dimethylformamide
DMSO	Dimethyl sulfoxide
DOS	Diversity-oriented synthesis
Dox	Doxorubicin
EDC	1-Ethyl-3-(3-dimethylaminopropyl)carbodiimide
E_{max}	Maximum effect
Equiv.	Equivalents
ESI	Electrospray ionisation
Et	Ethyl
Fab	Fragment antigen-binding
FAR	Fluorophore-to-antibody ratio
FBDD	Fragment-based drug discovery
Fc	Fragment crystallisable
FDA	Food and Drug Administration
Fmoc	Fluorenylmethoxycarbonyl
Fsp^3	Fraction sp^3
g	Gram
h	Hours
HBTU	*N,N,N',N'*-Tetramethyl-*O*-(1*H*-benzotriazol-1-yl)uronium hexafluorophosphate
HC	Heavy chain
HMBC	Heteronuclear multiple-bond correlation
HOBt	1-Hydroxybenzotriazole
HPLC	High performance liquid chromatography
HTS	High-throughput screening
Hz	Hertz
IC_{50}	Half maximal inhibitory concentration
IEDDA	Inverse electron demand Diels–Alder
IgG	Immunoglobulin
IR	Infrared
J	Coupling constant
L	Litre
LC	Light chain
LCMS	Liquid chromatography mass-spectrometry

LE	Ligand efficiency
μ	Micro
m	Milli/multiplet/medium
M	Molar
Mab	Monoclonal antibody
MBC	Metastatic breast cancer
Me	Methyl
MEC	Minimum effective concentration
mf	Monofunctional
MMAE	Monomethyl auristatin E
MMAF	Monomethyl auristatin F
MOA	Mechanism of action
MOE	Molecular Operating Environment
mol	Mole
m.p.	Melting point
Ms	Mesyl
MS	Mass spectroscopy
MSH	*O*-Mesitylenesulfonylhydroxylamine
mTG	Microbial transglutaminase
MTD	Maximum tolerated dose
MW	Molecular weight
mW	Microwave
ncAA	Non-canonical amino acid
NHS	*N*-Hydroxysuccinimide
NMO	*N*-Methylmorpholine *N*-oxide
NMR	Nuclear Magnetic Resonance
NOE	Nuclear Overhausser effect
NOESY	Nuclear Overhausser effect spectroscopy
NP	Natural product
Np	Nitrophenyl
NPR	Normalised principal moment of inertia ratio
NuBBE	Nuclei of bioassays, biosynthesis and ecophysiology of natural products
°C	Degrees centigrade
PAB	*para*-aminobenzyl

pAcF	*para*-acetyl-L-phenylalanine
PBD	Pyrrolobenzodiazepine
PEG	Polyethylene glycol
PG	Protecting group
Ph	Phenyl
PMI	Principal moment of inertia
ppm	Parts per million
py	Pyridine
q	Quartet
QTOF	Quadrupole time of flight
RCEYM	Ring closing enyne metathesis
R_f	Retardation factor
Ro3	Rule of three
rt	Room temperature
RuAAC	Ruthenium-catalysed azide alkyne cycloaddition
s	Singlet/strong
SDS-PAGE	Sodium dodecyl sulphate-polyacrylamide gel electrophoresis
SPAAC	Strain-promoted azide-alkyne cycloaddition
SM	Small molecule
S_NAr	Nucleophilic aromatic substitution
t	Triplet
TBAF	Tetra-n-butylammonium fluoride
TBS	*tert*-Butyldimethyl silyl
TBTA	Tris[(1-benzyl-1*H*-1,2,3-triazol-4-yl)methyl]amine
Teoc	2-(Trimethylsilyl)ethoxycarbonyl
TCEP	Tris(2-carboxyethyl)phosphine
TCO	Trans-cyclooctene
TFA	Trifluoroacetic acid
THF	Tetrahydrofuran
THP	Tetrahydropyran
THPTA	Tris-hydroxypropyltriazolylmethylamine
TLC	Thin layer chromatography
Ts	Tosyl
UV	Ultra-violet

v	Wavenumber
va	Valine-Alanine
vc	Valine-Citrulline
w	Weak
w/w	Weight/weight
δ	Chemical shift

Table of Contents

Section I:
Synthesis of a Diverse and Three-Dimensional Fragment Collection

1 Introduction

1.1 Introduction to Fragment-Based Drug Discovery

The discovery of small-molecule (SM) modulators of biological macromolecules is a key challenge of modern drug development.[1] One of the main approaches for the identification of such probes is high-throughput screening (HTS) – a technique that has led to the developed of numerous Food and Drug Administration (FDA) approved drugs (Figure 1.1).[2] This approach involves the use of automated equipment for rapid sample testing, with the aim of fast and efficient screening of large compound libraries (in the order of 10^5–10^6), either against a given target, or in a phenotypic setting.[3–5]

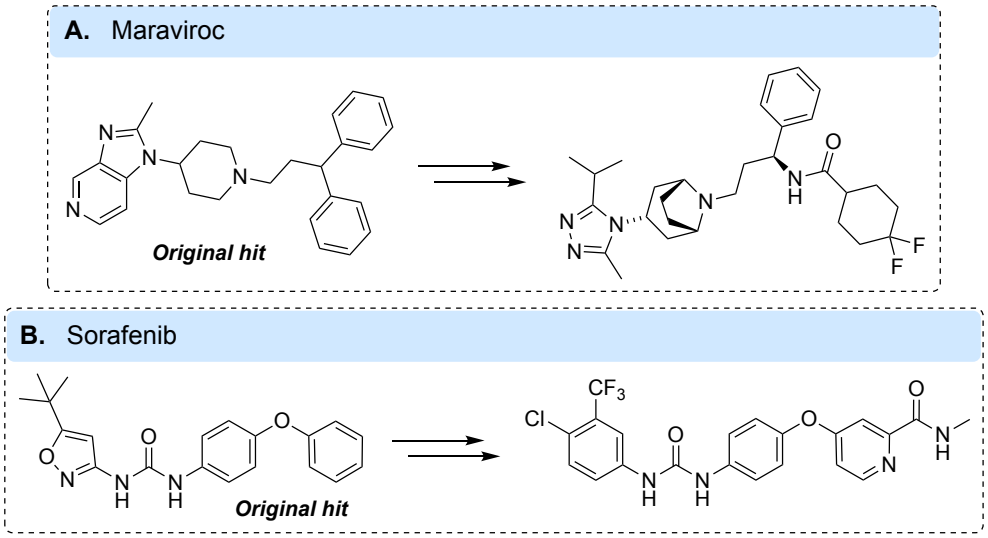

Figure 1.1. Examples of approved drugs with origins in HTS hits: (A) Maraviroc, a SM inhibitor of Chemokine Receptor CCR5 used in the treatment of human immunodeficiency virus.[6] (B) Sorafenib, a kinase inhibitor approved for the treatment of kidney, liver, and thyroid cancer.[7]

Whilst HTS is undeniably a powerful technique, particularly in the context of phenotypic screening, it also suffers from several drawbacks, such as the cost and challenges associated with maintaining multimillion-compound libraries.[2,8] Arguably the most significant problem facing HTS is the inefficiency with which these libraries sample chemical space. It is estimated that there are 10^{63} possible small drug-sized molecules, a number so astronomical that multimillion compound libraries are still vanishingly small in comparison.[9] This, along with the fact that these libraries are typically comprised of a high number of structurally similar compounds means that a significant proportion of chemical space is not covered by these collections. Consequently, although HTS libraries are successful against well-established targets, they often fail to yield hits against those that are newer and/or more

challenging.[10–12] Moreover, in addition to low hit rates, HTS screens frequently result in significant numbers of false positives.[11,13]

Over the past two decades fragment-based drug discovery (FBDD) has developed into a mainstream technique for the discovery of new biologically active compounds, offering an alternative approach to HTS for accessing lead compounds to seed drug discovery. The success of this strategy is now being realised; currently five FDA-approved drugs can trace their origins to a fragment-based screen (Table 1.1), whilst over forty further FBDD-derived compounds are currently in clinical studies.[14] Importantly, many of these successes have been achieved in areas where HTS has typically struggled to deliver leads, such as protein-protein interactions, e.g. Venetoclax, and hitherto 'undruggable targets', e.g. Sotorasib.[15–17] The power of this strategy can be attributed to three key concepts of improved chemical space sampling, higher hit rates, and increased ligand efficiency.

Table 1.1. Summary of FDA-approved drugs derived from FBDD.[18]

Drug	Indication	Year Approved	References
Vemurafenib	BRAF V600 mutation-positive unresectable or metastatic melanoma	2011	19,20
Venetoclax	Chronic lymphocytic leukemia	2016	21
Erdafitinib	Advanced or metastatic urothelial carcinoma	2019	22
Pexidartinib	Tenosynovial giant cell tumour	2019	23,24
Sotorasib	KRAS G12C-mutated advanced non-small cell lung cancer	2021	25,26

1.1.1 General Principles of FBDD

One key underlying principle of FBDD is that relatively small fragment libraries can be used to probe chemical space. With decreasing molecular weight (MW), the number of molecules in the corresponding chemical space decreases in an approximately exponential manner.[27] Thus, whilst the number of possible drug-like molecules with up to 30 heavy atoms is truly vast, there are just over 166 billion SMs with <17 heavy atoms.[28] Whilst this number is still high, chemical space can be much more efficiently sampled by screening collections of fragments (<17 heavy atoms) compared to HTS libraries.[27,29–32] Not only does this enable greater access to underexplored regions of chemical space but it also results in higher hit rates. Accordingly, whilst HTS involves the screening of large libraries of 'lead-like' compounds (MW 250–600 and binding affinities in the high-nM to low-µM range), FBDD

instead relies on the screening of smaller libraries of low MW (<300 Da) compounds to identify weak (μM to mM affinity) ligands for a given target.[33,34]

The high hit rates observed during fragment screens can also be explained by considering the concept of molecular complexity (often judged by number of chiral centres and/or the fraction of sp^3 carbons [Fsp^3] within a molecule).[35] According to a model proposed by Hann and co-worker, an increase in molecular complexity is associated with an increased chance of interactions forming with a given protein target.[30,36] Since these interactions are not always productive, as the complexity of a ligand increases the chance of complementarity is in turn decreased. It therefore follows that the screening of small fragments with reduced complexity should result in higher hit rates.

A further key advantage of FBDD is that fragments tend to form high-quality interactions, resulting in high binding energies relative to their small size.[37] As such, fragment-based approaches typically deliver high-quality starting points for drug development. One way in which the interactions of ligands with target proteins can be quantified is by measuring ligand efficiency (LE), which refers to the free energy of ligand binding divided by the number of heavy atoms.[38] Thus, compounds that achieve a particular potency with fewer heavy atoms are considered more efficient. By screening smaller, less complex compounds than HTS the chances of FBDD identifying ligands in which most atoms are involved in a given binding interaction is therefore increased.[37] Nevertheless, the low binding affinities (commonly in the mM to μM range) observed for fragments can make screening via standard biochemical methods extremely challenging. As a result, sensitive, and often several orthogonal, approaches are often required for hit identification and validation.[39–47]

1.1.2 Fragment Elaboration

Once validated, fragment hits can then undergo extensive optimisation to produce more potent lead-like compounds. During this stage, the binding affinity and other drug-like properties are improved through an iterative process of design, synthesis, and testing (Figure 1.2).[48]

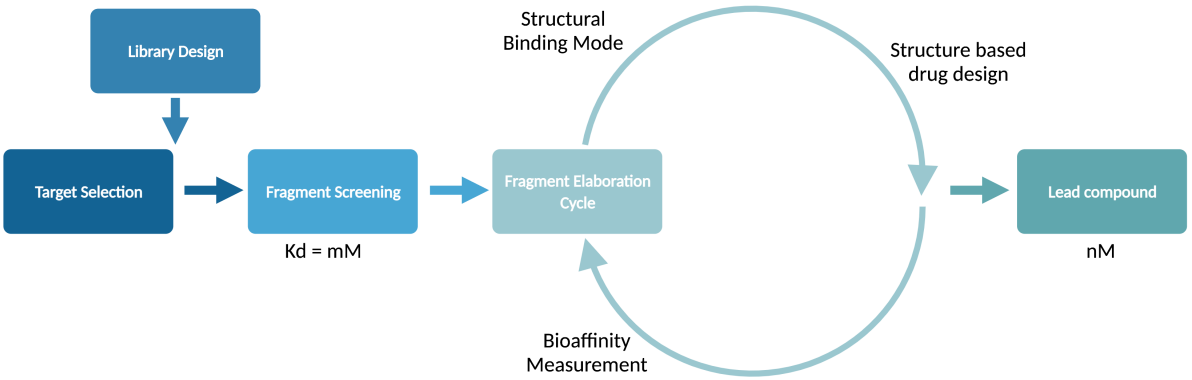

Figure 1.2. Overview of fragment-based drug discovery. Created with Biorender.com.

It is widely acknowledged that physicochemical properties, such as high MW, number of hydrogen bond donors and acceptors, and lipophilicity, contribute significantly to the attrition of small-molecule drug candidates due to their negative impact on ADMET[a] properties.[49–55] Thus, the ability of FBDD to allow careful control of these properties during this hit-to-lead stage (due to the high LEs and small size of fragments) is a key factor in its success in generating high-quality lead compounds. In contrast, although HTS hits are often more potent, their large size and poor LEs lead to far less efficient optimisations (Figure 1.3).[34]

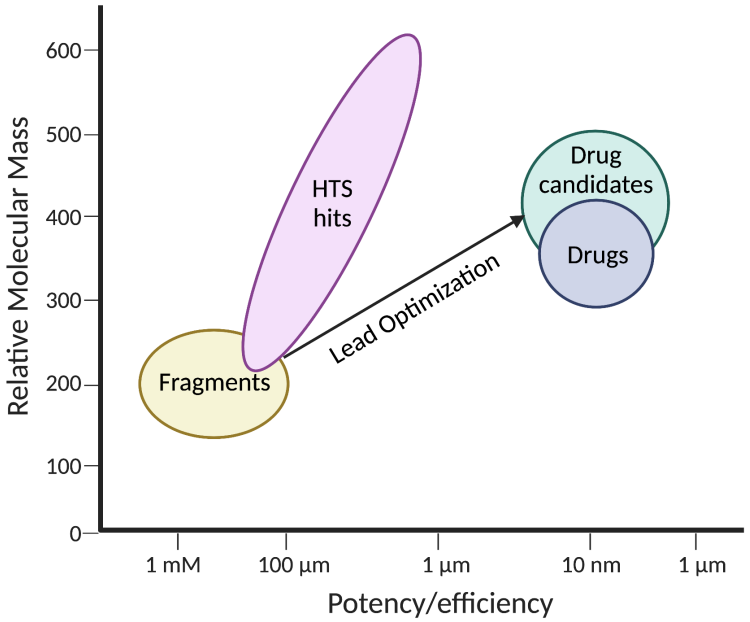

Figure 1.3. A generalisation of the differing size and binding potency characteristics for HTS and fragment screening collections, compared to drug candidates and oral drugs. Figure adapted from reference.[34] Created with Biorender.com.

[a] ADMET stands for 'absorption, distribution, metabolism, excretion, and toxicity', which play key roles in drug discovery and development.[49]

Often guided by structural information obtained through X-ray crystallography, NMR, and/or *in silico* approaches, the hit-to-lead stage typically employs one or more of three main strategies (Figure 1.4):[39,46]

- **Fragment growing:** the potency of a fragment can be increased by iteratively extending the molecule in such a way that it can make additional interactions with nearby residues within the binding site. This technique relies upon the presence of suitable growth vectors within the hit fragment and structural information about the target protein.

- **Fragment linking:** if several fragment hits are identified that bind to different sub-pockets of the same protein, they can be linked together to combine the contributions of both binding motifs. This technique can often be challenging as the individual fragment units must be able to retain their original minding modes without the introduction of a significant entropic cost through excessive linker flexibility.

- **Fragment merging:** if multiple fragment hits instead occupy overlapping regions of the same target protein, they can be merged into a single unit. Ideally, this should have an additive or synergistic effect on potency.

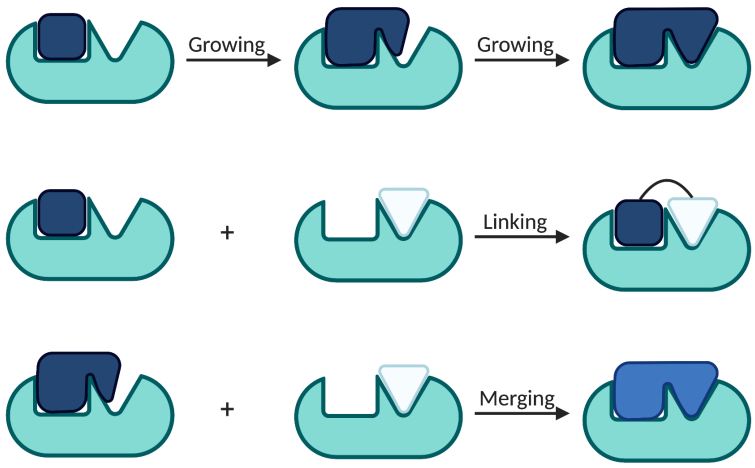

Figure 1.4. The main strategies for fragment elaboration: growing, linking, and merging. Created with Biorender.com.

Although in recent years successful campaigns devoid of structural information have also been demonstrated,[56,57] the presence of this data generally increases the efficiency of fragment elaboration. However, this requirement can also limit the applicability domain of FBDD, since deriving this information for certain biological targets is extremely challenging.

A general theme that will run throughout this chapter is the link between FBDD and synthetic chemistry. To enable all three of the described fragment elaboration processes, the available

chemistry around a given fragment hit is crucial. Therefore, to enable rapid hit derivatisation and improve the efficiency of the process from hit-to-lead, the quality of the FBDD starting points and therefore screening library design is critical.

1.2 Fragment Library Design

Since the composition of a fragment screening library plays a crucial role in determining the overall outcome of an FBDD campaign, several factors must therefore be considered to ensure the generation of high-quality fragments. A number of these factors are discussed below.

1.2.1 Physicochemical Properties

As previously discussed, the physiochemical properties of a drug candidate play a key role in determining its success in clinical development. In particular, both high lipophilicity and MW have been shown to have a significant deleterious effect on ADMET properties.[49,58–60] Furthermore, high lipophilicity is often associated with a lack of solubility, which can cause problems at the high concentrations required for fragment screening.[37] Thus, since fragments tend to become larger and more lipophilic as they are optimised, it is essential that these factors are controlled from the beginning of an FBDD campaign.[58]

Over the past two decades these new insights into the drug discovery process have aided in the development of numerous guidelines for the design of fragment libraries with appropriate physiochemical properties. In 2003, Cargreve *et al*. introduced a 'rule of three' (Ro3) for fragment-sized molecules. Based on the analysis of a diverse set of fragment hits, these guidelines stated that fragments should have MW <300, cLogP ≤3, number of hydrogen bond donors ≤3, and number of hydrogen bond acceptors ≤3.[61] The authors also noted that fragments should ideally have no more than three rotatable bonds and a polar surface area <60 Å. By restricting the number of possible fragments that can be formed, these limits to the physicochemical properties of fragments are also key to maintaining efficient chemical space sampling.

In recent years, Ro3 guidelines have been revised by Keserű *et al*., to further lower the MW to ~140−230.[8] The use of such small fragments is especially useful for the identification of probes for difficult and/or novel targets. Nevertheless, collections of larger fragments (~300 Da) still have a crucial role to play, in particular when targeting protein-protein interactions.[62]

1.2.2 Library Size and Diversity

The efficiency with which a given library samples chemical space is also dependent on the size of the collection. However, whilst the library must be large enough to provide a suitably high hit rate, the throughput of the desired screening method must also be taken into account.[8] As a result, fragment libraries typically range from a hundred to several thousand compounds, with most consisting of around 1,000–5,000.[8,11] If resources allow, the screening of larger libraries is often preferred due to the possibility of including numerous examples of a given chemotype, which can enable initial SAR identification and further hit validation.[11]

In addition, the structural diversity within a fragment collection also influences the efficiency of chemical space sampling, as well as the novelty of any potential hit compounds (which is particularly useful for novel and/or challenging target classes).[63] Although structural diversity can be difficult to define, the four types of structural diversity commonly identified in the literature are appendage, functional group, stereochemical, and scaffold.[1,64–66] Arguably, the most important of these is scaffold diversity, as this has the greatest impact on the shape of a molecule. Indeed, since proteins are large 3D environments that can only bind compounds with a complementary shape, it is the overall 3D shape of a SM that has the most significant impact on its biological behaviour.[1,67] An increase in scaffold diversity therefore correlates with an increased range of possible biological activities, and as such this diversity within a fragment library is now regarded as a key factor in determining the hit rate of a screening collection.

1.2.3 PAINS and False Positives

Due to the nature of their reactivity, a number of structural motifs have been identified as unsuitable for fragment screening (Figure 1.5).[68] This is because of their tendency to produce false positives through non-specific interactions with targets, for example via covalent attachment to proteins, redox activity, chelation, or aggregation.[69,70] Because of this ability to interfere with screening technologies, such species have been termed ‘pan-assay interference compounds’ (PAINS).[71] The avoidance of such species is therefore another important consideration in library design.

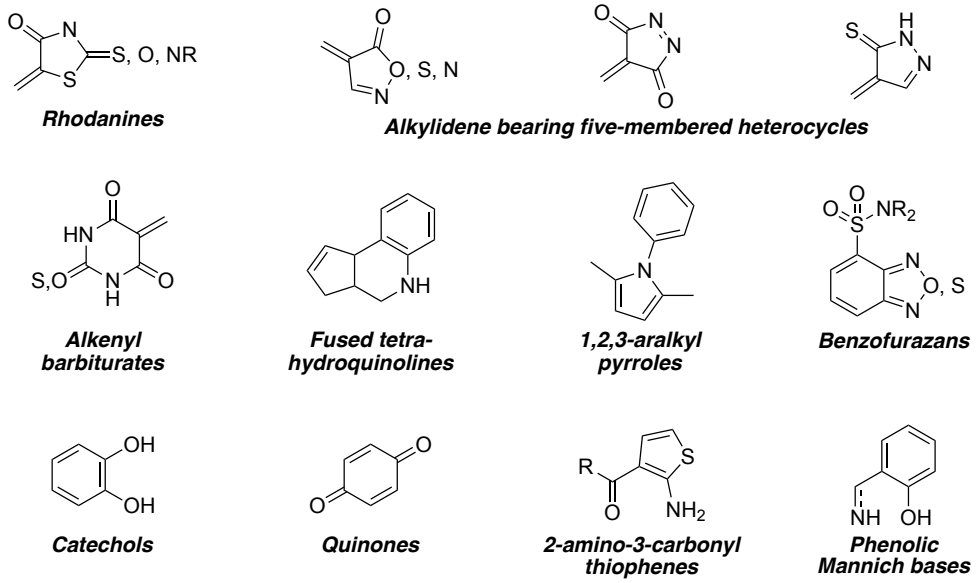

Figure 1.5. Examples of recognised PAINS. Figure adapted from reference.[68]

To avoid the unfruitful optimisation of false positives, it is important that PAINS are correctly identified as early as possible. However, whilst the presence of certain functional groups, such as epoxides and aldehydes, makes some PAINS easily recognisable, others are less easy to spot.[72] This has led to the development of computational filters that have been designed to identify these problematic compounds based on literature reports of known PAINS.[71,73]

1.2.4 Synthetic Tractability

Since a key concept of the FBDD process relies on the evolution of small, weakly potent hits into leads, fragment libraries must also be designed in such a way that any resulting hits are easily 'optimisable'.[74] In general, this requires fragments to have suitable functional handles (often referred to as 'growth/exit vectors') that can be used as starting points for fragment elaboration. Within recent years, it has been noted throughout the field that many fragment collections suffer from a lack of such vectors, which in-turn complicates the process of growing hits identified from these libraries (Figure 1.6).[75,76] As a result, calls for new synthetic methodologies capable of enabling fragment growth in multiple dimensions have been increasing.

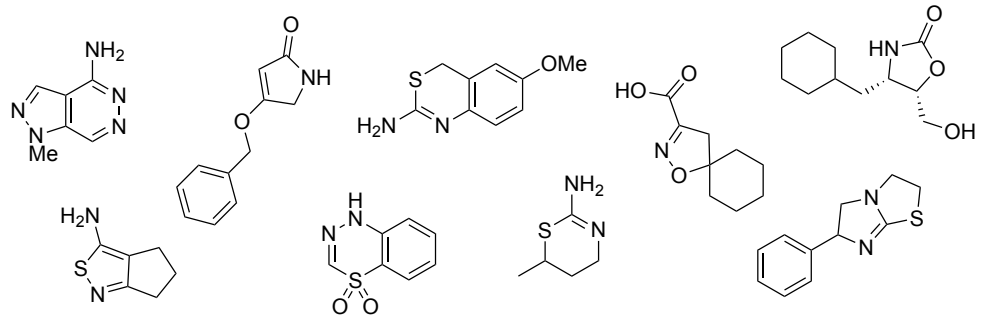

Figure 1.6. Example of fragments identified from Astex's libraries considered to be unsuitable for further elaboration (so-called 'unsociable' fragments).[75]

To alleviate this bottleneck in the FBDD process, in recent years the synthetic community have sought to generate 'poised' libraries containing fragments capable of undergoing rapid follow-up synthesis.[77,78] In one example, Twigg *et al*. were able to utilise a modular and divergent approach for the synthesis of a series of partially saturated pyrazole- and pyridine-based fragments (Scheme 1.1). The scaffolds were designed to have various saturated ring sizes and heteroatoms, with each also containing an alkene, amino, nitro, or chloro handle to provide a point for further elaboration.

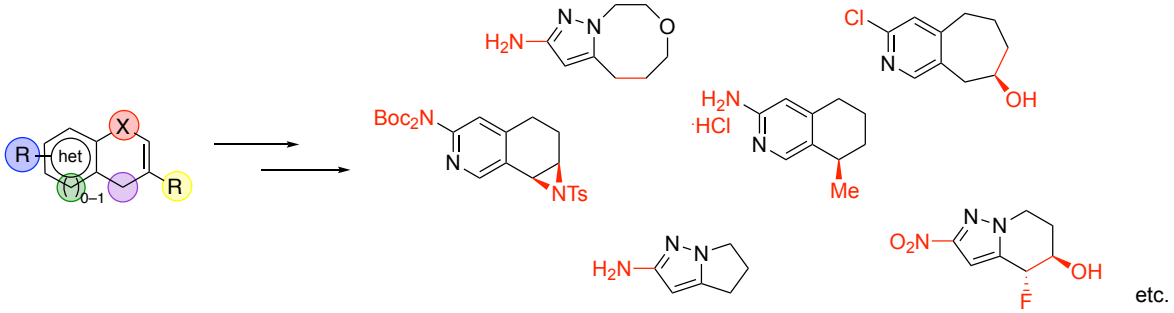

Scheme 1.1. Synthesis of a library of partially saturated bicyclic heteroaromatics designed for rapid follow-up chemistry.[79]

1.2.5 3D Fragments

Traditionally, many commercial screening libraries have relied on the use of flat, aromatic compounds based on a limited number of core scaffolds.[80–83] This is due, in part, to their greater commercial availability and more robust chemistry than their 3D counterparts. As a result, 3D fragments (which typically contain one or more chiral centres and/or high Fsp^3) tend to be underrepresented in screening collections.[35,84]

The extent to which libraries should include 3D structures is a long running debate within the field of FBDD. On one hand, since a more 3D shape results in more directional features, it is expected that greater three-dimensionality will increase compound complexity, and therefore lower the probability of a fragment matching a binding pocket.[36] However, on the other hand, this greater complexity may generate a clearer intellectual landscape, whilst enabling less promiscuous drug candidates to be built

from any hits.[85,86] Moreover, 3D fragments have the potential to access a greater number and range of growth vectors, and benefit from better physicochemical properties, such as solubility.[76,87] Perhaps most importantly, reports from both GSK and Pfizer have also demonstrated that an increase in the Fsp^3 of a molecule is associated with an increased likelihood of project progression.[35,88,89]

It should be noted that once a hit has been identified, sp^3-rich fragments can prove harder to optimise than their flatter counterparts.[75,86] Thus to avoid this it is often necessary for sp^3-rich fragments to incorporate heteroatom-centred growth vectors.[78,79,90] In one such example, Downes *et al*. generated a collection of 56 3D fragments based on disubstituted pyrrolidine and piperidine cores (Scheme 1.2). By assessing fragments prior to synthesis, the authors were able to maximise conformational and 3D shape diversity.[91] Importantly, the fragments possessed optimal physicochemical properties and numerous synthetic handles for fragment growth. In cases where sp^3-rich libraries lack such growth vectors, developments in $C(sp^3)$–H functionalisation offer a potential alternative for the advancement of sp^3-rich fragment hits.[86]

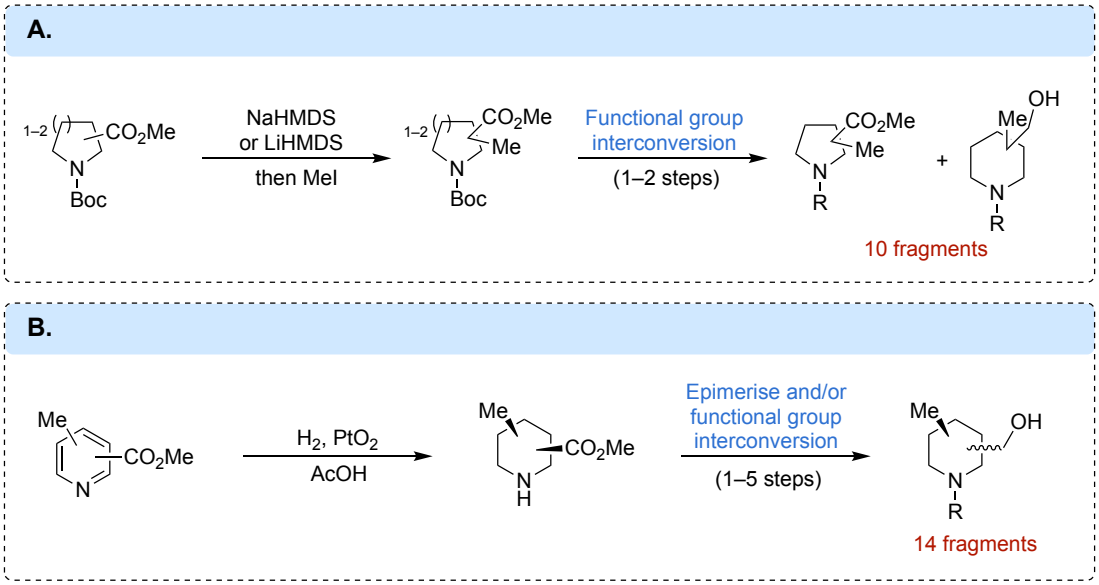

Scheme 1.2. Selected examples of (A) pyrrolidine and (B) piperidine fragments generated as part of a library of 56 shape-diverse 3D fragments.[91] R = H, Me, Ac, or Ms.

In summary, despite contrasting views, what is clear is that novel fragments containing multiple growth vectors are required to augment existing collections and alleviate the aforementioned bottlenecks. Furthermore, since fragment libraries are more commonly dominated by flat, achiral compounds, the development of novel synthetic strategies to more 3D fragments offers the opportunity to access underexplored regions of chemical space, which is key to the investigation of more challenging targets.

1.3 Sources of SMs

To ensure the key design principles required for FBDD are met, a suitable source of SMs to populate a given FBDD screening collection is required. Generally, this is obtained either from commercially available collections, the synthesis of novel compound collections, and/or derived from NPs.[92]

1.3.1 Natural Product-Based Libraries

It is often said that NPs are excellent, prevalidated starting points for the generation of screening collections.[93] Not only are NPs known for their exceptional diversity and three-dimensionality, but they are also a valuable proven source of medicinally relevant compounds from which many approved therapeutic agents have been derived.[94,95] However, despite these advantages, the utility of NPs in drug discovery has been severely limited by challenges associated with their identification, purification, and isolation from natural sources.[1,96] Notwithstanding those challenges, there has been significant interest in the laboratory synthesis of these compounds and their related analogues.

Although NPs are generally too large to fit within FBDD requirements, their substructures are often considered 'privileged' motifs, i.e. capable of acting as high-affinity ligands for multiple receptors.[97] With this in mind, several fragment libraries have been designed based on their substructures, with the aim of harnessing the improved molecular profiles and biological responses of NPs.[98–101] Examples include libraries based on modified low MW NPs,[102] fragments inspired by NPs ('NP-like' fragments),[90] or deconstructed NPs (Figure 1.7).[98]

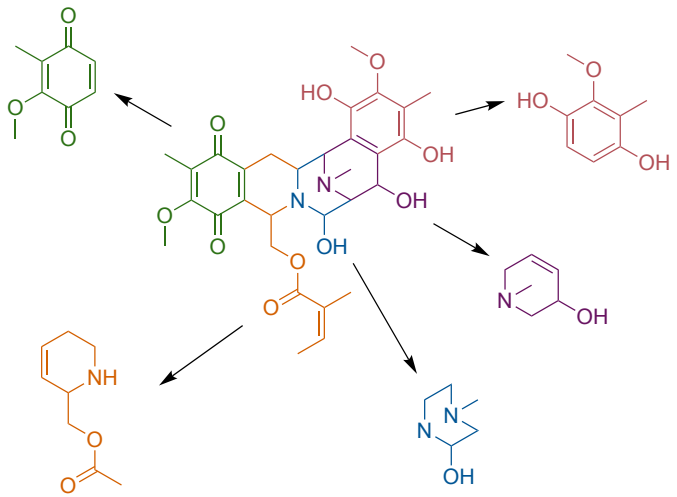

Figure 1.7. Fragments generated from the virtual deconstruction of the NP Renieramycin P.[98]

1.3.2 Diversity-Oriented Synthesis

As an alternative to NP libraries, commercially available libraries represent an important source of SMs.[103] However, these libraries often suffer from a lack of diversity and exit vectors for facile fragment elaboration (*vide supra*, section 1.2).[75,76,104] This has led to the development of several alternative synthetic approaches to library generation, with the overall aim of either: (1) accessing biologically relevant areas of chemical space (e.g. biology-oriented synthesis);[93] or (2) efficiently sampling large regions of chemical space simultaneously (e.g. diversity-oriented synthesis [DOS]).[81]

DOS, in particular, has emerged as a key technique for the efficient synthesis of large numbers of structurally diverse compounds, often for HTS purposes.[64,105–109] Typically, these campaigns take place via either a substrate- or reagent-based approach, and employ a forward synthetic analysis (Figure 1.8).[105,109] In a substrate-based approach a folding process is utilised to convert a collection of diverse substrates into distinct scaffolds via the use of common reaction conditions. In contrast, a reagent-based approach employs common starting materials that can then undergo a series of divergent, complexity-generating reactions to form diverse products. This requires either: (1) a densely functionalised molecule that can undergo a range of reactions at different functional groups; and/or (2) incorporation of a pluripotent functional group.

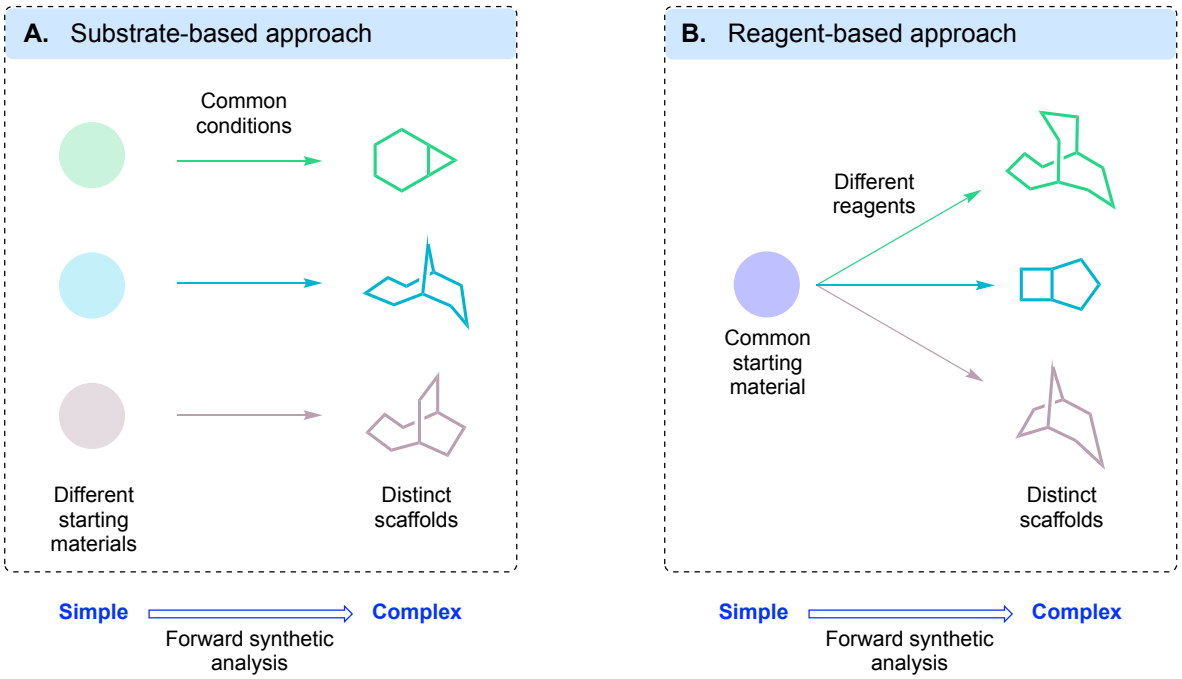

Figure 1.8. (A) Reagent-based approach to DOS. (B) Substrate-based approach to DOS. Both pathways require analysis in a forward direction. Figure adapted from reference.[92]

By employing these divergent approaches, DOS enables a small number of starting molecules to be transformed into numerous distinct and complex structures in only a few steps. In general, these steps can be divided into three stages (Scheme 1.3):[110]

1. **Build:** in the build stage the required building blocks are synthesised. Ideally, functional groups needed for subsequent reactions should already be present in these building blocks to minimise the overall number of synthetic steps.
2. **Couple:** in the second stage the building blocks undergo intermolecular reactions with other commercially available materials.
3. **Pair**: finally, intramolecular cyclisation reactions are used to pair functional groups, with the aim of producing rigid scaffolds. These final compounds should include numerous functional handles to enable further modification and diversification if required.[111]

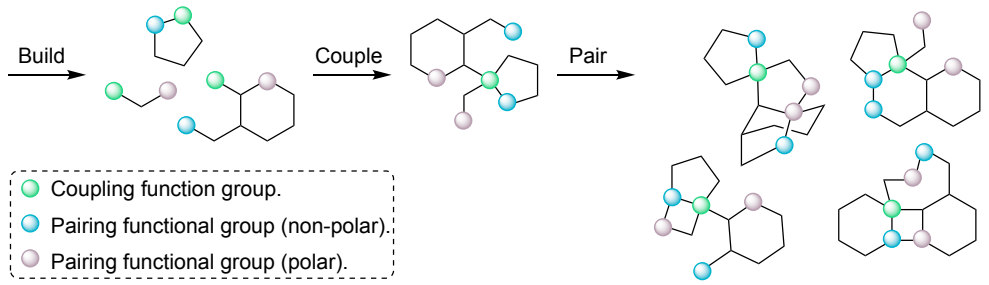

Scheme 1.3. The Build/Couple/Pair (B/C/P) strategy commonly employed in DOS. Figure adapted from reference.[110]

1.3.2.1 Applications of DOS in FBDD

Following on from the early success of DOS in lead generation of more HTS-like compounds,[112] DOS has since been applied to FBDD.[81] This has aided the population of underexplored areas of fragment space, which have largely been neglected by existing fragment collections.[113] Indeed, DOS offers a complementary approach to existing techniques, enabling the generation of libraries featuring high shape and structural diversity, increased 3D character, and numerous vectors for fragment growth.

Interestingly, due to high Fsp^3 and stereochemical content generated via DOS strategies, the resulting compounds are also often considered NP-like.[113,114] Such fragments have the potential to harness the biological relevance of NPs, thereby positively impacting the biological performance of the resulting fragment libraries.[114]

In 2011, Hung *et al*. described the first example of the application of DOS in FBDD.[81] Utilising a B/C/P pathway the authors were able to exploit three proline-derived building blocks for the formation of a collection of bicyclic compounds, including both fused and spirocyclic ring systems (Scheme 1.4). Each

library member contained multiple synthetic handles and desirable physical properties for fragment screening. Chemoinformatic analysis was also employed to confirm the greater three-dimensionality of the resulting compounds compared to more 'conventional' fragments.

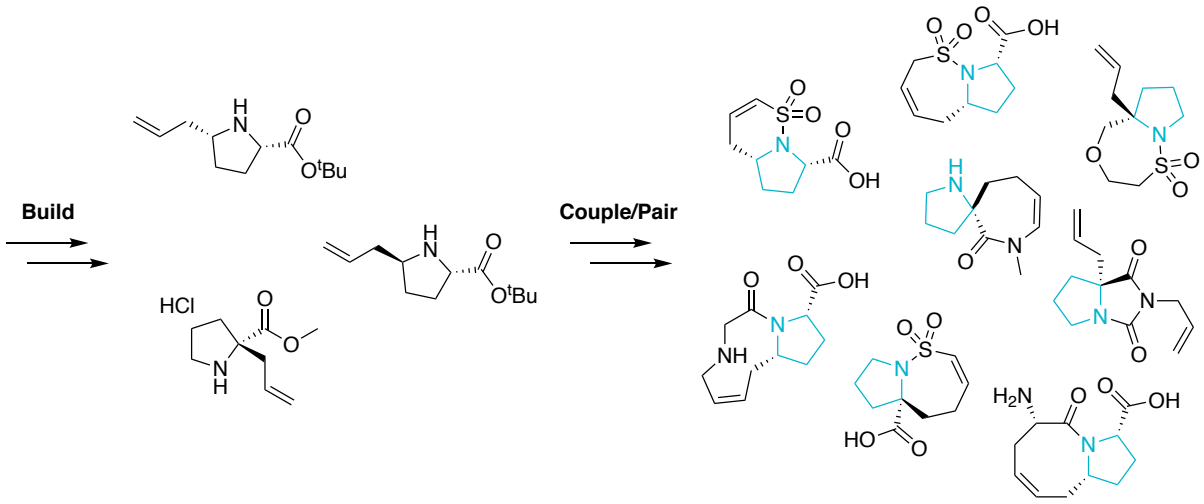

Scheme 1.4. DOS was employed for the generation of a library of highly sp^3-rich fragments from three proline-derived building blocks. Figure adapted from reference.[81]

More recently, Spring and co-workers have reported a library of 40 structurally diverse and rule of three-compliant DOS derived-fragments (Scheme 1.5).[78] Starting from racemic α-methyl propargylglycine, a B/C/P strategy was employed to enable library construction in a synthetically efficient manner. The resulting library was subsequently screened crystallographically at the XChem screening facility against three protein targets (a hydrolase, the growth factor TGF β , and a peptidase), leading to the identification of four hits.[115] Notably, these are the first reported SM binders for CFI_{25} and activin A, demonstrating the utility of DOS for the identification of hits against challenging target classes.

Despite these successes, the number of fragment libraries generated via DOS strategies remains low. Thus, continued exploration of these strategies for the development of novel fragment libraries is of significant interest.[113]

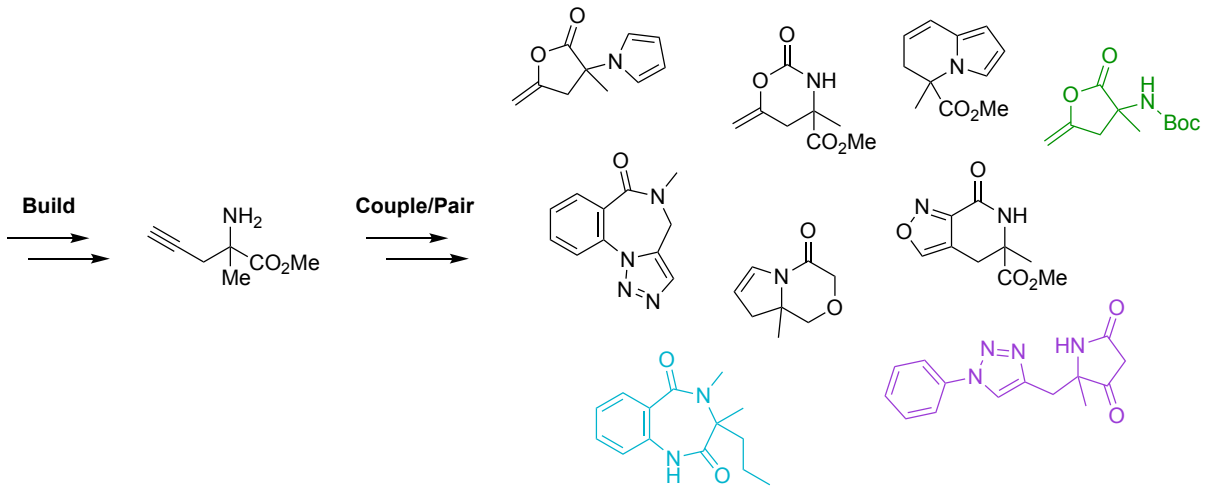

Scheme 1.5. Mateau *et al*. generated a DOS fragment library from racemic α-methyl propargylglycine.[81] The compound shown in green bound to penicillin binding protein 3 (PBP3), the compound shown in blue bound to a member of the transforming growth factor β superfamily and cleavage factor 25kDa (CFI_{25}), and the compound shown in purple bound CFI_{25}.[115]

1.4 Project Aims

Despite the previously discussed advances and examples, there is a requirement for the development of further novel fragments capable of addressing the issues of lack of diversity and/or three-dimensionality in many commercial collections. Indeed, it has been surmised that the limited shape diversity of traditional screening sets predisposes them to success against certain target classes, thereby restricting their utility against targets that require alternative substitution vectors.[84] Thus, the synthesis of diverse fragment collections, which have the potential to access underexplored regions of chemical space, is particularly important for the identification of probes against new and/or difficult targets.

There is also a need for the development of methodologies capable of enabling the rapid and efficient synthesis of novel fragments. Such methodologies would provide an easy route to the generation of analogues for rapid hit-to-lead optimisation. Importantly, calls within the field also remain for the generation of fragments bearing readily functionalisable handles for fragment growth and biological recognition.

With this in mind, the primary aim of this work was the efficient synthesis of a novel fragment library capable of overcoming some of the deficiencies observed in many traditional collections. Such a library, designed to incorporate greater diversity, three-dimensionality, and polar functionality for fragment growth and biological recognition, would have the potential to augment existing fragment collections.

2 Results and Discussion

Under my supervision, some of the compounds presented in this chapter were synthesised by Dr Nikolaj Sten Troelsen, a visiting PhD student in the Spring group. This work is published in Hanby *et al*.,[116] and is reported in the thesis of Dr Troelsen.[117] These reactions are indicated via footnotes and in scheme captions throughout.

2.1 Project Outline

A key way in which greater three-dimensionality can be incorporated into a fragment library is through the introduction of quaternary centre-containing molecules. These motifs are inherently 3D, and allow the simultaneous projection of substituents in multiple directions.[118] Thus, they are expected to enable more efficient navigation of underexplored regions of chemical space.[119] These centres are also of interest due to their prevalence in many NPs and small molecule drugs, as well as their ability to confer greater novelty, selectivity, and metabolic stability (Figure 2.1).[35,85,120–123] However, despite the many recent advances in methodologies for the synthesis of quaternary centres, the sterically-hindered nature of these centres mean that they remain a significant synthetic challenge.[118,124–126] Due to the constraints often imposed on the physicochemical properties of fragments, this challenge is increased in the context of fragment synthesis and, as such, scaffolds containing these motifs rarely feature in fragment collections.[61,78,126,127]

Inspired by recent work by Kidd *et al*., in which a DOS strategy was successfully employed for the generation of a diverse fragment library from which several hits were identified, it was hypothesised that a similar strategy could be employed utilising an all-carbon quaternary centre-containing building block.[78] Not only was this expected to increase the three-dimensionality and novelty of the resulting library, but also NP-likeness.

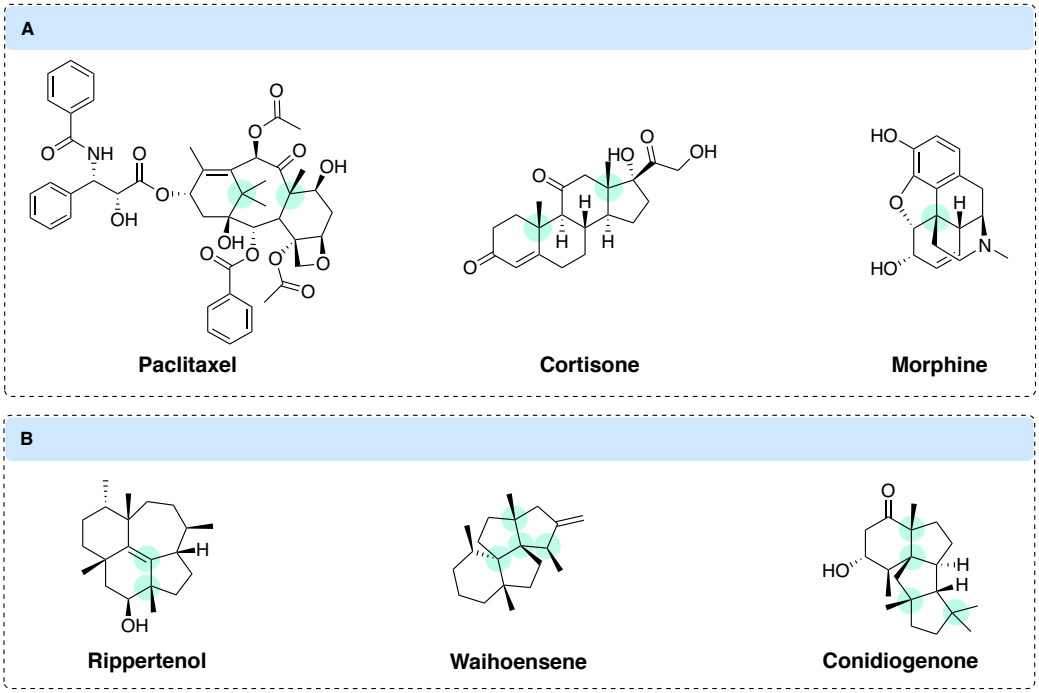

Figure 2.1. A selection of NPs possessing all-carbon quaternary stereocentres (highlighted in turquoise). (A) NPs used as drugs; (B) Additional examples of NPs.

In line with this vision, 3-hydroxy-2-methyl-2-(prop-2-yn-1-yl)cyclopentan-1-ones (**1**) were selected as the key building block for library generation. By exploiting the numerous synthetic handles (via a DOS strategy) and vicinal stereocentres, it was expected that these building blocks would enable the generation of extensive scaffold diversity, whilst simultaneously incorporating a range of functional handles for fragment growth.

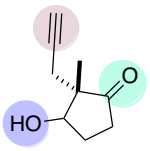

1

Figure 2.2. Pluripotent 3-hydroxy-2-methyl-2-(prop-2-yn-1-yl)cyclopentan-1-ones were selected as the building blocks for library generation.

Notably, 2,2-disubstituted-cyclopentanone/cyclopentanol motifs are present in numerous NPs and pharmaceutical agents, and as such they are often considered privileged scaffolds (Figure 2.3).[128–134] Indeed, the synthetic importance of 3-hydroxy-2,2-disubstituted-cyclopentan-1-ones has already been widely demonstrated through their use in the total synthesis of numerous 2,2-disubstituted-cyclopentanone/cycloalcohol motif-containing NPs.[133,134] It was therefore expected that incorporation of this motif within a novel fragment library would provide a potential means by which underexplored regions of biologically-relevant chemical space could be probed.

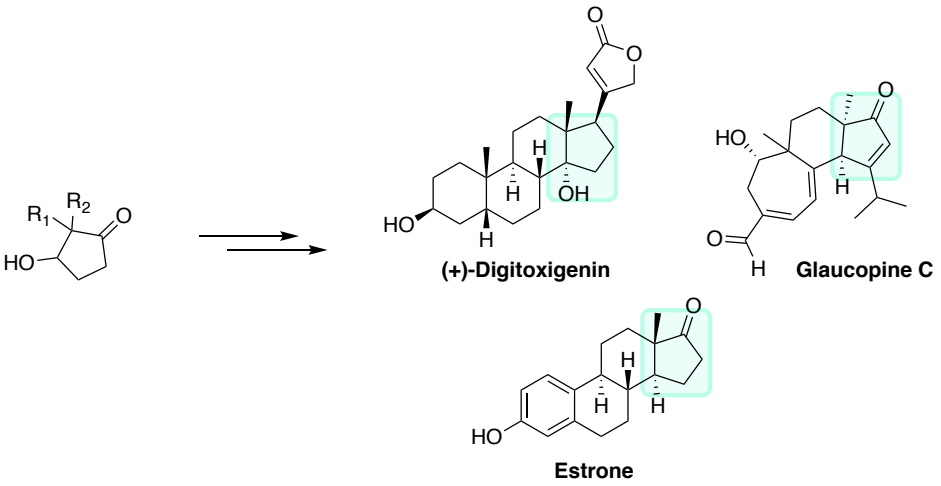

Figure 2.3. The synthetic importance of 3-hydroxy-2,2-disubstituted-cyclopentan-1-ones has been widely demonstrated through their use in the total synthesis of numerous 2,2-disubstituted-cycloketone/cycloalcohol motif-containing NPs.[133,134]

To maximise efficiency, a general strategy for library construction was proposed following the B/C/P approach commonly employed during DOS campaigns (Scheme 2.1).[110]

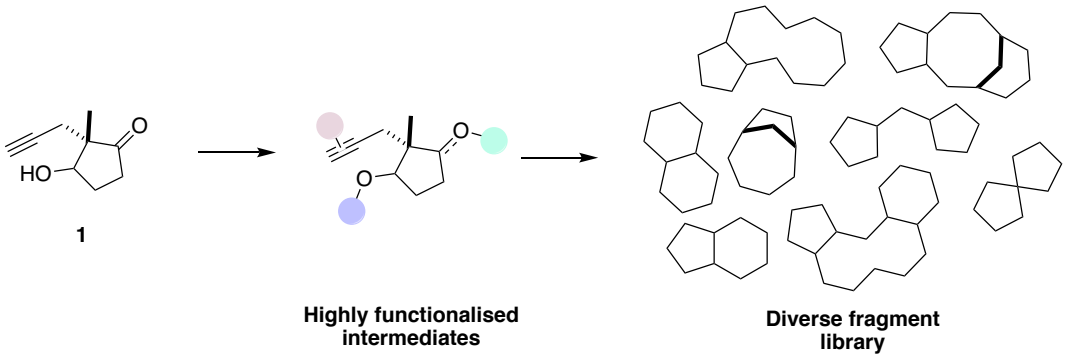

Scheme 2.1. Proposed strategy for the synthesis of a diverse and three-dimensional fragment library.

It was hypothesised that the first stage of the project would focus on the construction of building blocks *syn*-1 and *anti*-**1** via a two-step procedure starting from the diketone **2**. This would involve initial alkylation of **2**, followed by monoreduction of the resulting diketone **3** (Scheme 2.2). In this manner, both possible *syn*- and *anti*-diastereomers could be accessed and harnessed to introduce stereochemical diversity to the resulting library. Importantly, this approach could allow for a racemic strategy to be employed, facilitating downstream screening of both enantiomers.[8]

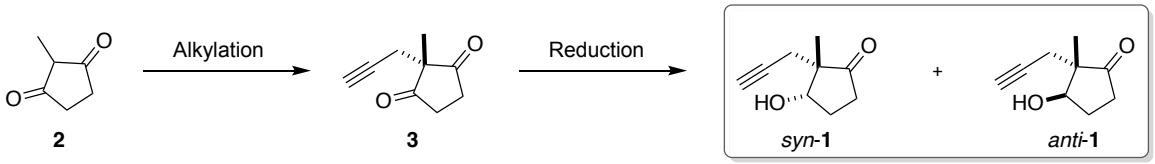

Scheme 2.2. Proposed strategy for building block synthesis.

The versatile nature of the proposed synthetic route would also allow for modification of both the R group at the quaternary stereocentre and ring size simply through selection of the desired diketone (Scheme 2.3). Thus, in future hit-to-lead campaigns rapid analogue synthesis could be facilitated, alleviating a common bottleneck in FBDD.[76]

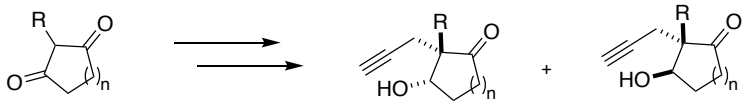

Scheme 2.3. The proposed synthetic strategy is expected to enable rapid analogue synthesis.

The second stage of the project would then focus on the generation of a range of diverse and 3D fragments from the key building blocks via a divergent strategy. To fully exploit the building block it was envisioned that four main pathways could be explored: (A) cyclisation between the alcohol and alkyne handles, either directly or via highly functionalised intermediates; (B) modification of the ketone carbonyl and subsequent cyclisation with the alkyne handle; (C) functionalisation at the α-position of the ketone, followed by cyclisation with the alkyne handle; or (D) intermolecular cyclisation at either the alkyne or the α-position following functionalisation (Figure 2.4). In this manner, numerous diverse scaffolds, each bearing a quaternary sp^3 carbon, could be efficiently constructed from a common pair of diastereomeric precursors in a limited number of steps.

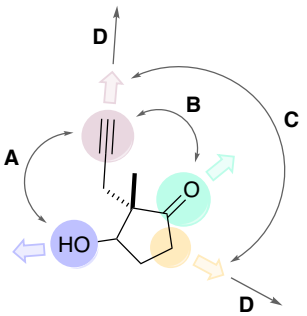

Figure 2.4. The pluripotent nature of 3-hydroxy-2-methyl-2-(prop-2-yn-1-yl)cyclopentan-1-one building blocks.

2.2 Building Block Synthesis

In line with the proposed building block synthesis detailed in Scheme 2.2, investigations began with the formation of *syn*-**1** and *anti*-**1** in two steps from cheap and commercially available cyclopentanone **2**. Thus, following a literature procedure, dione **2** was initially alkylated with propargyl bromide to form the key all-carbon quaternary centre (Scheme 2.4).[135] The resulting 2,2-disubstituted dione **3** was then subjected to reductive desymmetrisation with $NaBH_4$ to provide a separable 62:38

diastereomeric mixture of alcohols *syn*-**1** and *anti*-**1**[b] – consistent with the expected preferential attack of the least hindered face. Pleasingly, the use of sub-stoichiometric $NaBH_4$ (0.6 equiv.) was able to minimise diol formation, with less than 5% of the diol formed, and 23% of unreacted starting material successfully recovered.

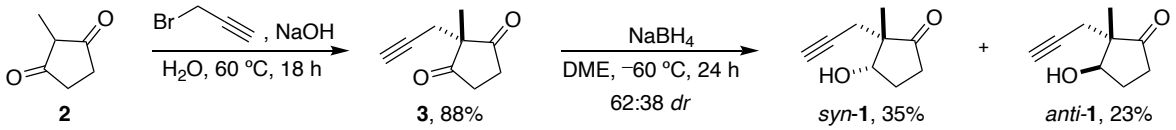

Scheme 2.4. Two-step procedure for the synthesis of building blocks *syn*-**1** and *anti*-**1**.

To probe whether improved *dr* could be achieved, both CBS and yeast reduction were also investigated; however, no improvement was observed (Scheme 2.5).[133,136] Since the preference for the DOS strategy was to include a racemic strategy, the original $NaBH_4$ conditions were repeated on scale to enable isolation of both the *syn*- and *anti*- products for use in downstream synthetic pathways.

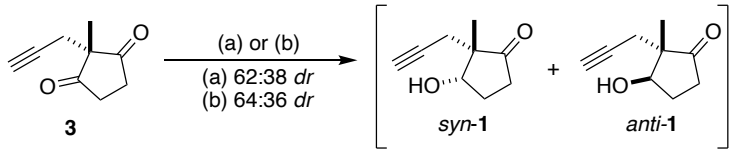

Scheme 2.5. *Reagents & conditions*: (a) (*S*)-CBS-*B*-Me, catecholborane, THF, –78 °C, 2 h; (b) Baker's yeast, sucrose, Triton-X, H_2O/EtOH (100:3), rt, 2 days. Ratios determined by crude ^{1}H NMR, products not isolated.

2.3 Preparation of Highly Functionalised Intermediates and Further Cyclisation: Couple and Pair Phases

2.3.1 Hydroxyl Group and Alkyne Cyclisation Strategies – Pathway A

With the building blocks *syn*-**1** and *anti*-**1** in hand, efforts first turned to fragment synthesis via pathway A (Figure 2.5).

[b] Determined by ^{1}H NMR spectroscopy.

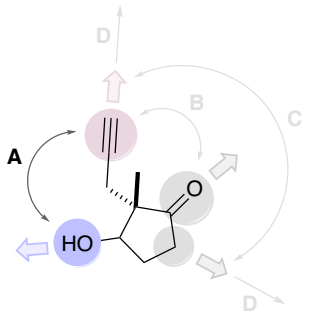

Figure 2.5. Investigations began with exploration of pathway A.

It was expected that three main strategies could be employed to enable cyclisation via this pathway (Figure 2.6):

1. **Hydroxyl group functionalisation:** the introduction of additional functionalities via alkylation/acylation of the hydroxyl motif would enable the formation of intermediates poised for intramolecular cyclisation reactions with the alkyne handle.
2. **Direct cyclisation:** the hydroxyl group could directly undergo intramolecular cyclisation reactions with the alkyne moiety.
3. **Hydroxyl group substitution**: finally, the hydroxyl group could undergo a substitution reaction to introduce an alternative functional group capable of undergoing an intramolecular cyclisation with the alkyne handle.

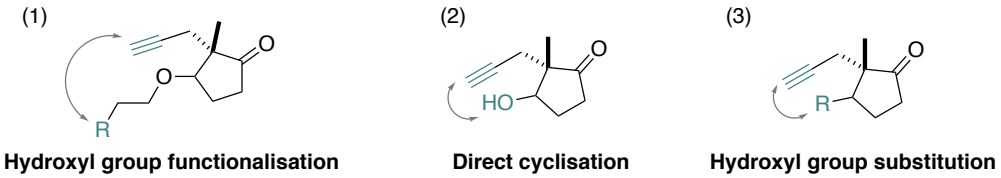

Figure 2.6. Three strategies were proposed for functionalisation via pathway A.

2.3.1.1 Introduction of Alkene Functionality

In accordance with the above proposal, attention was first directed towards the alkylation of building block *syn*-**1** with an alkene-containing coupling partner. It was hypothesised that this would allow for further cyclisation via ring-closing enyne metathesis (RCEYM) for the formation of a substituted cyclic ether. These motifs frequently occur as subunits of marine NPs, some of which exhibit important biological properties including anticancer, antibacterial, or antifungal activities.[137]

To this aim, attempts to transform *syn*-**1** into the corresponding allyl ether **4** were made using conditions adapted from related literature examples.[138,139] Unfortunately, however, treatment with NaH/allyl bromide in DMF led to the formation of a complex mixture (Table 2.1, entry 1). LCMS analysis and ^{1}H NMR spectroscopy indicated the formation of several species containing multiple allyl

groups; however, no identifiable products could be isolated via column chromatography. A similar result was also observed upon changing the base to K_2CO_3 (Table 2.1, entry 2).

It was hypothesised that this non-specific reactivity may be due to instability of the building block under basic conditions. As a result, further attempts to allylate *syn*-**1** were made using allyl trichloroacetimidate; a reagent capable of alkylating hydroxyl groups under mildly acidic conditions.[140] Disappointingly, however, the addition of *O*-allyl 2,2,2-trichloroacetimidate and TfOH to *syn*-**1** again led to the formation of a complex mixture (Table 2.1, entry 4). Likewise, reaction of *syn*-**1** with allyl bromide in the presence of $CaSO_4$ and Ag_2O did not appear to yield any of the desired product (Table 2.1, entry 5).

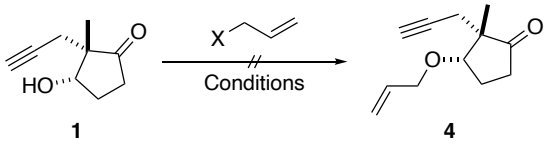

Table 2.1. Attempted allylation of **1** to form alkene-intermediate **4**.

Entry	R-X	Conditions	Results[a]
1	R-Br (1.1 equiv.)	NaH, DMF, 0 °C to rt, 2 h	Complex mixture
2	R-Br (1.1 equiv.)	K_2CO_3, DMF, rt, 18 h	Complex mixture
4	R-OC(NH)CCl_3 (1.1 equiv.)	TfOH, CH_2Cl_2/cyclohexane (2:1), 0 °C to rt, 5 h	Complex mixture
5	R-Br (1.1 equiv.)	$CaSO_4$, Ag_2O, DMF, 0 °C to rt, 18 h	Complex mixture

[a]As determined by ^{1}H NMR spectroscopy, TLC and LCMS analysis of the crude product. R = CH_2CHCH_2

To maintain focus on investigating the synthesis of diverse scaffolds as opposed to detailed optimisations, an alternate strategy for the introduction of alkene functionality was explored. Thus, *syn*-**1** was instead reacted with 5-hexenoic acid under esterification conditions to form the alkene-containing ester **5** in 91% yield (Scheme 2.6).

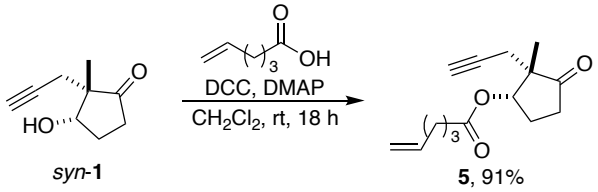

Scheme 2.6. Acylation of *syn*-**1**.

Having established an efficient route to **5**, attention then turned to pairing of the alkene and alkyne functionalities via RCEYM. Whilst medium sized ring systems (8–11 membered) are found widely in bioactive NPs, their synthesis is significantly more challenging compared to small- and large-ring compounds.[141–143] As such, medium-sized ring systems have historically been underrepresented in medicinal chemistry.[144] Nonetheless, there are several known examples of their synthesis via RCEYM, particularly when conformational constraints favour cyclisation.[143,145]

Direct RCEYM of enyne substrate **5** to form cyclised product **6** was initially attempted using the second-generation Grubbs' catalyst under a nitrogen atmosphere. Disappointingly, **5** was found to be inert under these conditions, affording only starting material (Scheme 2.7).

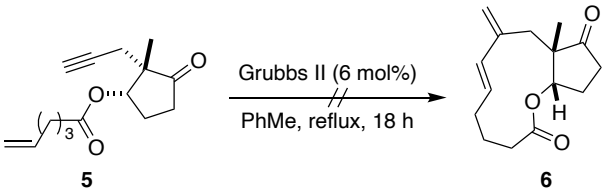

Scheme 2.7. Attempted RCEYM to form cyclised product **6**.

It has been widely reported that that the addition of ethylene to RCEYM reactions involving terminal alkynes results in higher yields, likely due to acceleration of the transformation of the alkyne to the corresponding diene, which can then undergo ring closing metathesis.[146–148] However, whilst efficient cross-metathesis of **5** with ethylene was possible to give diene **7**, none of the desired cyclised product was initially observed by LCMS or crude ^{1}H NMR spectroscopy on repeating the reaction under an ethylene atmosphere (Scheme 2.8).

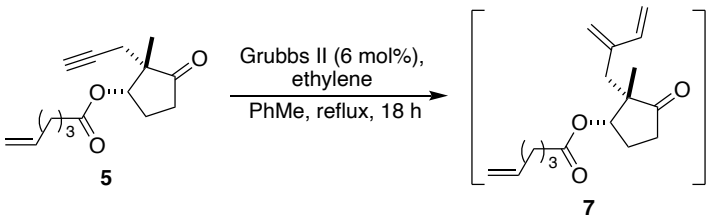

Scheme 2.8. RCEYM under an ethylene atmosphere led to the formation of diene **7** as the sole product.

Suspecting the excess of ethylene to be preventing subsequent cyclisation, the reaction was repeated once more under an ethylene atmosphere, with the reaction degassed following cross-metathesis with ethylene (Scheme 2.9). Pleasingly, this preferentially led to the generation of 11-membered ring **6** via an *endo*-cyclisation in good yield. It was envisioned that the embedded diene in the resulting fragment would provide a useful handle for fragment growth.

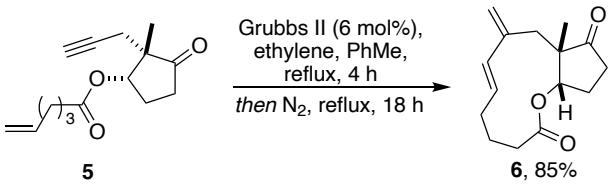

Scheme 2.9. Synthesis of 11-membered ring-containing fragment **6**.

Motivated by the successful generation of **6**, the same approach was then attempted for the generation of a seven-membered ring.[c] To this aim, *syn*-**1** was coupled with acrylic acid to give **8** in 51% yield (Scheme 2.10). It was expected that this ester could then be used to form a seven-membered ring lactone via *exo*-cylisation. Instead, however, **8** underwent a diastereoselective tandem cross enyne metathesis-intramolecular Diels-Alder reaction to form the bridged fragment **9** in 87% yield. Although this was unexpected, there are several known examples of the synthesis of similar bicyclo[5.3.1]undecenes via this reaction strategy.[149,150] Furthermore, such motifs are observed in many NPs, perhaps most notably the anti-cancer drug paclitaxel.[151]

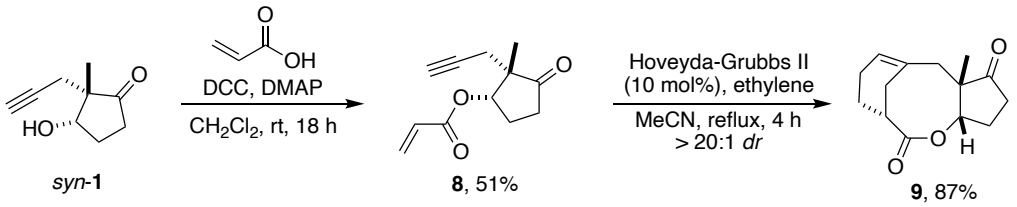

Scheme 2.10. Acylation of *syn*-**1** with acrylic acid and subsequent cyclisation. Reactions and analysis performed by Dr N. S. Troelsen.[116,117]

2.3.1.2 Introduction of Azide Functionality

Triazoles are an important class of biologically relevant heterocycle, with several marketed drugs possessing these motifs.[152] This includes the broad-spectrum antibiotic cefatrizine,[153] beta-lactamase inhibitor tazobactam,[154] and the anti-tumour agent carboxyamidotriazole (Figure 2.7).[155] It was therefore anticipated that the production of fragment-like, triazole-bearing scaffolds would be of great interest.

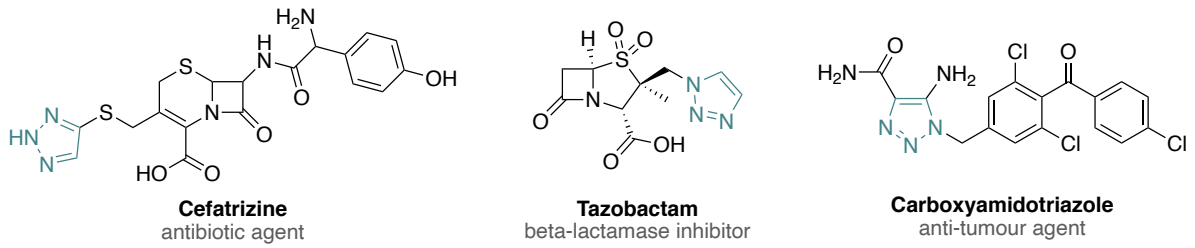

Figure 2.7. Examples of triazole containing marketed drugs.

[c] Reactions and analysis performed by Dr Nikolaj Sten Troelsen.[116,117]

Inspired by these reports, the introduction of azide-functionality to *syn*-**1** was next explored. It was hypothesised that this could allow for a subsequent [3+2] cycloaddition with the alkyne handle to form a fused triazole scaffold. Based on previous successful acylations of the hydroxyl group, it was expected that the desired azido group could be introduced through the coupling of *syn*-**1** with an azide-containing carboxylic acid. Indeed, DCC-mediated reaction of *syn*-**1** with 4-azidobutanoic acid gave the desired product **10** in good yield (Scheme 2.11). In this case, a larger alkyl chain was chosen with the aim of facilitating cyclisation via either RuAAC or CuAAC, such that both 1,4-disubstituted triazole and 1,5-disubstituted triazole motifs could be generated, respectively.[156]

With azide **10** in hand, it was then subjected to a RuAAC under high dilution conditions to form the 10-membered ring-containing fragment **11** in 87% yield (the regiochemistry of **11** was established through means of heteronuclear multiple-bond correlation [HMBC] 2D NMR spectral analysis). In contrast, subsequent attempts to form the more strained 11-membered ring system **12** via CuAAc were unsuccessful. No reaction was observed when refluxing **10** with CuI (10 mol%) and DIPEA for 48 hours, whilst attempts to increase catalyst loading to 20 mol% led to the eventual complete decomposition of the starting material after 72 hours (observed by ^{1}H NMR spectroscopy and LCMS analysis).

Nonetheless, inspired by the success of the RuAAC reaction, an 8-membered ring analogue was also synthesised to further expand the library. Alcohol *syn*-**1** was subjected to the previously established conditions using 2-azidoacetic acid.[c] Analogous to the previous acylation of this substrate, the reaction was found to be successful, delivering **13** in >95% yield. Ester **13** was then able to undergo Ru-catalysed cycloaddition to afford the 8-membered ring derivative **14**, the regiochemistry of which was established through analysis of the HMBC spectrum. Again, no reaction was observed under CuAAC conditions.

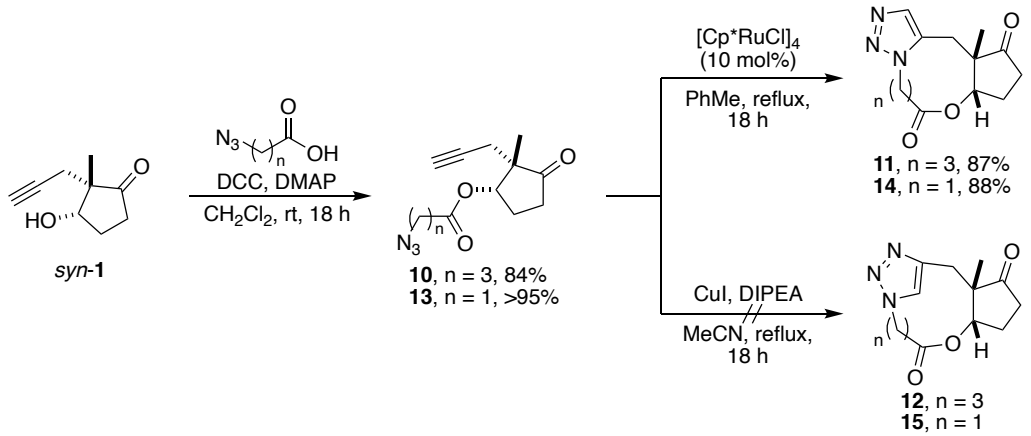

Scheme 2.11. Acylation of *syn*-**1** followed by 1,3-cycloaddition. Reactions and analysis towards the synthesis of **13**, **14**, and **15** was carried out by Dr N. S. Troelsen.[116,117]

2.3.1.3 Introduction of a Michael Acceptor

In a continued effort to exploit the hydroxyl functionality, attention was next directed towards the introduction of an α,β-unsaturated carbonyl moiety. Such an intermediate would be poised for radical cyclisation with the alkyne handle to generate substituted tetrahydropyran (THP) scaffolds. THPs and their partially unsaturated counterparts, dihydropyrans (DHPs), are important structural motifs found in many NPs of therapeutic interest (Scheme 2.11).[157–159]

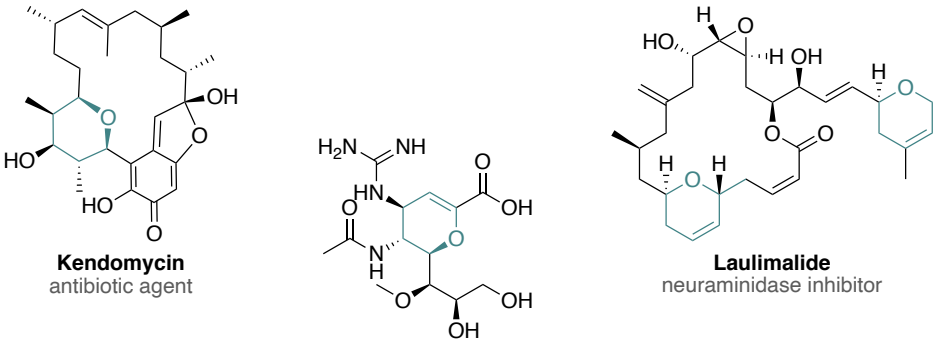

Figure 2.8. Examples of biologically active NPs containing THP or DHP motifs.[160–162]

Utilising a procedure adapted from the literature,[163] α,β-unsaturated carbonyl **16** was generated via *N*-methylmorpholine-mediated hetero-Michael addition of *syn*-**1** to ethyl propiolate (Scheme 2.12). The radical cyclisation was then achieved by dropwise addition of Bu_3SnH and AIBN to the Michael intermediate, followed by acidic destannylation of the resulting *cis*-fused 5,6-bicyclic vinylstannane derivative **17**. This afforded *cis*-fused bicycle **18** in 59% yield, the stereochemistry of which was established by NOE spectroscopy.

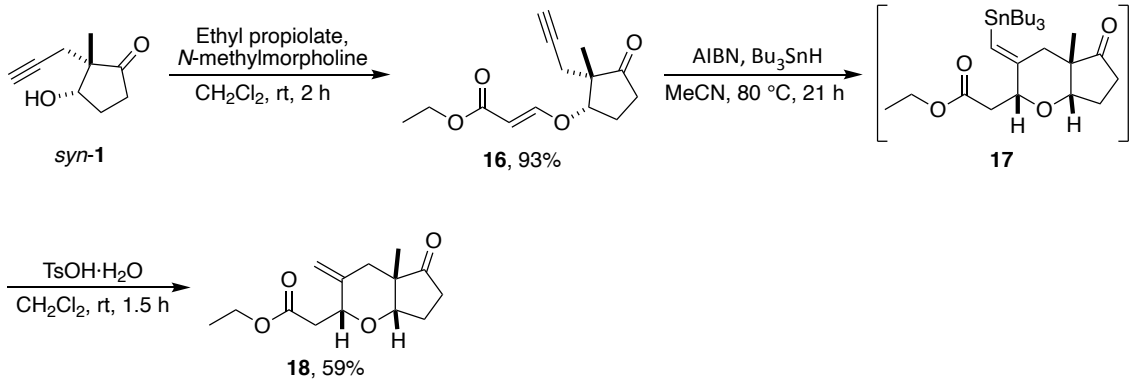

Scheme 2.12. Generation of THP scaffold **18** via radical cyclisation.

2.3.1.4 Direct Intramolecular Cyclisations

Having successfully developed a route for the synthesis of a THP-based fragment, focus then turned to the generation of DHPs. It was expected that these scaffolds could be achieved by the direct cyclisation of the hydroxyl and alkyne functionalities.

The Ru-catalysed cycloisomerisation of bis-homopropargylic alcohols via intramolecular *O*-trapping of a Ru vinylidene intermediate is a well-established strategy for the formation of DHPs.[78,164,165] With this transformation in mind, *syn*-**1** was subjected to conditions developed by Zacuto and co-workers to effect intramolecular cyclisation. Gratifyingly, despite the slow reaction, DHP **19** was successfully synthesised in good yield (Scheme 2.13).[165]

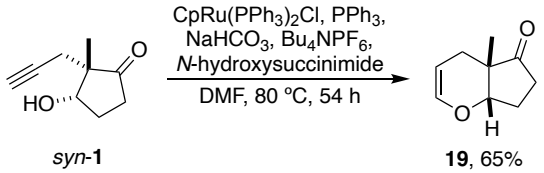

syn-**1** **19**, 65%

Scheme 2.13. The synthesis of the DHP scaffold **19**.

Inspired by the successful synthesis of a THP scaffold, attention next turned to 5-*exo* cyclisations for the formation of tetrahydrofuran (THF) ring systems. Our interest in this moiety again stemmed from its presence in many NPs, as well as FDA-approved drugs (Figure 2.9).[166–170]

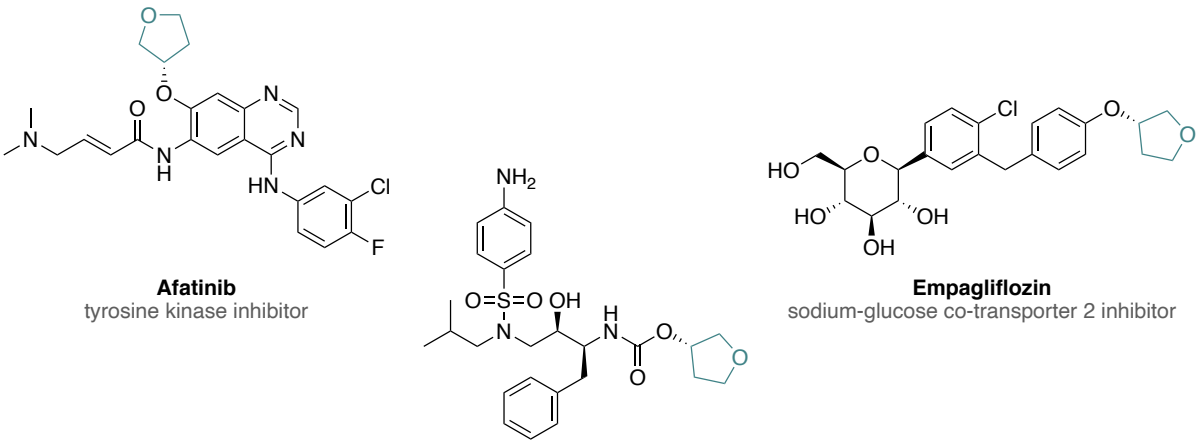

Figure 2.9. Examples of marketed drugs containing THF ring systems.[171–174]

Since these motifs frequently exhibit interesting biological activity, several routes have been developed for their synthesis.[175–177] Among these methods, the metal-catalysed cyclisation of acetylenic alcohols is one of the most widely employed. One such strategy involves the gold- and base-catalysed formation of α-alkylidene oxolanes.[175] Unfortunately, it was found that subjecting *syn*-**1** to these conditions led to decomposition of the starting material, with none of the desired cyclised product **20** observed (Scheme 2.14).

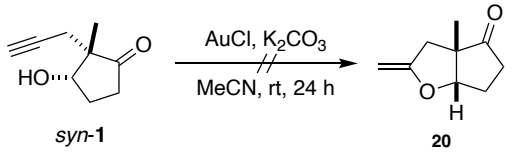

Scheme 2.14. Attempted gold-catalysed intramolecular cyclisation of *syn*-**1**.

As an alternative approach, iridium(I)-catalysed 5-*exo*-dig cyclisation in the presence of methanol was investigated. Pleasingly, these conditions led to the formation of adducts **21a** and **21b** as a separable mixture of isomers (Scheme 2.15).[178] The relative stereochemistry of each isomer was deduced by NOE correlation analysis. Similarly, palladium-catalysed cyclisation-methoxycarbonylation under mild conditions was successful for the generation of β-alkoxyacrylate **22**.[c,179] Some formation of **21a** and **21b** was also observed, but in this case these products were not isolated.

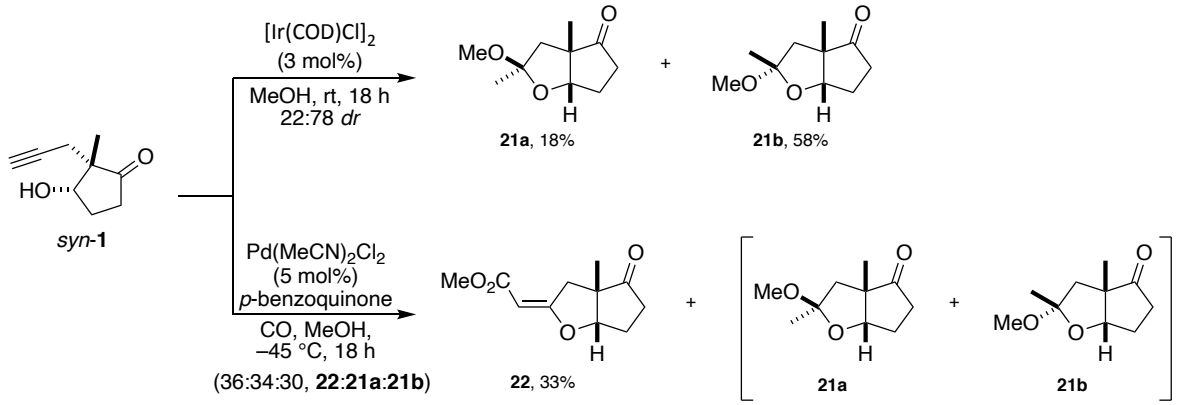

Scheme 2.15. Synthesis of THF-based fragments. Synthesis and analysis of **22** was carried out by Dr N. S. Troelsen.[116,117]

2.3.1.5 Hydroxyl Group Substitution

Having investigated methods for direct pairing of the hydroxyl and alkyne functionalities, efforts then turned to substitution of the hydroxyl group. It was expected that through this change of functionality access to a wider range of scaffolds would be possible. In particular, it was hoped that via introduction of a nitrile group several nitrogen-containing scaffolds could be accessed.

With the overall aim of eventually forming a *cis*-fused cyclic product, efforts focused on the synthesis of nitrile *syn*-**23**. It was envisioned this diastereomer could be formed from building block *anti*-**1** via the use of S_N2 displacement conditions. Thus, *anti*-**1** was first mesylated with MsCl to form *anti*-**24**, and subsequently treated with KCN to facilitate substitution (Scheme 2.16). Unfortunately, however, the reaction appeared to proceed with retention of configuration, resulting in the formation of the undesired product *anti*-**23**.

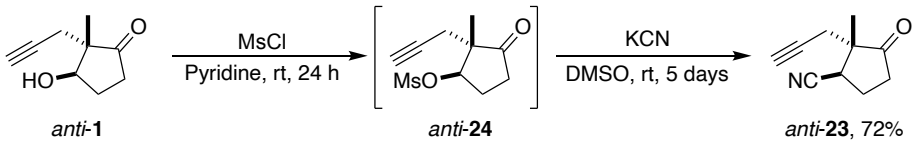

anti-**1** *anti*-**24** *anti*-**23**, 72%

Scheme 2.16. Generation of nitriles *anti*-**23** via displacement of the hydroxyl moiety.

To firmly establish the stereochemistry, the same reaction sequence was then applied to *syn*-**1**. Again, the mesylation and substitution sequence appeared to proceed with retention of configuration (Scheme 3.15). In this way, *syn*-**23** was synthesised in 60% yield.

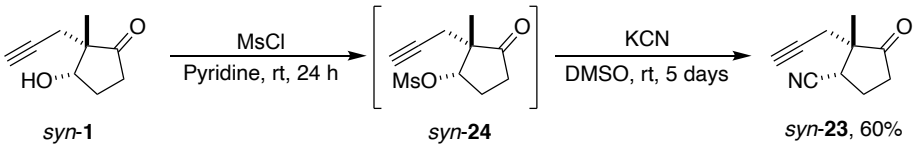

syn-**1** *syn*-**24** *syn*-**23**, 60%

Scheme 3.15. Generation of nitrile *syn*-**23** via displacement of the hydroxyl moiety.

This unexpected retention of configuration was confirmed by NOESY analysis of both *syn*-**23** and *anti*-**23**. The NOE spectrum of *syn*-**23** indicated coupling between H_6 and H_3, suggesting a *syn* relationship between the nitrile and propargyl group, which was not observed in the spectrum of diastereomer *anti*-**23** (Figure 2.10).

syn-**23** *anti*-**23**

Figure 2.10. Key NOE correlation supporting the stereochemical assignment of nitriles *syn*-**23** and *anti*-**23**.

Although this stereochemical outcome initially seemed surprising, comparable results have been reported by Stoltz and co-workers.[180] Indeed, it was observed that the treatment of mesylate **25** with KCN similarly affords the nitrile product **26** with overall retention of configuration (Scheme 2.17). A possible explanation for this is that the reaction proceeds via the formation of an oxetane intermediate generated by initial nucleophilic attack of the ketone. With *syn*-**23** in hand and the stereochemistry firmly established, the utility of the nitrile moiety within a pairing reaction was next investigated.

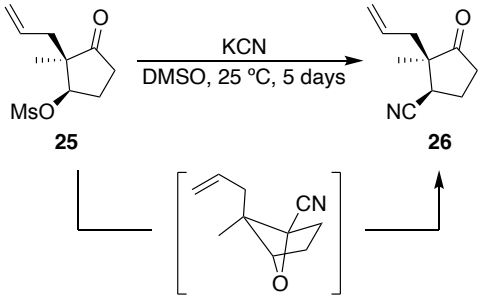

Scheme 2.17. Proposed substitution mechanism via an oxetane intermediate.

Transition-metal catalysed [2+2+2] cyclotrimerisations are an invaluable method for the synthesis of densely functionalised aromatics, enabling the generation of complex scaffolds in a single operational step.[181,182] As a result, these reactions have been extensively used to generate benzene derivatives, whilst more recent examples have demonstrated their utility in the generation of *N*-containing heterocycles.

Inspired by literature examples of the [2+2+2] cycloadditions of alkynes and nitriles, it was speculated that nitrile *syn*-**30** would make an excellent candidate for a [2+2+2] cycloaddition reaction with an alkyne.[78,183] With this in mind, *syn*-**30** was subjected to a [2+2+2] cyclotrimerisation with ethyl propiolate in the presence of catalytic $CpCo(CO)_2$ (Scheme 2.18). Although this led to the formation of a complex mixture of products (as observed by ^{1}H NMR spectroscopy and TLC analysis), **27** was successfully isolated in 10% yield as the only identifiable product. It was suspected that the low yield of this reaction may be due to the tendency of terminal alkynes to undergo undesired side reactions such as alkyne trimerisation.[183] Furthermore, the intermolecular nature of this reaction means that the possibility of formation of a second regioisomer must also be considered, however no evidence of a second isomer was observed by crude ^{1}H NMR spectroscopy. Despite the poor yield, scaffold **27** poses an important addition to the fragment library. Indeed, nitrogen heterocycles featuring a quaternary centre are ubiquitous in NPs and are considered useful building blocks for synthetic chemists,[184] whilst the ester and ketone functionalities provide further synthetic handles for growth. If required, upon hit identification, these [2+2+2] conditions could be optimised to improve the yield by exploiting the several known catalysts and reaction conditions reported in the literature.[185–188]

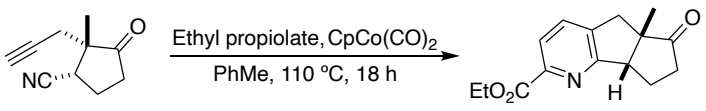

syn-**23** **27**, 10%

Scheme 2.18. Formation of tricyclic scaffold **27** via a cobalt-catalysed [2+2+2] cyclotrimerisation.

2.3.2 Carbonyl Modifications and Pairing Reactions – Pathway B

Satisfied by the successful cyclisation reactions via pathway A, attention then turned to pathway B (Figure 2.11). It was expected that the ketone could be readily exploited to form several highly functionalised intermediates capable of undergoing further cyclisation reactions with the alkyne handle.

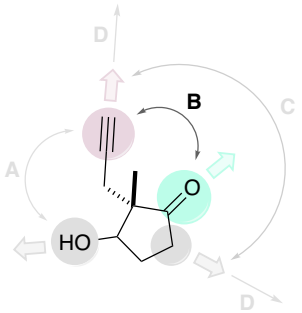

Figure 2.11. Proposed pathway B.

All reactions in this section, where reaction of the hydroxyl group was not required, employed TBS-protected building blocks *syn*-**28** and *anti*-**28** to prevent unwanted side reactions. These scaffolds could be readily synthesised from the corresponding free alcohols by reaction with TBSCl in the presence of imidazole (Scheme 2.19), providing the desired intermediates in excellent yield.

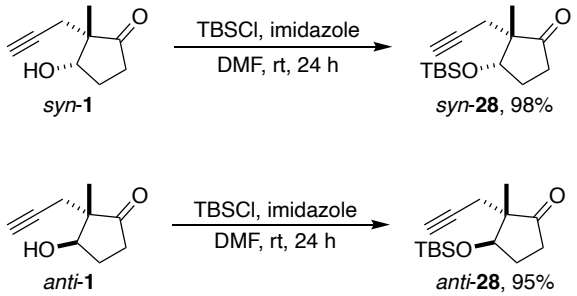

Scheme 2.19. Synthesis of TBS-protected building blocks *syn*-**28** and *anti*-**28**.

Given the utility of the building block *syn*-**1** has already been extensively demonstrated, further exploration was predominantly performed using the TBS protected derivative *anti*-**28**.

2.3.2.1 Ring Expansions

Ring expansions represented an attractive strategy for the modification of the ketone, providing a simple route by which further three-dimensional scaffolds could be accessed. Thus, inspired by the countless reports of Beckman rearrangements of cyclopentanones, it was envisioned that this reaction would enable access to a number of δ-lactam-based scaffolds.[189–191] To this end, the sterically hindered aminating reagent O-mesitylenesulfonylhydroxylamine (MSH), **29**,[190] was first synthesised via a two-step procedure from 2-mesitylenesulfonyl chloride, **30**, (Scheme 2.20).[192] The freshly prepared MSH

was then able to successfully mediate a one-pot Beckmann rearrangement of *anti*-**28**, to yield lactam **31**. To enable inclusion of this lactam scaffold in the final screening collection, **31** was subjected to standard TBS-deprotection conditions to afford the free alcohol **32**.

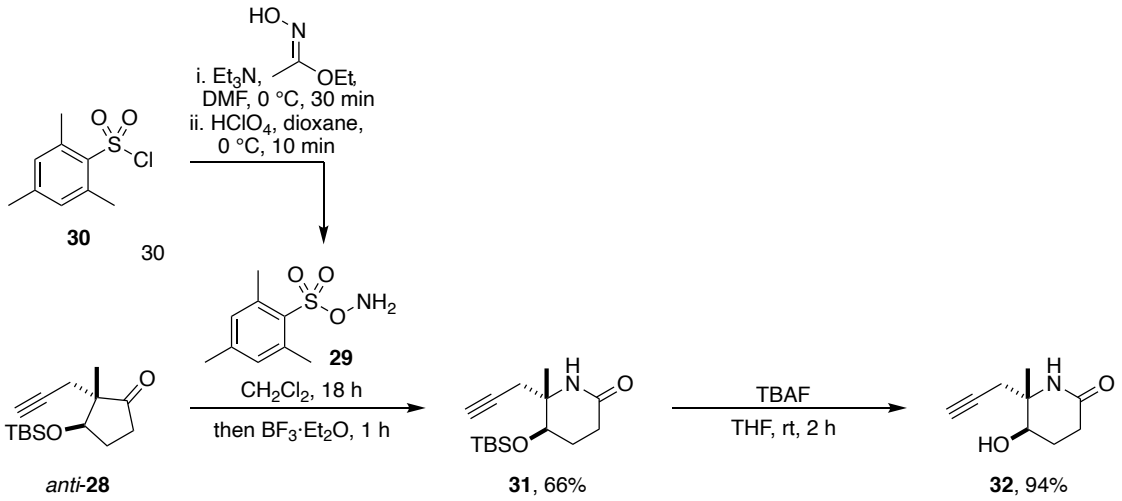

Scheme 2.20. Beckmann rearrangement of *anti*-**28**.

Looking to further exploit the lactam, methodology developed by Nicolai *et al.* for the synthesis indolizidinones was next explored.[193] This approach involved initial hydroindiation of **31** with $HInCl_2$ and subsequent quenching with iodine to yield a vinyl iodide intermediate (Scheme 2.21). Utilising conditions developed by Buchwald for the intermolecular vinylation of amides,[194] the vinyl intermediate was then transformed into bicyclic scaffold **33**, which was isolated in 64% yield. Finally, TBAF-mediated deprotection served to generate indolizidinone-derivative **34** in good yield. Importantly, it was envisaged that the alkene moiety in **34** could serve as a useful fragment growth vector.[79]

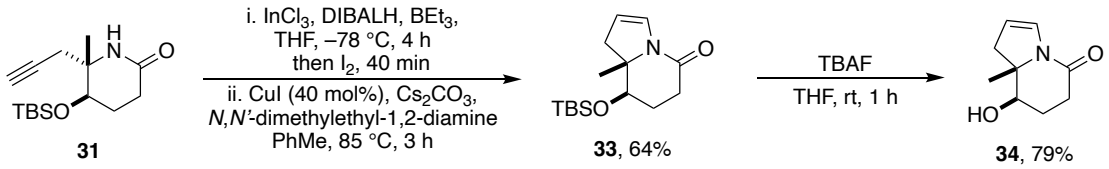

Scheme 2.21. Indolizidinone formation.

Alternatively, **31** was also able to undergo allylation by treatment with NaH and allyl bromide to afford lactam **35** — an intermediate poised for intramolecular cyclisation reactions (Scheme 2.22).[d] For example, RCEYM of **35** in the presence of ethylene proceeded smoothly to yield bicyclic fragment **36** after deprotection. In a second approach, a Pauson-Khand reaction of **35** was accomplished by

[d] Initial investigations into these reactions were carried out on the *syn*-diastereomer by Dr Nikolaj Sten Troelsen.[117]

treatment with $Co_2(CO)_8$ in the presence of the oxidant *N*-Methylmorpholine-*N*-Oxide (NMO), affording [5,6,6]-tricyclic scaffold **37** as a single isomer (the stereochemistry of **37** was deduced by NOE correlation analysis). Pleasingly, the resulting scaffold **37** possesses three stereocentres, thereby further increasing the complexity and diversity of the resulting fragment library.

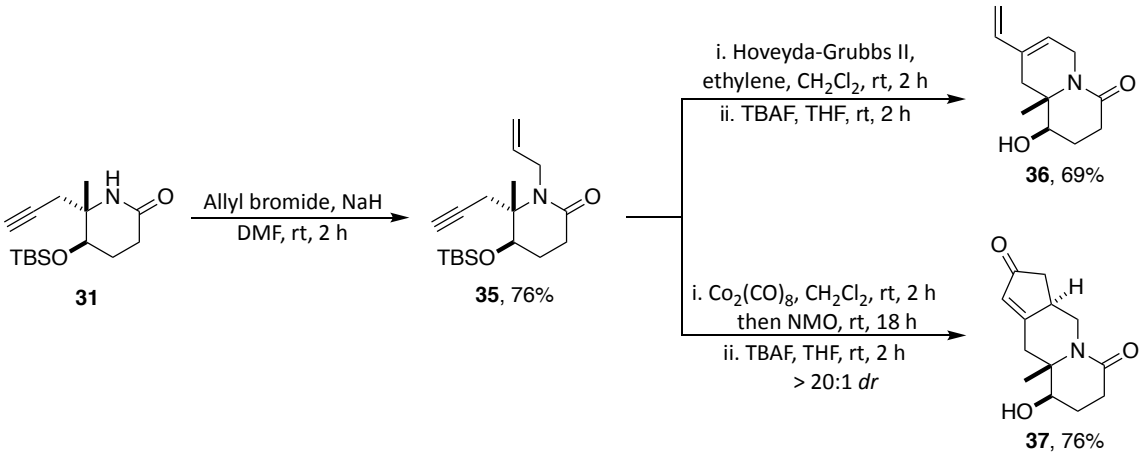

Scheme 2.22. Allylation and subsequent cyclisations of lactam **31**.

To further exploit ring expansion reactions, it was envisioned that a novel fragment could also be rapidly accessed via a Baeyer-Villiger oxidation (BVO). Indeed, in the presence of mCPBA, BVO of *syn*-**28** proceeded regioselectively to give the corresponding lactone **38** in a moderate 29% yield after TBS-deprotection (Scheme 2.23).[c]

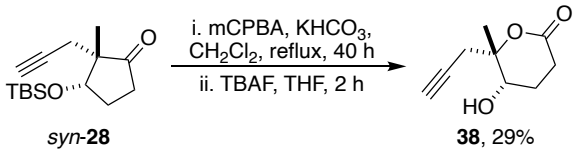

Scheme 2.23. Baeyer-Villiger oxidation of *syn*-**28**. Reactions and analysis performed by Dr N. S. Troelsen.[116,117]

2.3.2.2 Grignard Addition

In an additional effort to functionalise the ketone, it was anticipated that a vinyl group could be introduced to the ketone via Grignard addition. The resulting alkene-containing intermediate **39** would then be poised for cyclisation via either a RCEYM or Pauson-Khand reaction.

The addition of vinyl magnesium bromide to the ketone was carried out under strictly anhydrous conditions and in the presence of $CeCl_3$ to minimise the possibility of side reactions, such as enolisation.[195] Furthermore, to increase the likelihood of the successful formation of cyclised products the installation of the alkene moiety *syn* to the alkyne was required. Thus, to encourage formation of the desired *syn*-product the bulky TBS-protected building block *anti*-**28** was used to hinder attack from

the same face as the methyl group. Pleasingly, this resulted in the formation of a single diastereomer,[e] however only 13% conversion was achieved (Table 2.2, entry 1). Unfortunately, neither increasing the temperature or equivalents (equiv.) of vinyl magnesium bromide resulted in full conversion (Table 2.2, Entries 2–5),[f] and the vinyl product **39** was found to be inseparable from the starting material by column chromatography. Moreover, upon subjecting the crude reaction mixture to RCEYM conditions no cyclised product could be isolated.

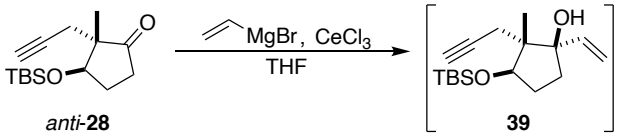

anti-**28** **39**

Table 2.2. Attempted Grignard addition to form **39**.

Entry	Equiv. of vinyl magnesium bromide	Temperature	Time	Percentage conversion[a]
1	3	–78 °C	18	13%
2	3.5	rt	18	30%
3	5	rt	48	38%
4	10	rt	48	50%
5	10	40 °C	18	-[b]

[a]As determined by ^{1}H NMR spectroscopy, TLC and LCMS analysis of the crude product. [b]Complex mixture.

Having failed to isolate vinyl product **39**, the introduction of an allyl group was instead pursued. Gratifyingly, introduction of the allyl group was more successful, with the major diastereomer, **40**, isolated in 62% yield using allylmagnesium bromide as the organometallic species (Scheme 2.24).[c] With **40** in hand, studies then focused on ring-closing reactions between the allyl and alkyne functionalities. In one such reaction, using previously described RCEYM and deprotection conditions (Section 2.3.2.1), the [5,6]-bicyclic scaffold **41** was synthesised in 66% yield. In a second example, the treatment of **40** with $Co_2(CO)_8$ and NMO, followed by deprotection, afforded tricyclic diastereomers **42a** and **42b** in 42% and 17% yield, respectively.

[e] Observed by ^{1}H NMR spectroscopy.
[f] Increasing the temperature to rt also led to a significant reduction in diastereoselectivity.

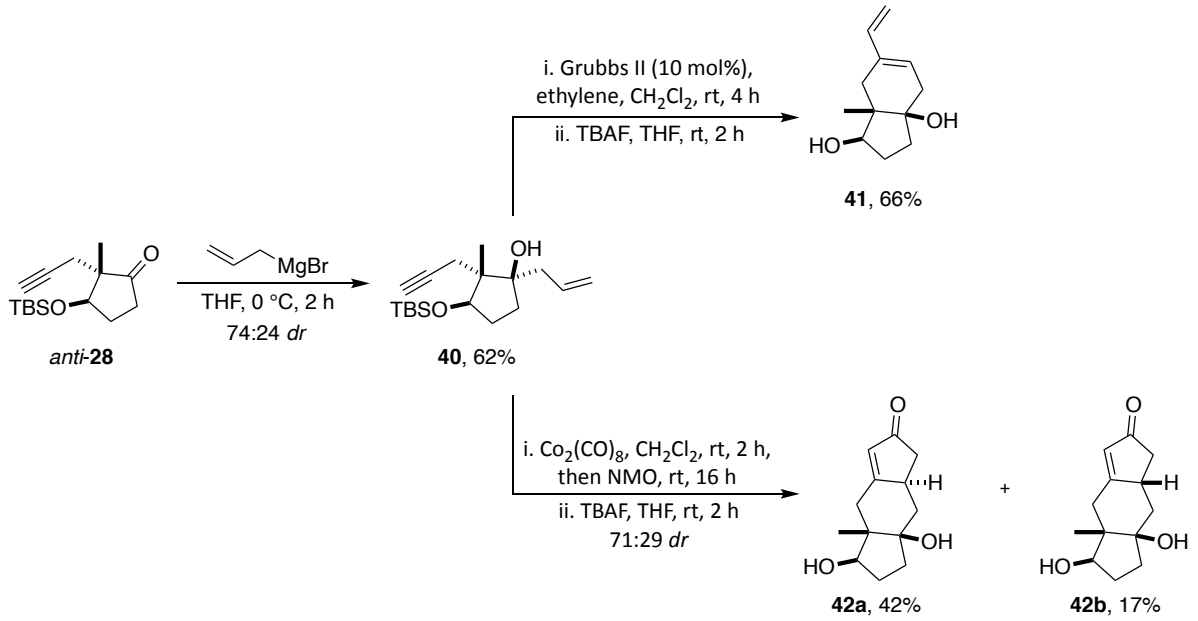

Scheme 2.24. Synthesis and cyclisation reactions of **40**. Reactions and analysis performed by Dr N. S. Troelsen.[116,117]

2.3.3 α-Allylation – Pathway C

Following on from the success of pairing pathway B, attention then turned to pathway C. It was expected that the α-position could be readily functionalised to enable intramolecular cyclisation with the alkyne handle (Figure 2.12).

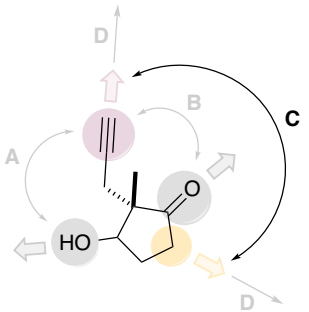

Figure 2.12. Proposed pathway C.

Thus, to exploit the α-carbon, allylation at this position was examined. It was expected that this would then enable cyclisation with the alkyne handle via RCEYM in a similar manner to described in Section 2.3.2.2. To this end, *anti*-**28** was alkylated with allyl bromide to provide intermediate **43** as an inseparable mixture of diastereoisomers (Scheme 2.25).[c] Thankfully, despite being a diastereomeric mixture, intermediate **43** (70:30 *syn:anti*) was able to undergo RCEYM and deprotection to form the corresponding bicyclic scaffold **44** as the only cyclised product in 33% yield.

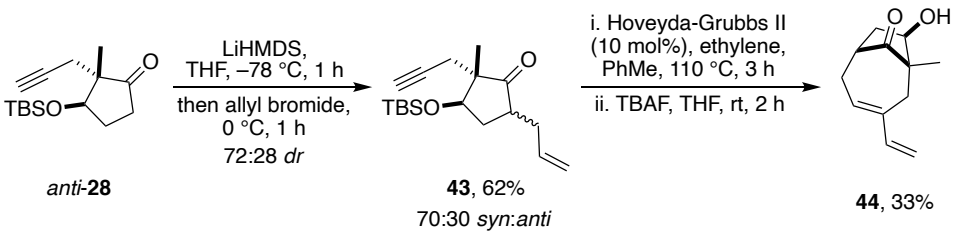

anti-**28** **43**, 62% (70:30 *syn*:*anti*) **44**, 33%

Scheme 2.25. Synthesis of bridge scaffold **44**. Reactions and analysis performed by Dr N. S. Troelsen.[116,117]

2.3.4 Intermolecular Cyclisation Strategies – Pathway D

Having investigated a wide range of intramolecular cyclisation strategies, final efforts focused on the formation of further diverse scaffolds via intermolecular cyclisations (pathway D, Figure 2.13). It was expected that this could be achieved via either direct reaction with the alkyne, or through reaction at the α-position of the ketone following initial functionalisation

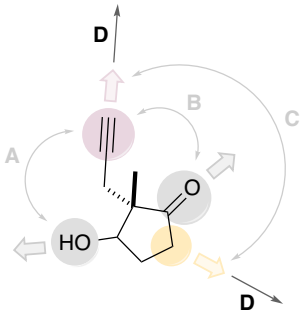

Figure 2.13. Proposed pathway D.

2.3.4.1 Exploitation of the α-Position

α,β-Unsaturated compounds are among the most important building blocks in medicinal chemistry, frequently acting as intermediates in the generation of pharmaceuticals.[196–199] Due to the diverse reactivity of these compounds, it was expected that the incorporation of such functionality into the building blocks would enable access to further biologically relevant ring systems.

Accordingly, based on literature precedent using similar substrates, TBS-protected building block *anti*-**28** was treated with IBX in DMSO/fluorobenzene to facilitate direct formation of the corresponding α,β-unsaturated system (Scheme 2.26).[200] Unfortunately, using these conditions only 50% conversion was achieved, and increasing reaction temperature to 85 °C or doubling the equiv. of IBX served only to generate a complex mixture. Nonetheless, **45** was successful isolated in 45% yield.

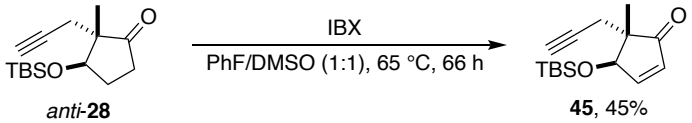

anti-**28** **45**, 45%

Scheme 2.26. IBX-mediated oxidation.

With **45** in hand, efforts then turned to exploitation of the newly formed unsaturated system. Disappointingly, attempts to subject **45** to a Diels-Alder reaction were unsuccessful; reaction with cyclohexa-1,3-diene, freshly distilled cyclopentadiene, or Danishefsky's diene resulted in complete return of unreacted starting material (Scheme 2.27).

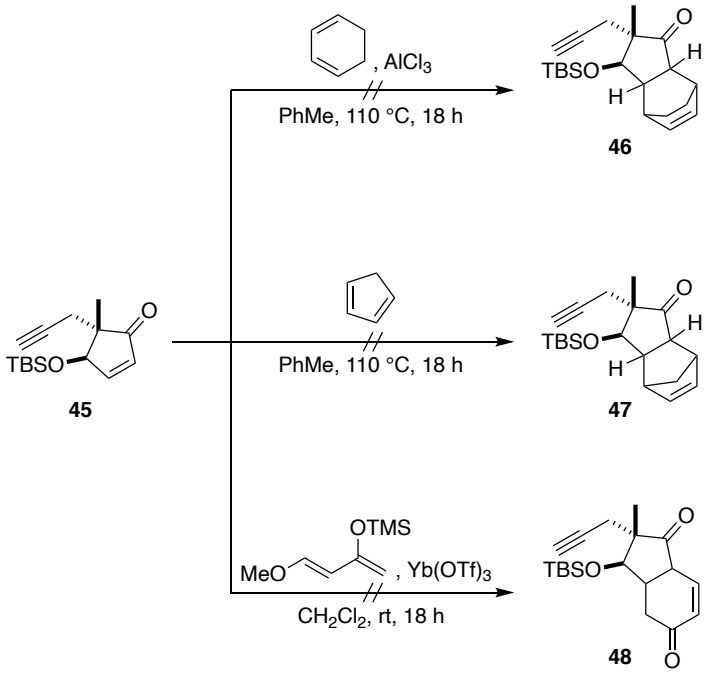

Scheme 2.27. Failed cycloadditions of **45**.

In an alternative approach, crude **45** was directly reacted with the azomethine ylide precursor **49** to avoid the challenging purification (Scheme 2.28).[c] This resulted in the formation of **50a** and **50b** as a separable mixture of diastereomers, in 12% and 10% yield, respectively. Cleavage of the silyl ether by TBAF then gave the bicyclic scaffolds **51a** and **51b** in high yields. Unfortunately, subsequent Pd/C-catalysed hydrogenation of the benzyl groups under a H_2 atmosphere was found to be unsuccessful, resulting in the formation of a complex mixture.

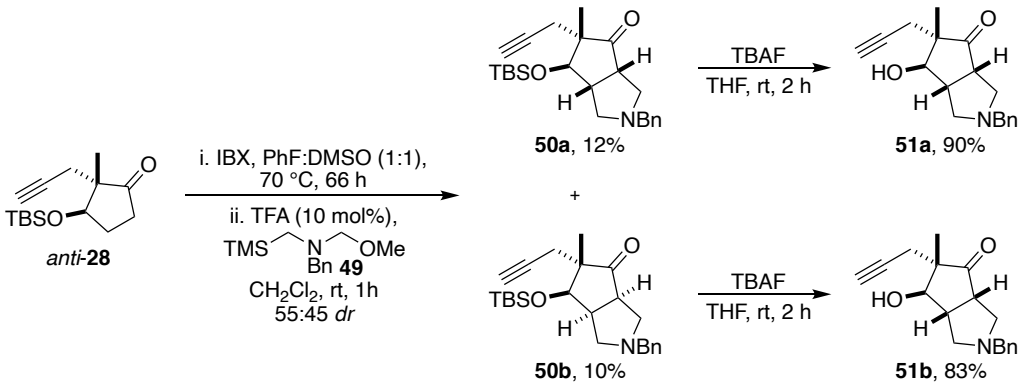

Scheme 2.28. One pot oxidation and cycloaddition. Reactions and analysis performed by Dr N. S. Troelsen.[116,117]

Following on from the previous successful synthesis of an endocyclic α,β-unsaturated ketone, a similar exocyclic system, **52**, was envisioned via α-methylenation. This was achieved in 68% yield through the treatment of *anti*-**28** with excess Et_2NH and CH_2Br_2 under microwave (mW) heating (Scheme 2.29).[c]

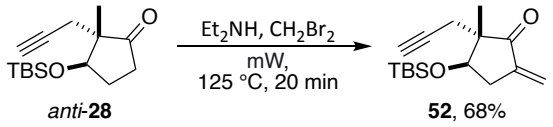

anti-**28** **52**, 68%

Scheme 2.29. Synthesis of exocyclic α,β-unsaturated ketone **52**. Reaction and analysis performed by Dr N. S. Troelsen.[116,117]

Using the previously established conditions, the resulting α,β-unsaturated system **52** was able to undergo a cycloaddition with azomethine ylide precursor **49** to generate spirocylic scaffolds **53a** and **53b** as a separable mixture of diastereomers (Scheme 2.30).[c] In this case both subsequent TBS-deprotection and *N*-debenzylation were successful, affording the fully deprotected fragments **54a** and **54b** in good yields.

Similarly, successful results were achieved by reacting with ethyl 2-chloro-2-(hydroxyimino)acetate to afford the spirocyclic isoxazoline product **55**. Pleasingly, this reaction proceeded with excellent diastereo-, regio-, and chemoselectivity to give **56** as the major product following successful deprotection.

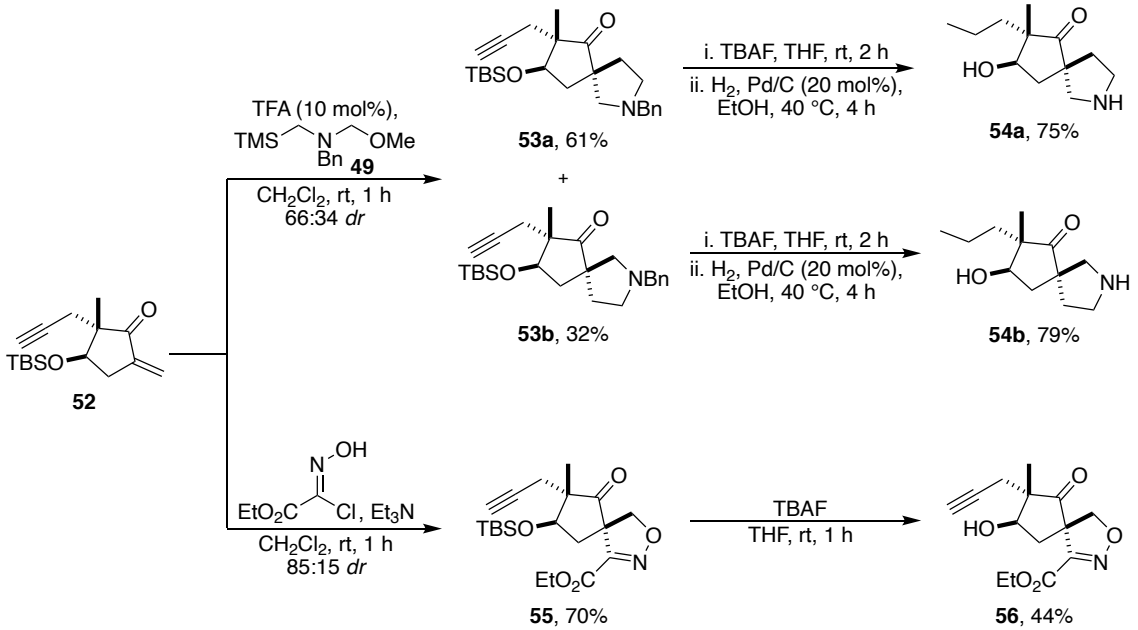

Scheme 2.30. Cycloadditions of α-methylenation product **52**. Reactions and analysis performed by Dr N. S. Troelsen.[116,117]

2.3.4.2 Alkyne Functionalisation

Finally, in an attempt to functionalise the alkyne handle intermolecularly, [3+2]-cycloadditions were investigated. It was expected that one such cycloaddition could be achieved by the Ru-catalysed

reaction of *syn*-**28** with ethyl 2-azidoacetate. Pleasingly, *syn*-**28** was able to undergo efficient Ru-catalysed cycloaddition with ethyl 2-azidoacetate, affording triazole **57** in 82% yield (Scheme 2.31). The regiochemical outcome was determined by HMBC analysis. Subsequent removal of the TBS group in the presence of acetic acid gave the desired triazole fragment **58**. Acetic acid was found to be a necessary addition during this reaction to prevent decomposition of the starting material, perhaps due to instability under the basic conditions created by the presence of water in the TBAF solution.[201,202] Importantly, the inclusion of an ester group in this scaffold was expected to provide a useful handle for fragment growth.

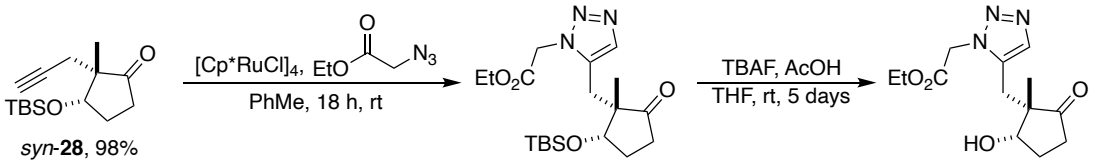

Scheme 2.31. Synthesis of 1,5-triazole **58** via RuAAc.

Encouraged by the success of the [3+2] cycloaddition within the above route, it was anticipated that the cycloaddition of other 1,3-dipoles, such as nitrile oxides, with the alkyne would provide the opportunity to form further complex scaffolds. The generation of isoxazoles through cycloaddition of nitrile oxides is of particular interest due to their presence as the main framework of numerous FDA-approved drugs such as leflunomide and isocarboxazid.[203,204] These motifs are also embedded in more complex drugs such as the antibacterial agent oxacillin (Figure 2.14).[205]

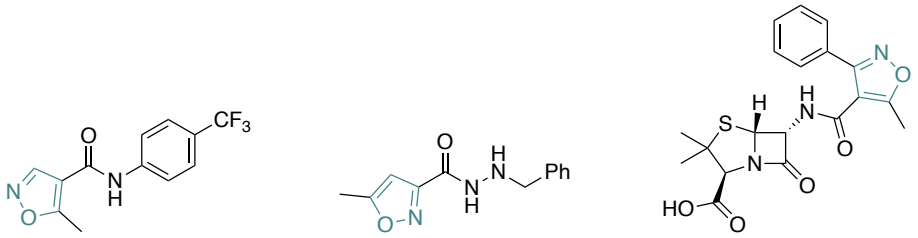

Figure 2.14. The structures of isoxazole-containing FDA-approved drugs.

Fokin *et al*. have reported a Ru-catalysed [3+2] cycloaddition of nitrile oxides (generated *in-situ* from hydroximoyl chlorides under basic conditions) and alkynes to afford 3,4-disubstituted isoxazoles with excellent regioselectivity.[206] Adapting this procedure, *syn*-**28** was subjected to Ru-catalysed cycloaddition conditions with ethyl 2-chloro-2-(hydroxyimino)acetate (1.2 equiv.). Disappointingly, this led to only 10% conversion after 48 hours (observed by crude ^{1}H NMR spectroscopy), with no improvement in conversion observed even upon increasing the number equiv. of ethyl 2-chloro-2-

(hydroxyimino)acetate to 10. This observed lack of reactivity may be due to the dimerisation of the nitrile oxide.

To limit any potential dimerisation the reaction was repeated with the dropwise addition of 10 equiv. of ethyl 2-chloro-2-(hydroxyimino)acetate (Scheme 2.32).[c] Whilst this technique served to increase conversion to ~50%, an inseparable mixture of the isomers **59a** and **59b** (7:5) was observed by crude ^{1}H NMR spectroscopy.

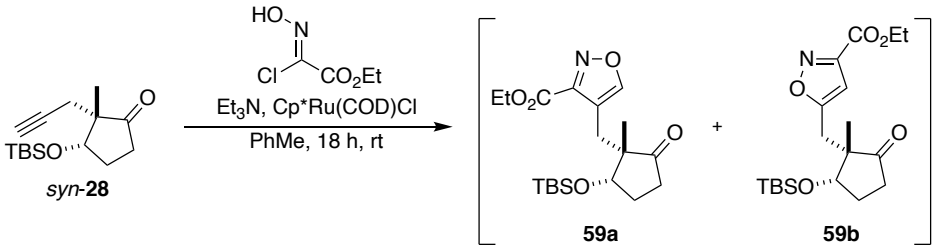

Scheme 2.32. Dropwise addition of ethyl 2-chloro-2-(hydroxyimino)acetate to *syn*-**28** led to an inseperable mixture of **59a** and **59b**. Reaction and analysis performed by Dr N. S. Troelsen.[116,117]

In a further attempt to reduce dimerisation, the bulkier reagent *N*-hydroxybenzimidoyl chloride was employed for isoxazole formation. Pleasingly, treatment of *anti*-**28** with *N*-hydroxybenzimidoyl chloride proceeded with full conversion, affording **60** as a single regioisomer (Scheme 2.33).[g] The regiochemistry of **60** was established through means of HMBC 2D NMR spectral analysis. TBAF-mediated deprotection of the resulting fragment served to generate isoxazole **61**.

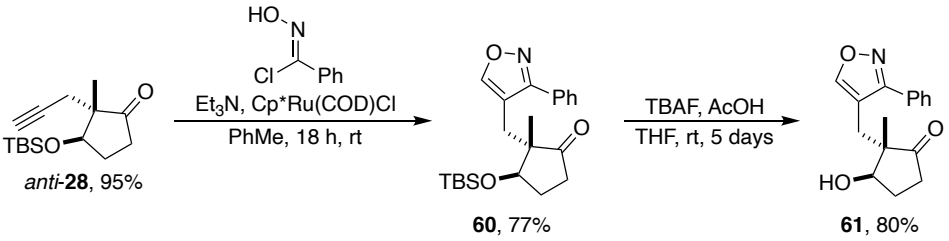

Scheme 2.33. [3+2]-cycloaddition of *N*-hydroxybenzimidoyl chloride with *anti*-**28**.

2.3.5 Exemplification of Building Block Versatility

As previously discussed, once a hit has been identified during fragment screening it must then undergo elaboration to enhance potency. To ensure success during this optimisation stage, it is vital that any fragments screened are supported by robust and general synthetic routes that enable every growth vector to be explored and a significant number of close analogues to be readily synthesised (and/or bought).[75]

[g] In this case the *anti*- isomer, *anti*-**28**, was used due to the greater availability of the building block.

2.3.5.1 Ring Size Modification

With the aim of rapid analogue synthesis in mind, efforts turned to demonstration of the versatile nature of the DOS strategy described in this chapter through altering the ring size of the core building block. It was also expected that inclusion of such analogues into our fragment library would serve to increase library diversity.

A core six-membered ring building block was selected for analogue synthesis. This was not only due to 2-methylcyclohexanone **62** being both cheap and commercially available, but 6-membered chiral cyclic 3-hydroxy ketones have also been used as key building blocks for the synthesis of many NPs and bioactive compounds (Scheme 2.34).[132,207–209]

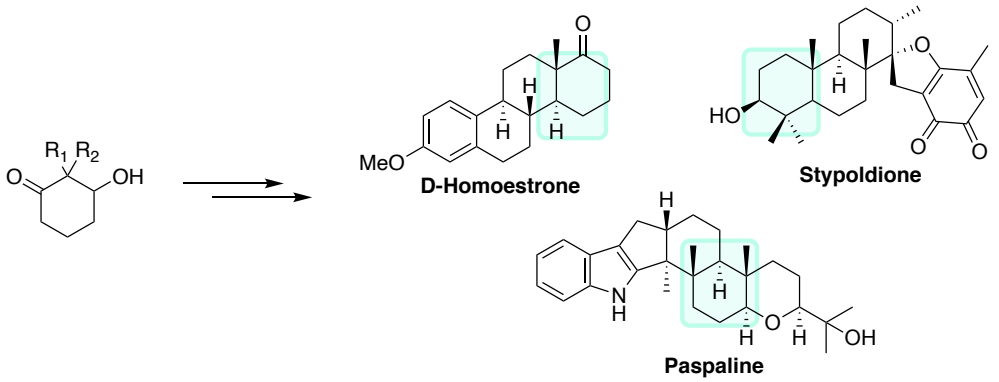

Scheme 2.34. Example of NPs and bioactive compounds synthesised from six-membered chiral cyclic 3-hydroxy ketones.

Applying the previously developed route for building block synthesis, 2-methylcyclohexan-1,3-dione **62** was alkylated with propargyl bromide to form dione **63** in 70% yield (Scheme 2.35). Next, cyclohexanedione **63** was treated with $NaBH_4$ to afford the desired secondary alcohols as a separable mixture of diastereomers *syn*-**64** and *anti*-**64** (57:43 *dr*). Whilst these conditions afforded less than 5% of the diol, consistent with the five-membered ring analogue, in this case lower selectivity and greater conversion were also observed.

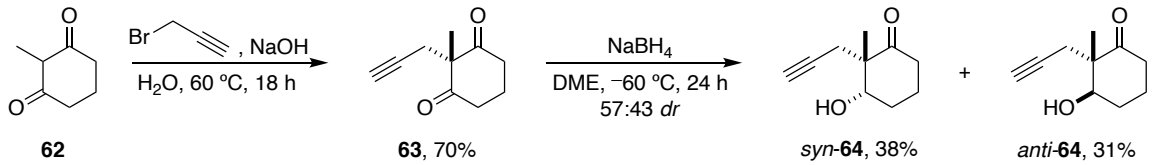

Scheme 2.35. Synthesis of 6-membered ring building block analogues *syn*-**64** and *anti*-**64**.

Following the successful synthesis of building blocks *syn*-**64** and *anti*-**64**, the poised nature of the fragment library was showcased through the generation of analogues of three previously synthesised fragments (Scheme 2.36). In one example, *syn*-**64** was readily acylated with either 5-hexenoic acid or 4-azidobutanoic acid to form **65** and **66**, respectively. Alkene-containing intermediate **65** was then

able to undergo efficient RCEYM to form cyclised product **67** in 83% yield, whilst azido-intermediate **66** underwent a Ru-catalysed click reaction to form **68** in 85% yield (the regiochemistry of which was established by analysis of the HMBC spectrum). Finally, in a further example, the Ru-catalysed intramolecular cyclisation of the alkyne and alcohol functionalities was demonstrated to afford **69** in 63% yield. In each case the resulting yields were comparable to the five-membered ring equivalents.

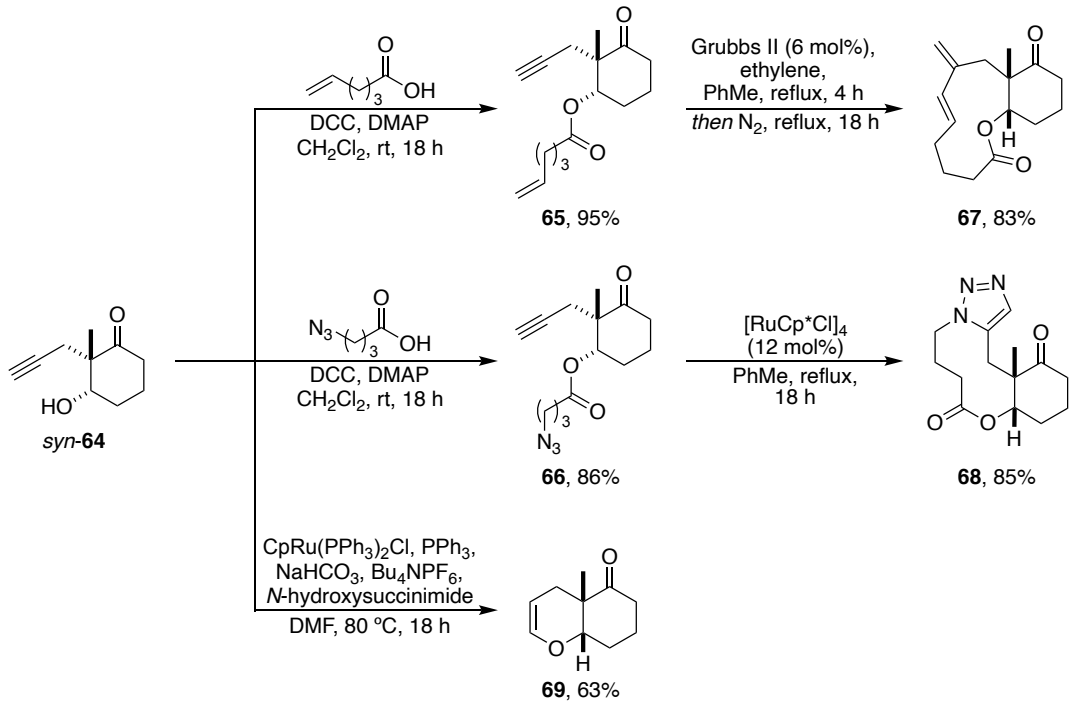

Scheme 2.36. Demonstration of the utility of *syn*-**64** for rapid analogue synthesis.

2.3.5.2 Modification of the Key All-Carbon Quaternary Centre

Variation of the substituent at the key all-carbon quaternary centre was next investigated to illustrate its possible use as a further growth vector (Figure 2.15).

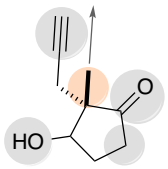

Figure 2.15. The substituent at the key all-carbon quaternary centre could serve as a synthetic growth point.

To this end, a pair of building block analogues bearing a benzyl group were synthesised from cyclopentane-1,3-dione **70**. This required initial installation of the benzyl group to **70** via a one-pot Knoevenagel condensation-reduction sequence (Scheme 2.37).[210] The resulting crude dione **71** was then able to undergo successful alkylation to give **72** in good yield. However, subsequent reduction gave building block **73** as an inseparable mixture of diastereomers (80:20 *dr*).

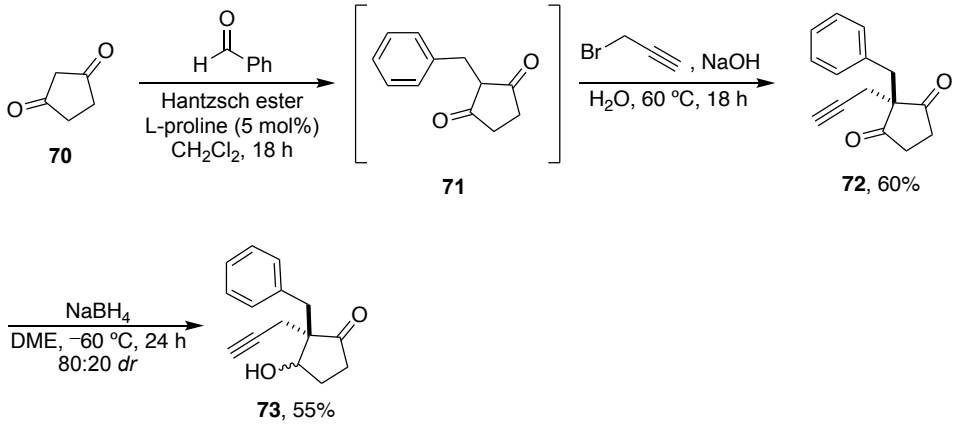

Scheme 2.37. Synthesis of benzyl building block analogue **73**.

In a second example, building block derivatives bearing a cyclopropylmethyl group were also synthesised (Scheme 2.38).[c] Following the previously developed route, the cyclopropylmethyl group was readily introduced to afford **74**, which was isolated in 91% yield. Gratifyingly, in this case, alkylation and reductive desymmetrisation of the resulting dione **75** formed a separable mixture of *anti*-**76** and *syn*-**76** in 54% and 19% yield, respectively. In contrast to the methyl analogues the major product possessed a *syn*-relationship between the R-group (cyclopropylmethyl) and alkynyl handle – a result that is consistent with greater size of the cyclopropylmethyl group relative to the alkynyl handle.

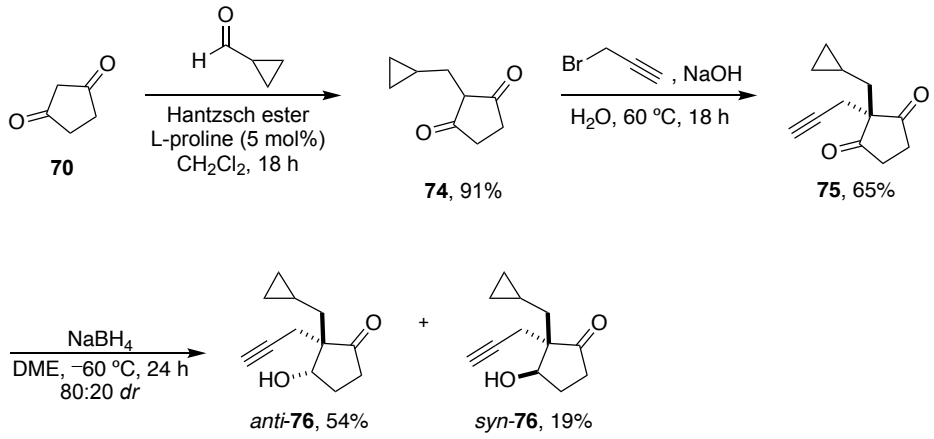

Scheme 2.38. Synthesis of *syn*- and *anti*- cyclopropylmethyl building block analogues. Reactions and analysis performed by Dr N. S. Troelsen.[116,117]

To demonstrate the suitability of the new building blocks for fragment analogue generation and to further expand our library, Ru-catalysed cyclisation of the cyclopropmethyl analogue was explored. Bicyclic fragment **77** was formed in 70% yield from *syn*-**76** using the previously described conditions (Scheme 2.39).[c]

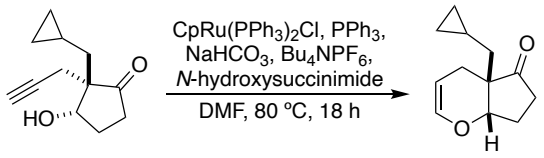

syn-**76** **77**, 70%

Scheme 2.39. Demonstration of fragment synthesis from building block *syn*-**76**. Reactions and analysis performed by Dr N. S. Troelsen.[116,117]

2.4 Library Analysis

In total, a library of 38 structurally diverse fragments based on 20 distinct frameworks was constructed in collaboration with Dr N. S. Troelsen. Only fragments considered suitable for screening were included in the final collection, a summary of which is provided in Scheme 2.40.

2.4.1 Diversity Analysis

One widely used computational method to visualise and compare the shape diversity within a compound collection is principal moment of inertia (PMI) analysis. This technique involves the computation of the moment of inertia of a particular conformation of a molecule around its three principal axes.[211] Sorting by ascending magnitude ($I_1>I_2>I_3$), these values are then converted into normalised ratios, NPR1 (I_1/I_3) and NPR2 (I_2/I_3) to remove the dependency of the results on the size of the molecule. Finally, NPR1 and NPR2 are plotted on a two-dimensional triangular scatterplot, with each corner of the graph representing an extreme of molecular shape (i.e., rod, sphere, or disc). In this manner, PMI plots provide a means by which the three-dimensionality of large compound collections can be rapidly assessed.

PMI analysis of the fragment library was conducted using LLAMA (Lead Likeness And Molecular Analysis), an open-access computational tool (see Appendix 1 for details).[212] Pleasingly, this data showed a high degree of shape diversity within the library, with rod-, disc-, and more sphere-like compounds all well-represented (Figure 3.11). Furthermore, only 8% of compounds were found to have NPR1 + NPR2 < 1.1, a boundary often referred to as 'flatland' due to the characteristic two-dimensional nature of molecules found below this boundary.[35,84,85]

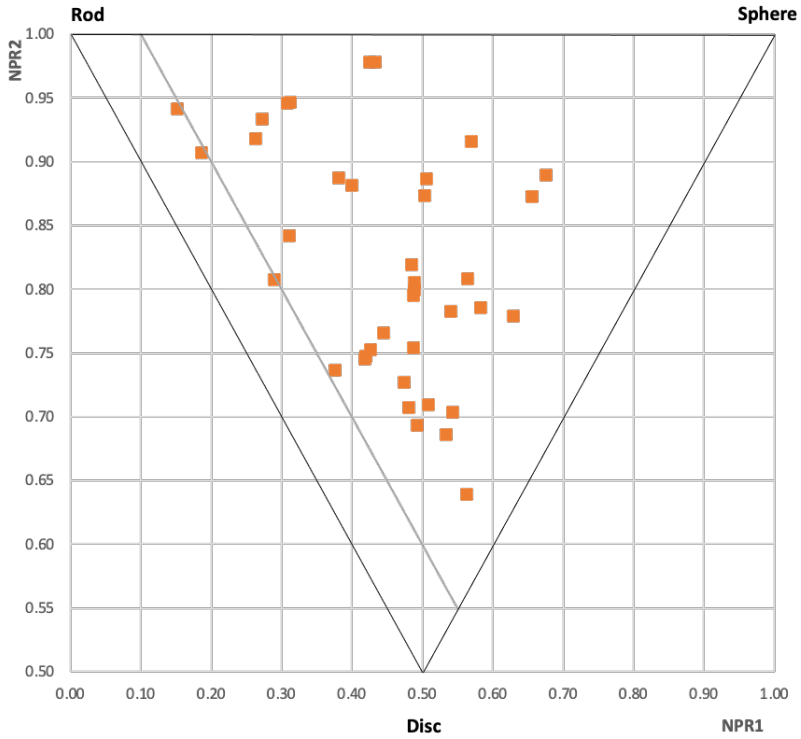

Figure 2.16. PMI plot of the fragment library (red squares). Grey line represents NPR1 + NPR2 = 1.1, the boundary of flatland.

Next, comparisons were made between this new fragment library and the commercially available Maybridge Diversity Set 1, comprising 500 compounds (Figure 2.17). Using the same analysis, a lower degree of three-dimensionality and overall molecular shape diversity was observed with the commercial collection. Moreover, a significant number of compounds within the Maybridge library were found to be two-dimensional, with a significant proportion situated in 'flatland'. This serves to illustrate that although there is growing awareness of the need for diverse libraries, many commercial libraries designed to be diverse, such as the Maybridge diversity set, still lack shape diversity.

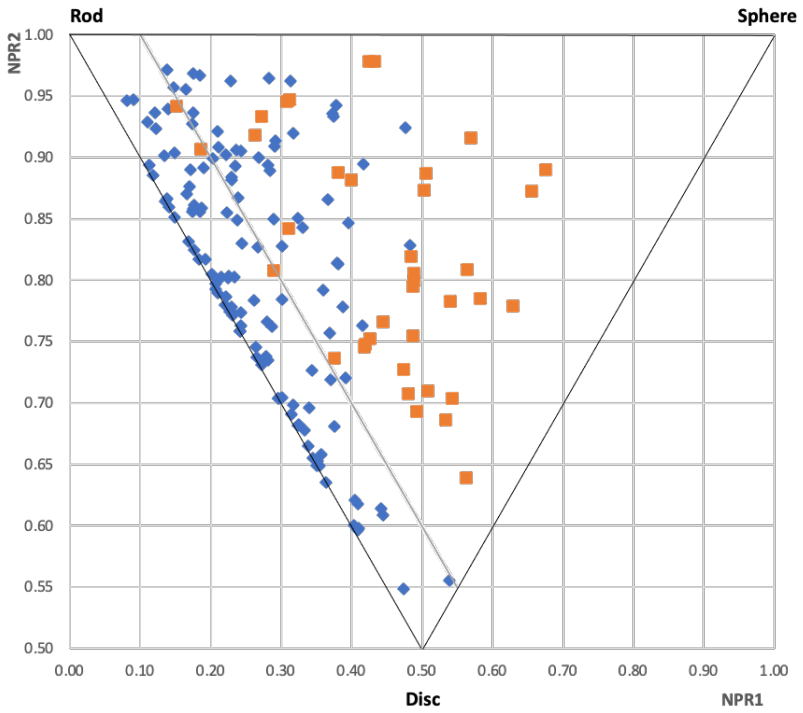

Figure 2.17. Comparative PMI plot analysis of this work (red squares) and the Maybridge diversity set 1 (blue diamonds).

As well as possessing excellent shape diversity, the fragment library generated as part of this work contains a broad range of cyclic scaffolds, such as bridged and spirocyclic structures, indicating good scaffold diversity (Figure 2.18).

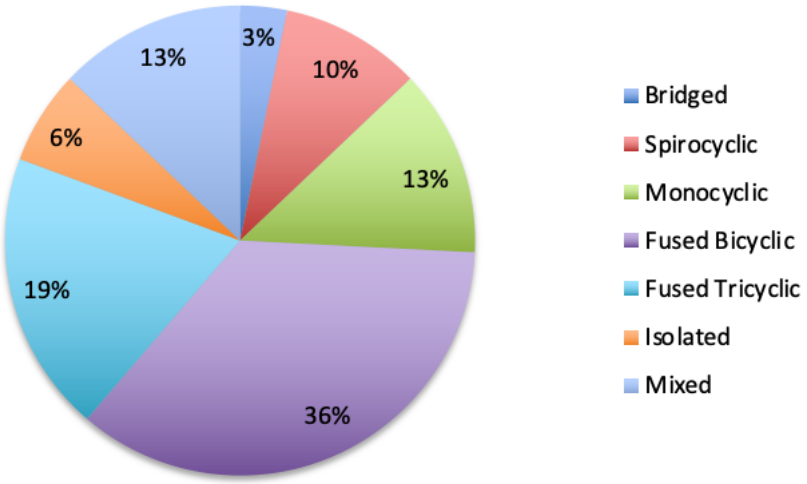

Figure 2.18. Distribution of ring systems within the fragment library.

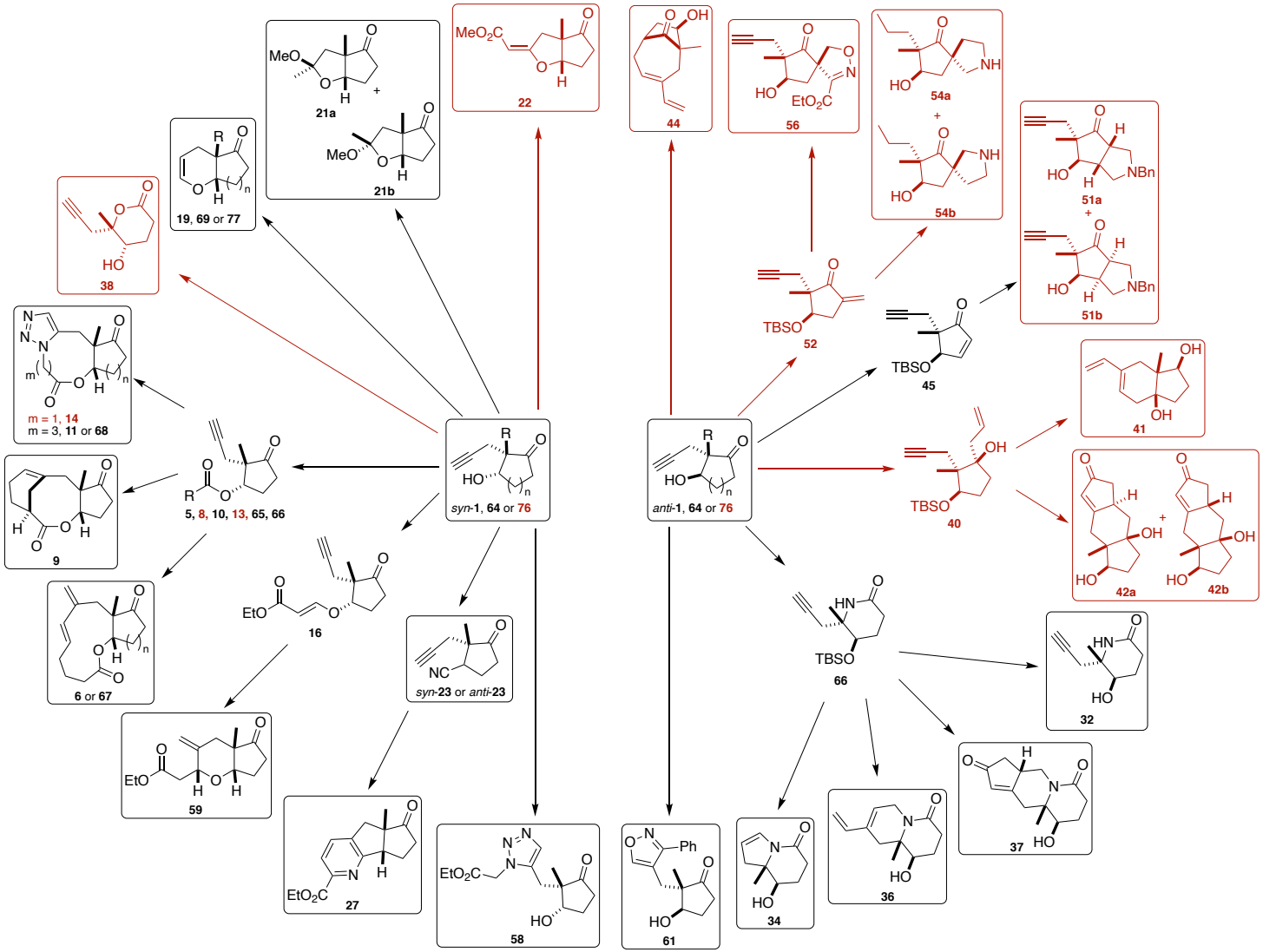

Scheme 2.40. The complete fragment library. Compounds shown in black were synthesised as part of this project, whilst those shown in red were synthesised by Dr N. S. Troelsen. Circled compounds were included in the final screening collection. n = 1 or 2; R = Me or cyclopropylmethyl. Figure adapted from reference.[116]

2.4.2 Analysis of Physicochemical Properties

As discussed in Section 1.2, a fragment library must possess suitable physicochemical properties to ensure optimal chemical space coverage and minimise attrition rates. Thus, to determine the suitability of the new fragment library as a screening collection it was assessed for the following physicochemical properties: MW, SlogP, number of HBA, number of HBD, number of chiral centres, Fsp^3, and fraction aromatic (the number of aromatic atoms expressed as a fraction of the total number of heavy atoms). The distribution of the data is displayed in a series of histograms in Figure 2.19.

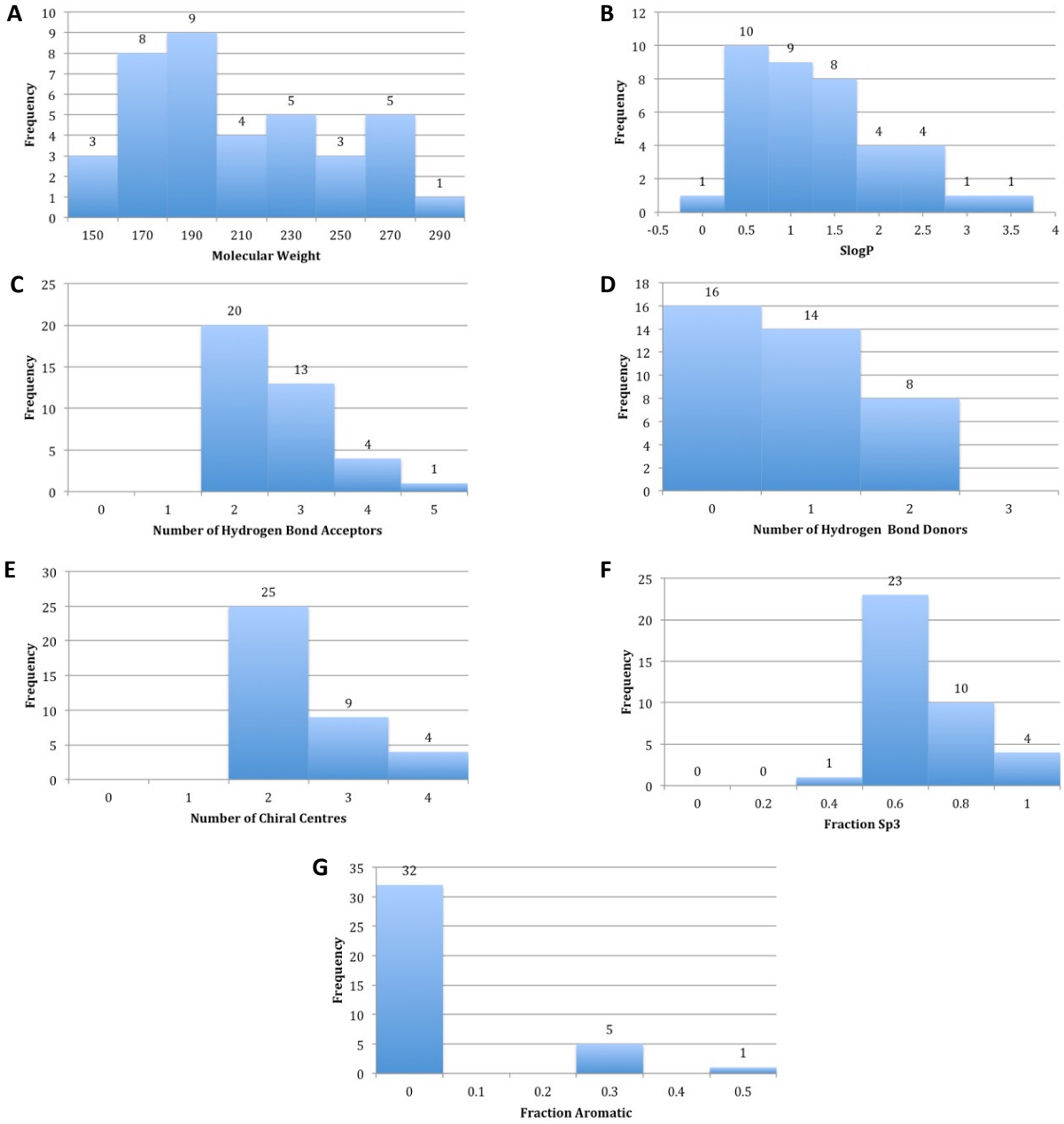

Figure 2.19. Histograms showing the distribution of physicochemical properties amongst the fragment collection. Figure adapted from reference.[116]

For the most part the resulting library adhered to the core Ro3 guidelines (MW <300, clogP <3, HBD/HBA <3), with only 3% of the library possessing a slightly higher SLogP than three (Figure 2.19, B), and all members complying with both the MW and HBD rules (Figure 2.19, A and D). Unfortunately, however, 13% of the library had a higher number of HBA than the upper guideline of three (Figure 2.19, C). Despite this, the library showed excellent fragment-like properties overall, demonstrating its applicability for fragment-based screening.

It should be noted that although the Ro3 provides useful guidelines to aid in the design of high-quality fragments, these rules should not be considered unbreakable.[213,214] In particular, whilst the limits to MW and clogP are largely accepted, the hydrogen bond criteria are much less frequently adopted. This is due, in part, to ambiguities in the definition of acceptors and donors.

Analysis of the 3D properties of the library also indicated a high level of saturation and low fraction of aromatic atoms within the new library. Both are highly desirable features, which have been correlated with the successful passage of molecules through the stages of clinical development.[8,35,85] Furthermore, the presence of multiple chiral centres in each fragment serves to generate stereochemical diversity.

To compare the new fragment library with recently developed complex and diverse commercial libraries, Maybridge Diversity Set 1 and Life Chemicals 3D, the mean values of the physicochemical properties for these libraries were also calculated (Table 2.3). In general, the new library compared near equally with both commercial collections. However, the new fragment library showed a significantly increased number of chiral centres, fraction sp^3, and decreased fraction aromatic – all common features in NPs. Thus, this successful generation of more complex, 3D fragments will undoubtedly provide access to novel areas of biologically relevant chemical space that might prove useful for the exploration of more challenging targets.

Table 2.3. Mean values of the physicochemical properties of this work compared to the Maybridge Diversity Set 1 and Life Chemicals 3D commercially available fragment libraries.

Property[a]	This work	Maybridge Diversity Set	Life Chemicals 3D	Ideal value[b]
MW	208	180	253	<300
SlogP	1.37	1.92	1.65	<3
HBA	2.63	2.46	2.72	<3
HBD	0.79	0.86	1.53	<3
Chiral centres	2.45	0.16	1.23	-
Fraction sp^3	0.70	0.29	0.65	>0.45
Fraction Ar	0.05	0.51	0.22	-

[a]MW = molecular weight, HBA = number of hydrogen bond acceptors, HBD = number of hydrogen bond donors.
[b]Ideal range based on guidelines of 'rule of three'.[61]

2.4.3 Natural Product-Likeness

Finally, the NP-likeness of the resulting library was assessed. These calculations were carried out by Dr N. S. Troelsen using the 'Natural Product-Likeness Scorer', a computational tool developed by Ertl and co-workers.[215,216] This technique involves each compound being divided into atom-centred 'fragments', which are then compared with the frequency with which they occur in two reference sets (lead-like molecules from the ZINC database and a representative collection of NPs[h]). The resulting scores typically range from –3 to 3, with a higher score indicating greater NP-likeness.

Using this approach, the NP-likeness score was calculated for our fragment library, Maybridge Diversity Set 1, Life Chemicals 3D, FDA-approved drugs, and a collection of 2712 NPs from the NuBBE database (Figure 2.20).[116] Comparison of these results showed that, as expected, the collection of NPs scored highly, whilst the commercial fragment libraries and FDA drugs were significantly less NP-like. The new fragment library, on the other hand, received similarly high scores to the NP collection, indicating good coverage of NP-like space.

[h] These are SMs from the ChEMBL database extracted from the *Journal of Natural Products.*

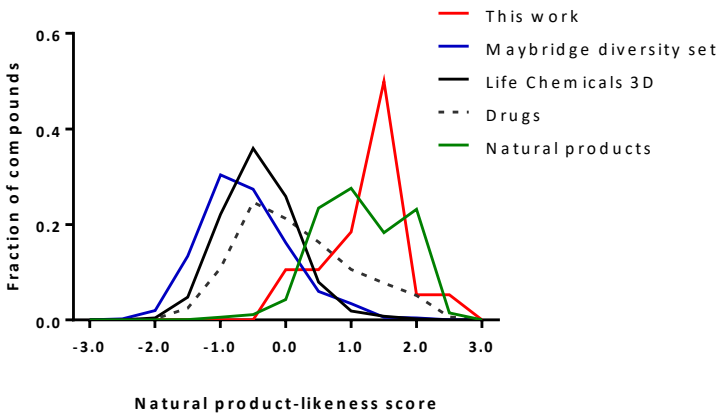

Figure 2.20. Comparison of the NP-likeness scores for this work, two commercially available collections, FDA-approved drugs, and a collection of NPs. Figure taken from reference.[116]

Despite this high NP-likeness score, only a few of the scaffolds within the new fragment library are found in known NPs. It could therefore be argued that these compounds are in fact 'pseudo NPs' – a term introduced by Waldmann *et al*. to refer to novel scaffolds that share many of the chemical and biological aspects of NPs but have not been accessed by nature.[114] Although not NPs themselves, pseudo NPs are expected to retain the biological relevance of NPs, facilitating the probing of areas of biologically relevant chemical space that have not been explored by nature.

3 Conclusions and Future Work

3.1 Conclusions

In total, a library of 38 structurally diverse fragments based on 20 distinct frameworks was constructed.[i] Whilst a B/C/P strategy was not strictly adhered to, the approach used was in-line with the general concept and efficiency of a DOS strategy, with each fragment synthesised in no more than five steps from the building blocks.

The resulting library is notable for its broad range of medicinally relevant motifs, polar functionality for biological recognition, and the presence of the key all-carbon quaternary centre in all fragments. Perhaps most importantly, each library member also includes multiple synthetic handles for fragment growth to address the current bottleneck in FBDD. The ability to alter both ring size and the quaternary substituent for rapid analogue synthesis has also been demonstrated through the synthesis of selected six-membered ring and methylcyclopropane-containing scaffolds.

Computational analysis of the final fragment library showed the fragments possess desirable physicochemical properties based on Ro3 guidelines, whilst displaying greater sp^3 character, stereochemical complexity, three-dimensionality, and diversity compared to commercially available fragment libraries. Finally, NP-likeness scoring suggests that the library possesses high NP-likeness, indicating good coverage of biologically-relevant chemical space.

3.2 Future Work

Future work on this project would focus on screening of the final fragment collection. A library designed to contain a high level of diversity would be expected to be able to access large areas of chemical space, and thus exhibit a wide range of biological activities.[1,106,217] Therefore, opportunities to screen the final fragment library against multiple targets are an attractive prospect. In recent years, the Spring group has established a successful collaboration with the fragment-based screening platform XChem,[113] which facilitates high-throughput methods of X-ray crystallographic screening using the i04-1 beamline at the Diamond Synchroton in Oxford.[44,218–220] An important aspect of this

[i] 15 of these fragments were synthesised by Dr N. S. Troelsen.

collaboration with XChem is the merging of chemistry groups specialising in library synthesis and fragment evolution with biochemistry groups specialising in investigation of novel biological targets and protein crystallography. As such, the DOS library and novel intermediates could be subjected to a primary X-ray screen using this platform against a variety of biological targets by several external XChem collaborators. Any hits that result from these campaigns would then undergo further biochemical and biophysical analysis to determine the significance of the binders that have been identified via quantification of the binding strength. In addition to this, the compounds synthesised will be included in the Spring Group Compound Collection, which is made accessible to other collaborators for traditional biochemical assay screening methods.

Following fragment screening, any hit compounds identified would then need to be synthesised in their enantiopure form to determine the enantiomer preference of the target. Guided by structural information gained through X-ray crystallography, the generation of a focused follow-up library would also be required. This would likely involve various substitutions, expansions, or fragment linkages to improve affinity and other physicochemical properties (Figure 3.1). Due to the large number of exit vectors within the fragments generated as part of this project it is expect that this hit-to-lead optimisation could be carried out both rapidly and efficiently.

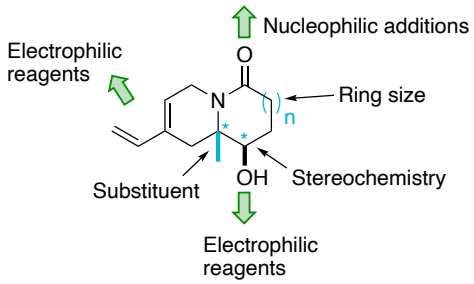

Figure 3.1. An example of the modifiable groups (highlighted in blue) and exit vectors (highlighted in green) that can be used for fragment elaboration.

Section II:
The Development of a Novel Platform for Antibody Dual Functionalisation

4 Introduction

4.1 Cancer Therapy

Cancer is a group of over 100 different diseases involving abnormal cell growth that can spread to other tissues and organs.[221,222] In 2020 cancer accounted for nearly 10 million deaths, making it a leading cause of death worldwide.[223] With the burden of cancer incidence and mortality rapidly increasing due, in part, to both ageing and growing populations, cancer poses an ever-increasing threat to health globally.[224]

Many types of cancer treatment have been developed, with most patients having a combination of chemotherapy, radiotherapy, and surgery.[225] Traditional chemotherapy is an aggressive form of drug therapy that is designed to employ a small molecule to target rapidly growing cells within the body through the disruption of the cell cycle. Although these treatments seek to exploit the rapid division of cancer cells, they inevitably also harm healthy cells that divide quickly.[226] This low selectivity can result in serious side effects and dosage is therefore limited.

To alleviate the adverse effects arising from the lack of selectivity of traditional therapeutic agents, more targeted approaches are now being explored. By ensuring that a cytotoxin only targets a specific cell type, these approaches can both decrease the minimum effective concentration (MEC) required for the drug to have the desired effect and increase the maximum tolerated dose (MTD).[227] Not only does this minimise off-target toxicity but it also facilitates the use of more potent drugs (Figure 4.1).

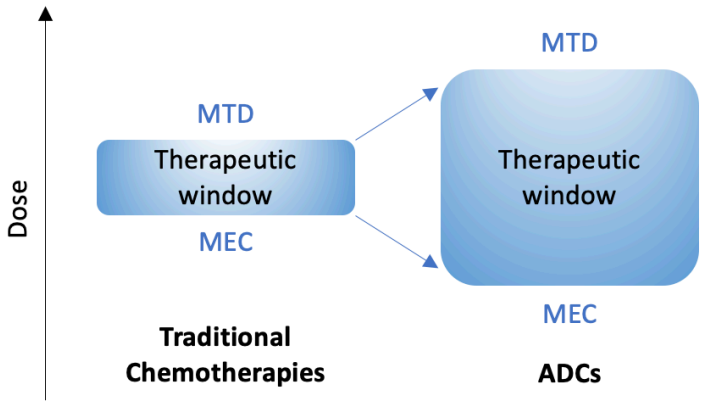

Figure 4.1. Graphical representation of the therapeutic windows for traditional chemotherapies and targeted therapeutics.

4.2 Antibody-Drug Conjugates

Antibody-drug conjugates (ADCs) are a class of targeted therapeutics, typically comprised of an antibody covalently bound to one or more cytotoxic drugs via a suitable linker (Figure 4.2). This allows the high specificity of monoclonal antibodies (mAbs) for a given target to be combined with the cytotoxicity of small molecule toxins, such that tumour cells can be selectively destroyed. The target, mAb, payload, and linker are all key factors which determine the overall success of the ADC, and careful consideration is therefore required for their selection.[228]

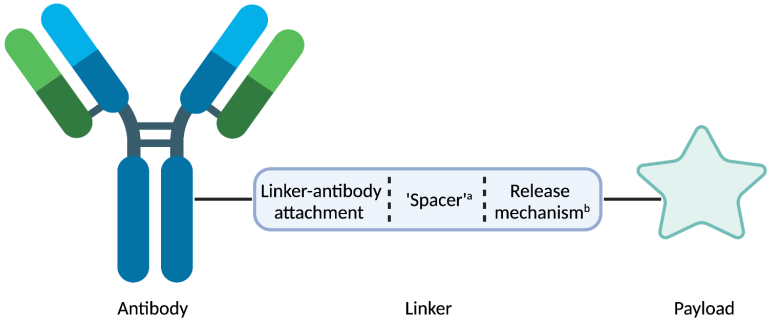

Figure 4.2. General structure of an ADC. [a]'Spacer' used to modulate linker properties. [b]Release mechanism not present in all ADCs. Created with Biorender.com.

4.2.1 Marketed ADCs

The use of antibodies for targeted drug delivery is not a new concept, with the first ADC having been developed by Mathe *et al*. in 1958.[229] However, it was not until 2000 that the first ADC (Mylotarg®) gained approval from the FDA for the treatment of acute myeloid leukemia.[230] Whilst preliminary results appeared promising, Mylotarg® was later voluntarily withdrawn after confirmatory trials failed to verify any clinical benefits over standard chemotherapy.[231,232] Nonetheless, Mylotarg® was able to gain reapproval in 2017 with a new dosing regimen for the same indication.[233]

Despite this initial setback, ADCs have shown significant promise over the last decade. A further nine ADCs have since gained FDA approval, with loncastuximab tesirine (Zynlonta®) having recently been granted accelerated approval for the treatment of relapsed or refractory B-cell lymphoma (Table 4.1).[234,235] In addition, more than 80 other ADCs are currently in active clinical trials.[236]

Table 4.1. ADCs approved by the FDA

ADC Product	Indication	Isotype	Target	Conjugation Method	Linker	Cytotoxin	Average DAR	Year(s) Approved	References
Mylotarg® (Gemtuzumab ozogamicin)	Acute myeloid leukemia	IgG4	CD33	Lys, NHS ester	Hydrazone (Cleavable)	N-acetyl calicheamicin γ1	2–3	2000[a], 2017	230–233,237
Adcetris® (Brentuximab vedotin)	Hodgkin lymphoma, anaplastic large cell lymphoma	IgG1	CD30	Interchain Cys, maleimide	Vc (Cleavable)	MMAE	~4	2011	238,239
Kadclya® (Trastuzumab emtansine)	HER2-positive breast cancer	IgG1	HER2	Lys, NHS ester	Thioether (Non-cleavable)	DM1	3.5	2013	239–242
Besponsa® (Inotuzumab ozogamicin)	B-cell precursor acute lymphoblastic leukemia	IgG4	CD22	Lys, NHS ester	Hydrazone (Cleavable)	N-acetyl calicheamicin γ1	5–7	2017	243,244
Polivy® (Polatuzumab vedotin)	Diffuse large B-cell lymphoma	IgG1	CD79b	Interchain Cys, maleimide	Vc (Cleavable)	MMAE	3.5	2019	245–247
Padcev® (Enfortumab vedotin)	Urothelial cancer	IgG1	Nectin-4	Interchain Cys, maleimide	Vc (Cleavable)	MMAE	~4	2019	248,249
Enhertu® (Trastuzumab deruxtecan)	HER2-positive breast and gastric cancer	IgG1	HER2	Interchain Cys, maleimide	GGFG (Cleavable)	DXd (exatecan)	~8	2019	250–253
Trodelvy® (Sacituzumab govitecan)	Triple-negative breast cancer	IgG1	Trop-2	Interchain Cys, maleimide	Carbonate (Cleavable)	SN-38	7.6	2020	254–257
Blenrep® (Belantamab mafodotin)	Relapsed or refractory multiple myeloma	IgG1	BCMA	Interchain Cys, maleimide	Amide (Non-cleavable)	MMAF	~4	2020	258,259
Zynlonta® (Loncastuximab tesirine)	Relapsed or refractory B-cell lymphoma	IgG1	CD19	Interchain Cys, maleimide	Va (Cleavable)	PBD Dimer	2.3	2021	260,261

[a]Withdrawn in 2010 and re-approved in 2017. Abbreviations: IgG = immunoglobulin G; Lys = Lysine; Cys = cysteine; Vc = valine-citrulline; Va = valine-alanine; GGFG = glycyn-glycyn-phenylalanyn-glycyn; NHS = *N*-hydroxysuccinimide; MMAE = monomethyl auristatin E; MMAF = monomethyl auristatin F; PBD = pyrrolobenzodiazepine.

4.2.2 Mechanism of Action

Due to their poor oral bioavailability, ADCs are administered intravenously.[262] Once in the bloodstream, ADCs can circulate throughout the body and selectively bind to the target cell surface antigens present on tumour cells.[263–266] In most cases, the resulting ADC-antigen complex is then internalised via receptor-mediated endocytosis (Figure 4.3.A). Subsequent trafficking of the ADC inside the cell and processing in either the lysosome or endosome can then lead to the release of the cytotoxic payload and subsequent apoptosis. If the released payload is sufficiently membrane-permeable it may also diffuse into neighbouring cells in a phenomenon known as the 'bystander effect'.[266] This effect enables neighbouring cells to be killed, regardless of whether they possess the target antigen, and is vital for the treatment of certain types of heterogeneous tumours where large areas of the tumour may not express the ADC target antigen. However, the 'bystander effect' can also lead to side effects if the payload enters neighbouring healthy cells.

It should also be noted that some ADCs employ non-internalising antibodies.[266] Non-internalising ADCs rely on labile linkers for extracellular payload release due to the inability of the ADC to be internalised into the target cells (Figure 4.3.B).

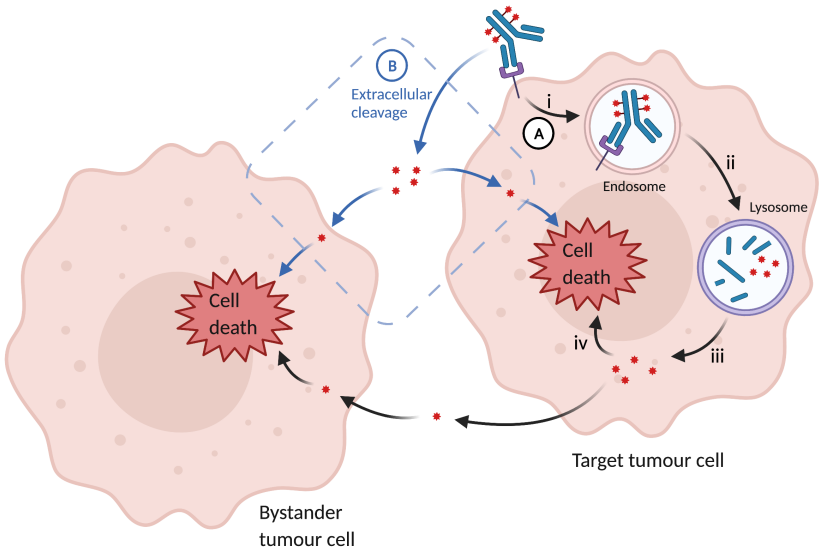

Figure 4.3. (A) Traditional mechanism of action: (i) endocytosis; (ii) lysosomal trafficking; (iii) lysosomal degradation; (iv) cell death. (B) Non-internalising mechanism of action. Figure adapted from reference.[264] Created with Biorender.com.

4.2.3 Monoclonal Antibodies

Monoclonal antibodies are synthetic antibodies that are typically produced in large quantities from homogeneous populations of B cell clones, resulting in their ability to bind to a single epitope.[267,268] The excellent selectivity with which these synthetic antibodies can bind, along with their favourable pharmacokinetics with respect to distribution, metabolism, and elimination, has led to their extensive use as targeted therapeutics, both alone, and as a key component of ADCs.[269] In particular, humanised or fully human mAbs make ideal delivery platforms for ADCs, offering high specificity, long half-life, and minimal immunogenicity.[270]

To date, all FDA-approved ADCs are comprised of mAbs of the immunoglobulin G (IgG) isotype — the most abundant isotype in serum. IgG antibodies are Y-shaped glycoproteins formed from four peptide chains — two heavy chains (HCs) and two light chains (LCs) that are connected via disulfide bonds (Figure 4.4). These large structures (~150 kDa) comprise two functional components:[271]

- **Fragment antigen-binding (Fab) region**: This region is responsible for antigen recognition via interactions at the complementarity-determining regions found at the tips of the Fabs.[272] IgG antibodies consist of two such Fab domains that are linked to a fragment crystallisable (Fc) region via a 'hinge' region.[273] They are formed of the entirety of the LCs (C_L and V_L) as well as both the V_H and C_H1 domains of the HCs.

- **Fragment crystallisable (Fc) region**: The Fc region is able to communicate with immune cells and bind to Fc receptors in order to generate a series of effector responses.[274,275] It is formed of the two constant domains of each of the HCs (C_H2 and C_H3) and bears a highly conserved glycosylation pattern at Asp297 of the C_H2 domains.[276,277]

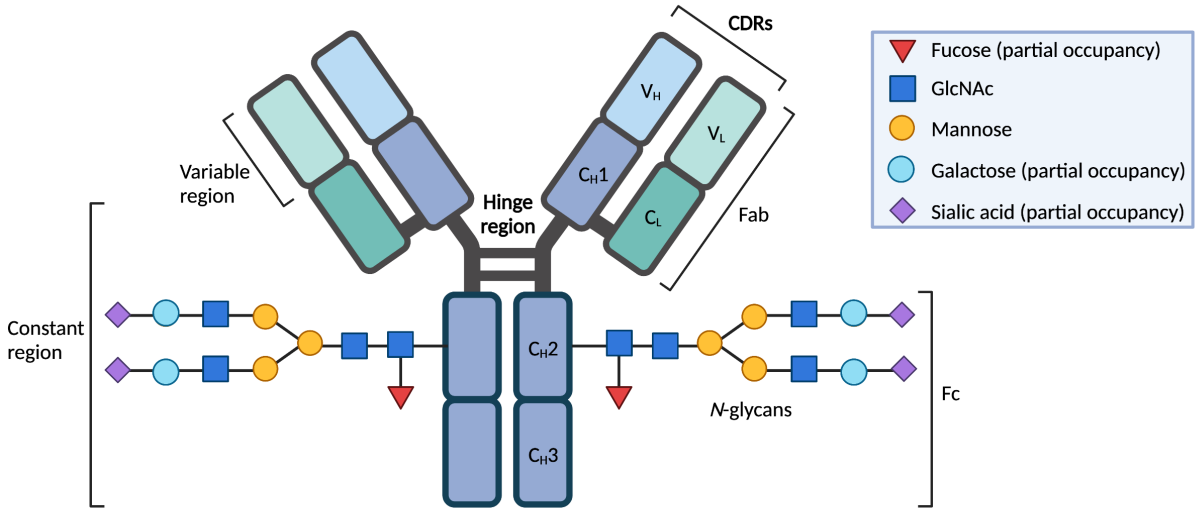

Figure 4.4. General structure of an IgG antibody (IgG1 is shown for illustrative purposes). Created with BioRender.com.

IgGs can be further divided into four subclasses: IgG1, IgG2, IgG3, and IgG4. These subclasses are approximately 90% identical on the amino acid level but vary in the number of interchain disulfide bonds, length of hinge-region, half-life, and ability to generate an immune response.[236,278] Of these subclasses, IgG1 is the most commonly used in ADCs due to its ease of production, moderate to strong immune activation, and long serum half-life (~21 days).[236] However, in some cases the pairing of IgG1 with potent warheads can result in issues of excessive toxicity, which has led to the development of some ADCs employing IgG2 or IgG4 isotypes.[279–281]

4.2.4 Target Selection

Appropriate target choice is a necessary requirement for the design of efficacious ADCs. The ADC target should ideally have a high level of expression compared to healthy cells, be efficiently internalised, and display minimal shedding from the membrane to prevent accumulation of extracellular ADC-antigen immune complexes and subsequent off-target toxicity.[282,283] Preferably, targets should also have consistently high expression on cancer cells throughout the tumour, particularly if non-cleavable linkers are employed (*vide infra*, Section 4.2.6.1).[284]

Lineage-specific antigens expressed by haematological malignancies are therefore considered good targets for ADCs, with five of the ten FDA-approved ADCs targeting such cancers.[285] For solid tumours, however, expressed antigens are predominantly tumour-associated (also expressed at low levels on healthy cells) rather than only being found on tumour cells. This lack of specificity, along with the IgG antibodies' poor tumour penetration often limits their broad clinical applicability as ADC targets.[286] In fact, until the approval of Kadcyla® in 2013 there were no FDA-approved ADCs directed against solid tumours. However, recent years have seen such ADCs experiencing increased success in the clinic.

With Padcev® and Enhertu® both approved in late 2019, Trodelvy® in 2020, and Zynlonta® in 2021, five ADCs are now FDA-approved for the treatment of solid tumours. Antibody fragments and other alternative formats are also being developed that exhibit an increased rate of diffusion, allowing for more efficient penetration of solid tumours.[287]

One ADC target that has been widely investigated is human epidermal growth factor receptor-2 (HER2/neu, c-erbB2). HER2 is a member of the ErbB family of transmembrane tyrosine kinase receptors and is overexpressed in a number of solid cancer types, including around 20% of human breast cancers.[288] Breast cancers can have up to two million of these receptors expressed at the tumour cell surface, 100 times more than healthy cells.[289] This overexpression induces greater cellular proliferation and is associated with both increased mortality and high rates of reoccurrence (Figure 4.5.A).[290,291] However, the difference in HER2 expression between normal tissues and tumours makes it an ideal candidate for targeted therapeutics.

Trastuzumab (Herceptin®), a humanised monoclonal antibody, acts as an effective treatment for tumours that overexpress the HER2 protein (Figure 4.5.B).[292] It is well-tolerated, significantly improving survival rates for patients with metastatic breast cancer (MBC) as well as those with early-stage HER2-positive breast cancer in the adjuvant setting. However, resistance to trastuzumab does develop in many patients with MBC.[293] ADCs based on trastuzumab, such as Enhertu® and Kadcyla®, offer an alternative approach to the treatment of HER2-positive breast cancer, potentiating the antitumour activity of trastuzumab through the addition of a cytotoxic drug. Such ADCs have also shown great promise as treatments for patients with heavily pre-treated disease or breast cancers with lower levels of HER2 expression.[253,294,295]

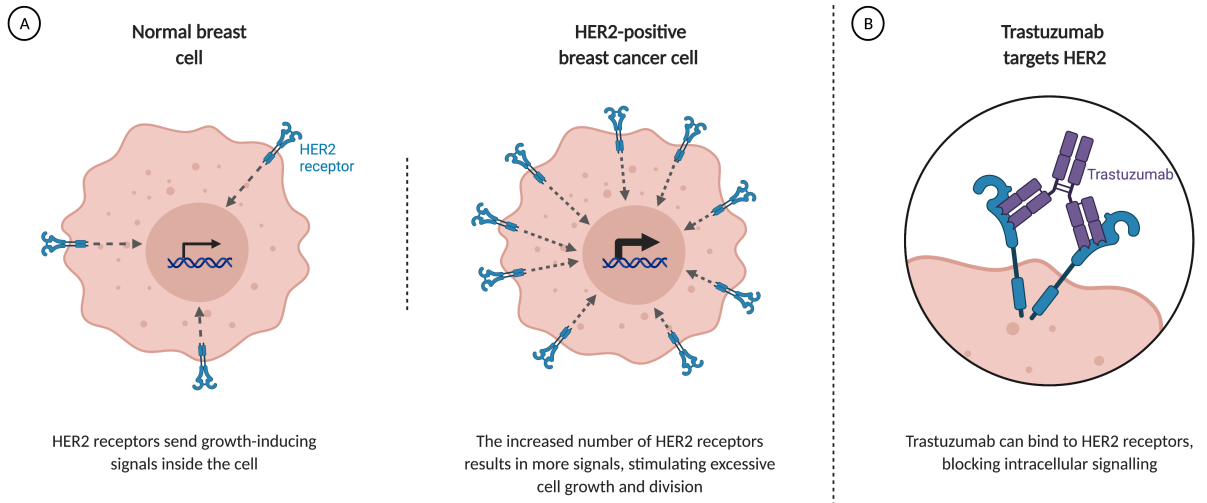

Figure 4.5. (A) Overexpression of HER2 receptors on breast cancer cells. (B) Effect of trastuzumab on HER2 receptors. Adapted from "HER2+ Breast Cancer", by BioRender.com (2021). Retrieved from https://app.biorender.com/biorender-templates.

4.2.5 Payloads

The choice of payload is another vital consideration when designing ADCs. A single antigen can only internalise one ADC molecule and in some cases this internalisation can be slow. This, along with inefficiencies in payload release, the limited number of target antigens on each given cell, as well as issues with biodistribution and tumour penetration, means that only a fraction of the administered drug ever reaches the desired target.[296] It is therefore crucial that the chosen cytotoxin is highly potent (sub-nanomolar IC_{50} values).[297] Drugs that are usually too potent for use in normal chemotherapy have been proven to be key for the generation of efficacious ADCs. Indeed, one of the major hurdles for early ADCs, which focused on the use of known anticancer drugs such as doxorubicin (Dox), was poor efficacy in comparison to the unconjugated cytotoxin.[298–300] Exceptional cytotoxicity is, however, not the only requirement for an effective ADC payload. Ideally, payloads should also have a defined mechanism of action, low immunogenicity, acceptable aqueous solubility, and good stability during preparation, storage, and circulation.[226,282] They should also be easily functionalised to allow attachment to an antibody.

Most ADC payloads under investigation belong to one of two main classes of drugs: anti-microtubule agents and DNA-damaging agents,[297] with anti-microtubule agents, such as the auristatins, making up a considerable proportion of the ADCs currently in clinical trials. Notably, auristatins alone account for 40% of FDA-approved ADCs. The auristatins include MMAE and MMAF, which are both synthetic derivatives of the natural anticancer agent dolastatin 10 (Figure 4.6.A).[301] These drugs act as antimitotic agents, inhibiting cellular division by blocking tubulin polymerisation.[302]

A second major group of microtubule-disrupting agents that have been widely used in ADC development is the maytansinoids. This includes the synthetic derivatives mertansine (the payload in Kadcyla®) and ravtansine (Figure 4.6.B).[241,303] As with the auristatins, the maytansinoids are highly potent microtubule-targeting agents that preferentially kill rapidly dividing cells.[304]

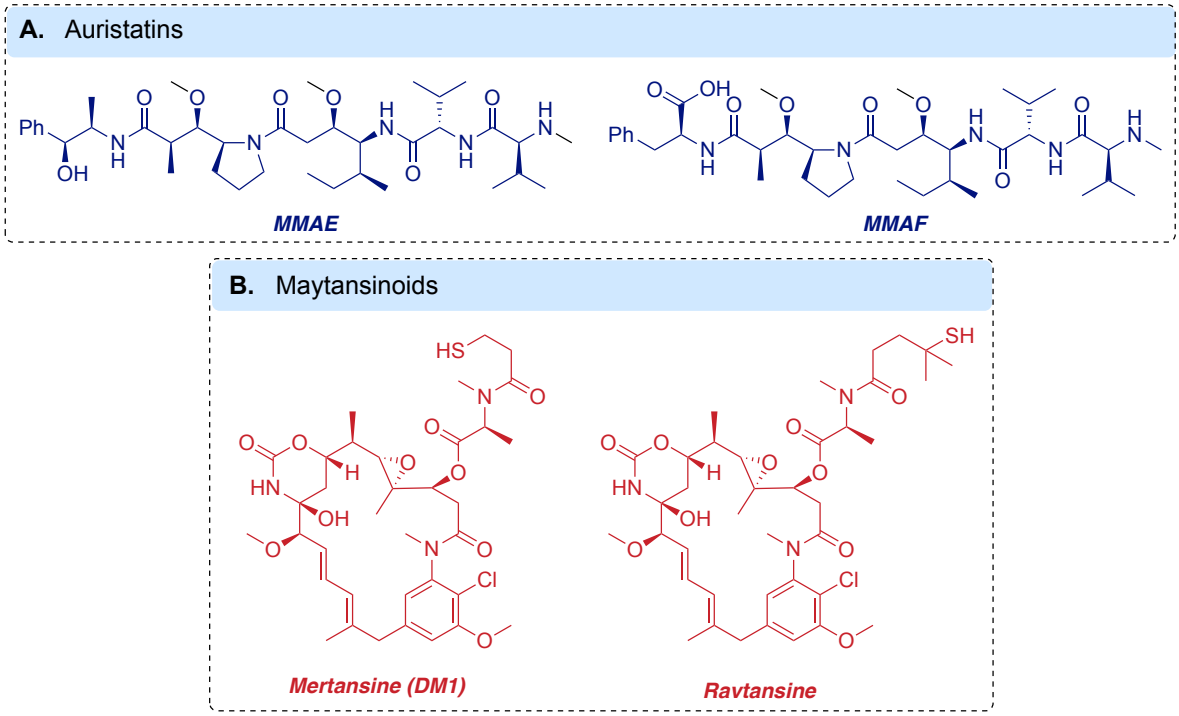

Figure 4.6. Examples of anti-microtubule agents used as ADC payloads.

The second class of cytotoxin commonly used in the generation of ADCs is DNA-damaging agents. DNA-damaging agents commonly used in ADCs include the DNA double-strand breaking calicheamicins,[237] DNA topoisomerase I inhibitors (such as the camptothecins),[305] the DNA alkylator duocarmycin,[306] and the DNA-cross-linking PBD dimers (Figure 4.7).[261] In fact, two camptothecin derivatives have successfully been used as payloads in marketed ADCs (SN-38 and exatecan [DXd]),[251,255] whilst *N*-acetyl calicheamicin γ_1^I, a calicheamicin derivative, is the payload in both Mylotarg® and Besponsa®.[233,244] In addition, ADC Therapeutics have recently gained approval for Zynlonta®, an ADC which incorporates a PBD-based cytotoxin.[260]

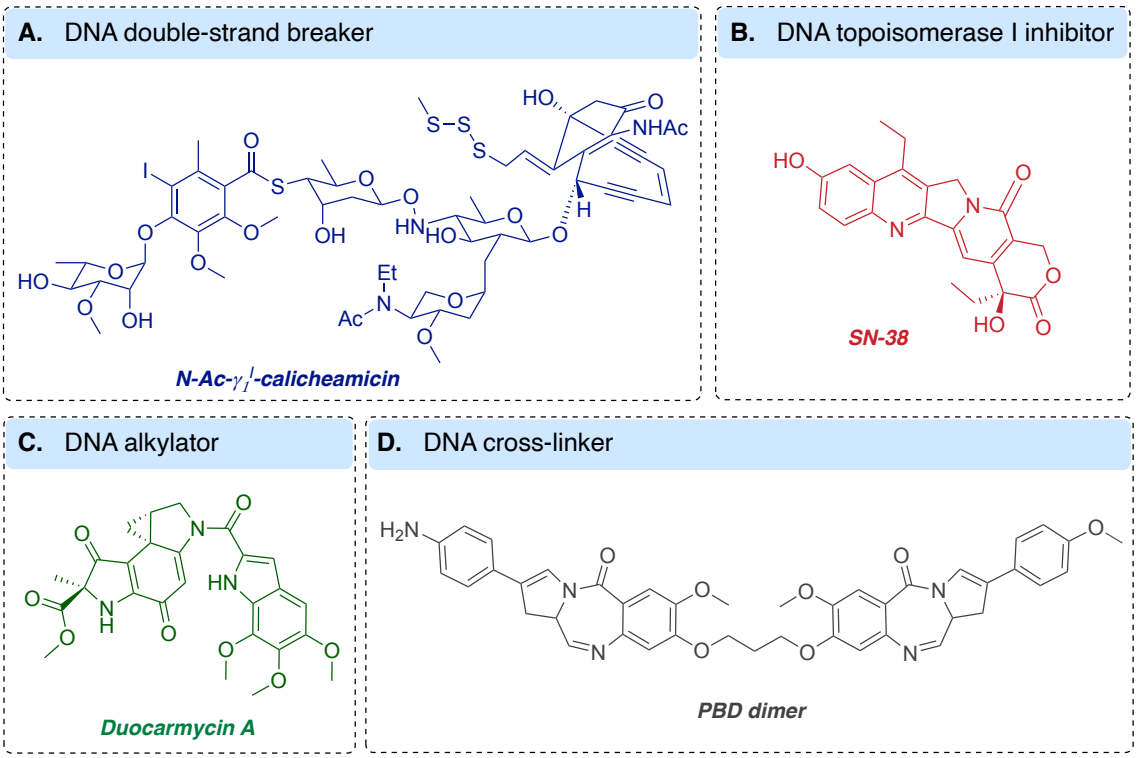

Figure 4.7. Examples of DNA-damaging agents used as ADC payloads.

4.2.6 Linker Technology

Linkers have a crucial role to play in ADCs; not only do linkers connect the cytotoxic warhead to the mAb, but they can also be used to modulate the properties of an ADC. To give an ADC the best chance of success, the linkers need to possess several key attributes:

- **High plasma stability:** the linker needs to be sufficiently stable in plasma so that the ADC can circulate in the bloodstream without premature cleavage of the drug, which can result in excess systemic toxicity and reduced efficacy as less of the payload reaches the desired target cell.[263]
- **Enable efficient release:** once reaching the desired target the linker must be able to release the payload-linker metabolite efficiently from the antibody.[236,264]
- **Good water solubility:**[307] Although increasing drug-to-antibody ratio (DAR) can increase *in vitro* potency, hydrophobic linker-payloads can cause antibody aggregation, which promotes rapid clearance and undesired immune responses.[308] ADC hydrophobicity has also been associated with increased rate of non-specific uptake, resulting in premature drug release.[309] Whilst historically, this has led to DARs being limited to 0–4, with appropriate linker design to minimise hydrophobicity ADCs, DARs as high as 8 can still be both safe and effective.[310,311]

4.2.6.1 Release Mechanism

Depending on the mechanism by which a payload is released, a linker can be considered either cleavable or non-cleavable. Cleavable linkers utilise the intrinsic properties of tumour cells (e.g. the low pH and high concentration of hydrolytic enzymes in lysosomes) to selectively release the free payload.[264] This may be via the use of an enzyme- (e.g. protease,[312] phosphatase,[313] glycosidase,[314] or sulfatase[315]), pH-,[237] or glutathione-sensitive trigger[316] (Figure 4.8). The resulting payload has the potential to diffuse out of the cells and into surrounding tumour cells, killing neighbouring cells via the bystander effect.[266]

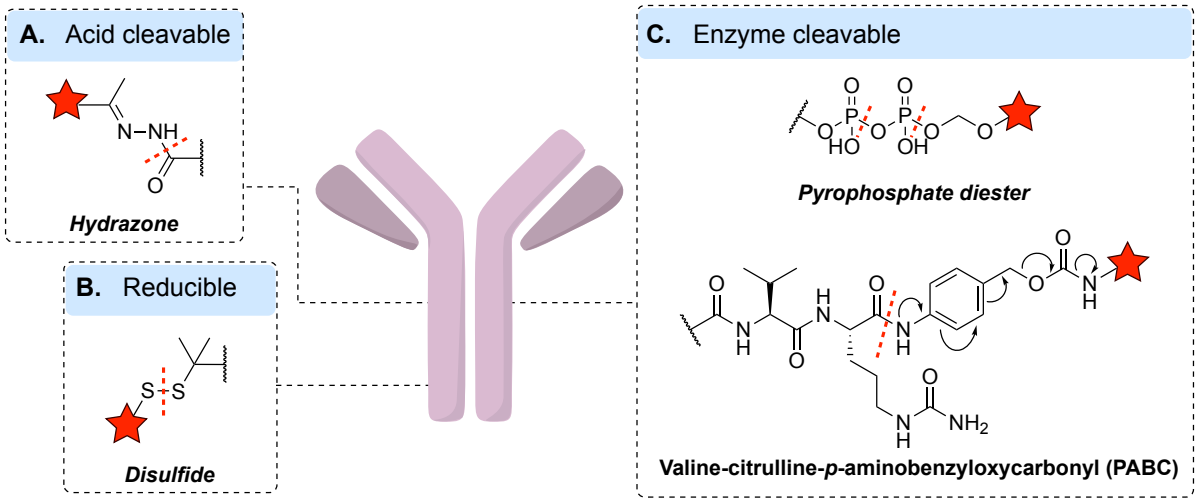

Figure 4.8. Cleavable linkers. (A) Acid-cleavable: these linkers, such as hydrazone linkers, are cleaved in acidic environments (i.e. endosome and lysosome). (B) Reducible linkers: these linkers contain disulfide bonds that can be reduced by intracellular reducing molecules (e.g. glutathione). (C) Enzyme-cleavable linkers: these include protease-cleavable peptide linkers, such as valine-citrulline-*p*-aminobenzyloxycarbonyl (vc-PABC), and phosphatase-cleavable pyrophosphate diester linkers. The red stars represent payloads.

In contrast to their cleavable counterparts, non-cleavable linkers have no traceless release mechanism.[317] These linkers instead utilise lysosomal degradation of the antibody into its constituent amino acids for the release of the linker-cytotoxin (Scheme 4.1).[318] This leaves the amino acid that was used for conjugation attached to the payload, so it is vital that the payload's pharmacophore is not affected by this alteration. The resulting cleaved payload is also zwitterionic, with poor membrane permeability and cannot diffuse out of the cell.[266] Thus, non-cleavable linkers often benefit from greater stability, whilst avoiding toxicity arising from the bystander effect on healthy cells.

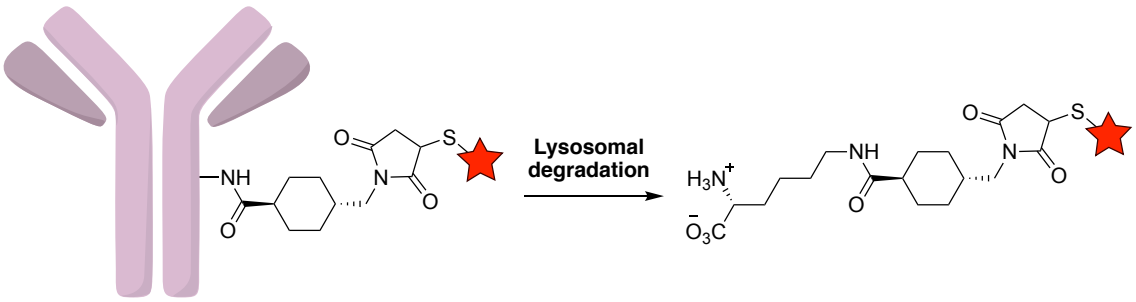

Scheme 4.1. Non-cleavable linkers such as maleimidomethyl cyclohexane-1-carboxylate utilise lysosomal degradation to release the payload. The resulting species is charged, preventing the 'bystander effect'.

4.2.7 Conjugation Site

The site of linker-payload attachment is another important consideration in ADC design as it must leave antibody binding and internalisation unchanged.[236] Early strategies for the attachment of cytotoxic payloads to antibodies involved the acylation of solvent-exposed lysine residues with *N*-hydroxysuccinimide esters or the alkylation of reduced interchain cysteine residues with maleimide (Scheme 4.2).[237,319,320] Unfortunately, these methods are usually not site-selective, and although stochastic cysteine conjugation offers marginally better control of DAR and conjugation site than lysine modification (with only eight available conjugation sites compared to *ca*. 30 modifiable lysine residues), both strategies produce a mixture of different ADC species.[319] As a result, early ADCs were heterogeneous (i.e. had a broad distribution of DARs and a range of antibody attachment sites) and often suffered from pharmacokinetic, efficacy, and stability issues associated with this heterogenity.[311,321,322]

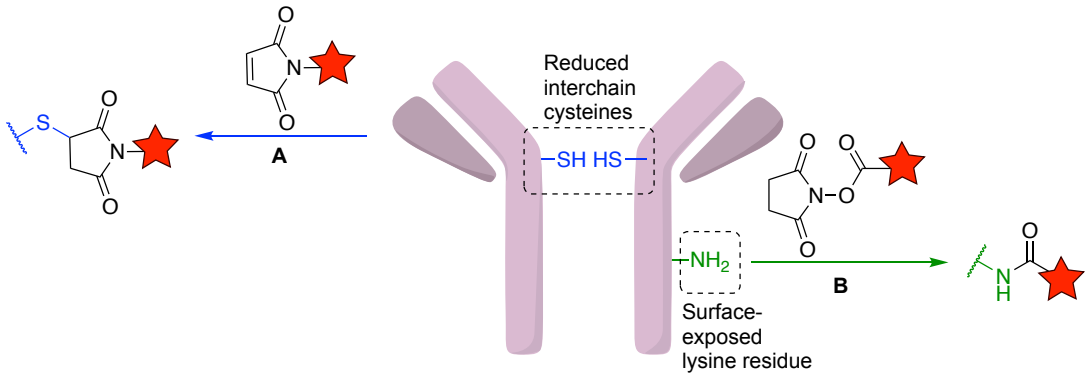

Scheme 4.2. (A) Disulfide bond reduction reveals thiol residues, which can then be modified by soft electrophiles. Partial reduction results in a mixture of products, whilst complete reduction and reaction of all eight thiols gives DAR 8 species. (B) Stochastic conjugation with surface-exposed lysine residues results in a heterogeneous mixture of conjugates. The stars represent payloads.

Although non-specific conjugation techniques have been employed for the generation of most FDA-approved ADCs, such as Kadcyla® and Mylotarg®, the use of non-selective approaches is now considered sub-optimal. In recent years, significant advances in antibody engineering and chemical conjugation methods have enabled the development of a new generation of ADCs with greater

homogeneity. These ADCs have been shown to have better pharmacological profiles than their heterogeneous counterparts.[311,322] Some of the methods for site-selective antibody modification, along with their advantages and limitations, are summarised in Table 4.2.[236,323] (Further discussion of these techniques can be found in Section 4.2.9).

Table 4.2. Summary of the main methods for the site-selective modification of antibodies.

	Technology	Advantages	Limitations	DAR[a]
Engineered mAbs	Engineered cysteines	Homogeneity, tuneability of reactivity/stability	Incorporation of a non-orthogonal group can be problematic, requires genetic engineering	2
	Non-canonical amino acid incorporation	Homogeneity, tuneability of reactivity/stability, chemoselectivity	Low antibody expression yields, potential immunogenicity issues, requires genetic engineering	2
	Enzymatic methods[b]	Homogeneity, ease of incorporation	Can be inefficient depending on site and antibody used, may require genetic engineering	Various
Native mAbs	Glycan modification	Homogeneity, ease of preparation, amino acid sequence unaltered	May affect immune recognition, requires multiple steps	2, 4
	Disulfide rebridging	Homogeneity, amino acid sequence and glycosylation unaltered	Potential for misbridging	4

[a]DAR values most commonly found for a given technology. [b]Not all enzymatic methods require the use of engineered mAbs.

4.2.8 Bioorthogonal Click Chemistry

The concept of bioorthogonal chemistry was first introduced in 2003 by Bertozzi and co-workers to refer to reactions that can be carried out in complex biological environments without interfering with any endogenous functional groups.[324,325] In practice, this means that the reaction must be highly chemo- and regioselective, proceed in aqueous media, and only use reagents that are both stable and non-toxic. Bioorthogonal chemistry, therefore, shares significant overlap with click chemistry, which uses only reactions that are modular, high-yielding, wide in scope, and generate inert by-products.[326] However, it should be noted that not all click reactions are bioorthogonal.

Over the past twenty years, bioorthogonal click chemistry has been widely used for bioconjugation, including for the development of targeted therapeutics, such as ADCs.[327,328] Indeed, following studies demonstrating the numerous benefits of increased ADC homogeneity, the exploration of click

chemistries for site-specific antibody-drug conjugation has increased dramatically. Through the introduction of a 'clickable' bioorthogonal handle onto a mAb (via either genetic engineering or chemical modification) ADCs can be generated with excellent control of DAR and conjugation site.

Several different click reactions have now been employed for the site-selective modification of antibodies, including both condensation reactions and cycloadditions.[327,329–332] One of the most prominent examples is the CuAAC (Figure 4.9.A), which benefits from moderately fast reaction rates, as well as employing stable and readily available reagents.[333] The use of CuAAC for protein modification is, however, hampered by its dependence on a metal catalyst. The use of such catalysts can lead to residual metal contaminants; low synthetic yields; and oxidation of certain amino acids on the antibody, which may cause an immunogenic response.[334,335]

To circumvent these issues, metal-free click reactions such as strain-promoted azide-alkyne cycloadditions (SPAAC) and inverse-electron-demand Diels-Alder (IEDDA) reactions, have been developed which allow rapid and selective covalent bond formation in aqueous conditions, whilst avoiding the issues associated with the use of cytotoxic metal catalysts.[336,337] Like CuAAC, SPAAC produces substituted triazoles via the 1,3-dipolar cycloaddition of an azide and alkyne. However, instead of the use of a copper catalyst, SPAAC relies on the ring strain of a cyclooctyne for its reactivity (Figure 4.9.B). Whilst this increases the applicability of SPAAC relative to CuAAC, many early applications of SPAAC suffered from issues associated with the limited water solubility of the strained alkyne and slow reaction kinetics. This led to the development of numerous cyclooctynes, e.g. bicyclo[6.1.0]nonyne (BCN), dibenzoazacyclooctyne (DBCO), or dibenzocyclooctyne (DIBO), that are capable of increasing solubility and reactivity without compromising on stability.[338] As a result, SPAAC has now been widely used for a number of biological applications, including the formation of homogeneous ADCs.[339–341] Several such ADCs are currently in clinical trials (e.g. STRO-001 and STRO-002 from Sutro Biopharma).[342,343]

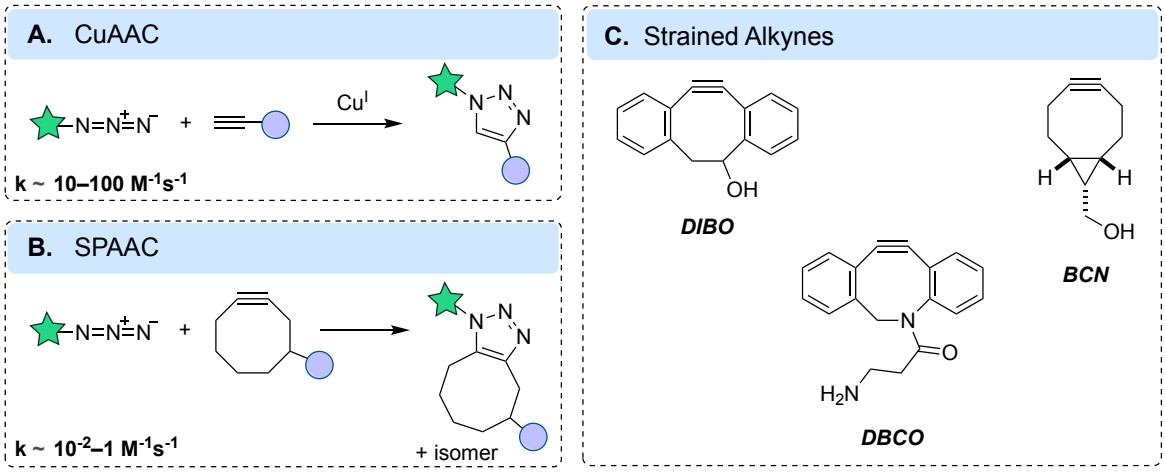

Figure 4.9. Click reactions based on the azide-alkyne cycloaddition. A. CuAAC. B. SPAAC. C. Examples of strained alkynes commonly employed.[344,345]

Application of IEDDA reactions for the site-selective modification of antibodies has also been demonstrated on a number of occasions.[327,346–349] These reactions involve a Diels-Alder [4+2] cycloaddition between a terminal or strained alkene, e.g. vinyl-, trans-cyclooctene- (TCO), or methylcyclopropene-functionalised molecules, and a tetrazine derivative and are notable for their exceptionally fast reaction kinetics (rate constant of up to 10^6 M^{-1} s^{-1}, Scheme 4.3).[345] Not only do IEDDA reactions constitute some of the fastest known biorthogonal reactions, but they also exhibit high biocompatibility. Furthermore, due to their orthogonality with SPAAC and CuAAC, they are also suitable for use in dual-labelling experiments.[350,351]

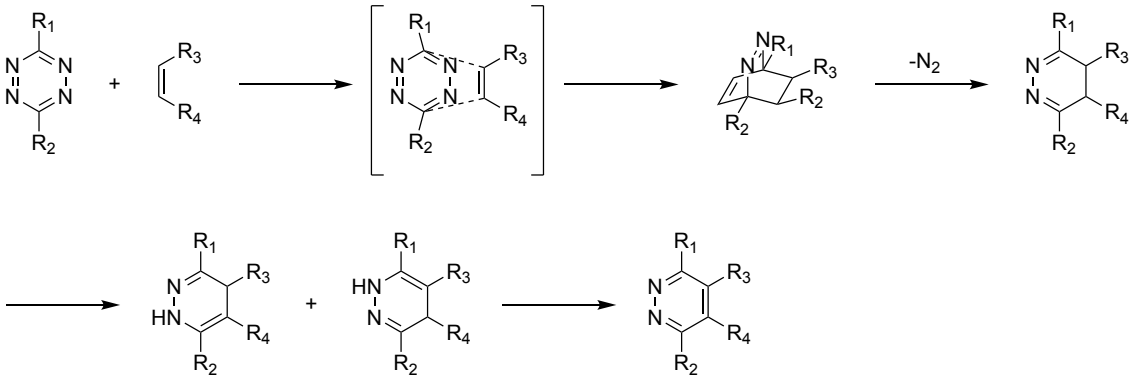

Scheme 4.3. Mechanism of the IEDDA reaction.

4.2.9 Dual Modification of Antibodies

Whilst recent years have seen significant advances in site-selective antibody modification, many strategies still only allow for modification of antibodies with a single type of payload.[352] Nonetheless, interest in the dual modification of antibodies for a variety of applications (e.g. combination therapies or theranostics) is rapidly increasing, which has led to the emergence of numerous techniques for the dual functionalisation of antibodies.[353]

The site-selective dual functionalisation of antibodies can be accomplished in two ways: through the modification of two different amino acids sites or via conjugation of a bifunctional linker to a single site.[352] In both instances, the choice of reagents and sequence of bioconjugation reactions needs to be carefully considered to maximise efficiency and avoid cross reactivity (Figure 4.10).

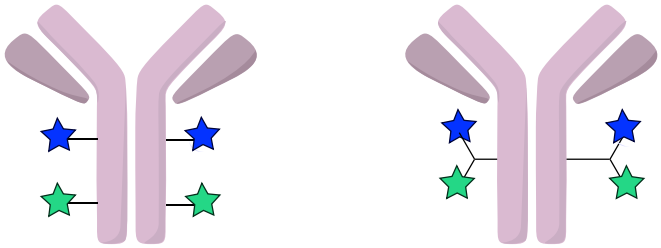

Figure 4.10. Approaches to the dual functionalisation of antibodies (A) at two different sites (B) at the same site using a multifunctional linker. The blue and green stars represent different payloads (e.g. dye or drug).

4.2.9.1 Genetic Engineering for Dual Functionalisation of Antibodies

To expand upon the natural reactivity of antibodies, many methods for dual modification require the recombinant incorporation of one or more amino acid residues or peptide tags.[352,353] These residues are carefully selected to prevent cross-reactivity with endogenous functional groups, resulting in excellent versatility and selectivity.

Engineered Cysteines

One approach for the dual functionalisation of antibodies involves the use of THIOMABs (antibodies bearing engineered cysteine residues).[354,355] Through the use of site-directed mutagenesis, THIOMAB technology enables the incorporation of additional cysteine residues at specific sites within antibodies.[322] The resulting free cysteines can then be reacted with suitable electrophiles to enable the site-selective conjugation of payloads with defined stoichiometry.[j] Kumar *et al*. utilised this technology to engineer free cysteines into trastuzumab for the generation of a dual-drug ADC (Scheme 4.4).[355] Initial cysteine conjugation with a heterotrifunctional *N*-aryl maleimide linker was employed to integrate ketone and alkyne handles. The resulting antibody-linker conjugate could then be subjected to oxime ligation with an aminooxy-Val-Cit(vc)-PABC-MMAE payload, followed by CuAAC with azido-Val-Ala(va)-PABC-PBD to generate a homogeneous DAR 4 ADC (two MMAE and two PBD payloads). Although *in vitro* studies showed that the resulting ADC failed to show any additive or synergistic cell killing effects, this study was able to successful demonstrate the utility of cysteine-engineering for the dual-modification of antibodies.

[j] All native cysteines in the antibody are present as disulfides, enabling selective modification of the genetically inserted free cysteines.

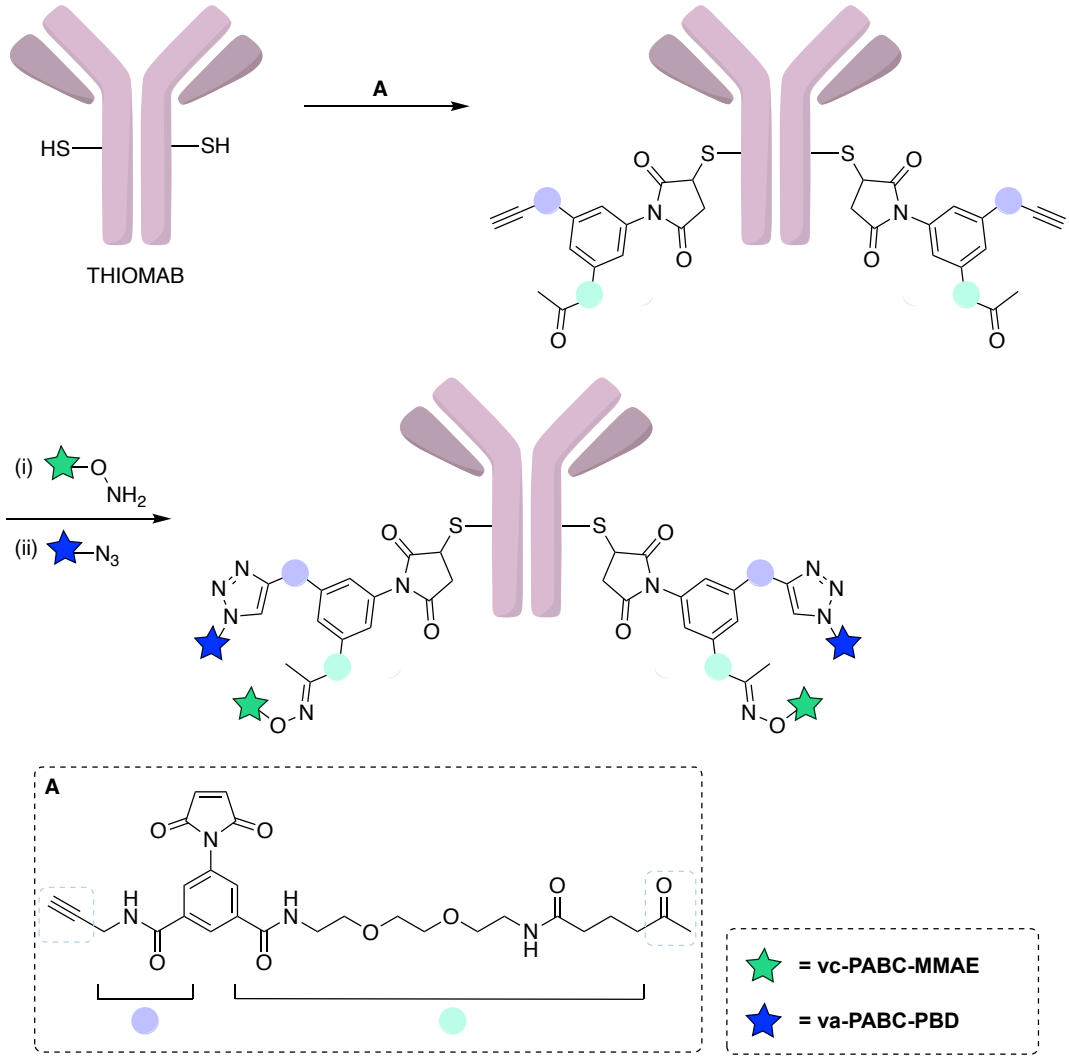

Scheme 4.4. Dual modification of a THIOMAB via conjugation to a bifunctional linker, followed by sequential oxime ligation and CuAAC.[355]

Non-Canonical Amino Acid Incorporation

Recent years have seen methods for the expansion of the genetic code beyond the 22 naturally occurring amino acids increase significantly, enabling non-canonical amino acids (ncAAs) to be site-selectively engineered into numerous proteins.[356–358] These techniques facilitate the incorporation of a limitless array of different functional handles, with high site-selectivity and flexible incorporation sites.

Although the majority of work has focused on the insertion of a single ncAA, a handful of examples have demonstrated the possibility of inserting two or potentially more different ncAAs into antibodies.[359–361] Indeed, Schultz *et al*. were able to introduce *p*-acetophenylalanine (*p*AcF) and azido-lysine (AzK) simultaneously and site-specifically into anti-HER2-IgG (Scheme 4.5).[360] The resulting antibody, was then able to undergo sequential oxime ligation to alkoxy-amine-derivatised auristatin F

and SPAAC with Alexa Fluor (AF) 488-DIBO alkyne to give the desired dual-labelled antibody in greater than 90% conjugation yield.

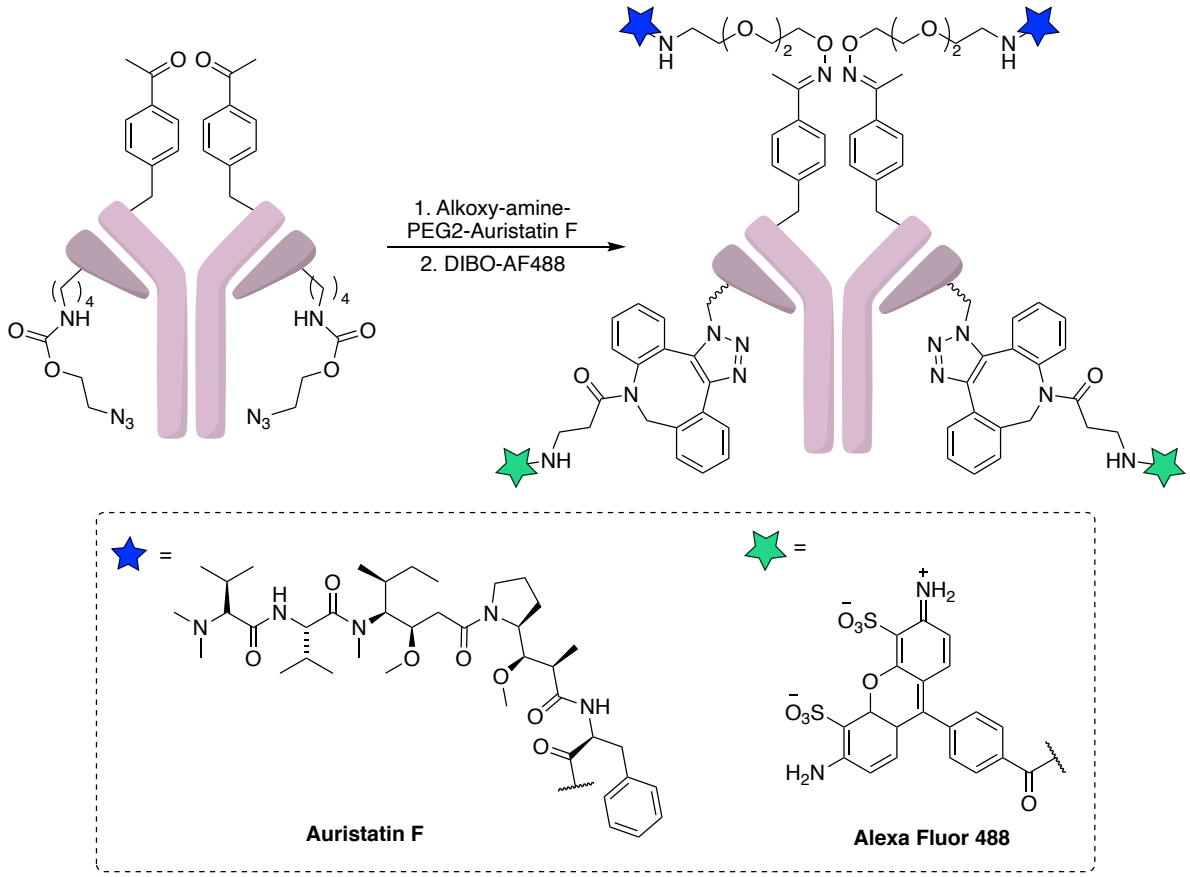

Scheme 4.5. Dual functional ADC generated via genetic code expansion. Tubulin inhibitor auristatin F and fluorescent dye AF488 were conjugated to a HER2-targeting antibody via site-specific conjugation at the engineered pAcF and AzK residues, respectively.[360] Wavy bonds represent the remainder of the azidolysine group. The conjugation product is formed as mixture of isomers, for illustrative purposes only one isomer is shown.

More recently, thio-selenomabs (antibodies with engineered selenocysteine and cysteine residues) have also facilitated the generation of dual functional antibodies.[359,361] Utilising the greater nucleophilicity of the selenoate group (p*K*a 5.2) relative to its thiolate counterpart (p*K*a 8.3), mildly acidic and reducing conditions can be employed to enable the site-selective conjugation of electrophilic compounds to engineered selenocysteine residues in the presence of free cysteine.[362] Subsequent reaction at the cysteine residues enables the formation of dual-labelled antibodies. This dual conjugation method was used by Nilchan and co-workers to generate an anti-HER2 ADC that combined two payloads with distinct mechanisms of action: tubulin-targeting payload MMAF and the DNA-damaging payload PNU-159682 (Scheme 4.6).[359]

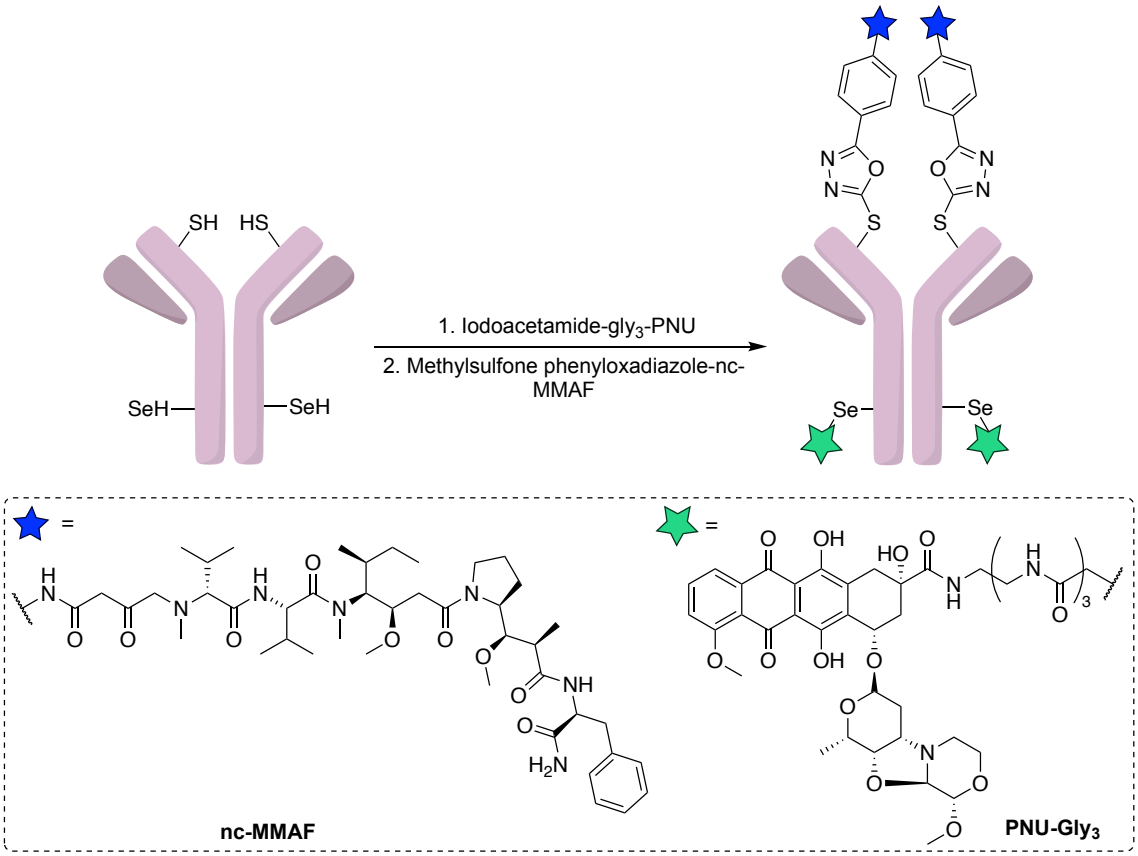

Scheme 4.6. Exploitation of a thio-selenomab for dual functionalisation: DNA crosslinking agent PNU-159682 and tubulin polymerisation inhibitor MMAF were conjugated to a HER2-targeting thio-selenomab via site-specific conjugation at the engineered selenocysteine and cysteine residues, respectively.[359] nc = non-cleavable.

Enzymatic Methods

By utilising their ability to selectively modify specific amino acids in a unique amino acid sequence, enzymes offer a useful alternative strategy for the site-selective modification of antibodies.[363] To provide suitable substrates for these enzyme-catalysed ligations, the genetic incorporation of suitable peptide tags into antibodies is often necessary.[364] Some examples of enzymes employed for dual functionalisation of antibodies are shown in Table 4.3 along with their tag sequences.

Table 4.3. Commonly used enzymes and peptide tags employed for dual modification of antibodies.[353]

Enzyme	Tag Sequence[a]
Butelase 1	NHV
Lipoate acid ligase A	GFEIDKVWYDLDA
Microbial transglutaminase (mTG)	LLQG
Sortase A	LPXTGG

[a]The reactive residue of each tag is underlined.

For this technology to be applied for the dual functionalisation of antibodies, the insertion of two orthogonal peptide tags that can be recognised by distinct enzymes is often required.[365–368] However, in one example, Spycher *et al*. were able demonstrate dual functionalisation by engineering a single short lysine-containing peptide tag into an aglycosylated IgG1 antibody. The mutant antibody was then treated with MTG, which can recognise glutamine 295 on aglycosylated IgGs, to facilitate modification of the exposed glutamine and lysine residues with primary amine and glutamine-containing peptide derivatives, respectively (Scheme 4.7).[369] By using this technique for the introduction of orthogonal TCO and azido motifs, simultaneous orthogonal click reactions with DBCO-PEG4-5/6-FAM dye and tetrazine-PEG4-DOTAGA metal chelator were enabled for the formation of a dual-labelled antibody for imaging purposes.

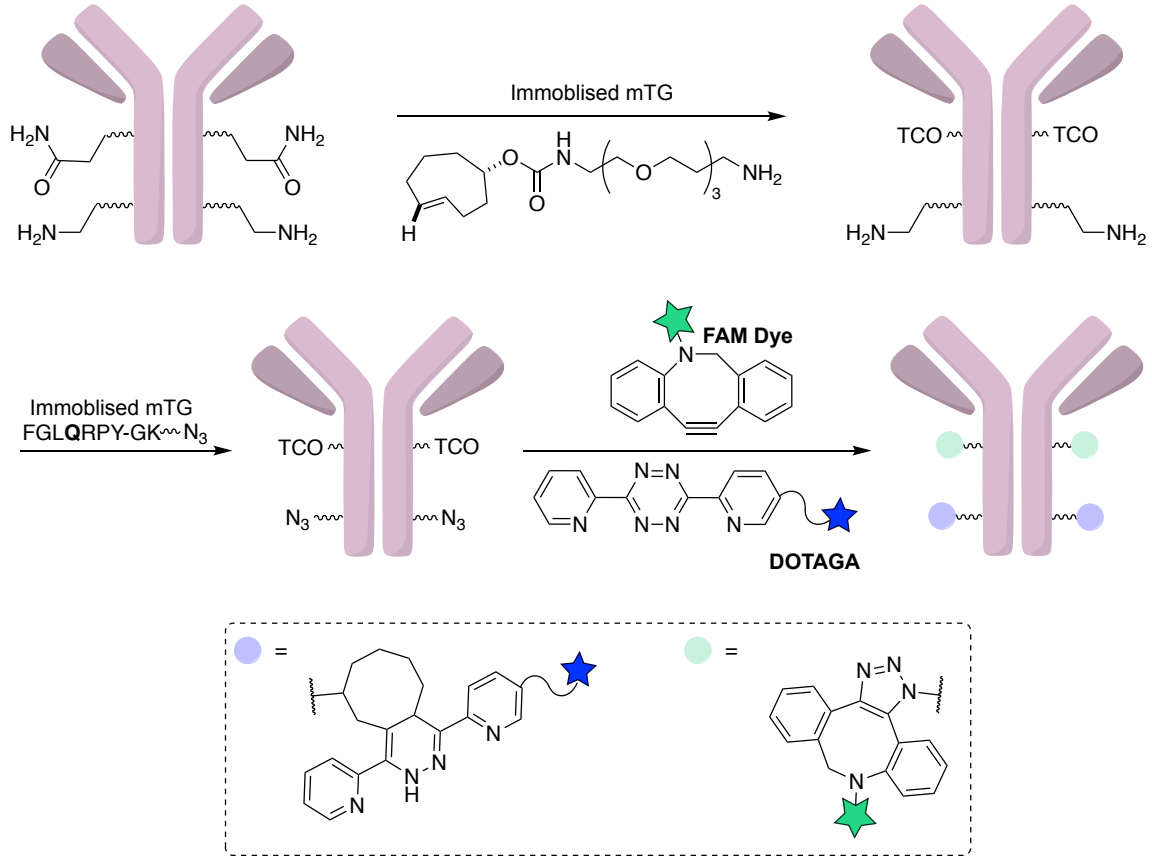

Scheme 4.7. MTG-mediated dual functionalisation of an aglycosylated IgG1 antibody.[369]

In some instances, the enzyme-mediated dual modification of antibodies can also be achieved without the need to engineer artificial peptide tags, or via the use of a single peptide tag in combination with a non-enzymatic modification strategy.[370–373] For example, Alabi and co-workers utilised mTG to facilitate the conjugation of a heterobifunctional linker containing both azide and methyltetrazine 'click' handles to deglycosylated trastuzumab (Figure 4.8).[372] The resulting antibody could then

undergo simultaneous SPAAC with a 'clickable' DBCO-modified PEG chain and IEDDA reaction with a TCO-PEG modified disulfide-linked version of DM1 to give the dually modified ADC.

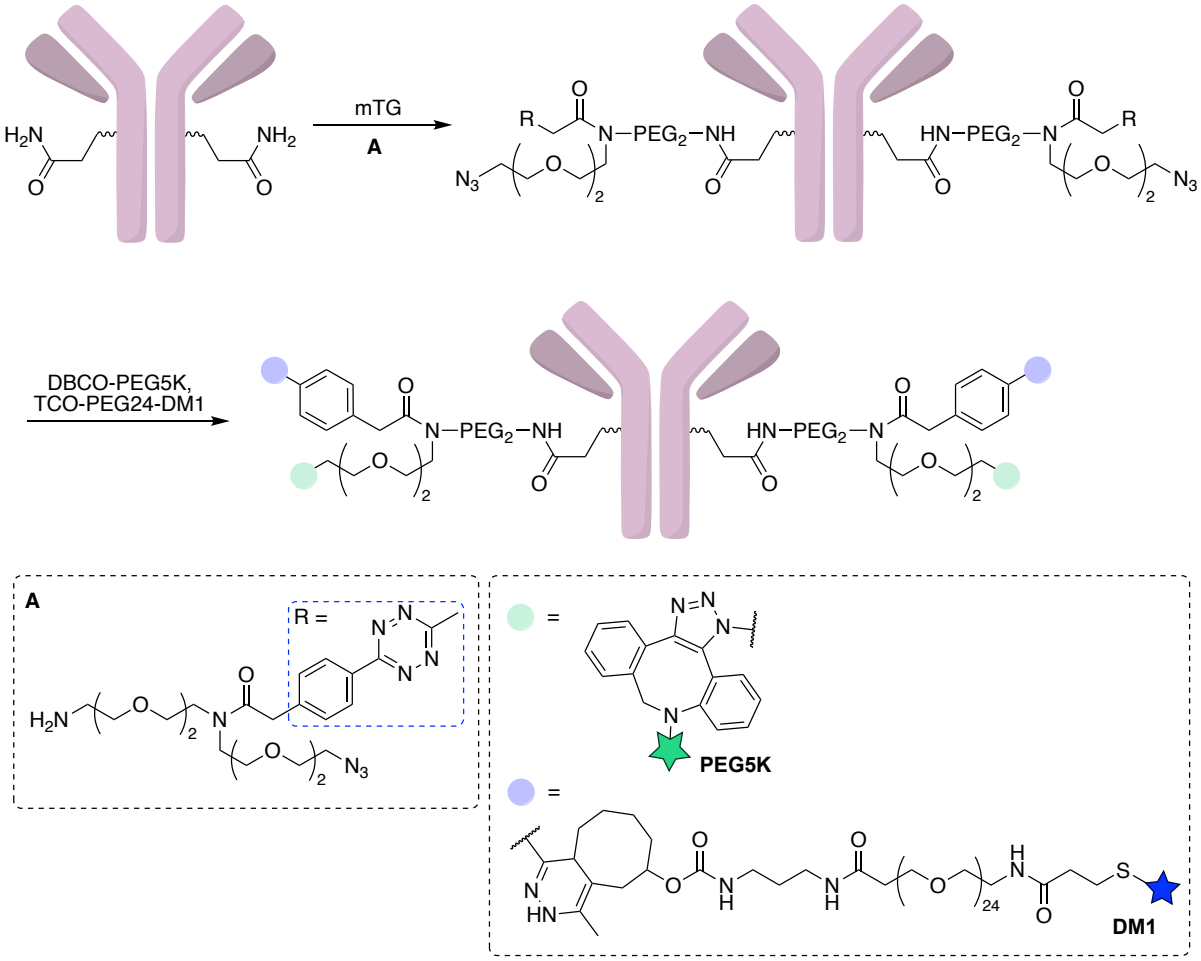

Scheme 4.8. Dual modification of an antibody using mTG.[372] Incorporation of a dual-functional linker bearing a tetrazine and an azido tag enabled simultaneous, one-pot synthesis of bifunctional antibody conjugates.

4.2.9.2 Synthetic Strategies for Dual Functionalisation of Antibodies

Although the use of genetically engineered mAbs for ADC construction allows excellent control of homogeneity, these approaches lack universal applicability and can be technically complicated and expensive when employed for dual functionalisation.[374] Modification of native, non-engineered, mAbs, on the other hand, is universal and operationally simpler, although control of homogeneity can be more of a challenge.[286] As a result, a number of synthetic strategies for the site-selective dual modification of antibodies have been developed.

Glycan Modification

Glycan-mediated conjugation provides a unique site-selective method for the modification of antibodies, which avoids the need for genetic engineering. As was discussed in Section 4.2.3, each heavy chain of an IgG antibody contains a conserved *N*-glycan at Asn297 of the Fc region.[375] These

glycans are both distant from the antigen-binding sites of the variable domain and well conserved across antibody type, making them extremely attractive and generic targets for site-selective modification.[227,376] As a result, several methods have been developed for the dual modification of antibodies at these sites.[377–379] For example, Zeglis and co-workers employed two sequential enzymatic reactions to introduce terminal azide-bearing monosaccharides to the heavy chain glycans of trastuzumab (Scheme 4.9).[377] To illustrate the utility of this platform for the generation of dual-labelled radio-ADCs, a SPAAC reaction was then employed to couple the azide-functionalised antibody to both the radiometal chelator desferrioxamine (DFO) and DIBO-modified MMAE (in a 1:1 molar ratio mixture). Subsequent labelling with ^{89}Zr resulted in the formation of a ^{89}Zr-trastuzumab-MMAE conjugate, which demonstrated good tumour targeting and therapeutic efficacy *in vivo*.

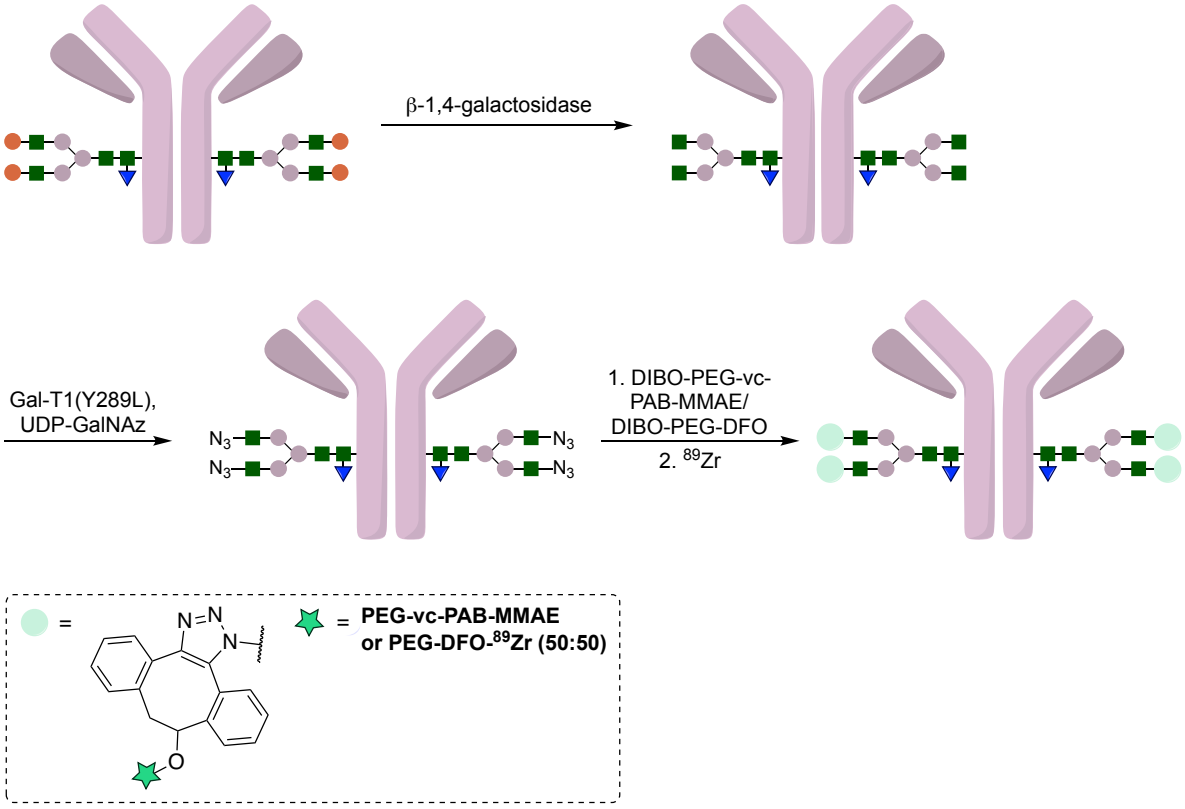

Scheme 4.9. β-1,4-galactosidase-catalysed trimming of native trastuzumab, followed by incubation with galactosyltransferase GalT(Y289L) and the azide-modified sugar GalNAz, afforded N_3-trastuzumab. Subsequent reaction with DIBO functionalised MMAE and DFO generated a ^{89}Zr-MMAE dual labelled ADC. Red circle = galactose.

Reduced Inter-Chain Disulfides

In recent years, disulfide rebridging has emerged as a leading strategy for the generation of near-homogeneous ADCs. This strategy avoids the need for genetic engineering or custom enzymes, instead reducing the four interchain disulfide bonds of a native IgG antibody.[236,380] The resulting free cysteines can then be reacted with electrophilic cross-linking reagents, thereby regaining the stabilising connection between the polypeptide chains. By installing the payloads away from any antibody-

antigen recognition sites this strategy also ensures that the affinity and specificity of an antibody for its target antigen is not diminished. Reagents developed for disulfide rebridging include bis-sulfones,[381] divinylpyrimidines (DVP),[382] dibromomaleimides,[383] and pyridazinediones (Scheme 4.10).[350] In general, these reagents install one linker molecule per disulfide, and hence DARs of 4, 8 or 16 are readily obtained (depending on the number of drug molecules per linker).

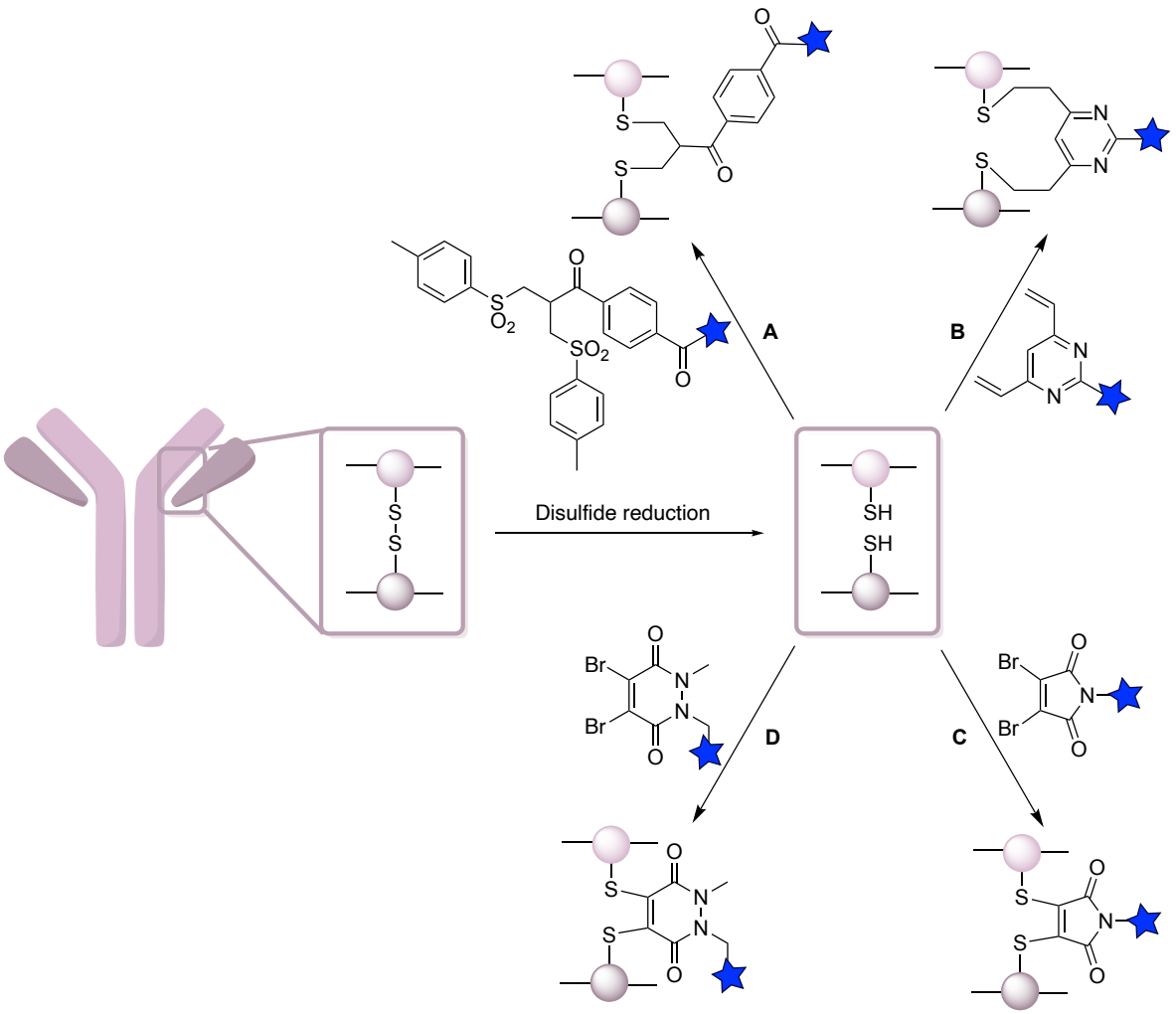

Scheme 4.10. Disulfide rebriding via the use of (A) bis-sulfones; (B) DVPs; (C) dibromomaleimides; (D) pyridazinediones. Stars represent payloads.

To enable dual modification of an antibody using a cysteine rebridging methodology, a multifunctional linker is required with three well-defined orthogonal handles to enable attachment to both a protein and two payloads. With this in mind, Chudasama and co-workers developed a dual-functional method where two orthogonal 'clickable' handles were directly introduced into both Fabs and IgG molecules using a dibromopyridazinedione linker (Scheme 4.11).[350] This approach allowed subsequent introduction of two distinct functionalities via sequential bioorthogonal reactions. In one example, the antibody-linker construct was reacted sequentially with sulfo-Cy5-N_3 and Dox-N_3, by applying SPAAC and CuAAC chemistry, respectively, to form a fluorescent ADC.

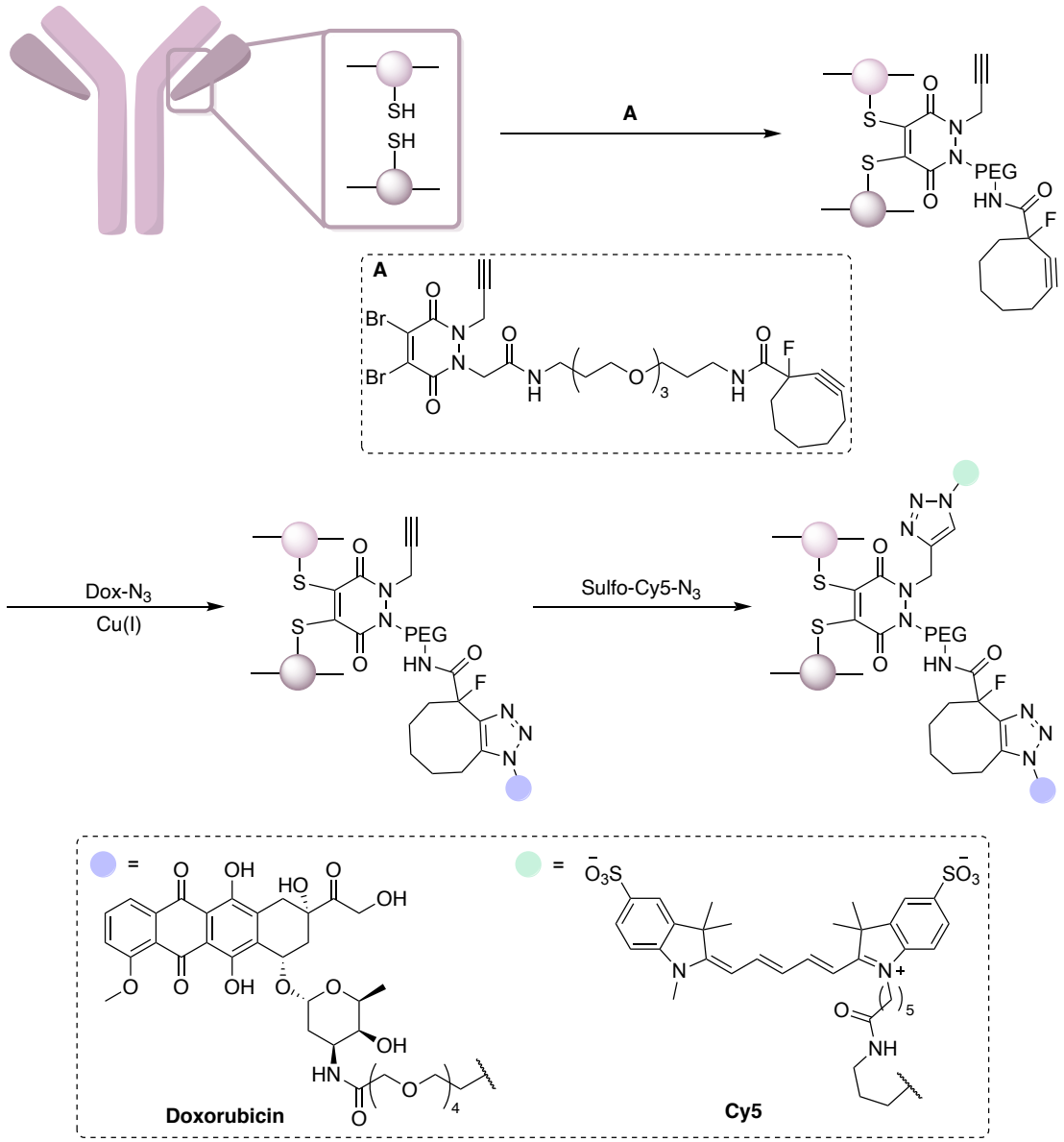

Scheme 4.11. A 'plug-and-play' approach to the site-selective dual modification of proteins developed by Chudasama and co-workers.[350] Cysteine rebridging of trastuzumab, followed by SPAAC with Sulfo-Cy5-N_3 and CuAAC with Dox-N_3 resulted in the formation of a fluorescent ADC.

As an alternative strategy to cysteine rebridging, Levengood *et al*. employed native cysteine-maleimide chemistry to introduce a multifunctional linker (Figure 4.11) at each of the eight interchain cysteines of anti-CD30 mAb cAC10.[384] The maleimide linker bears two orthogonally protected cysteine residues that can be sequentially unmasked and conjugated with two complementary payloads. Using this approach, the authors were able to introduce both MMAF and MMAE to form a homogeneous DAR 16 dual-drug ADC, with each drug having an individual DAR of 8.

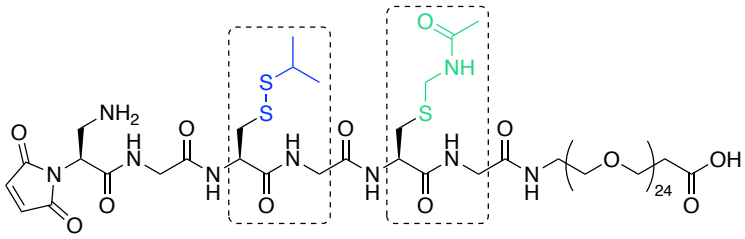

Figure 4.11. Trifunctional reagent used by Levengood and co-workers. After full reaction of the eight thiolates with the linker, the two orthogonally protected cysteine residues can then be sequentially unmasked to allow the introduction of two distinct payloads. This results in a total of 16 payloads/mAb.

More recently, in 2020, the Spring group reported the use of a DVP reagent for the dual modification of cysteine-containing biomacromolecules (Figure 4.12).[385] In addition to two cysteine-reactive centres, this linker was modified to incorporate fluorescein and an alkyne handle for further functionalisation.

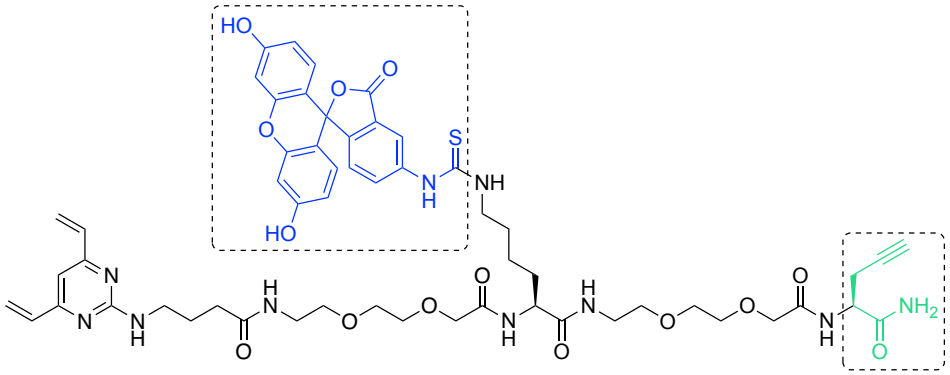

Figure 4.12. Linker developed within the Spring group for the site-selective dual modification of proteins.[385] Cysteine rebridging of trastuzumab with the linker, followed by CuAAC with azide-functionalised MMAE resulted in the formation of a fluorescent ADC.

4.2.9.3 Applications of Dual Antibody Modification

With the recent key advancements within the field of antibody dual functionalisation techniques, a range of homogeneous antibody conjugates with complex functionalities have been developed and applied for a variety of applications, which are discussed below.

ADCs, like traditional cancer chemotherapies, can suffer from inherited or acquired drug resistance.[353,386] This has led to increased interest in combination therapies that utilise complementary drug combinations designed to overcome or avoid resistance mechanisms. As a result, ADC are now being tested in combination with other established chemotherapeutics.[387,388] Current clinical data suggests that ADC resistance can also be overcome through delivery of an alternative cytotoxic payload using the same antibody.[389,390] Therefore, the attachment of two different cytotoxins with distinct mechanisms of action (MOA) to a single antibody has the potential to generate ADCs capable of avoiding resistance mechanisms. Notably, a recent study has demonstrated the ability of dual-drug

ADCs to exhibit greater treatment effect and survival benefit *in vivo* than two corresponding single-drug ADCs administered simultaneously.[373]

A second payload may also be added to an ADC to modulate pharmacokinetic properties and reduce ADC hydrophobicity.[353] This has been frequently demonstrated by the simultaneous introduction of a hydrophilic polyethylene glycol (PEG) chain alongside a cytotoxin.[350,372,391] These PEG chains can confer increased plasma half-life, improved stability, and reduced immunogenicity.[392]

Finally, dual modified antibodies can also be used as combined therapeutic and diagnostic agents, known as theranostics.[393,394] These agents have attracted widespread attention in recent years due to their ability to monitor treatments in real-time and potential application in personalised cancer medicines.

4.3 Project Aims

As discussed in the previous section, dual-modified antibodies have a multitude of uses both as diagnostics and therapeutics. Particularly in the field of ADCs, multifunctional scaffolds offer versatile platforms for the attachment of multiple warheads or stabilising groups. Unfortunately, most of the approaches that facilitate the site-selective, dual labelling of antibodies suffer from several drawbacks due to problems with stability, solubility, partial conversions, low yield, and/or the use of cytotoxic metal catalysts.[352,360,367,371,372] Thus, as demand for these multifunctional scaffolds increases, there is a need for more flexible and straightforward approaches that can enable rapid screening of payload and antibody combinations, whilst overcoming these problems.

Accordingly, the aim of this work was the development of novel DVP-based linkers capable of undergoing efficient metal-free post-rebridging conjugation, with a particular focus on the synthesis of a novel platform for the dual modification of antibodies. Crucially, it was proposed that this platform could be designed in such a way as to address some of the known issues faced by such dual-modification strategies. Thus, it was vital that several criteria were satisfied:

- The linker design should not negatively impact the ability of the DVP moiety to undergo fast, efficient rebridging, with high conversions.
- The post-rebridging chemistry should not impact the structure or biological activity of the native antibody.
- Functionalisation of the linker with a variety of payloads should involve robust and efficient metal-free chemistry.

- The linker should not affect the main characteristics of the payload (e.g. cytotoxicity or fluorescence).
- The linker should be compatible with a range of payloads, such that the linker provides a modular platform to rapidly access a broad range of bioconjugates.
- The resulting conjugates should be stable and soluble in aqueous media.

5 Results and Discussion

5.1 Project Outline

In recent years, the development of DVP linkers for the efficient rebridging of the reduced disulfides of native antibodies has been reported by the Spring group for the mono- and dual-functionalisation of antibodies (*vide supra,* Section 4.2.9.2).[382,385] These studies have not only confirmed the high plasma-stability of the cysteine-DVP linkage, but also that DVP modification does not have a detrimental effect on the cellular specificity and receptor affinity of the antibody. However, to date, post-rebridging conjugation reactions using this DVP-technology have relied upon the use of CuAAC chemistry, whilst dual-functionalisation has been limited to the introduction of a drug and fluorescein to trastuzumab with only partial conversions.[385]

Thus, in line with the project aims, it was proposed that a DVP linker containing two orthogonal 'clickable' handles for metal-free click reactions could be synthesised to facilitate antibody modification (Figure 5.1). By enabling this conjugation to take place post-rebridging, this linker could provide a versatile platform for the generation of dual functionalised antibodies with various applications as diagnostic and/or therapeutic agents.[350,359]

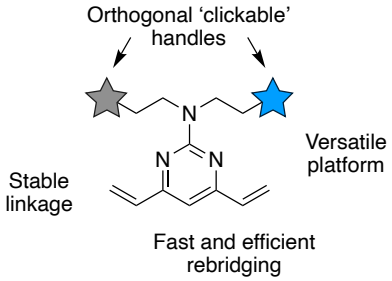

Figure 5.1. General dual functional (df) linker design.

For these purposes, it was envisioned that two orthogonal metal-free click reactions, SPAAC and IEDDA, could be employed sequentially to enable efficient dual modification of antibodies. Although both IEDDA and SPAAC reactions have already been applied for the site-selective modification of antibodies this has mainly been *via* the incorporation of unnatural amino acids or through enzymatic modifications,[347,395,396] whilst cysteine rebridging methods have been largely limited to the modification of Fab fragments.[397,398] Thus, investigations first began by combining IEDDA or SPAAC chemistry with cysteine rebridging technology, to form DVP-based linkers with only one 'clickable' handle (monofunctional [mf] DVPs). Not only was this expected to aid in the optimisation of the

conditions for the click reactions on antibodies prior to dual functional (df) linker formation, but such linkers also serve to expand the toolbox of cysteine rebridging linkers.

To this end, it was envisioned that DVP linkers containing metal-free click handles, such as strained alkyne **78** or strained alkene **79** could be explored, allowing tetrazine- or azide-functionalised payloads to then be installed after rebridging (Figure 5.2). This strategy would benefit from the commercial availability of a catalogue of payloads containing azide or tetrazine groups.

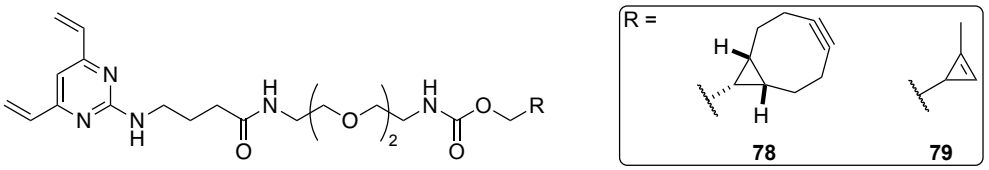

Figure 5.2. Proposed mf-DVP linkers.

For ease of synthesis, the design of this linker was such that it could be generated in a single step from DVP-acid **80** — a compound whose synthesis has been previously reported by the Spring group (Scheme 5.1).[399] The linker was also designed to incorporate a short PEG spacer to ensure sufficient water solubility of the final linker construct and provide adequate spacing between the DVP and the 'clickable' handle.

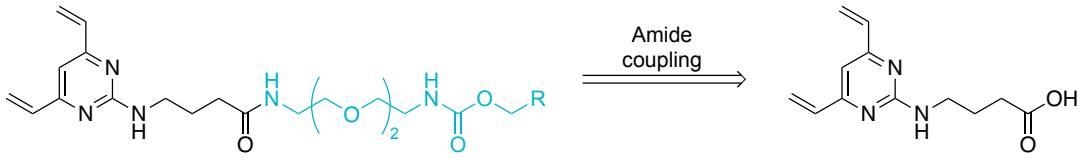

Scheme 5.1. The novel linkers were designed to be accessed in a single step from the previously synthesised DVP-acid **80**.

5.2 Synthesis of Monofunctional DVP Linkers

5.2.1 DVP Synthesis

To provide a common intermediate capable of being coupled to different 'clickable' handles, investigations began with the exploration of DVP-acid **80**. Following the reported procedure, DVP-acid **80** was synthesised in three steps from 2,4,6-trichloropyrimidine **81** (Scheme 5.2).[399] Briefly, this required S_NAr with ethyl 4-aminobutyrate hydrochloride to give dichloropyrimidine **82**, followed by a Suzuki cross-coupling coupling with vinyl trifluoroborate to form DVP-derivative **83** in 73% yield. Previous experience in the Spring group has shown the propensity of this intermediate to polymerise, thus immediate hydrolysis to the more stable acid **80** was required, which was achieved in 80% yield.

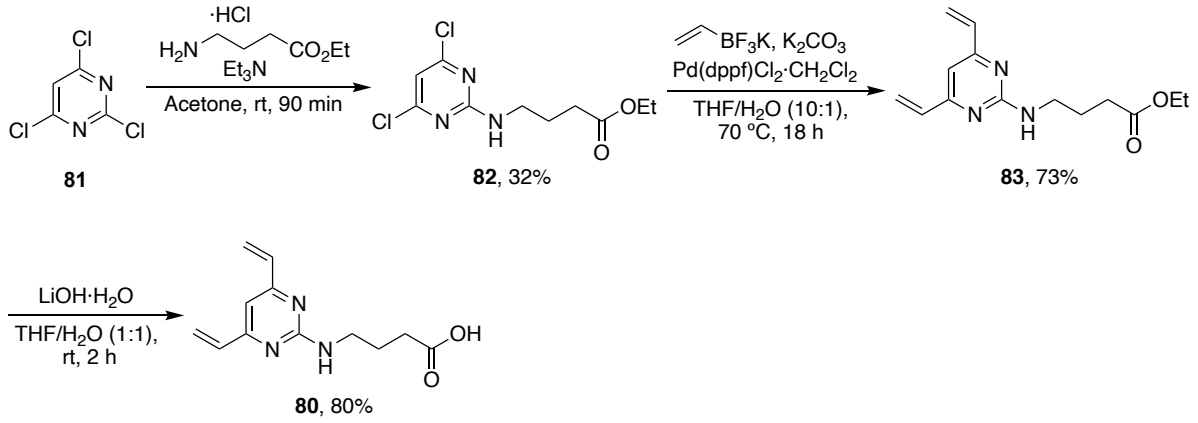

Scheme 5.2. Synthesis of DVP-acid **80**.

5.2.2 Synthesis a BCN-DVP Linker

Having successfully synthesised DVP-acid **80**, efforts then turned to the generation of a linker containing a strained alkyne. For this purpose, BCN was selected due its low lipophilicity, good stability, and excellent SPAAC kinetics.[338,400] BCN can also be readily synthesised from cyclooctadiene, **84**, in only four steps. Indeed, following a previously reported synthetic route, diene **84** underwent a Rh-catalysed cycloaddition with ethyl diazoacetate to afford a separable mixture of *endo*- and *exo*-isomers (Scheme 5.3).[400] Notably, although both *endo*- and *exo*-BCN can undergo SPAAC, the *exo*-isomer is known to react much more slowly.[400] Thus, only the *endo*- isomer **85** was isolated and carried through to the next step. Cyclooctene **85** was then reduced with $LiAlH_4$ followed by bromination and elimination to give BCN (**86**) in 40% yield.

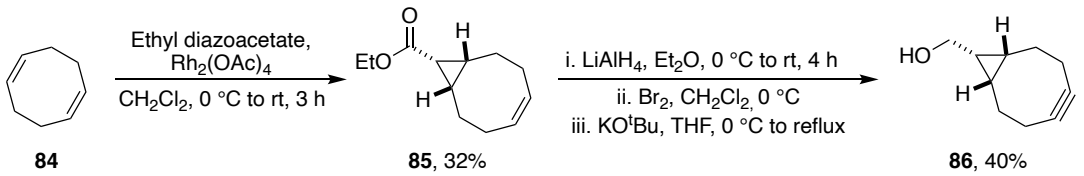

Scheme 5.3. BCN (**86**) synthesis.

With BCN in hand, synthetic efforts then moved towards the formation of a BCN-functionalised PEG chain capable of undergoing amide coupling with DVP-acid **80**. Again, following a literature route, BCN was transformed into the activated mixed carbonate **87** using 4-nitrophenyl chloroformate and pyridine (py) in 78% yield (Scheme 5.4).[400] Although subsequent conversion of **87** to the desired carbamate proceeded smoothly upon reaction with 1,8-diamino-3,6-dioxaoctane, purification of **88** via flash column chromatography proved challenging, with the compound streaking even with addition of Et_3N. Thus, crude **88** was instead directly coupled with DVP-acid **80**. This amide coupling was initially attempted under *N*,*N*,*N*',*N*'-tetramethyl-O-(1H-benzotriazol-1-yl)uraniumhexafluorophosphate (HBTU) conditions, however difficulties arose separating the product from unidentified by-products. Gratifyingly, by swapping to a 1-Ethyl-3-(3-

dimethylaminopropyl)carbodiimide (EDC)-mediated coupling the by-products were easily removed by aqueous extraction, enabling isolation of the desired BCN-DVP linker **78** in 61% yield.

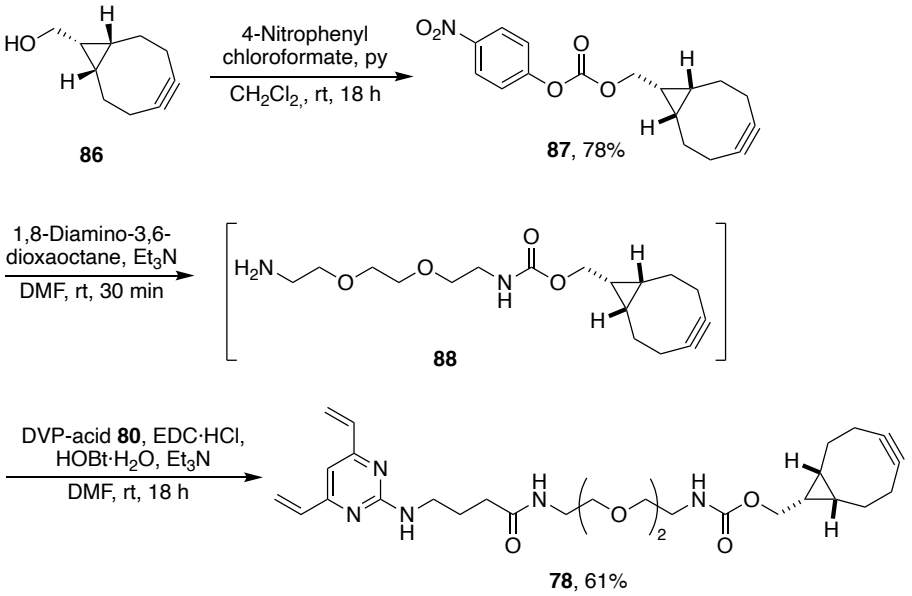

Scheme 5.4. BCN-DVP linker (**78**) synthesis.

5.2.3 Synthesis of a Cyclopropene-DVP Linker

Having successfully developed a route for the synthesis of a BCN-containing linker, the development of a second linker only capable of undergoing IEDDA was then required. In recent years, cyclopropenes (cyps) have emerged as alternative tetrazine coupling partners for IEDDA reactions, capable of reacting selectively in complex biological environments.[401,402] Although the rate constant of their reaction with tetrazine is significantly lower than the classic IEDDA dienophile TCO, their small size and greater stability make them ideal for use in biological applications.[403,404] For example, Chin and co-workers used genetic code expansion to introduce a non-canonical cyp-lysine derivative into trastuzumab, which underwent subsequent IEDDA with a tetrazine-modified MMAE to generate a HER2-targeted ADC.[347] Encouraged by this work, it was decided that cyp would make an ideal choice for the generation of a linker containing a strained alkene.

To this end, activated cyp-derivative **89** was synthesised according to a synthetic route adapted from the literature (Scheme 5.5).[402,405–407] This required Rh-catalysed cyclopropenation of ethyl diazoacetate (**90**) to give TMS-propene **91**,[405] followed by ester reduction. Notably, when this reaction was carried out using $LiAlH_4$,[402] an inseparable mixture of cyclopropane **92** and the desired cyp **93** were formed (as observed by ^1H NMR spectroscopy). However, following a different procedure that employed a DIBAL-H reduction only the desired product **93** was generated.[406] Finally, sequential one-

pot TMS-deprotection and reaction with 4-nitrophenyl chloroformate afforded the mixed activated carbonate **89** in 81% yield.[407]

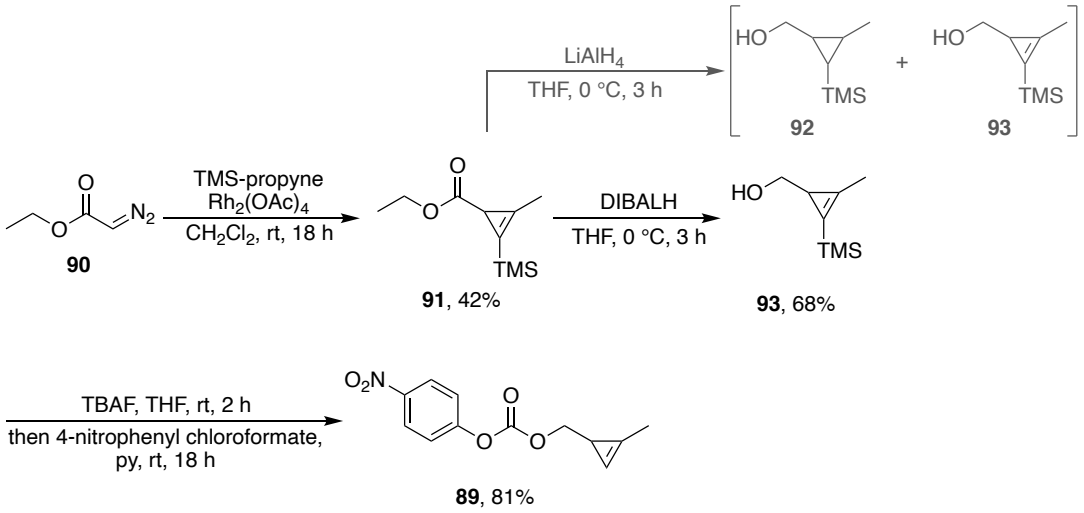

Scheme 5.5. Synthesis of activated cyp-derivative **89**.

Applying the previously established synthetic route, carbonate **89** was reacted with 1,8-diamino-3,6-dioxaoctane to generate the cyp-functionalised PEG chain **94** (Scheme 5.6). The crude material was then immediately reacted with DVP-acid **80** under EDC/HOBt coupling conditions to give the DVP-cyp linker **79** in 63% yield.

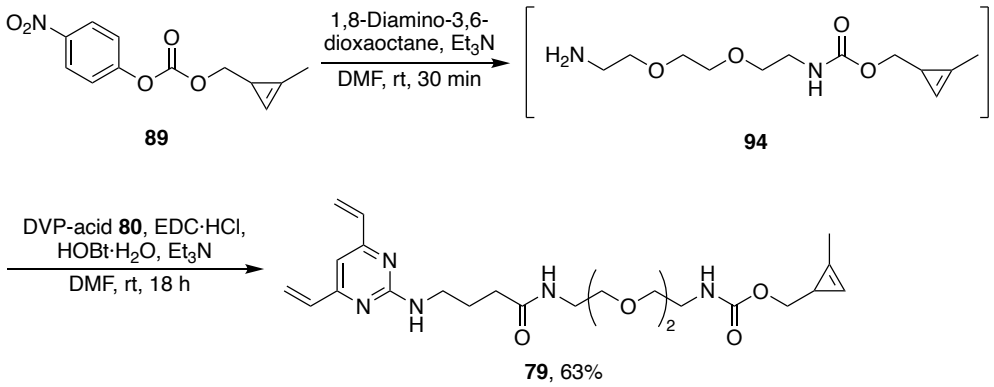

Scheme 5.6. Cyp linker (**79**) synthesis.

5.2.4 Synthesis Alkyne-DVP Linker

To provide a means by which the CuAAC and metal-free click reactions could be directly compared post-rebridging, the analogous alkyne-DVP linker **95** was also synthesised (Scheme 5.7). Accordingly, commercially available hex-5-yn-1-ol (**96**) was treated with 4-nitrophenyl chloroformate to give carbonate **97**. This was then reacted with 1,8-diamino-3,6-dioxaoctane to form the crude PEG chain **98**, and subsequently coupled with DVP-acid **80** to afford the alkyne-DVP linker **95** in 57% yield.

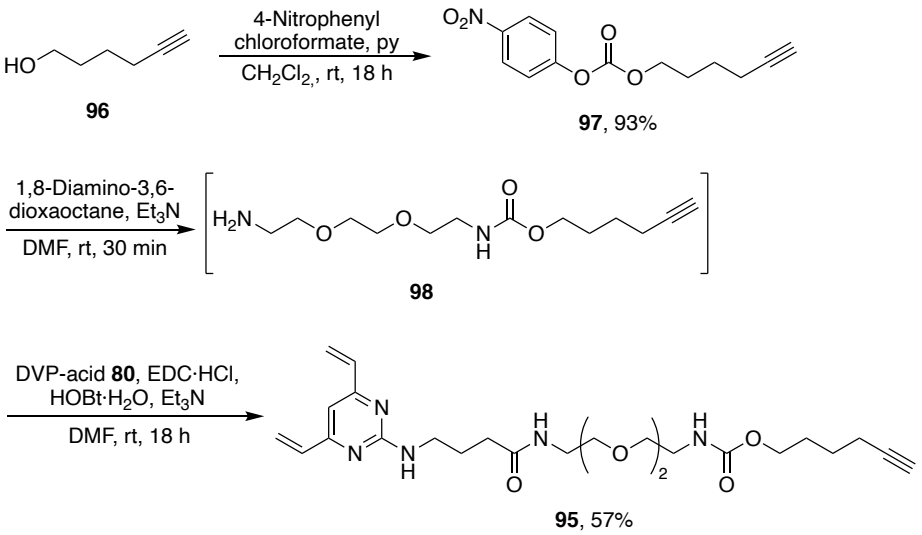

Scheme 5.7. Alkyne linker (**95**) synthesis.

5.3 Antibody Bioconjugation

5.3.1 Trastuzumab Rebridging

With the three linkers **78**, **79**, and **95** in hand, investigation of their suitability as cysteine rebridging reagents commenced. Given that trastuzumab is a clinically validated antibody for ADCs, and the volume of literature in which trastuzumab is used for bioconjugation method development, it was considered a suitable model for these studies.[243,347,350,382] In addition, the availability of HER2-positive and HER2-negative breast carcinoma cell lines meant that biological evaluation could be carried out in-house, allowing for rapid conjugate evaluation.

The ability of DVP-based linkers to successfully rebridge trastuzumab has been demonstrated by the Spring group on a number of occasions.[315,382,385] Indeed, following the tris(2-carboxyethyl)phosphine (TCEP)-mediated reduction of the four disulfides of trastuzumab **99**, DVP-based linkers have been shown to undergo rapid reaction with the resulting eight free thiols to give a mixture of full and half-antibody conjugates (Scheme 5.8). The predominant species in this mixture is half-antibody (**100**), which stems from competitive intra-chain cross-linking of the reduced heavy chain (HC) cysteines with DVP. However, despite being undesired, these 'half-antibody' conjugates are held together by non-covalent interactions and as such have been shown to retain their receptor affinity and cellular selectivity.[382,408–410] In fact, most FDA approved ADCs use conjugation techniques that result in removal of the interchain disulfide bridges.[236,307] In each case the antibody remains functional, despite no interchain disulfide bridges remaining to stabilise the structure.

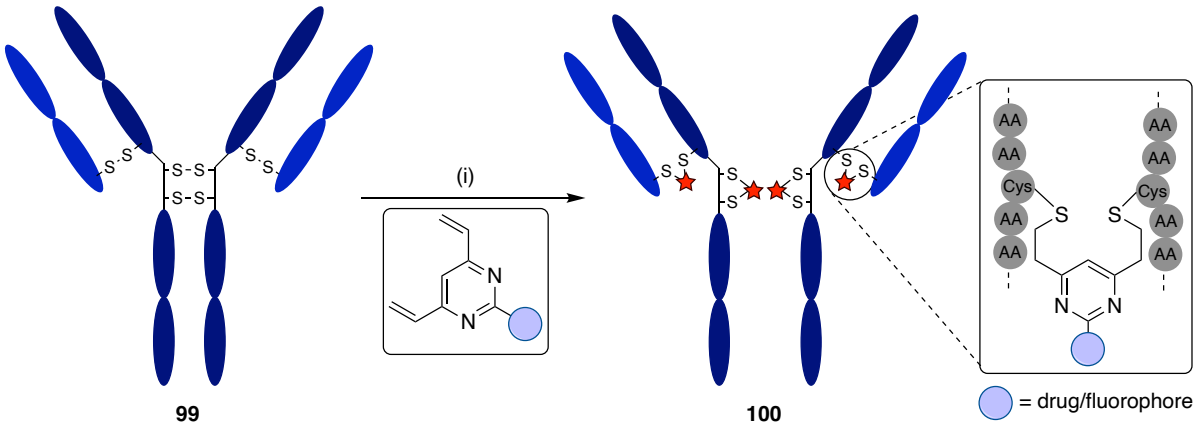

Scheme 5.8. DVP linkers developed within the Spring group have been shown to undergo efficient cysteine rebridging to give half antibody **100** as the predominant species. *Reagents and Conditions*: (i) TCEP (10 equiv.), TBS buffer, 37 °C, 1 h, then DVP linker (40 equiv.), DMSO (10% v/v), 37 °C, 2 h.

Studies began by exploring the rebridging potential of BCN-DVP linker **78**. Thus, using the reduction-rebridging protocol previously developed within the Spring group,[382] initial TCEP-mediated reduction of the four interchain disulfide bonds in trastuzumab (2.5 mg/mL) was carried out at 37 °C in TBS buffer (25 mM Tris HCl pH 8, 25 mM NaCl, 0.5 mM EDTA) to reveal eight free thiols. The reduced antibody was then treated with a stock solution of BCN-DVP linker **78** in DMSO (40 equiv.). To monitor reaction progression, aliquots were drawn from the reaction mixture after 1, 2, 3, and 4 hours and analysed by protein LCMS and sodium dodecyl sulfate polyacrylamide gel electrophoresis (SDS-PAGE) under reducing conditions (Table 5.1, entries 1–4). Pleasingly, in all cases significant rebridging was observed. SDS-PAGE analysis indicated that conversion from unmodified HC and LC to rebridged antibody **101** improved up to 2 hours, after which time no significant increase in conversion was observed. Thus, 2 hours was selected as the optimum reaction time. Consistent with previous observations using DVP-based rebridging linkers,[382] both protein LCMS and SDS-PAGE also revealed that the predominant species formed was the half antibody (covalently linked LC and HC). Small amounts of the HC-HC and HC-HC-LC were also observed by SDS-PAGE analysis.

Considering the objective of this project was dual functionalisation and analysis thereof, rather than rebridging optimisation, extensive optimisation for the new linkers was not deemed necessary. Nonetheless, following on from these results, a small screen varying the number of equiv. of linker **78** was carried out (Table 5.1, entries 5–7, and 2). In each case the predominant species observed by SDS-PAGE was half-antibody (Figure 5.3). With 10 equiv. of linker the prevalence of the HC and LC species appeared to increase, whilst the differences between 20, 40 and 80 were marginal. Hence, all further rebridging reactions were therefore carried out with 20 equiv. of linker.

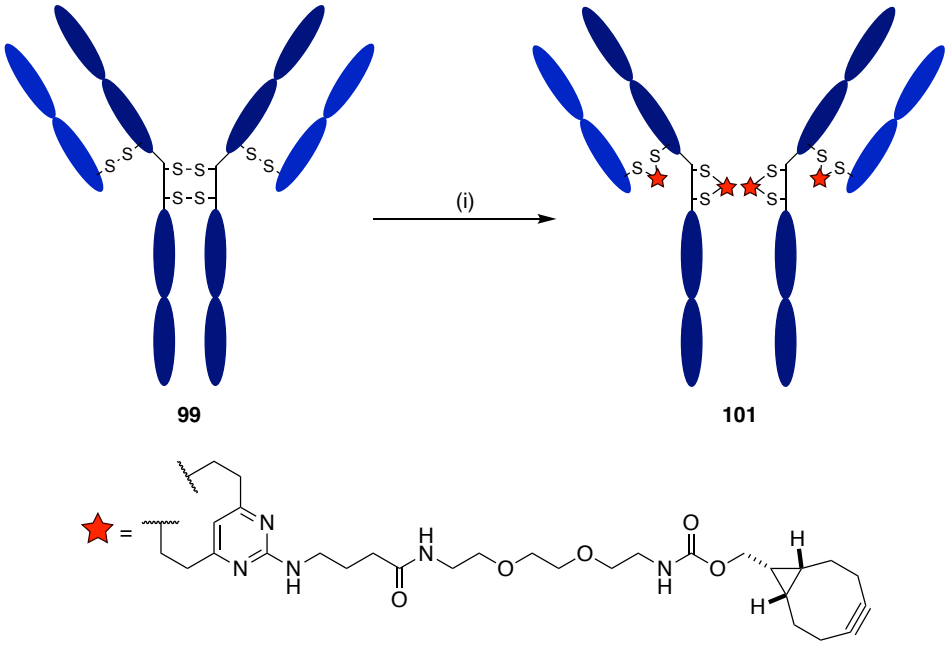

Table 5.1. Conditions trialled for the synthesis of trastuzumab bioconjugate **101**. *Reagents and Conditions:* (i) TCEP (10 equiv.), TBS buffer, 37 °C, 1 h, then BCN-DVP linker **78**, DMSO (10% v/v), 37 °C.

Entry	Equiv. of **78**	Time (h)	Conversion[a]
1	20	1	Moderate
2	20	2	Good
3	20	3	Good
4	20	4	Good
5	10	2	Moderate
6	40	2	Good
7	80	2	Good

[a]As observed by SDS-PAGE analysis.

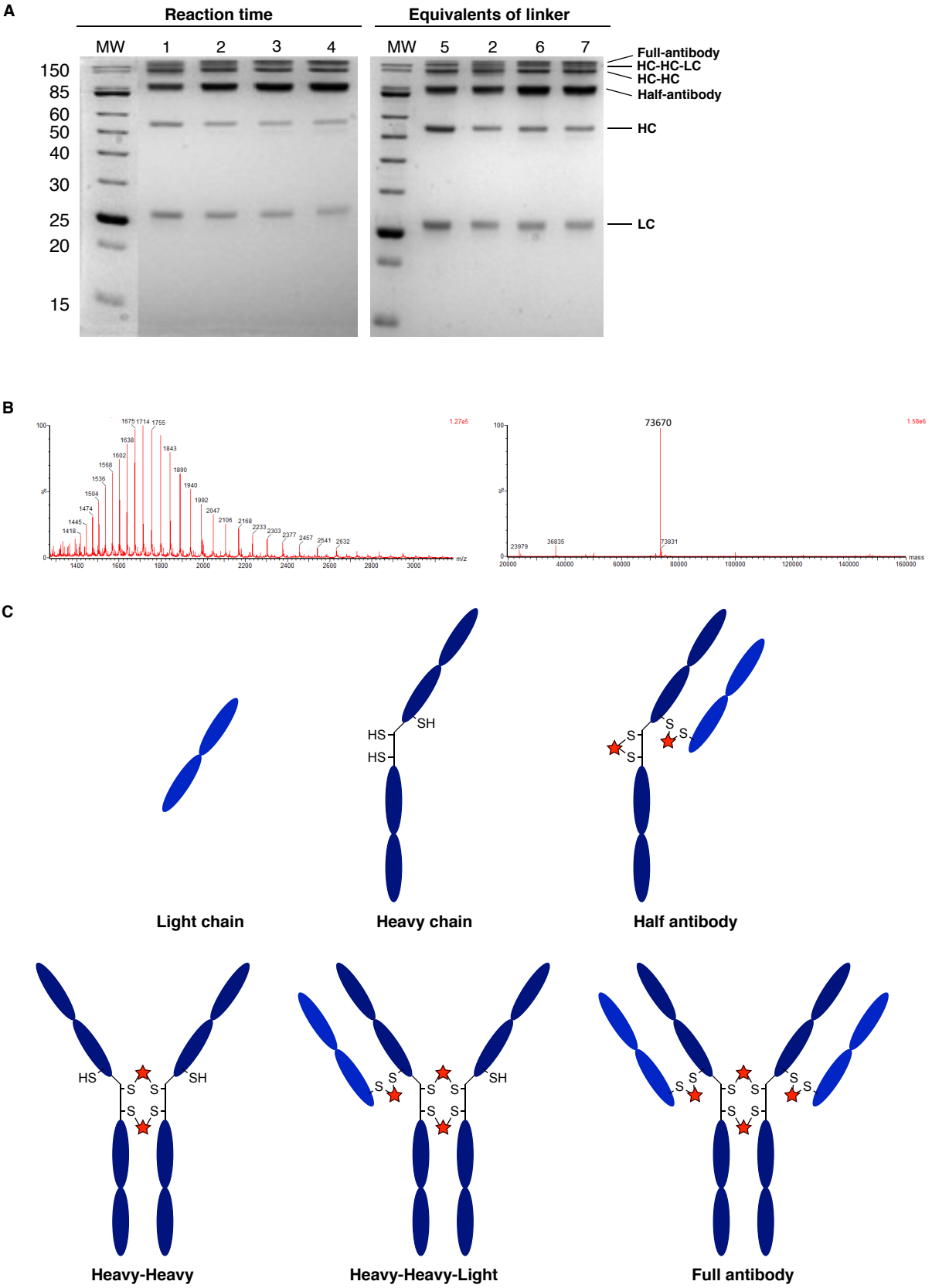

Figure 5.3. (A) SDS-PAGE analysis of the reaction between reduced trastuzumab and linker **78**. The numbers above lanes represent entry number in Table 5.1, MW = molecular weight marker. (B) Non-deconvoluted and deconvoluted MS of an exemplary sample of bioconjugate **101**. Expected mass: 73669 Da (Table 5.1, entry 2). (C) The observed antibody fragments.

Having optimised the conditions for linker **78**, the same conditions were then applied to linkers **79** and **95**. Accordingly, trastuzumab was reduced with TCEP at 37 °C for 1 hour in TBS, and subsequently treated with either cyp-DVP **79** or alkyne-DVP **95** (20 equiv.) in DMSO (Scheme 5.9). After incubating for 2 hours, the reaction mixture was diafiltrated and analysed.

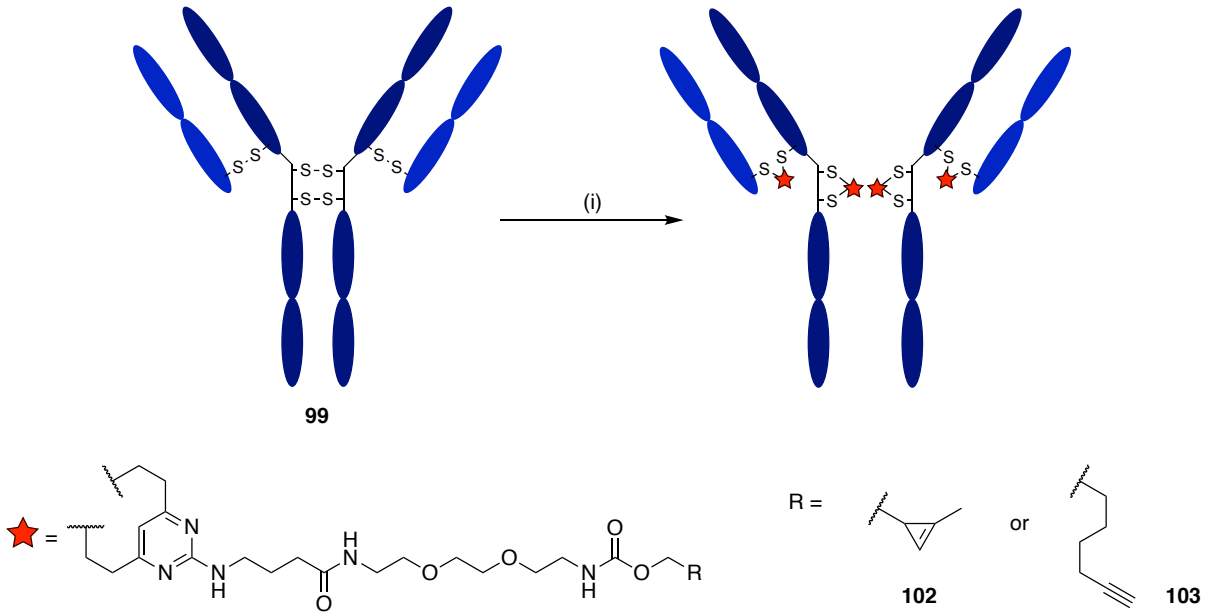

Scheme 5.9. Cysteine rebridging of trastuzumab with cyp-DVP **79** or alkyne-DVP **95** gave mAbs **102** and **103**, respectively. *Reagents and Conditions*: (i) TCEP (10 equiv.), TBS buffer, 37 °C, 1 h, then DVP linker **79** or **95** (20 equiv.), DMSO (10% v/v), 37 °C, 2 h.

Pleasingly, the optimised conditions translated well to linkers **79** and **95**, with analysis by LCMS and SDS-PAGE indicating >95 % rebridging of the antibody (Figure 5.4).

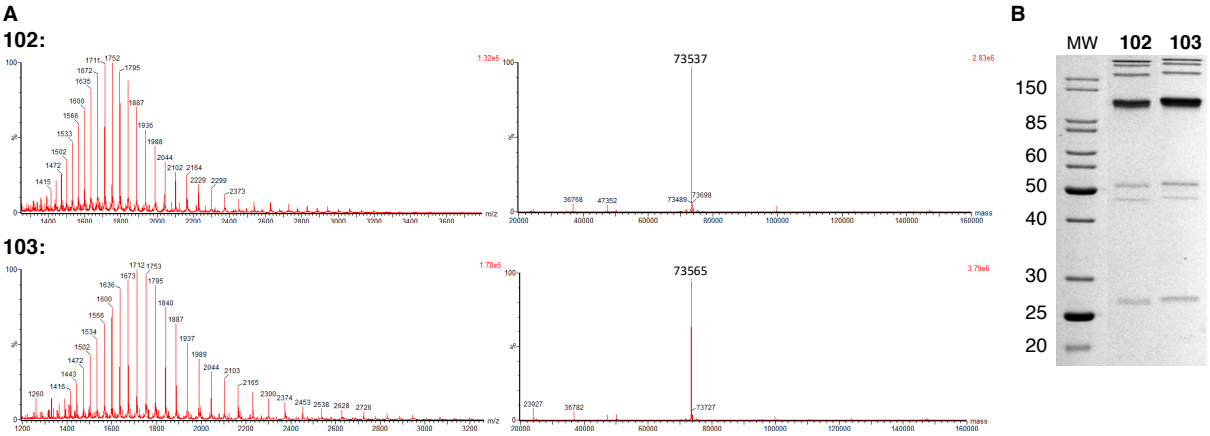

Figure 5.4. (A) Non-deconvoluted (left) and deconvoluted (right) MS of conjugates **102** (expected mass: 73537 Da) and **103** (expected mass: 73565 Da). (B) Analysis of conjugates **102** and **103** by SDS-PAGE. Lanes: MW) molecular weight marker, 102) bioconjugate **102**, 103) bioconjugate **103**.

5.3.2 Post-Rebridging Functionalisation

5.3.2.1 Metal-free click chemistry

Following on from successful antibody rebridging, it was anticipated that the bioorthogonal handles present in conjugates **101** and **102** would enable modular and divergent copper-free functionalisation. To explore this chemistry and enable optimisation of the relevant reaction conditions, the commercially available dyes AF488 azide, **104**, and AZDye 488 tetrazine, **105**, were selected as model payloads (Figure 5.5).[k] These dyes were chosen for several reasons: first, they are readily obtainable from commercial sources; second, they display good photostability; and finally, their chromophoric properties enable facile reaction analysis.[411]

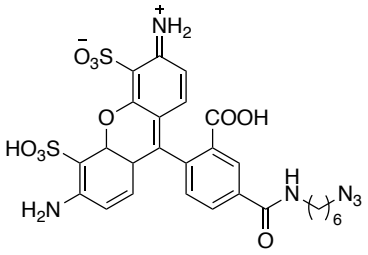

Alexa Fluor® 488 azide, **104**

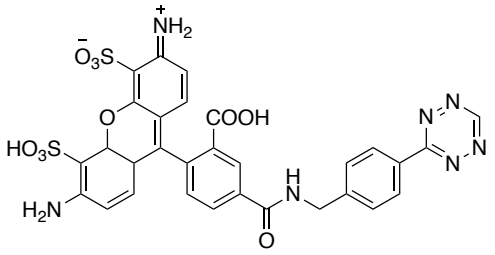

AZDye 488 tetrazine, **105**

Figure 5.5. Structure of AF488 azide and AZDye 488 tetrazine.

Using trastuzumab-BCN **101** as the 'clickable' antibody and AF488 azide as the azide model, SPAAC conditions were first explored. To provide a suitable starting point, conditions previously reported by Chudasama *et al*. for the SPAAC of the BCN-modified Fab domain of trastuzumab with AF488 **104** were adapted and tested on the full antibody model.[397] Thus, bioconjugate **101** was initially treated with 12 molar equiv. of AF488 **104** in PBS at 37 °C, however even after 24 hours a significant amount of starting material could still be observed by protein LCMS. Gratifyingly, increasing the number of equiv. of AF488 **104** to 16 and incubating for 8 hours was sufficient to overcome this hurdle and convert trastuzumab-BCN **101** to antibody-fluorophore conjugate (AFC) **106** in near quantitative yield (Scheme 5.10).[l]

[k] AZDye 488 is structurally identical to AF488, which is a registered trademark of Thermo Fisher Scientific.
[l] Based on protein mass return.

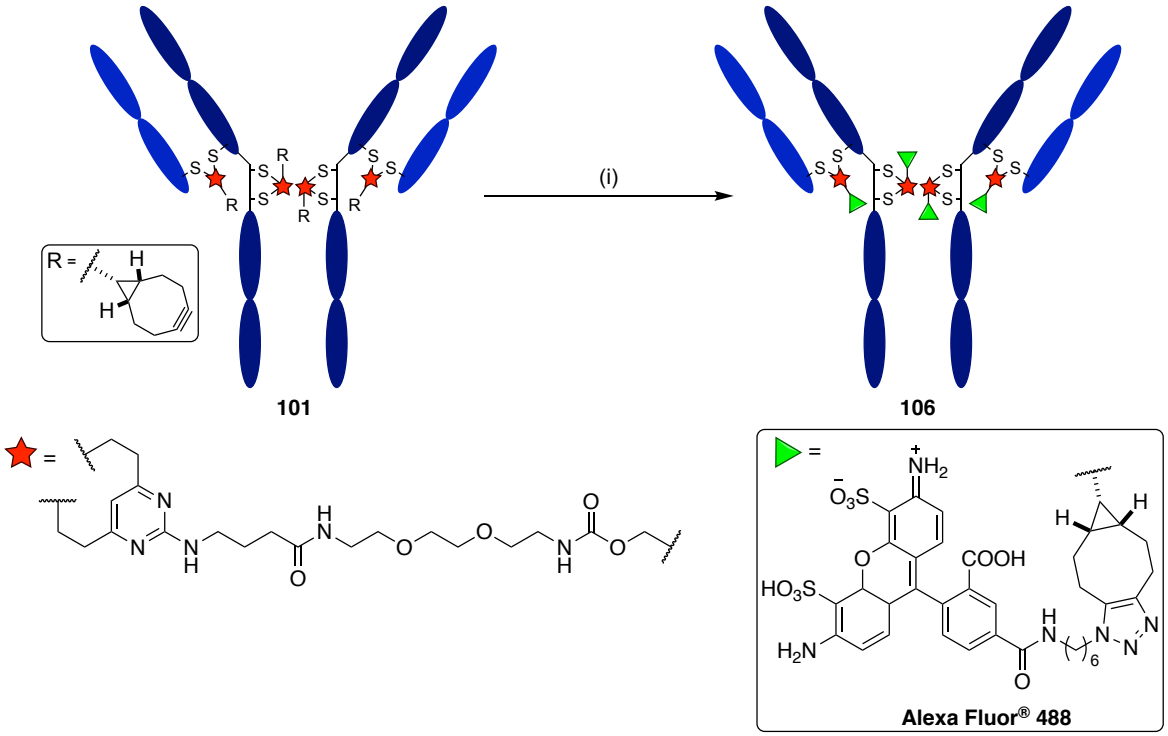

Scheme 5.10. SPAAC of BCN-modified trastuzumab **101** and AF488 azide **104**. *Reagents and Conditions*: (i) AF488 azide **104** (16 equiv.), PBS buffer, DMSO (10% v/v), 37 °C, 8 h.

Subsequent analysis by SDS-PAGE and protein LCMS indicated conversion to **106**, with UV-vis data confirming an average fluorophore to antibody ratio (FAR) of 4.0 (Figure 5.6). Thus, satisfied with these results, no further optimisation of the SPAAC was required.

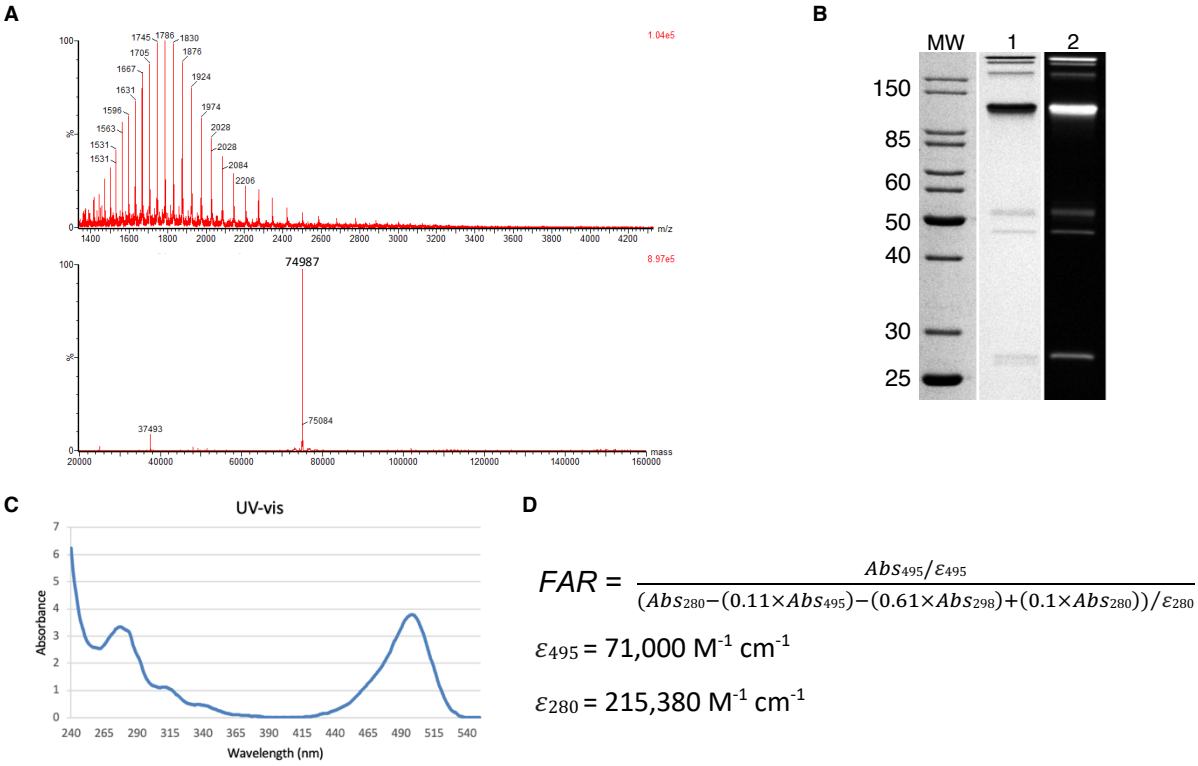

Figure 5.6. (A) Non-deconvoluted (top) and deconvoluted (bottom) MS of bioconjugate **106**. Expected mass: 74983 Da. (B) Analysis of bioconjugate **106** by SDS-PAGE. Lanes: MW) molecular weight marker, 1) Coomassie stain of bioconjugate **106**, 2) in-gel fluorescent image of bioconjugate **106**. (C) UV-vis spectrum of conjugate bioconjugate **106**. (D) FAR calculation. A correction factor (cf) of 0.61 was used to account for DVP absorbance at 280 nm, a cf of 0.1 was used to account for trastuzumab absorbance at 298 nm, and a further cf of 0.11 was used for AF488 at 280 nm.[399,412]

Next, attention turned to exploration of IEDDA conditions on-antibody and demonstration of the applicability of the cyp-functionalised DVP reagent **79** for antibody modification. To this aim, cyp-modified trastuzumab **102** was reacted with fluorescent tetrazine reagent AZDye 488 tetrazine **105** in PBS and incubated at 37 °C (Scheme 5.11). Owing to the exceptionally fast kinetics of the IEDDA reaction, excellent conversion to AFC **107** was achieved in only 1 hour.

Surprisingly, subsequent analysis by protein LCMS appeared to indicate a greater presence of the full antibody, whilst SDS-PAGE analysis required stronger denaturing conditions to fully dissociate the antibody — heating for 5 minutes at 90 °C was required, in contrast to the 5 minutes at 80 °C previously used (Figure 5.7). Although the full reasoning behind this is not fully understood, it appears to suggest the presence of stronger non-covalent bonding between the half antibody species. Nonetheless, protein LCMS, UV-vis analysis, and SDS-PAGE in-gel fluorescence analysis all confirmed conversion to the corresponding antibody-fluorophore conjugate **107**, with an average FAR of 4.0, and so no further optimisation was considered necessary.

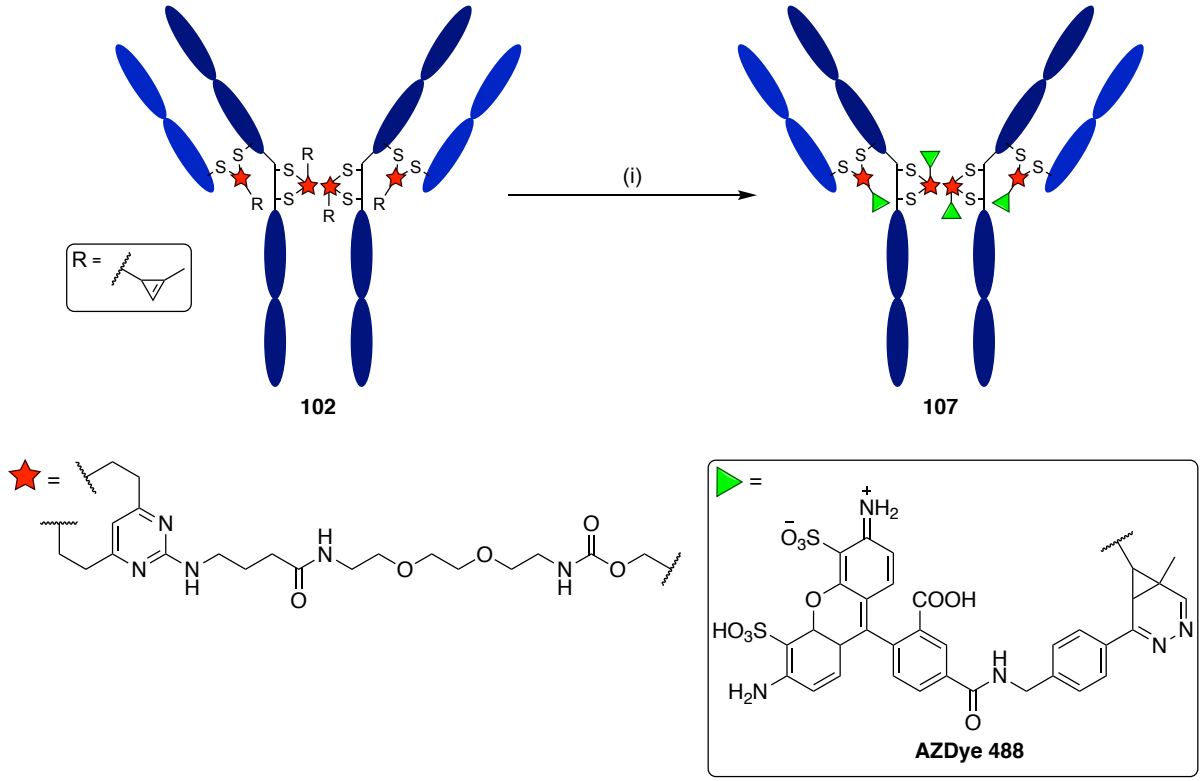

Scheme 5.11. IEDDA of cyp-modified trastuzumab **102** and AZDye 488 tetrazine **105**. *Reagents and Conditions*: (i) AZDye 488 tetrazine **105** (16 equiv.), PBS buffer, DMSO (10% v/v), 37 °C, 1 h.

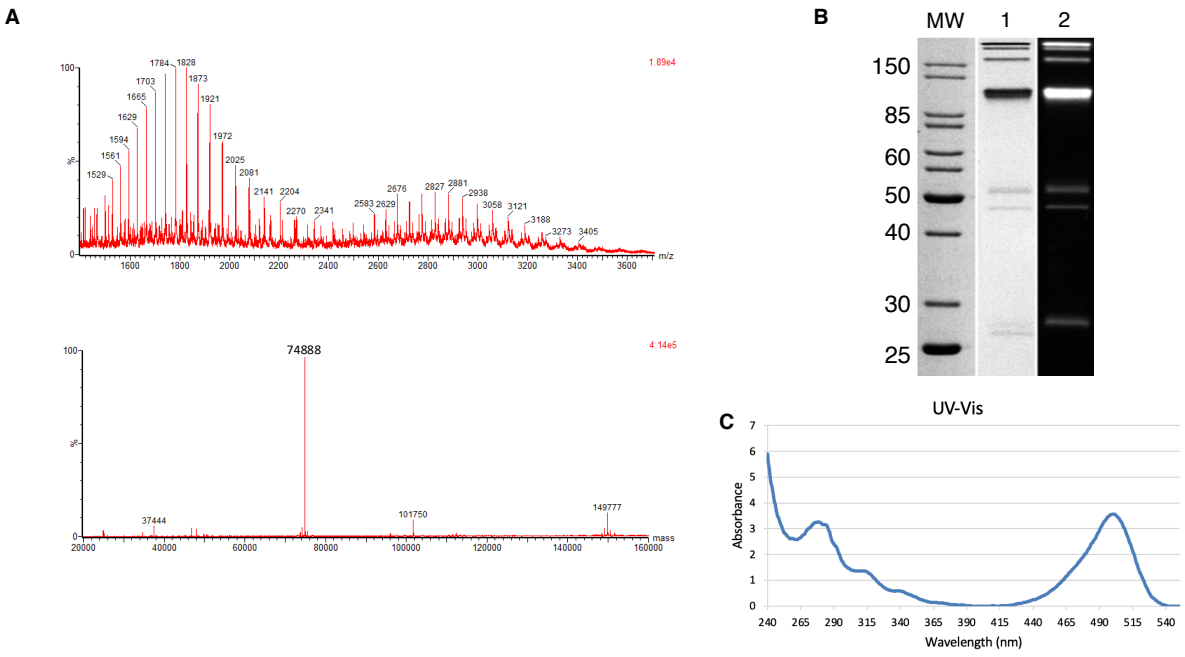

Figure 5.7. (A) Non-deconvoluted (top) and deconvoluted (bottom) MS of bioconjugate **107**. Expected mass: 74885 Da. (B) Analysis of bioconjugate **107** by SDS-PAGE. Lanes: MW) molecular weight marker, 1) coomassie stain of bioconjugate **107**, 2) in-gel fluorescent image of bioconjugate **107**. (C) UV-vis spectrum of bioconjugate **107**.

Interested by these results, and to demonstrate the versatility of BCN-modified trastuzumab **101**, the decision was made to also carry out a similar IEDDA reaction on this species. Thus, BCN-trastuzumab conjugate **101** was treated with AZDye 488 tetrazine **105** and incubated for 1 hour at 37 °C to form AFC **108** (Scheme 5.12).

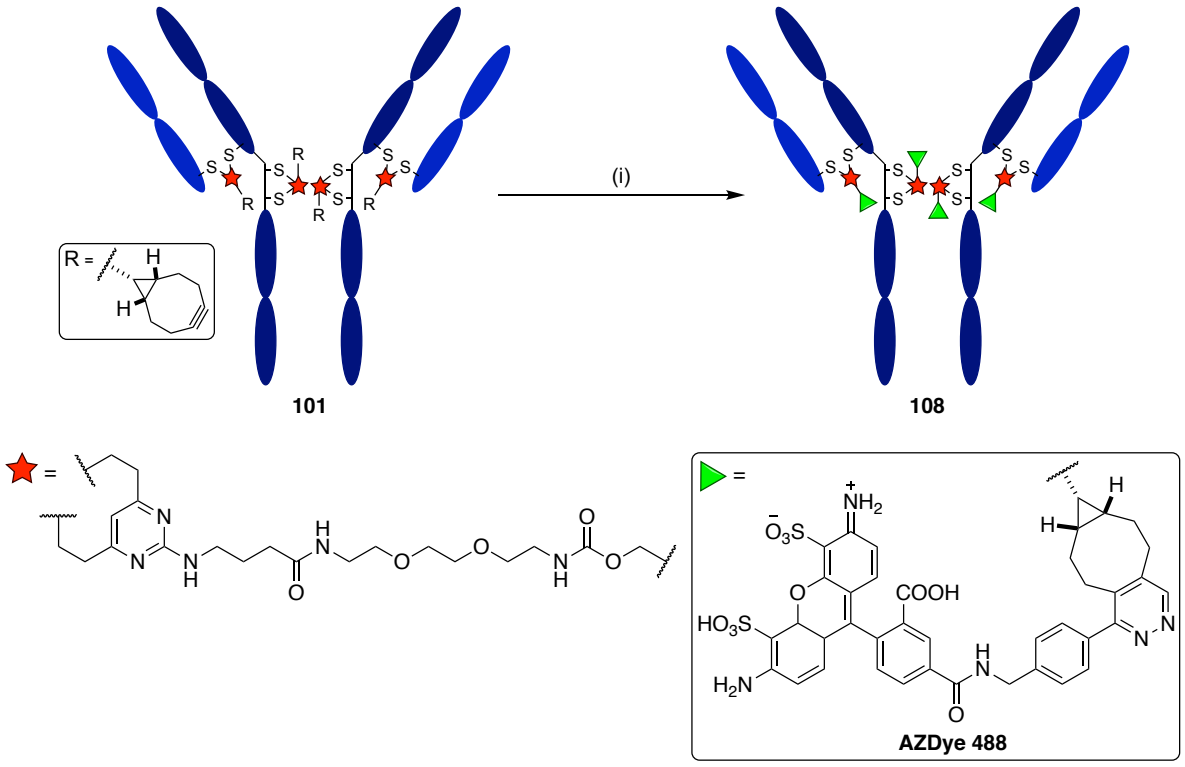

Scheme 5.12. IEDDA of BCN-modified trastuzumab **101** and AZDye 488 tetrazine **105**. *Reagents and Conditions*: (i) AZDye 488 tetrazine **105** (16 equiv.), PBS buffer, DMSO (10% v/v), 37 °C, 1 h.

Again, IEDDA led to excellent conversion to the desired AFC, with an average FAR of 4.1 (Figure 5.8). Curiously, in this case the proportion of full antibody observed did not appear to increase relative to what was observed for the rebridged antibody **101**, nor were the harsher denaturing conditions for SDS-PAGE required.

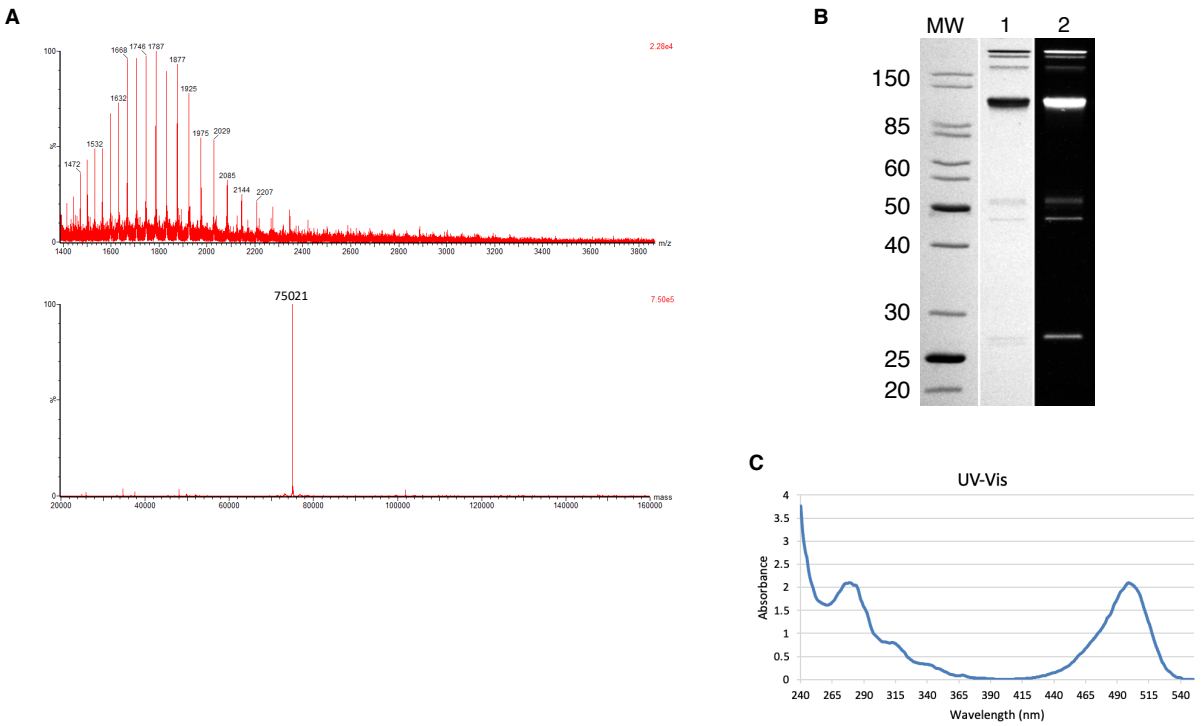

Figure 5.8. (A) Non-deconvoluted (top) and deconvoluted (bottom) MS of bioconjugate **108**. Expected mass: 75020 Da. (B) Analysis of bioconjugate **108** by SDS-PAGE. Lanes: MW) molecular weight marker, 1) coomassie stain of bioconjugate **108**, 2) in-gel fluorescent image of bioconjugate **108**. (C) UV-vis spectrum of bioconjugate **108**.

5.3.2.2 Copper Click Chemistry

For comparative purposes, a CuAAC reaction was then carried out on trastuzumab-alkyne conjugate **102**. Following a synthetic procedure optimised within the Spring group, bioconjugate **103** was treated with AF488 azide **104** in PBS in the presence of $CuSO_4 \cdot H_2O$, tris(3-hydroxpyropyltriazolylmethyl)amine (THPTA), and sodium ascorbate, and incubated at 37 °C for 4 hours (Scheme 5.13).

Pleasingly, UV-vis spectroscopy, protein LCMS, and SDS-PAGE analysis all confirmed the successful formation of AFC **109**, which was found to have an average FAR of 3.9 (Figure 5.9). However, in contrast to the near quantitative yields obtained for the four metal-free click reactions, only 74% of protein was recovered after purification following CuAAC, confirming the need for the use of metal-free click chemistry in subsequent dual functionalisation experiments.

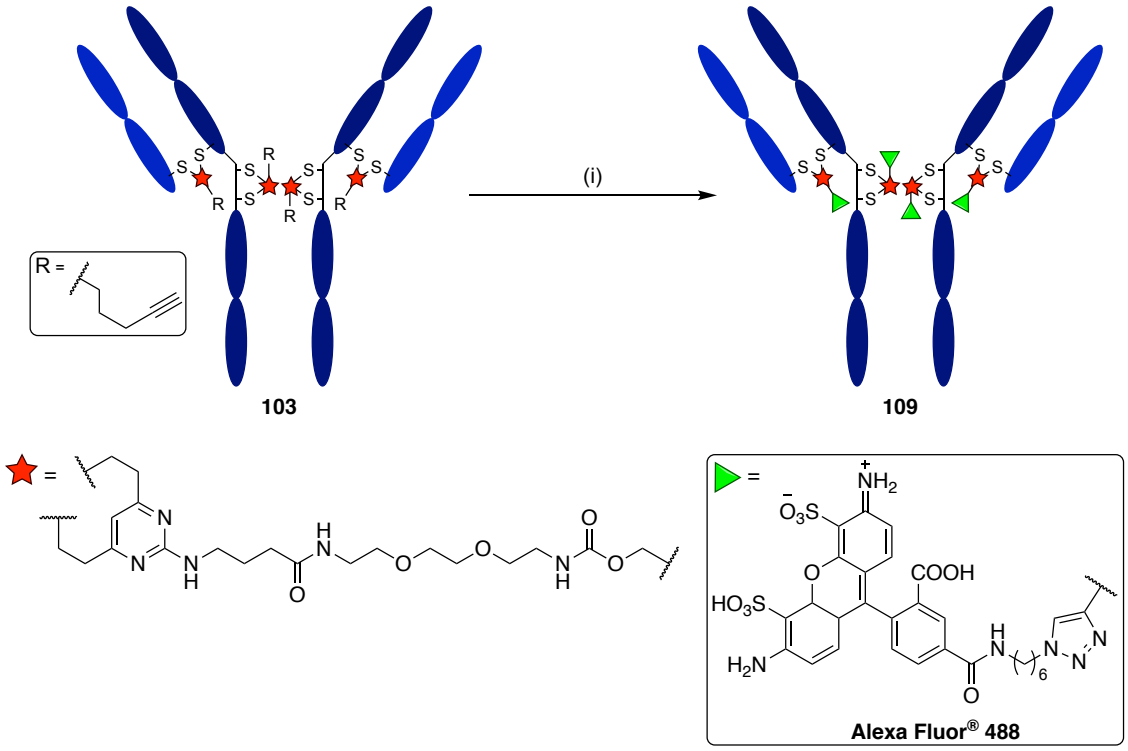

Scheme 5.13. CuAAc of alkyne-modified trastuzumab **103** and AF488 azide **104**. *Reagents and Conditions*: (i) AF488 azide **104** (16 equiv.), $CuSO_4 \cdot H_2O$, THPTA, sodium ascorbate, PBS buffer, DMSO (10% v/v), 37 °C, 4 h.

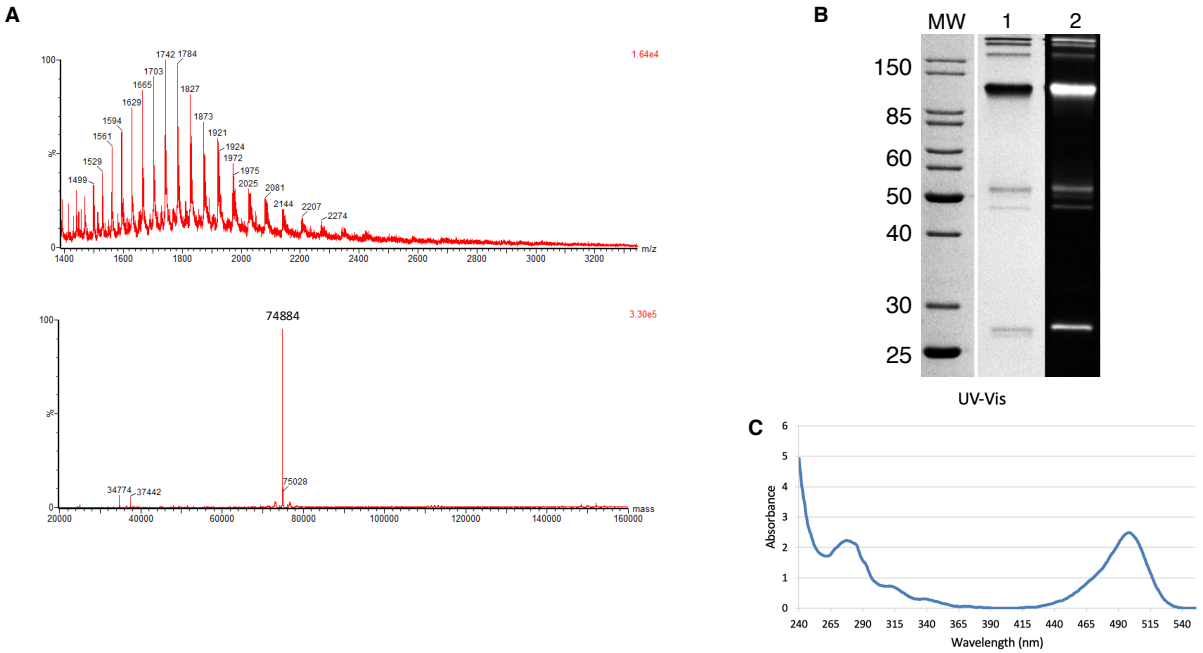

Figure 5.9. (A) Non-deconvoluted (top) and deconvoluted (bottom) MS of conjugate **109**. Expected mass: 74879 Da. (B) Analysis of conjugate **109** by SDS-PAGE. Lanes: MW) molecular weight marker, 1) coomassie stain of **109**, 2) in-gel fluorescent image of bioconjugate **109**. (C) UV-vis spectrum of bioconjugate **109**.

5.3.3 Summary

These results serve to demonstrate the utility of the developed method. Indeed, through this work the ability of both BCN- and cyp-DVP linkers **78** and **79** to efficiently modify trastuzumab without the need for harsh metal catalysts has been successfully demonstrated. Not only does this strategy prevent the need for the for removal of potentially toxic transition metals from the biotherapeutic product, but it has also been shown to significantly increase recovery of the extremely valuable bioconjugate.

5.4 Dual Functional Linker Design

With the suitability of the individual 'clickable' handles confirmed, and conditions for both IEDDA and SPAAC reactions explored, the synthesis of the corresponding dual functional (df) linker was next considered.

At the time this project commenced, studies in the Spring group towards the synthesis of DVP-based df linkers had focused on the model structure **110**, which was synthesised in three steps from secondary amine **111** and 2,4,6-trichloropyrimidine **81** (Scheme 5.14).[399] These studies had successfully demonstrated that **110** efficiently rebridges reduced trastuzumab.

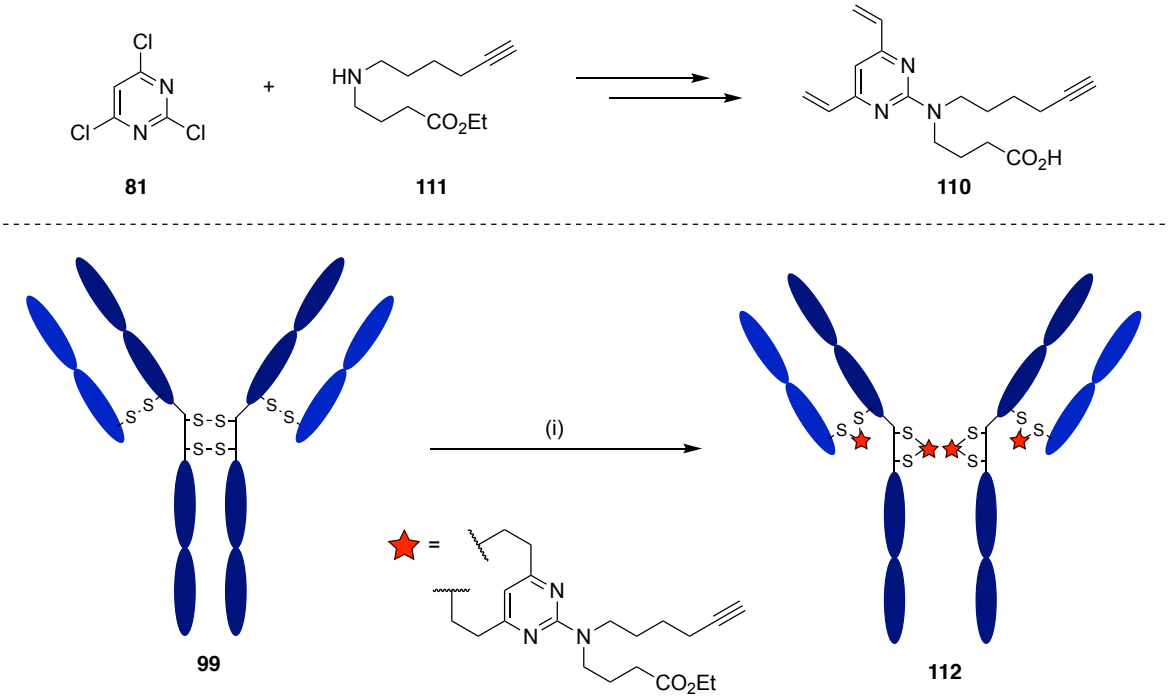

Scheme 5.14. Previous work using model df linker **110** for trastuzumab rebridging.[399] *Reagents and Conditions:* (i) TCEP (10 equiv.), TBS buffer, 37 °C, 1 h, then df-DVP linker **110** (40 equiv.), DMSO (10% v/v), 37 °C, 2 h.

Inspired by this strategy, it was proposed that a similar method could be employed for the generation of a novel df linker containing both BCN and cyp moieties. By designing a linker to incorporate these handles it was envisioned that antibody modification could take place via sequential SPAAC and IEDDA reactions. It was proposed that this could take place via a one-pot strategy, avoiding the need for stepwise purification. However, since BCN can undergo both SPAAC and IEDDA reactions, whilst cyp can only undergo IEDDA reactions, it was expected that full conversion during an initial SPAAC reaction would be required prior to IEDDA to prevent cross-reactivity.

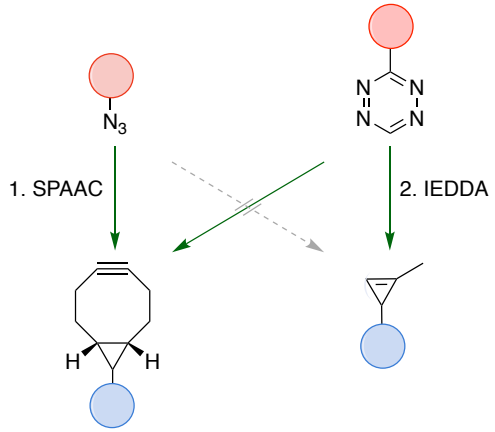

Figure 5.10. Sequential SPAAC and IEDDA reactions could be exploited for the efficient dual modification of antibodies. Solid arrows represent moieties that can react, whilst dashed arrows represent those that do not.

Adapting the conditions previously used for monofunctional linker synthesis, it was proposed that the BCN handle could be introduced via amide coupling of BCN-PEG-NH_2 **88** to a DVP moiety with general structure **113** (Figure 5.11). The cyp handle could then be incorporated via carbamate formation.

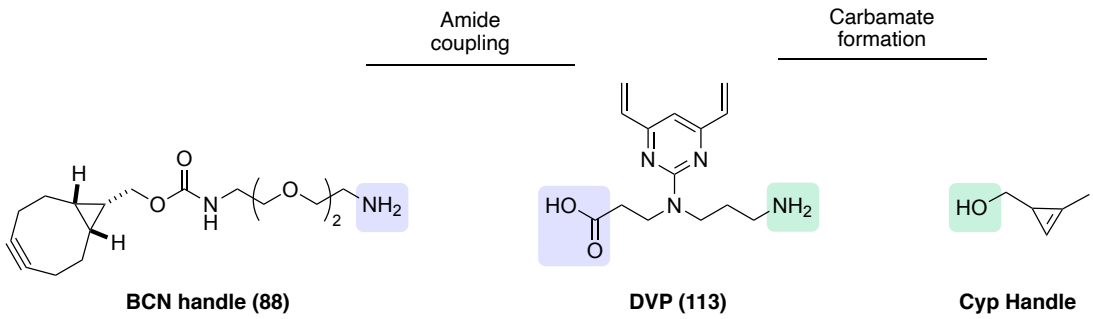

Figure 5.11. An overview of possible connections between the three different portions of the dual functional linker. The DVP and BCN handle could be attached via amide coupling, whilst the cyp and DVP could be connected via carbamate formation.

Taking these considerations into account, the first-generation df linker **114** was designed (Figure 5.12). It was noted that the length, lipophilicity, and flexibility of the spacers between the DVP moiety and functional handles could all impact the ability of the linker to facilitate antibody dual modification. However, the major consideration for the first generation of df linker was synthetic tractability.

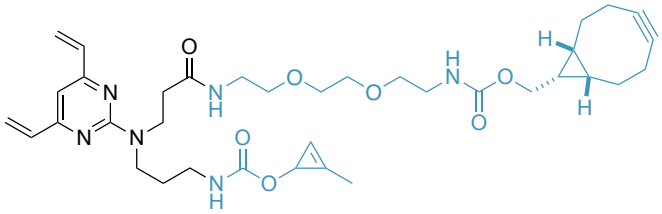

114

Figure 5.12. The structure of first-generation df linker **114**.

5.4.1 Retrosynthetic Analysis

In devising a retrosynthetic strategy for accessing df-DVP **114**, it was vital that both the cyp and BCN handles were introduced at the latest stage due to their intricate reactivities and laborious syntheses. Thus, it was proposed that df linker **114** could be derived from DVP-derivative **115** after deprotection and subsequent carbamate formation to introduce the cyp handle (Scheme 5.15). Disconnection at the amide bond within **115** would then lead back to precursors **116** and **88**.

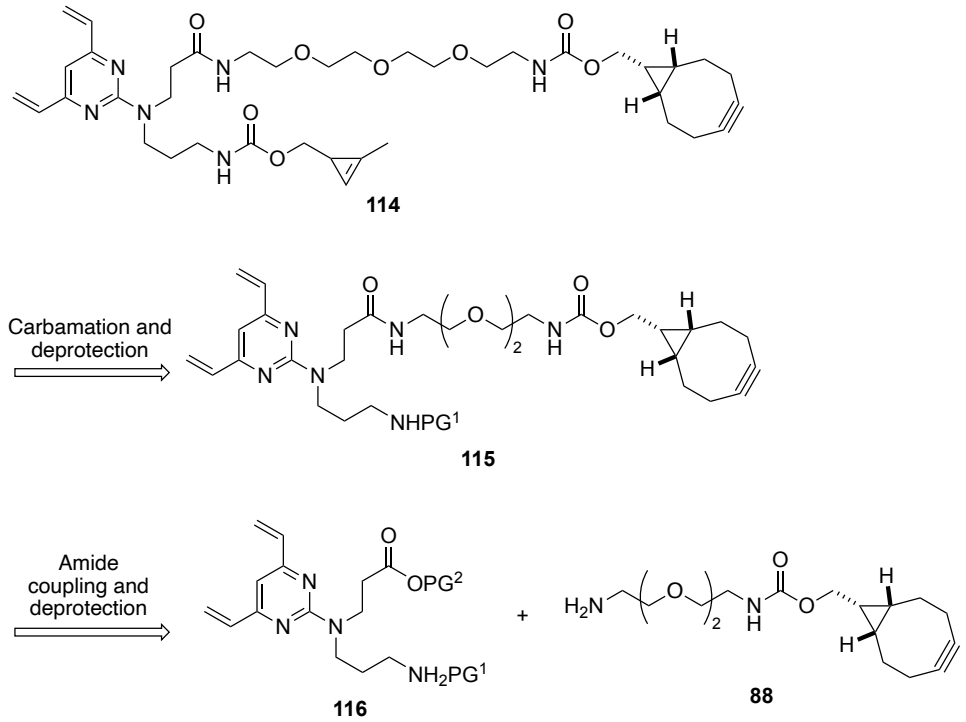

Scheme 5.15. Retrosynthetic analysis of df-DVP **114**. PG = protecting group.

DVP **116** was then retrosynthetically traced back to amine **117**, whose transformation to **116** would rely on the S_NAr and Suzuki cross-coupling sequence previously employed for the synthesis of monofunctional linkers **78**, **79** and **95** (Scheme 5.16).

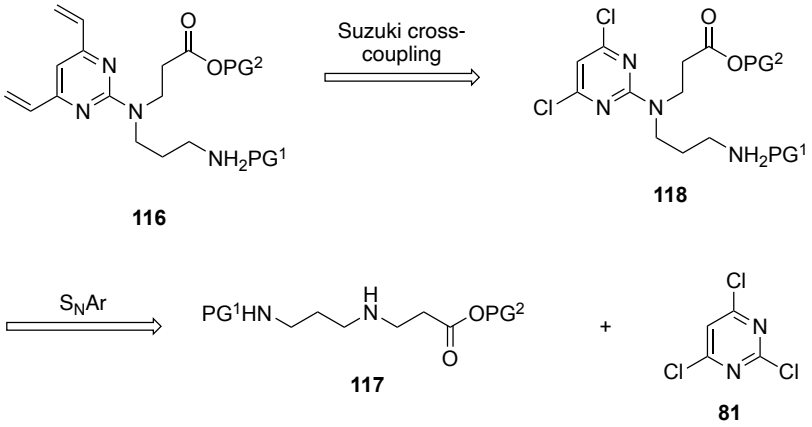

Scheme 5.16. Retrosynthetic analysis of protected intermediate **116**.

Finally, it was proposed that precursor **117** could be synthesised from commercially available 1,3-diaminopropane (**119**) and methyl acrylate (**120**) via an aza-Michael addition and amine protection (Scheme 5.17). This reaction has predominately been reported for the synthesis of polymers,[413–415] nonetheless it was hypothesised that with judicious selection of reaction conditions the mono-functionalised adduct of methyl acrylate and 1,3-diamino propane could be formed.[416]

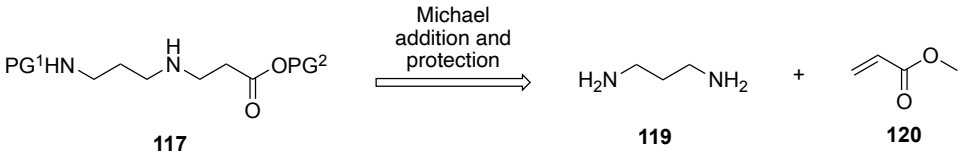

Scheme 5.17. Retrosynthetic analysis of S_NAr precursor **117**.

5.4.2 Protecting Group Strategy

Prior to commencing the synthesis of dual functional linker **114**, a suitable protecting group strategy was required. Whilst the methyl ester protection of methyl acrylate was considered suitable for the subsequent reaction steps and thus was retained in the route design, a second protecting group was required for protection of the amine. Due to the known acid-instability of the DVP moiety, a base-sensitive Fmoc protecting group was selected.

To test the suitability of the chosen protecting group strategy, conditions for the selective cleavage of the carboxyl-protecting group in the presence of Fmoc were investigated. Several literature conditions have been reported for such transformations,[417,418] including the use of $CaCl_2$ as an additive to suppress Fmoc cleavage under basic conditions.[419] Using the Fmoc-protected substrate **121** as a model system, selective hydrolysis with $CaCl_2$ and NaOH was attempted, however this led to the gradual decomposition of the starting material over 8 hours (Table 5.2, entry 1). In contrast, no reaction was observed upon attempted hydrolysis with Me_3SnOH at 80 °C (Table 5.2, entry 2),[417] or with MgI_2 under mW conditions (Table 5.2, entry 3).[418]

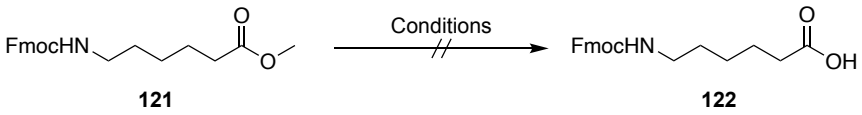

121 **122**

Table 5.2. Attempts at selective ester cleavage from model substrate **121**.

Entry	Reagents	Solvent	Temp	Time (h)	Observation[a]
1	NaOH, $CaCl_2$	^{i}PrOH/MeOH	rt	8	Decomposition
2	Me_3SnOH	DCE	80 °C	8	Returned starting material
3	MgI_2	THF	mW, 120 °C	2	Returned starting material

[a]as observed via ^{1}H NMR spectroscopy.

Alongside these experiments the stability of the Fmoc protecting group under Suzuki cross-coupling conditions was also explored. For the synthesis of DVP-acid **80**, Suzuki cross-coupling was carried out at 70 °C under basic conditions. Thus, to simulate these conditions, the model compound **123** was treated with K_2CO_3 at 70 °C for 18 hours (Scheme 5.18). During the course of this reaction significant base-mediated Fmoc deprotection was observed via LCMS and TLC analysis.

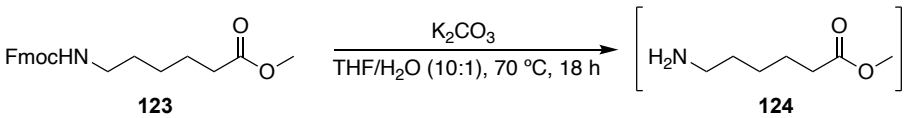

123 **124**

Scheme 5.18. The stability of the Fmoc group was tested under the basic conditions used for Suzuki cross-coupling.

Given the challenges associated with the use of Fmoc in this context, an alternative approach using the 2-(trimethylsilyl)ethoxycarbonyl (Teoc) was investigated. It was anticipated that not only would this protecting group be readily cleaved under mild conditions (fluoride-source), but since it is stable to mild base, it would also be inert during both ester hydrolysis and Suzuki cross-coupling.[420] Using 3-(teoc-amino)-1-propanol, **125**, as a test substrate the stability of the of Teoc group under both reactions conditions was surveyed. As expected, Teoc was found to be stable to both treatment with LiOH at rt, and K_2CO_3 at 70 °C (Scheme 5.19).

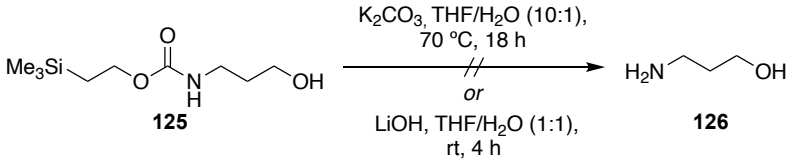

125 **126**

Scheme 5.19. The stability of the Teoc group was tested under the basic conditions used for ester hydrolysis and Suzuki cross-coupling.

Finally, since the removal of Teoc typically requires the use of a suitable fluoride source, the compatibility of DVP-derivatives with TBAF deprotection conditions needed to be assessed. Pleasingly, no reaction was observed upon treatment of DVP-acid **80** with TBAF at rt for 8 h, confirming the suitability of this protecting group for df linker synthesis (Scheme 5.20).

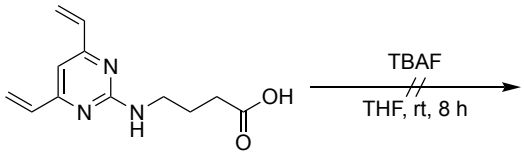

80

Scheme 5.20. The stability of DVP-derivatives to TBAF-deprotection conditions was tested on model substrate DVP-acid **80**.

5.5 Synthesis and Evaluation of a First-Generation Dual-Functional Linker

5.5.1 Synthesis of Df-DVP 114

With a suitable protecting group strategy in place, studies toward the synthesis of df linker **114** commenced.

In line with the retrosynthetic analysis, synthesis started with the formation of bis-protected intermediate **127**. Pleasingly, dropwise addition of an equimolar amount of methyl acrylate (**120**) to diamine **119** occurred rapidly at 0 °C and delivered a single product, as indicated by ^{1}H NMR spectroscopy of the crude reaction mixture (Scheme 5.21). Cautious of the potential for aminolysis, 4-nitrophenyl 2-(trimethylsilyl)ethyl carbonate (Teoc-ONp) and Et_3N were then immediately added to the reaction to effect the transformation to **127** via a sequential one-pot strategy. Gratifyingly, this reaction enabled facile installation of both desired protecting groups in a single step.

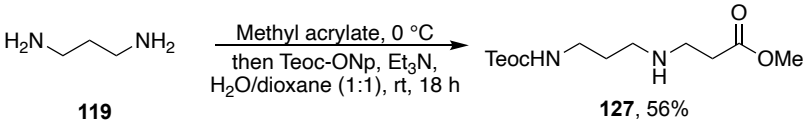

119 **127**, 56%

Scheme 5.21. Synthesis of precursor **127** via a one-pot procedure.

S_NAr of amine **127** with pyrimidine **81** proceeded smoothly to yield a mixture of regioisomers (Scheme 5.22). Thankfully, the desired dichloropyrimidine **128** could readily be separated by column chromatography from the other isomers in 28% yield. Next, installation of the vinyl groups via Suzuki cross-coupling was performed to yield DVP-derivative **129**, which was in turn hydrolysed by treatment with LiOH. The subsequent installation of the BCN motif first required reaction of activated carbonate **87** with 1,8-diamino-3,6-dioxaoctane under the previously established conditions (Section 5.2.2) to

afford BCN-derivative **88**. With both reactants in hand, EDC-mediated amide coupling was then successfully achieved, affording BCN-functionalised DVP **130** in 40% yield.

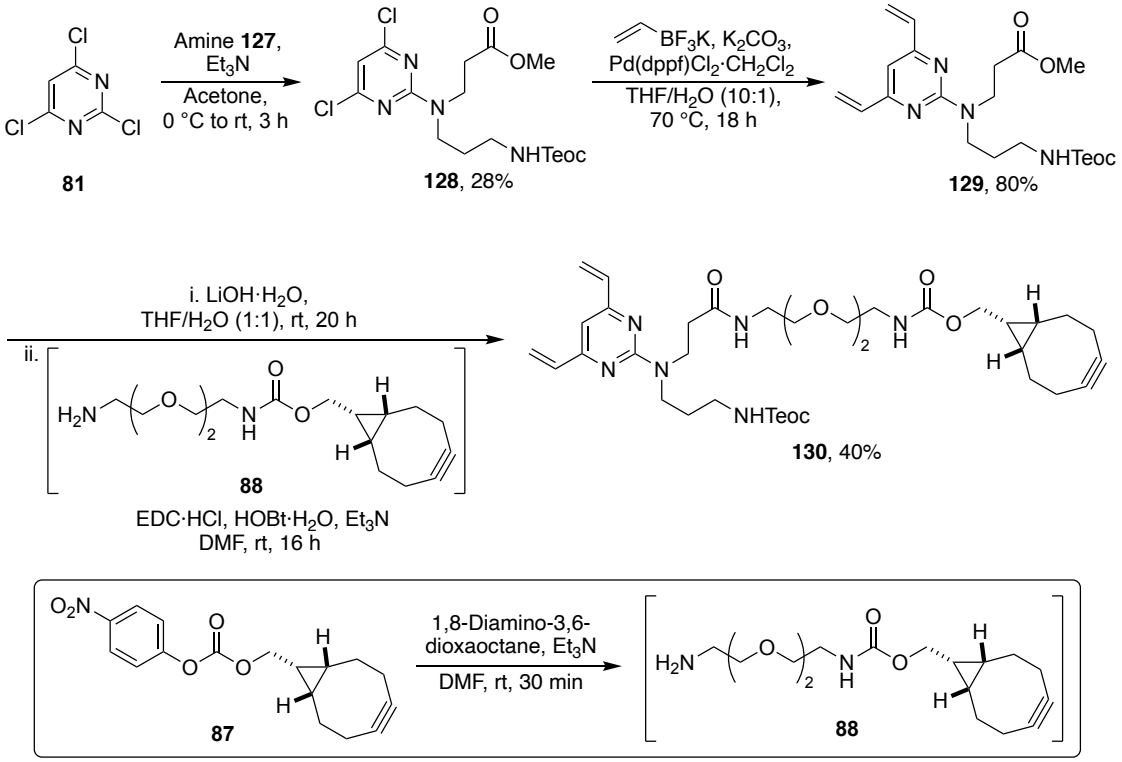

Scheme 5.22. Synthetic route towards the advanced intermediate linker **130**.

During the course of this project it was observed by members of the Spring group that steric bulk near the vinyl groups of a DVP motif may result in poor conversions during bioconjugation.[399] Thus, prior to optimisation of the final Teoc-deprotection step and cyclopropene handle installation, the ability of the general linker structure to rebridge reduced trastuzumab was assessed.

5.5.2 Trastuzumab Rebridging

Using the previously established conditions (Section 5.3.1), df linker **130** (20 equiv.) was reacted with reduced trastuzumab in 10% DMSO (v/v) in TBS buffer and shaken at 37 °C for 2 hours (Scheme 5.23). Disappointingly, under these conditions, linker **130** demonstrated poor rebridging efficiency, as evidenced by LCMS and SDS-PAGE analysis. Unsuccessful rebridging was also observed on increasing the number of equiv. of linker to 80 and the reaction time to 4 hours. Thus, these results provide further evidence that increasing steric bulk close to the DVP can limit its ability to rebridge the interchain disulfides of trastuzumab.

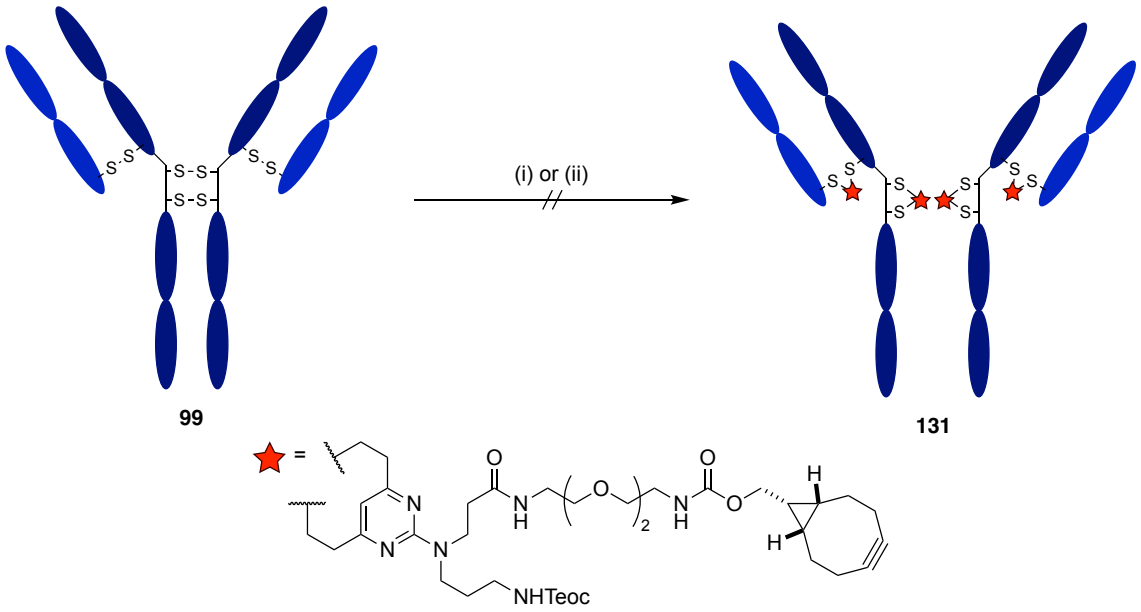

Scheme 5.23. Attempted rebridging of trastuzumab with linker **130**. *Reagents and Conditions*: TCEP (10 equiv.), TBS buffer, 37 °C, 1 h, then df-DVP linker **130**, (i) 20 equiv., 1 h, or (ii) 80 equiv., 4 h, DMSO (10% v/v), 37 °C

5.6 Synthesis and Evaluation of a Second-Generation Dual-Functional Linker

Faced with the issue of steric hindrance around the DVP moiety, a partial redesign of the linker was deemed necessary. It was proposed that the introduction of an additional PEG chain spacer between the click handles and the DVP (Figure 5.13) would reduce any hindrance around the vinyl groups.

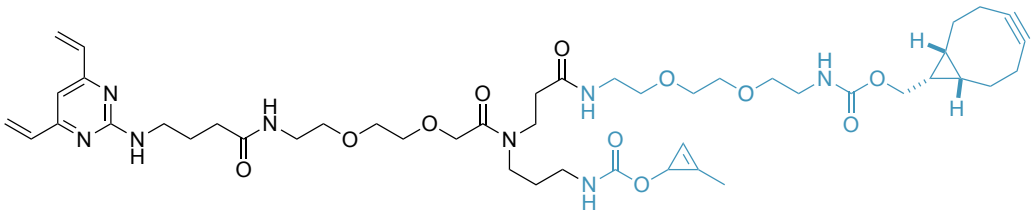

131

Figure 5.13. The structure of second-generation df linker **131**.

5.6.1 Retrosynthetic Analysis of Second-Generation Linker

The retrosynthetic analysis of second-generation linker **131**, outlined below, followed similar procedures to first-generation linker **114** (Scheme 5.24). However, whilst disconnection of the BCN and cyp handles remained the same, the protected precursor, **132**, was retrosynthetically be traced back to DVP-acid **80** and branched amine **133**. It was expected that this would enable the incorporation of the branched amine via amide coupling to DVP-acid **80** rather than employing a low-yielding S_NAr reaction. Finally, by disconnecting at the amide bond in **133**, it was envisioned that

branched amine **133** could be formed from the amide coupling of Fmoc-PEG-COOH **134** and the previously synthesised precursor **127**.

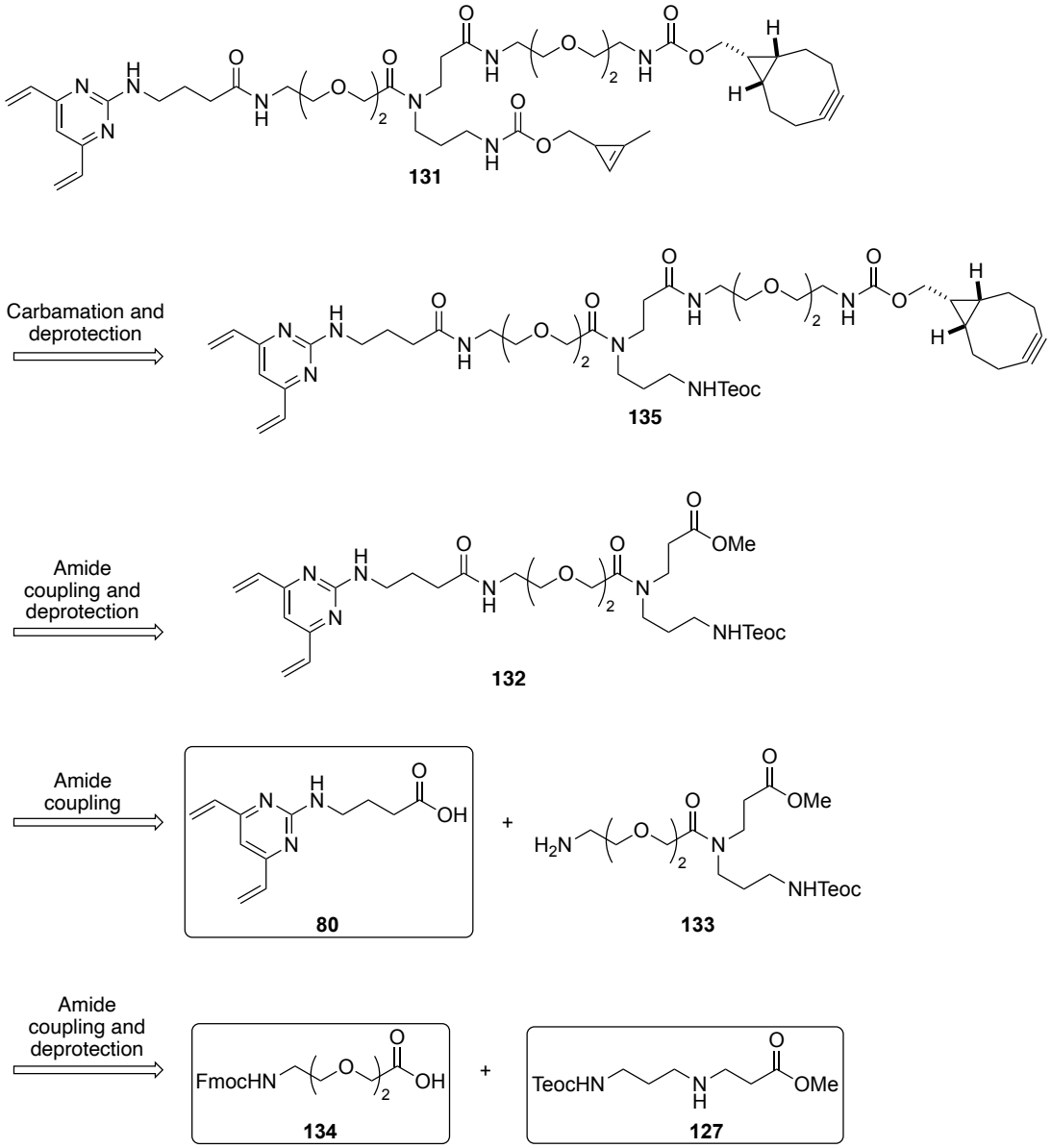

Scheme 5.24. Retrosynthetic analysis of second-generation df linker **131**.

5.6.2 Synthesis of Df-DVP 131

Efforts towards the synthesis of the second generation df linker **131** began with the attempted synthesis of branched tertiary amine **136** via amide coupling of Fmoc-amino-3,6-dioxaoctanoic acid (**134**) and secondary amine **127** (Scheme 5.25). Disappointingly, this reaction led to the formation of a complex mixture, with starting material decomposition observed by ^{1}H NMR spectroscopy.

Scheme 5.25. Attempted EDC-mediated amide coupling for the formation of intermediate **136**.

Due to the observed incompatibility of the Fmoc-protected PEG chain with secondary amine **127**, the use of a Boc protecting group was instead pursued. Pleasingly, EDC-mediated amide coupling of secondary amine **127** and 8-(Boc-amino)-3,6-dioxaoctanoic acid·DCHA led to the desired branched amine **137** in 95% yield (Scheme 5.26). With tertiary amine **137** in hand, it was then subjected to a *p*-TsOH-mediated selective Boc deprotection, and amide coupling with DVP-acid **80** to afford the advanced intermediate **132** in good yield.

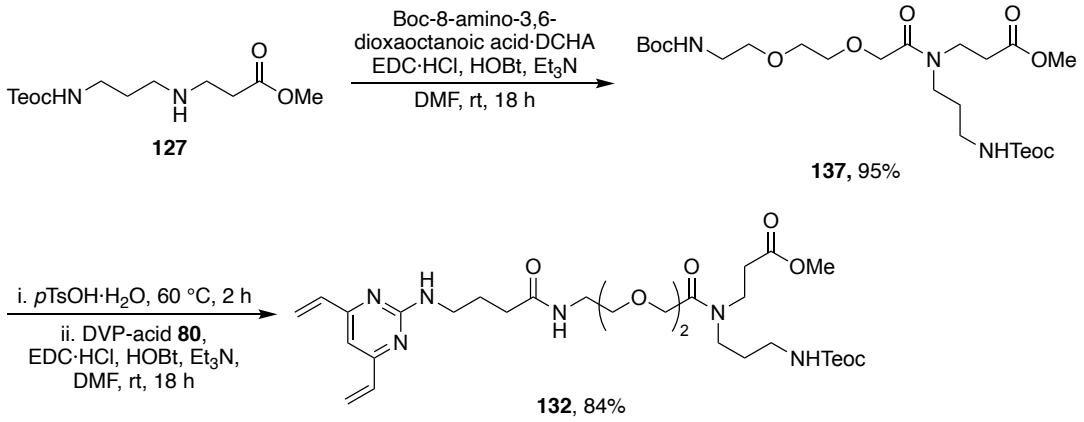

Scheme 5.26. Synthesis of DVP-derivative **132** from a Boc-protected starting material.

Next, incorporation of the BCN and cyp handles was investigated. As expected, introduction of the BCN motif proceeded smoothly using the previously established ester hydrolysis and amide coupling conditions (Scheme 5.27).

Unfortunately, subsequent removal of the Teoc-group proved much more challenging. A variety of reaction variables for this transformation were surveyed (time, equiv. of TBAF, and temperature) and are summarised in Table 5.3. In each case the conditions were either too mild to effect complete deprotection or led to degradation of the BCN moiety.

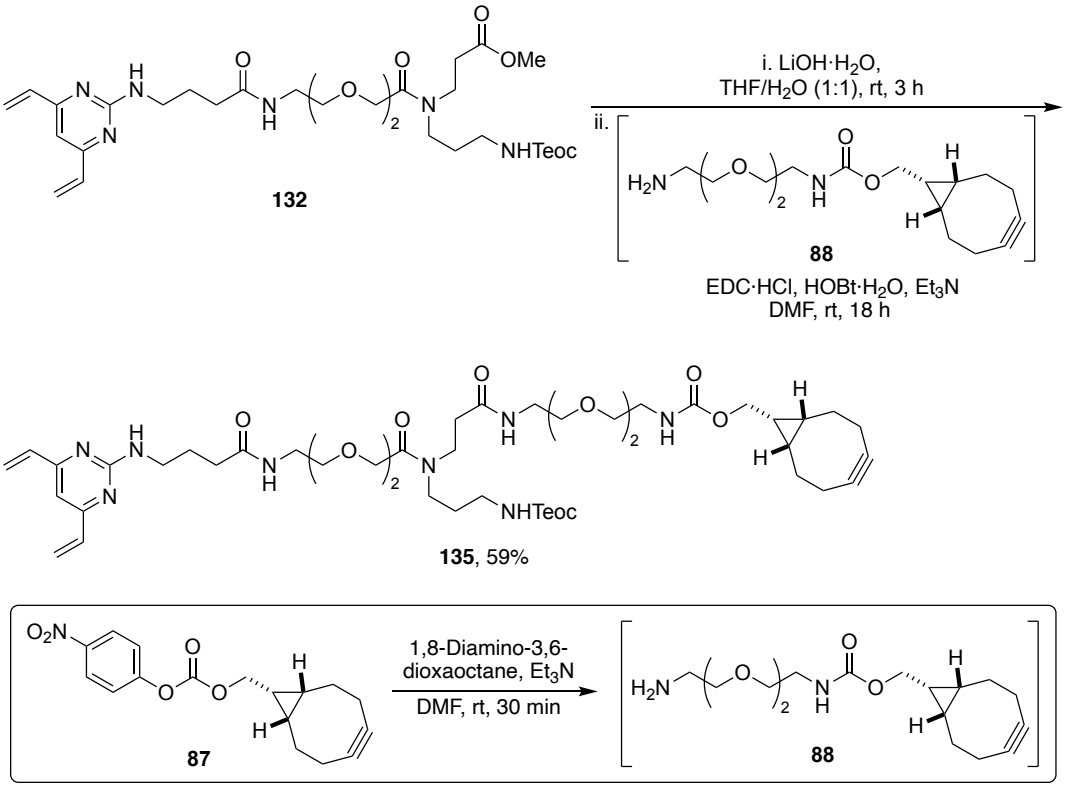

Scheme 5.27. Synthesis of DVP scaffold **135**.

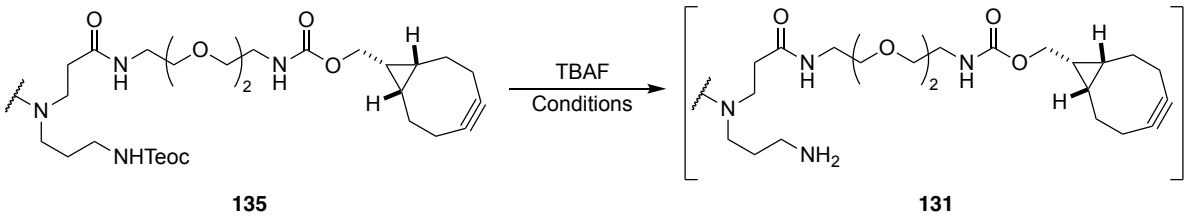

Table 5.3. Unsuccessful optimisation of the TBAF-mediated Teoc deprotection of **135**.

Entry	Equiv. of TBAF	Time (h)	Temp	Conversion[a]	Observations[a]
1	2	16	rt	20%	-
2	5	16	rt	60%	Minor decomposition
3	5	24	rt	-	Significant decomposition
4	7	12	rt	63%	Minor decomposition
6	20	4	40 °C	-	Significant decomposition

[a]As observed by crude ^{1}H NMR spectroscopy.

To circumvent this problem, the order of addition of the 'clickable' handles was reversed to enable Teoc removal prior to the incorporation of BCN. Thankfully, this enabled TBAF-mediated deprotection to be carried out at 50 °C without any observable decomposition (Scheme 5.28). After stirring for 6 h, nitrophenyl activated cyclopropene **89** (cyp-ONp) and Et_3N were added to the reaction mixture to enable generation of DVP-derivative **131** via a sequential one-pot deprotection-carbamate formation strategy. As before, subsequent ester hydrolysis and amide coupling with crude BCN-PEG **88** was unproblematic, affording the desired df-DVP linker **131** in 38% yield.

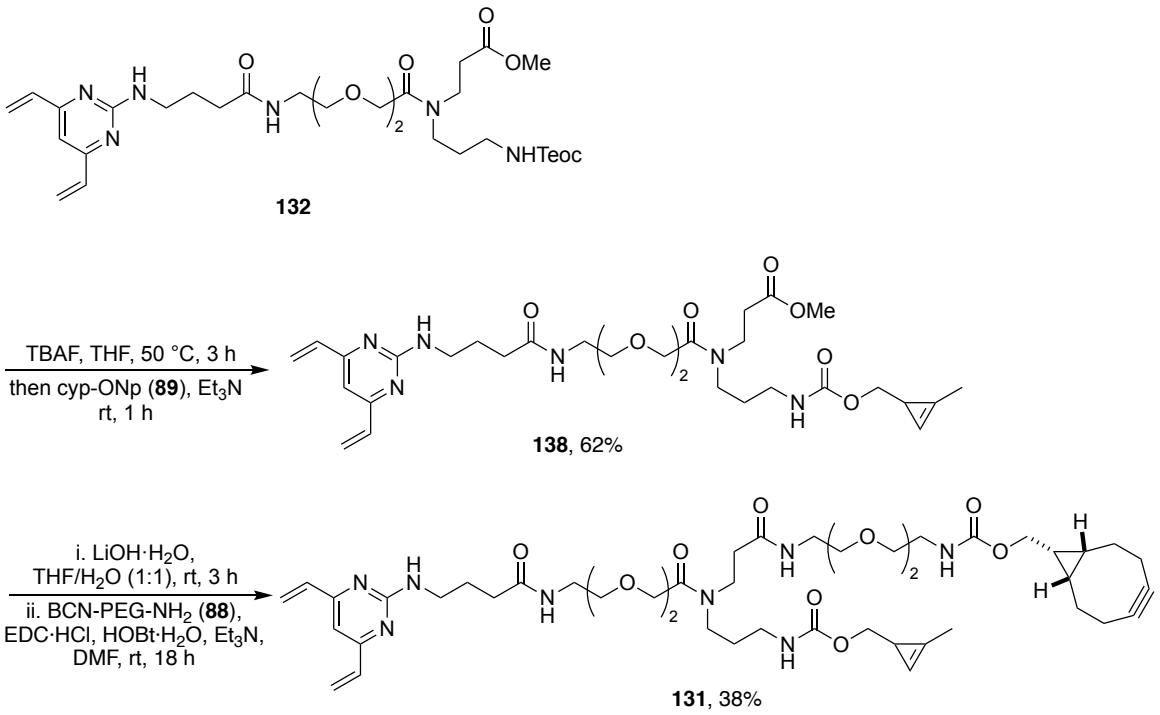

Scheme 5.28. Revised strategy for the synthesis of df linker **131**.

5.6.3 Trastuzumab Rebridging

Having successfully synthesised the second-generation linker **131**, conjugation to trastuzumab was investigated. To this end, trastuzumab was treated with TCEP in TBS buffer to facilitate reduction of the interchain disulfides (Scheme 5.29). After stirring for 1 hour, df-DVP linker **131** was then added, and the reaction mixture was shaken at 37 °C for a further 2 hours. Gratifyingly, subsequent analysis by protein LCMS and SDS-PAGE confirmed >90% rebridging to give bioconjugate **139** as the predominate species (Figure 5.14).

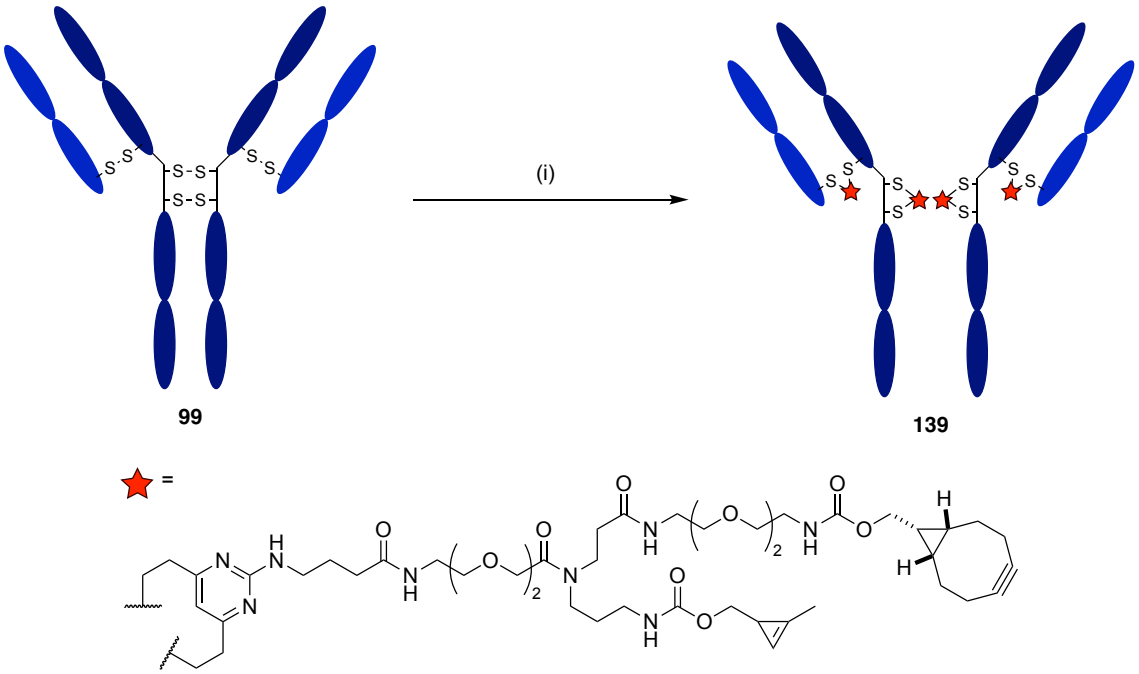

Scheme 5.29. Cysteine rebridging of trastuzumab with df-DVP **131** gave predominantly antibody conjugate **139**. *Reagents and Conditions*: (i) TCEP (10 equiv.), TBS buffer, 37 °C, 1 h, then df-DVP linker **131** (20 equiv.), DMSO (10% v/v), 37 °C, 2 h.

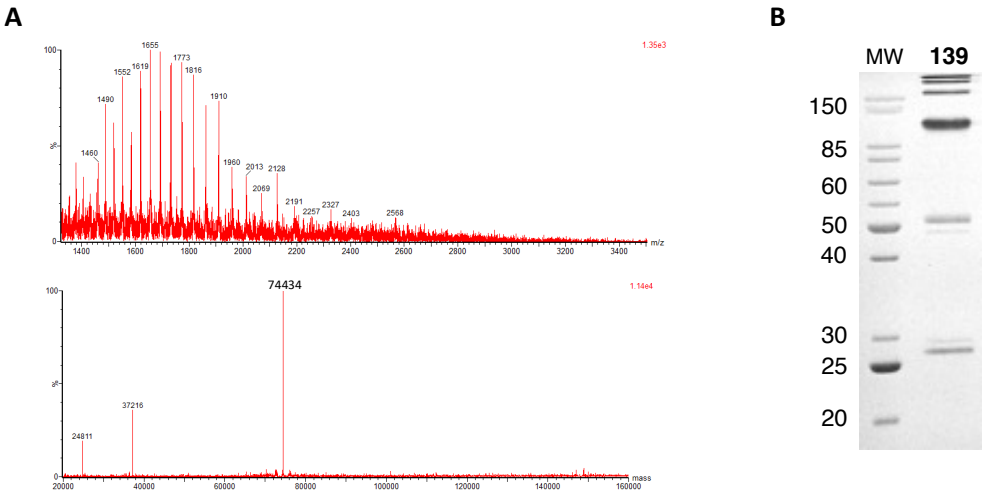

Figure 5.14. (A) Non-deconvoluted (top) and deconvoluted (bottom) MS of bioconjugate **139**. Expected Mass: 74437 Da (B) Analysis of bioconjugate **139** by SDS-PAGE. Lanes: MW) molecular weight marker, 139) bioconjugate **139**.

5.7 ADC Generation – Theranostics

Following on from these promising results, the utility of the linker-platform for antibody dual modification was next investigated.

As previously discussed in Section 4.2.9.3, theranostic ADCs are considered highly valuable targets because of their joint therapeutic and imaging capabilities.[393,394] Thus, as a proof of concept, efforts first focused on the synthesis of a fluorescent ADC containing both a cytotoxic payload and fluorescent dye such as AF488. It was hypothesised that such a conjugate would have potential use in several *in vitro* applications, including enabling cellular uptake studies using confocal microscopy or monitoring of cellular selectivity via flow cytometry.

5.7.1 Synthesis and Evaluation of a First-Generation Fluorescent ADC

To demonstrate the utility of the novel linker-platform for the generation of theranostic agents, the highly potent anti-cancer drug MMAE (IC_{50}: 10^{-11}–10^{-9} M) was chosen as a model payload.[421] As discussed in section 4.2.5, MMAE is tubulin inhibitor that is widely used in ADC research. In fact, many ADCs currently in clinical development utilise MMAE as their payload, as well as three that are FDA-approved.[238,245,309,422] At present, all FDA-approved MMAE-based ADCs operate via the use of a protease-labile vc linker to enable efficient intracellular release of the free drug.[238,245,309] Traceless release of MMAE further ensures its excellent potency and bystander effect – the killing of surrounding cells due to MMAE's excellent cell permeability.[266]

As an alternative to dipeptide-based linkers, the Spring group have reported the development of sulfatase-cleavable linkers and demonstrated their utility in several MMAE-containing ADCs.[315,385,423] These linkers not only facilitate efficient release of MMAE, but they also exhibit improved mouse plasma stability compared to their dipeptidic counterparts.[315] As such, they were considered a suitable choice in this context. To enable initial SPAAC with the BCN handle, the azide-functionalised payload azido-sulfate-MMAE **140** was selected (Figure 5.15).

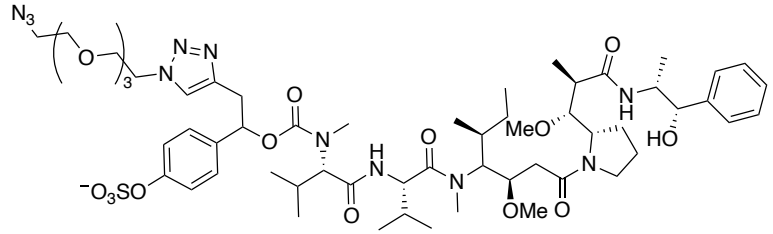

140

Figure 5.15. Structure of azido-sulfate-MMAE, **140**.

5.7.1.1 Synthesis of a Fluorescent ADC

As previously discussed, due to the ability of BCN to undergo both SPAAC and IEDDA reactions, the linker platform was designed to enable sequential cycloadditions. To prevent the BCN moiety undergoing IEDDA it was vital that full conversion was achieved in the SPAAC reaction with azido-sulfate-MMAE **140** prior to incorporation of the tetrazine-functionalised fluorophore. With this in mind, efforts first focused on optimisation of the SPAAC.

Using the previously optimised conditions, bioconjugate **139** was treated with 16 equiv. of azido-sulfate-MMAE **140**[m] in PBS (containing 10% v/v DMSO) and shaken for 8 hours. Unfortunately, analysis by protein LCMS indicated approximately 70% conversion to the corresponding ADC **141** (Table 5.4, entry 1).[n] Whilst increasing the reaction time to 16 hours led to increased conversion, a significant amount of starting material remained (Table 5.4, entry 2). Further improvements were made by increasing the number of equiv. of azido-sulfate-MMAE **140** (Table 5.4, entries 3–6), although no significant change was observed above 24 equiv. Similarly, only a marginal difference in conversion was observed upon doubling the reaction concentration (Table 5.4, entry 7) or increasing reaction time to 24 hours (Table 5.4, entry 8). Nonetheless, having successfully achieved >90% conversion (Table 5.4, entry 4), no further optimisation was considered necessary.

[m] Synthesised by Dr Jonathan Bargh, Spring Group, Department of Chemistry, University of Cambridge.
[n] Due to the potential different ionisation potentials of **139** and the various partially clicked species, stated conversions can only be considered a rough approximation.

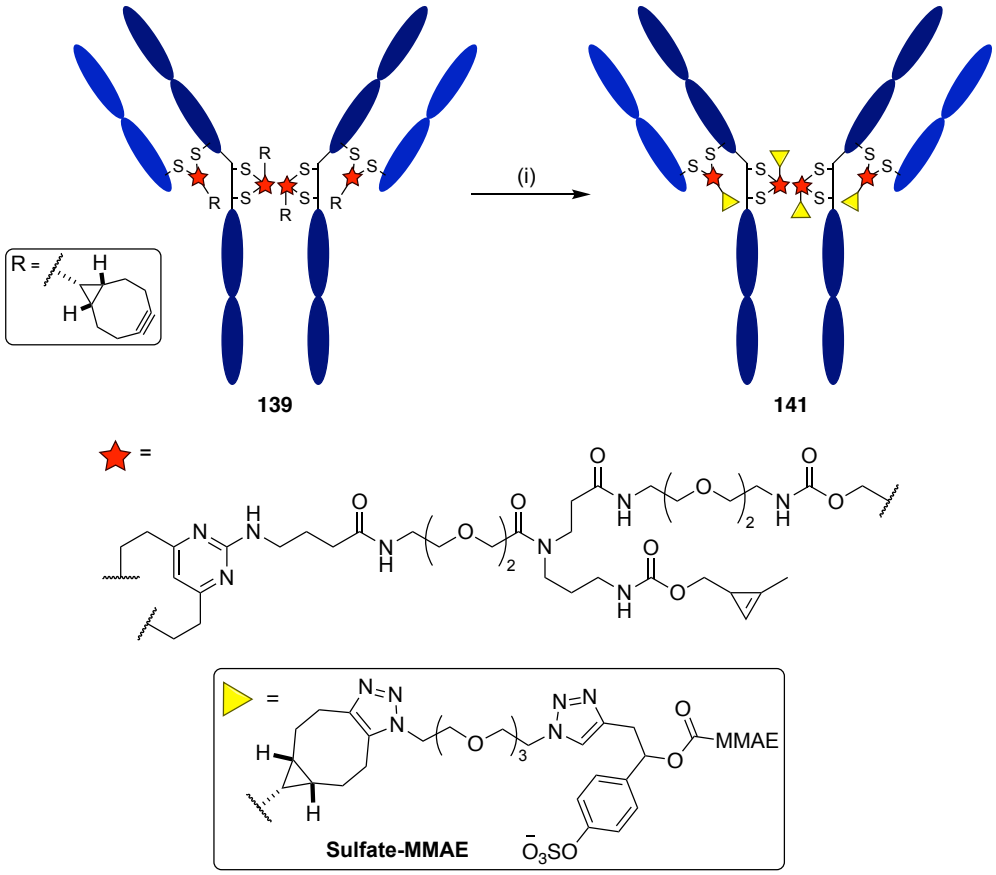

Table 5.4. Optimisation of the SPAAC of MMAE **140** and antibody conjugate **139**. *Reagents and Conditions:* (i) azido-sulfate-MMAE **140**, PBS buffer, 37 °C, DMSO (10% v/v), 37 °C.

Entry	Equiv. of MMAE	Concentration (mg/mL)	Time (h)	Conversion[a]
1	16	2.5	8	71%
2	16	2.5	16	84%
3	20	2.5	16	85%
4	24	2.5	16	92%
5	40	2.5	16	92%
6	80	2.5	16	94%
7	24	5	16	92%
8	24	2.5	24	92%

[a]Approximate values obtained from protein LCMS analysis.

Going forward, Table 5.4, entry 4 was selected as the optimum reaction conditions as very little change was observed upon further increasing the time or number of equiv. Analytical data of the product obtained under these conditions is shown in (Figure 5.16).

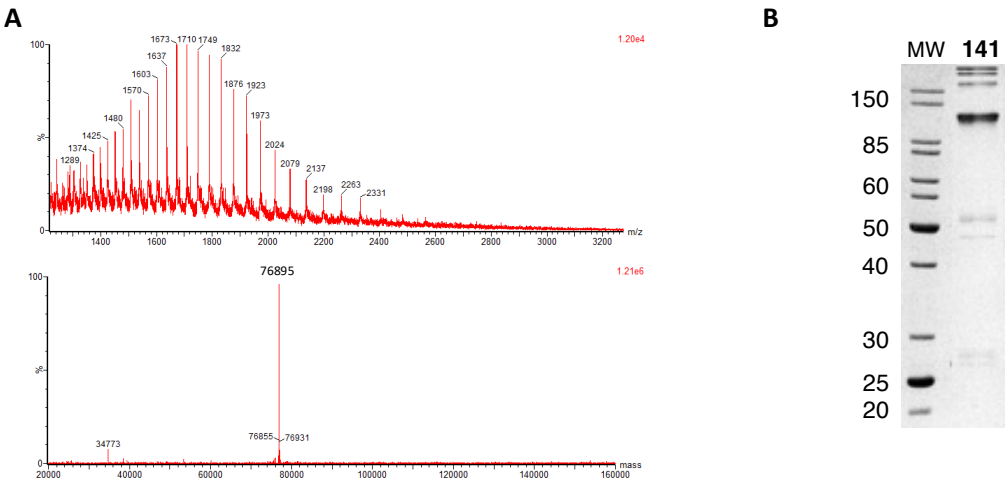

Figure 5.16. (A) Non-deconvoluted (top) and deconvoluted (bottom) MS of bioconjugate **141**. Expected mass: 76898 Da. (B) Analysis of conjugate **141** by SDS-PAGE. Lanes: MW) molecular weight, 141) bioconjugate **141**.

Having optimised the SPAAC, efforts then turned to the subsequent IEDDA with AZDye 488 tetrazine **105**. Thus, to effect a one-pot transformation, tras-df-DVP **139** was treated with 24 equiv. of azido-sulfate-MMAE in PBS (10% v/v DMSO). After constant agitation at 37 °C for 16 h, a stock solution of AZDye 488 tetrazine **105** in DMSO (24 equiv.) was added to the reaction mixture. Aliquots were taken at 2, 3 and 4 hours after the addition of tetrazine **105** to monitor reaction progression by protein LCMS.

Pleasingly, after 4 hours complete consumption of the tras-MMAE precursor **141** was observed by LCMS analysis (Figure 5.16). Successful conjugation of both substrates was confirmed *via* SDS-PAGE in-gel fluorescence, and analysis via UV-vis spectroscopy indicated an average FAR of 3.9.

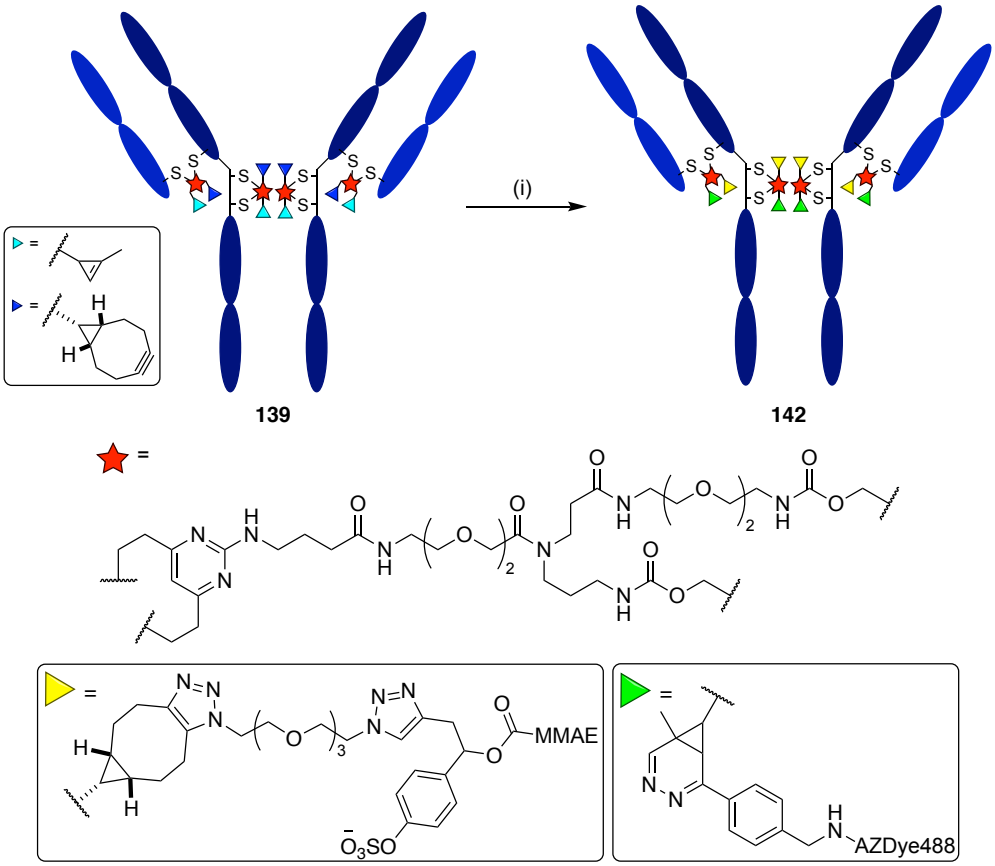

Scheme 5.30. One-pot synthesis of fluorescent ADC **142**. *Reagents and Conditions*: (i) Azido-sulfate-MMAE **140** (24 equiv.), DMSO (10% v/v), 37 °C, 16 h then AZDye 488 tetrazine **105** (24 equiv.), 37 °C, 4 h.

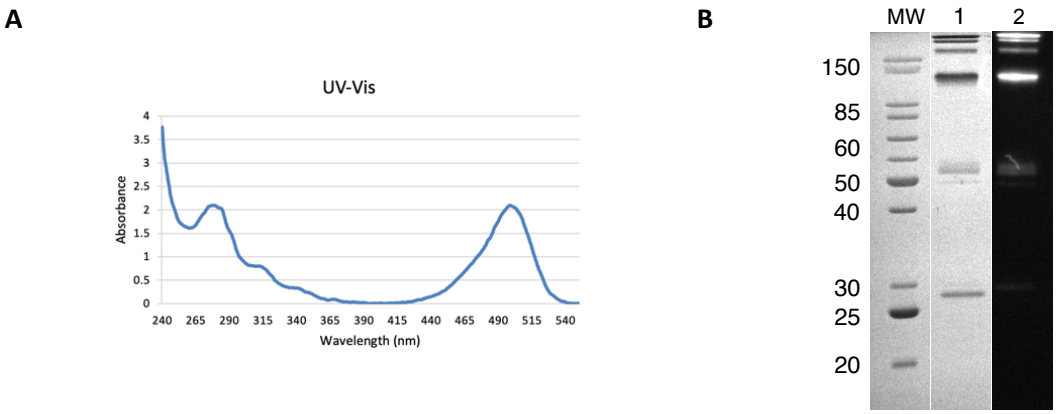

Figure 5.17. (A) UV-vis spectrum of bioconjugate **142**. (B) Analysis of bioconjugate **142** by SDS-PAGE. Lanes: MW) molecular weight marker, 1) coomassie stain of **142**, 2) in-gel fluorescent image of biconjugate **142**.

5.7.1.2 Cytotoxicity Assay

The work in this subsection was carried out by Dr Stephen Walsh, Spring Group, Department of Chemistry, University of Cambridge.

To evaluate the cytotoxicity and selectivity of tras-MMAE-AZDye488 **142** *in vitro*, its effect on cell viability in both HER2-positive (SKBR3) and HER2-negative (MCF7) cell lines was assessed. Both cell lines are reported to be sensitive to MMAE with sub-nanomolar IC_{50}s.[382]

Gratifyingly, tras-MMAE-AZDye488 **142** exhibited toxicity against the SKBR3 cell line, whilst activity against the MCF7 (HER2 low) cells was negligible at the tested concentration range (Figure 5.18). Thus, these results serve to demonstrate the cell-selective cytotoxicity of conjugate **142**.

Unfortunately, previous work in the Spring group has shown that DAR 4 tras-MMAE ADCs with a sulfatase-cleavable moiety have IC_{50}s ~200 pM against SKBR3 cells.[315] However, it was observed that tras-MMAE-AZDye488 **142** had very little activity below 1 nM and had a significantly lower maximum effect (E_{max}) on cell viability than the earlier generation ADCs (Figure 5.18). The exact reason for this lower level of cell cytotoxicity is unknown, although it was hypothesised that it may be due to inefficient release of MMAE or a reduction in antibody binding affinity following modification.

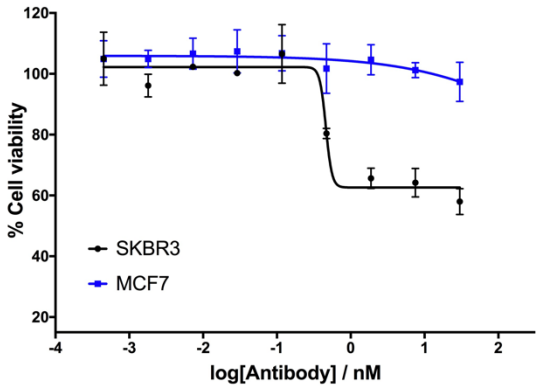

Figure 5.18. *In vitro* potency of ADC **142** on SKBR3 (black) and MCF7 (blue) cells. Cell viability was plotted against the log of bioconjugate **142** concentration. SKBR3 and MCF7 cell lines were treated with varying concentrations of fluorescent ADC **142**, incubated for 96 hours, and subsequently assessed for cell viability via a CellTiter-Glo® assay.

5.7.2 Synthesis and Evaluation of a Second-Generation Fluorescent ADC

It was hypothesised that the low level of cytotoxicity observed for ADC **142** may be caused by the complex and bulky structure of the df linker. Thus, following on from these results, it was proposed that a further spacer could be introduced between the dye and 'clickable' handle to provide greater space between payloads. For this purpose, the commercially available dye TAMRA-PEG2-tetrazine was selected (Figure 5.19).

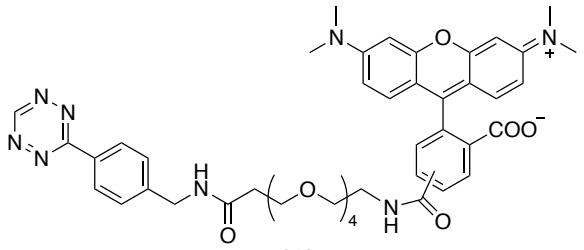

143

Figure 5.19. Structure of TAMRA-PEG4-tetrazine, **143**.

The cleavable linker used for MMAE was also changed to the well-established protease-labile vc-PABC, with a longer PEG spacer (Figure 5.20).

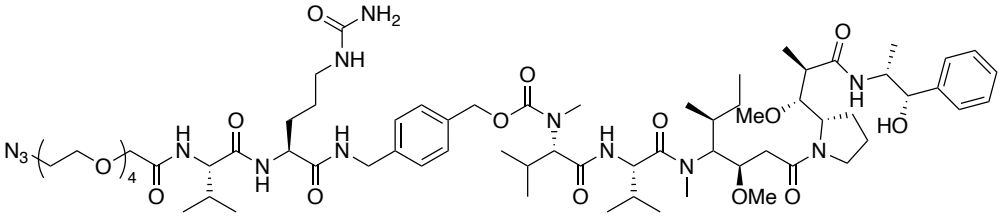

144

Figure 5.20. Structure of azido-PEG4-vc-PAB-MMAE, **144**.

5.7.2.1 Synthesis of Second-Generation Fluorescent ADC

Having selected the new payloads, the one-pot synthesis of second-generation ADC **145** was carried out under the previously developed dual click conditions. Briefly, SPAAC of tras-dfDVP **139** and azido-vc-PAB-MMAE **144** (24 equiv.)[o] in PBS (10% v/v DMSO), followed by IEDDA with TAMRA-tetrazine **143** (24 equiv.) gave the desired conjugate **145** (Scheme 5.31).

Although analysis by protein LCMS and SDS-PAGE with in-gel fluorescence indicated conversion to the desired conjugate, a measured FAR of 2.16 was obtained (Figure 5.21). Notably, the relative intensity of the shoulder band at 520 nm in the visible absorption spectrum appeared unusually high, which is consistent with TAMRA forming a non-covalent dimer.[424–428] This phenomenon has been observed on several occasions where TAMRA moieties are sufficiently close to each other, and is associated with significant quenching. Thus, in this case UV-vis analysis could not be used to quantitatively confirm the FAR, nonetheless, protein LCMS and SDS-PAGE analysis were sufficient to confirm the successful formation of the desired conjugate.

[o] Synthesised by Dr Stephen Walsh, Spring Group, Department of Chemistry, University of Cambridge.

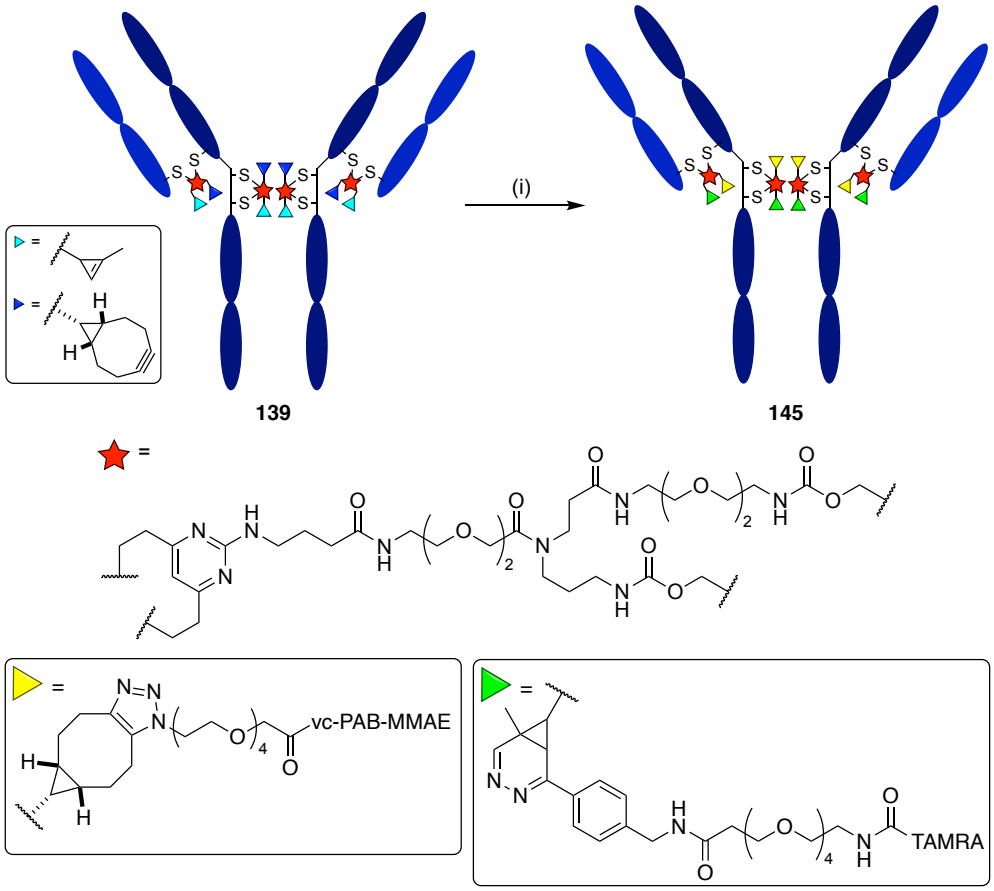

Scheme 5.31. One-pot synthesis of fluorescent ADC **145** via sequential SPAAC and IEDDA reactions. *Reagents and Conditions*: (i) Azido-PEG4-vc-PAB-MMAE **144** (24 equiv.), DMSO (10% v/v), 37 °C, 16 h then TAMRA tetrazine **143** (24 equiv.), 37 °C, 4 h.

A

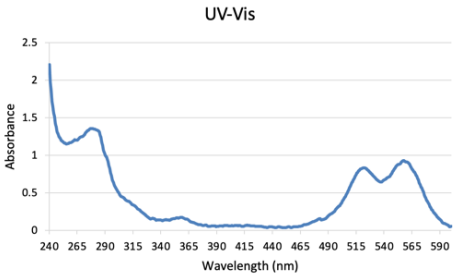

B

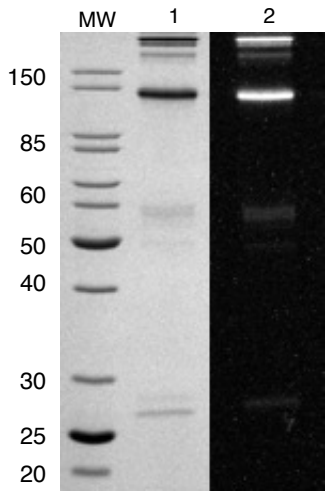

Figure 5.21. (A) UV-vis spectrum of **145**; (B) Analysis of bioconjugate **145** by SDS-PAGE. Lanes: MW) molecular weight marker, 1) coomassie stain of bioconjugate **145**, 2) in-gel fluorescent image of bioconjugate **145**.

5.7.2.2 Synthesis of Monofunctional MMAE-Based ADC

To enable a means of comparison of the effect of dual modification on ADC cytotoxicity, the analogous mf-MMAE ADC **146** was also synthesised (Scheme 5.32). This required SPAAC of BCN-conjugate **101**

and azido-PEG4-vc-PAB-MMAE **144** under the conditions developed for mono-functionalisation. Excellent conversion to the desired ADC **146** was confirmed by protein LCMS (Figure 5.22).

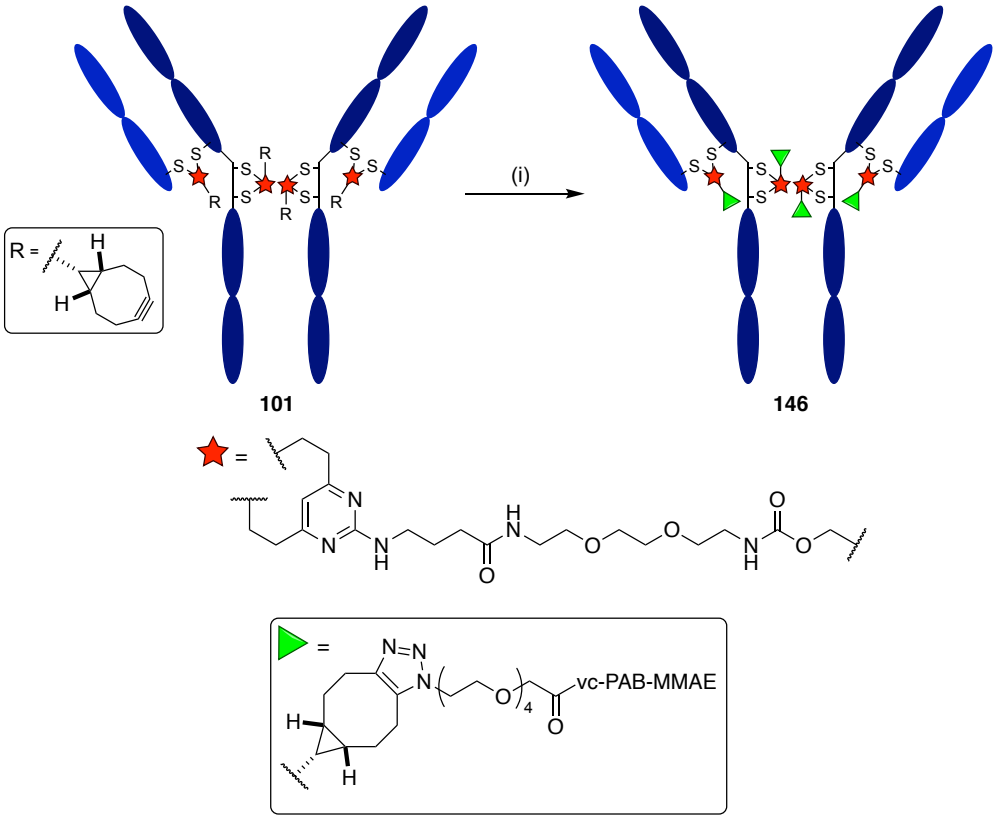

Scheme 5.32. SPAAC of BCN-modified trastuzumab **101** and azide-vc-PAB-MMAE, **144**. *Reagents and Conditions*: (i) azide-vc-PAB-MMAE **144** (16 equiv.), PBS buffer, DMSO (10% v/v), 37 °C, 8 h.

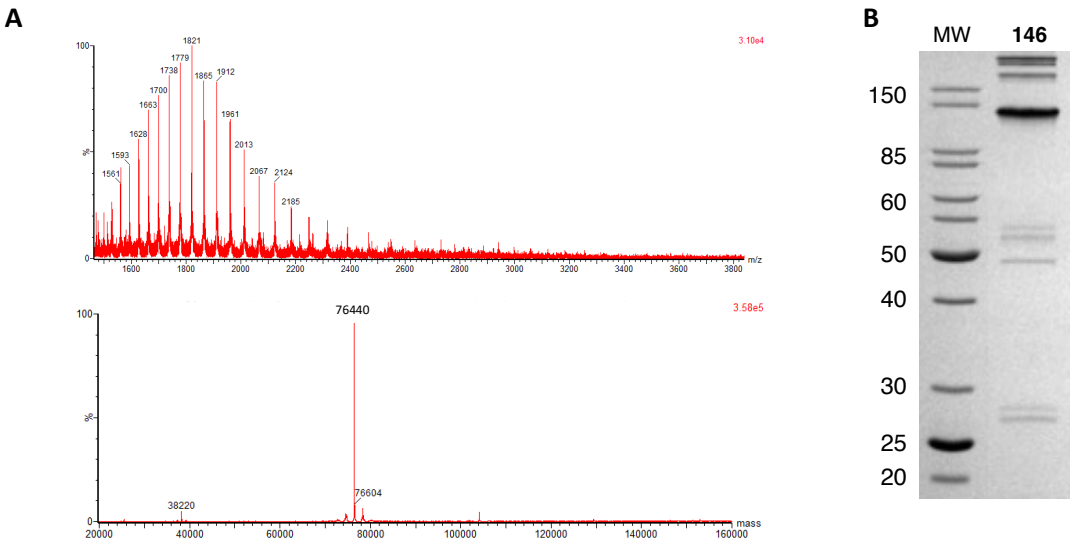

Figure 5.22. (A) Non-deconvoluted (top) and deconvoluted (bottom) MS of bioconjugate **146** after deglycosylation by PNGaseF. Expected mass: 76434 Da. (B) Analysis of bioconjugate **146** by SDS-PAGE. Lanes: MW) molecular weight marker, 146) bioconjugate **146**.

5.7.2.3 Cytotoxicity Assay

The work in this subsection was carried out by Dr Stephen Walsh, Spring Group, Department of Chemistry, University of Cambridge.

In possession of two ADCs bearing MMAE, **145** and **146**, *in vitro* cytotoxicity was next assessed. Again, the SKBR3- and MCF7-cells were selected to represent HER2-positive and HER2-negative cell lines, respectively.

Gratifyingly, both mf-ADC **146** and fluorescent ADC **145** exhibited sub-nanomolar toxicity against the SKBR3 cell line, with IC_{50} values of 26.4 pM and 40.0 pM obtained for mf-ADC **146** and df-ADC **145**, respectively (Figure 5.23.A). E_{max} of both ADCs was significantly higher than the first generation df-ADC, and in line with previous ADCs developed in the group. Moreover, both ADCs also displayed negligible activity against the HER2 negative cell line (IC_{50}s > 30 nM), thereby confirming their selectivity for HER2 expressing cell lines (Figure 5.23.B). These results serve to demonstrate not only the exceptional potency and selectivity of both ADCs, but also that dual modification has no significant detrimental effect on cytotoxicity.

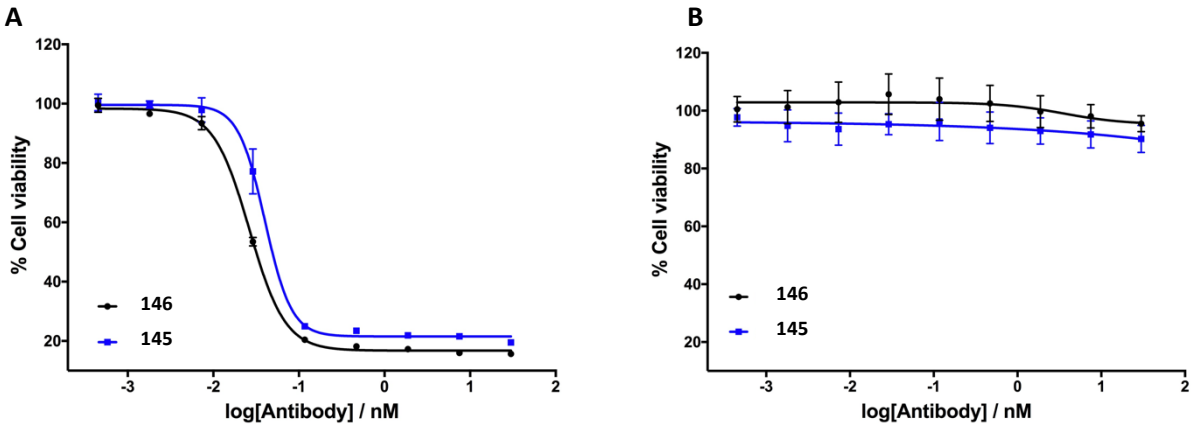

Figure 5.23. *In vitro* potency of mf-ADC **146** (black) and df-ADC **145** (blue) on (A) SKBR3 and (B) MCF7 cells. SKBR3 and MCF7 cell lines were treated with varying concentrations of ADC **146** or **145**, incubated for 96 hours, and subsequent assessed for cell viability via a CellTiter-Glo® assay.

5.8 Dual-Drug ADCs

Whilst all FDA-approved ADCs currently only contain a single type of drug payload, interest in dual-drug ADCs has dramatically increased in recent years in the hopes of overcoming issues of tumour heterogeneity and circumventing ADC-drug resistance (*vide supra*, Section 4.2.9.3).[359,373,384] Such ADCs also have the potential to benefit from lower dosing of each individual drug, which, with appropriate drug selection, may lead to reduced side effects.[429,430]

An additional interesting application of dual-drug ADCs is the delivery of two cytotoxins that interact synergistically. Although there are currently no reports of ADC payload synergism, such an ADC would have the potential for much greater potency.[359,384] Alternatively, dual-drug ADCs may also offer an approach by which synthetic lethality in cancer cells could be achieved, resulting in enhanced therapeutic indexes.[431]

With these benefits in mind, and to further demonstrate the versatility of the novel linker platform, attention turned to the generation of a dual-drug ADC. As an initial proof-of-principle, the tyrosine kinase inhibitor crizotinib (Criz) and DNA-intercalating agent Dox were selected as model payloads.[432,433] Not only do these payloads have distinct MOA, providing a means by which resistance could be potentially circumvented, but both also display significant activity against the SKBR3 cell-line.[433,434] Moreover, the payloads were expected to be readily functionalised with either azide- or tetrazine-handles to enable efficient attachment to the antibody via metal-free click chemistry.

Although Criz has not been widely used as an ADC payload, its suitability for this purpose has previously been demonstrated by Bernardes and co-workers via the formation of a DAR 2 thiomab-Criz conjugate.[433] Notably, compared to the free drug, a 10-fold improvement in cell-killing ability was observed in SKBR3 cells upon conjugation of Criz.

Dox, on the other hand, has been extensively used in ADC development.[435,436] In fact, several Dox-based ADCs have undergone clinical evaluation; however, issues of dose-liming toxicity and insufficient efficacy have prevented their further development.[299] Thus, it was hypothesised that Dox may benefit from the potential lower dosing enabled by the formation of a dual-drug ADC.

5.8.1 Crizotinib-Based ADC

Investigations began with the functionalisation of Criz. Following the successful incorporation of an azido-functionalised vc linker into fluorescent ADC **145**, it was hypothesised that a similar linker could be employed for the functionalisation of Criz. However, for these purposes the use of the va motif was favoured due to its tendency to generate more soluble linker-payload constructs.[264] Thus, the synthesis of azido-va-PAB-Criz **147** was pursued (Figure 5.24).

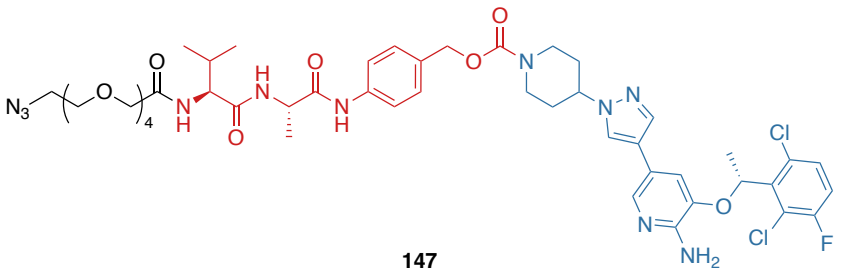

147

Figure 5.24. Structure of azido-va-PAB-Criz **147**. Criz highlighted in blue, cleavable motif in red, and spacer in black.

Synthetic routes to va-MMAE linker-drugs are well established and were found to be readily adapted for Criz.[399,437] Starting from Alloc-protected valine-alanine-4-aminobenzyl alcohol (Alloc-va-PABA, **148**), which was readily available from AstraZeneca, the corresponding activated carbonate was formed upon treatment with bis(4-nitrophenyl) carbonate (Scheme 5.33). This was then converted to the desired carbamate via reaction with Criz, HOBt and py, affording Criz-derivative **149** in 84% yield. Finally, Alloc removal by treatment with [$Pd(PPh_3)_4$], followed by HBTU-mediated amide coupling of the resulting deprotected amine with 14-azido-3,6,9,12-tetraoxatetradecanoic acid produced va-PAB-Criz **147** in excellent yield.

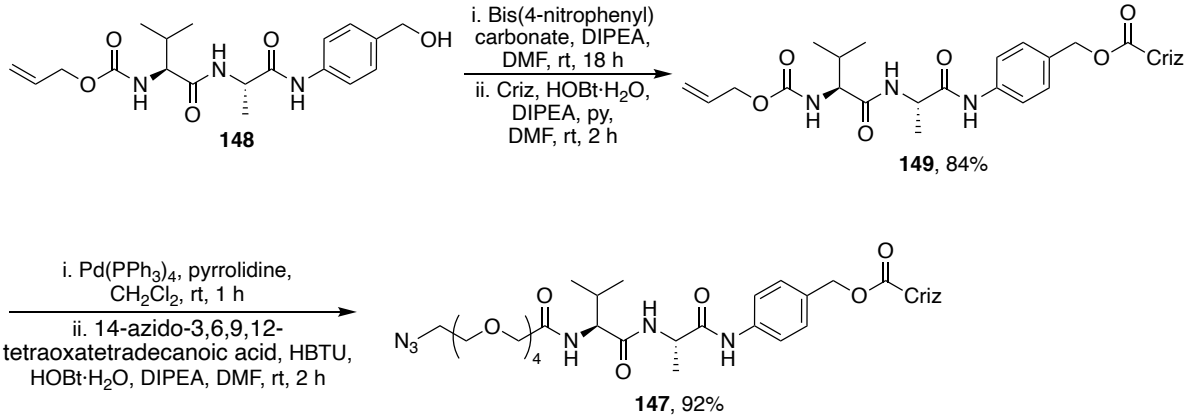

Scheme 5.33. Synthesis of azido-functionalised Criz **147**.

With azide-functionalised Criz **147** in hand, investigation of its ability to undergo post-rebridging SPAAC commenced by employing tras-BCN **101** as a model system. Accordingly, tras-BCN **101** was reacted with Criz **147** in PBS (10% v/v DMSO) to yield ADC **150** (Scheme 5.34). Although the linker-payload **147** appeared to be poorly soluble in the solvent system, the reaction proceeded smoothly, with protein LCMS analysis indicating complete consumption of tras-BCN **101** after 8 hours (Figure 5.25).

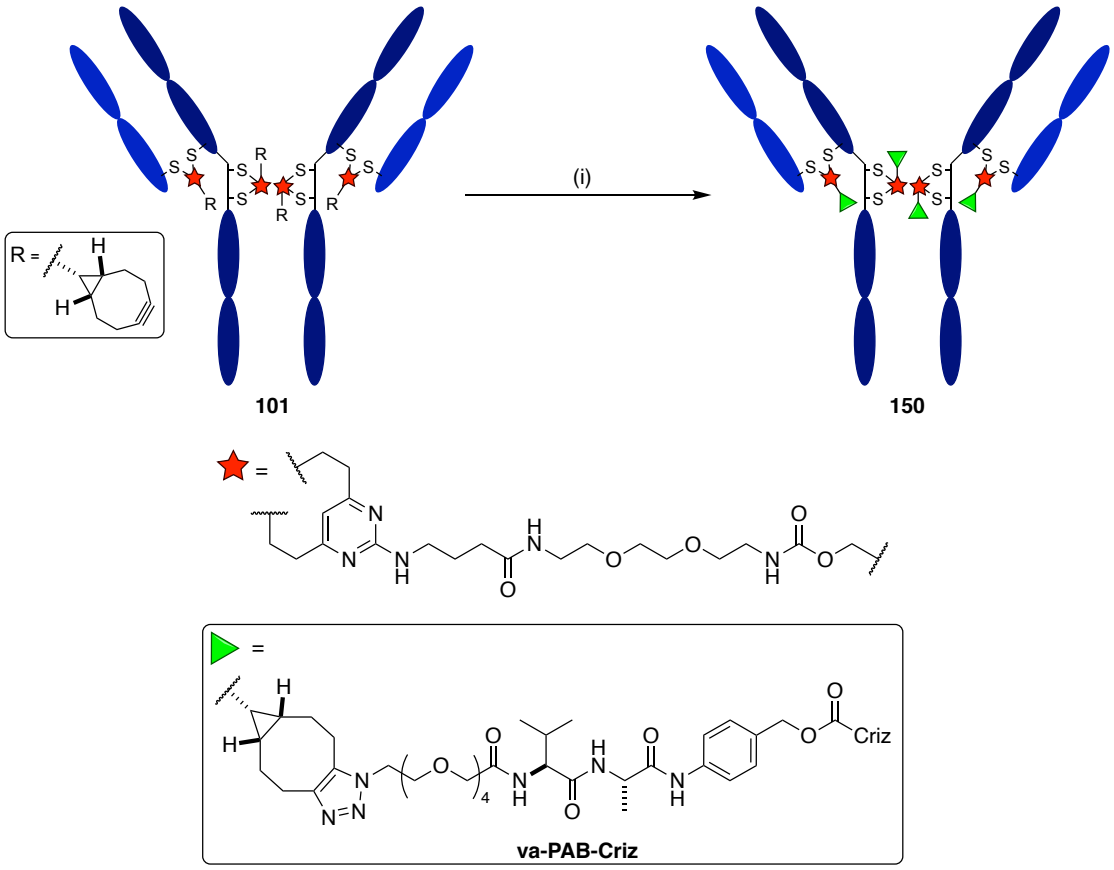

Scheme 5.34. SPAAC of BCN-modified trastuzumab **101** and azide-va-PAB-Criz **147**. *Reagents and Conditions*: (i) azide-va-PAB-Criz **147** (16 equiv.), PBS buffer, DMSO (10% v/v), 37 °C, 8 h.

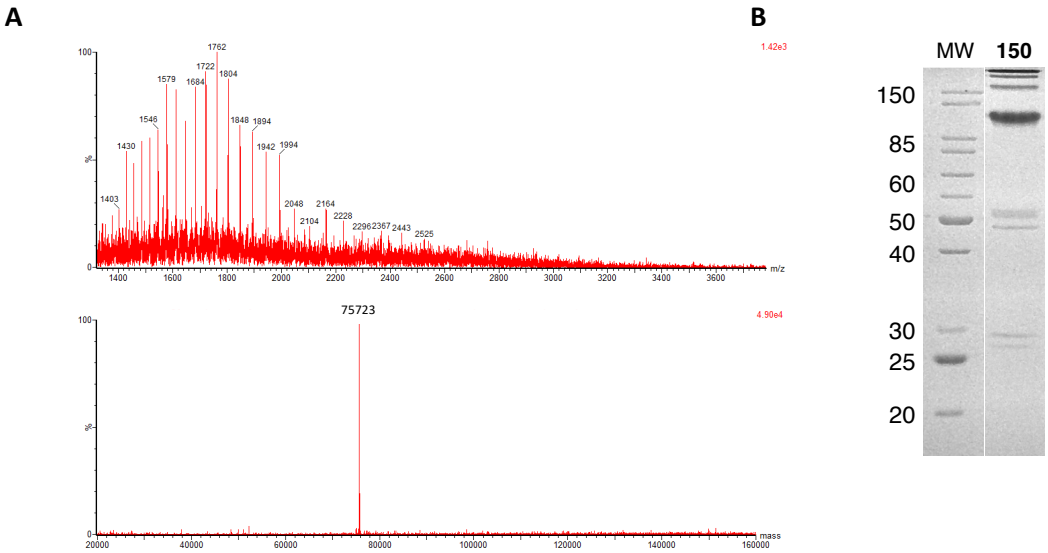

Figure 5.25. (A) Non-deconvoluted (top) and deconvoluted (bottom) MS of ADC **150**. Expected mass: 75725 Da. (B) Analysis of ADC **150** by SDS-PAGE. Lanes: MW) molecular weight marker, 150) bioconjugate **150**.

5.8.2 Doxorubicin-Based ADC

After the successful formation and SPAAC of azide-functionalised Criz, focus then turned to a tetrazine-functionalised payload.

To enable efficient IEDDA on the antibody, the tetrazine-functionalised payload required good water-solubility. Thus, investigations began with the formation of a tetrazine-functionalised PEG chain. For these purposes, the synthesis of methyl-substituted reagent **151** was pursued due to its greater stability, and hence greater ease of handling, compared to the more reactive unsubstituted tetrazines.[438] Following a literature procedure described by Devaraj *et al*,[439] tetrazine **152** was synthesised in moderate yield via the $Zn(OTf)_2$-catalysed reaction of 4-cyanophenylacetic acid (**153**), hydrazine, and acetonitrile, to form a dihydrotetrazine intermediate, which was then directly oxidised with $NaNO_2$ (Scheme 5.35). The resulting acid **152** was then reacted with *tert*-butyl 12-amino-4,7,10-trioxadodecanoate to generate the tetrazine-functionalised PEG chain **154**. Finally, TFA-mediated *tert*-Butyl-deprotection enabled rapid formation of the corresponding tetrazine-PEG-acid **151** in 99% yield.

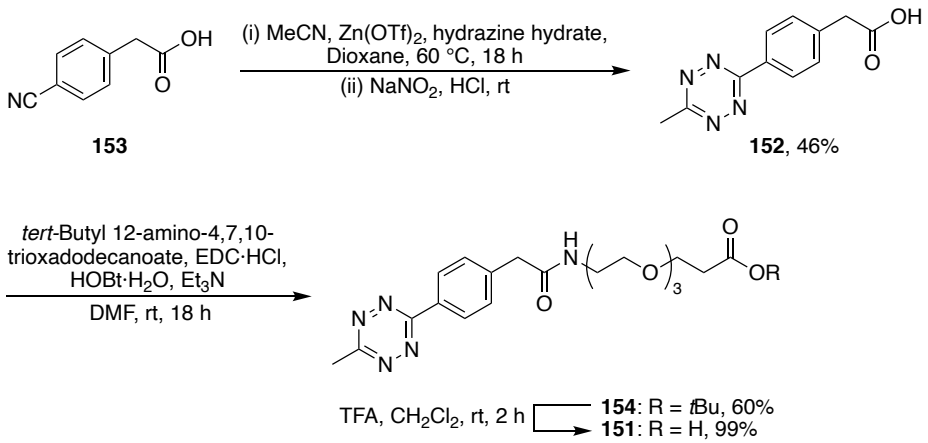

Scheme 5.35. Synthesis of tetrazine-functionalised PEG chain **151**.

Having developed a viable route to the formation of tetrazine-PEG-acid chain **151**, it was then proposed that tetrazine-va-PAB-Dox **155** could be synthesised via a similar strategy as established for Criz functionalisation (Figure 5.26).

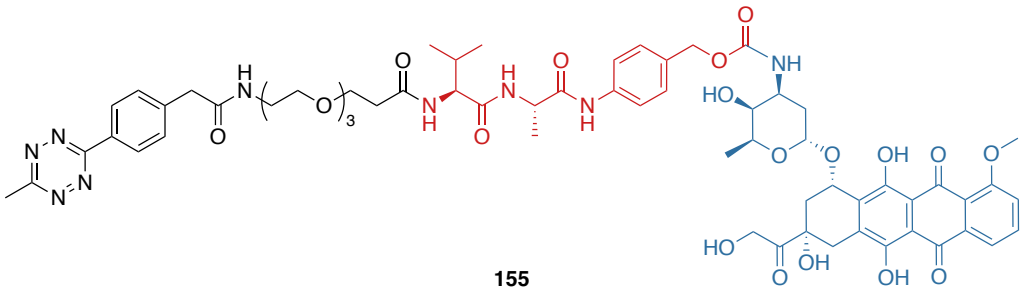

155

Figure 5.26. Structure of tetrazine-va-PAB-Dox **155**. Dox highlighted in blue, cleavable motif in red, and spacer in black.

In the first step, Alloc-va-PABA, **148** was treated with bis(nitrophenyl)carbonate, followed by reaction with Dox to form the Alloc-protected intermediate **156** in moderate yield (Scheme 5.36). Notably, despite the reaction proceeding cleanly and in high conversion, the yield was significantly lower than

that obtained for Criz. This significant mass loss was attributed to product streaking during chromatography purification. Nonetheless, sufficient material was obtained for the deprotection of Alloc-protected intermediate **156**, and subsequent amide coupling with tetrazine-PEG-acid **151**. Pleasingly, the desired tetrazine-functionalised Dox **155** was obtained in 80% yield.

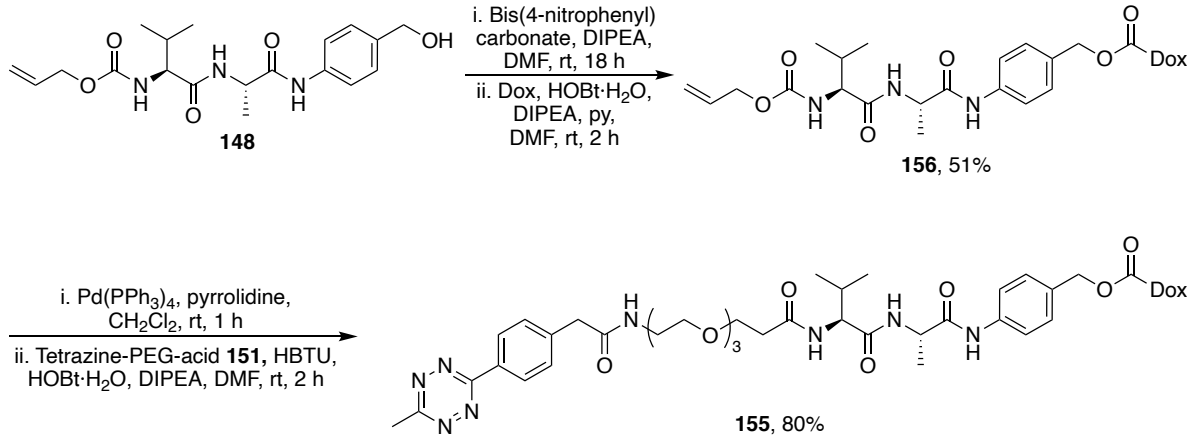

Scheme 5.36. Synthesis of methyltetrazine-PEG3-va-PAB-Dox **155**.

Next, the IEEDA reaction between a cyp-conjugated antibody and tetrazine-modified Dox **155** was tested using tras-cyp **102** as a model system. Thus, cleavable Dox-derivative **155** was subjected to a IEDDA reaction with df-DVP tras-cyp **102** under the previously established conditions (Table 5.5, entry 1). Unfortunately, Dox appeared to be completely insoluble in the solvent system and no evidence of the desired conjugate **157** was observed by LCMS after 2 hours. The reaction was then repeated increasing the number of equiv. to 80, with aliquots removed at 4, 8 and 16 hours (Table 5.5, entries 2–4). Whilst this served to marginally increase conversion, a significant amount of starting material remained.

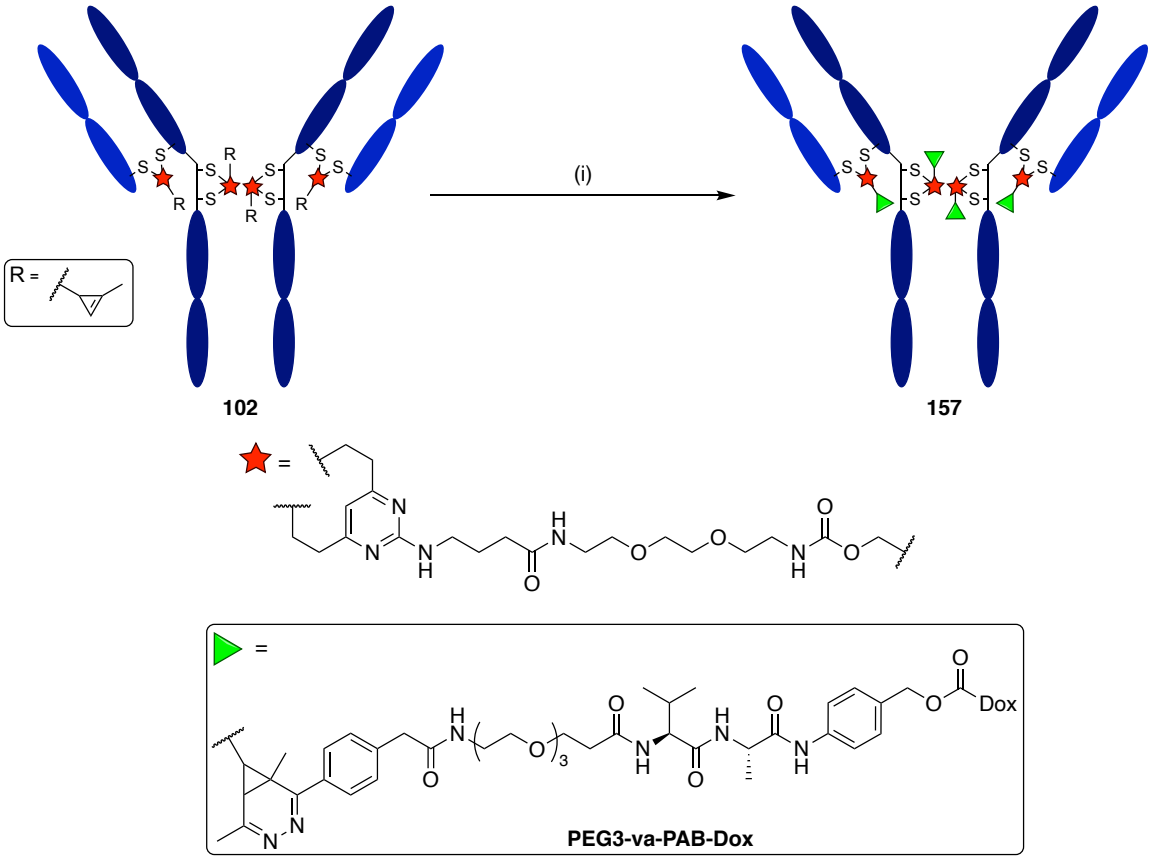

Table 5.5. Optimisation of the SPAAC of Dox **155** and antibody conjugate **102**. *Reagents and Conditions*: (i) PEG3-va-PAB-Dox **155**, PBS buffer, DMSO (10% v/v), 37 °C.

Entry	Equiv. of **155**	Time (h)	Conversion[a]
1	16	2	Negligible
2	80	4	Poor
3	80	8	Poor
4	80	24	Poor

[a]As observed by protein LCMS analysis.

Given the apparent solubility issues faced by PEG3-va-PAB-Dox **155**, it was postulated that increasing the PEG chain length would potentially increase aqueous solubility. Based on this hypothesis, Alloc-protected intermediate **148** was amide coupled to the commercially available methyltetrazine-PEG12-acid, **158**, using HBTU as the coupling agent (Scheme 5.37). This afforded the tetrazine-functionalised Dox **159** in 76% yield.

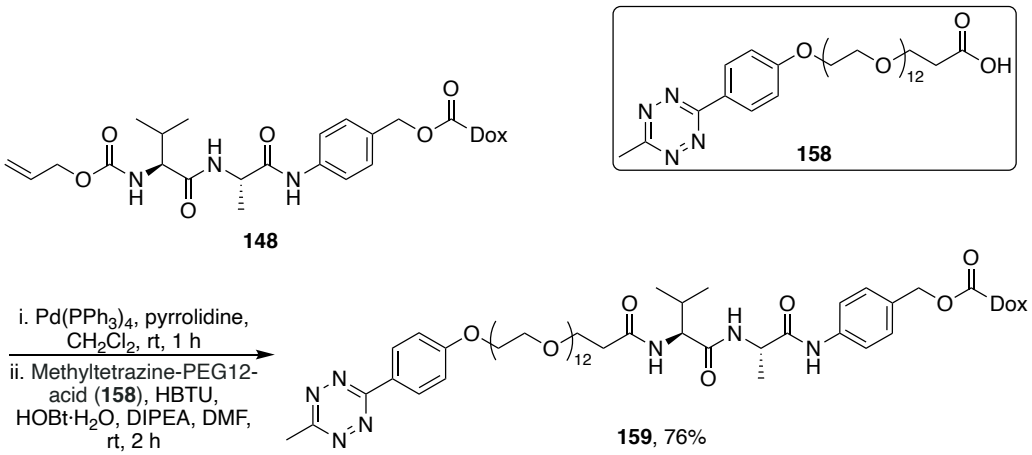

Scheme 5.37. Synthesis of methyltetrazine-PEG12-va-PAB-Dox **159**.

With Dox-derivative **159** in hand, IEDDA with tras-cyp **102** was attempted. Again, no reactivity was observed using the conditions previously optimised for AZDye 488 **105** (Table 5.6, entry 1). A screen of conditions was then attempted by varying equiv. of **159**, time, DMSO percentage (10 or 15% v/v) and reaction concentration (Table 5.6, entries 2–7). Unfortunately, in each case the payload appeared to be poorly soluble, and no significant increase in conversion was observed compared to the shorter PEG chain analogue. Further optimisation of this reaction is on-going.

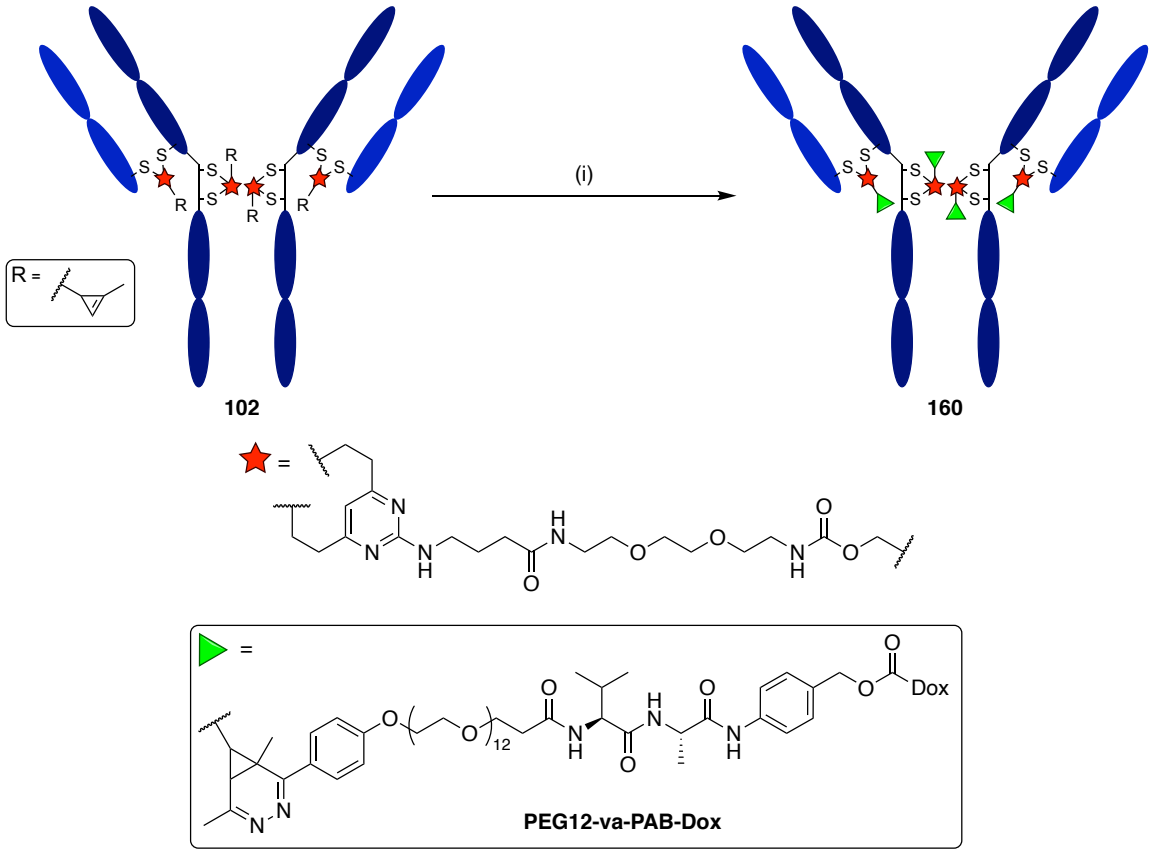

Table 5.6. Optimisation of the SPAAC of Dox **159** and cyp-functionalised tras **102**. *Reagents and Conditions*: (i) PEG12-va-PAB-Dox **159**, PBS buffer, DMSO, 37 °C.

Entry	Equiv. of **159**	DMSO percentage	Concentration (mg/mL)	Time (h)	Conversion[a]
1	16	10	2.5	2	Negligible
2	80	10	2.5	4	Poor
3	80	10	2.5	8	Poor
4	80	10	2.5	16	Moderate
5	80	15	2.5	4	Poor
6	80	15	2.5	8	Significant degradation
7	24	10	1	16	Poor

[a]As observed by protein LCMS analysis.

6 Conclusions and Future Work

6.1 Conclusions

Early work on this project led to the synthesis of two novel mf DVP-based linkers containing either a BCN or cyp handle. The ability of these linkers to efficiently rebridge reduced disulfides in antibodies was then successfully demonstrated, resulting in the formation of both BCN- and cyp-functionalised trastuzumab. Using metal-free click chemistry, these handles were then leveraged for post-rebridging functionlisation to generate several AFCs and ADCs.

Following on from this work, a df-DVP linker containing orthogonal 'clickable' handles was successfully synthesised and its ability to rebridge reduced trastuzumab was subsequently demonstrated. By harnessing the orthogonality of SPAAC and IEDDA chemistry, the efficient one-pot synthesis of a fluorescent ADC bearing MMAE and the fluorescent dye TAMRA was achieved. Biological evaluation of the resulting conjugate indicated exceptional cell-specific toxicity, with a measured IC_{50} obtained that was comparable to its mf counterpart. Taken together, these results demonstrate the power of this approach for the efficient, metal-free, one-pot dual functionalisation of antibodies.

Finally, in the last part of this project, studies towards the synthesis of a dual-drug ADC containing both Dox and Criz were undertaken. Whilst the synthesis of azide-functionalised Criz was successfully achieved and its suitability for antibody conjugation demonstrated through the generation of a Criz-based ADC, preliminary conjugation studies with tetrazine-functionalised Dox were unfruitful. This is likely due to issues of poor solubility. Nevertheless, provided the payloads are sufficiently water-soluble and unhindered, the high versatility and modular nature of this linker-platform provides a potential means by which multiple dual-drug ADCs could be readily accessed.

6.2 Future Work

Future work on this project would initially focus on continued efforts towards the formation of a dual-drug ADC containing payloads with non-overlapping MOA. Following the unsuccessful results obtained from attempted trastuzumab functionalisation with tetrazine-Dox, these studies would begin with the synthesis of an azide-functionalised Dox analogue. It is expected that since such species have been previously reported in the literature the likelihood of them succeeding is greater than their novel tetrazine-functionalised counterparts.[350,382,440] This would then require tetrazine-functionalisation of Criz. However, if these payloads still suffer from issues of poor solubility either longer PEG spacers could be used and/or more hydrophilic payloads. Furthermore, to assess to what extent sterics is preventing reactivity, the click reactions should also be tested on the Fab fragment of trastuzumab. Due to the far smaller size of the Fab fragment (~50 kDa) and single native disulfide,[287,441] these systems are far less hindered and thus have the potential to be more easily modified.

Following the successful generation of a dual-drug ADC, an additional interesting application of this linker platform would be the delivery of two cytotoxins that either interact synergistically or that achieve synthetic lethality. With this aim in mind, it is expected that the modular approach provided by this novel linker platform could provide a means by which payload combinations could be rapidly screened (following initial studies on the free drugs), enabling the identification of a range of dual-drug ADCs with improved activities.

Apart from the formation of the dual-drug ADCs it is also envisaged that this linker could be used to introduce a range of other payloads (e.g. cleavable fluorophores, radiolabels or half-life extending PEG chains) to antibodies and/or antibody fragments to combine different functions as required.

Finally, it is also expected that this platform would have applications outside the field of ADCs, such as for the formation of dual functionalised peptide-drug conjugates (PDCs). Given that peptides have a significantly shorter half-life than biologics,[442] a particularly useful application in this area is the attachment of both a cytotoxin and half-life extending PEG chain. However, other applications including dual warhead incorporation are also envisioned.

7 Experimental

7.1 General Experimental Procedures

Solvents

Except as otherwise indicated, reactions were carried out in oven- or flame-dried glassware under nitrogen or argon with dry, freshly distilled solvents. Tetrahydrofuran was distilled from calcium hydride and $LiAlH_4$ in the presence of triphenyl methane. Diethyl ether was distilled from calcium hydride and $LiAlH_4$. CH_2Cl_2, MeOH, PhMe, MeCN, and hexane were distilled from calcium hydride. All other reagents were used as supplied by commercial sources. Petroleum ether refers to petroleum ether 40–60°C.

Infrared Spectroscopy

Infrared spectra were recorded on a Perkin-Elmer Spectrum One spectrometer with internal referencing as neat films. Absorption maxima (ν_{max}) are reported in wavenumbers (cm^{-1}) and the following abbreviations are used: w, weak; m, medium; s, strong; br, broad.

NMR Spectroscopy

Proton magnetic resonance spectra were recorded at 298 K using either an internal deuterium lock on Bruker DPX (400 MHz; DUL probe), Bruker Avance III HD (400 MHz; Smart probe), Bruker Avance III HD (500 MHz; Smart probe), Bruker Avance III HD (500 MHz; DCH Cryoprobe) or 600 MHz Avance (600 MHz; Smart probe) BBI spectrometers. Whilst all compounds were formed as racemates (unless stated otherwise) stereochemistry is indicated to demonstrate relative relationships between multiple stereocentres. Chemical shifts (δ_H) are quoted in ppm to the nearest 0.01 ppm and are referenced to the residual non-deuterated solvent peak ($CDCl_3$: 7.26, DMSO-d_6: 2.50, CD_3OD: 3.31). Coupling constants (*J*) are reported in Hertz to the nearest 0.5 Hz. Data are reported as follows: chemical shift, integration, multiplicity [br, broad; app, apparent; s, singlet; d, doublet; t, triplet; q, quartet; p, pentet; sept, septet; m, multiplet; or as a combination of these (e.g. app s, dd, dt, etc.)] and coupling constant(s). Carbon magnetic resonance spectra were recorded on Bruker Avance 400 QNP (101 MHz), Bruker DRX-400 (100 MHz), Bruker Avance 500 BB ATM (125 MHz) and Bruker Avance 500 Cryo Ultrashield (125 MHz) spectrometers. Chemical shifts (δ_C) are quoted in ppm to the nearest 0.1 ppm and are referenced to the deuterated solvent ($CDCl_3$: 77.2, DMSO-d_6, 39.5, CD_3OD: 49.0).

Proton assignments are supported by $^{1}H^{1}H$ COSY, $^{1}H^{13}C$ HSQC or $^{1}H^{13}C$ HMBC spectra. Diastereotopic protons are referred to as H_A and H_B. Cis and trans protons are referred to as H_c and H_t, respectively.

Mass Spectrometry

High resolution mass spectrometry (HRMS) measurements were recorded on a Micromass QTOF mass spectrometer or a Waters LCT Premier Time of Flight mass spectrometer. Mass values are quoted within the error limits of ± 5 ppm mass units. ESI refers to the electrospray ionisation technique. LCMS was carried out using a Waters ACQUITY H-Class UPLC with an ESCi Multi- Mode Ionisation Waters SQ Detector 2 spectrometer using MassLynx 4.1 software; ESI refers to the electrospray ionisation technique; LC system: solvent A: 2 mM NH_4OAc in H_2O/MeCN (95:5); solvent B: MeCN; solvent C: 2% formic acid; column: ACQUITY UPLC® CSH C18 (2.1 mm × 50 mm, 1.7 µm, 130 Å) at 40 °C; gradient: 5 – 95 % B with constant 5 % C over 1 min at flow rate of 0.6 mL/min; detector: PDA eλ Detector 220 – 800 nm, interval 1.2 nm.

Analytical high performance liquid chromatography (HPLC)

HPLC analysis was performed on an Agilent 1260 Infinity machine, using a Supelcosil™ ABZ+PLUS column (150 mm × 4.6 mm, 3 µm) with a linear gradient system (solvent A: 0.05% (v/v) TFA in H_2O; solvent B: 0.05% (v/v) TFA in MeCN) over 20 min at a flow rate of 1 mL/min, and UV detection (λ_{max} = 220 – 254 nm).

Miscellaneous

Organic layers were dried over $MgSO_4$, unless otherwise stated. Yields refer to chromatographically and spectroscopically pure compounds. Thin layer chromatography was performed on glass plates coated with 60 F_{254} silica. Plates were visualised using UV light (254 nm) or 1% aq $KMnO_4$. Retention factors (R_f) are quoted to 0.01. Flash chromatography was carried out using slurry-packed Merck 9385 Kieselgel 60 silica gel or Combiflash Rf200 automated chromatography system with Redisep® reverse-phase C18-silica flash columns (20-40 µm). Melting points were obtained using a Büchi Melting Point B-545 melting point apparatus and are uncorrected. All reactions were carried out under an N_2 atmosphere using oven-dried glassware at rt unless otherwise stated.

7.2 Procedures and Analytical Data

General Procedure A

Propargyl bromide (1.0 equiv.) was added to a stirred solution of the diketone (1.0 equiv.) and NaOH (1.0 equiv.) in H_2O (1.06 M). The resultant mixture was stirred at 60 °C for 18 h after which the aqueous layer was extracted with CH_2Cl_2 (3 ×) and the combined organic extracts were washed with brine, then dried and concentrated *in vacuo* to give a crude material.

General Procedure B

$NaBH_4$ (0.5 equiv.) was added to a stirred solution of the α,α-disubstituted ketone (1.0 equiv.) in DME (0.5 M). The resultant mixture was stirred at 60 °C for 24 h before 1 M HCl (aq.) was added. The mixture was diluted with EtOAc, the phases were separated, and the aqueous phase was extracted with EtOAc (3 ×). The combined organic extracts were washed with brine, then dried and concentrated *in vacuo* to give a crude material.

General Procedure C

Imidazole (9.5 equiv.) and *tert*-butyldimethylsilyl chloride (5.0 equiv.) were added to a stirred solution of the alcohol (1.0 equiv.) in DMF (0.1 M) and the resultant mixture was stirred for 24 h at rt. H_2O was added, and the aqueous phase was extracted with petroleum ether (3 ×). The combined organic extracts were dried and concentrated *in vacuo* to give a crude material.

General Procedure D

TBAF (1.0 M in THF, 2 equiv.) was added to a stirred solution of the silyl ether (1 equiv.) in anhydrous THF (0.05 M). The reaction mixture was stirred at rt until TLC showed complete consumption of the starting material. The mixture was concentrated *in vacuo* to give a crude material.

General Procedure E

10% Pd/C (20 mol%) was added to a stirred solution of the benzylamine (1.0 equiv.) in EtOH (0.05 M), and the reaction mixture was stirred under an atmosphere of H_2 at 40 °C for 4 h. The mixture was filtered through a pad of Celite® and concentrated *in vacuo* to give the title compound.

General Procedure F

DCC (1.35 equiv.) was added to a stirred solution of the alcohol (1.0 equiv.), the carboxylic acid (1.35 equiv.), and DMAP (0.1 equiv.) at 0 °C in anhydrous CH_2Cl_2 (0.1 M). The reaction mixture was stirred at rt for 18 h. Then, the precipitate was filtered off and the mixture was concentrated *in vacuo* to give a crude material.

General Procedure G

EDC·HCl (2.0 equiv.) was added to a stirred solution of the amine (2.0 equiv.), the carboxylic acid (1.0 equiv.), Et_3N (2.0 equiv.) and HOBt·H_2O (2.0 equiv.) at 0 °C in anhydrous DMF (0.1 M). The reaction mixture was stirred at rt for 18 h. Then, EtOAc was added, and the organic layer was washed with brine (8 ×). The organic extract was dried and concentrated *in vacuo* to give a crude material.

2-Methyl-2-(prop-2-yn-1-yl)cyclopentane-1,3-dione (3)

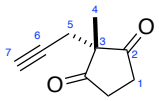

3

According to General Procedure A, propargyl bromide (80 wt. % in toluene, 9.94 mL, 89.2 mmol), 2-methylcyclopentane-1,3-dione, **2**, (10.0 g, 89.2 mmol) and NaOH (3.57 g, 89.2 mmol) gave a crude material. Purification *via* flash column chromatography (EtOAc/hexane, 16:84) gave **3** as an amorphous white solid (11.8 g, 78.5 mmol, 88%). $\mathbf{R_f}$ = 0.25 (EtOAc/hexane, 20:80); **^{1}H NMR** (400 MHz, $CDCl_3$): δ_H 2.90–2.75 (4H, m, C(1)H_2), 2.47 (2H, d, *J* 2.8, C(5)H_2), 1.98 (1H, t, *J* 2.5, C(7)*H*), 1.14 (3H, s, C(4)H_3); **^{13}C NMR** (101 MHz, $CDCl_3$): δ_C 215.0 (*C*(2)), 78.8 (*C*(6)), 70.8 (*C*(7)), 55.1 (*C*(3)), 35.6 (*C*(1)), 24.0 (*C*(5)), 19.1 (*C*(4)); **IR** ν_{max}: 3280 (m, C≡C–H), 1749, 1723 (C=O); These characterisation data are in accordance with that previously reported in the literature.[135]

(2*S,3*S**)-3-Hydroxy-2-methyl-2-(prop-2-yn-1-yl)cyclopentan-1-one (*syn*-1) and (2*S**,3*R**)-3-hydroxy-2-methyl-2-(prop-2-yn-1-yl)cyclopentan-1-one (*anti*-1)**

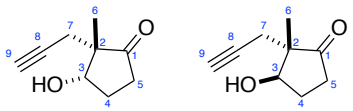

syn-**1** *anti*-**1**

According to General Procedure B, $NaBH_4$ (630 mg, 16.5 mmol) and **3** (5.00 g, 33.3 mmol) gave a crude material (62:38 *dr*). Purification *via* flash column chromatography (EtOAc/hexane, 20:80) gave *syn*-**1** (1.78 g, 11.7 mmol, 35%) and *anti*-**1** (1.16 g, 7.66 mmol, 23%) both as colourless oils.

Data of *syn*-**1**:

$\mathbf{R_f}$ = 0.19 (EtOAc/hexane, 20:80); **^{1}H NMR** (400 MHz, $CDCl_3$): δ_H 4.27 (1H, dd, *J* 4.6, 1.9, C(3)*H*), 2.56–2.32 (4H, m, C(5)H_AH_B, C(7)H_AH_B), 2.23 (1H, dddd, *J* 13.9, 10.3, 9.2, 4.5, C(4)H_AH_B), 2.09–1.99 (2H, m, C(4)H_AH_B, C(9)*H*), 1.96 (1H, br s, O*H*), 1.12 (3H, s, C(6)H_3); **^{13}C NMR** (101 MHz, $CDCl_3$): δ_C 219.7 (*C*(1)), 81.2 (*C*(8)), 77.0 (*C*(3)), 70.8 (*C*(9)), 53.3 (*C*(2)), 34.3 (*C*(5)), 27.6 (*C*(4)), 21.1 (*C*(7)), 20.1 (*C*(6)); **IR** ν_{max}: 3435 (br, O–H), 3289 (m, C≡C–H), 1729 (s, C=O).

Data of *anti*-**1**:

$\mathbf{R_f}$ = 0.17 (EtOAc/hexane, 20:80); **^{1}H NMR** (400 MHz, $CDCl_3$): δ_H 4.41 (1H, ddd, *J* 9.5, 6.4, 3.5, C(3)*H*), 2.59–2.24 (4H, m, C(5)H_AH_B, C(7)H_AH_B), 2.22–2.09 (2H, m, C(4)H_AH_B), 2.05 (1H, t, *J* 2.7, C(9)*H*), 1.93–1.79 (1H, m, C(4)H_AH_B), 1.06 (3H, s, C(6)H_3); **^{13}C NMR** (101 MHz, $CDCl_3$): δ_C 218.4 (*C*(1)), 80.8

(*C*(8)), 75.7 (*C*(3)), 71.3 (*C*(9)), 51.8 (*C*(2)), 35.0 (*C*(5)), 27.3 (*C*(4)), 25.1 (*C*(7)), 15.2 (*C*(6)); **IR** ν_{max}: 3439 (br, O–H), 3287 (m, C≡C–H), 1731 (s, C=O).

These characterisation data are in accordance with that previously reported in the literature.[135]

(1*S,2*S**)-2-Methyl-3-oxo-2-(prop-2-yn-1-yl)cyclopentyl hex-5-enoate (5)**

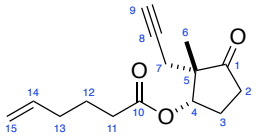

5

According to General Procedure F, *syn*-**1** (100 mg, 0.658 mmol), 5-hexenoic acid (106 µL, 0.891 mmol), DMAP (8.0 mg, 0.066 mmol) and DCC (184 mg, 0.891 mmol) gave a crude material. Purification *via* flash column chromatography (EtOAc/petroleum ether, 12:88) gave **5** as a colourless oil (149 mg, 0.600 mmol, 91%). $\mathbf{R}_f$ = 0.20 (EtOAc/petroleum ether, 8:92); **^{1}H NMR** (400 MHz, $CDCl_3$): δ_H 5.77 (1H, ddt, *J* 17.0, 10.2, 6.7, C(14)*H*), 5.25 (1H, dd, *J* 4.6, 1.8, C(4)*H*), 5.08–4.95 (2H, m, C(15)H_2), 2.48–2.36 (4H, m, C(7)H_AH_B), C(2)H_2), 2.36–2.22 (3H, m, C(3)H_AH_B, C(11)H_2), 2.08 (3H, m, C(3)H_AH_B, C(13)H_2), 1.94 (1H, t, *J* 2.6, C(9)*H*), 1.73 (2H, p, *J* 7.4, C(12)H_2), 1.19 (3H, s, C(6)H_3); **^{13}C NMR** (100 MHz, $CDCl_3$): δ_C 218.2 (*C*(1)), 172.6 (*C*(10)), 137.7 (*C*(14)), 115.7 (*C*(15)), 80.3 (*C*(8)), 78.2 (*C*(4)), 70.4 (*C*(9)), 51.9 (*C*(5)), 34.1 (*C*(2)), 33.8 (*C*(11)), 33.1 (*C*(13)), 25.7 (*C*(3)), 24.2 (*C*(12)), 21.3 (*C*(7)), 20.1 (*C*(6)); **IR** ν_{max}: 1733 (m, 2 × C=O), 1641 (m, C=C); **HRMS** (ESI): $[M+H]^+$ calcd. for $C_{15}H_{21}O_3^+$: 249.1485, found: 249.1487.

(9a*S,12a*S**,*E*)-9a-methyl-8-methylene-4,5,8,9,9a,11,12,12a-octahydro-2*H*-cyclopenta[*b*][1]oxacycloundecine-2,10(3*H*)-dione (6)**

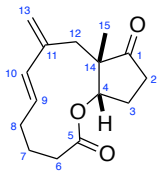

6

Grubbs 2nd generation catalyst (30.0 mg, 35.3 µmol) was added to a stirred solution of **5** (138 mg, 0.556 mmol) in PhMe (70 mL). The reaction mixture was stirred under an ethylene atmosphere at reflux for 4 h, then degassed with N_2 and stirred for a further 18 h. The resultant mixture was filtered through Celite® then concentrated *in vacuo*. Purification *via* flash column chromatography (EtOAc/petroleum ether, 10:90) gave **6** as a white amorphous solid (117 mg, 0.472 mmol, 85%). $\boldsymbol{R_f}$ = 0.24 (EtOAc/ petroleum ether, 10:90); **^{1}H NMR** (400 MHz, $CDCl_3$): δ_H 5.91 (1H, d, *J* 15.8, C(10)*H*), 5.63 (1H, dt, *J* 15.6, 7.7, C(9)*H*), 5.17–4.99 (2H, m, C(4)*H*, (14)H_AH_B), 4.84 (1H, d, *J* 2.0, C(14)H_AH_B), 2.50–2.09

(8H, m, C(2)H_2, C(3)H_AH_B, C(6)H_2, C(8)H_AH_B, C(12)H_2), 2.08–1.80 (4H, m, C(3)H_AH_B, C(7)H_2, C(8)H_AH_B), 1.10 (3H, s, C(15)H_3); **^{13}C NMR** (101 MHz, $CDCl_3$): δ_C 220.2 (*C*(1)), 175.1 (*C*(5)), 142.4 (*C*(11)), 136.5 (*C*(10)), 128.1 (*C*(9)), 116.3 (*C*(14)), 78.4 (*C*(4)), 53.3 (*C*(13)), 35.4 (*C*(12)), 34.4 (*C*(2)), 33.8 (*C*(6)), 31.4 (*C*(8)), 26.2 (*C*(3)), 24.8 (*C*(7)), 22.0 (*C*(15)); **IR** ν_{max}: 1729 (m, 2 × C=O); **HRMS** (ESI): $[M+H]^+$ calcd. for $C_{15}H_{21}O_3^+$: 249.1485, found: 249.1491.

(1*S,2*S**)-2-methyl-3-oxo-2-(prop-2-yn-1-yl)cyclopentyl 4-azidobutanoate (10)**

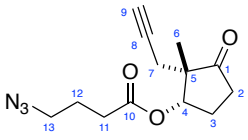

10

According to General Procedure F, *syn*-**1** (100 mg, 0.658 mmol), 4-azidobutanoic acid (115 mg, 0.891 mmol), DMAP (8.0 mg, 0.066 mmol) and DCC (184 mg, 0.891 mmol) gave a crude material. Purification *via* flash column chromatography (EtOAc/hexane, 12:88) gave **10** as a colourless oil (145 mg, 0.551 mmol, 84%). $\mathbf{R_f}$ = 0.11 (EtOAc/hexane, 8:92); **^{1}H NMR** (400 MHz, $CDCl_3$): δ_H 5.27 (1H, dd, *J* 4.6, 1.9, C(4)*H*), 3.36 (2H, t, *J* 6.7, C(13)H_2), 2.42 (4H, m, C(2)H_2, C(7)H_AH_B), 2.38 (2H, d, *J* 2.7, C(11)H_AH_B), 2.29 (1H, m, C(3)H_AH_B), 2.12–2.03 (1H, m, C(3)H_AH_B), 1.96–1.87 (3H, m, C(9)*H,* C(12)H_2), 1.19 (3H, s, C(6)H_3); **^{13}C NMR** (100 MHz, $CDCl_3$): δ_C 217.9 (*C*(1)), 171.8 (*C*(10)), 80.3 (*C*(8)), 78.6 (*C*(4)), 70.4 (*C*(9)), 51.9 (*C*(5)), 50.7 (*C*(13)), 34.1 (*C*(2)), 31.4 (*C*(11)), 25.7 (*C*(3)), 24.4 (*C*(12)), 21.4 (*C*(7)), 20.2 (*C*(6)); **IR** ν_{max}: 2099 (s, N=N=N), 1732 (m, 2 × C=O); **HRMS** (ESI): $[M+H]^+$ calcd. for $C_{13}H_{18}N_3O_3^+$: 264.1343, found: 264.1343.

(9a*S,12a*S**)-12a-Methyl-6,7,10,11,12a,13-hexahydrocyclopenta[*b*][1,2,3]triazolo[5,1-*e*][1,6]oxazecine-8,12(5*H*,9a*H*)-dione (11)**

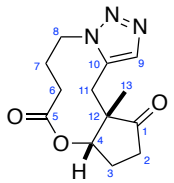

11

$[RuCp^*Cl]_4$ (37.1 mg, 34.1 µmol) was added to a degassed solution of **10** (82.0 mg, 0.313 mmol) in PhMe (120 mL). The resultant solution heated under refluxed for 18 h before being cooled to rt. The crude mixture was filtered through Celite® and concentrated *in vacuo*. Purification *via* flash column chromatography (MeOH, 97:3) gave **11** as an amorphous yellow solid (71.6 mg, 0.272 mmol, 87%). $\mathbf{R_f}$

= 0.24 (EtOAc/hexane, 90:10); **^{1}H NMR** (400 MHz, $CDCl_3$):[p] δ_H 7.47 (1H, s, C(9)*H*), 4.87 (1H, app s, C(4)*H*), 4.27 (2H, app s, C(8)H_AH_B), 3.01 (1H, app s, C(11)H_AH_B), 2.73 (1H, d, *J* 13.9, C(11)H_AH_B), 2.64–2.32 (5H, m, C(6)H_2, C(7)H_2, C(3)H_AH_B), 2.30–2.14 (2H, m, C(2)H_AH_B, C(3)H_AH_B), 2.02–1.91 (1H, m, C(2)H_AH_B), 1.26 (3H, s, C(13)H_3); **^{13}C NMR** (101 MHz, $CDCl_3$):[q] δ_C 218.4 (*C*(1)), 170.7 (*C*(5)), 134.3 (*C*(10)), 132.8 (*C*(9)), 78.4 (*C*(4)), 52.9 (*C*(12)), 45.7 (*C*(8)), 34.4 (*C*(2)), 29.7 (*C*(11)), 29.3 (*C*(6)), 26.5 (*C*(3)), 25.8 (*C*(7)), 22.0 (*C*(13)); **IR** ν_{max}: 1736 (m, 2 × C=O); **HRMS** (ESI): $[M+H]^+$ calcd. for $C_{13}H_{18}N_3O_3^+$: 264.1343, found 264.1345.

Ethyl (*E*)-3-(((1*S,2*S**)-2-methyl-3-oxo-2-(prop-2-yn-1-yl)cyclopentyl)oxy)acrylate (16)**

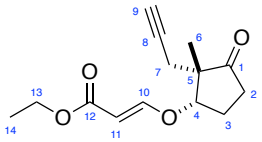

16

Ethyl propiolate (133 µL, 1.32 mmol) and NMM (145 µL, 1.32 mmol) were added to a stirred solution of *syn*-**1** (100 mg, 0.658 mmol) in CH_2Cl_2 (2.0 mL). The mixture was stirred at rt for 2 h then concentrated *in vacuo*. Purification *via* flash column chromatography (EtOAc/hexane, 18:82) gave **16** as a colourless oil (153 mg, 0.612 mmol, 93%). $\mathbf{R_f}$ = 0.10 (EtOAc/hexane, 10:90); **^{1}H NMR** (400 MHz, $CDCl_3$): δ_H 7.54 (1H, d, *J* 12.5, C(10)*H*), 5.29 (1H, d, *J* 12.5, C(11)*H*), 4.43 (1H, t, *J* 2.8, C(4)*H*), 4.17 (2H, q, *J* 7.1, C(13)H_2), 2.50–2.35 (4H, m, C(2)H_2, C(7)H_2), 2.29–2.17 (2H, m, C(3)H_2), 1.98 (1H, t, *J* 2.7, C(9)*H*), 1.27 (3H, t, *J* 7.1, C(14)H_3), 1.19 (3H, s, C(6)H_3); **^{13}C NMR** (100 MHz, $CDCl_3$): δ_C 217.1 (*C*(1)), 167.8 (*C*(12)), 161.0 (*C*(10)), 98.6 (*C*(11)), 86.1 (*C*(4)), 80.3 (*C*(8)), 70.6 (*C*(9)), 60.1 (*C*(13)), 52.8 (*C*(5)), 33.7 (*C*(2)), 24.7 (*C*(3)), 20.8 (*C*(7)), 20.0 (*C*(6)), 14.5 (*C*(14)); **IR** ν_{max}: 1743 (s, C=O ketone), 1705 (s, C=O ester), 1643 (m, C=C), 1622 (m, C=C); **HRMS** (ESI): $[M+H]^+$ calcd. for $C_{14}H_{19}O_4^+$: 251.1278, found: 251.1279.

[p] Peaks in ^{1}H-NMR spectrum broad and split due to the presence of residual metal catalyst.
[q] Peaks in ^{13}C-NMR spectrum broad and split due to the presence of residual metal catalyst.

Ethyl 2-((2*R,4a*S**,7a*S**)-4a-methyl-3-methylene-5-oxooctahydrocyclopenta[*b*]pyran-2-yl)acetate (18)**

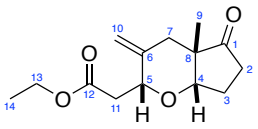

18

A degassed solution of Bu_3SnH (78.0 µL, 0.290 mmol) and AIBN (5.9 mg, 36.0 µmol) in PhMe (0.70 mL) was added dropwise over 5 h to a degassed solution of **16** (36.0 mg, 0.144 mmol) in PhMe (2.20 mL) at 80 °C. The reaction mixture was stirred for a further 12 h at 80 °C, then concentrated *in vacuo*. *p*-Toluenesulfonic acid monohydrate (14.6 mg, 76.5 µmol) was added to a stirred solution of the crude material in CH_2Cl_2 (0.30 mL) at rt. The mixture was stirred for 1.5 h, then poured into satd. $NaHCO_3$ (5 mL) and extracted with CH_2Cl_2 (3 × 5 mL). The combined organic extracts were dried and concentrated *in vacuo*. Purification *via* flash column chromatography (EtOAc/hexane, 10:90) gave **18** as a colourless oil (21.4 mg, 85.0 µmol, 59%). $\mathbf{R_f}$ = 0.18 (EtOAc/hexane, 10:90); **^{1}H NMR** (400 MHz, $CDCl_3$): δ_H 4.87 (1H, d, *J* 1.7, C(10)H_AH_B), 4.74 (1H, d, *J* 1.7, C(10)H_AH_B), 4.26 (1H, dd, *J* 8.2, 5.2, C(5)*H*), 4.16 (2H, m, C(13)H_2), 3.95 (1H, d, *J* 4.0, C(4)*H*), 2.70 (1H, d, *J* 14.0, C(7)H_AH_B), 2.67–2.48 (2H, m, C(11)H_2), 2.47–2.24 (2H, m, C(2)H_AH_B), 2.20–1.96 (3H, m, C(3)H_AH_B), C(7)H_AH_B), 1.26 (3H, t, *J* 7.1, C(14)H_3), 0.96 (3H, s, C(9)H_3); **^{13}C NMR** (100 MHz, $CDCl_3$): δ_C 220.0 (*C*(1)), 171.4 (*C*(12)), 142.8 (*C*(6)), 108.9 (*C*(10)), 83.1 (*C*(4)), 74.2 (*C*(5)), 60.7 (*C*(13)), 51.5 (*C*(8)), 38.2 (*C*(11)), 37.8 (*C*(7)), 34.0 (*C*(2)), 25.7 (*C*(3)), 21.2 (*C*(9)), 14.3 (*C*(14)); **IR** ν_{max}: 1738 (br, 2 ×C=O); **HRMS** (ESI): $[M+H]^+$ calcd. for $C_{14}H_{20}O_4Na^+$: 275.1254, found: 275.1249.

(4a*S,7a*S**)-4a-Methyl-4a,6,7,7a-tetrahydrocyclopenta[b]pyran-5(4H)-one (19)**

19

$CpRu(PPh_3)_2Cl$ (57.0 mg, 78.5 µmol) and PPh_3 (42.1 mg, 0.161 mmol) were added to a degassed solution of *N*-hydroxy succinimide (45.0 mg, 0.391 mmol), NBu_4PF_6 (38.7 mg, 0.100 mmol), $NaHCO_3$ (33.1 mg, 0.394 mmol) and *syn*-**1** (120 mg, 0.788 mmol) in DMF (8.0 mL). The reaction was degassed once more and then sealed in a vial. The resultant mixture was stirred at 80 °C for 18 h. Further $CpRu(PPh_3)_2Cl$ (57.0 mg, 78.5 µmol) was added and the reaction was stirred at 80 °C for 38 h. Upon completion, the reaction was filtered through Celite® and partitioned between EtOAc (20 mL) and brine (20 mL). The organic layer was separated, dried, and concentrated *in vacuo*. Purification *via* flash column chromatography (EtOAc/hexane, 10:90) gave **19** as a colourless oil (78.1 mg, 0.513 mmol,

65%). $\mathbf{R}_f$ = 0.30 (EtOAc/hexane, 10:90); **^{1}H NMR** (400 MHz, $CDCl_3$): δ_H 6.32 (1H, dt, *J* 6.3, 2.1 C(5)*H*), 4.62 (1H, ddd, *J* 6.3, 4.3, 3.2, C(6)*H*), 4.17 (1H, t, *J* 3.7, C(4)*H*), 2.48–2.30 (3H, m, C(2)H_AH_B, C(7)H_AH_B), 2.28–2.19 (1H, m, C(3)H_AH_B), 2.13–2.06 (1H, m, C(3)H_AH_B), 1.82–1.77 (1H, m, C(7)H_AH_B), 1.07 (3H, s, C(9)H_3); **^{13}C NMR** (101 MHz, $CDCl_3$): δ_C 218.0 (*C*(1)), 142.6 (*C*(5)), 98.3 (*C*(6)), 79.7 (*C*(4), 47.4 (*C*(8)), 32.9 (*C*(2)), 25.8 (*C*(3)), 24.6 (*C*(7)), 21.7 (*C*(9)); **IR** ν_{max}: 1742 (s, C=O), 1659 (m, C=C); **HRMS** (ESI): $[M+H]^+$ calcd. for $C_9H_{13}O_2^+$: 153.0910, found: 153.0910.

(2*S,3a*S**,6a*S**)-2-Methoxy-2,3a-dimethylhexahydro-4*H*-cyclopenta[*b*]furan-4-one (21a) and (2*R**,3a*S**,6a*S**)-2-methoxy-2,3a-dimethylhexahydro-4*H*-cyclopenta[*b*]furan-4-one (21b)**

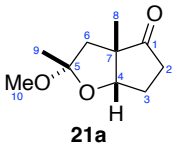

21a

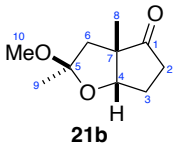

21b

$[Ir(cod)Cl]_2$ (4.0 mg, 6.0 µmol) was added to a stirred solution of *syn*-**1** (33.4 mg, 0.220 mmol) in MeOH (0.6 mL). The resultant mixture was stirred at rt for 4 h. Upon completion, the reaction was filtered through Celite® and concentrated *in vacuo* to give a mixture of diastereomers (22:78 *dr*). Purification *via* flash column chromatography (EtOAc/hexane, 10:90) gave **21a** (7.4 mg, 40 µmol, 18%) and **21b** (23.4 mg, 0.127 mmol, 58%) both as colourless oils.

Data of **21a**:

$\mathbf{R}_f$ = 0.24 (EtOAc/hexane, 10:90); **^{1}H NMR** (400 MHz, $CDCl_3$): 4.35 (1H, app d, *J* 4.3, C(4)*H*), 3.21 (3H, s, C(10)H_3), 2.54–2.42 (1H, m, C(2)H_AH_B), 2.37–2.27 (1H, m, C(2)H_AH_B), 2.25–2.13 (2H, m, C(3)H_AH_B, C(6)H_AH_B), 2.04–1.94 (2H, m, C(3)H_AH_B, C(6)H_AH_B), 1.33 (3H, s, C(9)H_3), 1.15 (3H, s, C(8)H_3); **^{13}C NMR** (126 MHz, $CDCl_3$): δ_C 222.9 (*C*(1)), 108.3 (*C*(5)), 86.6 (*C*(4)), 56.5 (*C*(7)), 50.8 (*C*(6)), 48.7 (*C*(10)), 34.6 (*C*(2)), 23.9 (*C*(3)), 21.5 (*C*(9)), 18.6 (*C*(8)); **IR** ν_{max}: 1738 (s, C=O); **HRMS** (ESI): $[M+Na]^+$ calcd. for $C_{10}H_{16}O_3Na^+$: 207.0992, found: 207.0993.

Data of **21b**:

$\mathbf{R}_f$ = 0.13 (EtOAc/hexane, 10:90); **^{1}H NMR** (400 MHz, $CDCl_3$): δ_H 4.47 (1H, app d, *J* 5.1, C(4)*H*), 3.13 (3H, s, C(10)H_3), 2.59–2.41 (2H, m, C(2)H_AH_B, C(6)H_AH_B), 2.37–2.23 (1H, m, C(2)H_AH_B), 2.20–2.01 (2H, m, C(3)H_AH_B), 1.79 (1H, d, *J* 12.7, C(6)H_AH_B), 1.39 (3H, s, C(9)H_3), 1.12 (3H, s, C(8)H_3); **^{13}C NMR** (126 MHz, $CDCl_3$): δ_C 221.9 (*C*(1)), 107.7 (*C*(5)), 88.8 (*C*(4)), 55.5 (*C*(7)), 50.8 (*C*(6)), 48.4 (*C*(10)), 35.3 (*C*(2)), 26.2 (*C*(3)), 20.9 (*C*(9)), 19.4 (*C*(8)); **IR** ν_{max}: 1739 (s, C=O); **HRMS** (ESI): $[M+Na]^+$ calcd. for $C_{10}H_{16}O_3Na^+$: 207.0992, found: 207.0998.

(1*R,2*S**)-2-Methyl-3-oxo-2-(prop-2-yn-1-yl)cyclopentane-1-carbonitrile (*anti*-23)**

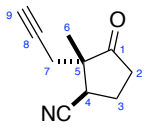

anti-**23**

MsCl (76.4 μL, 0.987 mmol) was added to a stirred solution of *anti*-**1** (50.2 mg, 0.329 mmol) in pyridine (2.25 mL) at 0 °C, and the resultant mixture was stirred at rt for 24 h. After addition of 1 M HCl (20 mL, aq.), the aqueous layer was extracted with EtOAc (3 × 20 mL). The combined organic extracts were dried and concentrated *in vacuo* to give the crude mesylate, which was used in the next step without further purification.

KCN (41.7 mg, 0.640 mmol) was added to a stirred solution of the crude material in DMSO (3.0 mL) at rt, and the resultant mixture was stirred for 5 days. After addition of brine (20 mL), the aqueous layer was extracted with EtOAc (3 × 20 mL), and the combined organic extracts were dried and concentrated *in vacuo*. Purification *via* flash column chromatography (EtOAc/hexane, 15:85) gave *anti*-**23** as an amorphous white solid (38.2 mg, 0.237 mmol, 72%). $\mathbf{R}_f$ = 0.16 (EtOAc/hexane, 15:85); **^{1}H NMR** (400 MHz, $CDCl_3$): δ_H 3.47 (1H, dd, *J* 11.0, 6.8, C(4)*H*), 2.63–2.52 (2H, m, C(2)H_AH_B, C(7)H_AH_B), 2.52–2.32 (1H, m, C(3)H_AH_B), 2.36 (1H, dd, *J* 17.0, 2.7, C(7)H_AH_B), 2.29–2.09 (2H, m, C(2)H_AH_B, C(3)H_AH_B), 2.07 (1H, t, *J* 2.7, C(9)*H*), 1.22 (3H, s, C(6)H_3); **^{13}C NMR** (101 MHz, $CDCl_3$): δ_C 214.7 (*C*(1)), 119.0 (*C*N), 79.1 (*C*(8)), 72.4 (*C*(9)), 50.7 (*C*(5)), 36.2 (*C*(2)), 34.9 (*C*(4)), 25.7 (*C*(7)), 23.5 (*C*(3)), 19.5 (*C*(6)); **IR** ν_{max}: 3291 (C≡C–H), 2242 (m, C≡N), 1746 (s, C=O); **HRMS** (ESI): $[M+H]^+$ calcd. for $C_{10}H_{12}NO^+$: 162.0913, found: 162.0914.

(1*S,2*S**)-2-Methyl-3-oxo-2-(prop-2-yn-1-yl)cyclopentane-1-carbonitrile (*syn*-23)**

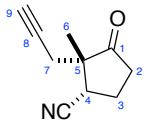

syn-**23**

MsCl (95.2 μL, 1.23 mmol) was added to a stirred solution of *syn*-**1** (63.0 mg, 0.414 mmol) in pyridine (2.80 mL) at 0 °C, and the resultant mixture was stirred at rt for 24 h. After addition of 1 M HCl (20 mL, aq.), the aqueous layer was extracted with EtOAc (3 × 20 mL). The combined organic extracts were dried and concentrated *in vacuo* to give the crude mesylate, which was used in the next step without further purification.

KCN (49.2 mg, 0.770 mmol) was added to a stirred solution of the crude material in DMSO (3.5 mL) at rt, and the resultant mixture was stirred for 5 days. After addition of brine (20 mL), the aqueous layer

was extracted with EtOAc (3 × 20 mL), and the combined organic extracts were dried and concentrated *in vacuo*. Purification *via* flash column chromatography (EtOAc/hexane, 20:80) gave *syn*-**23** as an amorphous white solid (40.0 mg, 0.248 mmol, 60%). $\mathbf{R_f}$ = 0.19 (EtOAc/hexane, 20:80); **^{1}H NMR** (400 MHz, $CDCl_3$): δ_H 3.10–3.05 (1H, m, C(4)*H*), 2.65–2.27 (6H, m, C(2)H_AH_B, C(3)H_AH_B, C(7)H_AH_B), 2.09 (1H, t, *J* 2.7, C(9)*H*), 1.24 (3H, s, C(6)H_3); **^{13}C NMR** (101 MHz, $CDCl_3$): δ_C 215.2 (*C*(1)), 119.1 (*C*N), 78.9 (*C*(8)), 71.9 (*C*(9)), 50.6 (*C*(5)), 37.9 (*C*(2)), 35.5 (*C*(4)), 24.9 (*C*(7)), 23.6 (*C*(3)), 21.6 (*C*(6)); **IR** ν_{max}: 3291 (s, C≡C–H), 2242 (m, C≡N), 1744 (s, C=O); **HRMS** (ESI): $[M+H]^+$ calcd. for $C_{10}H_{12}NO^+$: 162.0913, found: 162.0914.

Ethyl (5a*S,8a*S**)-5a-methyl-6-oxo-5,5a,6,7,8,8a-hexahydropentaleno[1,2-b]pyridine-2-carboxylate (27)**

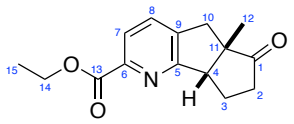

27

$CpCo(CO)_2$ (8.30 µL, 62.0 µmol) was added to a degassed solution of *syn*-**1** (20.0 mg, 124 µmol) and ethyl propiolate (62.8 µL, 620 µmol) in PhMe (1.0 mL) in a vial. The vial was sealed and the reaction mixture was stirred at 110 °C for 18 h. Upon completion, the reaction mixture was filtered through Celite®, washed with EtOAc (20 mL) and the filtrate concentrated *in vacuo*. Purification *via* flash column chromatography (EtOAc/hexane, 30:70) gave **27** as a yellow oil (3.1 mg, 12 µmol, 10%). $\mathbf{R_f}$ = 0.21 (EtOAc/hexane, 35:75); **^{1}H NMR** (400 MHz, $CDCl_3$): δ_H 7.94 (1H, d, *J* 7.9, C(7)*H*), 7.55 (1H, d, *J* 7.9, C(8)*H*), 4.56–4.40 (2H, m, C(14)H_2), 3.66 (1H, d, *J* 6.7, C(4)*H*), 3.29 (1H, d, *J* 17.3, C(10)H_AH_B), 2.88 (1H, d, *J* 17.3, C(10)H_AH_B), 2.71–2.58 (1H, m, C(3)H_AH_B), 2.49–2.30 (2H, m, C(3)H_AH_B, C(2)H_AH_B), 2.00–1.85 (1H, m, C(2)H_AH_B), 1.44 (3H, t, *J* 7.1, C(15)H_3), 1.34 (3H, s, C(12)H_3); **^{13}C NMR** (101 MHz, $CDCl_3$): δ_C 223.7 (*C*(1)), 165.7 (*C*(13)), 165.5 (*C*(5)), 148.0 (*C*(6)), 140.1 (*C*(9)), 132.9 (*C*(8)), 124.1 (*C*(7)), 62.0 (*C*(14)), 54.8 (*C*(11)), 54.4 (*C*(4)), 40.6 (*C*(10)), 36.6 (*C*(2)), 23.9 (*C*(3)), 21.2 (*C*(12)), 14.5 (*C*(15)); **IR** ν_{max}: 1735 (m, C=O), 1447, 1410 (C=C); **HRMS** (ESI): $[M+H]^+$ calcd. for $C_{15}H_{18}NO_3^+$: 260.1281, found: 260.1280.

(2*S,3*S**)-3-((*tert*-Butyldimethylsilyl)oxy)-2-methyl-2-(prop-2-yn-1-yl)cyclopentan-1-one (*syn*-28)**

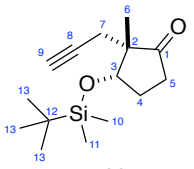

syn-**28**

According to General Procedure C, imidazole (811 mg, 11.9 mmol), *tert*-butyldimethylsilyl chloride (939 mg, 6.23 mmol) and *syn*-**1** (190 mg, 1.25 mmol) gave a crude material. Purification *via* flash

column chromatography (EtOAc/hexane, 10:90) gave *syn*-**28** as a colourless oil (327 mg, 1.23 mmol, 98%). $\mathbf{R}_f$ = 0.42 (EtOAc/hexane, 10:90); **^{1}H NMR** (400 MHz, $CDCl_3$): δ_H 4.15 (1H, m, C(3)*H*), 2.49–2.30 (4H, m, C(5)H_AH_B, C(7)H_AH_B), 2.17 (1H, m, C(4)H_AH_B), 1.95 (2H, m, C(4)H_AH_B, C(9)*H*), 1.09 (3H, s, C(6)H_3), 0.87 (9H, s, C(13)H_3), 0.12 (3H, s, C(10/11)H_3) 0.11 (3H, s, C(10/11)H_3); **^{13}C NMR** (101 MHz, $CDCl_3$): δ_C 219.5 (*C*(1)), 81.6 (*C*(8)), 76.8 (*C*(3)), 70.1 (*C*(9)), 53.7 (*C*(2)), 33.6 (*C*(5)), 28.1 (*C*(4)), 25.7 (*C*(13)), 20.6 (*C*(7)), 19.2 (*C*(6)), 18.0 (*C*(12)), –4.5 (*C*(10/11)), –5.0 (*C*(10/11)); **IR** ν_{max}: 3307 (s, C≡C–H), 2930 (m, C–H), 1744 (s, C=O); **HRMS** (ESI): $[M+H]^+$ calcd. for $C_{15}H_{27}O_2Si^+$: 267.1775, found: 267.1775.

(2S*,3R*)-3-((*tert*-Butyldimethylsilyl)oxy)-2-methyl-2-(prop-2-yn-1-yl)cyclopentan-1-one (*anti*-28)

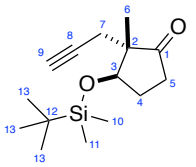

anti-**28**

According to General Procedure C, imidazole (427 mg, 6.23 mmol), *tert*-butyldimethylsilyl chloride (494 mg, 3.28 mmol) and *anti*-**1** (100 mg, 0.657 mmol) gave a crude material. Purification *via* flash column chromatography (EtOAc/hexane, 10:90) gave *anti*-**28** as a colourless oil (167 mg, 0.627 mmol, 95%). $\mathbf{R}_f$ = 0.42 (EtOAc/hexane, 10:90); **^{1}H NMR** (400 MHz, $CDCl_3$): δ_H 4.50–4.42 (1H, m, C(3)*H*), 2.53–2.35 (2H, m, C(5)H_AH_B, C(7)H_AH_B), 2.18–2.06 (3H, m, C(4)H_AH_B, C(5)H_AH_B, C(7)H_AH_B), 1.95 (1H, t, *J* 2.6, C(9)*H*), 1.88–1.73 (1H, m, C(4)H_AH_B), 0.96 (3H, s, C(6)H_3), 0.89 (9H, s, C(13)H_3), 0.10 (6H, 2 × s, C(10)H_3, C(11)H_3); **^{13}C NMR** (101 MHz, $CDCl_3$): δ_C 218.6 (*C*(1)), 80.6 (*C*(8)), 74.4 (*C*(3)), 70.7 (*C*(9)), 53.1 (*C*(2)), 35.6 (*C*(5)), 28.5 (*C*(4)), 25.9 (*C*(13)), 24.5 (*C*(7)), 18.1 (*C*(12)), 16.2 (*C*(6)), –4.3 (*C*(10/11)), –4.8 (*C*(10/11)); **IR** ν_{max}: 3309 (s, C≡C–H), 2930 (s, C–H), 1747 (s, C=O); **HRMS** (ESI): $[M+H]^+$ calcd. for $C_{15}H_{27}O_2Si^+$: 267.1775, found: 267.1775.

***O*-Mesitylsulfonylhydroxylamine (29)**

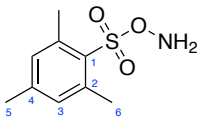

29

Et_3N (1.51 mL, 10.8 mmol) was added to a stirred solution of ethyl *N*-hydroxyacetamidate (1.18 g, 11.4 mmol) in DMF (6.0 mL) and the solution was cooled to 0 °C. 2-Mesitylensulfonylchloride (2.49 g, 11.4 mmol) was added in small portions and the mixture was stirred vigorously for 30 min at 0 °C. The reaction was then diluted with Et_2O (100 mL) and washed with H_2O (5 × 50 mL). The organic extract

was dried and concentrated *in vacuo*. Ethyl-*O*-(mesitylensulfonyl)acetohydroxamate (2.20 g) was obtained and used in the next step without further purification.

Perchloric acid (70%, 0.950 mL, 22.5 µmol) was added dropwise to a stirred solution of ethyl-*O*-(mesitylsulfonyl)-acetohydroxamate (2.20 g, 7.72 mmol) in 1,4-dioxane (3.0 mL) at 0 °C. The reaction was stirred for 10 min, then transferred onto ice water (100 mL). The aqueous layer was extracted with Et_2O (3 × 30 mL) and the combined organic extracts were washed with brine (2 × 50 mL) then dried/neutralized with K_2CO_3. After filtration, the solution was concentrated to a volume less than 10 mL and poured into 20 mL of ice-cold petroleum ether. After crystallisation, **29** was obtained (805 mg, 4.04 mmol, 37%) as a white crystalline solid. $\mathbf{R}_f$ = 0.32 (hexane/EtOAc, 80:20); **m**.**p**. 93 °C [Lit. 90–91 °C];[443] **^{1}H NMR** (400 MHz, $CDCl_3$): δ_H 7.00 (2H, s, C(3)*H*), 2.65 (6H, s, C(6)H_3), 2.33 (3H, s, C(5)H_3); **^{13}C NMR** (101 MHz, $CDCl_3$): δ_C 143.9 (*C*(1)), 141.1 (*C*(2)), 131.9 (*C*(3)), 129.3 (*C*(4)), 22.9 (*C*(6)), 21.2 (*C*(5)); **IR** ν_{max}: 3469, 3198 (m, N–H stretch), 2980 (br, Ar C–H), 1603 (s, N–H bend), 1170 (s, S=O). These characterisation data are in accordance with that previously reported in the literature.[443]

(5*R,6*S**)-5-((*tert*-Butyldimethylsilyl)oxy)-6-methyl-6-(prop-2-yn-1-yl)piperidin-2-one (31)**

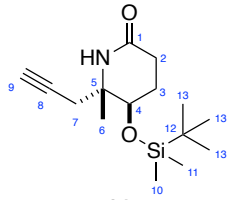

31

MSH**, 29**, (636 mg, 2.95 mmol) was added to a stirred solution of *anti*-**28** (432 mg, 1.62 mmol) in CH_2Cl_2 (5.0 mL) at 0 °C. After 20 min the temperature was raised to rt and the solution was stirred for a further 18 h. $BF_3{\cdot}Et_2O$ (0.63 mL, 5.10 mmol) was then added, and the mixture was stirred at rt for 1 h. The reaction mixture was diluted with CH_2Cl_2 (50 mL) and washed with saturated aqueous $NaHCO_3$ (2 × 50 mL). The aqueous layers were re-extracted with Et_2O (3 × 50 mL), and the combined organic extracts were dried and concentrated *in vacuo*. Purification *via* flash column chromatography (EtOAc/hexane, 50:50) gave **31** as a white crystalline solid (300 mg, 1.07 mmol, 66%); $\mathbf{R}_f$ = 0.20 (EtOAc/hexane, 50:50); **m**.**p**. 125 °C; **^{1}H NMR** (400 MHz, $CDCl_3$): δ_H 5.95 (1H, br s, N*H*), 3.84 (1H, dd, *J* 7.8, 4.9, C(4)*H*), 2.58–2.26 (4H, m, C(2)H_AH_B, C(7)H_AH_B), 2.11 (1H, t, *J* 2.7, C(9)*H*), 1.90 (2H, td, *J* 8.0, 5.1, C(3)H_AH_B), 1.28 (3H, s, C(6)H_3), 0.89 (9H, s, C(13)H_3), 0.09 (6H, s, C(10)H_3, C(11)H_3); **^{13}C NMR** (101 MHz, $CDCl_3$): δ_C 171.0 (*C*(1)), 79.3 (*C*(8)), 72.6 (*C*(9)), 70.7 (*C*(4)), 58.0 (*C*(5)), 31.7 (*C*(7)), 28.3 (*C*(2)), 25.8 (*C*(3), *C*(13)), 22.3 (*C*(6)), 18.1 (*C*(12)), –4.1 (*C*(10/11)), –4.9 (*C*(10/11)); **IR** ν_{max}: 3313 (s, C≡C–H), 1660 (s, C=O); **HRMS** (ESI): $[M+H]^+$ calcd. for $C_{15}H_{28}NO_2Si^+$: 282.1884, found: 282.1879.

(5*R,6*S**)-5-Hydroxy-6-methyl-6-(prop-2-yn-1-yl)piperidin-2-one (32)**

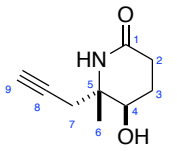

32

According to General Procedure D, **31** (30.0 mg, 0.107 mmol) and TBAF (1.0 M in THF, 0.168 mL, 0.168 mmol) gave a crude material. Purification *via* flash column chromatography (MeOH/EtOAc, 5:95) gave **32** as a colourless oil (16.7 mg, 0.10 mmol, 94%). R_f = 0.21 (MeOH/EtOAc, 5:95); **^{1}H NMR** (400 MHz, $CDCl_3$): δ_H 5.95 (1H, br s, N*H*), 3.88 (1H, td, *J* 6.6, 3.4, C(4)*H*), 2.59–2.36 (4H, m, C(7)H_2, C(2)H_2), 2.29 (1H, br s, O*H*), 2.14 (1H, t, *J* 2.7, C(9)*H*), 2.06–1.91 (2H, m, C(3)H_2), 1.34 (3H, s, C(6)H_3); **^{13}C NMR** (101 MHz, $CDCl_3$): δ_c 171.0 (*C*(1)), 79.1 (*C*(8)), 72.8 (*C*(9)), 70.4 (*C*(4)), 57.5 (*C*(5)), 31.8 (*C*(7)), 28.3 (*C*(2)), 25.6 (*C*(3)), 21.7 (*C*(6)); **IR** ν_{max}: 3305 (m, N–H), 1638 (s, C=O); **HRMS** (ESI): $[M+H]^+$ calcd. for $C_9H_{14}NO_2^+$: 168.1019, found 168.1018.

(8R*,8aS*)-8-((*tert*-Butyldimethylsilyl)oxy)-8a-methyl-6,7,8,8a-tetrahydroindolizin-5(1H)-one (33)

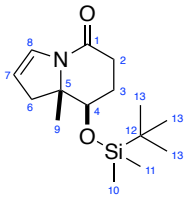

33

$InCl_3$ (101 mg, 0.457 mmol) was introduced into a 10 mL flask and heated with a heat gun (150 °C) under vacuum for 2 min. After being allowed to cool to room temperature, THF (1.2 mL) was added. The mixture was stirred at rt for 10 min and then cooled to −78 °C. DIBAL-H (1.0 M in hexane, 0.44 mL, 0.44 mmol) was added dropwise and the mixture was stirred at −78 °C for 40 min. Lactam **31** (83.0 mg, 0.295 mmol) was then added, followed by Et_3B (1.0 M in THF, 0.17 mL, 0.17 mmol) and the mixture was stirred at −78 °C for 4 h. A solution of iodine (449 mg, 1.78 mmol) in THF (0.75 mL) was then added. After 40 min, the mixture was poured onto satd. $NaHCO_3$ (5 mL). $Na_2S_2O_3$ was added under stirring until complete decolouration and the aqueous layer was extracted with EtOAc (5 × 10 mL). The combined organic extracts were washed with brine (50 mL), dried and concentrated *in vacuo*.

Cs_2CO_3 (115 mg, 0.35 mmol), CuI (23.0 mg, 0.121 mmol) and *N*,*N*′-dimethylethyl-1,2-diamine (25.0 µL, 0.232 mmol) were added to a stirred solution of the crude product in PhMe (2.0 mL) and the mixture was heated to 85 °C for 3 h. H_2O (10 mL) was added, and the reaction extracted with CH_2Cl_2 (5 × 10 mL). The combined organic extracts were washed with brine (10 mL), dried and concentrated *in vacuo*.

Purification *via* flash column chromatography (EtOAc/petroleum ether, 40:60) gave **33** as a white amorphous solid (53.2 mg, 0.189 mmol, 64%). $\mathbf{R}_f$ = 0.32 (EtOAc/petroleum ether, 50:50); **^{1}H NMR** (400 MHz, $CDCl_3$): δ_H 6.81 (1H, t, *J* 4.1, C(8)*H*), 5.19 (1H, dt, *J* 4.8, 2.6, C(7)*H*), 3.85 (1H, t, *J* 8.4, C(4)*H*), 2.70–2.51 (2H, m, C(2)H_AH_B, C(6)H_AH_B), 2.51–2.32 (2H, m, C(2)H_AH_B, C(6)H_AH_B), 1.87 (2H, td, *J* 7.9, 7.1, 5.3, C(3)H_AH_B), 1.23 (3H, s, C(9)H_3), 0.87 (9H, s, C(13)H_3), 0.06 (6H, 2 × s, C(10)H_3, C(11)H_3); **^{13}C NMR** (101 MHz, $CDCl_3$): δ_C 165.5 (*C*(1)), 128.0 (*C*(8)), 110.3 (*C*(7)), 73.4 (*C*(4)), 65.3 (*C*(5)), 44.8 (*C*(6)), 29.1 (*C*(2)), 26.5 (*C*(3)), 25.7 (*C*(13)), 19.5 (*C*(9)), 18.0 (*C*(12)), –3.9 (*C*(10/11)), –4.8 (*C*(10/11)); **IR** ν_{max}: 1664 (s, C=O), 1629 (s, C=C); **HRMS** (ESI): $[M+H]^+$ calcd. for $C_{15}H_{28}NO_2Si^+$: 282.1884, found: 282.1882.

(8*R,8a*S**)-8-Hydroxy-8a-methyl-6,7,8,8a-tetrahydroindolizin-5(1H)-one (34)**

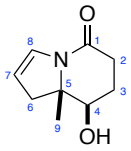

34

According to General Procedure D, **33** (53.2 mg, 0.189 mmol) and TBAF (1.0 M in THF, 0.27 mL, 0.27 mmol) gave a crude material. Purification *via* flash column chromatography (MeOH/EtOAc, 5:95) gave **34** as a colourless oil (25.1 mg, 0.150 mmol, 79%). $\boldsymbol{R_f}$ = 0.36 (MeOH/EtOAc, 5:95); **^{1}H NMR** (400 MHz, $CDCl_3$): δ_H 6.80 (1H, ddd, *J* 4.4, 2.9, 1.4, C(8)*H*), 5.28–5.21 (1H, m, C(7)*H*), 3.88 (1H, dd, *J* 11.6, 5.4, C(4)*H*), 2.78 (1H, dt, *J* 16.3, 2.5, C(6)H_AH_B), 2.58 (1H, ddd, *J* 18.9, 9.3, 2.3, C(2)H_AH_B), 2.52–2.41 (2H, m, C(2)H_AH_B, C(6)H_AH_B), 2.04–1.83 (2H, m, C(3)H_AH_B), 1.25 (3H, s, C(9)H_3); **^{13}C NMR** (101 MHz, $CDCl_3$): δ_C 165.8 (*C*(1)), 127.8 (*C*(8)), 111.0 (*C*(7)), 72.4 (*C*(4)), 65.1 (*C*(5)), 44.3 (*C*(6)), 29.1 (*C*(2)), 25.8 (*C*(3)), 19.2 (*C*(9)); **IR** ν_{max}: 3341 (br, O–H bend), 1603 (m, C=O), 1440 (m, O–H bend); **HRMS** (ESI): $[M+H]^+$ calcd. for $C_9H_{14}NO_2^+$: 168.1019, found: 168.1025.

(5*R,6*S**)-1-Allyl-5-((*tert*-butyldimethylsilyl)oxy)-6-methyl-6-(prop-2-yn-1-yl)piperidin-2-one (35)**

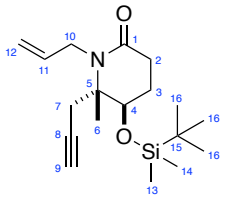

35

NaH (60% in mineral oil, 33.0 mg, 0.825 mmol) was added to a stirred solution of lactam **31** (190 mg, 0.676 mmol) in anhydrous DMF (7.0 mL) at 0 °C. The mixture was stirred at rt for 30 min, then allyl bromide (0.126 mL, 1.46 mmol) was added and the reaction mixture was stirred for another 2 h. The mixture was diluted with EtOAc (200 mL), washed with H_2O (2 × 150 mL) and brine (1 × 150 mL), and

the organic extract was dried and concentrated *in vacuo*. Purification *via* flash column chromatography (EtOAc/petroleum ether, 20:80) gave **35** as a colourless oil (165 mg, 0.514 mmol, 76%). R_f = 0.19 (EtOAc/petroleum ether, 80:20); **^{1}H NMR** (400 MHz, $CDCl_3$): δ_H 5.88 (1H, dddd, *J* 17.3, 10.3, 5.9, 5.0, C(11)H_2), 5.19–5.05 (2H, m, C(12)H_AH_B), 4.26 (1H, ddt, *J* 16.1, 5.1, 1.8, C(10)*H*), 4.09 (1H, dd, *J* 8.2, 3.0, C(4)*H*), 3.77 (1H, ddt, *J* 16.1, 5.9, 1.6, C(10)*H*), 2.66–2.55 (2H, m, C(7)H_AH_B, C(2)H_AH_B), 2.48–2.34 (2H, m, C(7)H_AH_B, C(2)H_AH_B), 2.06 (1H, t, *J* 2.7, C(9)*H*), 1.95 (1H, dtd, *J* 13.8, 6.9, 3.0, C(3)H_AH_B), 1.83 (1H, dddd, *J* 13.7, 8.2, 7.3, 6.7, C(3)H_AH_B), 1.29 (3H, s, C(6)H_3), 0.90 (9H, s, C(16)H_3), 0.11 (6H, 2 × s, C(13)H_3, C(14)H_3); **^{13}C NMR** (151 MHz, $CDCl_3$): δ_C 170.0 (*C*(1)), 135.7 (*C*(11)), 115.8 (*C*(12)), 79.8 (*C*(8)), 72.3 (*C*(9)), 70.3 (*C*(4)), 63.6 (*C*(5)), 45.0 (*C*(10)), 28.8 (*C*(7)), 28.7 (*C*(2)), 25.9 (*C*(16)), 24.9 (*C*(3)), 21.7 (*C*(6)), 18.1 (*C*(15)), –4.1 (*C*(13/14)), –4.9 (*C*(13/14)); **IR** ν_{max}: 3314 (s, C≡C–H), 1639 (m, C=O); **HRMS** (ESI): $[M+H]^+$ calcd. for $C_{18}H_{32}NO_2Si^+$: 322.2197, found 322.2198.

(1*R,9a*S**)-1-Hydroxy-9a-methyl-8-vinyl-1,2,3,6,9,9a-hexahydro-4H-quinolizin-4-one (36)**

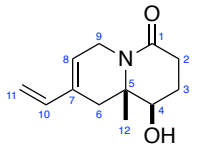

36

Grubbs 2nd generation catalyst (12.0 mg, 14.2 µmol) was added to a stirred solution of lactam **35** (45.6 mg, 0.142 mmol) in anhydrous CH_2Cl_2 (25.0 mL). The reaction mixture was stirred under an ethylene atmosphere at rt for 4 h then concentrated *in vacuo*. TBAF (1.0 M in THF, 0.25 mL, 0.25 mmol) was added to a solution of the crude product in anhydrous THF (3.0 mL). The solution was stirred at rt for 2 h, then concentrated *in vacuo*. Purification *via* flash column chromatography (MeOH/EtOAc, 2:98) gave **36** as a white amorphous solid (20.3 mg, 98.0 µmol, 69%). R_f = 0.39 (MeOH/EtOAc, 10:90); **^{1}H NMR** (400 MHz, CD_3OD): δ_H 6.49 (1H, dd, *J* 17.5, 10.8, C(10)*H*), 5.79 (1H, q, *J* 3.2, C(8)*H*), 5.22 (1H, d, *J* 17.5, C(11)H_AH_B), 5.06 (1H, d, *J* 10.8, C(11)H_AH_B), 4.70 (1H, dt, *J* 20.5, 3.6, C(9)H_AH_B), 3.83 (1H, t, *J* 6.7, C(4)*H*), 3.68–3.57 (1H, m, C(9)H_AH_B), 2.65–2.53 (2H, m, C(2)H_AH_B, C(6)H_AH_B), 2.53–2.42 (1H, m, C(2)H_AH_B), 2.21 (1H, dd, *J* 16.7, 3.1, C(6)H_AH_B), 2.07–1.87 (2H, m, C(3)H_2), 1.28 (3H, s, C(12)H_3); **^{13}C NMR** (101 MHz, CD_3OD): δ_C 171.8 (*C*(1)), 139.6 (*C*(10)), 133.7 (*C*(7)), 124.1 (*C*(8)), 112.4 (*C*(11)), 73.9 (*C*(4)), 59.8 (*C*(5)), 41.5 (*C*(9)), 36.7 (*C*(6)), 30.3 (*C*(2)), 25.6 (*C*(3)), 18.6 (*C*(12)); **IR** ν_{max}: 3370 (br, O–H), 1611 (s, C=O), 1600 (s, C=C), 1408 (s, O–H); **HRMS** (ESI): $[M+H]^+$ calcd. for $C_{12}H_{18}NO_2^+$ 208.1332, found 208.1328.

(3a*R,9*R**,9a*S**)-9-Hydroxy-9a-methyl-3a,4,8,9,9a,10-hexahydrocyclopenta[b]quinolizine-2,6(3H,7H)-dione (37)**

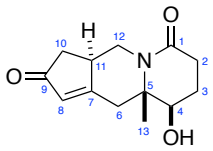

37

Lactam **35** (38.0 mg, 0.118 mmol) in CH_2Cl_2 (1.0 mL) was added to a stirred solution of $Co_2(CO)_8$ (50.5 mg, 0.147 mmol) in CH_2Cl_2 (4.25 mL) at rt. The reaction mixture was stirred at rt for 2 h, then 4-methylmorpholine *N*-oxide (138 mg, 1.18 mmol) was added portion-wise and the mixture was stirred for a further 18 h. The violet Co precipitate was removed by filtration through a short plug of silica (washed with CH_2Cl_2/MeOH, 19:1) and the filtrate was concentrated *in vacuo*. TBAF (1.0 M in THF, 0.21 mL, 0.21 mmol) was added to a solution of the crude material in anhydrous THF (5.4 mL). The solution was stirred at rt for 2 h, then concentrated *in vacuo*. Purification *via* flash column chromatography (MeOH/EtOAc, 5:95) gave **37** as a colourless oil (21.1 mg, 89.8 µmol, 76%). R_f = 0.34 (MeOH/EtOAc, 10:90); **^{1}H NMR** (400 MHz, CD_3OD): δ_H 6.02 (1H, d, *J* 1.8, C(8)*H*), 5.05 (1H, dd, *J* 13.2, 6.6, C(12)H_AH_B), 3.89 (1H, app p, *J* 7.5, C(4)*H*), 3.03 (1H, d, *J* 13.5, C(6)H_AH_B), 2.78 (1H, dt, *J* 13.0, 6.7, C(11)*H*), 2.73–2.37 (5H, m, C(2)H_AH_B, C(6)H_AH_B, C(10)H_AH_B, C(12)H_AH_B), 2.10–2.02 (1H, m, C(10)H_AH_B), 1.98 (2H, tt, *J* 8.5, 4.7, C(3)H_2), 1.24 (3H, s, C(13)H_3); **^{13}C NMR** (101 MHz, CD_3OD): δ_C 207.6 (*C*(9)), 177.5 (*C*(7)), 169.1 (*C*(1)), 130.1 (*C*(8)), 74.0 (*C*(4)), 61.2 (*C*(5)), 43.9 (*C*(12)), 41.9 (*C*(6)), 40.2 (*C*(11)), 39.0 (*C*(10)), 29.8 (*C*(2)), 25.5 (*C*(3)), 17.8 (*C*(13)); **IR** ν_{max}: 3361 (br, O–H), 1702 (s, C=O), 1673 (s, C=O), 1614 (s, C=C), 1407 (s. O–H); **HRMS** (ESI): $[M+H]^+$ calcd. for $C_{13}H_{18}NO_3^+$: 236.1281, found 236.1283.

(4*R,5*S**)-4-((*tert*-Butyldimethylsilyl)oxy)-5-methyl-5-(prop-2-yn-1-yl)cyclopent-2-en-1-one (45)**

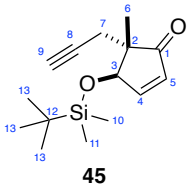

45

IBX (45% wt., 460 mg, 0.739 mmol) was added to a stirred solution of *anti*-**28** (100 mg, 0.376 mmol) in a mixture of fluorobenzene (1.70 mL) and DMSO (0.85 mL), and the resultant solution was stirred at 65 °C for 24 h. The reaction mixture was cooled to rt and diluted with Et_2O (100 mL) and then washed successively with satd. $NaHCO_3$, H_2O, and brine. The organic extract was then dried and concentrated *in vacuo*. Purification *via* flash column chromatography (EtOAc/hexane, 1:99) gave **45** as a colourless oil (45.1 mg, 0.171 mmol, 45%). R_f = 0.15 (EtOAc/hexane, 1:99); **^{1}H NMR** (400 MHz,

$CDCl_3$): δ_H 7.37 (1H, dd, *J* 5.9, 2.1, C(4)*H*), 6.17 (1H dd, *J* 5.9, 1.7, C(5)*H*), 4.94 (1H, app t, *J* 1.7, C(3)*H*), 2.48 (1H, dd, *J* 16.9, 2.7, C(7)H_AH_B), 2.30 (1H, dd, *J* 16.9, 2.7, C(7)H_AH_B), 1.92 (1H, t, *J* 2.7, C(9)*H*), 1.04 (3H, s, C(6)H_3), 0.93 (9H, s, C(13)H_3), 0.17 (3H, s, C(10/11)H_3), 0.16 (3H, s, C(10/11)H_3); **^{13}C NMR** (100 MHz, $CDCl_3$): δ_C 209.5 (*C*(1)), 162.8 (*C*(4)), 132.2 (*C*(5)), 80.6 (*C*(8)), 76.6 (*C*(3)), 70.6 (*C*(9)), 51.9 (*C*(2)), 25.9 (*C*(13)), 25.2 (*C*(7)), 19.6 (*C*(6)), 18.2 (*C*(12)), –4.4 (*C*(10/11)), –4.6 (*C*(10/11)); **IR** ν_{max}: 1717 (s, C=O); **HRMS** (ESI): $[M+H]^+$ calcd. for $C_{15}H_{24}O_2NaSi^+$: 287.1438, found: 287.1424.

Ethyl 2-(5-(((1*S,2*S**)-2-((*tert*-butyldimethylsilyl)oxy)-1-methyl-5-oxocyclopentyl)methyl)-1H-1,2,3-triazol-1-yl)acetate (57)**

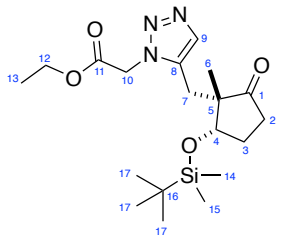

57

$[Cp^*RuCl]_4$ (59.0 mg, 0.0543 mmol) was added to a degassed solution of *syn*-**28** (130 mg, 0.488 mmol) and ethyl 2-azidoacetate (114 mg, 0.883 mmol) in PhMe (8.0 mL) under argon. The reaction mixture was stirred at rt for 18 h before being concentrated *in vacuo*. Purification *via* flash column chromatography (EtOAc/hexane, 40:60) gave **57** as a yellow oil (160 mg, 0.404 mmol, 82%). $\mathbf{R_f}$ = 0.26 (EtOAc/hexane, 40:60); **^{1}H NMR** (400 MHz, $CDCl_3$): δ_H 7.52 (1H, s, C(9)*H*), 5.19 (1H, d, *J* 17.7, C(10)H_AH_B), 5.12 (1H, d, *J* 17.7, C(10)H_AH_B), 4.27–4.16 (3H, m, C(12)H_2, C(4)*H*), 2.79 (2H, app s, C(7)H_AH_B), 2.41–2.22 (2H, m, C(2)H_AH_B), 2.15 (1H, m, C(3)H_AH_B), 1.78 (1H, m, C(3)H_AH_B), 1.27 (3H, t, *J* 7.1, C(13)H_3), 0.98 (3H, s, C(6)H_3), 0.84 (9H, s, C(17)H_3), 0.11 (3H, s, C(14/15)H_3), 0.03 (3H, s, C(14/15)H_3); **^{13}C NMR** (101 MHz, $CDCl_3$): δ_C 219.6 (*C*(1)), 166.6 (*C*(11)), 134.9 (*C*(8)), 133.7 (*C*(9)), 78.1 (*C*(4)), 62.5 (*C*(12)), 53.7 (*C*(5)), 49.1 (*C*(10)), 33.9 (*C*(2)), 28.4 (*C*(3)), 25.9 (*C*(17)), 24.6 (*C*(7)), 20.0 (*C*(6)), 18.2 (*C*(16)), 14.3 (*C*(13)), –4.0 (*C*(14/15)), –4.8 (*C*(14/15)); **IR** ν_{max}: 1743 (s, C=O); **HRMS** (ESI): $[M+H]^+$ calcd. for $C_{19}H_{34}N_3O_4Si^+$: 396.2313, found: 396.2313.

Ethyl 2-(5-(((1*S,2*S**)-2-hydroxy-1-methyl-5-oxocyclopentyl)methyl)-1H-1,2,3-triazol-1-yl)acetate (58)**

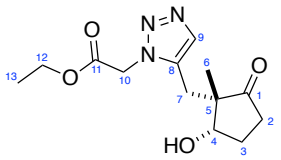

58

TBAF (3.3 mL, 1 M in THF, 3.3 mmol) was added to a stirred solution of **57** (125 mg, 0.316 mmol) and AcOH (0.33 mL, 5.7 mmol) in THF (12.5 mL) under argon. The reaction mixture was stirred at rt for 5 days, then concentrated *in vacuo*. The residue was treated with brine (4 mL) and satd. $NaHCO_3$ to adjust the pH to 7. The aqueous layer was extracted with Et_2O (3 × 10 mL), and the combined extracts were dried and concentrated *in vacuo*. Purification *via* flash column chromatography (EtOAc/hexane, 30:70) gave **58** as a yellow oil (67.0 mg, 0.238 mmol, 75%). $\mathbf{R_f}$ = 0.09 (EtOAc/hexane, 40:60); **^{1}H NMR** (400 MHz, $CDCl_3$): δ_H 7.55 (1H, s, C(9)*H*), 5.30 (1H, d, *J* 17.6, C(10)H_AH_B), 5.15 (1H, d, *J* 17.6, C(10)H_AH_B), 4.22 (2H, q, *J* 7.1, C(12)H_2), 4.06 (1H, dd, *J* 4.1, 1.7, C(4)*H*), 2.93 (1H, d, *J* 15.6, C(7)H_AH_B), 2.79 (1H, d, *J* 15.6, C(7)H_AH_B), 2.50–2.34 (2H, m, C(2)H_AH_B), 2.27–2.13 (1H, m, C(3)H_AH_B), 1.97–1.88 (1H, m, C(3)H_AH_B), 1.26 (3H, t, *J* 7.1, C(13)H_3), 1.00 (3H, s, C(6)H_3); **^{13}C NMR** (101 MHz, $CDCl_3$): δ_C 220.1 (*C*(1)), 166.9 (*C*(11)), 135.4 (*C*(8)), 133.5 (*C*(9)), 75.5 (*C*(4)), 62.3 (*C*(12)), 53.7 (*C*(5)), 49.0 (*C*(10)), 33.4 (*C*(2)), 28.3 (*C*(3)), 24.2 (*C*(7)), 19.8 (*C*(6)), 14.0 (*C*(13)); **IR** ν_{max}: 3338 (br, O–H), 1741 (s, C=O); **HRMS** (ESI): $[M+H]^+$ calcd. for $C_{13}H_{20}N_3O_4^+$: 282.1448, found: 282.1445.

(2*S,3*R**)-3-((*tert*-Butyldimethylsilyl)oxy)-2-methyl-2-((3-phenylisoxazol-4-yl)methyl)cyclopentan-1-one (60)**

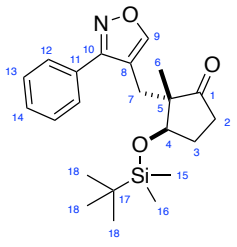

60

Cp*Ru(COD)Cl (10.8 mg, 28.5 µmol) and NEt_3 (72.2 µL, 0.518 mmol) were added to a degassed solution of α-chlorobenzaldoxime (200 mg, 1.29 mmol) and *anti*-**28** (69.0 mg, 0.259 mmol) in DCE (5.0 mL). The mixture was stirred at 80 °C for 24 h before being concentrated *in vacuo*. Purification *via* flash column chromatography (EtOAc/hexane, 7:93) gave **60** (76.6 mg, 0.199 mmol, 77%) as a colourless oil. $\mathbf{R_f}$ = 0.28 (EtOAc/hexane, 10:90); **^{1}H NMR** (400 MHz, $CDCl_3$): δ_H 8.29 (1H, s, C(9)*H*), 7.56–7.50 (2H, m,

C(12)*H*), 7.50–7.46 (3H, m, C(13)*H*, C(14)*H*), 3.87 (1H, t, *J* 5.8, C(4)*H*), 2.69 (1H, d, *J* 15.1, C(7)H_AH_B), 2.58 (1H, d, *J* 15.1, C(7)H_AH_B), 2.39 (1H, ddd, *J* 18.8, 9.6, 5.7, C(2)H_AH_B), 1.98–1.80 (2H, m, C(2)H_AH_B, C(3)H_AH_B), 1.68 (1H, dddd, *J* 12.9, 9.6, 7.2, 5.8, C(3)H_AH_B), 0.90 (3H, s, C(6)H_3), 0.75 (9H, s, C(18)H_3), –0.08 (3H, s, C(15/16)H_3), –0.20 (3H, s, C(15/16)H_3); **^{13}C NMR** (101 MHz, $CDCl_3$): δ_C 220.4 (*C*(1)), 162.7 (*C*(10)), 157.7 (*C*(9)), 129.6 (*C*(13/14)), 129.1 (C(11)), 129.0 (*C*(13/14)), 128.9 (*C*(12)), 113.6 (*C*(8)), 75.3 (*C*(4)), 54.4 (*C*(5)), 35.1 (*C*(2)), 28.4 (*C*(3)), 27.0 (*C*(7)), 25.7 (*C*(18)), 18.0 (*C*(12)), 16.3 (*C*(6)), –4.3 (*C*(15/16)), –5.1 (*C*(15/16)); **IR** ν_{max}: 3619 (br, O–H), 1739 (s, C=O); **HRMS** (ESI): $[M+H]^+$ calcd. for $C_{22}H_{32}O_3NSi^+$: 386.2146, found: 386.2154.

(2*S,3*R**)-3-Hydroxy-2-methyl-2-((3-phenylisoxazol-4-yl)methyl)cyclopentan-1-one (61)**

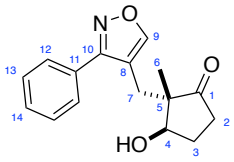

61

TBAF (1.0 M in THF, 2.0 mL, 2.0 mmol) was added to a stirred solution of **60** (77.0 mg, 0.200 mmol) and AcOH (0.20 mL) in THF (7.8 mL) under argon. The reaction mixture was stirred at rt for 5 days, then concentrated *in vacuo*. The residue was treated with brine (4 mL) and satd. $NaHCO_3$ to adjust the pH to 7. The aqueous layer was extracted with Et_2O (3 × 10 mL), and the combined extracts were dried and concentrated *in vacuo*. Purification *via* flash column chromatography (EtOAc/petroleum ether, 45:55) gave **61** as a yellow oil (43.4 mg, 0.160 mmol, 80%). $\mathbf{R_f}$ = 0.24 (EtOAc/petroleum ether, 50:50); **^{1}H NMR** (400 MHz, $CDCl_3$): δ_H 8.22 (1H, s, C(9)*H*), 7.58 (2H, dd, *J* 6.7, 3.0, C(12)*H*), 7.53–7.43 (3H, m, C(14)*H*, C(13)*H*,), 3.82 (1H, dd, *J* 8.8, 6.5, C(4)*H*), 2.86 (1H, d, *J* 5.1, C(7)H_AH_B), 2.65 (1H, d, *J* 15.1, C(7)H_AH_B), 2.40 (1H, ddd, *J* 19.2, 9.3, 2.7, C(2)H_AH_B), 2.00 (1H, dddd, *J* 11.9, 9.0, 6.3, 2.6, C(3)H_AH_B), 1.89 (1H, dt, *J* 19.0, 9.3, C(2)H_AH_B), 1.71 (1H, dq, *J* 12.0, 9.2, C(3)H_AH_B), 1.37 (1H, br s, O*H*), 0.93 (3H, s, C(6)H_3); **^{13}C NMR** (101 MHz, $CDCl_3$): δ_C 219.2 (*C*(1)), 162.7 (*C*(10)), 158.0 (*C*(9)), 129.9 (*C*(13/14)), 129.2 (*C*(13/14)), 129.0 (*C*(11)), 128.8 (*C*(12)), 113.8 (*C*(8)), 73.4 (*C*(4)), 54.3 (*C*(5)), 35.5 (*C*(2)), 27.2 (*C*(3)), 26.3 (*C*(7)), 16.0 (*C*(6)); **IR** ν_{max}: 3422 (br, O–H), 1732 (s, C=O); **HRMS** (ESI): $[M+H]^+$ calcd. for $C_{16}H_{18}NO_3^+$: 272.1281, found: 272.1281.

2-Methyl-2-(prop-2-yn-1-yl)cyclohexane-1,3-dione (63)

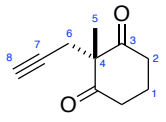

63

According to General Procedure A, propargyl bromide (80 wt. % in toluene, 5.76 mL, 53.5 mmol), 2-methylcyclohexane-1,3-dione, **62**, (6.75 g, 53.5 mmol) and NaOH (2.14 g, 53.5 mmol) gave a crude material. Purification *via* flash column chromatography (EtOAc/hexane, 16:84) gave **63** as a yellow oil (6.14 g, 37.4 mmol, 70%). $\mathbf{R_f}$ **=** 0.27 (EtOAc/hexane, 20:80); **^{1}H NMR** (400 MHz, $CDCl_3$): δ_H 2.73–2.52 (6H, m, C(2)H_2, C(6)H_2), 2.02–1.80 (3H, m, C(1)H_2 C(8)H), 1.24 (3H, s, C(5)H_3); **^{13}C NMR** (101 MHz, $CDCl_3$): δ_C 208.8 (*C*(3)), 80.4 (*C*(7)), 70.5 (*C*(8)), 64.0 (*C*(4)), 38.1 (*C*(2)), 24.3 (*C*(6)), 22.3 (*C*(1)), 17.2 (*C*(7)); **IR** ν_{max}: 3276 (m, C≡C–H), 1728, 1694 (C=O). These characterisation data are in accordance with that previously reported in the literature.[135]

(2*S,3*S**)-3-Hydroxy-2-methyl-2-(prop-2-yn-1-yl)cyclohexan-1-one (*syn*-64) and (2*S**,3*R**)-3-hydroxy-2-methyl-2-(prop-2-yn-1-yl)cyclohexan-1-one (*anti*-64)**

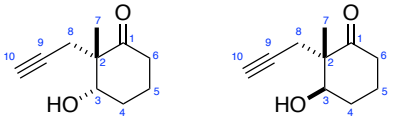

syn-**64** *anti*-**64**

According to General Procedure B, $NaBH_4$ (680 mg, 18.0 mmol) and **63** (5.88 g, 35.8 mmol) gave a crude material (57:43 *dr*). Purification *via* flash column chromatography (EtOAc/hexane, 20:80) gave *syn*-**64** (2.26 g, 13.6 mmol, 38%) and *anti*-**64** (1.84 g, 11.1 mmol, 31%) both as colourless oils.

Data of *syn*-**64**:

$\mathbf{R_f}$ = 0.19 (EtOAc/hexane, 20:80); **^{1}H NMR** (400 MHz, $CDCl_3$): δ_H 4.19 (1H, m, C(3)H), 2.69 (1H, dd, *J* 17.3, 2.7, C(8)H_AH_B), 2.59–2.41 (2H, m, C(6)H_AH_B, C(8)H_AH_B), 2.37–2.29 (1H, m, C(6)H_AH_B), 2.15–2.02 (2H, m, C(4)H_AH_B, C(5)H_AH_B), 2.01 (1H, t, *J* 2.7, C(10)H), 1.94 (1H, d, *J* 4.0, OH), 1.92–1.76 (2H, m, C(4)H_AH_B, C(5)H_AH_B), 1.27 (3H, s, C(7)H_3); **^{13}C NMR** (101 MHz, $CDCl_3$): δ_C 213.1 (*C*(1)), 81.2 (*C*(9)), 75.1 (*C*(3)), 71.9 (*C*(10)), 52.5 (*C*(2)), 37.8 (*C*(6)), 28.2 (*C*(4)), 23.0 (*C*(8)), 21.3 (*C*(7)), 20.7 (*C*(5)); **IR** ν_{max}: 3505 (br, O–H), 3393 (s, C≡C–H), 1696 (s, C=O).

Data of *anti*-**64**:

$\mathbf{R_f}$ = 0.16 (EtOAc/hexane, 20:80); **^{1}H NMR** (400 MHz, $CDCl_3$): δ_H 4.07 (1H, dd, *J* 10.3, 3.8, C(3)H), 2.60 (1H, d, *J* 16.8, C(8)H_AH_B), 2.52–2.41 (2H, m, C(6)H_AH_B, C(8)H_AH_B), 2.33–2.26 (2H, m, OH, C(6)H_AH_B),

2.07–1.91 (3H, m, C(4)H_AH_B, C(5)H_AH_B, C(10)H), 1.91–1.79 (1H, m, C(4)H_AH_B), 1.63–1.50 (1H, m, C(5)H_AH_B), 1.24 (3H, s, C(7)H_3); **^{13}C NMR** (101 MHz, $CDCl_3$): δ_C 211.9 (*C*(1)), 81.7 (*C*(9)), 74.7 (*C*(3)), 71.4 (*C*(10)), 54.4 (*C*(2)), 37.2 (*C*(6)), 29.2 (*C*(4)), 24.9 (*C*(8)), 20.2 (*C*(5)), 17.2 (*C*(7)); **IR** ν_{max}: 3448 (br, O–H), 3289 (s, C≡C–H), 1702 (s, C=O).

These characterisation data are in accordance with that previously reported in the literature.[135]

(1*S,2*S**)-2-Methyl-3-oxo-2-(prop-2-yn-1-yl)cyclohexyl hex-5-enoate (65)**

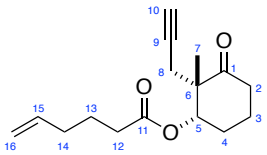

65

According to General Procedure F, *syn*-**64** (109 mg, 0.658 mmol), 5-hexenoic acid (106 µL, 0.891 mmol), DMAP (8.0 mg, 0.066 mmol) and DCC (184 mg, 0.891 mmol) gave a crude material. Purification *via* flash column chromatography (EtOAc/petroleum ether, 12:88) gave **65** as a colourless oil (164 mg, 0.625 mmol, 95%). $\mathbf{R_f}$ = 0.20 (EtOAc/petroleum ether, 8:92); **^{1}H NMR** (400 MHz, $CDCl_3$): δ_H 5.76 (1H, ddt, *J* 17.0, 10.2, 6.7, C(15)*H*), 5.25 (1H, t, *J* 3.4, C(5)*H*), 5.07–4.94 (2H, m, C(16)H_2), 2.63–2.22 (6H, m, C(2)H_2, C(8)H_AH_B, C(12)H_2), 2.12–1.98 (4H, m, C(14)H_2, C(4)H_AH_B), 1.96 (1H, t, *J* 2.7, C(10)*H*), 1.93–1.84 (2H, m, C(3)H_2), 1.78–1.63 (2H, m, C(13)H_2), 1.33 (3H, s, C(7)H_3); **^{13}C NMR** (100 MHz, $CDCl_3$): δ_C 211.9 (*C*(1)), 172.4 (*C*(11)), 137.7 (*C*(15)), 115.7 (*C*(16)), 80.1 (*C*(9)), 77.2 (*C*(5)), 71.4 (*C*(10)), 50.9 (*C*(6)), 37.6 (*C*(2)), 33.8 (*C*(12)), 33.1 (*C*(14)), 25.2 (*C*(4)), 24.2 (*C*(13)), 23.3 (*C*(8)), 21.3 (*C*(7)), 20.9 (*C*(3)); **IR** ν_{max}: 1733 (s, C=O), 1710 (s, C=O), 1640 (m, C=C); **HRMS** (ESI): $[M+H]^+$ calcd. for $C_{16}H_{23}O_3^+$: 263.1642, found: 263.1643.

(1*S,2*S**)-2-Methyl-3-oxo-2-(prop-2-yn-1-yl)cyclohexyl 4-azidobutanoate (66)**

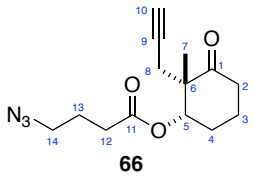

66

According to General Procedure F, *syn*-**64** (109 mg, 0.658 mmol), 4-azidobutanoic acid (115 mg, 0.891 mmol), DMAP (8.0 mg, 0.066 mmol) and DCC (184 mg, 0.891 mmol) gave a crude material. Purification *via* flash column chromatography (EtOAc/hexane, 12:88) gave **66** as a colourless oil (157 mg, 0.566 mmol, 86%). $\mathbf{R_f}$ = 0.11 (EtOAc/hexane, 8:92); **^{1}H NMR** (400 MHz, $CDCl_3$): δ_H 5.27 (1H, dd, *J* 4.1, 2.7, C(5)*H*), 3.34 (2H, td, *J* 6.7, 1.4, C(14)H_2), 2.67–2.30 (6H, m, C(2)H_2, C(8)H_AH_B, C(12)H_2), 2.15–2.01 (2H,

m, C(4)H_AH_B), 1.97 (1H, t, *J* 2.7, C(10)*H*), 1.93–1.85 (4H, m, C(3)H_2, C(13)H_2), 1.33 (3H, s, C(7)H_3); **^{13}C NMR** (101 MHz, $CDCl_3$): δ_C 211.7 (*C*(1)), 171.5 (*C*(11)), 80.1 (*C*(9)), 77.6 (*C*(5)), 71.4 (*C*(10)), 50.9 (*C*(6)), 50.7 (*C*(14)), 37.6 (*C*(2)), 31.4 (*C*(12)), 25.2 (*C*(4)), 24.4 (*C*(13)), 23.3 (*C*(8)), 21.4 (*C*(7)), 20.9 (*C*(3)); **IR** ν_{max}: 2097 (s, N=N=N), 1733 (s, C=O), 1709 (s, C=O); **HRMS** (ESI): $[M+H]^+$ calcd. for $C_{14}H_{20}O_3N_3^+$: 278.1499, found: 278.1488.

(9a*S,13a*S**,*E*)-9a-Methyl-8-methylene-3,4,5,8,9,9a,11,12,13,13a-decahydrobenzo[*b*][1]oxacycloundecine-2,10-dione (67)**

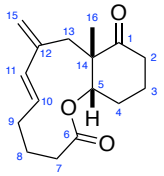

67

Grubbs 2nd generation catalyst (9.5 mg, 11 µmol) was added to a stirred solution of **65** (45.1 mg, 0.172 mmol) in PhMe (22 mL). The reaction mixture was stirred under an ethylene atmosphere at reflux for 4 h, then degassed with N_2 and stirred for a further 18 h. The resultant mixture was filtered through Celite® then concentrated *in vacuo*. Purification *via* flash column chromatography (EtOAc/petroleum ether, 10:90) gave **67** as a white amorphous solid (37.5 mg, 0.143 mmol, 83%). ***R*$_f$** = 0.26 (EtOAc/ petroleum ether, 10:90); **^{1}H NMR** (400 MHz, $CDCl_3$): δ_H 5.93 (1H, d, *J* 15.9, C(11)*H*), 5.78 (1H, app s, C(10)*H*), 5.12 (1H, app s, C(15)H_AH_B), 4.84 (1H, app s, C(15)H_AH_B), 4.77– 4.70 (1H, m, C(5)*H*), 2.64 (1H, ddd, *J* 15.1, 12.7, 7.3, C(2)H_AH_B), 2.38–2.14 (6H, m, C(2)H_AH_B, C(7)H_2, C(9)H_AH_B, C(13)H_2), 2.05–1.81 (7H, m, C(3)H_2, C(4)H_AH_B, C(8)H_2, C(9)H_AH_B), 1.31 (3H, s, C(16)H_3); **^{13}C NMR** (101 MHz, $CDCl_3$): δ_C 213.9 (*C*(1)), 175.3 (*C*(6)), 142.2 (*C*(12)), 135.7 (*C*(11)), 128.7 (*C*(10)), 116.2 (*C*(15)), 78.5 (*C*(5)), 51.9 (*C*(14)), 37.7 (*C*(2)), 33.2 (*C*(7), *C*(13)), 29.8 (*C*(9)), 25.2 (*C*(4)), 24.7 (*C*(8)), 23.8 (*C*(16)), 20.8 (*C*(3)); **IR** ν_{max}: 1726 (s, C=O), 1706 (s, C=O), 1622 (m, C=C); **HRMS** (ESI): $[M+H]^+$ calcd. for $C_{16}H_{22}O_3^+$: 263.1642, found: 263.1643.

(9a*S,13a*S**)-13a-Methyl-6,7,9a,10,11,12,13a,14-octahydro-13*H*-benzo[*b*][1,2,3]triazolo[5,1-*e*][1,6]oxazecine-8,13(5*H*)-dione (68)**

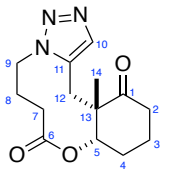

68

$[RuCp^*Cl]_4$ (42.0 mg, 38.6 µmol) was added to a degassed solution of **66** (92.1 mg, 0.332 mmol) in PhMe (134 mL). The resultant solution heated under refluxed for 24 h before being cooled to rt. The crude mixture was filtered through Celite® and concentrated *in vacuo*. Purification *via* flash column chromatography gave **68** as an amorphous yellow solid (77.9 mg, 0.281 mmol, 85%). $\mathbf{R_f}$ = 0.20 (EtOAc/hexane, 90:10); **^{1}H NMR** (400 MHz, $CDCl_3$): δ_H 7.52 (1H, s, C(10)*H*), 4.42 (2H, m, C(5)*H*, C(9)H_AH_B), 4.29–4.17 (1H, m, C(9)H_AH_B), 3.36 (1H, d, *J* 15.6, C(12)H_AH_B), 2.86–2.55 (3H, m, C(12)H_AH_B, C(2)H_AH_B, C(4)H_AH_B), 2.47–2.29 (4H, m, C(2)H_AH_B, C(4)H_AH_B, C(7)H_2), 2.02–1.79 (4H, m, C(3)H_2, C(8)H_2), 1.46 (3H, s, C(14)H_3); **^{13}C NMR** (101 MHz, $CDCl_3$): δ_C 212.8 (*C*(1)), 171.0 (*C*(6)), 133.4 (*C*(11)), 132.4 (*C*(10)), 77.4 (*C*(5))[r], 50.9 (*C*(13)), 46.8 (*C*(9)), 37.6 (*C*(2)), 33.8 (*C*(7)), 27.5 (*C*(12)), 26.9 (*C*(4)), 25.4 (*C*(8)), 23.2 (*C*(14)), 20.9 (*C*(3)); **IR** ν_{max}: 1735 (s, C=O ester), 1703 (s, C=O ketone); **HRMS** (ESI): $[M+H]^+$ calcd. for $C_{14}H_{20}N_3O_3^+$: 278.1499, found 278.1499.

(4a*S,8a*S**)-4a-Methyl-4,4a,6,7,8,8a-hexahydro-5H-chromen-5-one (69)**

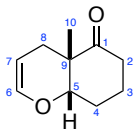

69

$CpRu(PPh_3)_2Cl$ (61.1 mg, 84.2 µmol) and PPh_3 (44.1 mg, 0.168 mmol) were added to a degassed solution of *N*-hydroxysuccinimide (48.2 mg, 0.419 mmol), NBu_4PF_6 (42.7 mg, 0.110 mmol), $NaHCO_3$ (36.1 mg, 0.430 mmol) and *syn*-**64** (140 mg, 0.842 mmol) in DMF (8.5 mL). The reaction was degassed once more and then sealed in a vial. The resultant mixture was stirred at 80 °C for 18 h. Further $CpRu(PPh_3)_2Cl$ (67.1 mg, 84.2 µmol) was added and the reaction was stirred at 80 °C for 38 h. Upon completion, the reaction was filtered through Celite® and partitioned between EtOAc (20 mL) and brine (20 mL). The organic layer was separated, dried and concentrated *in vacuo*. Purification *via* flash column chromatography (EtOAc/hexane, 10:90) gave **69** as a colourless oil (88.1 mg, 0.530 mmol,

[r] Observed in 2D NMR spectra.

63%). $\mathbf{R_f}$ = 0.30 (EtOAc/hexane, 10:90); **^{1}H NMR** (400 MHz, $CDCl_3$): δ_H 6.26 (1H, dt, *J* 6.2, 2.0, C(6)*H*), 4.63 (1H, ddd, *J* 6.2, 4.5, 3.0, C(7)*H*), 3.96 (1H, dd, *J* 5.5, 2.2, C(5)*H*), 2.61–2.44 (2H, m, C(2)H_AH_B, C(8)H_AH_B), 2.41–2.30 (1H, m, C(2)H_AH_B), 2.15–2.00 (2H, m, C(3)H_AH_B, C(4)H_AH_B), 1.99–1.87 (1H, m, C(4)H_AH_B), 1.85–1.72 (1H, m, C(3)H_AH_B), 1.60 (1H, dt, *J* 17.2, 2.6, C(8)H_AH_B), 1.20 (3H, s, C(10)H_3); **^{13}C NMR** (101 MHz, $CDCl_3$): δ_C 212.2 (*C*(1)), 142.4 (*C*(6)), 98.8 (*C*(7)), 80.1 (*C*(5)), 47.6 (*C*(9)), 36.9 (*C*(2)), 27.7 (*C*(8)), 25.8 (*C*(4)), 23.0 (*C*(10)), 20.9 (*C*(3)); **IR** ν_{max}: 1708 (s, C=O), 1661 (m, C=C); **HRMS** (ESI): $[M+H]^+$ calcd. for $C_{10}H_{15}O_2^+$: 167.1067, found: 167.1066.

2-Phenyl-2-(prop-2-yn-1-yl)cyclopentane-1,3-dione (72)

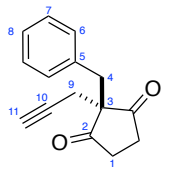

72

L-Proline (18.0 mg, 0.156 mmol) was added to a stirred suspension of cyclopentane-1,3-dione, **70**, (300 mg, 3.06 mmol), phenylacetaldehyde (1.10 g, 9.18 mmol) and Hantzsch ester (775 mg, 3.06 mmol) in anhydrous CH_2Cl_2 (8.0 mL) at rt. The resultant mixture was stirred at rt for 24 h, then concentrated *in vacuo*. 2-Phenylcyclopentane-1,3-dione **71** (499 mg) was obtained as a brown solid and used in the next step without further purification.

According to General Procedure A, propargyl bromide (0.21 mL, 2.21 mmol), crude **71** (499 mg) and NaOH (88 mg, 2.21 mmol) gave a crude material. Purification *via* flash column chromatography (petroleum ether/EtOAc, 90:10) gave **72** as a colourless oil (377 mg, 1.84 mmol, 60%). $\boldsymbol{R_f}$ = 0.29 (petroleum ether/EtOAc, 90:10); **^{1}H NMR** (400 MHz, $CDCl_3$): δ_H 7.22 (3H, m, C(8)*H*, C(6/7)*H*), 7.06–6.99 (2H, m, C(6/7)*H*), 2.93 (2H, s, C(4)H_2), 2.61–2.54 (3H, m, C(1)H_AH_B, C(9)H_AH_B), 2.52 (1H, d, *J* 6.4, C(9)H_AH_B), 2.13–1.98 (2H, m, C(1)H_AH_B), 1.95 (1H, t, *J* 2.6, C(11)*H*); **^{13}C NMR** (101 MHz, $CDCl_3$): δ_C 216.3 (*C*(2)), 134.9 (*C*(5)), 129.8 (*C*(7)), 128.9 (*C*(6)), 127.6 (*C*(8)), 78.8 (*C*(10)), 71.0 (*C*(11)), 61.6 (*C*(3)), 42.0 (*C*(4)), 37.1 (*C*(1)), 24.4 (*C*(9)); **IR** ν_{max}: 3282 (s, C≡C–H), 1723 (s, C=O), 1495 (s, Ar C=C), 1455 (s, Ar C=C); **HRMS** (ESI): calcd. for $C_{15}H_{15}O_2^+$ $[M+H]^+$: 227.1067, found**:** 227.1062.

(2*R)-2-(Cyclopropylmethyl)-3-hydroxy-2-(prop-2-yn-1-yl)cyclopentan-1-one (73)**

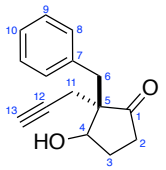

73

According to General Procedure B, $NaBH_4$ (10.9 mg, 0.288 mmol) and diketone **72** (130 mg, 0.575 mmol) gave a crude material (4:1 *dr*). Purification *via* flash column chromatography (EtOAc/petroleum ether, 20:80) gave **73** as a colourless oil (72.1 mg, 0.316 mmol, 55%). The compound was isolated as an inseparable 4:1 mixture of diastereomers, referred to below as x and y respectively. $\boldsymbol{R_f}$ = 0.21 (EtOAc/petroleum ether, 20:80); **^{1}H NMR** (400 MHz, $CDCl_3$): δ_H 7.36–7.11 (6.25H, m, $C^{x,y}$(8)*H*, $C^{x,y}$(9)*H*, $C^{x,y}$(10)*H*), 4.44 (1.25H, m, $C^{x,y}$(4)*H*), 3.05 (1H, d, *J* 13.9, C^x(6)H_AH_B), 3.01–2.89 (1.50H, m, C^x(6)H_A*H*$_B$, C^y(6)H_AH_B), 2.56–2.36 (2.75H, m, C^x(2)H_AH_B, C^y(2)H_AH_B, C^y(11)H_AH_B, C^x(11)H_AH_B), 2.34–2.13 (5.5H, O^x*H,* C^x(2)H_a*H*$_b$, C^y(2)H_A*H*$_B$, C^x(3)H_AH_B, C^x(11)H_A*H*$_B$, $C^{x,y}$(13)*H*), 1.96 (0.85H, m, O^y*H,* C^y(3)H_A*H*$_B$), 1.85–1.73 (1H, m, C^x(3)H_A*H*$_B$); **^{13}C NMR** (101 MHz, $CDCl_3$): δ_C 218.2 (C^y(2)), 217.1 (C^x(2)), 136.3 (C^x(7)), 136.2 (C^y(7)), 130.7 (C^x(9)), 130.1 (C^y(9)), 128.7(C^y(8)), 128.3 (C^x(8)), 127.2 (C^y(10)), 126.9 (C^x(10)), 81.2 (C^y(12)), 80.9 (C^x(12)), 76.4 (C^x(4)), 75.7 (C^y(4)), 72.1 (C^x(13)), 71.7 (C^y(13)), 57.4 (C^y(5)), 56.1 (C^x(5)), 39.5 (C^y(6)), 35.5 (C^y(2)), 35.0 (C^x(2)), 34.7 (C^x(6)), 27.6 (C^y(3)), 27.1 (C^x(3)), 23.4 (C^x(11)), 19.7 (C^y(11)); IR ν_{max}: 3475 (br, O–H), 3294 (m, C≡C–H), 1735 (s, C=O), 1496 (s, Ar C=C), 1454 (s, Ar C=C); **HRMS** (ESI): $[M+H]^+$ calcd. for $C_{15}H_{17}O_2^+$: 229.1223, found: 229.1220.

Ethyl 4-((4,6-dichloropyrimidin-2-yl)amino)butanoate (82)

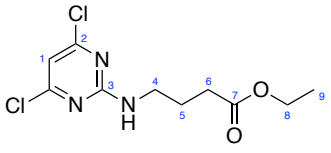

82

Et_3N (3.80 mL, 27.3 mmol) was added dropwise to a stirred solution of 2,4,6-trichloropyrimidine, **81**, (2.00 g, 10.9 mmol) and ethyl 4-aminobutyrate hydrochloride (2.19 g, 13.1 mmol) in acetone (40 mL) at 0 °C. After 5 min, the reaction mixture was warmed to rt and stirred for a further 90 min. The reaction mixture was concentrated *in vacuo*, then redissolved in EtOAc (30 mL) and washed with H_2O (2 × 30 mL) and brine (30 mL). The organic extract was dried and concentrated *in vacuo*. Purification *via* flash column chromatography (EtOAc/petroleum ether, 8:92) gave **82** as an amorphous white solid (971 mg, 3.49 mmol, 32%). $\mathbf{R}_f$ = 0.17 (EtOAc/petroleum ether, 10:90); **^{1}H NMR** (400 MHz, $CDCl_3$): δ_H 6.57 (1H, s, C(1)*H*), 5.95 (1H, t, *J* 6.1, N*H*), 4.12 (2H, q, *J* 7.1, C(8)H_2), 3.47 (2H, q, *J* 6.6, C(4)H_2), 2.37

(2H, t, *J* 7.2, C(6)H_2), 1.92 (2H, t, *J* 7.0, C(5)H_2), 1.24 (3H, t, *J* 7.2, C(9)H_3); **^{13}C NMR** (101 MHz, $CDCl_3$): δ_C 173.2 (*C*(7)), 162.3 (*C*(2)), 161.8 (*C*(3)), 161.5 (*C*(2)), 109.0 (*C*(1)), 60.7 (*C*(8)), 41.0 (*C*(4)), 31.6 (*C*(6)), 24.6 (*C*(5)), 14.3 (*C*(9)); **IR** ν_{max}: 3372 (m, N–H), 2987 (w, Ar C–H), 2937 (w, C–H), 1735 (s, C=O), 1583 (s, Ar C=C); **LRMS** (ESI): $[M+H]^+$ calcd. for $C_{10}H_{14}{}^{35}Cl_2N_3O_2^+$: 278.0, found: 278.0. These characterisation data are in accordance with that previously reported in the literature.[315]

Ethyl 4-((4,6-divinylpyrimidin-2-yl)amino)butanoate (83)

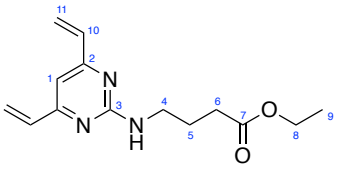

83

Potassium vinyltrifluoroborate (788 mg, 5.88 mmol), Pd(dppf)Cl_2·CH_2Cl_2 (160 mg, 0.196 mmol) and K_2CO_3 (1.63 g, 11.8 mmol) were added to a stirred solution of **82** (545 mg, 1.96 mmol) in THF/H_2O (10:1, 6.60 mL) and heated to 70 °C for 18 h. Then, the reaction mixture was filtered through Celite® and concentrated *in vacuo*. Purification *via* flash column chromatography (EtOAc/petroleum ether, 20:80) gave **83** (377 mg, 1.44 mmol, 73%) as a pale-yellow oil. $\mathbf{R}_f$ = 0.23 (EtOAc/petroleum ether, 20:80); **^{1}H NMR** (400 MHz, $CDCl_3$): δ_H 6.60–6.47 (3H, m, C(1)*H*, C(10)*H*), 6.33 (2H, d, *J* 17.4, C(11)H_t), 5.52 (2H, dd, *J* 10.6, 1.5, C(11)H_c), 5.30 (1H, m, N*H*), 4.09 (2H, q, *J* 7.2, C(8)H_2), 3.50 (2H, q, *J* 6.6, C(4)H_2), 2.37 (2H, dd, *J* 8.3, 6.3, C(6)H_2), 1.93 (2H, p, *J* 7.0, C(5)H_2), 1.21 (3H, t, *J* 7.2, C(9)H_3); **^{13}C NMR** (101 MHz, $CDCl_3$): δ_C 173.5 (*C*(7)), 163.7 (*C*(2)), 162.7 (*C*(3)), 136.0 (*C*(10)), 121.4 (*C*(11)), 105.7 (*C*(1)), 60.4 (*C*(8)), 40.7 (*C*(4)), 31.8 (*C*(6)), 25.2 (*C*(5)), 14.3 (*C*(9)); **IR** ν_{max}: 2982 (w, C–H), 1730 (s, C=O), 1636 (w, C=C), 1541 (m, Ar C=C); **LRMS** (ESI): $[M+H]^+$ calcd. for $C_{14}H_{20}N_3O_2^+$: 262.2, found: 262.2. These characterisation data are in accordance with that previously reported in the literature.[315]

4-((4,6-Divinylpyrimidin-2-yl)amino)butanoic acid (80)

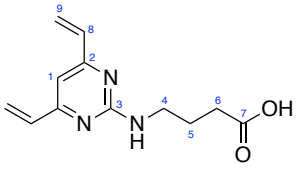

80

$LiOH·H_2O$ (123 mg, 2.94 mmol) was added to a stirred solution of **83** (640 mg, 2.45 mmol) in THF/H_2O (1:1, 3.50 mL) at rt. The reaction mixture was stirred for 3 h, then concentrated *in vacuo* to remove the organics. The crude mixture was then diluted with satd. NH_4Cl (40 mL), and the pH adjusted to 4 with 1 M HCl. The resulting solution was extracted with 10% ^{i}PrOH/EtOAc (4 × 120 mL) and the

combined organic extracts were dried and concentrated *in vacuo* to yield **80** (457 mg, 1.96 mmol, 80%) as an amorphous yellow solid. $\mathbf{R}_f$ = 0.56 (MeOH/CH_2Cl_2, 10:90); **^{1}H NMR** (400 MHz, CD_3OD): δ_H 6.68 (1H, s, C(1)*H*), 6.66–6.54 (2H, m, C(8)*H*), 6.36 (2H, d, *J* 17.4, C(9)H_t), 5.56 (2H, d, *J* 10.9, C(9)H_c), 3.47 (2H, t, *J* 6.9, C(4)H_2), 2.37 (2H, t, *J* 7.4, C(6)H_2), 1.92 (2H, p, *J* 7.3, C(5)H_2); **^{13}C NMR** (101 MHz, CD_3OD): δ_C 177.5 (*C*(7)), 165.4 (*C*(2)), 164.1 (*C*(3)), 137.1 (*C*(8)), 122.2 (*C*(9)), 105.8 (*C*(1)), 41.6 (*C*(4)), 32.5 (*C*(6)), 26.2 (*C*(5)); **IR** ν_{max}: 3310 (m, N–H), 2981 (w, Ar C–H), 2925 (w, C–H), 1735 (s, C=O), 1697 (w, C=C), 1567 (m, Ar C=C); **LRMS** (ESI): $[M–H]^-$ calcd. for $C_{12}H_{14}N_3O_2^-$: 232.1, found: 232.1. These characterisation data are in accordance with that previously reported in the literature.[315]

Ethyl (1*R*,8*S*,9*s*,*Z*)-bicyclo[6.1.0]non-4-ene-9-carboxylate (85)

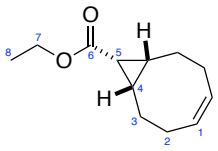

85

Ethyl diazoacetate (≥13 wt. % CH_2Cl_2, 0.727 mL, 5.99 mmol) in CH_2Cl_2 (3 mL) was added dropwise over 18 h to a stirred solution of 1,5-cyclooctadiene, **84**, (5.88 mL, 47.9 mmol) and rhodium tetraacetate (114 mg, 0.258 mmol) in CH_2Cl_2 (5.0 mL). After the addition was complete, the stirring was continued for a further 3 h at rt. The resulting mixture was filtered through Celite® and concentrated *in vacuo*. Purification *via* flash column chromatography (EtOAc/petroleum ether, 1:99) gave **85** (373 mg, 1.92 mmol, 32%) as colourless oil. $\mathbf{R}_f$ **=** 0.21 (EtOAc/petroleum ether, 10:90); **^{1}H NMR** (400 MHz, $CDCl_3$): δ_H 5.67–5.55 (2H, m, *C*(1)*H*), 4.12 (2H, q, *J* 7.1, (*C*(7)H_2), 2.51 (2H, ddt, *J* 15.9, 8.3, 4.0, C(2)H_AH_B), 2.20 (2H, dtd, *J* 13.7, 8.4, 5.0, C(3)H_AH_B), 2.12–1.99 (2H, m, C(2)H_AH_B), 1.83 (2H, dtd, *J* 14.0, 6.7, 4.5, C(3)H_AH_B), 1.71 (1H, t, *J* 8.8, *C*(5)*H*), 1.40 (2H, dddt, *J* 11.6, 8.6, 6.8, 2.9, C(4)*H*), 1.26 (3H, t, *J* 7.1, *C*(8)H_3); **^{13}C NMR** (101 MHz, $CDCl_3$): δ_C 172.5 (*C*(6)), 129.6 (*C*(1)), 59.9 (*C*(7)), 27.2 (*C*(2)), 24.3 (*C*(4)), 22.8 (*C*(3)), 21.4 (*C*(5)), 14.6 (*C*(8)); **IR** ν_{max}: 2973, 2901 (m, C–H), 1719 (s, C=O); **LRMS** (ESI): $[M+H]^+$ calcd. for $C_{12}H_{19}O_2^+$: 195.1, found: 195.1. These characterisation data are in accordance with that previously reported in the literature.[400]

((1*R*,8*S*,9*s*)-Bicyclo[6.1.0]non-4-yn-9-yl)methanol (86)

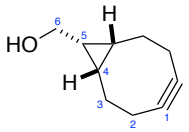

86

$LiAlH_4$ (1.0 M in THF, 4.51 mL, 4.51 mmol) was added dropwise to a stirred solution of **85** (350 mg, 1.80 mmol) in THF (3.00 mL) at 0 °C. After stirring for a further 4 h at rt the reaction mixture was quenched by dropwise addition of a solution of AcOH/MeOH/H_2O (1:3:1, 2.00 mL), followed by AcOH (0.30 mL). The resulting solution was poured onto ice (20 g) containing brine (5 mL) and extracted with EtOAc (3 × 20 mL). The combined organic extracts were washed with brine (3 × 20 mL), then dried and concentrated *in vacuo* to give a crude material.

The resulting crude material was redissolved in CH_2Cl_2 (14.0 mL) and cooled to 0 °C. A solution of Br_2 (101 µL, 1.97 mmol) in CH_2Cl_2 (1.35 mL) was added dropwise to the solution at 0 °C until a yellow colour persisted. The reaction mixture was quenched with a 10% aq. $Na_2S_2O_3$ (5 mL) and extracted with CH_2Cl_2 (2 × 20 mL). The organic extract was dried and concentrated *in vacuo* to afford a crude material.

Without further purification the crude material was dissolved in THF (17.0 mL), and a solution of KO^tBu (1 M in THF, 4.97 mL, 4.97 mmol) was added dropwise to the solution at 0 °C. The solution was then refluxed for 2 h before being cooled to rt, quenched with satd. NH_4Cl (20 mL), and extracted with CH_2Cl_2 (3 × 20 mL). The organic extract was dried and concentrated *in vacuo*. Purification *via* flash column chromatography (EtOAc/petroleum ether, 20:80) gave **86** as an amorphous white solid (108 mg, 0.724 mmol, 40%). $\mathbf{R_f}$ = 0.12 (EtOAc/petroleum ether, 20:80); **^{1}H NMR** (400 MHz, $CDCl_3$): δ_H 3.73 (2H, d, *J* 7.9, C(6)H_2), 2.36–2.17 (6H, m, C(2)H_2, C(3)H_2), 1.68–1.54 (2H, m, C(3)H_2), 1.48 (1H, br s, O*H*), 1.34 (1H, tt, *J* 9.1, 7.9, C(5)*H*), 0.99–0.89 (2H, m, C(4)H_2); **^{13}C NMR** (101 MHz, $CDCl_3$): δ_C 99.0 (*C*(1)), 60.2 (*C*(6)), 29.2 (*C*(3)), 21.7 (*C*(2)), 21.6 (*C*(5)), 20.2 (*C*(4)); **IR** ν_{max}: 3346 (br, O–H), 2910, 2849 (m, C–H); **LRMS** (ESI): $[M–H]^–$ calcd. for $C_{10}H_{12}O^–$: 149.1, found: 149.1. These characterisation data are in accordance with that previously reported in the literature.[400]

((1*R*,8*S*,9*s*)-Bicyclo[6.1.0]non-4-yn-9-yl)methyl (4-nitrophenyl) carbonate (87)

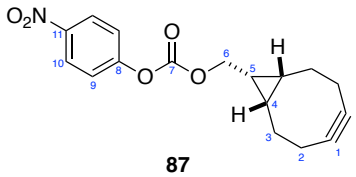

87

Pyridine (85.4 µL, 1.06 mmol) and 4-nitrophenyl chloroformate (107 mg, 0.532 mmol) were added to a stirred solution of BCN, **86**, (63.9 mg, 0.426 mmol) in CH_2Cl_2 (10 mL). After stirring for 1 h at rt the mixture was quenched with satd. NH_4Cl (10 mL) and extracted with CH_2Cl_2 (3 × 10 mL). The organic extract was dried and concentrated *in vacuo*. Purification *via* flash column chromatography (EtOAc/petroleum ether, 10:90) gave **87** as an amorphous white solid (105 mg, 0.333 mmol, 78%). **R_f =** 0.21 (EtOAc/petroleum ether, 10:90); **^{1}H NMR** (400 MHz, $CDCl_3$): δ_H 8.27 (2H, d, *J* 8.9, C(10)H_2), 7.38 (2H, *J* 8.9, C(9)H_2), 4.40 (2H, d, *J* 8.2, C(6)H_2), 2.36–2.17 (6H, m, C(2)H_2, C(3)H_2), 1.67–1.44 (3H, m, C(3)H_2, C(5)*H*), 1.11–0.98 (2H, m, C(4)H_2); **^{13}C NMR** (101 MHz, $CDCl_3$): δ_C 155.7 (*C*(8)), 152.7 (*C*(7)), 145.5 (*C*(11)), 125.4 (*C*(10)), 121.9 (*C*(9)), 98.8 (*C*(1)), 68.1 (*C*(6)), 29.2 (*C*(3)), 21.5 (*C*(2)), 20.6 (*C*(5)), 17.4 (*C*(4)); **IR** ν_{max}: 2926 (m, C–H), 1748 (s, C=O), 1517 (s, NO_2), 1346 (s, NO_2); **LRMS** (ESI): $[M+H]^+$ calcd. for $C_{17}H_{18}NO_5^+$: 316.1, found: 316.1. These characterisation data are in accordance with that previously reported in the literature.[400]

Bicyclo[6.1.0]non-4-yn-9-ylmethyl (2-(2-(2-(4-((4,6-divinylpyrimidin-2-yl)amino)butanamido)ethoxy)ethoxy)ethyl)- carbamate (78)

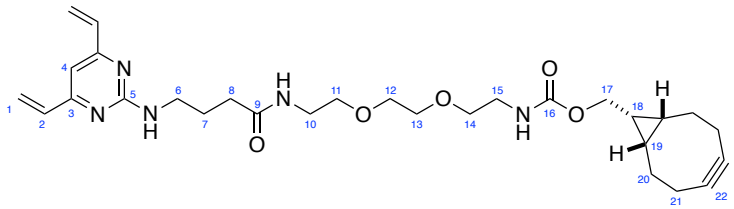

78

1,8-Diamino-3,6-dioxaoctane (358 µL, 2.44 mmol) and NEt_3 (170 µL, 1.22 mmol) were added to a stirred solution of **87** (128 mg, 0.406 mmol) in DMF (2.0 mL). The reaction mixture was stirred at rt for 15 min, before being concentrated *in vacuo*. The resulting residue was redissolved in CH_2Cl_2 (5 mL) and washed with 1 M NaOH (5 × 5 mL), followed by water (5 × 5 mL). The organic extract was then dried and concentrated *in vacuo* to give crude (2-methylcycloprop-2-en-1-yl)methyl (2-(2-(2-aminoethoxy)ethoxy)ethyl)carbamate **88**, which was used in the next step without further purification.

According to General Procedure G, EDC·HCl (38.9 mg, 0.203 mmol), the crude amine **88**, carboxylic acid **80** (47.3 mg, 0.203 mmol), Et_3N (28.3 µL, 0.203 mmol) and HOBt·H_2O (31.1 mg, 0.203 mmol) gave a crude material. Purification *via* flash column chromatography (MeOH/CH_2Cl_2, 3:97) gave **78** as a yellow oil (66.4 mg, 0.123 mmol, 61%). $\mathbf{R_f}$ = 0.14 (MeOH/CH_2Cl_2, 3:97); **^{1}H NMR** (700 MHz, MeOD): δ_H 6.71 (1H, s, C(4)*H*), 6.63 (2H, dd, *J* 17.4, 10.7, C(2)*H*), 6.38 (2H, d, *J* 17.4, C(1)H_t), 5.59 (2H, d, *J* 10.7, C(1)H_c), 4.14 (2H, d, *J* 8.1, C(17)H_2), 3.61 (4H, app s, C(12)H_2 C(13)H_2,), 3.54 (4H, q, *J* 5.9, C(11)H_2, C(14)H_2), 3.48 (2H, t, *J* 6.8, C(6)H_2), 3.38 (2H, d, *J* 5.5, C(10)H_2), 3.29 (2H, t, *J* 5.5, C(15)H_2), 2.32 (2H, t, *J* 7.4, C(8)H_2), 2.28–2.19 (4H, m, C(20)H_AH_B, C(21)H_AH_B), 2.18–2.14 (2H, m, C(21)H_AH_B), 1.94 (2H, dt, *J* 13.6, 6.6, C(7)H_2), 1.59 (2H, d, *J* 11.0, C(20)H_AH_B), 1.34 (1H, s, C(18)*H*), 0.95–0.90 (2H, m, C(19)*H*); **^{13}C NMR** (176 MHz, MeOD): δ_C 174.5 (*C*(9)), 163.9 (*C*(3)), 162.7 (*C*(5)), 157.8 (*C*(16)), 135.8 (*C*(2)), 120.7 (*C*(1)), 104.4 (*C*(4)), 98.2 (*C*(22)), 69.9 (*C*(11/12/13/14)), 69.7 (*C*(11/12/13/14)), 69.2 (2C, *C*(11/12/13/14)), 62.3 (*C*(17)), 40.3 (2C, *C*(6), *C*(15)), 39.0 (*C*(10)), 33.2 (*C*(8)), 28.8 (*C*(20)), 25.6 (*C*(7)), 20.6 (*C*(21)), 20.0 (*C*(19)), 17.6 (*C*(18)); **IR** ν_{max}: 3316 (m, N–H), 2919 (w, C–H), 1703 (s, C=O), 1648 (s, C=O), 1539 (m, Ar C=C); **HRMS** (ESI): $[M+Na]^+$ calcd. for $C_{29}H_{41}N_5NaO_5^+$: 562.3000, found: 562.3008.

Ethyl 2-methyl-3-(trimethylsilyl)cycloprop-2-ene-1-carboxylate (91)

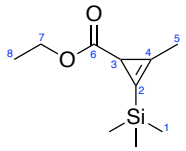

91

A solution of ethyl diazoacetate, **90**, (≥13 wt. % CH_2Cl_2, 0.901 mL, 7.42 mmol) in CH_2Cl_2 (12.3 mL) was added dropwise over 18 h to a stirred mixture of trimethylsilyl acetylene (3.17 mL, 22.3 mmol) and rhodium tetraacetate (33.1 mg, 74.9 µmol). After the addition was complete, the stirring was continued for a further 30 min. The resulting mixture was filtered through Celite® and concentrated *in vacuo*. Purification *via* flash column chromatography (Et_2O/petroleum ether, 2:98) gave **91** as a colourless oil (618 mg, 3.12 mmol, 42%). $\mathbf{R_f}$ = 0.28 (Et_2O/petroleum ether, 5:95); **^{1}H NMR** (400 MHz, $CDCl_3$): δ_H 4.13–4.00 (2H, m, C(7)H_2), 2.16 (3H, s, C(5)H_3), 1.94 (1H, s, C(3)*H*), 1.20 (3H, t, *J* 7.1, C(8)H_3), 0.16 (9H, s, C(1)H_3); **^{13}C NMR** (101 MHz, $CDCl_3$): δ_C 177.1 (*C*(6)), 122.7 (*C*(4)), 104.2 (*C*(2)), 59.9 (*C*(7)), 21.3 (*C*(5)), 14.5 (*C*(8)), 11.9 (*C*(3)), –1.50 (*C*(1)); **IR** ν_{max}: 1730 (s, C=O), 1694 (m, C=C); **LRMS** (ESI): $[M+H]^+$ calcd. for $C_{10}H_{19}O_2Si^+$**:** 199.1, found**:** 199.1. These characterisation data are in accordance with that previously reported in the literature.[444]

(2-Methyl-3-(trimethylsilyl)cycloprop-2-en-1-yl)methanol (93)

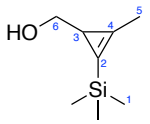

93

DIBAL-H (1.0 M in THF, 5.90 mL, 5.90 mmol) was added dropwise to a stirred solution of **91** (468 mg, 2.36 mmol) in THF (5.9 mL) at 0 °C. The reaction mixture was stirred for a further 3 h at 0 °C before being carefully quenched with H_2O. The precipitate was filtered, and the filtrate was concentrated *in vacuo*. Purification *via* flash column chromatography (EtOAc/petroleum ether, 10:90) gave **93** as a colourless oil (251 mg, 1.61 mmol, 68%). $\mathbf{R_f}$ = 0.21 (EtOAc/petroleum ether, 10:90); **^{1}H NMR** (400 MHz, $CDCl_3$): δ_H 3.48 (2H, d, *J* 4.6, C(6)H_2), 2.21 (3H, s, C(5)H_3), 1.56 (1H, t, *J* 4.6, C(3)*H*), 0.17 (9H, s, C(1)H_3); **^{13}C NMR** (101 MHz, $CDCl_3$): δ_C 135.6 (*C*(4)), 111.5 (*C*(2)), 69.4 (*C*(6)), 22.3 (*C*(3)), 13.6 (*C*(5)), –1.0 (*C*(1)); **IR** ν_{max}: 3310 (br, O–H), 2956, 2915 (m, C–H); **LRMS** (ESI): $[M–H]^-$ calcd. for $C_8H_{15}OSi^-$: 155.1, found: 155.1. These characterisation data are in accordance with that previously reported in the literature.[444]

(2-Methylcycloprop-2-en-1-yl)methyl (4-nitrophenyl) carbonate (89)

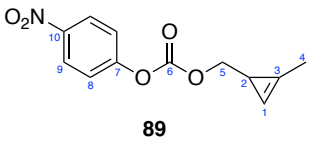

89

TBAF (1.0 M in THF, 0.352 mL, 0.352 mmol) was added to a stirred solution of **93** (50.0 mg, 0.320 mmol) in THF (2.50 mL). The reaction mixture was stirred at rt for 2 h before pyridine (1.30 mL) and 4-nitrophenyl chloroformate (175 mg, 0.868 mmol) were added at 0 °C. The reaction mixture was warmed to rt and stirred for a further 18 h. Upon completion the mixture was quenched with satd. NH_4Cl (5 mL) and extracted with CH_2Cl_2 (3 × 5 mL). The organic extract was dried and concentrated *in vacuo*. Purification *via* flash column chromatography (EtOAc/petroleum ether, 3:97) gave **89** (64.5 mg, 0.259 mmol, 81%) as an amorphous white solid. $\mathbf{R_f}$ = 0.31 (EtOAc/petroleum ether, 3:97); **^{1}H NMR** (400 MHz, $CDCl_3$): δ_H 8.27 (2H, d, *J* 9.1, C(9)*H*), 7.38 (2H, d, *J* 9.1, C(8)*H*), 6.61 (1H, app s, C(1)*H*), 4.21 (1H, dd, *J* 10.9, 5.2, C(5)H_AH_B), 4.13 (1H, dd, 10.9, 5.4, C(5)H_AH_B), 2.17 (3H, s, C(4)H_3), 1.78 (1H, app td, *J* 5.4, 2.6, C(2)*H*); **^{13}C NMR** (101 MHz, $CDCl_3$): δ_C 155.9 (*C*(7)), 152.8 (*C*(6)), 145.4 (*C*(10)), 125.4 (*C*(9)), 122.0 (*C*(8)), 120.3 (*C*(3)), 101.8 (*C*(1)), 77.5 (*C*(5)), 16.8 (*C*(4)), 11.8 (*C*(2)); **IR** ν_{max}: 2924 (m, C–H), 1761 (s, C=O), 1523 (s, NO_2), 1346 (s, NO_2); **LRMS** (ESI): $[M+H]^+$ calcd. for $C_{12}H_{12}NO_5^+$: 250.1, found: 250.1. These characterisation data are in accordance with that previously reported in the literature.[444]

(2-Methylcycloprop-2-en-1-yl)methyl (2-(2-(2-(4-((4,6-divinylpyrimidin-2-yl)amino)butanamido)ethoxy)ethoxy)- ethyl)carbamate (79)

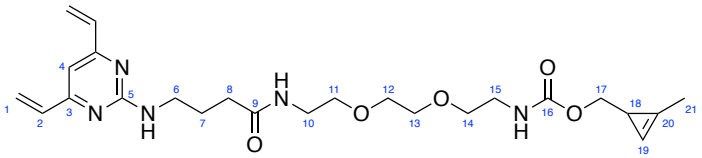

79

1,8-Diamino-3,6-dioxaoctane (358 µL, 2.44 mmol) and NEt_3 (170 µL, 1.22 mmol) were added to a stirred solution of **89** (101 mg, 0.406 mmol) in DMF (2.00 mL). The reaction mixture was stirred at rt for 15 min, before being concentrated *in vacuo*. The resulting residue was redissolved in CH_2Cl_2 (5 mL) and washed with 1 M NaOH (5 × 5 mL), followed by H_2O (5 × 5 mL). The organic extract was then dried and concentrated *in vacuo* to give crude (2-methylcycloprop-2-en-1-yl)methyl (2-(2-(2-aminoethoxy)ethoxy)ethyl)carbamate **94**, which was used in the next step without further purification.

According to General Procedure G, EDC·HCl (38.9 mg, 0.203 mmol), the crude amine **94**, carboxylic acid **80** (47.3 mg, 0.203 mmol), Et_3N (28.3 µL, 0.203 mmol) and HOBt·H_2O (31.1 mg, 0.203 mmol) gave a crude material. Purification *via* flash column chromatography (MeOH/CH_2Cl_2, 3:97) gave **79** as a yellow oil (60.6 mg, 0.128 µmol, 63%). $\mathbf{R_f}$ = 0.38 (MeOH/CH_2Cl_2, 3:97); **^{1}H NMR** (400 MHz, $CDCl_3$): δ_H 6.62–6.50 (4H, m, C(2)*H*, C(4)*H*, C(19)*H*), 6.34 (2H, dd, *J* 17.3, 1.5, C(1)H_t), 6.23 (1H, br s, C(5)N*H*), 5.55 (2H, dd, *J* 10.6, 1.6, C(1)H_c), 5.35 (2H, br s, C(9)N*H*, C(10)N*H*), 3.92 (2H, d, *J* 5.0, C(17)H_2), 3.60–3.49 (10H, m, C(6)H_2, C(11)H_2, C(12)H_2 C(13)H_2, C(14)H_2), 3.47–3.41 (2H, m, C(10)H_2), 3.35 (2H, q, *J* 5.4, C(15)H_2), 2.29 (2H, t, *J* 7.3, C(8)H_2), 2.11 (3H, d, *J* 1.1, C(21)H_3), 1.97 (2H, p, *J* 7.0, C(7)H_2), 1.69–1.59 (1H, m, C(18)*H*); **^{13}C NMR** (101 MHz, $CDCl_3$): δ_C 172.9 (*C*(9)), 163.8 (*C*(3)), 162.7 (*C*(5)), 157.1 (*C*(16)), 136.0 (*C*(2)), 121.6 (*C*(1)), 120.8 (*C*(20)), 105.6 (*C*(4)), 102.4 (*C*(19)), 72.5 (*C*(17)), 70.4 (*C*(11/12/13/14)), 70.3 (2C, *C*(11/12/13/14)), 70.1 (*C*(11/12/13/14)), 40.8 (2C, *C*(6), *C*(15)), 39.4 (*C*(10)), 33.9 (*C*(8)), 25.8 (*C*(7)), 17.4 (*C*(18)), 11.8 (*C*(21)); **IR** ν_{max}: 3382 (m, N–H), 2958 (w, C–H), 1705 (s, C=O), 1653 (s, C=O), 1546 (m, Ar C=C); **HRMS** (ESI): $[M+Na]^+$ calcd. for $C_{24}H_{35}N_5NaO_5^+$: 496.2530, found: 496.2544.

Hex-5-yn-1-yl (4-nitrophenyl) carbonate (97)

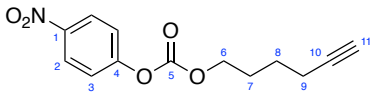

97

Pyridine (0.411 mL, 5.10 mmol) and 4-nitrophenyl chloroformate (1.23 g, 6.12 mmol) were added to a stirred solution of 5-hexyn-1-ol, **96**, (0.562 mL, 5.10 mmol) in CH_2Cl_2 (100 mL). After stirring for 1 h at rt the mixture was quenched with satd. NH_4Cl (100 mL) and extracted with CH_2Cl_2 (3 × 50 mL). The organic extract was dried and concentrated *in vacuo*. Purification *via* flash column chromatography (EtOAc/petroleum ether, 10:90) gave **97** as an amorphous white solid (1.25 g, 4.75 mmol, 93%). **R_f =** 0.28 (EtOAc/petroleum ether, 10:90); **^{1}H NMR** (400 MHz, $CDCl_3$): δ_H 8.32–8.24 (2H, d, *J* 9.0, C(2)*H*), 7.42–7.34 (2H, d, *J* 9.0, C(3)*H*), 4.33 (2H, t, *J* 6.5, C(6)H_2), 2.29 (2H, td, *J* 6.9, 2.6, C(9)H_2), 1.99 (1H, t, *J* 2.7, C(11)*H*), 1.91 (2H, ddt, *J* 9.8, 8.1, 6.3, C(7)H_2), 1.75–1.64 (2H, m, C(8)H_2); **^{13}C NMR** (101 MHz, $CDCl_3$): δ_C 155.5 (*C*(4)), 152.4 (*C*(5)), 145.3 (*C*(1)), 125.2 (*C*(2)), 121.7 (*C*(3)), 83.5 (*C*(10)), 69.0 (*C*(11)), 68.9 (*C*(6)), 27.4 (*C*(7)), 24.5 (*C*(8)), 17.9 (*C*(9)); **IR** ν_{max}: 3304 (s, alkyne C–H), 2971 (m, C–H), 1763 (s, C=O), 1524 (s, NO_2), 1347 (s, NO_2); **HRMS** (ESI): $[M+Na]^+$ calcd. for $C_{13}H_{13}NNaO_5^+$: 286.0686, found: 286.0680.

Hex-5-yn-1-yl (2-(2-(2-(4-((4,6-divinylpyrimidin-2 yl)amino)butanamido)ethoxy)ethoxy)ethyl)carbamate (95)

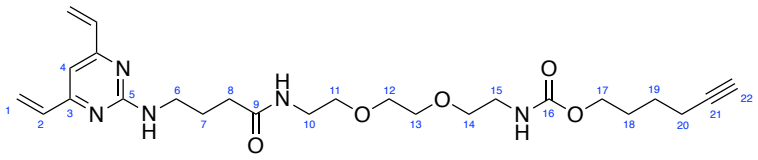

95

1,8-Diamino-3,6-dioxaoctane (358 µL, 2.44 mmol) and NEt_3 (170 µL, 1.22 mmol) were added to a stirred solution of **97** (107 mg, 0.406 mmol) in DMF (2.00 mL). The reaction mixture was stirred at rt for 15 min, before being concentrated *in vacuo*. The resulting residue was redissolved in CH_2Cl_2 (5 mL) and washed with 1 M NaOH (5 × 5 mL), followed by H_2O (5 × 5 mL). The organic extract was then dried and concentrated *in vacuo* to give crude hex-5-yn-1-yl (2-(2-(2-aminoethoxy)ethoxy)ethyl)carbamate **98**, which was used in the next step without further purification.

According to General Procedure G, EDC·HCl (38.9 mg, 0.203 mmol), the crude amine **98**, carboxylic acid **80** (47.3 mg, 0.203 mmol), Et_3N (28.3 µL, 0.203 mmol) and HOBt·H_2O (31.1 mg, 0.203 mmol) gave a crude material. Purification *via* flash column chromatography (MeOH/CH_2Cl_2, 3:97) gave **95** as a yellow oil (56.6 mg, 0.116 mmol, 57%). **R_f** = 0.39 (MeOH/CH_2Cl_2, 3:97); **^{1}H NMR** (400 MHz, $CDCl_3$): δ_H

6.62–6.50 (3H, m, C(2)*H*, C(4)*H*), 6.34 (2H, dd, *J* 17.3, 1.5, C(1)H_t), 6.16 (1H, br s, C(5)N*H*), 5.55 (2H, dd, *J* 10.5, 1.5, C(1)H_c), 5.25 (2H, br s, C(9)N*H*, C(15)N*H*), 4.07 (2H, t, *J* 6.4, C(17)H_2), 3.62–3.49 (10H, m, C(6)H_2, C(11)H_2, C(12)H_2 C(13)H_2, C(14)H_2), 3.45 (2H, td, *J* 5.5, 4.2, C(10)H_2), 3.36 (2H, q, *J* 5.6, C(15)H_2), 2.29 (2H, t, *J* 7.3, C(8)H_2), 2.22 (2H, td, *J* 6.9, 2.6, C(20)H_2), 2.03–1.92 (3H, m, C(7)H_2, C(22)*H*), 1.72 (2H, s, C(18)H_2), 1.61 (2H, d, *J* 7.2, C(19)H_2); **^{13}C NMR** (101 MHz, $CDCl_3$): δ_C 172.8 (*C*(9)), 163.9 (*C*(3)), 162.9 (*C*(5)), 156.9 (*C*(16)), 136.1 (*C*(2)), 121.6 (*C*(1)), 105.7 (*C*(4)), 84.1 (*C*(22)), 70.4 (*C*(11/12/13/14)), 70.3 (*C*(11/12/13/14)), 70.2 (*C*(11/12/13/14)), 70.1 (*C*(11/12/13/14)), 68.8 (*C*(21)), 64.5 (*C*(17)), 40.8 (2C, *C*(6), *C*(15)), 39.4 (*C*(10)), 34.0 (*C*(8)), 28.2 (*C*(18)), 25.9 (*C*(7)), 25.0 (*C*(19)), 18.2 (*C*(20)); **IR** ν_{max}: 3331 (m, N–H), 2935 (w, C–H), 1701 (s, C=O), 1644 (m, C=O), 1540 (m, Ar C=C); **HRMS** (ESI): $[M+Na]^+$ calcd. for $C_{25}H_{37}N_5NaO_5^+$: 510.2687, found: 510.2699.

Methyl 2,2-dimethyl-6-oxo-5-oxa-7,11-diaza-2-silatetradecan-14-oate (127)

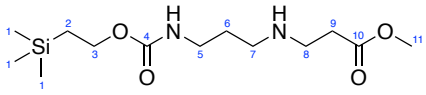

127

Methyl acrylate (2.94 mL, 32.1 mmol) was added dropwise to neat propane-1,3-diamine, **119**, (2.70 mL, 32.1 mmol) at 0 °C. The resulting mixture was then immediately dissolved in dioxane/H_2O (1:1, 100 mL). Et_3N (11.5 mL, 8.25 mmol) and 4-nitrophenyl 2-(trimethylsilyl)ethyl carbonate (10.0 g, 35.2 mmol) were then added and the mixture was stirred for a further 18 h at rt. Upon completion, CH_2Cl_2 (10 mL) was added, and the organic layer was washed with brine (3 × 10 mL). The organic layer was then dried and concentrated *in vacuo*. Purification *via* flash column chromatography (Et_3N/MeOH/CH_2Cl_2, 1:3:96) gave **127** as a yellow oil (5.48 g, 18.0 mmol, 56%). $\mathbf{R_f}$ = 0.11 (MeOH/CH_2Cl_2, 4:96); **^{1}H NMR** (400 MHz, $CDCl_3$): δ_H 4.13 (2H, t, *J* 8.4, C(3)H_2), 3.69 (3H, s, C(11)H_3), 3.25 (2H, q, *J* 6.3, C(5)H_2), 2.87 (2H, t, *J* 6.5, C(8)H_2), 2.69 (2H, t, *J* 6.5, C(7)H_2), 2.51 (2H, t, *J* 6.4, C(9)H_2), 1.65 (2H, p, *J* 6.5, C(6)H_2), 0.96 (2H, t, *J* 8.4, C(2)H_2), 0.03 (9H, s, C(1)H_3); **^{13}C NMR** (101 MHz, $CDCl_3$): δ_C 173.4 (*C*(10)), 157.0 (*C*(4)), 62.9 (*C*(3)), 51.8 (*C*(11)), 47.7 (*C*(7)), 45.1 (*C*(8)), 39.9 (*C*(5)), 34.6 (*C*(9)), 29.8 (*C*(6)), 17.9 (*C*(2)), –1.3 (*C*(1)); **IR** ν_{max}: 3309 (m, N–H), 2954 (m, C–H), 1711 (m, 2 × C=O); **HRMS** (ESI): $[M+H]^+$ calcd. for $C_{13}H_{29}N_2O_4Si^+$: 305.1891, found: 305.1895.

Methyl 3-((4,6-dichloropyrimidin-2-yl)(3-(3-(trimethylsilyl)propanamido)propyl)amino)propanoate (128)

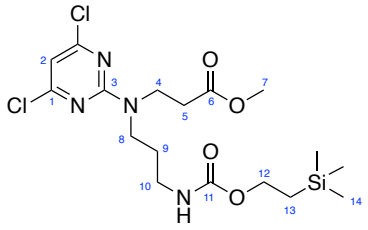

128

Et_3N (2.86 mL, 20.5 mmol) was added dropwise to a stirred solution of 2,4,6-trichloropyrimidine, **81**, (1.51 g, 8.23 mmol) and amine **127** (3.00 g, 9.86 mmol) in MeOH (50 mL) at 0 °C. After 5 min, the reaction mixture was warmed to rt and stirred for a further 3 h. The reaction mixture was concentrated *in vacuo*, then redissolved in EtOAc (30 mL) and washed with H_2O (2 × 30 mL) and brine (30 mL). The organic extract was dried and concentrated *in vacuo*. Purification *via* flash column chromatography (EtOAc/petroleum ether, 15:85) gave **128** as a yellow oil (1.04 g, 2.30 mmol, 28%). $\mathbf{R_f}$ = 0.12 (EtOAc/petroleum ether, 20:80); **^{1}H NMR** (400 MHz, $CDCl_3$): δ_H 6.57 (1H, d, *J* 1.1, C(2)*H*), 5.42 (1H, br s, N*H*), 4.15 (2H, t, *J* 8.4, C(12)H_2), 3.80 (2H, t, *J* 7.0, C(4)H_2), 3.71–3.61 (5H, m, C(7)H_3, C(8)H_2), 3.14 (2H, q, *J* 6.3, C(10)H_2), 2.68 (2H, t, *J* 7.0, C(5)H_2), 1.78 (2H, p, *J* 6.3, C(9)H_2), 1.02–0.94 (2H, m, C(13)H_2), 0.03 (9H, s, C(14)H_3); **^{13}C NMR** (101 MHz, $CDCl_3$): δ_C 172.4 (*C*(6)), 161.9 (C(1)), 161.7 (*C*(1)) 160.9 (*C*(3)), 157.0 (*C*(11), 108.4 (*C*(2)), 63.0 (*C*(12)), 51.9 (*C*(7)), 45.5 (*C*(8)), 44.1 (*C*(4)), 37.6 (*C*(10)), 32.3 (*C*(5)), 28.1 (*C*(9)), 17.9 (*C*(13)), –1.3 (*C*(14)); **IR** ν_{max}: 3378 (m, N–H), 2954 (m, C–H), 1716 (m, 2 × C=O), 1569 (s, Ar C=C); **HRMS** (ESI): $[M+H]^+$ calcd. for $C_{17}H_{29}{}^{35}Cl_2N_4O_4Si^+$: 451.1330, found: 451.1330.

Methyl 3-((4,6-divinylpyrimidin-2-yl)(3-(3-(trimethylsilyl)propanamido)propyl)amino)propanoate (129)

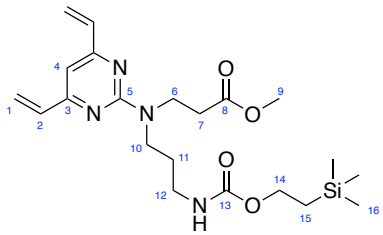

129

Potassium vinyltrifluoroborate (535 mg, 3.99 mmol), $Pd(dppf)Cl_2{\cdot}CH_2Cl_2$ (109 mg, 0.133 mmol) and K_2CO_3 (1.10 g, 7.98 mmol) were added to a stirred solution of pyrimidine **128** (600 mg, 1.33 mmol) in THF/H_2O (10:1, 55 mL) and heated to 70 °C for 18 h. Then, the reaction mixture was filtered through Celite® and concentrated *in vacuo*. Purification *via* flash column chromatography (EtOAc/petroleum

ether, 15:85) gave **129** (464 mg, 1.07 mmol, 80%) as a pale-yellow oil. $\mathbf{R_f}$ = 0.26 (EtOAc/petroleum ether, 15:85); **^{1}H NMR** (400 MHz, $CDCl_3$): δ_H 6.61 (2H, dd, *J* 17.3, 10.6, C(2)*H*), 6.51 (1H, s, C(4)*H*), 6.37 (2H, d, *J* 17.3, C(1)H_t), 5.93 (1H, br s, N*H*), 5.57 (2H, d, *J* 10.5, C(1)H_c), 4.14 (2H, dd, *J* 8.4, 3.2, C(14)H_2), 3.86 (2H, t, *J* 7.2, C(6)H_2), 3.77 (2H, t, *J* 6.3, C(10)H_2), 3.67 (3H, d, *J* 2.0, C(9)H_3), 3.16–3.10 (2H, m, C(12)H_2), 2.72 (2H, t, *J* 7.2, C(7)H_2), 1.77 (2H, t, *J* 6.3, C(11)H_2), 0.98 (2H, t, *J* 8.5. C(15)H_2), 0.03 (9H, s, C(16)H_3); **^{13}C NMR** (101 MHz, $CDCl_3$): δ_C 173.0 (*C*(8)), 163.6 (*C*(3)), 161.8 (*C*(5)), 157.0 (*C*(13)), 136.1 (*C*(2)), 121.6 (*C*(1)), 105.1 (*C*(4)), 62.7 (*C*(14)), 51.7 (*C*(9)), 44.3 (*C*(10)), 43.7 (*C*(6)), 37.3 (*C*(12)), 32.6 (*C*(7)), 28.2 (*C*(11)), 17.9 (*C*(15)), –1.3 (*C*(16)); **IR** ν_{max}: 2953 (w, C–H), 1717 (s, C=O), 1638 (w, C=C), 1542 (m, Ar C=C); **HRMS** (ESI): $[M+H]^+$ calcd. for $C_{21}H_{35}N_4O_4Si^+$: 435.2422, found: 435.2415.

Bicyclo[6.1.0]non-4-yn-9-ylmethyl (2-(trimethylsilyl)ethyl) (13-(4,6-divinylpyrimidin-2-yl)-10-oxo-3,6-dioxa-9,13-diazahexadecane-1,16-diyl)dicarbamate (130)

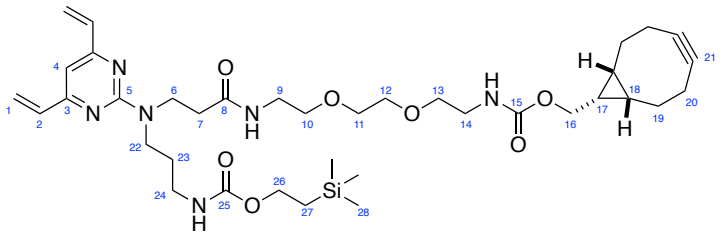

130

1,8-Diamino-3,6-dioxaoctane (251 µL, 1.71 mmol) and NEt_3 (126 µL, 0.906 mmol) were added to a stirred solution of **87** (125 mg, 0.396 mmol) in DMF (7.0 mL). The reaction mixture was stirred at rt for 15 min, before being concentrated *in vacuo*. The resulting residue was redissolved in CH_2Cl_2 (20 mL) and washed with 1 M NaOH (5 × 20 mL), followed by H_2O (5 x 20 mL). The organic extract was then dried and concentrated *in vacuo* to give crude ((1*R*,8*S*,9*s*)-bicyclo[6.1.0]non-4-yn-9-yl)methyl (2-(2-(2-aminoethoxy)ethoxy)ethyl)carbamate **88**, which was used in the next step without further purification.

LiOH·H_2O (16.6 mg, 0.396 mmol) was added to a stirred solution of **129** (86.0 mg, 0.198 mmol) in THF/H_2O (1:1, 283 µL) at rt. The reaction mixture was stirred for 3 h, then concentrated *in vacuo* to remove the organics. The crude mixture was then diluted with satd. NH_4Cl (5 mL) and the pH adjusted to 4 with 1 M HCl. The resulting solution was extracted with 10% ^{i}PrOH/EtOAc (4 x 5 mL) and the combined organic extracts were dried and concentrated *in vacuo*. The resulting crude carboxylic acid was dissolved in DMF (3.95 mL) and cooled to 0 °C. EDC·HCl (75.9 mg, 0.396 mmol), the crude amine **88**, Et_3N (55.2 µL, 0.396 mmol) and HOBt·H_2O (60.6 mg, 0.396 mmol) were added to the solution at 0 °C. The resultant mixture was warmed to rt and stirred for a further 18 h. Then, EtOAc was added (20 mL), and the organic layer was washed with brine (8 × 20 mL). The organic extract was dried and

concentrated *in vacuo*. Purification *via* flash column chromatography (MeOH/CH_2Cl_2, 2:98) gave **130** as a yellow oil (57.3 mg, 78.8 µmol, 40%). $\mathbf{R_f}$ = 0.16 (MeOH/CH_2Cl_2, 3:97); **^{1}H NMR** (400 MHz, $CDCl_3$): δ_H 6.62 (2H, dd, *J* 17.3, 10.6, C(2)*H*), 6.52 (1H, s, C(4)*H*), 6.37 (2H, d, *J* 17.3, C(1)H_t), 5.87 (1H, br s, C(8)N*H*), 5.58 (2H, d, *J* 10.6, C(1)H_c), 5.15 (1H, br s, C(15/25)N*H*), 4.13 (4H, t, *J* 7.8, C(16)H_2, C(26)H_2), 3.88 (2H, t, *J* 6.8, C(6)H_2), 3.76 (2H, t, *J* 6.3, C(22)H_2), 3.54 (8H, m, C(10)H_2, C(11)H_2 C(12)H_2, C(13)H_2), 3.44 (2H, q, *J* 5.3, C(9)H_2), 3.36–3.32 (2H, m, C(14)H_2), 3.12 (2H, d, *J* 6.3, C(24)H_2), 2.60 (2H, t, *J* 6.8, C(7)H_2), 2.33–2.23 (6H, m, C(19)H_AH_B, C(20)H_2), 1.77 (2H, t, *J* 6.3, C(23)H_2), 1.56 (2H, m, C(19)H_AH_B),[s] 1.37–1.22 (1H, m, C(17)*H*), 1.01–0.78 (4H, m, C(18)*H*, C(27)H_2), 0.03 (9H, s, C(28)H_3); **^{13}C NMR** (101 MHz, $CDCl_3$): δ_C 171.8 (*C*(8)), 163.7 (*C*(3)), 161.9 (*C*(5)), 157.0 (*C*(15/25), 156.9 (*C*(15/25)), 136.1 (*C*(2)), 121.7 (*C*(1)), 104.9 (*C*(4)), 99.0 (*C*(21)), 70.4 (2C, *C*(10/11/12/13)), 70.2 (*C*(10/11/12/13)), 70.1 (*C*(10/11/12/13)), 62.9 (*C*(16/26)), 62.8 (*C*(16/26)), 53.6 (CH_2Cl_2), 44.3 (*C*(22)), 44.2 (*C*(6)), 40.9 (*C*(14)), 39.4 (*C*(9)), 37.4 (*C*(24)), 35.2 (*C*(7)), 31.1 (acetone), 29.2 (*C*(19)), 28.1 (*C*(23)), 21.6 (*C*(20)), 20.2 (*C*(18)), 17.9 (2C, *C*(17), *C*(27)), –1.3 (*C*(23)); **IR** ν_{max}: 3320 (m, N–H), 2926 (w, C–H), 1705 (s, C=O), 1660 (s, C=O), 1542 (m, Ar C=C); **HRMS** (ESI): $[M+H]^+$ calcd. for $C_{37}H_{59}N_6O_7Si^+$: 727.4209, found: 727.4208.

Methyl 2,2-dimethyl-4,13-dioxo-14-(3-(((2-(trimethylsilyl)ethoxy)carbonyl)amino)propyl)-3,8,11-trioxa-5,14-diazaheptadecan-17-oate (137)

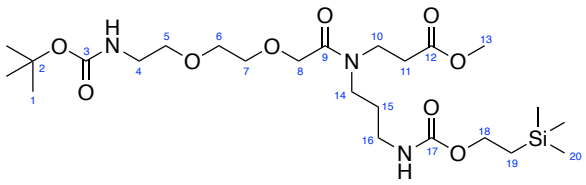

137

According to General Procedure G, EDC·HCl (347 mg, 1.81 mmol), Boc-8-amino-3,6-dioxaoctanoic acid·DCHA (803 mg, 1.81 mmol), carboxylic acid **80** (500 mg, 1.64 mmol), Et_3N (145 µL, 1.81 mmol) and HOBt·H_2O (277 mg, 1.81 mmol) gave a crude material. Purification *via* flash column chromatography (MeOH/CH_2Cl_2, 2:98) gave **137** as a yellow oil (858 mg, 1.56 mmol, 95%). $\mathbf{R_f}$ = 0.38 (MeOH/CH_2Cl_2, 5:95); **^{1}H NMR** (400 MHz, $CDCl_3$):[t] δ_H 4.28–4.07 (4H, m, C(8)H_2, C(18)H_2), 3.73–3.49 (11H, m, C(5)H_2, C(6)H_2, C(7)H_2, C(10)H_2, C(13)H_3), 3.44–3.24 (4H, m, C(4)H_2, C(14)H_2), 3.18 (1H, d, *J* 6.2, C(16)H_2), 3.10 (1H, q, *J* 6.2, C(16)H_2), 2.62 (2H, td, *J* 7.2, 4.3, C(11)H_2), 1.82–1.66 (2H, m, C(15)H_2), 1.43 (9H, s, C(1)H_3), 0.96 (2H, dq, *J* 8.9, 4.3, C(19)H_2), 0.02 (9H, s, C(20)H_3); **^{13}C NMR** (101 MHz, $CDCl_3$):[u]

[s] Observed in 2D NMR spectra.
[t] Peaks in ^{1}H NMR spectrum broad and split due to the presence of rotamers, compound **130** was unstable to high temperature NMR.
[u] Peaks in ^{13}C NMR spectrum broad and split due to the presence of rotamers.

δ_C 172.5 (*C*(12)), 171.6 (*C*(12)), 169.9 (*C*(9)), 169.1 (*C*(9)), 157.1 (*C*(17)), 156.1 (*C*(3)), 79.3 (*C*(2)), 70.9 (*C*(5/6/7/8)), 70.8 (*C*(5/6/7/8)), 70.6 (*C*(5/6/7/8)), 70.5 (*C*(5/6/7/8)), 70.4 (2C, C(5/6/7/8), 63.2 (*C*(18)), 62.9 (*C*(18)), 52.1 (*C*(13)), 51.9 (*C*(13)), 45.7 (*C*(14)), 42.6 (*C*(10)), 42.3 (*C*(10)), 42.2 (*C*(14)), 40.6 (*C*(4)), 38.3 (*C*(16)), 37.7 (*C*(16)), 33.5 (*C*(11)), 32.5 (*C*(11)), 29.4 (*C*(15)), 28.5 (*C*(1)), 27.8 (*C*(15)), 17.9 (*C*(19)), –1.3 (*C*(20)); **IR** ν_{max}: 3340 (br, N–H), 2954 (w, C–H), 1706 (s, C=O), 1645 (s, C=O); **HRMS** (ESI): $[M+Na]^+$ calcd. for $C_{24}H_{47}N_3NaO_9Si^+$: 572.2974, found: 572.2980.

Methyl 17-((4,6-divinylpyrimidin-2-yl)amino)-5,14-dioxo-4-(3-(((2-(trimethylsilyl)ethoxy)carbonyl)amino)propyl)-7,10-dioxa-4,13-diazaheptadecanoate (132)

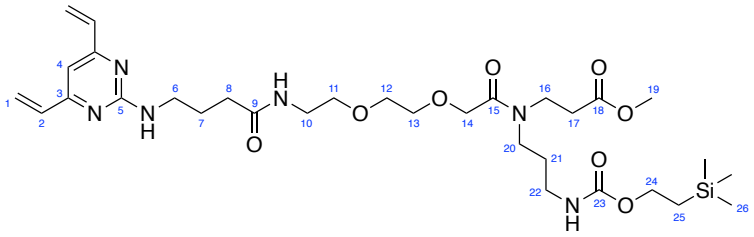

132

*p*TsOH·H_2O (223 mg, 1.17 mmol) was added to a stirred solution of tertiary amine **137** (215 mg, 0.391 mmol) in MeOH (5.0 mL). The reaction mixture was stirred at 60 °C for 2 h, then quenched with satd. $NaHCO_3$ (5 mL) and concentrated *in vacuo* to remove the organics. The crude mixture was then diluted with satd. $NaHCO_3$ (10 mL) and extracted with CH_2Cl_2 (3 × 15 mL). The combined organic extracts were then dried and concentrated *in vacuo* to give the corresponding crude amine, which was used in the next step without further purification.

According to General Procedure G, EDC·HCl (150 mg, 0.782 mmol), the crude amine, carboxylic acid **80** (182 mg, 0.782 mmol), Et_3N (109 µL, 0.782 mmol) and HOBt·H_2O (120 mg, 0.782 mmol) gave a crude material. Purification *via* flash column chromatography (MeOH/CH_2Cl_2, 4:96–10:90) gave **132** as a yellow oil (218 mg, 0.328 mmol, 84%). $\mathbf{R}_f$ = 0.68 (MeOH/CH_2Cl_2, 10:90); **^{1}H NMR** (400 MHz, $CDCl_3$):[v] δ_H 6.77–6.66 (1H, br s, N*H*), 6.61–6.49 (3H, m, C(2)*H*, C(4)*H*), 6.37–6.28 (2H, m, C(1)H_t), 5.54 (2H, dd, *J* 10.5, 1.6, C(1)H_c), 5.35 (1H, br s, N*H*), 4.28–4.06 (4H, m, C(14)H_2, C(24)H_2), 3.72–3.59 (7H, m, C(12)H_2, C(13)H_2, C(19)H_3), 3.59–3.48 (6H, m, C(6)H_2, C(11)H_2, C(16)H_2), 3.44 (2H, q, *J* 5.2, C(10)H_2), 3.34 (2H, dt, *J* 26.2, 7.4, C(20)H_2), 3.21–3.06 (2H, m, C(22)H_2), 2.61 (2H, t, *J* 7.1, C(17)H_2), 2.32 (2H, t, *J* 7.3, C(8)H_2), 1.97 (2H, ddd, *J* 9.0, 5.7, 2.2, C(7)H_2), 1.87–1.64 (2H, m, C(21)H_2), 1.01–0.91 (2H, m, C(25)H_2), 0.02 (9H,

[v] Peaks in ^{1}H NMR spectrum broad and split due to the presence of rotamers, compound **132** was unstable to high temperature NMR.

s, C(26)*H*$_3$); **^{13}C NMR** (101 MHz, $CDCl_3$):[w] δ_C 173.1 (*C*(9)), 172.6 (*C*(18)), 171.6 (*C*(18)), 169.9 (*C*(15)), 169.3 (*C*(15)), 163.8 (*C*(3)), 162.9 (*C*(5)), 157.1 (*C*(23)), 136.1 (*C*(2)), 121.5 (*C*(1)), 105.5 (*C*(4)), 70.8 (*C*(11/12/13/14)), 70.3 (*C*(11/12/13/14)), 70.2 (*C*(11/12/13/14)), 70.1 (*C*(11/12/13/14)), 63.0 (*C*(24)), 52.2 (*C*(19)), 51.9 (*C*(19)), 45.6 (*C*(20)), 42.5 (*C*(16)), 41.0 (*C*(6)), 39.4 (*C*(10)), 37.8 (*C*(22)), 33.9 (*C*(8)), 33.5 (*C*(17)), 32.5 (*C*(17)), 27.8 (*C*(21)), 25.8 (*C*(7)), 17.9 (*C*(25)), –1.3 (*C*(26)); **IR** ν_{max}: 3323 (m, N–H), 2950 (w, C–H), 1713 (m, C=O), 1639 (m, C=O/C=C), 1542 (m, Ar C=C); **HRMS** (ESI): $[M+H]^+$ calcd. for $C_{31}H_{53}N_6O_8Si^+$: 665.3689, found: 665.3696.

Bicyclo[6.1.0]non-4-yn-9-ylmethyl (2-(trimethylsilyl)ethyl) (13-(2-(2-(2-(4-((4,6-divinylpyrimidin-2-yl)amino)butanamido)ethoxy)ethoxy)acetyl)-10-oxo-3,6-dioxa-9,13-diazahexadecane-1,16-diyl)dicarbamate (135)

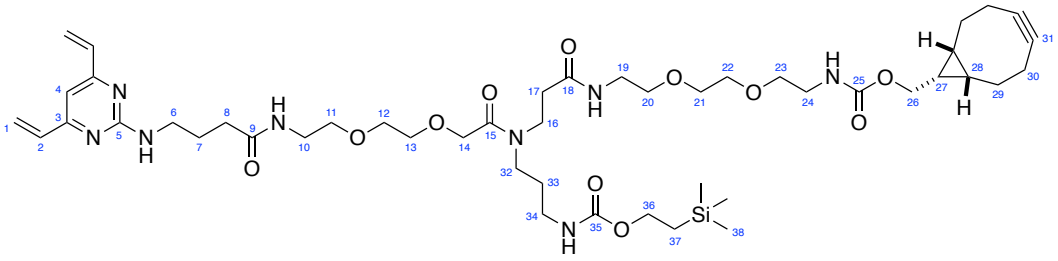

135

1,8-Diamino-3,6-dioxaoctane (195 µL, 1.33 mmol) and NEt_3 (99.4 µL, 0.713 mmol) were added to a stirred solution of BCN-ONp **87** (206 mg, 0.310 mmol) in DMF (5.5 mL). The reaction mixture was stirred at rt for 15 min, before being concentrated *in vacuo*. The resulting residue was then dissolved in CH_2Cl_2 (10 mL) and washed with 1 M NaOH (5 × 10 mL), followed by H_2O (5 x 10 mL). The organic extract was dried and concentrated *in vacuo* to give crude ((1*R*,8*S*,9*s*)-bicyclo[6.1.0]non-4-yn-9-yl)methyl (2-(2-(2-aminoethoxy)ethoxy)ethyl)carbamate **88**, which was used in the next step without further purification.

LiOH·H_2O (7.80 mg, 0.186 mmol) was added to a stirred solution of DVP **132** (103 mg, 0.155 mmol) in THF/H_2O (1:1, 0.50 mL) at rt. The reaction mixture was stirred for 3 h, then concentrated *in vacuo* to remove the organics. The crude mixture was then diluted with satd. NH_4Cl (5 mL), and the pH adjusted to 4 with 1 M HCl. The resulting solution was extracted with 10% ^{i}PrOH/EtOAc (4 x 5 mL) and the combined organic extracts were dried and concentrated *in vacuo*. The resulting crude carboxylic acid was dissolved in DMF (2.0 mL) and cooled to 0 °C. EDC·HCl (59.4 mg, 0.310 mmol), the crude amine **88**, Et_3N (43.2 µL, 0.310 mmol) and HOBt·H_2O (47.5 mg, 0.310 mmol) were added to the solution 0 °C.

[w] Peaks in ^{13}C NMR spectrum broad and split due to the presence of rotamers.

The resultant mixture was warmed to rt and stirred for a further 18 h. Then, EtOAc was added (20 mL), and the organic layer was washed with brine (8 × 20 mL). The organic extract was dried and concentrated *in vacuo*. Purification *via* flash column chromatography (CH_2Cl_2/MeOH, 95:5) gave **135** as a yellow oil (152 mg, 915 µmol, 59%). $\mathbf{R_f}$ = 0.29 (CH_2Cl_2/MeOH 93:7); **^{1}H NMR** (500 MHz, MeOD):[x] δ_H 6.70 (1H, s, C(4)*H*), 6.61 (2H, dd, *J* 17.4, 10.7, C(2)*H*), 6.37 (2H, d, *J* 17.4, C(1)H_t), 5.57 (2H, dd, *J* 10.7, 1.5, C(1)H_c), 4.32 (1H, s, C(14)H_2), 4.22 (1H, s, C(14)H_2), 4.14–4.08 (4H, m, C(26)H_2, C(36)H_2), 3.69–3.49 (16H, m, C(16)H_2, C(11)H_2, C(12)H_2, C(13)H_2, C(20)H_2, C(21)H_2, C(22)H_2, C(23)H_2), 3.47 (2H, t, *J* 6.8, C(6)H_2), 3.36 (5H, m, C(19)H_2, C(10)H_2, C(32)H_2), 3.28 (3H, app t, *J* 5.7, C(24)H_2 , C(32)H_2), 3.10 (2H, dt, *J* 17.4, 6.7, C(34)H_2), 2.49 (2H, dt, *J* 16.2, 7.0, C(17)H_2), 2.38–2.11 (8H, m, C(8)H_2, C(29)H_AH_B, C(30)H_2), 1.97–1.88 (2H, m, C(7)H_2) 1.74 (2H, dp, *J* 27.9, 7.0, 6.6, C(33)H_2), 1.65–1.53 (2H, m, C(29)H_AH_B), 1.36 (1H, p, *J* 8.5, C(27)*H*), 1.01–0.88 (4H, m, C(28)*H*, C(37)H_2), 0.05 (9H, d, *J* 1.7, C(38)H_3); **^{13}C NMR** (126 MHz, MeOD):[y] 176.0 (*C*(9)), 173.7 (*C*(18)), 173.1 (*C*(18)), 171.9 (*C*(15)), 171.5 (*C*(15)), 165.3 (*C*(5)), 164.0 (*C*(5)), 159.2 (*C*(25/35)), 159.1 (*C*(25/35)), 137.1 (*C*(2)), 122.1 (*C*(1)), 105.8 (*C*(4)), 99.5 (*C*(31)), 71.8 (2C, *C*(13), *C*(13)), 71.3 (3C, *C*(10/11/12/20/21/22/23)), 71.2 (2C, *C*(10/11/12/20/21/22/23)), 71.0 (*C*(10/11/12/20/21/22/23)), 70.6 (*C*(10/11/12/20/21/22/23)), 70.5 (*C*(14)), 70.4 (*C*(14)), 63.9 (*C*(36)), 63.8 (C(36)), 63.7 (C(26)), 46.3 (*C*(32)), 44.3 (*C*(16)), 44.1 (*C*(19)), 44.0 (*C*(16)), 41.7 (*C*(6)), 41.6 (*C*(24)), 40.5 (*C*(10)), 40.4 (*C*(10)), 39.2 (*C*(34)), 39.1 (*C*(34)), 35.9 (*C*(17)), 35.2 (*C*(17)), 34.5 (*C*(8)), 30.2 (*C*(29)), 30.0 (*C*(33)), 28.7 (*C*(33)), 27.0 (*C*(7)), 21.9 (*C*(30)), 21.4 (*C*(28)), 19.0 (*C*(27)), 18.7 (2C, (*C*(37)), –1.4 (C(38)); **IR** ν_{max}: 3326 (m, N–H), 2920 (w, C–H), 1705 (s, C=O), 1681 (s, C=O), 1546 (m, Ar C=C); **HRMS** |ESI): $[M+H]^+$ calcd. for $C_{47}H_{77}N_8O_{11}Si^+$: 957.5476, found: 957.5533.

[x] Peaks in ^{1}H NMR spectrum broad and split due to the presence of rotamers, compound **135** was unstable to high temperature NMR.

[y] Peaks in ^{13}C NMR spectrum broad and split due to the presence of rotamers.

Methyl 17-((4,6-divinylpyrimidin-2-yl)amino)-4-(3-((((2-methylcycloprop-2-en-1-yl)methoxy)carbonyl)amino)propyl)-5,14-dioxo-7,10-dioxa-4,13-diazaheptadecanoate (138)

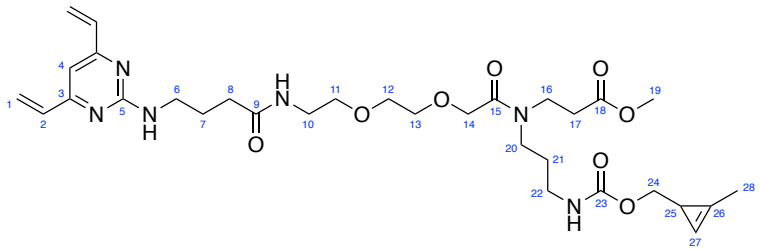

138

TBAF (1.0 M in THF, 575 µL, 575 µmol) was added to a stirred solution of DVP **132** (76.5 mg, 0.115 mmol) in THF (5.00 mL). The reaction mixture was stirred at 50 °C for 3 h before cyp-ONP, **89**, (31.7 mg, 0.127 mmol) and Et_3N (17.7 µL, 0.127 mmol) was added. After stirring for 1 h at rt the mixture was quenched with satd. NH_4Cl (5 mL) and extracted with CH_2Cl_2 (3 × 5 mL). The combined organic extracts were dried and concentrated *in vacuo*. Purification *via* flash column chromatography (CH_2Cl_2/MeOH, 97:3–95:5) gave **138** as a yellow oil (45.0 mg, 71.3 µmol, 62%). $\mathbf{R_f}$ = 0.53 (CH_2Cl_2/MeOH, 90:10); **^{1}H NMR** (500 MHz, MeOD):[z] δ_H 6.69–6.55 (4H, m, C(2)*H*, C(4)*H*, C(27)*H*), 6.37 (2H, d, *J* 17.1, C(1)H_t), 5.57 (2H, dd, *J* 10.7, 1.5, C(1)H_c), 4.31 (1H, s, C(14)H_2), 4.21 (1H, s, C(14)H_2), 3.99–3.91 (1H, m, C(24)H_2), 3.86–3.76 (1H, m, C(24)H_2), 3.70–3.62 (7H, m, C(12)H_2, C(13)H_2, C(19)H_3), 3.62–3.56 (2H, m, C(16)H_2), 3.54 (2H, ddd, *J* 7.1, 4.7, 2.0, C(11)H_2), 3.46 (2H, t, *J* 6.8, C(6)H_2), 3.36 (4H, m, C(10)H_2, C(20)H_2), 3.10 (2H, dt, *J* 17.9, 6.2, C(22)H_2), 2.67 (1H, t, *J* 7.1, C(17)H_2), 2.60 (1H, t, *J* 7.1, C(17)H_2), 2.30 (2H, td, *J* 7.4, 4.3, C(8)H_2), 2.12 (3H, app s, C(28)H_3), 1.93 (2H, p, *J* 7.1, C(7)H_2), 1.82–1.65 (2H, m, C(21)H_2), 1.61 (1H, t, *J* 5.8, C(25)*H*); **^{13}C NMR** (126 MHz, MeOD):[aa] δ_C 176.0 (*C*(9)), 173.8 (*C*(15)), 173.3 (*C*(15)), 171.8 (*C*(18)), 171.5 (*C*(18)), 165.3 (*C*(3)), 164.0 (*C*(5)), 159.4 (*C*(23)), 159.3 (*C*(23)), 137.1 (*C*(2)), 122.2 (*C*(1)), 122.1 (*C*(26)), 105.8 (*C*(4)), 102.9 (*C*(27)), 73.2 (*C*(24)), 73.1 (*C*(24)), 71.8 (*C*(12/13)), 71.7 (*C*(12/13)), 71.1 (*C*(12/13)), 70.7 (*C*(14)), 70.5 (*C*(11)), 70.5 (*C*(14)), 52.3 (*C*(19)), 52.2 (*C*(19)), 46.3 (*C*(20)), 44.0 (*C*(20)), 43.6 (*C*(16)), 43.3 (*C*(16)), 41.6 (*C*(6)), 40.4 (*C*(10)), 39.2 (*C*(22)), 39.1 (*C*(22)), 34.5 (*C*(8)), 33.8 (*C*(17)), 33.1 (*C*(17)), 30.0 (*C*(21)), 28.7 (*C*(21)), 27.0 (*C*(7)), 18.3 (*C*(25)), 11.6 (*C*(28)); **IR** ν_{max}: 3306 (m, N–H), 2923 (m, C–H), 1732 (s, C=O), 1698 (s, C=O), 1638 (s, C=O), 1542 (m, Ar C=C); **HPLC** (5–95% MeCN/H_2O over 15 min) retention time 8.242 min; **HRMS** (ESI): $[M+H]^+$ calcd. for $C_{31}H_{47}N_6O_8^+$: 631.3450, found: 631.3461.

[z] Peaks in ^{1}H NMR spectrum broad and split due to the presence of rotamers, compound **138** was unstable to high temperature NMR.

[aa] Peaks in ^{13}C NMR spectrum broad and split due to the presence of rotamers.

Bicyclo[6.1.0]non-4-yn-9-ylmethyl ((2-methylcycloprop-2-en-1-yl)methyl) (13-(2-(2-(2-(4-((4,6-divinylpyrimidin-2-yl)amino)butanamido)ethoxy)ethoxy)acetyl)-10-oxo-3,6-dioxa-9,13-diazahexadecane-1,16-diyl)dicarbamate (131)

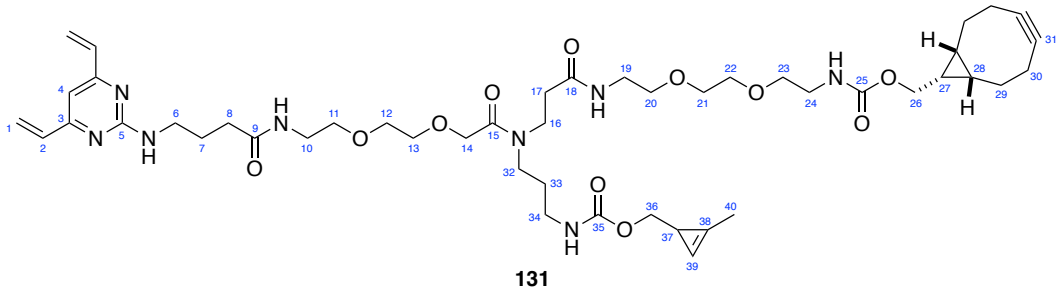

131

1,8-Diamino-3,6-dioxaoctane (119 µL, 0.813 mmol) and NEt_3 (60.6 µL, 0.435 mmol) were added to a stirred solution of BCN-ONp, **87**, (59.6 mg, 0.189 mmol) in DMF (5.5 mL). The reaction mixture was stirred at rt for 15 min, before being concentrated *in vacuo*. The resulting residue was then dissolved in CH_2Cl_2 (10 mL) and washed with 1 M NaOH (5 × 10 mL), followed by H_2O (5 x 10 mL). The organic extract was dried and concentrated *in vacuo* to give crude ((1*R*,8*S*,9*s*)-bicyclo[6.1.0]non-4-yn-9-yl)methyl (2-(2-(2-aminoethoxy)ethoxy)ethyl)carbamate **88**, which was used in the next step without further purification.

$LiOH{\cdot}H_2O$ (3.3 mg, 79 µmol) was added to a stirred solution of DVP **138** (59.7 mg, 94.6 µmol) in THF/H_2O (1:1, 1.00 mL) at rt. The reaction mixture was stirred for 3 h, then concentrated *in vacuo* to remove the organics. The crude mixture was then diluted with satd. NH_4Cl (5 mL), and the pH adjusted to 4 with 1 M HCl. The resulting solution was extracted with 10% ^{i}PrOH/EtOAc (4 x 5 mL) and the combined organic extracts were dried and concentrated *in vacuo*. The resulting crude carboxylic acid was dissolved in DMF (2.0 mL) and cooled to 0 °C. EDC·HCl (36.3 mg, 0.189 mmol), the crude amine **88**, Et_3N (26.3 µL, 0.189 mmol) and $HOBt{\cdot}H_2O$ (25.6 mg, 0.189 mmol) were added to the solution at 0 °C. The resultant mixture was warmed to rt and stirred for a further 18 h. Then, EtOAc was added (20 mL), and the organic layer was washed with brine (8 × 20 mL). The organic extract was dried and concentrated *in vacuo*. Purification *via* flash column chromatography ($MeOH/CH_2Cl_2$, 15:85–20:80) gave **131** as a yellow oil (33.4 mg, 36.2 µmol, 38%). $\mathbf{R_f}$ = 0.28 ($MeOH/CH_2Cl_2$, 15:85); **^{1}H NMR** (500 MHz, $CDCl_3$):[bb] δ_H 6.64 (1H, s, C(4)*H*), 6.61–6.51 (3H, m, C(2)*H,* C(39)*H*), 6.31 (2H, *J* 17.3, C(1)H_t), 5.51 (2H, d, *J* 11.4, C(1)H_c), 4.26 (1H, C(14)H_2), 4.16 (1H, s, C(14)H_2), 4.08 (2H, d, *J* 8.1, C(26)H_2), 3.91–3.85 (1H, m, C(36)H_2), 3.79–3.73 (1H, m, C(36)H_2), 3.60–3.46 (16H, m, C(16)H_2, C(11)H_2, C(12)H_2, C(13)H_2, C(20)H_2,

[bb] Peaks in ^{1}H NMR spectrum broad and split due to the presence of rotamers, compound **131** was unstable to high temperature NMR.

C(21)H_2, C(22)H_2, C(23)H_2), 3.41 (2H, t, *J* 6.8, C(6)H_2), 3.31 (5H, dt, *J* 10.8, 6.8, C(19)H_2, C(10)H_2, C(32)H_2), 3.22 (3H, m, C(24)H_2, C(32)H_2), 3.08–3.00 (2H, m, C(34)H_2), 2.43 (2H, dt, *J* 22.6, 6.9, C(17)H_2), 2.25 (2H, t, *J* 7.4, C(8)H_2), 2.18 (4H, q, *J* 12.9, 11.8, C(29)H_AH_B, C(30)H_AH_B), 2.09 (5H, d, *J* 30.8, C(30)H_AH_B, C(40)H_3), 1.86 (2H, q, *J* 7.0, C(7)H_2), 1.74–1.65 (2H, m, C(33)H_2), 1.55 (3H, s, C(29)H_AH_B, C(37)*H*)), 1.34–1.27 (1H, m, C(27)*H*), 0.86 (2H, dd, *J* 19.9, 9.7, C(28)*H*); **^{13}C NMR** (126 MHz, $CDCl_3$):[cc] 176.1 (*C*(9)), 173.7 (*C*(18)), 173.1 (*C*(18)), 171.9 (*C*(15)), 171.5 (*C*(15)), 165.3 (*C*(3)), 164.0 (*C*(5)), 159.3 (*C*(25/35)), 159.3 (*C*(25/35), 137.1 (*C*(2)), 122.1 (*C*(1)), 105.8 (*C*(4)), 103.0 (*C*(38/39)), 102.9 (*C*(38/39)), 99.5 (*C*(31)), 73.3 (*C*(36)), 73.2 (*C*(36)), 71.8, 71.7, 71.3, 71.3, 71.3, 71.2, 71.2, 71.0, 70.6 (7C, *C*(11/13/12/20/21/22/23)) 70.5 (*C*(14)), 63.7 (*C*(26)), 46.3 (*C*(32)), 44.3 (*C*(16)), 44.1 (*C*(19)), 44.0 (*C*(16)), 41.7 (*C*(6)), 41.6 (*C*(24)), 40.5 (*C*(10), 40.4 (*C*(10)), 39.3 (*C*(34), 39.1 (*C*(34), 35.9 (*C*(17)), 35.2 (*C*(17)), 34.5 (*C*(8)), 30.2 (*C*(29)), 30.0 (*C*(33)), 28.7 (*C*(33)), 27.0 (*C*(7)), 21.9 (*C*(30)), 21.4 (*C*(28)), 19.0 (*C*(27), 18.3 (*C*(37)), 11.6 (*C*(40)); **IR** ν_{max}: 3318 (m, N–H), 1698 (s, C=O), 1648 (s, C=O), 1552 (m, Ar C=C); **HPLC** (5–95% MeCN/H_2O over 15 min) retention time 9.664 min; **HRMS** (ESI): $[M+H]^+$ calcd. for $C_{47}H_{71}N_8O_{11}^+$: 923.5237, found: 923.5232.

2-(4-(6-Methyl-1,2,4,5-tetrazin-3-yl)phenyl)acetic acid (152)

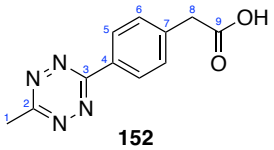

152

MeCN (0.497 mL, 9.31 mmol), and $Zn(OTf)_2$ (169 mg, 0.466 mmol) were added to a stirred solution of 4-cyanophenylacetic acid, **153**, (150 mg, 0.931 mmol) in dioxane (0.43 mL) at rt. Next, hydrazine hydrate (2.25 mL, 46.6 mmol) was added dropwise, and the reaction mixture was stirred for 18 h at 60 °C. After cooling the reaction mixture to rt, $NaNO_2$ (1.59 g, 23.0 mmol) in H_2O (13.3 mL) was added. Next, 1 M HCl was added dropwise to the solution until gas evolution stopped and the pH became acidic (caution: this reaction produces toxic nitrous fumes). The reaction mixture was extracted six times with CH_2Cl_2 (15 mL), followed by washing of the combined organic layers with brine (50 mL). The organic extract was dried and concentrated *in vacuo*. Purification *via* flash column chromatography (MeOH/CH_2Cl_2, 5:95) gave **152** as an amorphous pink solid (99.4 mg, 0.432 mmol, 46%). $\mathbf{R}_f$ = 0.30 (MeOH/CH_2Cl_2, 5:95); **^{1}H NMR** (700 MHz, $CDCl_3$): δ_H 8.58 (2H, d, *J* 8.3, C(5)*H*), 7.54 (2H, d, *J* 8.3, C(6)*H*), 3.80 (2H, s, C(8)H_2), 3.10 (3H, s, C(1)H_3); **^{13}C NMR** (176 MHz, $CDCl_3$): δ_C 176.3 (C(9)), 167.4 (C(2)), 164.0 (C(3)), 138.1 (C(7)), 131.1 (C(4)), 130.5 (C(6)), 128.4 (C(5)), 41.0 (C(8)), 21.3 (C(1)); **IR** ν_{max}: 2900 (w, C–H), 2518 (br, O–H), 1697 (s, C=O), 1556 (m, Ar C=C), 1401 (s, O–H, carboxylic acid); **LRMS** (ESI): $[M+H]^+$

[cc] Peaks in ^{13}C NMR spectrum broad and split due to the presence of rotamers.

calcd. for $C_{11}H_{11}N_4O_2^+$: 231.1 found: 231.1. These characterisation data are in accordance with that previously reported in the literature.[439]

***tert*-Butyl 1-(4-(6-methyl-1,2,4,5-tetrazin-3-yl)phenyl)-2-oxo-6,9,12-trioxa-3-azapentadecan-15-oate (154)**

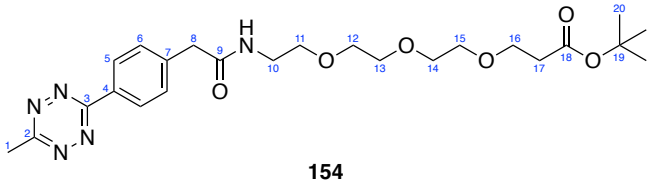

154

According to General Procedure G, EDC·HCl (32.5 mg, 0.170 mmol), *tert*-butyl 12-amino-4,7,10-trioxadodecanoate (44.6 µL, 0.170 mmol), carboxylic acid **152** (35.5 mg, 0.150 mmol), Et_3N (23.7 µL, 0.170 mmol) and HOBt·H_2O (31.1 mg, 0.203 mmol) gave a crude material. Purification *via* flash column chromatography (MeOH/CH_2Cl_2, 5:95) gave **154** as an amorphous pink solid (44.0 mg, 89.9 µmol, 60%). $\mathbf{R_f}$ = 0.56 (MeOH/CH_2Cl_2, 10:90); **^{1}H NMR** (400 MHz, $CDCl_3$): δ_H 8.55 (2H, d, *J* 8.2, C(5)*H*), 7.52 (2H, d, *J* 8.2, C(6)*H*), 6.31 (1H, br s, N*H*), 3.69 (2H, t, *J* 6.5, C(16)H_2), 3.66 (2H, s, C(8)H_2), 3.60–3.56 (8H, m, C(12)H_2, C(13)H_2, C(14)H_2, C(15)H_2), 3.54 (2H, t, *J* 5.0, C(11)H_2), 3.45 (2H, d, *J* 4.7, C(10)H_2), 3.09 (3H, s, C(1)H_3), 2.48 (2H, t, *J* 6.5, C(17)H_2), 1.43 (9H, C(20)H_3); **^{13}C NMR** (101 MHz, $CDCl_3$): δ_C 171.0 (*C*(18)), 170.3 (*C*(9)), 167.4 (*C*(2)), 164.0 (*C*(3)), 140.2 (*C*(7)), 130.8 (*C*(4)), 130.4 (*C*(6)), 128.4 (*C*(5)), 80.8 (*C*(19)), 70.7 (*C*(12/13/14/15), 70.6 (*C*(12/13/14/15), 70.5 (*C*(12/13/14/15), 70.4 (*C*(12/13/14/15), 69.8 (*C*(11)), 67.0 (*C*(16)), 43.7 (*C*(8)), 39.7 (*C*(10)), 36.4 (*C*(17)), 28.2 (*C*(20)), 21.3 (*C*(1)); **IR** ν_{max}: 2870 (w, C–H), 1725 (s, C=O), 1650 (s, C=O), 1546 (m, Ar C=C); **HRMS** (ESI): $[M+H]^+$ calcd. for $C_{24}H_{36}N_5O_6^+$: 490.2660, found: 490.2651.

1-(4-(6-Methyl-1,2,4,5-tetrazin-3-yl)phenyl)-2-oxo-6,9,12-trioxa-3-azapentadecan-15-oic acid (151)

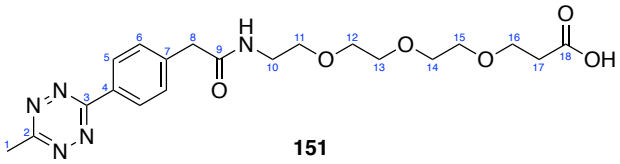

151

TFA (0.10 mL, 2.61 mmol) was added to a stirred solution of **154** (14.3 mg, 29.2 µmol) in CH_2Cl_2 (0.90 mL) at rt. The mixture was stirred at rt for 2 h before being concentrated under a stream of N_2. Purification *via* flash column chromatography (AcOH/MeOH/CH_2Cl_2, 1:10:89) gave **151** as an amorphous pink solid (12.5 mg, 28.8 µmol, 99%). $\mathbf{R_f}$ = 0.35 (MeOH/CH_2Cl_2, 10:90); **^{1}H NMR** (400 MHz, MeOD): δ_H 8.49 (2H, d, *J* 7.1, C(5)*H*), 7.56 (2H, d, *J* 7.1, C(6)*H*), 3.71 (2H, t, *J* 6.3, C(16)H_2), 3.66 (2H, s, C(8)H_2), 3.64–3.54 (10H, m, C(11)H_2, C(12)H_2, C(13)H_2, C(14)H_2, C(15)H_2), 3.41 (2H, d, *J* 5.0, C(10)H_2),

3.03 (3H, s, C(1)H_3), 2.51 (2H, app s, C(17)H_2); **^{13}C NMR** (101 MHz, MeOD): δ_C 172.0 (2C, *C*(9), *C*(18)), 167.3 (*C*(2)), 163.8 (*C*(3)), 140.6 (*C*(7)), 130.7 (*C*(4)), 129.7 (*C*(6)), 127.5 (*C*(5)), 70.2 (*C*(12/13/14/15), 70.1 (*C*(12/13/14/15), 69.9 (*C*(12/13/14/15), 69.8 (*C*(12/13/14/15), 69.2 (*C*(11)), 67.2 (*C*(16)), 42.3 (*C*(8)), 39.3 (2C, *C*(10), *C*(17)), 19.7 (*C*(1)); **IR** ν_{max}: 2901 (w, C–H), 1717 (s, C=O), 1644 (s, C=O), 1567 (m, Ar C=C); **HRMS** (ESI): $[M+H]^+$ calcd. for $C_{20}H_{28}N_5O_6^+$: 434.2034, found: 434.2039.

Alloc-va-PAB-Crizotinib (149)

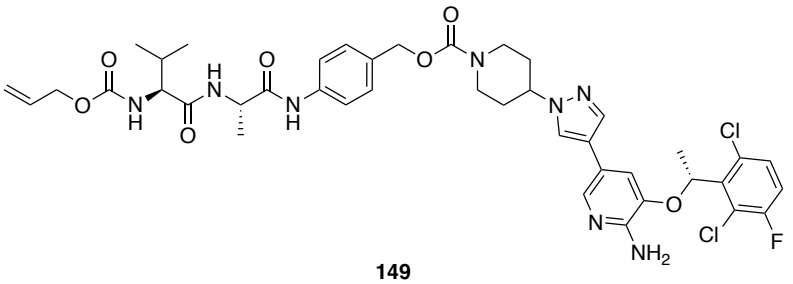

149

Bis(4-nitrophenyl) carbonate (22.9 mg, 75.2 µmol) and DIPEA (43.7 µL, 0.251 mmol) were added to a stirred solution of Alloc-va-PABA (18.9 mg, 50.1 µmol) in CH_2Cl_2 (5 mL) at rt. The mixture was stirred for 18 h before being concentrated under a stream of N_2. The crude residue was then redissolved in CH_2Cl_2 (10 mL) and washed with satd. $NaHCO_3$ (15 mL). The aqueous phase was then extracted with further CH_2Cl_2 (3 × 10 mL). The combined organic fractions were dried and concentrated *in vacuo* to give a crude material.

The crude material, HOBt·H_2O (16.6 mg, 123 µmol), pyridine (50.0 µL, 621 µmol) and DIPEA (50.0 µL, 387 µmol) were added to a stirred solution of crizotinib (33.3 mg, 74.0 µmol) in DMF (0.5 mL) at rt. After stirring for 2 h, the reaction mixture was concentrated under a stream of N_2. Purification *via* flash column chromatography (MeOH/CH_2Cl_2, 5:95) gave **149** as an amorphous white solid (35.9 mg, 42.0 µmol, 84%). **HPLC** (5–95% MeCN/H_2O over 15 min) retention time 10.145 min; **HRMS** (ESI): $[M+H]^+$ calcd. for $C_{41}H_{48}Cl_2FN_8O_7^+$: 853.3002, found: 853.2996.

N_3-PEG$_4$-va-PAB-Crizotinib (147)

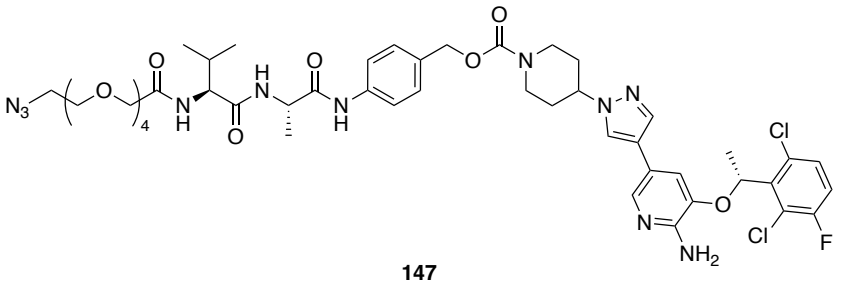

147

$Pd(PPh_3)_4$ (4.3 mg, 3.72 µmol) and pyrrolidine (11.9 µL, 145 µmol) were added to a stirred solution of alloc-va-PABC-crizotinib **149** (60.8 mg, 71.2 µmol) in CH_2Cl_2 (1.3 mL) at rt. After stirring for 1 h, the reaction mixture was diluted with CH_2Cl_2 (5 mL) and satd. $NaHCO_3$ (5 mL). The layers were separated, and the aqueous phase was extracted with further CH_2Cl_2 (3 × 5 mL). The combined organic fractions were dried and concentrated *in vacuo* to give the crude amine, which was carried through without further purification.

A solution of the crude amine, 14-azido-3,6,9,12-tetraoxatetradecanoic acid (0.5 M in TBME, 285 µL, 142 µmol), HBTU (54.2 mg, 143 µmol), HOBt·H_2O (21.9 mg, 143 µmol) and DIPEA (24.9 µL, 143 µmol) in DMF (1.0 mL) was stirred at rt for 2 h. Upon completion, the solvent was removed under a stream of N_2. Purification *via* flash column chromatography (MeOH/CH_2Cl_2, 5:95) gave **147** as an amorphous white solid (67.7 mg, 65.8 µmol, 92%). **HPLC** (5–95% MeCN/H_2O over 15 min) retention time 10.228 min; **HRMS** (ESI): $[M+H]^+$ calcd. for $C_{47}H_{61}Cl_2FN_{11}O_{10}^+$: 1028.3958, found: 1028.3953.

Alloc-va-PAB-Doxorubicin (156)

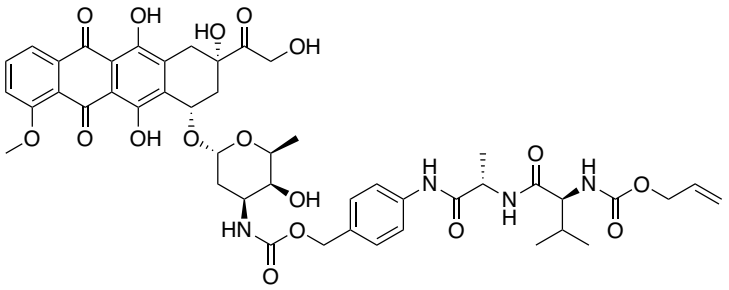

156

Bis(4-nitrophenyl) carbonate (22.9 mg, 75.2 µmol) and DIPEA (43.7 µL, 0.251 mmol) were added to a stirred solution of Alloc-va-PABA (18.9 mg, 50.1 µmol) in CH_2Cl_2 (5 mL) at rt. The mixture was stirred for 18 h before being concentrated under a stream of N_2. The crude residue was then redissolved in CH_2Cl_2 (10 mL) and washed with satd. $NaHCO_3$ (15 mL). The aqueous phase was then extracted with

further CH_2Cl_2 (3 × 10 mL). The combined organic fractions were dried and concentrated *in vacuo* to give a crude material.

The crude material, HOBt·H_2O (16.6 mg, 123 µmol), pyridine (50.0 µL, 621 µmol) and DIPEA (50.0 µL, 387 µmol) were added to a stirred solution of doxorubicin hydrochloride (40.2 mg, 74.0 µmol) in DMF (0.5 mL) at rt. Upon completion, the solvent was removed under a stream of N_2. Purification *via* flash column chromatography (MeOH/CH_2Cl_2, 5:95) gave **156** as an amorphous red solid (41.0 mg, 43.3 µmol, 51%). **HPLC** (5–95% MeCN/H_2O over 15 min) retention time 10.338 min; **HRMS** (ESI): $[M+H]^+$ calcd. for $C_{47}H_{55}N_4O_{17}^+$: 947.3557, found: 947.3545.

6-Methyl-Tetrazine-PEG3-va-PAB-Doxorubicin (155)

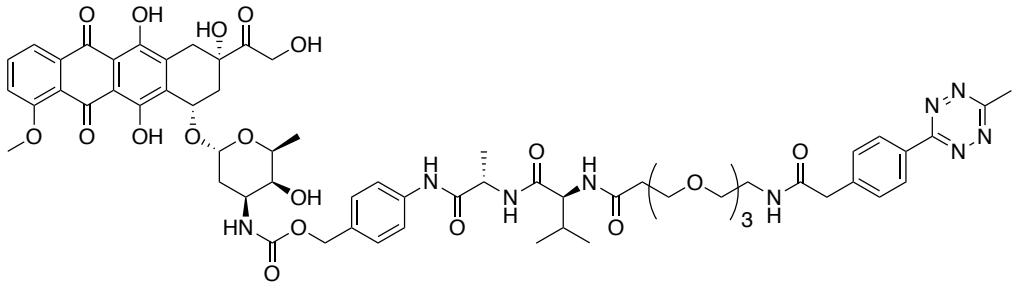

155

$Pd(PPh_3)_4$ (1.0 mg, 0.865 µmol) and pyrrolidine (2.72 µL, 32.6 µmol) were added to a stirred solution of Alloc-va-PABC-doxorubicin **156** (15.7 mg, 16.3 µmol) in CH_2Cl_2 (0.3 mL) at rt. After stirring for 1 h, the reaction mixture was diluted with CH_2Cl_2 (5 mL) and satd. $NaHCO_3$ (5 mL). The layers were separated, and the aqueous phase was extracted with further CH_2Cl_2 (3 × 5 mL). The combined organic fractions were dried and concentrated *in vacuo* to give the crude amine, which was carried through without further purification.

A solution of the crude amine, methyltetrazine-PEG3-acid **151** (14.1 mg, 32.6 µmol), HBTU (12.3 mg, 32.6 µmol), HOBt·H_2O (5.5 mg, 33 µmol) and DIPEA (5.66 µL, 32.6 µmol) in DMF (1.0 mL) was stirred at rt for 2 h. Upon completion, the solvent was removed under a stream of N_2. Purification *via* flash column chromatography (MeOH/CH_2Cl_2, 5:95) gave **155** as an amorphous red solid (4.0 mg, 13 µmol, 80%). **HPLC** (5–95% MeCN/H_2O over 15 min) retention time 9.946 min; **HRMS** (ESI): $[M+H]^+$ calcd. for $C_{59}H_{68}N_9O_{18}^+$: 1190.4677, found: 1190.4670.

6-Methyltetrazine-PEG12-va-PAB-Doxorubicin (159)

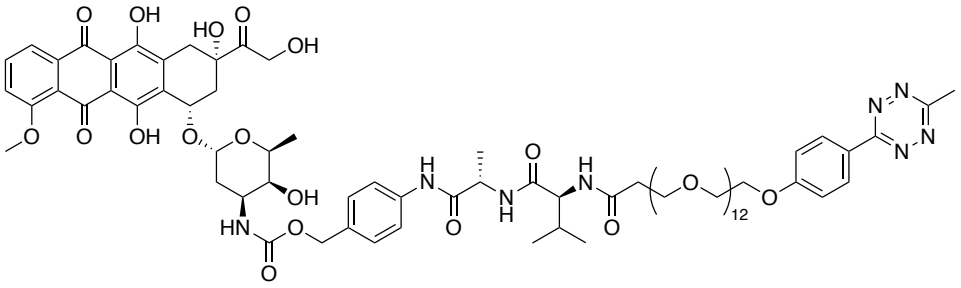

159

$Pd(PPh_3)_4$ (0.22 mg, 0.19 µmol) and pyrrolidine (0.62 µL, 7.6 µmol) were added to a stirred solution of Alloc-va-PABC-doxorubicin **156** (3.6 mg, 3.8 µmol) in CH_2Cl_2 (0.2 mL) at rt. After stirring for 1 h, the reaction mixture was diluted with CH_2Cl_2 (5 mL) and satd. $NaHCO_3$ (5 mL). The layers were separated, and the aqueous phase was extracted with further CH_2Cl_2 (3 × 5 mL). The combined organic fractions were dried and concentrated *in vacuo* to give the crude amine, which was carried through without further purification.

A solution of the crude amine, methyltetrazine-PEG12-acid, **158**, (1.50 mg, 1.9 µmol), HBTU (1.44 mg, 3.8 µmol), HOBt·H_2O (0.68 mg, 3.8 µmol) and DIPEA (0.66 µL, 3.8 µmol) in DMF (0.2 mL) was stirred at rt for 2 h. Upon completion, the solvent was removed under a stream of N_2. The resulting crude material was purified via reverse phase flash column chromatography (30-60% solvent B in solvent A. Solvent A: 0.1 M NH_4OAc (aq). Solvent B: MeCN) and lyophilised to yield **159** as an amorphous red solid (XX mg, XX µmol, XX%). **HPLC** (5–95% MeCN/H_2O over 15 min) retention time 9.946 min; **HRMS** (ESI): $[M+H]^+$ calcd. for $C_{63}H_{75}N_9O_{20}^+$: 1633.7295, found: 1633.7289.

7.3 Antibody Modification

Protein LCMS Analysis

Protein LCMS was performed on a Xevo G2-S TOF mass spectrometer coupled to an Acquity UPLC system using an Acquity UPLC BEH300 C4 column (1.7 µm, 2.1 × 50 mm). H_2O with 0.1% formic acid (solvent A) and 95% MeCN and 5% H_2O with 0.1% formic acid (solvent B), were used as the mobile phase at a flow rate of 0.2 mL/min. The gradient was programmed as follows: 95% A for 0.93 min, then a gradient to 100% B over 4.28 min, then 100% B for 1.04 minutes, then a gradient to 95% A over 1.04 min. The electrospray source was operated with a capillary voltage of 2.0 kV and a cone voltage of 150 V. Nitrogen was used as the desolvation gas at a total flow of 850 L/h. Total mass spectra were reconstructed from the ion series using the MaxEnt algorithm preinstalled on MassLynx software (v4.1 from Waters) according to the manufacturer's instructions. ADC samples were deglycosylated with PNGase F (New England Biolabs) prior to LCMS analysis. Ion series were generated by integration of the total ion chromatogram (TIC) over the appropriate range. Analysis was conducted in the same way for all protein LCMS traces.

SDS Page

Non-reducing Tris-Glycine SDS-PAGE with 12% acrylamide with 4% stacking gel was performed as standard. Broad range molecular weight marker (10-200 kDa, New England BioLabs) was run in all gels. Samples (10 µL of 0.4 mg/mL) were prepared with reducing loading dye (10 µL, containing β-mercaptoethanol) and heated to either 80 °C or 90 °C for 5 min. Gels were run at constant voltage (200 V) for 48 min in 1× Laemmli running buffer (LRB). All gels were stained with Coomassie dye and imaged on a Syngene gel imaging system.

Ultraviolet-Visible Spectroscopy

Ultraviolet-visible spectra were recorded on a NanoDrop™ One UV-Visible spectrophotometer, operating at rt. Sample buffer was used as blank for baseline correction.

After bioconjugation and purification by desalting and filtration, the concentration of the resulting ADCs was determined by UV-Vis according to the calculation previously employed by Walsh et al.[399]; 0.61 is used as a correction factor to account for DVP absorbance at 280 nm, and 0.1 is used to account for trastuzumab absorbance at 298 nm.

$$ADC\ (mg/mL) = \frac{Abs_{280} - (0.61 \times Abs_{298}) + (0.1 \times Abs_{280}))}{1.46}$$

Trastuzumab General Rebridging Procedure

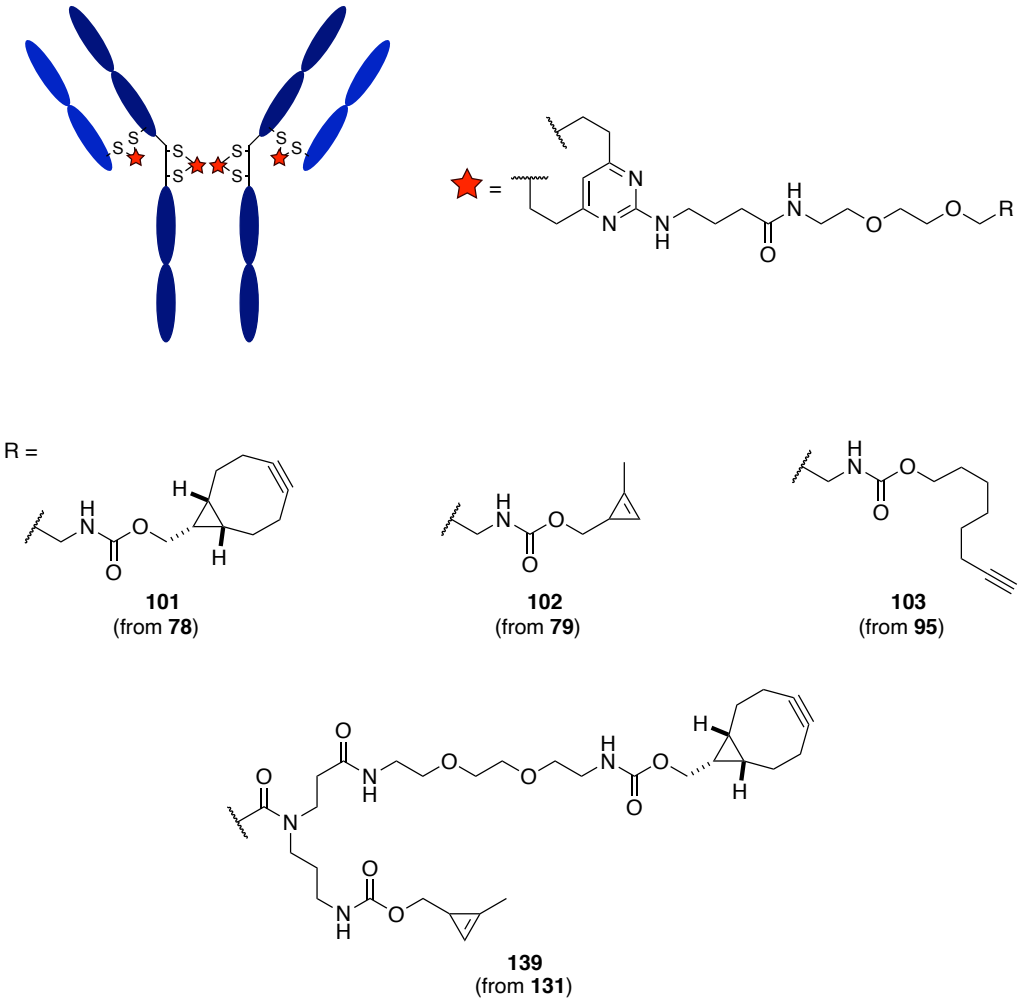

To a solution of trastuzumab (30.0 µL, 16.9 µM, 2.50 mg/mL) in TBS (25 mM Tris HCl pH 8, 25 mM NaCl, 0.5 mM EDTA) was added TCEP (10 equiv.). The mixture was vortexed and incubated at 37 °C for 1 h with shaking at 1000 rpm. A solution of linker **78**, **79**, **95** or **131** (10 mM in DMSO) was added with additional DMSO (final concentration of 0.319 mM, 10% DMSO (v/v), 20 equiv.) and the reaction mixture incubated at 37 °C for 2 h with shaking at 1000 rpm. The excess reagents were then removed with a Zeba Spin desalting column (40K MWCO, 0.5 mL) and exchanged into PBS with an Amicon-Ultra centrifugal filter (10K MWCO, Merck Millipore). Samples were either stored at 4 °C or flash frozen and stored at –20 °C until analysis.

General SPAAC Procedure

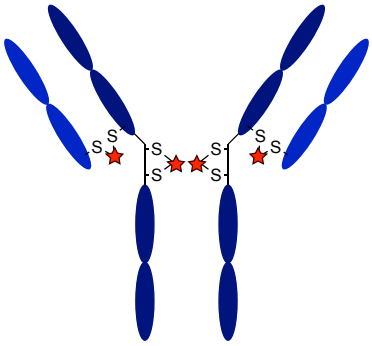

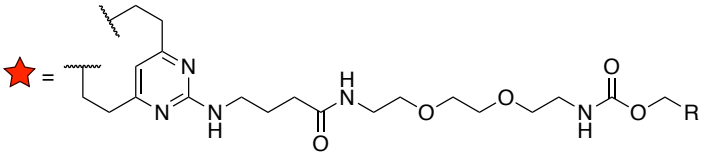

R =

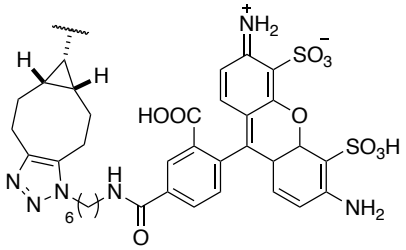

106
(from **104**)

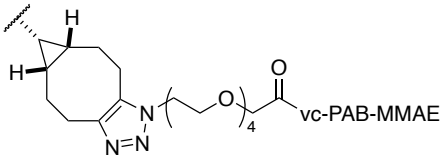

146
(from **144**)

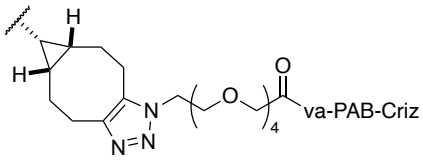

150
(from **147**)

To a solution of trastuzumab-BCN **101** (40 µL, 16.6 µM, 2.50 mg/mL) in PBS was added AlexaFluor® 488 azide **104**, azide-PEG4-vc-PAB-MMAE **144**, or azide-PEG4-va-PAB-Criz **147** (20 mM in DMSO) with additional DMSO (final concentration of 0.362 mM, 10% DMSO (v/v), 16 equiv.). The mixture was vortexed and incubated at 37 °C for 8 h with shaking at 1000 rpm. The excess reagents were then removed with a Zeba Spin desalting column (10K MWCO, 0.5 mL) and exchanged into PBS with an Amicon-Ultra centrifugal filter (10K MWCO, Merck Millipore). Samples were either stored at 4 °C or flash frozen and stored at –20 °C until analysis.

General IEDDA Procedure

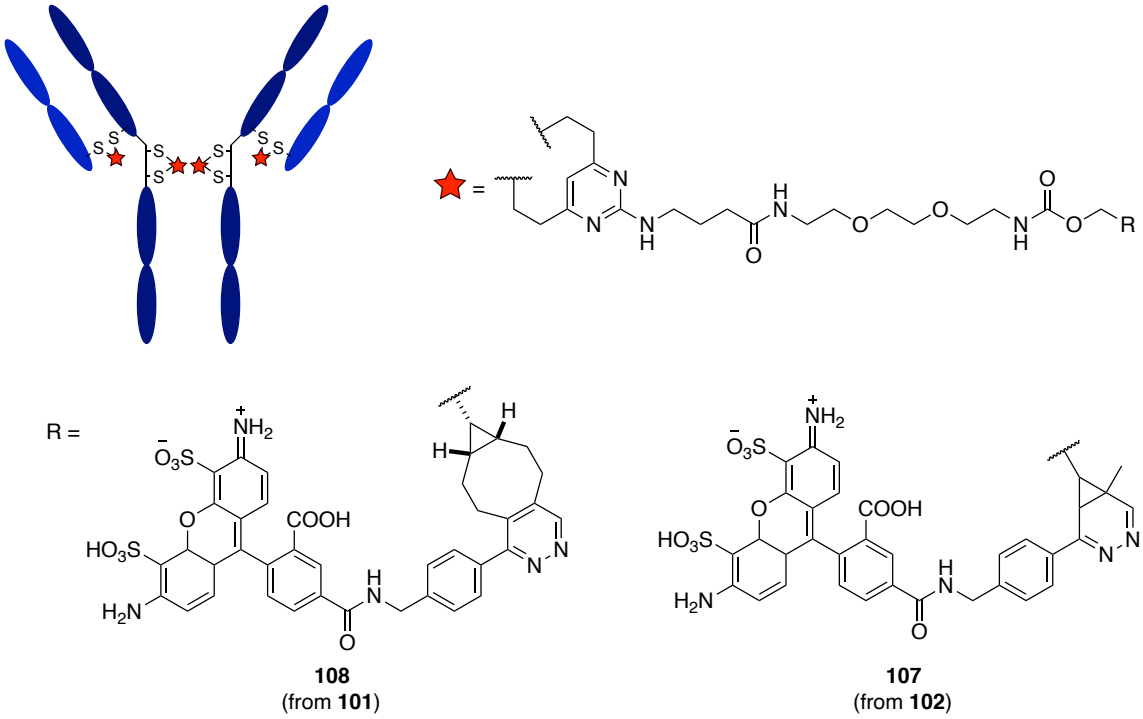

To a solution of trastuzumab-BCN **101** or trastuzumab-cyp **102** (40 µL, 16.6 µM, 2.50 mg/mL) in PBS was added AZDye 488 tetrazine **105** (20 mM in DMSO) with additional DMSO (final concentration of 0.398 mM, 10% DMSO (v/v), 16 equiv.). The mixture was vortexed and incubated at 37 °C for 2 h with shaking at 1000 rpm. The excess reagents were then removed with a Zeba Spin desalting column (40K MWCO, 0.5 mL) and exchanged into PBS with an Amicon-Ultra centrifugal filter (10K MWCO, Merck Millipore). Samples were either stored at 4 °C or flash frozen and stored at –20 °C until analysis.

Trastuzumab-alkyne (103) AlexaFluor™ 488 (104) CuAAC

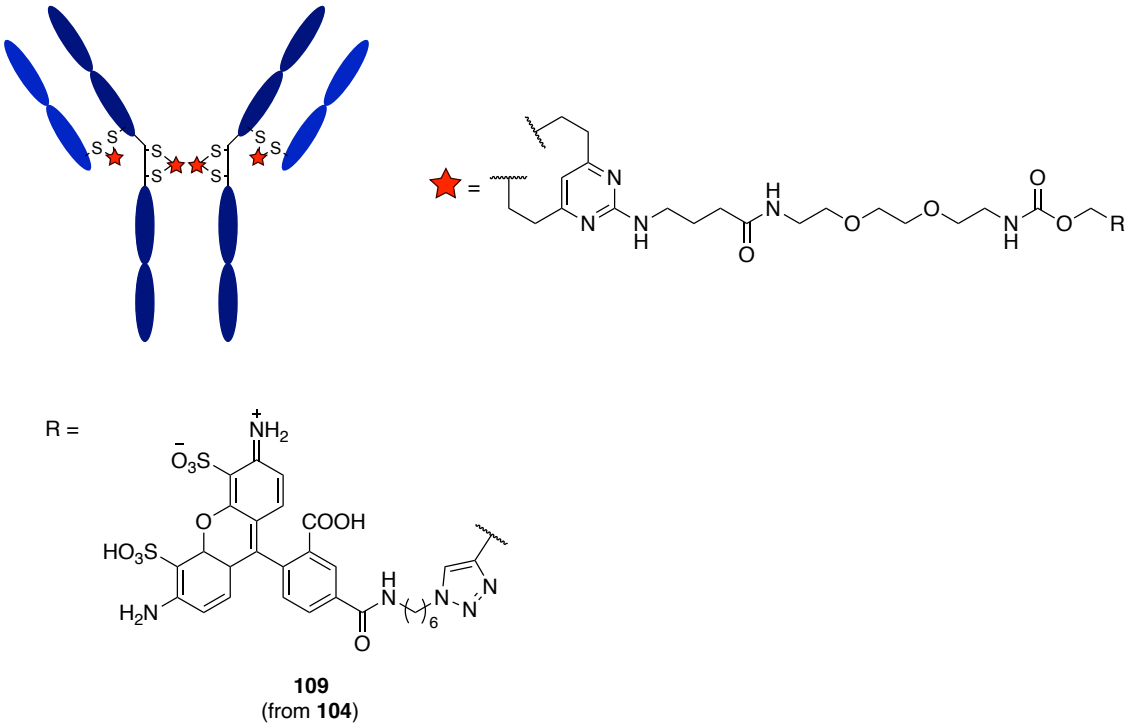

109
(from **104**)

To a solution of trastuzumab-alkyne **103** (40 µL, 16.6 µM, 2.50 mg/mL) in PBS was added AlexaFluor® 488 azide **104** (20 mM in DMSO) with additional DMSO (final concentration of 0.398 mM, 10% DMSO (v/v), 24 equiv.), $CuSO_4 \cdot 5H_2O$ (final concentration of 0.302 mM, 20 equiv.), THPTA (final concentration of 1.51 mM, 100 equiv.) and sodium ascorbate (final concentration of 2.26 mM, 150 equiv.). The mixture was vortexed and incubated at 37 °C for 4 h with shaking at 1000 rpm. The excess reagents were then removed with a Zeba Spin desalting column (10K MWCO, 0.5 mL) and exchanged into PBS with an Amicon-Ultra centrifugal filter (10K MWCO, Merck Millipore). Sample was either stored at 4 °C or flash frozen and stored at –20 °C until analysis.

Trastuzumab-dfDVP MMAE/AZDye 488 (142)

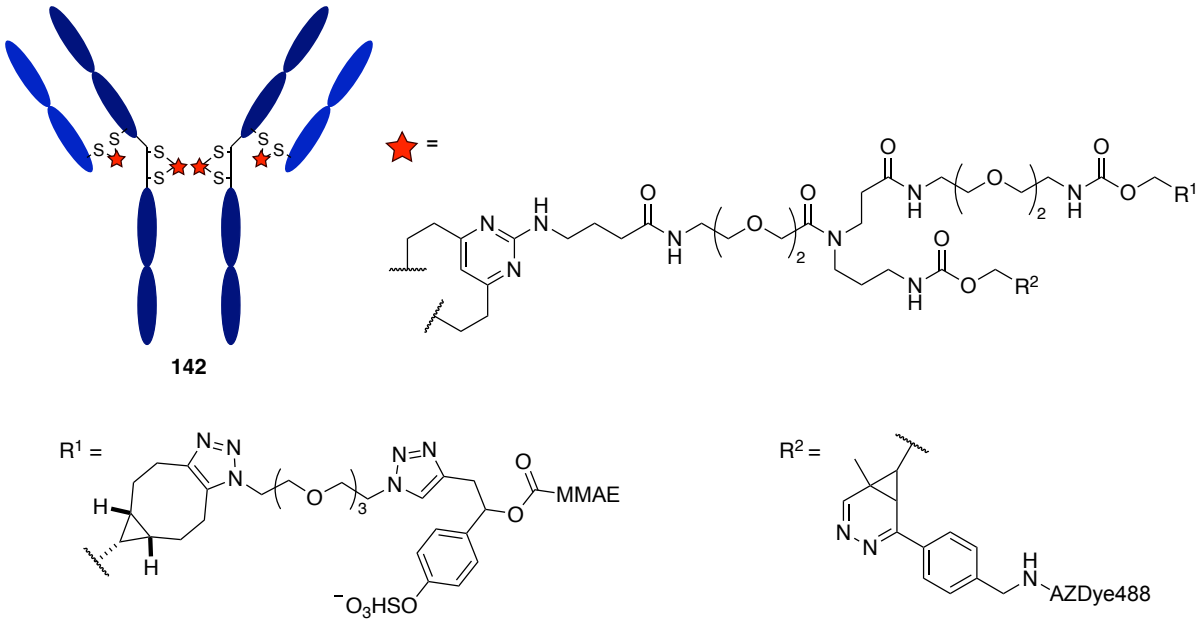

To a solution of trastuzumab-dfDVP **139** (60 µL, 16.4 µM, 2.50 mg/mL) in PBS was added azido-sulfate MMAE **140** (20 mM in DMSO) with additional DMSO (final concentration of 0.358 mM, 10% DMSO (v/v), 24 equiv.). The mixture was vortexed and incubated at 37 °C for 8 h with shaking at 1000 rpm. To this solution, AZDye 488 tetrazine **105** (25 mM in DMSO, final concentration of 0.353 mM, 24 equiv.) was added, and the reaction mixture was incubated for a further 4 h at 37 °C with shaking at 1000 rpm. The excess reagents were then removed with a Zeba Spin desalting column (10K MWCO, 0.5 mL) and exchanged into PBS with an Amicon-Ultra centrifugal filter (10K MWCO, Merck Millipore). Samples were either stored at 4 °C or flash frozen and stored at –20 °C until analysis.

Trastuzumab-dfDVP MMAE/TAMRA (145)

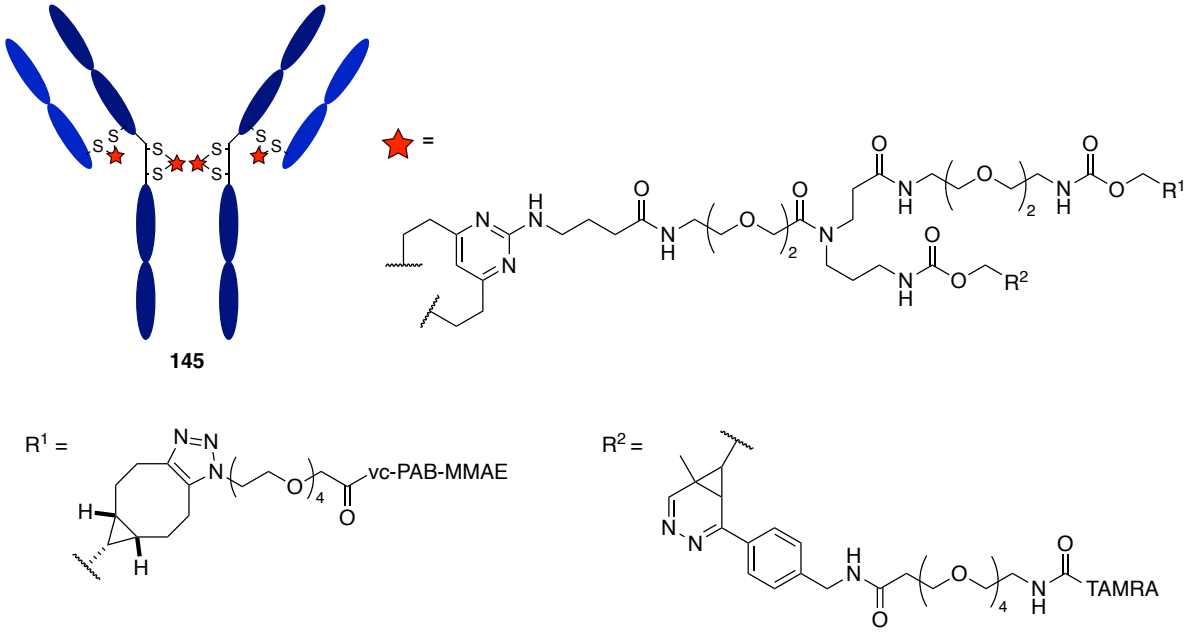

To a solution of trastuzumab-dfDVP **139** (60 µL, 16.4 µM, 2.50 mg/mL) in PBS was added azide-PEG4-vc-PAB-MMAE **144** (20 mM in DMSO) with additional DMSO (final concentration of 0.358 mM, 10% DMSO (v/v), 24 equiv.). The mixture was vortexed and incubated at 37 °C for 8 h with shaking at 1000 rpm. To this solution, TAMRA-PEG_2-tetrazine **143** (25 mM in DMSO, final concentration of 0.353 mM, 24 equiv.) was added, and the reaction mixture was incubated for a further 4 h at 37 °C with shaking at 1000 rpm. The excess reagents were then removed with a Zeba Spin desalting column (10K MWCO, 0.5 mL) and exchanged into PBS with an Amicon-Ultra centrifugal filter (10K MWCO, Merck Millipore). Samples were either stored at 4 °C or flash frozen and stored at –20 °C until analysis.

8 References

1 W. R. J. D. Galloway, A. Isidro-Llobet and D. R. Spring, *Nat. Commun.*, 2010, **1**, 1–13.

2 R. Macarron, M. N. Banks, D. Bojanic, D. J. Burns, D. A. Cirovic, T. Garyantes, D. V. S. Green, R. P. Hertzberg, W. P. Janzen, J. W. Paslay, U. Schopfer and G. S. Sittampalam, *Nat. Rev. Drug Discov.*, 2011, **10**, 188–195.

3 C. M. Dobson, *Nature*, 2004, **432**, 824–828.

4 W. P. Walters and M. Namchuk, *Nat. Rev. Drug Discov.*, 2003, **2**, 259–266.

5 E. A. Martis, R. Radhakrishnan and R. R. Badve, *J. Appl. Pharm. Sci.*, 2011, **1**, 2–10.

6 P. Dorr, M. Westby, S. Dobbs, P. Griffin, B. Irvine, M. Macartney, J. Mori, G. Rickett, C. Smith-Burchnell, C. Napier, R. Webster, D. Armour, D. Price, B. Stammen, A. Wood and M. Perros, *Antimicrob. Agents Chemother.*, 2005, **49**, 4721–4732.

7 S. Wilhelm, C. Carter, M. Lynch, T. Lowinger, J. Dumas, R. A. Smith, B. Schwartz, R. Simantov and S. Kelley, *Nat. Rev. Drug Discov.*, 2006, **5**, 835–844.

8 G. M. Keserű, D. A. Erlanson, G. G. Ferenczy, M. M. Hann, C. W. Murray and S. D. Pickett, *J. Med. Chem.*, 2016, **59**, 8189–8206.

9 R. S. Bohacek, C. McMartin and W. C. Guida, *Med. Res. Rev.*, 1996, **16**, 3–50.

10 D. E. Scott, A. G. Coyne, S. A. Hudson and C. Abell, *Biochemistry*, 2012, **51**, 4990–5003.

11 D. A. Erlanson, S. W. Fesik, R. E. Hubbard, W. Jahnke and H. Jhoti, *Nat. Rev. Drug Discov.*, 2016, **15**, 605–619.

12 A. Barker, J. G. Kettle, T. Nowak and J. E. Pease, *Drug Discov. Today*, 2013, **18**, 298–304.

13 S. L. McGovern, E. Caselli, N. Grigorieff and B. K. Shoichet, *J. Med. Chem.*, 2002, **45**, 1712–1722.

14 J. Osborne, S. Panova, M. Rapti, T. Urushima and H. Jhoti, *Biochem. Soc. Trans.*, 2020, **48**, 271–280.

15 A. R. Moore, S. C. Rosenberg, F. McCormick and S. Malek, *Nat. Rev. Drug Discov.*, 2020, **19**, 533–552.

16 X. Ran and J. E. Gestwicki, *Curr. Opin. Chem. Biol.*, 2018, **44**, 75–86.

17 A. D. Cox, S. W. Fesik, A. C. Kimmelman, J. Luo and C. J. Der, *Nat. Rev. Drug Discov.*, 2014, **13**, 828–851.

18 J. Coyle and R. Walser, *SLAS Discov. Adv. Sci. Drug Discov.*, 2020, **25**, 471–490.

19 J. Tsai, J. T. Lee, W. Wang, J. Zhang, H. Cho, S. Mamo, R. Bremer, S. Gillette, J. Kong, N. K. Haass, K. Sproesser, L. Li, K. S. M. Smalley, D. Fong, Y.-L. Zhu, A. Marimuthu, H. Nguyen, B. Lam, J. Liu, I. Cheung, J. Rice, Y. Suzuki, C. Luu, C. Settachatgul, R. Shellooe, J. Cantwell, S.-H. Kim, J. Schlessinger, K. Y. J. Zhang, B. L. West, B. Powell, G. Habets, C. Zhang, P. N. Ibrahim, P. Hirth, D. R. Artis, M. Herlyn and G. Bollag, *Proc. Natl. Acad. Sci.*, 2008, **105**, 3041–3046.

20 G. Bollag, P. Hirth, J. Tsai, J. Zhang, P. N. Ibrahim, H. Cho, W. Spevak, C. Zhang, Y. Zhang, G. Habets, E. A. Burton, B. Wong, G. Tsang, B. L. West, B. Powell, R. Shellooe, A. Marimuthu, H. Nguyen, K. Y. J. Zhang, D. R. Artis, J. Schlessinger, F. Su, B. Higgins, R. Iyer, K. D'Andrea, A. Koehler, M. Stumm, P. S. Lin, R. J. Lee, J. Grippo, I. Puzanov, K. B. Kim, A. Ribas, G. A. McArthur, J. A. Sosman, P. B. Chapman, K. T. Flaherty, X. Xu, K. L. Nathanson and K. Nolop, *Nature*, 2010, **467**, 596–599.

21 A. J. Souers, J. D. Leverson, E. R. Boghaert, S. L. Ackler, N. D. Catron, J. Chen, B. D. Dayton, H. Ding, S. H. Enschede, W. J. Fairbrother, D. C. S. Huang, S. G. Hymowitz, S. Jin, S. L. Khaw, P. J. Kovar, L. T. Lam, J. Lee, H. L. Maecker, K. C. Marsh, K. D. Mason, M. J. Mitten, P. M. Nimmer, A. Oleksijew, C. H. Park, C.-M. Park, D. C. Phillips, A. W. Roberts, D. Sampath, J. F. Seymour, M. L. Smith, G. M. Sullivan, S. K. Tahir, C. Tse, M. D. Wendt, Y. Xiao, J. C. Xue, H. Zhang, R. A. Humerickhouse, S. H. Rosenberg and S. W. Elmore, *Nat. Med.*, 2013, **19**, 202–208.

22 C. W. Murray, D. R. Newell and P. Angibaud, *Med. Chem. Commun.*, 2019, **10**, 1509–1511.

23 C. Zhang, P. N. Ibrahim, J. Zhang, E. A. Burton, G. Habets, Y. Zhang, B. Powell, B. L. West, B. Matusow, G. Tsang, R. Shellooe, H. Carias, H. Nguyen, A. Marimuthu, K. Y. J. Zhang, A. Oh, R. Bremer, C. R. Hurt, D. R. Artis, G. Wu, M. Nespi, W. Spevak, P. Lin, K. Nolop, P. Hirth, G. H. Tesch and G. Bollag, *Proc. Natl. Acad. Sci.*, 2013, **110**, 5689–5694.

24 H. Gelderblom and M. van de Sande, *Futur. Oncol.*, 2020, **16**, 2345–2356.

25 Y. Shin, J. W. Jeong, R. P. Wurz, P. Achanta, T. Arvedson, M. D. Bartberger, I. D. G. Campuzano, R. Fucini, S. K. Hansen, J. Ingersoll, J. S. Iwig, J. R. Lipford, V. Ma, D. J. Kopecky, J. McCarter, T.

San Miguel, C. Mohr, S. Sabet, A. Y. Saiki, A. Sawayama, S. Sethofer, C. M. Tegley, L. P. Volak, K. Yang, B. A. Lanman, D. A. Erlanson and V. J. Cee, *ACS Med. Chem. Lett.*, 2019, **10**, 1302–1308.

26 J. M. Ostrem, U. Peters, M. L. Sos, J. A. Wells and K. M. Shokat, *Nature*, 2013, **503**, 548–551.

27 A. R. Leach, M. M. Hann, J. N. Burrows and E. J. Griffen, *Mol. BioSyst.*, 2006, **2**, 429–446.

28 L. Ruddigkeit, R. van Deursen, L. C. Blum and J.-L. Reymond, *J. Chem. Inf. Model.*, 2012, **52**, 2864–2875.

29 M. Congreve, G. Chessari, D. Tisi and A. J. Woodhead, *J. Med. Chem.*, 2008, **51**, 3661–3680.

30 D. A. Erlanson, R. S. McDowell and T. O'Brien, *J. Med. Chem.*, 2004, **47**, 3463–3482.

31 W. A. Warr, *J. Comput. Aided. Mol. Des.*, 2009, **23**, 453–458.

32 S. Vajda, A. Whitty and D. Kozakov, *Oncotarget*, 2015, **6**, 18740–18741.

33 P. Kirsch, A. M. Hartman, A. K. H. Hirsch and M. Empting, *Molecules*, 2019, **24**, 4309.

34 D. C. Rees, M. Congreve, C. W. Murray and R. Carr, *Nat. Rev. Drug Discov.*, 2004, **3**, 660.

35 F. Lovering, J. Bikker and C. Humblet, *J. Med. Chem.*, 2009, **52**, 6752–6756.

36 M. M. Hann, A. R. Leach and G. Harper, *J. Chem. Inf. Comput. Sci.*, 2001, **41**, 856–864.

37 C. W. Murray and D. C. Rees, *Nat. Chem.*, 2009, **1**, 187–192.

38 S. D. Bembenek, B. A. Tounge and C. H. Reynolds, *Drug Discov. Today*, 2009, **14**, 278–283.

39 Q. Li, *Front. Mol. Biosci.*, 2020, **7**, 180.

40 K. Gao, R. Oerlemans and M. R. Groves, *Biophys. Rev.*, 2020, **12**, 85–104.

41 J. E. Ladbury, G. Klebe and E. Freire, *Nat. Rev. Drug Discov.*, 2010, **9**, 23–27.

42 M. Bentley, B. C. Doak, B. Mohanty and M. J. Scanlon, in *Applications of NMR Spectroscopy in FBDD*, Springer International Publishing, 2018, pp. 2211–2231.

43 T. Neumann, H. Junker and K. S. and R. Sekul, *Curr. Top. Med. Chem.*, 2007, 7, 1630–1642.

44 D. Patel, J. D. Bauman and E. Arnold, *Prog. Biophys. Mol. Biol.*, 2014, **116**, 92–100.

45 M. Pellecchia, *Nat. Chem. Biol.*, 2009, **5**, 274–275.

46 L. R. de Souza Neto, J. T. Moreira-Filho, B. J. Neves, R. L. B. R. Maidana, A. C. R. Guimarães, N. Furnham, C. H. Andrade and F. P. Silva, *Front. Chem.*, 2020, **8**, 93.

47 D. Stumpfe and J. Bajorath, *J. Chem. Inf. Model.*, 2020, **60**, 4112–4115.

48 B. C. Doak, R. S. Norton and M. J. Scanlon, *Pharmacol. Ther.*, 2016, **167**, 28–37.

49 M. P. Gleeson, *J. Med. Chem.*, 2008, **51**, 817–834.

50 P. D. Leeson and B. Springthorpe, *Nat. Rev. Drug Discov.*, 2007, **6**, 881–890.

51 S. J. Teague, A. M. Davis, P. D. Leeson and T. Oprea, *Angew. Chemie Int. Ed.*, 1999, **38**, 3743–3748.

52 M. Vieth, M. G. Siegel, R. E. Higgs, I. A. Watson, D. H. Robertson, K. A. Savin, G. L. Durst and P. A. Hipskind, *J. Med. Chem.*, 2004, **47**, 224–232.

53 J. D. Hughes, J. Blagg, D. A. Price, S. Bailey, G. A. DeCrescenzo, R. V Devraj, E. Ellsworth, Y. M. Fobian, M. E. Gibbs, R. W. Gilles, N. Greene, E. Huang, T. Krieger-Burke, J. Loesel, T. Wager, L. Whiteley and Y. Zhang, *Bioorg. Med. Chem. Lett.*, 2008, **18**, 4872–4875.

54 M. C. Wenlock, R. P. Austin, P. Barton, A. M. Davis and P. D. Leeson, *J. Med. Chem.*, 2003, **46**, 1250–1256.

55 C. A. Lipinski, F. Lombardo, B. W. Dominy and P. J. Feeney, *Adv. Drug Deliv. Rev.*, 2001, **46**, 3–26.

56 D. A. Erlanson, B. J. Davis and W. Jahnke, *Cell Chem. Biol.*, 2019, **26**, 9–15.

57 G. Szabó, G. I. Túrós, S. Kolok, M. Vastag, Z. Sánta, M. Dékány, G. I. Lévay, I. Greiner, M. Natsumi, W. Tatsuya and G. M. Keserű, *J. Med. Chem.*, 2019, **62**, 234–246.

58 Z. Konteatis, *Expert Opin. Drug Discov.*, 2021, **16**, 723–726.

59 S. Lobo, *Expert Opin. Drug Discov.*, 2020, **15**, 261–263.

60 C. P. Tinworth and R. J. Young, *J. Med. Chem.*, 2020, **63**, 10091–10108.

61 M. Congreve, R. Carr, C. Murray and H. Jhoti, *Drug Discov. Today*, 2003, **8**, 876–877.

62 D. C. Fry, C. Wartchow, B. Graves, C. Janson, C. Lukacs, U. Kammlott, C. Belunis, S. Palme, C. Klein and B. Vu, *ACS Med. Chem. Lett.*, 2013, **4**, 660–665.

63 Y. Shi and M. von Itzstein, *Molecules*, 2019, **24**, 2838.

64 W. R. J. D. Galloway, D. Wilcke, F. Nie, K. Hadje-georgiou, L. Laraia and D. R. Spring, in *Concepts and Case Studies in Chemical Biology*, Wiley-VCH, 2014, 379–389.

65 W. R. J. D. Galloway, A. Bender, M. Welch and D. R. Spring, *Chem. Commun.*, 2009, 2446–2462.

66 W. R. J. D. Galloway, R. J. Spandl, A. Bender, G. L. Thomas, M. Diaz-gavilan, K. M. G. O'Connell and D. R. Spring, in *Chemical Genomics*, Cambridge University Press, 2011, 39–59.

67 W. R. J. D. Galloway, in *Solid-Phase Organic Synthesis: Concepts, Strategies, and Applications*, eds. P. H. Toy and Y. Lam, Wiley, 2012, 131–150.

68 B. J. Davis and D. A. Erlanson, *Bioorg. Med. Chem. Lett.*, 2013, **23**, 2844–2852.

69 J. Seidler, S. L. McGovern, T. N. Doman and B. K. Shoichet, *J. Med. Chem.*, 2003, **46**, 4477–4486.

70 J. L. Dahlin, J. W. M. Nissink, J. M. Strasser, S. Francis, L. Higgins, H. Zhou, Z. Zhang and M. A. Walters, *J. Med. Chem.*, 2015, **58**, 2091–2113.

71 J. B. Baell and G. A. Holloway, *J. Med. Chem.*, 2010, **53**, 2719–2740.

72 G. M. Rishton, *Drug Discov. Today*, 2003, **8**, 86–96.

73 J. B. Baell and J. W. M. Nissink, *ACS Chem. Biol.*, 2018, **13**, 36–44.

74 N. Palmer, T. M. Peakman, D. Norton and D. C. Rees, *Org. Biomol. Chem.*, 2016, **14**, 1599–1610.

75 J. D. St. Denis, R. J. Hall, C. W. Murray, T. D. Heightman and D. C. Rees, *RSC Med. Chem.*, 2021, **12**, 321–329.

76 C. W. Murray and D. C. Rees, *Angew. Chemie Int. Ed.*, 2016, **55**, 488–492.

77 O. B. Cox, T. Krojer, P. Collins, O. Monteiro, R. Talon, A. Bradley, O. Fedorov, J. Amin, B. D. Marsden, J. Spencer, F. von Delft and P. E. Brennan, *Chem. Sci.*, 2016, **7**, 2322–2330.

78 N. Mateu, S. L. Kidd, L. Kalash, H. F. Sore, A. Madin, A. Bender and D. R. Spring, *Chem. Eur. J.*, 2018, **24**, 13681–13687.

79 D. G. Twigg, N. Kondo, S. L. Mitchell, W. R. J. D. Galloway, H. F. Sore, A. Madin and D. R. Spring, *Angew. Chemie Int. Ed.*, 2016, **55**, 12479–12483.

80 P. J. Hajduk, W. R. J. D. Galloway and D. R. Spring, *Nature*, 2011, **470**, 42–43.

81 A. W. Hung, A. Ramek, Y. Wang, T. Kaya, J. A. Wilson, P. A. Clemons and D. W. Young, *Proc. Natl. Acad. Sci.*, 2011, **108**, 6799–6804.

82 S. R. Langdon, N. Brown and J. Blagg, *J. Chem. Inf. Model.*, 2011, **51**, 2174–2185.

83 J. Hert, J. J. Irwin, C. Laggner, M. J. Keiser and B. K. Shoichet, *Nat. Chem. Biol.*, 2009, **5**, 479–483.

84 A. D. Morley, A. Pugliese, K. Birchall, J. Bower, P. Brennan, N. Brown, T. Chapman, M. Drysdale, I. H. Gilbert, S. Hoelder, A. Jordan, S. V Ley, A. Merritt, D. Miller, M. E. Swarbrick and P. G. Wyatt, *Drug Discov. Today*, 2013, **18**, 1221–1227.

85 F. Lovering, *Med. Chem. Commun.*, 2013, **4**, 515–519.

86 M. J. Caplin and D. J. Foley, *Chem. Sci.*, 2021, **12**, 4646–4660.

87 N. C. Firth, N. Brown and J. Blagg, *J. Chem. Inf. Model.*, 2012, **52**, 2516–2525.

88 T. J. Ritchie and S. J. F. Macdonald, *Drug Discov. Today*, 2009, **14**, 1011–1020.

89 T. J. Ritchie, S. J. F. Macdonald, R. J. Young and S. D. Pickett, *Drug Discov. Today*, 2011, **16**, 164–171.

90 D. J. Foley, P. G. E. Craven, P. M. Collins, R. G. Doveston, A. Aimon, R. Talon, I. Churcher, F. von Delft, S. P. Marsden and A. Nelson, *Chem. A Eur. J.*, 2017, **23**, 15227–15232.

91 T. D. Downes, S. P. Jones, H. F. Klein, M. C. Wheldon, M. Atobe, P. S. Bond, J. D. Firth, N. S. Chan, L. Waddelove, R. E. Hubbard, D. C. Blakemore, C. De Fusco, S. D. Roughley, L. R. Vidler, M. A. Whatton, A. J.-A. Woolford, G. L. Wrigley and P. O'Brien, *Chem. Eur. J.*, 2020, **26**, 8969–8975.

92 B. M. Ibbeson, L. Laraia, E. Alza, C. J. O'Connor, Y. S. Tan, H. M. L. Davies, G. Mckenzie, A. R. Venkitaraman and D. R. Spring, *Nat. Commun.*, 2014, **5**, 1–8.

93 S. Wetzel, R. S. Bon, K. Kumar and H. Waldmann, *Angew. Chemie Int. Ed.*, 2011, **50**, 10800–

10826.

94 D. J. Newman and G. M. Cragg, *J. Nat. Prod.*, 2020, **83**, 770–803.

95 A. G. Atanasov, S. B. Zotchev, V. M. Dirsch, I. E. Orhan, M. Banach, J. M. Rollinger, D. Barreca, W. Weckwerth, R. Bauer, E. A. Bayer, M. Majeed, A. Bishayee, V. Bochkov, G. K. Bonn, N. Braidy, F. Bucar, A. Cifuentes, G. D'Onofrio, M. Bodkin, M. Diederich, A. T. Dinkova-Kostova, T. Efferth, K. El Bairi, N. Arkells, T.-P. Fan, B. L. Fiebich, M. Freissmuth, M. I. Georgiev, S. Gibbons, K. M. Godfrey, C. W. Gruber, J. Heer, L. A. Huber, E. Ibanez, A. Kijjoa, A. K. Kiss, A. Lu, F. A. Macias, M. J. S. Miller, A. Mocan, R. Müller, F. Nicoletti, G. Perry, V. Pittalà, L. Rastrelli, M. Ristow, G. L. Russo, A. S. Silva, D. Schuster, H. Sheridan, K. Skalicka-Woźniak, L. Skaltsounis, E. Sobarzo-Sánchez, D. S. Bredt, H. Stuppner, A. Sureda, N. T. Tzvetkov, R. A. Vacca, B. B. Aggarwal, M. Battino, F. Giampieri, M. Wink, J.-L. Wolfender, J. Xiao, A. W. K. Yeung, G. Lizard, M. A. Popp, M. Heinrich, I. Berindan-Neagoe, M. Stadler, M. Daglia, R. Verpoorte, C. T. Supuran and the I. N. P. S. Taskforce, *Nat. Rev. Drug Discov.*, 2021, **20**, 200–216.

96 R. J. Spandl, G. L. Thomas, M. Diaz-gavilan, K. M. G. O. Connell and D. R. Spring, in *Linker Strategies in Solid-Phase Organic Synthesis*, 2010, 239–262.

97 B. E. Evans, K. E. Rittle, M. G. Bock, R. M. DiPardo, R. M. Freidinger, W. L. Whitter, G. F. Lundell, D. F. Veber, P. S. Anderson, R. S. L. Chang, V. J. Lotti, D. J. Cerino, T. B. Chen, P. J. Kling, K. A. Kunkel, J. P. Springer and J. Hirshfield, *J. Med. Chem.*, 1988, **31**, 2235–2246.

98 B. Over, S. Wetzel, C. Grütter, Y. Nakai, S. Renner, D. Rauh and H. Waldmann, *Nat. Chem.*, 2013, **5**, 21–28.

99 H. Prescher, G. Koch, T. Schuhmann, P. Ertl, A. Bussenault, M. Glick, I. Dix, F. Petersen and D. E. Lizos, *Bioorg. Med. Chem.*, 2017, **25**, 921–925.

100 C. Abell and C. Dagostin, in *Fragment-Based Drug Discovery*, The Royal Society of Chemistry, 2015, 1–18.

101 A. Nelson and G. Karageorgis, *RSC Med. Chem.*, 2021, **12**, 353–362.

102 H. Oh, D. C. Swenson, J. B. Gloer and C. A. Shearer, *J. Nat. Prod.*, 2003, **66**, 73–79.

103 W. R. J. D. Galloway and D. R. Spring, *Expert Opin. Drug Discov.*, 2009, **4**, 467–472.

104 J. A. Johnson, C. A. Nicolaou, S. E. Kirberger, A. K. Pandey, H. Hu and W. C. K. Pomerantz, *ACS*

Med. Chem. Lett., 2019, **10**, 1648–1654.

105 M. D. Burke and S. L. Schreiber, *Angew. Chemie Int. Ed.*, 2004, **43**, 46–58.

106 M. D. Burke, E. M. Berger and S. L. Schreiber, *Science*, 2003, **302**, 613–618.

107 P. A. Clemons, N. E. Bodycombe, H. A. Carrinski, J. A. Wilson, A. F. Shamji, B. K. Wagner, A. N. Koehler and S. L. Schreiber, *Proc. Natl. Acad. Sci.*, 2010, **107**, 18787–18792.

108 D. S. Tan, *Nat. Chem. Biol.*, 2005, **1**, 74–84.

109 W. R. J. D. Galloway and D. R. Spring, *Divers. Oriented Synth.*, 2013, **1**, 21–28.

110 T. E. Nielsen and S. L. Schreiber, *Angew. Chem. Int. Ed. Engl.*, 2007, **47**, 48–56.

111 A. Isidro-Llobet, T. Murillo, P. Bello, A. Cilibrizzi, J. T. Hodgkinson, W. R. J. D. Galloway, A. Bender, M. Welch and D. R. Spring, *Proc. Natl. Acad. Sci.*, 2011, **108**, 6793–6798.

112 C. J. Gerry and S. L. Schreiber, *Nat. Rev. Drug Discov.*, 2018, **17**, 333–352.

113 S. L. Kidd, T. J. Osberger, N. Mateu, H. F. Sore and D. R. Spring, *Front. Chem.*, 2018, **6**, 460.

114 G. Karageorgis, D. J. Foley, L. Laraia and H. Waldmann, *Nat. Chem.*, 2020, **12**, 227–235.

115 S. L. Kidd, E. Fowler, T. Reinhardt, T. Compton, N. Mateu, H. Newman, D. Bellini, R. Talon, J. McLoughlin, T. Krojer, A. Aimon, A. Bradley, M. Fairhead, P. Brear, L. Díaz-Sáez, K. McAuley, H. F. Sore, A. Madin, D. H. O'Donovan, K. V. M. Huber, M. Hyvönen, F. von Delft, C. G. Dowson and D. R. Spring, *Chem. Sci.*, 2020, **11**, 10792–10801.

116 A. R. Hanby, N. S. Troelsen, T. J. Osberger, S. L. Kidd, K. T. Mortensen and D. R. Spring, *Chem. Commun.*, 2020, **56**, 2280–2283.

117 N. S. Troelsen, PhD Thesis, Technical University of Denmark, 2020.

118 T. T. Talele, *J. Med. Chem.*, 2020, **63**, 13291–13315.

119 J. Kim, H. Kim and S. B. Park, *J. Am. Chem. Soc.*, 2014, **136**, 14629–14638.

120 M. Ishikawa and Y. Hashimoto, *J. Med. Chem.*, 2011, **54**, 1539–1554.

121 Z. Fang, Y. Song, P. Zhan, Q. Zhang and X. Liu, *Future Med. Chem.*, 2014, **6**, 885–901.

122 P. A. Clemons, N. E. Bodycombe, H. A. Carrinski, J. A. Wilson, A. F. Shamji, B. K. Wagner, A. N. Koehler and S. L. Schreiber, *Proc. Natl. Acad. Sci.*, 2010, **107**, 18787–18792.

123 B. Cox, V. Zdorichenko, P. B. Cox, K. I. Booker-Milburn, R. Paumier, L. D. Elliott, M. Robertson-Ralph and G. Bloomfield, *ACS Med. Chem. Lett.*, 2020, **11**, 1185–1190.

124 P. Hu, H. M. Chi, K. C. DeBacker, X. Gong, J. H. Keim, I. T. Hsu and S. A. Snyder, *Nature*, 2019, **569**, 703–707.

125 Y. Liu, S.-J. Han, W.-B. Liu and B. M. Stoltz, *Acc. Chem. Res.*, 2015, **48**, 740–751.

126 H. Zheng, Y. Wang, C. Xu, X. Xu, L. Lin, X. Liu and X. Feng, *Nat. Commun.*, 2018, **9**, 1968.

127 C. J. Douglas and L. E. Overman, *Proc. Natl. Acad. Sci.*, 2004, **101**, 5363–5367.

128 K. Mori and H. Mori, *Tetrahedron*, 1985, **41**, 5487–5493.

129 S. N. Ananchenko, Y. Y. Limanov, V. N. Leonov, V. N. Rzheznikov and I. V Torgov, *Tetrahedron*, 1962, **18**, 1355–1367.

130 P. D. Thornton and D. J. Burnell, *Org. Lett.*, 2006, **8**, 3195–3198.

131 D. W. Brooks, P. G. Grothaus and W. L. Irwin, *J. Org. Chem.*, 1982, **47**, 2820–2821.

132 A.-S. Chapelon, D. Moraléda, R. Rodriguez, C. Ollivier and M. Santelli, *Tetrahedron*, 2007, **63**, 11511–11616.

133 Yeung, R.-J. Chein and E. J. Corey, *J. Am. Chem. Soc.*, 2007, **129**, 10346–10347.

134 G.-J. Wu, Y.-H. Zhang, D.-X. Tan, L. He, B.-C. Cao, Y.-P. He and F.-S. Han, *J. Org. Chem.*, 2019, **84**, 3223–3238.

135 D. W. Brooks, H. Mazdiyasni and P. G. Grothaus, *J. Org. Chem.*, 1987, **52**, 3223–3232.

136 S. Breitler and E. M. Carreira, *Angew. Chemie Int. Ed.*, 2013, **52**, 11168–11171.

137 Q. Lu, D. S. Harmalkar, Y. Choi and K. Lee, *Molecules*, 2019, **24**, 3778.

138 C.-Y. Ho and L. He, *J. Org. Chem.*, 2014, **79**, 11873–11884.

139 C. Su and P. G. Williard, *Org. Lett.*, 2010, **12**, 5378–5381.

140 H.-P. Wessel, T. Iversen and D. R. Bundle, *J. Chem. Soc. Perkin Trans. 1*, 1985, 2247–2250.

141 G. Illuminati and L. Mandolini, *Acc. Chem. Res.*, 1981, **14**, 95–102.

142 D.-W. Gao, C. S. Jamieson, G. Wang, Y. Yan, J. Zhou, K. N. Houk and Y. Tang, *J. Am. Chem. Soc.*, 2021, **143**, 80–84.

143 I. Shiina, *Chem. Rev.*, 2007, **107**, 239–273.

144 K. Y. Palate, R. G. Epton, A. C. Whitwood, J. M. Lynam and W. P. Unsworth, *Org. Biomol. Chem.*, 2021, **19**, 1404–1411.

145 S. K. Chattopadhyay, S. Karmakar, T. Biswas, K. C. Majumdar, H. Rahaman and B. Roy, *Tetrahedron*, 2007, **63**, 3919–3952.

146 M. Mori, N. Sakakibara and A. Kinoshita, *J. Org. Chem.*, 1998, **63**, 6082–6083.

147 G. C. Lloyd-Jones, A. J. Robinson, L. Lefort and J. G. de Vries, *Chem. Eur. J.*, 2010, **16**, 9449–9452.

148 A. G. D. Grotevendt, J. A. M. Lummiss, M. L. Mastronardi and D. E. Fogg, *J. Am. Chem. Soc.*, 2011, **133**, 15918–15921.

149 K. P. Kaliappan, V. Ravikumar and S. A. Pujari, *Tetrahedron Lett.*, 2006, **47**, 981–984.

150 V. V Betkekar, A. A. Sayyad and K. P. Kaliappan, *Org. Lett.*, 2014, **16**, 5540–5543.

151 D. G. I. Kingston, *Chem. Commun.*, 2001, 867–880.

152 M. S. Malik, S. A. Ahmed, I. I. Althagafi, M. A. Ansari and A. Kamal, *RSC Med. Chem.*, 2020, **11**, 327–348.

153 G. L. Dunn, J. R. E. Hoover, D. A. Berges, J. J. Taggart, L. D. Davis, E. M. Dietz, D. R. Jakas, N. Yim, P. Actor, J. V Uri and J. A. Weisbach, *J. Antibiot.*, 1976, **29**, 65–80.

154 Y. Yang, B. A. Rasmussen and D. M. Shlaes, *Pharmacol. Ther.*, 1999, **83**, 141–151.

155 W. D. Figg, K. A. Cole, E. Reed, S. M. Steinberg, S. C. Piscitelli, P. A. Davis, M. J. Soltis, J. Jacob, S. Boudoulas and B. Goldspiel, *Clin. Cancer Res.*, 1995, **1**, 797–803.

156 T. M. A. Barlow, D. Tourwé and S. Ballet, *Eur. J. Org. Chem.*, 2017, **2017**, 4678–4694.

157 A. Budakoti, P. K. Mondal, P. Verma and J. Khamrai, *Beilstein J. Org. Chem.*, 2021, **17**, 932–963.

158 A. E. Wright, J. C. Botelho, E. Guzmán, D. Harmody, P. Linley, P. J. McCarthy, T. P. Pitts, S. A. Pomponi and J. K. Reed, *J. Nat. Prod.*, 2007, **70**, 412–416.

159 A. Aragão Craveiro, A. da Costa Prado, O. R. Gottlieb and P. C. Welerson de Albuquerque, *Phytochemistry*, 1970, **9**, 1869–1875.

160 J. Mulzer and M. Hanbauer, *Tetrahedron Lett.*, 2000, **41**, 33–36.

161 J. T. Lowe and J. S. Panek, *Org. Lett.*, 2008, **10**, 3813–3816.

162 M. Yamashita, *Antivir. Chem. Chemother.*, 2010, **21**, 71–84.

163 M. A. Leeuwenburgh, R. E. J. N. Litjens, J. D. C. Codée, H. S. Overkleeft, G. A. van der Marel and J. H. van Boom, *Org. Lett.*, 2000, **2**, 1275–1277.

164 B. M. Trost and Y. H. Rhee, *J. Am. Chem. Soc.*, 2002, **124**, 2528–2533.

165 M. J. Zacuto, D. Tomita, Z. Pirzada and F. Xu, *Org. Lett.*, 2010, **12**, 684–687.

166 F. Q. Alali, X.-X. Liu and J. L. McLaughlin, *J. Nat. Prod.*, 1999, **62**, 504–540.

167 G. W. Gribble, *Chem. Soc. Rev.*, 1999, **28**, 335–346.

168 M. M. Faul and B. E. Huff, *Chem. Rev.*, 2000, **100**, 2407–2474.

169 A. Bermejo, B. Figadère, M.-C. Zafra-Polo, I. Barrachina, E. Estornell and D. Cortes, *Nat. Prod. Rep.*, 2005, **22**, 269–303.

170 R. A. Fernandes, R. S. Pathare and D. A. Gorve, *Chem. Asian J.*, 2020, **15**, 2815–2837.

171 G.-F. Ho, C.-S. Chai, A. Alip, M. I. A. Wahid, M. M. Abdullah, Y.-C. Foo, S.-H. How, A. Zaatar, K.-S. Lam, K.-W. Leong, J.-S.-H. Low, M. M. Yusof, E. C.-Y. Lee, Y.-Y. Toh and C.-K. Liam, *BMC Cancer*, 2019, **19**, 896.

172 T. Kovacevic, M. Mesic, A. Avdagic and M. Zegarac, *Tetrahedron Lett.*, 2018, **59**, 4180–4182.

173 S. Noble and K. L. Goa, *Drugs*, 2000, **60**, 1383–1410.

174 A. J. Scheen, *Clin. Pharmacokinet.*, 2014, **53**, 213–225.

175 H. Harkat, J.-M. Weibel and P. Pale, *Tetrahedron Lett.*, 2007, **48**, 1439–1442.

176 P. Pale and J. Chuche, *Eur. J. Org. Chem.*, 2000, **2000**, 1019–1025.

177 F. E. McDonald and M. M. Gleason, *J. Am. Chem. Soc.*, 1996, **118**, 6648–6659.

178 E. Genin, S. Antoniotti, V. Michelet and J.-P. Genêt, *Angew. Chemie Int. Ed.*, 2005, **44**, 4949–4953.

179 K. Kato, A. Nishimura, Y. Yamamoto and H. Akita, *Tetrahedron Lett.*, 2001, **42**, 4203–4205.

180 C. Baumgartner, S. Ma, Q. Liu and B. M. Stoltz, *Org. Biomol. Chem.*, 2010, **8**, 2915–2917.

181 D. Broere and E. Ruijter, *Synthesis*, 2012, **44**, 2639–2672.

182 S. Kotha, K. Lahiri and G. Sreevani, *Synlett*, 2018, **29**, 2342–2361.

183 N. Nicolaus and H. G. Schmalz, *Synlett*, 2010, **14**, 2071–2074.

184 T. Inukai, T. Kano and K. Maruoka, *Angew. Chemie Int. Ed.*, 2020, **59**, 2211–2214.

185 A. Geny, N. Agenet, L. Iannazzo, M. Malacria, C. Aubert and V. Gandon, *Angew. Chemie Int. Ed.*, 2009, **48**, 1810–1813.

186 P. Kumar, S. Prescher and J. Louie, *Angew. Chemie Int. Ed.*, 2011, **50**, 10694–10698.

187 R. M. Stolley, H. A. Duong, D. R. Thomas and J. Louie, *J. Am. Chem. Soc.*, 2012, **134**, 15154–15162.

188 B. Heller and M. Hapke, *Chem. Soc. Rev.*, 2007, **36**, 1085–1094.

189 E. V Tret'yakova, O. B. Flekhter, F. Z. Galin, I. P. Baikova and G. A. Tolstikov, *Chem. Nat. Compd.*, 2003, **39**, 16–18.

190 C. E. Elliott, D. O. Miller and D. J. Burnell, *J. Chem. Soc. Perkin Trans. 1*, 2002, 217–226.

191 S. Kotha, O. Ravikumar and J. Majhi, *Beilstein J. Org. Chem.*, 2015, **11**, 1503–1508.

192 A. Kitowski, E. Jiménez-Moreno, M. Salvadó, J. Mestre, S. Castillón, G. Jiménez-Osés, O. Boutureira and G. J. L. Bernardes, *Org. Lett.*, 2017, **19**, 5490–5493.

193 N. Stefano, P. Cyril and W. Jérôme, *Angew. Chemie Int. Ed.*, 2011, **50**, 4680–4683.

194 L. Jiang, G. E. Job, A. Klapars and S. L. Buchwald, *Org. Lett.*, 2003, **5**, 3667–3669.

195 T. Imamoto, N. Takiyama, K. Nakamura, T. Hatajima and Y. Kamiya, *J. Am. Chem. Soc.*, 1989, **111**, 4392–4398.

196 Z. Shi, C. Grohmann and F. Glorius, *Angew. Chemie Int. Ed.*, 2013, **52**, 5393–5397.

197 R. Buffa, P. Šedová, I. Basarabová, M. Moravcová, L. Wolfová, T. Bobula and V. Velebný, *Carbohydr. Polym.*, 2015, **134**, 293–299.

198 J. W. Choi, B. K. Jang, N. Cho, J.-H. Park, S. K. Yeon, E. J. Ju, Y. S. Lee, G. Han, A. N. Pae, D. J. Kim and K. D. Park, *Bioorg. Med. Chem.*, 2015, **23**, 6486–6496.

199 R. S. Gouhar, E. F. Ewies, M. F. El-Shehry, M. N. F. Shaheen and E.-M. M. E. Ibrahim, *J. Heterocycl. Chem.*, 2018, **55**, 2368–2380.

200 K. C. Nicolaou, T. Montagnon, P. S. Baran and Y.-L. Zhong, *J. Am. Chem. Soc.*, 2002, **124**, 2245–2258.

201 D. S. Siegel, G. Piizzi, G. Piersanti and M. Movassaghi, *J. Org. Chem.*, 2009, **74**, 9292–9304.

202 A. M. DiLauro, W. Seo and S. T. Phillips, *J. Org. Chem.*, 2011, **76**, 7352–7358.

203 B. Rozman, *Clin. Pharmacokinet.*, 2002, **41**, 421–430.

204 M. A. Schwartz, *J. Pharmacol. Exp. Ther.*, 1960, **130**, 157–165.

205 R. Sutherland, E. A. Croydon and G. N. Rolinson, *Br. Med. J.*, 1970, **4**, 455–460.

206 G. Scott and F. Valery V., *Angew. Chemie Int. Ed.*, 2008, **47**, 8285–8287.

207 K. Mori, *Synlett*, 1995, **11**, 1097–1109.

208 C. R. Johnson, *Acc. Chem. Res.*, 1998, **31**, 333–341.

209 R. J. Sharpe and J. S. Johnson, *J. Org. Chem.*, 2015, **80**, 9740–9766.

210 S. Cuadros, L. Dell'Amico and P. Melchiorre, *Angew. Chemie Int. Ed.*, 2017, **56**, 11875–11879.

211 W. H. B. Sauer and M. K. Schwarz, *J. Chem. Inf. Comput. Sci.*, 2003, **43**, 987–1003.

212 I. Colomer, C. J. Empson, P. Craven, Z. Owen, R. G. Doveston, I. Churcher, S. P. Marsden and A.

Nelson, *Chem. Commun.*, 2016, **52**, 7209–7212.

213 H. Köster, T. Craan, S. Brass, C. Herhaus, M. Zentgraf, L. Neumann, A. Heine and G. Klebe, *J. Med. Chem.*, 2011, **54**, 7784–7796.

214 H. Jhoti, G. Williams, D. C. Rees and C. W. Murray, *Nat. Rev. Drug Discov.*, 2013, **12**, 644.

215 P. Ertl, S. Roggo and A. Schuffenhauer, *J. Chem. Inf. Model.*, 2008, **48**, 68–74.

216 K. Vanii Jayaseelan, P. Moreno, A. Truszkowski, P. Ertl and C. Steinbeck, *BMC Bioinformatics*, 2012, **13**, 106.

217 F. Nie, D. L. Kunciw, D. Wilcke, J. E. Stokes, W. R. J. D. Galloway, S. Bartlett, H. F. Sore and D. R. Spring, *Angew. Chemie Int. Ed.*, 2016, **55**, 11139–11143.

218 P. M. Collins, J. T. Ng, R. Talon, K. Nekrosiute, T. Krojer, A. Douangamath, J. Brandao-Neto, N. Wright, N. M. Pearce and F. von Delft, *Acta Crystallogr. Sect. D*, 2017, **73**, 246–255.

219 T. Krojer, R. Talon, N. Pearce, P. Collins, A. Douangamath, J. Brandao-Neto, A. Dias, B. Marsden and F. von Delft, *Acta Crystallogr. Sect. D*, 2017, **73**, 267–278.

220 N. M. Pearce, T. Krojer, A. R. Bradley, P. Collins, R. P. Nowak, R. Talon, B. D. Marsden, S. Kelm, J. Shi, C. M. Deane and F. von Delft, *Nat. Commun.*, 2017, **8**, 15123.

221 D. Hanahan and R. A. Weinberg, *Cell*, 2000, **100**, 57–70.

222 D. Hanahan and R. A. Weinberg, *Cell*, 2011, **144**, 646–674.

223 H. Sung, J. Ferlay, R. L. Siegel, M. Laversanne, I. Soerjomataram, A. Jemal and F. Bray, *CA. Cancer J. Clin.*, 2021, **71**, 209–249.

224 G. B. of D. C. Collaboration, *JAMA Oncol.*, 2015, **1**, 505–527.

225 V. T. DeVita and E. Chu, *Cancer Res.*, 2008, **68**, 8643–8653.

226 R. V. J. Chari, M. L. Miller and W. C. Widdison, *Angew. Chemie Int. Ed.*, 2014, **53**, 3796–3827.

227 A. Beck, L. Goetsch, C. Dumontet and N. Corvaïa, *Nat. Rev. Drug Discov.*, 2017, **16**, 315–337.

228 H. Tang, Y. Liu, Z. Yu, M. Sun, L. Lin, W. Liu, Q. Han, M. Wei and Y. Jin, *Front. Pharmacol.*, 2019, **10**, 373.

229 G. Mathe, L. O. C. Tran Ba and J. Bernard, *C. R. Hebd. Seances Acad. Sci.*, 1958, **246**, 1626–1628.

230 P. F. Bross, J. Beitz, G. Chen, X. H. Chen, E. Duffy, L. Kieffer, S. Roy, R. Sridhara, A. Rahman, G. Williams and R. Pazdur, *Clin. Cancer Res.*, 2001, **7**, 1490–1496.

231 P. Zhao, Y. Zhang, W. Li, C. Jeanty, G. Xiang and Y. Dong, *Acta Pharm. Sin. B*, 2020, **10**, 1589–1600.

232 S. H. Petersdorf, K. J. Kopecky, M. Slovak, C. Willman, T. Nevill, J. Brandwein, R. A. Larson, H. P. Erba, P. J. Stiff, R. K. Stuart, R. B. Walter, M. S. Tallman, L. Stenke and F. R. Appelbaum, *Blood*, 2013, **121**, 4854–4860.

233 F. R. Appelbaum and I. D. Bernstein, *Blood*, 2017, **130**, 2373–2376.

234 N. Joubert, A. Beck, C. Dumontet and C. Denevault-Sabourin, *Pharmaceuticals*, 2020, 13.

235 L. Gauzy-Lazo, I. Sassoon and M.-P. Brun, *SLAS Discov. Adv. Sci. Drug Discov.*, 2020, **25**, 843–868.

236 S. J. Walsh, J. D. Bargh, F. M. Dannheim, A. R. Hanby, H. Seki, A. J. Counsell, X. Ou, E. Fowler, N. Ashman, Y. Takada, A. Isidro-Llobet, J. S. Parker, J. S. Carroll and D. R. Spring, *Chem. Soc. Rev.*, 2021, **50**, 1305–1353.

237 P. R. Hamann, L. M. Hinman, I. Hollander, C. F. Beyer, D. Lindh, R. Holcomb, W. Hallett, H.-R. Tsou, J. Upeslacis, D. Shochat, A. Mountain, D. A. Flowers and I. Bernstein, *Bioconjug. Chem.*, 2002, **13**, 47–58.

238 N. W. C. J. van de Donk and E. Dhimolea, *MAbs*, 2012, **4**, 458–465.

239 A. Deslandes, *MAbs*, 2014, **6**, 859–870.

240 P. F. Peddi and S. A. Hurvitz, *Futur. Oncol.*, 2013, **9**, 319–326.

241 J. M. Lambert and R. V. J. Chari, *J. Med. Chem.*, 2014, **57**, 6949–6964.

242 G. von Minckwitz, C.-S. Huang, M. S. Mano, S. Loibl, E. P. Mamounas, M. Untch, N. Wolmark, P. Rastogi, A. Schneeweiss, A. Redondo, H. H. Fischer, W. Jacot, A. K. Conlin, C. Arce-Salinas, I. L. Wapnir, C. Jackisch, M. P. DiGiovanna, P. A. Fasching, J. P. Crown, P. Wülfing, Z. Shao, E. Rota Caremoli, H. Wu, L. H. Lam, D. Tesarowski, M. Smitt, H. Douthwaite, S. M. Singel and C. E. Geyer, *N. Engl. J. Med.*, 2018, **380**, 617–628.

243 I. Pysz, P. J. M. Jackson and D. E. Thurston, in *Cytotoxic Payloads for Antibody–Drug Conjugates*, The Royal Society of Chemistry, eds. D. Thurston, P. Jackson, 2019, 1–30.

244 Y. N. Lamb, *Drugs*, 2017, **77**, 1603–1610.

245 H. Tilly, F. Morschhauser, N. L. Bartlett, A. Mehta, G. Salles, C. Haioun, J. Munoz, A. I. Chen, K. Kolibaba, D. Lu, M. Yan, E. Penuel, J. Hirata, C. Lee and J. P. Sharman, *Lancet Oncol.*, 2019, **20**, 998–1010.

246 L. H. Sehn, A. F. Herrera, M. J. Matasar, M. Kamdar, S. Assouline, M. Hertzberg, T. M. Kim, W.-S. Kim, A. McMillan, M. Özcan, J. M. Hirata, E. Penuel, J. Cheng, G. Ku and C. R. Flowers, *Blood*, 2018, **132**, 1683.

247 M. Akaiwa, J. Dugal-Tessier and B. A. Mendelsohn, *Chem. Pharm. Bull.*, 2020, **68**, 201–211.

248 P. M. Challita-Eid, D. Satpayev, P. Yang, Z. An, K. Morrison, Y. Shostak, A. Raitano, R. Nadell, W. Liu, D. R. Lortie, L. Capo, A. Verlinsky, M. Leavitt, F. Malik, H. Aviña, C. I. Guevara, N. Dinh, S. Karki, B. S. Anand, D. S. Pereira, I. B. J. Joseph, F. Doñate, K. Morrison and D. R. Stover, *Cancer Res.*, 2016, **76**, 3003–3013.

249 T. K. Burki, *Lancet Oncol.*, 2020, **21**, e133.

250 Y. Ogitani, T. Aida, K. Hagihara, J. Yamaguchi, C. Ishii, N. Harada, M. Soma, H. Okamoto, M. Oitate, S. Arakawa, T. Hirai, R. Atsumi, T. Nakada, I. Hayakawa, Y. Abe and T. Agatsuma, *Clin. Cancer Res.*, 2016, **22**, 5097–5108.

251 T. N. Iwata, C. Ishii, S. Ishida, Y. Ogitani, T. Wada and T. Agatsuma, *Mol. Cancer Ther.*, 2018, **17**, 1494–1503.

252 K. Shitara, Y.-J. Bang, S. Iwasa, N. Sugimoto, M.-H. Ryu, D. Sakai, H.-C. Chung, H. Kawakami, H. Yabusaki, J. Lee, K. Saito, Y. Kawaguchi, T. Kamio, A. Kojima, M. Sugihara and K. Yamaguchi, *N. Engl. J. Med.*, 2020, **382**, 2419–2430.

253 S. Modi, C. Saura, T. Yamashita, Y. H. Park, S.-B. Kim, K. Tamura, F. Andre, H. Iwata, Y. Ito, J. Tsurutani, J. Sohn, N. Denduluri, C. Perrin, K. Aogi, E. Tokunaga, S.-A. Im, K. S. Lee, S. A. Hurvitz, J. Cortes, C. Lee, S. Chen, L. Zhang, J. Shahidi, A. Yver and I. Krop, *N. Engl. J. Med.*, 2019, **382**, 610–621.

254 W. Dong, J. Shi, T. Yuan, B. Qi, J. Yu, J. Dai and L. He, *Eur. J. Med. Chem.*, 2019, **167**, 583–593.

255 T. M. Cardillo, S. V Govindan, R. M. Sharkey, P. Trisal, R. Arrojo, D. Liu, E. A. Rossi, C.-H. Chang and D. M. Goldenberg, *Bioconjug. Chem.*, 2015, **26**, 919–931.

256 R. M. Sharkey, W. J. McBride, T. M. Cardillo, S. V Govindan, Y. Wang, E. A. Rossi, C.-H. Chang and D. M. Goldenberg, *Clin. Cancer Res.*, 2015, **21**, 5131–5138.

257 D. M. Goldenberg and R. M. Sharkey, *Expert Opin. Biol. Ther.*, 2020, **20**, 871–885.

258 S. Lonial, H. C. Lee, A. Badros, S. Trudel, A. K. Nooka, A. Chari, A.-O. Abdallah, N. Callander, N. Lendvai, D. Sborov, A. Suvannasankha, K. Weisel, L. Karlin, E. Libby, B. Arnulf, T. Facon, C. Hulin, K. M. Kortüm, P. Rodríguez-Otero, S. Z. Usmani, P. Hari, R. Baz, H. Quach, P. Moreau, P. M. Voorhees, I. Gupta, A. Hoos, E. Zhi, J. Baron, T. Piontek, E. Lewis, R. C. Jewell, E. J. Dettman, R. Popat, S. D. Esposti, J. Opalinska, P. Richardson and A. D. Cohen, *Lancet Oncol.*, 2020, **21**, 207–221.

259 Y.-T. Tai, P. A. Mayes, C. Acharya, M. Y. Zhong, M. Cea, A. Cagnetta, J. Craigen, J. Yates, L. Gliddon, W. Fieles, B. Hoang, J. Tunstead, A. L. Christie, A. L. Kung, P. Richardson, N. C. Munshi and K. C. Anderson, *Blood*, 2014, **123**, 3128–3138.

260 F. Zammarchi, S. Corbett, L. Adams, P. C. Tyrer, K. Kiakos, N. Janghra, T. Marafioti, C. E. Britten, C. E. G. Havenith, S. Chivers, F. D'Hooge, D. G. Williams, A. Tiberghien, P. W. Howard, J. A. Hartley and P. H. van Berkel, *Blood*, 2018, **131**, 1094–1105.

261 M. Hamadani, J. Radford, C. Carlo-Stella, P. F. Caimi, E. G. Reid, O. A. O'Connor, J. Feingold, K. M. Ardeshna, W. M. Townsend, M. Solh, L. T. Heffner, D. Ungar, L. Wang, J. P. Boni, K. Havenith, Y. G. Qin and B. Kahl, *Blood*, 2021, **137**, 2634–2645.

262 C. H. Chau, P. S. Steeg and W. D. Figg, *Lancet*, 2019, **394**, 793–804.

263 J. Lu, F. Jiang, A. Lu and G. Zhang, *Int. J. Mol. Sci.*, 2016, **17**, 561.

264 J. D. Bargh, A. Isidro-Llobet, J. S. Parker and D. R. Spring, *Chem. Soc. Rev.*, 2019, **48**, 4361–4374.

265 M. Ritchie, L. Tchistiakova and N. Scott, *MAbs*, 2013, **5**, 13–21.

266 A. H. Staudacher and M. P. Brown, *Br. J. Cancer*, 2017, **117**, 1736–1742.

267 S. A. Frank, in *Immunology and Evolution of Infectious Disease*, Princeton University Press, 2002, 33–35.

268 P. J. Kennedy, C. Oliveira, P. L. Granja and B. Sarmento, *Pharmacol. Ther.*, 2017, **177**, 129–145.

269 C. Peters and S. Brown, *Biosci. Rep.*, 2015, **35**, e00225.

270 F. A. Harding, M. M. Stickler, J. Razo and R. B. DuBridge, *MAbs*, 2010, **2**, 256–265.

271 H. Liu and K. May, *MAbs*, 2012, **4**, 17–23.

272 C. Lo Nigro, M. Macagno, D. Sangiolo, L. Bertolaccini, M. Aglietta and M. C. Merlano, *Ann. Transl. Med.*, 2019, **7**, 105.

273 M. L. Chiu, D. R. Goulet, A. Teplyakov and G. L. Gilliland, *Antibodies*, 2019, **8**, 55.

274 T. Kubota, R. Niwa, M. Satoh, S. Akinaga, K. Shitara and N. Hanai, *Cancer Sci.*, 2009, **100**, 1566–1572.

275 B. Heyman, *Immunol. Lett.*, 1996, **54**, 195–199.

276 V. Chudasama, A. Maruani and S. Caddick, *Nat. Chem.*, 2016, **8**, 114–119.

277 P. Agarwal and C. R. Bertozzi, *Bioconjug. Chem.*, 2015, **26**, 176–192.

278 G. Vidarsson, G. Dekkers and T. Rispens, *Front. Immunol.*, 2014, **5**, 520.

279 R. M. Hoffmann, B. G. T. Coumbe, D. H. Josephs, S. Mele, K. M. Ilieva, A. Cheung, A. N. Tutt, J. F. Spicer, D. E. Thurston, S. Crescioli and S. N. Karagiannis, *Oncoimmunology*, 2018, **7**, e1395127.

280 P. Herbener, K. Schönfeld, M. König, M. Germer, J. M. Przyborski, K. Bernöster and J. Schüttrumpf, *PLoS One*, 2018, **13**, e0195823.

281 L. Liu-Shin, A. Fung, A. Malhotra and G. Ratnaswamy, *MAbs*, 2018, **10**, 583–595.

282 M.-R. Nejadmoghaddam, A. Minai-Tehrani, R. Ghahremanzadeh, M. Mahmoudi, R. Dinarvand and A.-H. Zarnani, *Avicenna J. Med. Biotechnol.*, 2019, **11**, 3–23.

283 P. J. Carter and P. D. Senter, *Cancer J.*, 2008, **14**, 154–169.

284 Y. V Kovtun, C. A. Audette, Y. Ye, H. Xie, M. F. Ruberti, S. J. Phinney, B. A. Leece, T. Chittenden, W. A. Blättler and V. S. Goldmacher, *Cancer Res.*, 2006, **66**, 3214–3221.

285 C. Criscitiello, S. Morganti and G. Curigliano, *J. Hematol. Oncol.*, 2021, **14**, 20.

286 P. Chames, M. Van Regenmortel, E. Weiss and D. Baty, *Br. J. Pharmacol.*, 2009, **157**, 220–233.

287 K. T. Xenaki, S. Oliveira and P. M. P. van Bergen en Henegouwen, *Front. Immunol.*, 2017, **8**, 1287.

288 D.-Y. Oh and Y.-J. Bang, *Nat. Rev. Clin. Oncol.*, 2020, **17**, 33–48.

289 O. P. Kallioniemi, A. Kallioniemi, W. Kurisu, A. Thor, L. C. Chen, H. S. Smith, F. M. Waldman, D. Pinkel and J. W. Gray, *Proc. Natl. Acad. Sci.*, 1992, **89**, 5321–5325.

290 D. J. Slamon, G. M. Clark, S. G. Wong, W. J. Levin, A. Ullrich and W. L. McGuire, *Science*, 1987, **235**, 177–182.

291 W. F. Symmans, C. Wei, R. Gould, X. Yu, Y. Zhang, M. Liu, A. Walls, A. Bousamra, M. Ramineni, B. Sinn, K. Hunt, T. A. Buchholz, V. Valero, A. U. Buzdar, W. Yang, A. M. Brewster, S. Moulder, L. Pusztai, C. Hatzis and G. N. Hortobagyi, *J. Clin. Oncol.*, 2017, **35**, 1049–1060.

292 R. Nahta and F. J. Esteva, *Oncogene*, 2007, **26**, 3637–3643.

293 P. R. Pohlmann, I. A. Mayer and R. Mernaugh, *Clin. Cancer Res.*, 2009, **15**, 7479–7491.

294 C. Saura, F. Thistlethwaite, U. Banerji, S. Lord, V. Moreno, I. MacPherson, V. Boni, C. D. Rolfo, E. G. E. de Vries, C. M. L.- Van Herpen, S. Rottey, J. J. J. Geenen, F. Eskens, M. Gil Martin, E. Mommers, N. P. Koper, R. Mulder and P. G. Aftimos, *J. Clin. Oncol.*, 2018, **36**, 1014.

295 S. Modi, H. Park, R. K. Murthy, H. Iwata, K. Tamura, J. Tsurutani, A. Moreno-Aspitia, T. Doi, Y. Sagara, C. Redfern, I. E. Krop, C. Lee, Y. Fujisaki, M. Sugihara, L. Zhang, J. Shahidi and S. Takahashi, *J. Clin. Oncol.*, 2020, **38**, 1887–1896.

296 A. A. Epenetos, D. Snook, H. Durbin, P. M. Johnson and J. Taylor-Papadimitriou, *Cancer Res.*, 1986, **46**, 3183–3191.

297 M. Abdollahpour-Alitappeh, M. Lotfinia, T. Gharibi, J. Mardaneh, B. Farhadihosseinabadi, P. Larki, B. Faghfourian, K. S. Sepehr, K. Abbaszadeh-Goudarzi, G. Abbaszadeh-Goudarzi, B. Johari, M. R. Zali and N. Bagheri, *J. Cell. Physiol.*, 2019, **234**, 5628–5642.

298 P. A. Trail, D. Willner, S. J. Lasch, A. J. Henderson, S. Hofstead, A. M. Casazza, R. A. Firestone, I. Hellstrom and K. E. Hellstrom, *Science*, 1993, **261**, 212–215.

299 A. W. Tolcher, S. Sugarman, K. A. Gelmon, R. Cohen, M. Saleh, C. Isaacs, L. Young, D. Healey, N. Onetto and W. Slichenmyer, *J. Clin. Oncol.*, 1999, **17**, 478–484.

300 K. C. Nicolaou and S. Rigol, *Angew. Chemie Int. Ed.*, 2019, **58**, 11206–11241.

301 J. Dugal-Tessier, S. D. Barnscher, A. Kanai and B. A. Mendelsohn, *J. Nat. Prod.*, 2017, **80**, 2484–2491.

302 K. Miyazaki, M. Kobayashi, T. Natsume, M. Gondo, T. Mikami, K. Sakabibara and S. Tsukagoshi, *Chem. Pharm. Bull.*, 1995, **43**, 1706–1718.

303 E. E. Hong, H. Erickson, R. J. Lutz, K. R. Whiteman, G. Jones, Y. Kovtun, V. Blanc and J. M. Lambert, *Mol. Pharm.*, 2015, **12**, 1703–1716.

304 W. C. Widdison, in *Cytotoxic Payloads for Antibody–Drug Conjugates*, The Royal Society of Chemistry, 2019, 100–116.

305 M. Ryan, R. Lyski, L. Bou, R. Heiser, B. Grogan, D. Meyer, S. Jin, J. Simmons, M. Conerly, P. Senter and S. Jeffrey, *Blood*, 2020, **136**, 41–42.

306 L. Yu, Y. Lu, Y. Yao, Y. Liu, Y. Wang, Q. Lai, R. Zhang, W. Li, R. Wang, Y. Fu, Y. Tao, S. Yi, L. Gou, L. Chen and J. Yang, *Oncotarget*, 2017, **9**, 5197–5207.

307 K. Tsuchikama and Z. An, *Protein Cell*, 2018, **9**, 33–46.

308 K. J. Hamblett, P. D. Senter, D. F. Chace, M. M. C. Sun, J. Lenox, C. G. Cerveny, K. M. Kissler, S. X. Bernhardt, A. K. Kopcha, R. F. Zabinski, D. L. Meyer and J. A. Francisco, *Clin. Cancer Res.*, 2004, **10**, 7063–7070.

309 J. K. Simmons, P. J. Burke, J. H. Cochran, P. G. Pittman and R. P. Lyon, *Toxicol. Appl. Pharmacol.*, 2020, **392**, 114932.

310 R. P. Lyon, T. D. Bovee, S. O. Doronina, P. J. Burke, J. H. Hunter, H. D. Neff-LaFord, M. Jonas, M. E. Anderson, J. R. Setter and P. D. Senter, *Nat. Biotechnol.*, 2015, **33**, 733–735.

311 P. Strop, K. Delaria, D. Foletti, J. M. Witt, A. Hasa-Moreno, K. Poulsen, M. G. Casas, M. Dorywalska, S. Farias, A. Pios, V. Lui, R. Dushin, D. Zhou, T. Navaratnam, T.-T. Tran, J. Sutton, K. C. Lindquist, B. Han, S.-H. Liu, D. L. Shelton, J. Pons and A. Rajpal, *Nat. Biotechnol.*, 2015, **33**, 694–696.

312 S. O. Doronina, B. E. Toki, M. Y. Torgov, B. A. Mendelsohn, C. G. Cerveny, D. F. Chace, R. L. DeBlanc, R. P. Gearing, T. D. Bovee, C. B. Siegall, J. A. Francisco, A. F. Wahl, D. L. Meyer and P. D. Senter, *Nat. Biotechnol.*, 2003, **21**, 778–784.

313 J. C. Kern, M. Cancilla, D. Dooney, K. Kwasnjuk, R. Zhang, M. Beaumont, I. Figueroa, S. Hsieh, L. Liang, D. Tomazela, J. Zhang, P. E. Brandish, A. Palmieri, P. Stivers, M. Cheng, G. Feng, P. Geda, S. Shah, A. Beck, D. Bresson, J. Firdos, D. Gately, N. Knudsen, A. Manibusan, P. G. Schultz, Y. Sun and R. M. Garbaccio, *J. Am. Chem. Soc.*, 2016, **138**, 1430–1445.

314 S. C. Jeffrey, J. B. Andreyka, S. X. Bernhardt, K. M. Kissler, T. Kline, J. S. Lenox, R. F. Moser, M. T. Nguyen, N. M. Okeley, I. J. Stone, X. Zhang and P. D. Senter, *Bioconjug. Chem.*, 2006, **17**, 831–840.

315 J. D. Bargh, S. J. Walsh, A. Isidro-Llobet, S. Omarjee, J. S. Carroll and D. R. Spring, *Chem. Sci.*, 2020, **11**, 2375–2380.

316 T. H. Pillow, J. D. Sadowsky, D. Zhang, S.-F. Yu, G. Del Rosario, K. Xu, J. He, S. Bhakta, R. Ohri, K. R. Kozak, E. Ha, J. R. Junutula and J. A. Flygare, *Chem. Sci.*, 2017, **8**, 366–370.

317 N. Jain, S. W. Smith, S. Ghone and B. Tomczuk, *Pharm. Res.*, 2015, **32**, 3526–3540.

318 H. K. Erickson, P. U. Park, W. C. Widdison, Y. V Kovtun, L. M. Garrett, K. Hoffman, R. J. Lutz, V. S. Goldmacher and W. A. Blättler, *Cancer Res.*, 2006, **66**, 4426–4433.

319 L. Wang, G. Amphlett, W. A. Blättler, J. M. Lambert and W. Zhang, *Protein Sci.*, 2005, **14**, 2436–2446.

320 M. M. C. Sun, K. S. Beam, C. G. Cerveny, K. J. Hamblett, R. S. Blackmore, M. Y. Torgov, F. G. M. Handley, N. C. Ihle, P. D. Senter and S. C. Alley, *Bioconjug. Chem.*, 2005, **16**, 1282–1290.

321 P. Akkapeddi, S.-A. Azizi, A. M. Freedy, P. M. S. D. Cal, P. M. P. Gois and G. J. L. Bernardes, *Chem. Sci.*, 2016, **7**, 2954–2963.

322 J. R. Junutula, H. Raab, S. Clark, S. Bhakta, D. D. Leipold, S. Weir, Y. Chen, M. Simpson, S. P. Tsai, M. S. Dennis, Y. Lu, Y. G. Meng, C. Ng, J. Yang, C. C. Lee, E. Duenas, J. Gorrell, V. Katta, A. Kim, K. McDorman, K. Flagella, R. Venook, S. Ross, S. D. Spencer, W. Lee Wong, H. B. Lowman, R. Vandlen, M. X. Sliwkowski, R. H. Scheller, P. Polakis and W. Mallet, *Nat. Biotechnol.*, 2008, **26**, 925–932.

323 E. A. Hoyt, P. M. S. D. Cal, B. L. Oliveira and G. J. L. Bernardes, *Nat. Rev. Chem.*, 2019, **3**, 147–171.

324 E. M. Sletten and C. R. Bertozzi, *Angew. Chemie Int. Ed.*, 2009, **48**, 6974–6998.

325 H. C. Hang, C. Yu, D. L. Kato and C. R. Bertozzi, *Proc. Natl. Acad. Sci.*, 2003, **100**, 14846–14851.

326 H. C. Kolb, M. G. Finn and K. B. Sharpless, *Angew. Chemie Int. Ed.*, 2001, **40**, 2004–2021.

327 T. I. Chio and S. L. Bane, *Methods Mol. Biol.*, 2020, **2078**, 83–97.

328 C. S. McKay and M. G. Finn, *Chem. Biol.*, 2014, **21**, 1075–1101.

329 P. M. Drake, A. E. Albers, J. Baker, S. Banas, R. M. Barfield, A. S. Bhat, G. W. de Hart, A. W. Garofalo, P. Holder, L. C. Jones, R. Kudirka, J. McFarland, W. Zmolek and D. Rabuka, *Bioconjug. Chem.*, 2014, **25**, 1331–1341.

330 R. Kudirka, R. M. Barfield, J. McFarland, A. E. Albers, G. W. de Hart, P. M. Drake, P. G. Holder, S. Banas, L. C. Jones, A. W. Garofalo and D. Rabuka, *Chem. Biol.*, 2015, **22**, 293–298.

331 R. A. Kudirka, R. M. Barfield, J. M. McFarland, P. M. Drake, A. Carlson, S. Bañas, W. Zmolek, A. W. Garofalo and D. Rabuka, *ACS Med. Chem. Lett.*, 2016, **7**, 994–998.

332 P. Thompson, E. Ezeadi, I. Hutchinson, R. Fleming, B. Bezabeh, J. Lin, S. Mao, C. Chen, L. Masterson, H. Zhong, D. Toader, P. Howard, H. Wu, C. Gao and N. Dimasi, *ACS Med. Chem. Lett.*, 2016, **7**, 1005–1008.

333 V. V Rostovtsev, L. G. Green, V. V Fokin and K. B. Sharpless, *Angew. Chemie Int. Ed.*, 2002, **41**, 2596–2599.

334 R. van Geel, M. A. Wijdeven, R. Heesbeen, J. M. M. Verkade, A. A. Wasiel, S. S. van Berkel and F. L. van Delft, *Bioconjug. Chem.*, 2015, **26**, 2233–2242.

335 J. C. Jewett and C. R. Bertozzi, *Chem. Soc. Rev.*, 2010, **39**, 1272–1279.

336 N. J. Agard, J. A. Prescher and C. R. Bertozzi, *J. Am. Chem. Soc.*, 2004, **126**, 15046–15047.

337 M. L. Blackman, M. Royzen and J. M. Fox, *J. Am. Chem. Soc.*, 2008, **130**, 13518–13519.

338 J. Dommerholt, F. P. J. T. Rutjes and F. L. van Delft, *Top. Curr. Chem.*, 2016, **374**, 16.

339 E. S. Zimmerman, T. H. Heibeck, A. Gill, X. Li, C. J. Murray, M. R. Madlansacay, C. Tran, N. T. Uter, G. Yin, P. J. Rivers, A. Y. Yam, W. D. Wang, A. R. Steiner, S. U. Bajad, K. Penta, W. Yang, T. J. Hallam, C. D. Thanos and A. K. Sato, *Bioconjug. Chem.*, 2014, **25**, 351–361.

340 Y. Wu, H. Zhu, B. Zhang, F. Liu, J. Chen, Y. Wang, Y. Wang, Z. Zhang, L. Wu, L. Si, H. Xu, T. Yao, S. Xiao, Q. Xia, L. Zhang, Z. Yang and D. Zhou, *Bioconjug. Chem.*, 2016, **27**, 2460–2468.

341 X. Li, T. Fang and G.-J. Boons, *Angew. Chemie Int. Ed.*, 2014, **53**, 7179–7182.

342 C. L. Abrahams, X. Li, M. Embry, A. Yu, S. Krimm, S. Krueger, N. Y. Greenland, K. W. Wen, C. Jones, V. DeAlmeida, W. A. Solis, S. Matheny, T. Kline, A. Y. Yam, R. Stafford, A. P. Wiita, T. Hallam, M. Lupher and A. Molina, *Oncotarget*, 2018, **9**, 37700–37714.

343 X. Li, C. Abrahams, S. Zhou, S. Krimm, R. Henningsen, H. Stephenson, J. Hanson, M. R. Masikat, K. Bajjuri, T. Heibeck, C. Tran, G. Yin, J. Zawada, G. Sarma, J. Chen, M. Bruhns, W. Solis, A. Steiner, A. Galan, T. Kline, R. Stafford, A. Yam, V. I. De Almeida, M. Lupher and T. Hallam, in *Cancer Research*, 2018, vol. 78, 1782–1782.

344 J. Li and P. R. Chen, *Nat. Chem. Biol.*, 2016, **12**, 129–137.

345 B. L. Oliveira, Z. Guo and G. J. L. Bernardes, *Chem. Soc. Rev.*, 2017, **46**, 4895–4950.

346 B. J. Umlauf, K. A. Mix, V. A. Grosskopf, R. T. Raines and E. V Shusta, *Bioconjug. Chem.*, 2018, **29**, 1605–1613.

347 B. Oller-Salvia, G. Kym and J. W. Chin, *Angew. Chemie Int. Ed.*, 2018, **57**, 2831–2834.

348 V. F. C. Ferreira, B. L. Oliveira, A. D'Onofrio, C. M. Farinha, L. Gano, A. Paulo, G. J. L. Bernardes and F. Mendes, *Bioconjug. Chem.*, 2021, **32**, 121–132.

349 B. E. Cook, P. Adumeau, R. Membreno, K. E. Carnazza, C. Brand, T. Reiner, B. J. Agnew, J. S. Lewis and B. M. Zeglis, *Bioconjug. Chem.*, 2016, **27**, 1789–1795.

350 A. Maruani, M. E. B. Smith, E. Miranda, K. A. Chester, V. Chudasama and S. Caddick, *Nat. Commun.*, 2015, **6**, 6645.

351 Y. Liang, J. L. Mackey, S. A. Lopez, F. Liu and K. N. Houk, *J. Am. Chem. Soc.*, 2012, **134**, 17904–17907.

352 A. Maruani, D. A. Richards and V. Chudasama, *Org. Biomol. Chem.*, 2016, **14**, 6165–6178.

353 L. Xu, S. L. Kuan and T. Weil, *Angew. Chemie Int. Ed.*, 2021, **60**, 13757–13777.

354 B.-C. Lee, C. Chalouni, S. Doll, S. C. Nalle, M. Darwish, S. P. Tsai, K. R. Kozak, G. Del-Rosario, S.-F. Yu, H. Erickson and R. Vandlen, *Bioconjug. Chem.*, 2018, **29**, 2468–2477.

355 A. Kumar, K. Kinneer, L. Masterson, E. Ezeadi, P. Howard, H. Wu, C. Gao and N. Dimasi, *Bioorg. Med. Chem. Lett.*, 2018, **28**, 3617–3621.

356 J. W. Chin, *Nature*, 2017, **550**, 53–60.

357 C. C. Liu and P. G. Schultz, *Annu. Rev. Biochem.*, 2010, **79**, 413–444.

358 H. Neumann, A. L. Slusarczyk and J. W. Chin, *J. Am. Chem. Soc.*, 2010, **132**, 2142–2144.

359 N. Nilchan, X. Li, L. Pedzisa, A. R. Nanna, W. R. Roush and C. Rader, *Antib. Ther.*, 2019, **2**, 71–78.

360 H. Xiao, A. Chatterjee, S. Choi, K. M. Bajjuri, S. C. Sinha and P. G. Schultz, *Angew. Chemie Int. Ed.*, 2013, **52**, 14080–14083.

361 X. Li, J. T. Patterson, M. Sarkar, L. Pedzisa, T. Kodadek, W. R. Roush and C. Rader, *Bioconjug. Chem.*, 2015, **26**, 2243–2248.

362 T. Hofer, J. D. Thomas, T. R. Burke and C. Rader, *Proc. Natl. Acad. Sci.*, 2008, **105**, 12451–12456.

363 E. M. Milczek, *Chem. Rev.*, 2018, **118**, 119–141.

364 P. Adumeau, S. K. Sharma, C. Brent and B. M. Zeglis, *Mol. Imaging Biol.*, 2016, **18**, 153–165.

365 C. M. Le Gall, J. M. S. van der Schoot, I. Ramos-Tomillero, M. P. Khalily, F. J. van Dalen, Z. Wijfjes, L. Smeding, D. van Dalen, A. Cammarata, K. M. Bonger, C. G. Figdor, F. A. Scheeren and M. Verdoes, *Bioconjug. Chem.*, 2021, **32**, 301–310.

366 T. J. Harmand, D. Bousbaine, A. Chan, X. Zhang, D. R. Liu, J. P. Tam and H. L. Ploegh, *Bioconjug. Chem.*, 2018, **29**, 3245–3249.

367 D. N. Thornlow, E. C. Cox, J. A. Walker, M. Sorkin, J. B. Plesset, M. P. DeLisa and C. A. Alabi, *Bioconjug. Chem.*, 2019, **30**, 1702–1710.

368 C. Wollschlaeger, I. Meinhold-Heerlein, X. Cong, K. Bräutigam, S. Di Fiore, F. Zeppernick, T. Klockenbring, E. Stickeler, S. Barth and A. F. Hussain, *Bioconjug. Chem.*, 2018, **29**, 3586–3594.

369 P. R. Spycher, C. A. Amann, J. E. Wehrmüller, D. R. Hurwitz, O. Kreis, D. Messmer, A. Ritler, A. Küchler, A. Blanc, M. Béhé, P. Walde and R. Schibli, *ChemBioChem*, 2017, **18**, 1923–1927.

370 M. D. Lee, W. Y. Tong, T. Nebl, L. A. Pearce, T. M. Pham, A. Golbaz-Hagh, S. Puttick, S. Rose, T. E. Adams and C. C. Williams, *Bioconjug. Chem.*, 2019, **30**, 2539–2543.

371 S. Puthenveetil, S. Musto, F. Loganzo, L. N. Tumey, C. J. O'Donnell and E. Graziani, *Bioconjug. Chem.*, 2016, **27**, 1030–1039.

372 J. A. Walker, J. J. Bohn, F. Ledesma, M. R. Sorkin, S. R. Kabaria, D. N. Thornlow and C. A. Alabi, *Bioconjug. Chem.*, 2019, **30**, 2452–2457.

373 C. M. Yamazaki, A. Yamaguchi, Y. Anami, W. Xiong, Y. Otani, J. Lee, N. T. Ueno, N. Zhang, Z. An and K. Tsuchikama, *Nat. Commun.*, 2021, **12**, 3528.

374 A. M. Sochaj, K. W. Świderska and J. Otlewski, *Biotechnol. Adv.*, 2015, **33**, 775–784.

375 M. Kiyoshi, K. Tsumoto, A. Ishii-Watabe and J. M. M. Caaveiro, *Int. Immunol.*, 2017, **29**, 311–317.

376 F. S. Ekholm, H. Pynnönen, A. Vilkman, V. Pitkänen, J. Helin, J. Saarinen and T. Satomaa, *ChemMedChem*, 2016, **11**, 2501–2505.

377 P. Adumeau, D. Vivier, S. K. Sharma, J. Wang, T. Zhang, A. Chen, B. J. Agnew and B. M. Zeglis, *Mol. Pharm.*, 2018, **15**, 892–898.

378 J. L. Houghton, B. M. Zeglis, D. Abdel-Atti, R. Aggeler, R. Sawada, B. J. Agnew, W. W. Scholz and J. S. Lewis, *Proc. Natl. Acad. Sci.*, 2015, **112**, 15850–15855.

379 B. M. Zeglis, C. B. Davis, D. Abdel-Atti, S. D. Carlin, A. Chen, R. Aggeler, B. J. Agnew and J. S. Lewis, *Bioconjug. Chem.*, 2014, **25**, 2123–2128.

380 N. Forte, V. Chudasama and J. R. Baker, *Drug Discov. Today Technol.*, 2018, 30, 11–20.

381 G. Badescu, P. Bryant, M. Bird, K. Henseleit, J. Swierkosz, V. Parekh, R. Tommasi, E. Pawlisz, K. Jurlewicz, M. Farys, N. Camper, X. Sheng, M. Fisher, R. Grygorash, A. Kyle, A. Abhilash, M. Frigerio, J. Edwards and A. Godwin, *Bioconjug. Chem.*, 2014, **25**, 1124–1136.

382 S. J. Walsh, S. Omarjee, W. R. J. D. Galloway, T. T.-L. Kwan, H. F. Sore, J. S. Parker, M. Hyvönen, J. S. Carroll and D. R. Spring, *Chem. Sci.*, 2019, **10**, 694–700.

383 C. R. Behrens, E. H. Ha, L. L. Chinn, S. Bowers, G. Probst, M. Fitch-Bruhns, J. Monteon, A. Valdiosera, A. Bermudez, S. Liao-Chan, T. Wong, J. Melnick, J.-W. Theunissen, M. R. Flory, D. Houser, K. Venstrom, Z. Levashova, P. Sauer, T.-S. Migone, E. H. van der Horst, R. L. Halcomb and D. Y. Jackson, *Mol. Pharm.*, 2015, **12**, 3986–3998.

384 M. R. Levengood, X. Zhang, J. H. Hunter, K. K. Emmerton, J. B. Miyamoto, T. S. Lewis and P. D. Senter, *Angew. Chem. Int. Ed. Engl.*, 2017, **56**, 733–737.

385 S. J. Walsh, J. Iegre, H. Seki, J. D. Bargh, H. F. Sore, J. S. Parker, J. S. Carroll and D. R. Spring, *Org. Biomol. Chem.*, 2020, **18**, 4224–4230.

386 S. García-Alonso, A. Ocaña and A. Pandiella, *Cancer Res.*, 2018, **78**, 2159–2165.

387 M. A. Fanale, S. M. Horwitz, A. Forero-Torres, N. L. Bartlett, R. H. Advani, B. Pro, R. W. Chen, A. Davies, T. Illidge, D. Huebner, D. A. Kennedy and A. R. Shustov, *J. Clin. Oncol.*, 2014, **32**, 3137–3143.

388 A. Younes, J. M. Connors, S. I. Park, M. Fanale, M. M. O'Meara, N. N. Hunder, D. Huebner and S. M. Ansell, *Lancet Oncol.*, 2013, **14**, 1348–1356.

389 F. Loganzo, X. Tan, M. Sung, G. Jin, J. S. Myers, E. Melamud, F. Wang, V. Diesl, M. T. Follettie, S. Musto, M.-H. Lam, W. Hu, M. B. Charati, K. Khandke, K. S. K. Kim, M. Cinque, J. Lucas, E. Graziani, A. Maderna, C. J. O. Donnell, K. T. Arndt and H.-P. Gerber, *Mol. Cancer Ther.*, 2015, **14**, 952–963.

390 S.-F. Yu, B. Zheng, M. Go, J. Lau, S. Spencer, H. Raab, R. Soriano, S. Jhunjhunwala, R. Cohen, M. Caruso, P. Polakis, J. Flygare and A. G. Polson, *Clin. Cancer Res.*, 2015, **21**, 3298–3306.

391 P. J. Burke, J. Z. Hamilton, S. C. Jeffrey, J. H. Hunter, S. O. Doronina, N. M. Okeley, J. B. Miyamoto, M. E. Anderson, I. J. Stone, M. L. Ulrich, J. K. Simmons, E. E. McKinney, P. D. Senter and R. P. Lyon, *Mol. Cancer Ther.*, 2017, **16**, 116–123.

392 M. Swierczewska, K. C. Lee and S. Lee, *Expert Opin. Emerg. Drugs*, 2015, **20**, 531–536.

393 N. Crawley, M. Thompson and A. Romaschin, *Anal. Chem.*, 2014, **86**, 130–160.

394 J. Zhang, L. Ning, J. Huang, C. Zhang and K. Pu, *Chem. Sci.*, 2020, **11**, 618–630.

395 A. Ebenig, N. E. Juettner, L. Deweid, O. Avrutina, H.-L. Fuchsbauer and H. Kolmar,

ChemBioChem, 2019, **20**, 2411–2419.

396 M. P. VanBrunt, K. Shanebeck, Z. Caldwell, J. Johnson, P. Thompson, T. Martin, H. Dong, G. Li, H. Xu, F. D'Hooge, L. Masterson, P. Bariola, A. Tiberghien, E. Ezeadi, D. G. Williams, J. A. Hartley, P. W. Howard, K. H. Grabstein, M. A. Bowen and M. Marelli, *Bioconjug. Chem.*, 2015, **26**, 2249–2260.

397 M. K. Greene, D. A. Richards, J. C. F. Nogueira, K. Campbell, P. Smyth, M. Fernández, C. J. Scott and V. Chudasama, *Chem. Sci.*, 2018, **9**, 79–87.

398 L. Xu, M. Raabe, M. M. Zegota, J. C. F. Nogueira, V. Chudasama, S. L. Kuan and T. Weil, *Org. Biomol. Chem.*, 2020, **18**, 1140–1147.

399 S. J. Walsh, PhD Thesis, University of Cambridge, 2019.

400 J. Dommerholt, S. Schmidt, R. Temming, L. J. A. Hendriks, F. P. J. T. Rutjes, J. C. M. van Hest, D. J. Lefeber, P. Friedl and F. L. van Delft, *Angew. Chemie Int. Ed.*, 2010, **49**, 9422–9425.

401 D. M. Patterson, L. A. Nazarova, B. Xie, D. N. Kamber and J. A. Prescher, *J. Am. Chem. Soc.*, 2012, **134**, 18638–18643.

402 J. Yang, J. Šečkutė, C. M. Cole and N. K. Devaraj, *Angew. Chemie Int. Ed.*, 2012, **51**, 7476–7479.

403 S. S. Nguyen and J. A. Prescher, *Nat. Rev. Chem.*, 2020, **4**, 476–489.

404 J. M. J. M. Ravasco, C. M. Monteiro and A. F. Trindade, *Org. Chem. Front.*, 2017, **4**, 1167–1198.

405 M. K. Pallerla and J. M. Fox, *Org. Lett.*, 2005, **7**, 3593–3595.

406 L. Qian, S. Pan, J.-S. Lee, J. Ge, L. Li and S. Q. Yao, *Chem. Commun.*, 2019, **55**, 1092–1095.

407 A.-K. Späte, H. Bußkamp, A. Niederwieser, V. F. Schart, A. Marx and V. Wittmann, *Bioconjug. Chem.*, 2014, **25**, 147–154.

408 C. Bahou, E. A. Love, S. Leonard, R. J. Spears, A. Maruani, K. Armour, J. R. Baker and V. Chudasama, *Bioconjug. Chem.*, 2019, **30**, 1048–1054.

409 S. Shao, M.-H. Tsai, J. Lu, T. Yu, J. Jin, D. Xiao, H. Jiang, M. Han, M. Wang and J. Wang, *Bioorg. Med. Chem. Lett.*, 2018, **28**, 1363–1370.

410 F. F. Schumacher, J. P. M. Nunes, A. Maruani, V. Chudasama, M. E. B. Smith, K. A. Chester, J. R.

Baker and S. Caddick, *Org. Biomol. Chem.*, 2014, **12**, 7261–7269.

411 N. Panchuk-Voloshina, R. P. Haugland, J. Bishop-Stewart, M. K. Bhalgat, P. J. Millard, F. Mao, W.-Y. Leung and R. P. Haugland, *J. Histochem. Cytochem.*, 1999, **47**, 1179–1188.

412 D. Willner, P. A. Trail, S. J. Hofstead, H. D. King, S. J. Lasch, G. R. Braslawsky, R. S. Greenfield, T. Kaneko and R. A. Firestone, *Bioconjug. Chem.*, 1993, **4**, 521–527.

413 J. López-Andarias, J. Guerra, G. Castañeda, S. Merino, V. Ceña and P. Sánchez-Verdú, *Eur.J. Org. Chem.*, 2012, **2012**, 2331–2337.

414 J. Chu, J. Chen and K. Zhang, *J. Polym. Sci. Part A Polym. Chem.*, 2004, **42**, 1963–1969.

415 G. González, X. Fernández-Francos, À. Serra, M. Sangermano and X. Ramis, *Polym. Chem.*, 2015, **6**, 6987–6997.

416 S. C. Dickerman and J. Simon, *J. Org. Chem.*, 1957, **22**, 259–261.

417 K. C. Nicolaou, A. A. Estrada, M. Zak, S. H. Lee and B. S. Safina, *Angew. Chemie Int. Ed.*, 2005, **44**, 1378–1382.

418 M. Berthet, F. Davanier, G. Dujardin, J. Martinez and I. Parrot, *Chem. Eur. J.*, 2015, **21**, 11014–11016.

419 M. L. Di Gioia, A. Leggio, A. Le Pera, C. Siciliano, A. Liguori and G. Sindona, *J. Pept. Res.*, 2004, **63**, 383–387.

420 P. G. M. Wuts, T. W. Greene, *Greene's Prot. Groups Org. Synth.*, John Wiley & Sons, 2006, 533–646.

421 N. Diamantis and U. Banerji, *Br. J. Cancer*, 2016, **114**, 362–367.

422 C. Li, C. Zhang, Z. Li, D. Samineni, D. Lu, B. Wang, S.-C. Chen, R. Zhang, P. Agarwal, B. M. Fine and S. Girish, *MAbs*, 2020, **12**, 1699768.

423 H. Seki, S. J. Walsh, J. D. Bargh, J. S. Parker, J. Carroll and D. R. Spring, *Chem. Sci.*, 2021, **12**, 9060–9068.

424 I. López Arbeloa and P. Ruiz Ojeda, *Chem. Phys. Lett.*, 1982, **87**, 556–560.

425 A. Shiba, E. Kinoshita-Kikuta, E. Kinoshita and T. Koike, *Sensors*, 2017, 17.

426 R. J. Christie, C. J. Tadiello, L. M. Chamberlain and D. W. Grainger, *Bioconjug. Chem.*, 2009, **20**, 476–480.

427 M. J. Blackman, J. E. T. Corrie, J. C. Croney, G. Kelly, J. F. Eccleston and D. M. Jameson, *Biochemistry*, 2002, **41**, 12244–12252.

428 T. Förster and E. König, *Phys Chem Chem Phys*, 1957, **61**, 344–348.

429 T.-C. Chou, *Pharmacol. Rev.*, 2006, **58**, 621 LP – 681.

430 J. Jia, F. Zhu, X. Ma, Z. W. Cao, Y. X. Li and Y. Z. Chen, *Nat. Rev. Drug Discov.*, 2009, **8**, 111–128.

431 D. A. Chan and A. J. Giaccia, *Nat. Rev. Drug Discov.*, 2011, **10**, 351–364.

432 H. Taymaz-Nikerel, M. E. Karabekmez, S. Eraslan and B. Kırdar, *Sci. Rep.*, 2018, **8**, 13672.

433 A. M. Freedy, M. J. Matos, O. Boutureira, F. Corzana, A. Guerreiro, P. Akkapeddi, V. J. Somovilla, T. Rodrigues, K. Nicholls, B. Xie, G. Jiménez-Osés, K. M. Brindle, A. A. Neves and G. J. L. Bernardes, *J. Am. Chem. Soc.*, 2017, **139**, 18365–18375.

434 N. M. Ayoub, K. M. Al-Shami, M. A. Alqudah and N. M. Mhaidat, *Onco. Targets. Ther.*, 2017, **10**, 4869–4883.

435 S. V Govindan, T. M. Cardillo, R. M. Sharkey, F. Tat, D. V Gold and D. M. Goldenberg, *Mol. Cancer Ther.*, 2013, **12**, 968–978.

436 Z. Ma, H. He, F. Sun, Y. Xu, X. Huang, Y. Ma, H. Zhao, Y. Wang, M. Wang and J. Zhang, *J. Cancer Res. Clin. Oncol.*, 2017, **143**, 1929–1940.

437 S. Cazzamalli, A. D. Corso and D. Neri, *J. Control. Release*, 2017, **246**, 39–45.

438 M. R. Karver, R. Weissleder and S. A. Hilderbrand, *Bioconjug. Chem.*, 2011, **22**, 2263–2270.

439 J. Yang, M. R. Karver, W. Li, S. Sahu and N. K. Devaraj, *Angew. Chemie Int. Ed.*, 2012, **51**, 5222–5225.

440 S. Das, K. Haedicke and J. Grimm, *J. Nucl. Med.*, 2018, **59**, 58 LP – 65.

441 E. A. Hull, M. Livanos, E. Miranda, M. E. B. Smith, K. A. Chester and J. R. Baker, *Bioconjug. Chem.*, 2014, **25**, 1395–1401.

442 B. M. Cooper, J. Iegre, D. H. O' Donovan, M. Ölwegård Halvarsson and D. R. Spring, *Chem. Soc. Rev.*, 2021, **50**, 1480–1494.

443 Y. A. Lin, J. M. Chalker, N. Floyd, G. J. L. Bernardes and B. G. Davis, *J. Am. Chem. Soc.*, 2008, **130**, 9642–9643.

444 M. Baalmann, L. Neises, S. Bitsch, H. Schneider, L. Deweid, P. Werther, N. Ilkenhans, M. Wolfring, M. J. Ziegler, J. Wilhelm, H. Kolmar and R. Wombacher, *Angew. Chemie Int. Ed.*, 2020, **59**, 12885–12893.

Appendices

9 Appendices

9.1 Appendix 1: Computational Analysis of Fragment Library

9.1.1 Compound Collections Analysed

Collection 1: This Work.

Only final compounds in their fully deprotected forms were analysed. The relevant structures are shown in Figure 9.1.

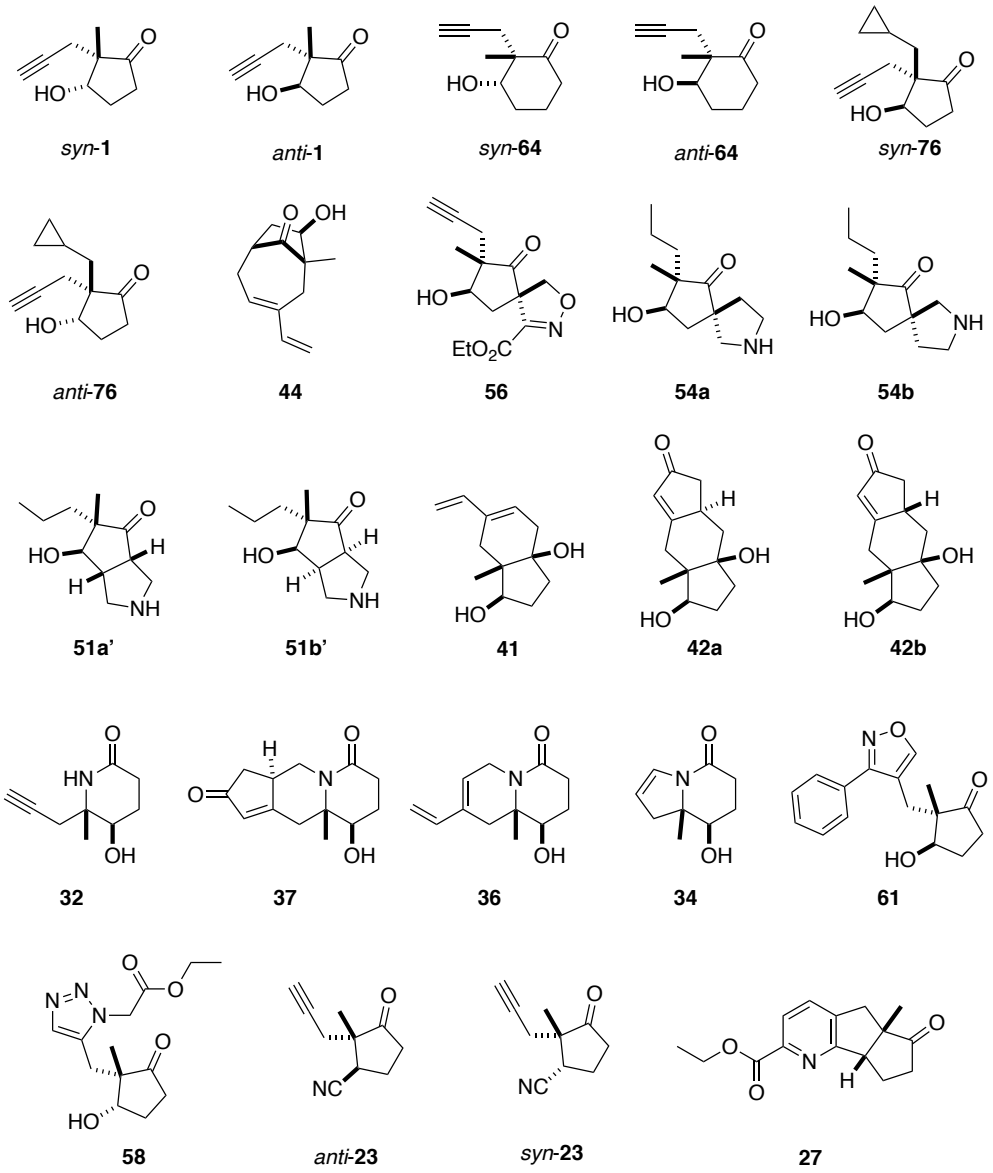

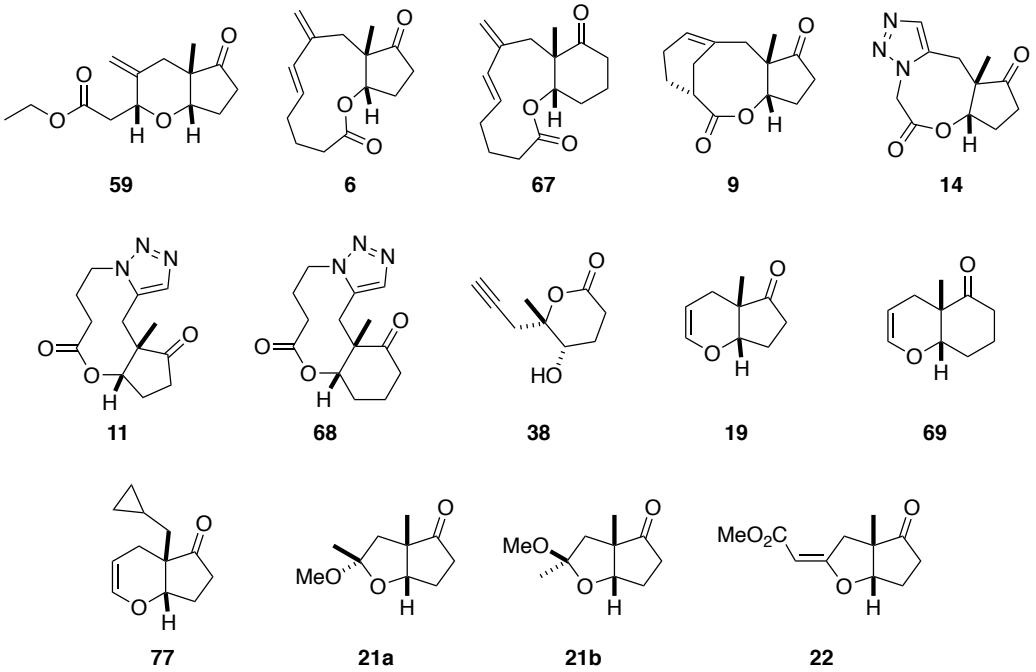

Figure 9.1. The structures of the analysed final compounds. When applicable protecting groups were virtually removed.

Collection 2: Maybridge 'Ro3' Diversity Set 1 Fragment Collection

This library is based on the Maybridge 'Ro3' Diversity Set 1 within the Maybridge Fragment collection. Details of the library (including SMILES and SDF) are available from 'http://www.maybridge.com/' under the Fragment collection 'Maybridge Ro3 Diversity Sets' section.

Collection 3: Life Chemicals 3D Fragment Library

This library is based on the 3D Fragment library within the Life chemicals Fragment collection. Details of the library (including SMILES and SDF) are available from 'http://www.lifechemicals.com/' under the Fragment libraries '3D fragment library' section.

9.1.2 Calculation of Physicochemical Properties

Calculation of the physicochemical properties of library members was carried out using a Molecular Operating Environment (MOE) software package version 2012.10 from the Chemical Computing Group. Merck molecular force field Amber 10 EHT, an all-atom force field parameterised for small organic molecules with the Generalised Born solvation model, was used to minimise the energy potential. A LowModeMD search was employed for conformation generation. Detailed settings for conformational search are listed below (Table 9.1).

Table 9.1. Conformational Search Settings

Conformation Search Settings	
Rejection Limit	100
RMS Gradient	0.005
Iteration Limit	10000
MM Iteration Limit	500
RMSD Limit	0.15
Energy Window	3
Conformation Limit	100

Our library compounds were analysed for the following properties: SlogP, molecular weight (MW), number of hydrogen-bond acceptors (HBA), number of hydrogen-bond donors (HBD), number of chiral centres and fraction aromatic (the number of aromatic atoms expressed as a fraction of the total number of heavy atoms). Fraction sp^3 (the number of sp^3 hybridised carbon atoms expressed as a fraction of the total number of carbon atoms) was calculated using the LLAMA web tool.

By means of comparison with existing libraries, the percentage of the library complying with the fragment 'rule of three' properties is shown alongside those of two popular commercially available fragment libraries, Maybridge Diversity Set 1 and Life Chemicals 3D, in Table 9.2.

Table 9.2. Percentage of each library complying with the fragment 'rule of three'.

Property[a]	This Work	Maybridge Diversity Set 1	Life Chemicals 3D	Ideal Value[b]
MW	68%	87%	25%	≤230
SlogP	97%	91%	92%	≤3
HBA	87%	100%	78%	≤3
HBD	100%	100%	100%	≤3

[a] MW = molecular weight, HBA = number of hydrogen bond acceptors, HBD = number of hydrogen bond donors. [b] Ideal range based on guidelines of 'rule of three'.[3,4]

9.1.3 Principal Moment of Inertia

The principal moments of inertia (PMI) of the lowest energy conformations of the virtual library was performed using the LLAMA web tool and the data replotted in excel.[5]

Table 9.3. Normalised PMI ratio values of conformers of compounds in Figure 9.1 with the lowest energy.

Canonical SMILES	PMI x (NPR1)	PMI y (NPR2)
O[C@H]([C@@]1(CC#C)C)CCC1=O	0.48903	0.7995
O[C@@H]([C@@]1(CC#C)C)CCC1=O	0.44513	0.76579
O[C@H]([C@@]1(CC#C)C)CCCC1=O	0.56362	0.80854
O[C@@H]([C@@]1(CC#C)C)CCCC1=O	0.42554	0.75246
O[C@@H]([C@@]1(CC#C)CC2CC2)CCC1=O	0.58255	0.78519
O[C@H]([C@@]1(CC#C)CC2CC2)CCC1=O	0.54026	0.78265
O[C@@H]([C@@]1(CC(C=C)=CC2)C)C[C@@H]2C1=O	0.50541	0.88669
O[C@@H]([C@@]1(CC#C)C)C[C@]2(CON=C2C(OCC)=O)C1=O	0.50782	0.70959
O[C@@H]([C@@]1(CCC)C)C[C@]2(CCNC2)C1=O	0.31222	0.94676
O[C@@H]([C@@]1(CCC)C)C[C@]2(CNCC2)C1=O	0.30808	0.94576
O[C@@H]([C@@]1(CCC)C)[C@](CNC2)([H])[C@]2([H])C1=O	0.39961	0.88123
O[C@@H]([C@@]1(CCC)C)[C@@](CNC2)([H])[C@@]2([H])C1=O	0.31094	0.84209
O[C@@H]1CC[C@]2(O)[C@]1(CC(C=C)=CC2)C	0.40534	0.8956
O[C@@H]1CC[C@@](O)(C[C@@]2([H])C3)[C@]1(CC2=CC3=O)C	0.381	0.88754
O[C@@H]1CC[C@@](O)(C[C@]2([H])C3)[C@]1(CC2=CC3=O)C	0.27281	0.93321
O=C1CC[C@@H](O)[C@@](CC#C)(C)N1	0.62855	0.77882
O=C1CC[C@@H](O)[C@@](C2)(C)N1C[C@@]3([H])C2=CC(C3)=O	0.2911	0.79301
O=C1CC[C@@H](O)[C@@]2(C)N1CC=C(C=C)C2	0.37601	0.73635
O=C1CC[C@@H](O)[C@@]2(C)N1C=CC2	0.56255	0.639
O=C1CC[C@@H](O)[C@@]1(CC2=CON=C2C3=CC=CC=C3)C	0.48685	0.75436
O[C@H]([C@@]1(CC2=CN=NN2CC(OCC)=O)C)CCC1=O	0.18636	0.90693
O=C1CC[C@H](C#N)[C@@]1(CC#C)C	0.67563	0.88966
O=C1CC[C@@H](C#N)[C@@]1(CC#C)C	0.48064	0.70721
O=C1CC[C@@]2([H])[C@]1(C)CC3=C2N=C(C(OCC)=O)C=C3	0.15122	0.94161
O=C1CC[C@@](O[C@]2([H])CC(OCC)=O)([H])[C@@]1(CC2=C)C	0.4243	0.97837
O=C1CC[C@@](OC(CCC/C=C/2)=O)([H])[C@@]1(CC2=C)C	0.4175	0.74513
O=C1CCC[C@@](OC(CCC/C=C/2)=O)([H])[C@@]1(CC2=C)C	0.49196	0.69301
O=C1CC[C@@](OC2=O)([H])[C@@]1(CC3=CCC[C@H]2C3)C	0.50253	0.87337
O=C1CC[C@@](OC2=O)([H])[C@@]1(CC3=CN=NN3C2)C	0.41922	0.74743
O=C1CC[C@@](OC2=O)([H])[C@@]1(CC3=CN=NN3CCC2)C	0.54235	0.70377
O=C1CCC[C@@](OC2=O)([H])[C@@]1(CC3=CN=NN3CCC2)C	0.47444	0.72708
O=C(O1)CC[C@H](O)[C@@]1(CC#C)C	0.53357	0.6862
O=C1CC[C@@]2(OC=CC[C@]12C)[H]	0.48472	0.8194
O=C1CCC[C@@]2(OC=CC[C@]12C)[H]	0.65594	0.87239
O=C1CC[C@@]2(OC=CC[C@]12CC3CC3)[H]	0.48683	0.79487
C[C@]12[C@](O[C@](C)(OC)C2)([H])CCC1=O	0.56959	0.91568
C[C@]12[C@](O[C@@](C)(OC)C2)([H])CCC1=O	0.43335	0.97777
C[C@]12[C@](O/C(C2)=C/C(OC)=O)([H])CCC1=O	0.26256	0.91833

9.2 Appendix 2: Selected NMR Spectra

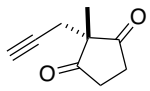

3

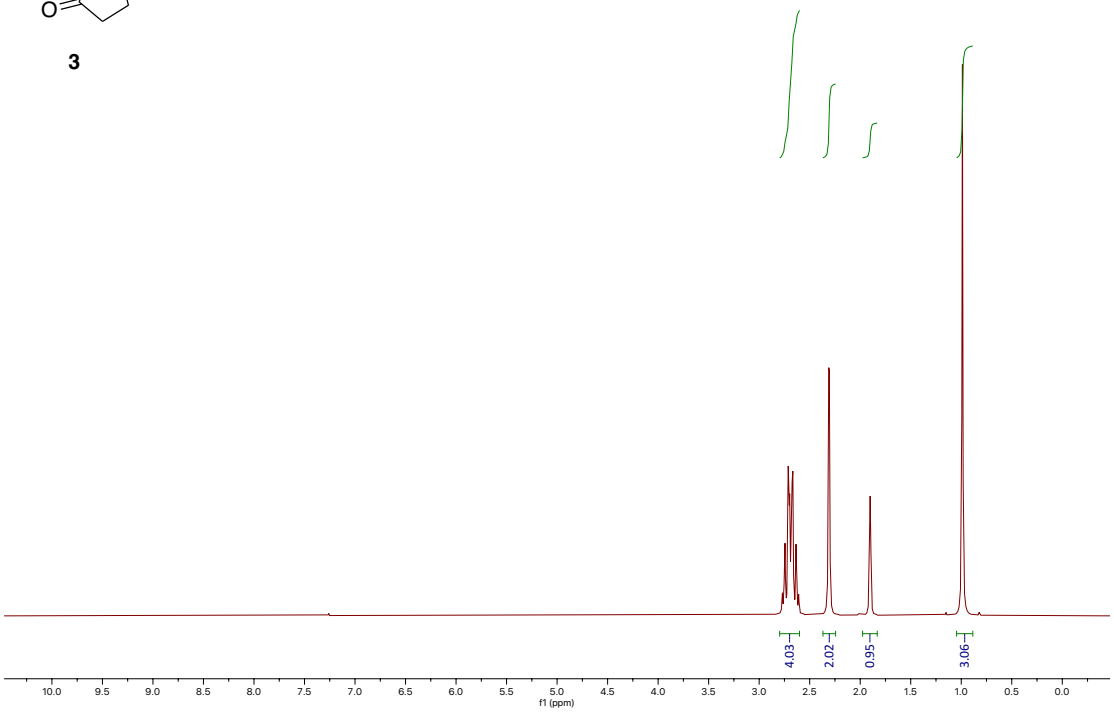

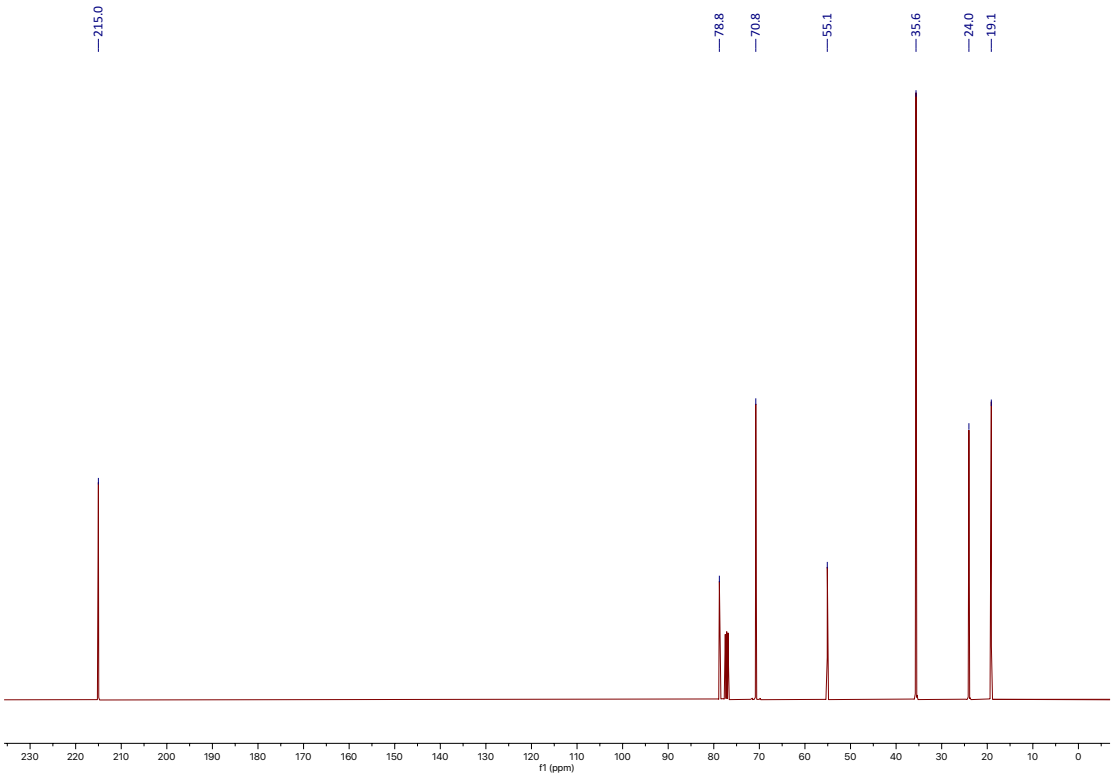

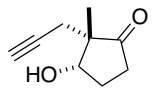
O
HO

syn-**1**

0.95
4.00
1.07
2.03
1.16
2.96
f1 (ppm)

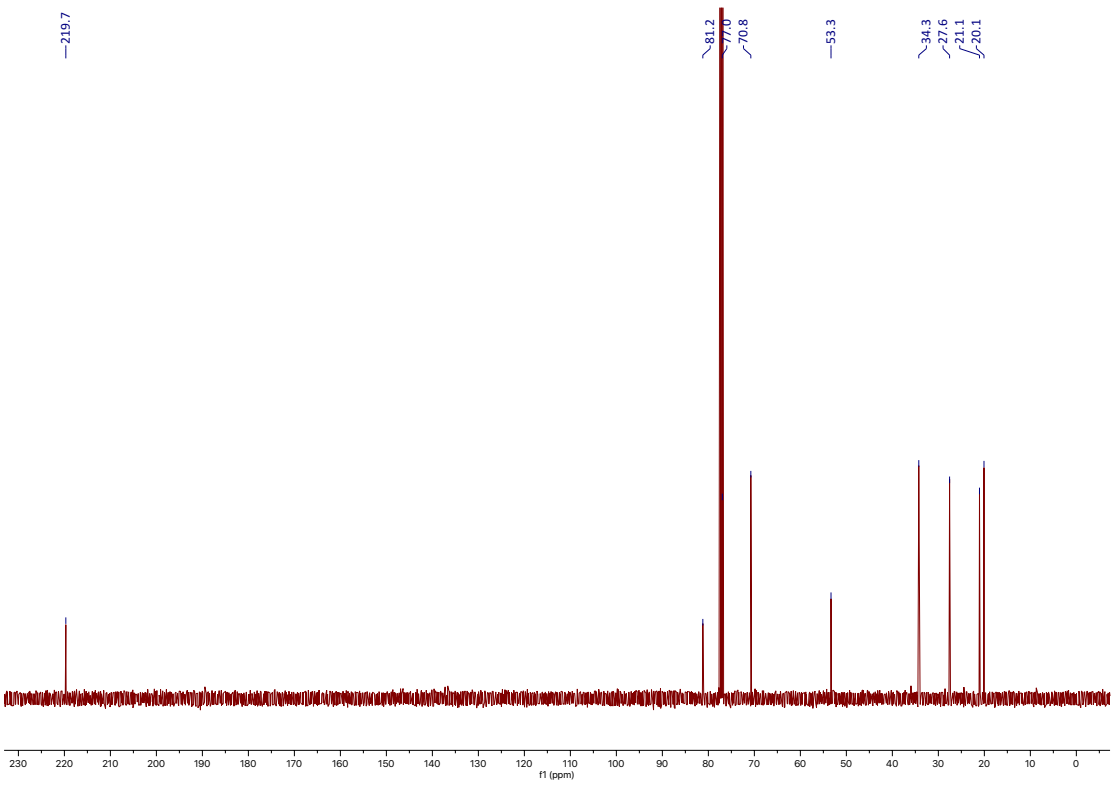
219.7
81.2
77.0
70.8
53.3
34.3
27.6
21.1
20.1
f1 (ppm)

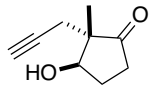
O
HO

anti-**1**

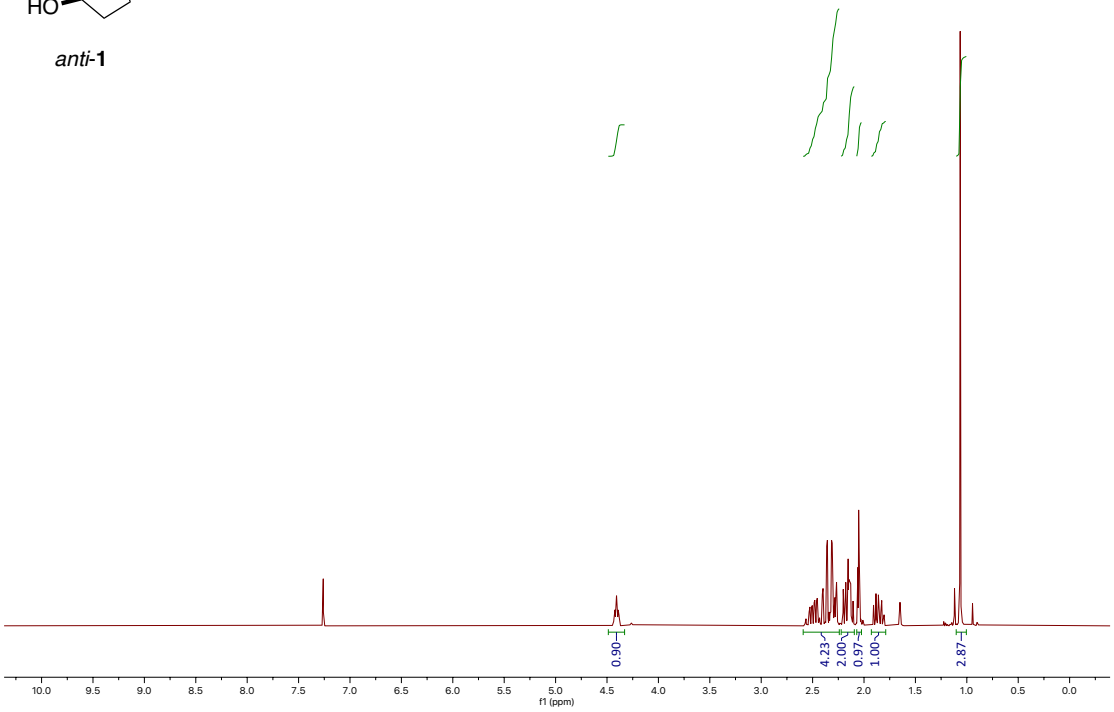
0.90
4.23
2.00
0.97
1.00
2.87
10.0 9.5 9.0 8.5 8.0 7.5 7.0 6.5 6.0 5.5 5.0 4.5 4.0 3.5 3.0 2.5 2.0 1.5 1.0 0.5 0.0
f1 (ppm)

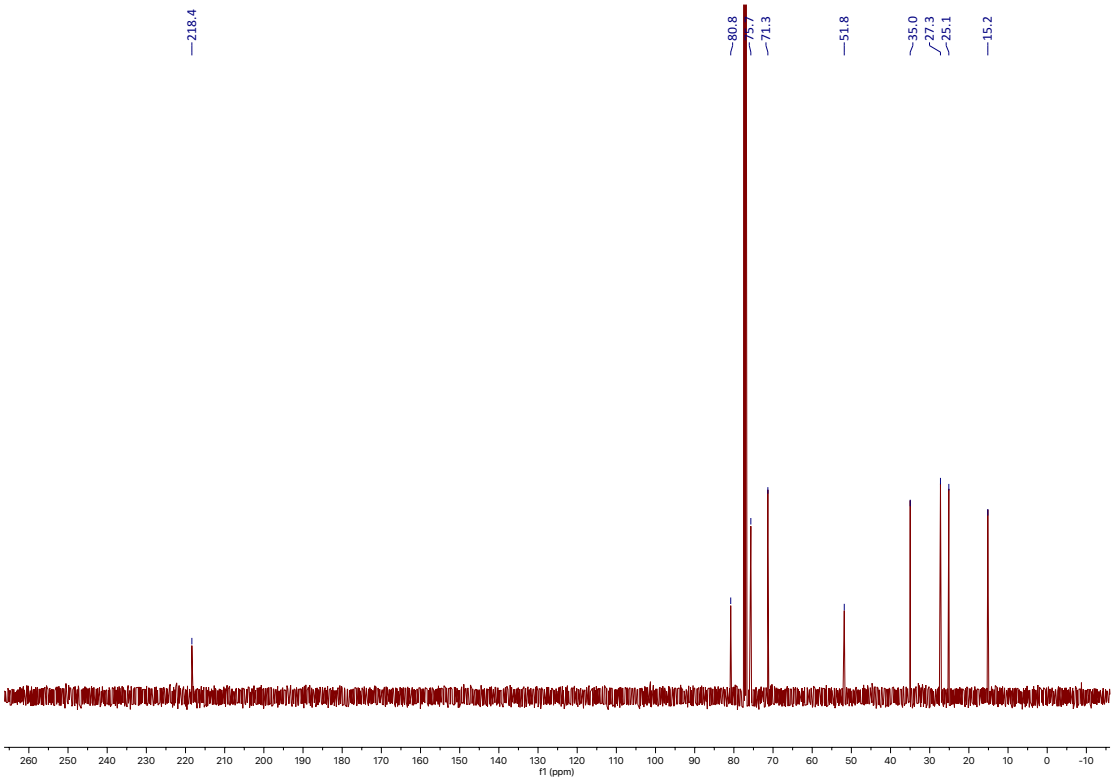
218.4
80.8
75.7
71.3
51.8
35.0
27.3
25.1
15.2
260 250 240 230 220 210 200 190 180 170 160 150 140 130 120 110 100 90 80 70 60 50 40 30 20 10 0 -10
f1 (ppm)

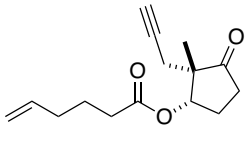

5

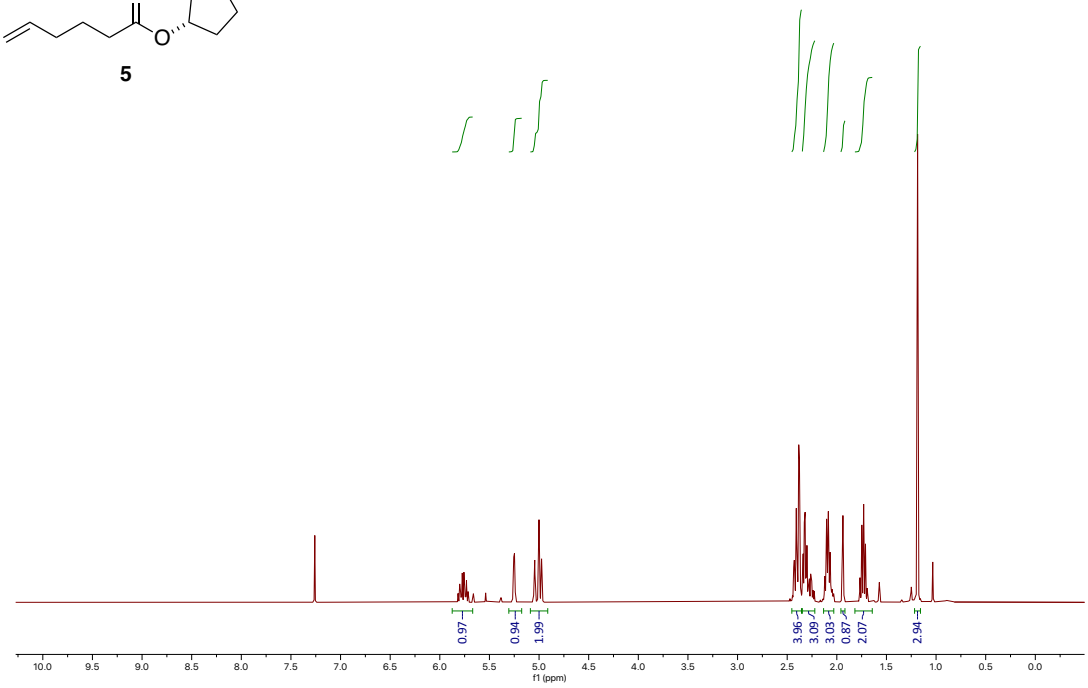
0.97
0.94
1.99
3.96
3.09
3.03
0.87
2.07
2.94
f1 (ppm)

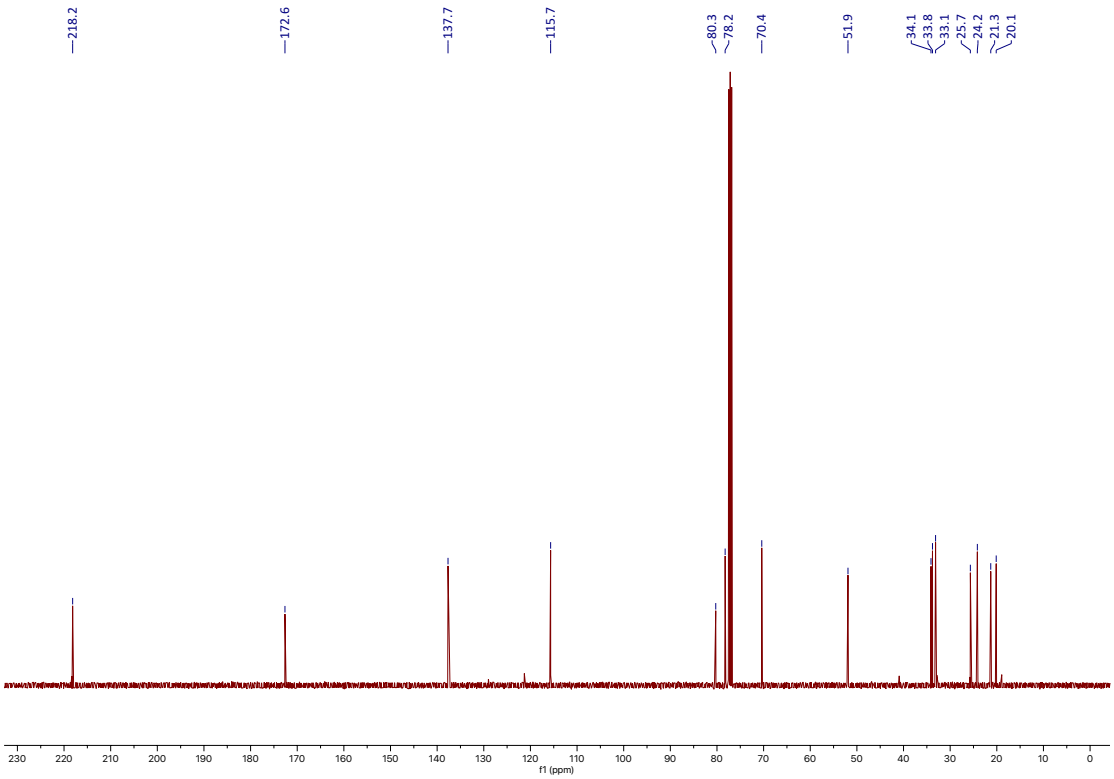
218.2
172.6
137.7
115.7
80.3
78.2
70.4
51.9
34.1
33.8
33.1
25.7
24.2
21.3
20.1
f1 (ppm)

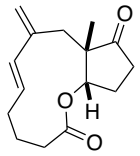
O
O
H
O

6

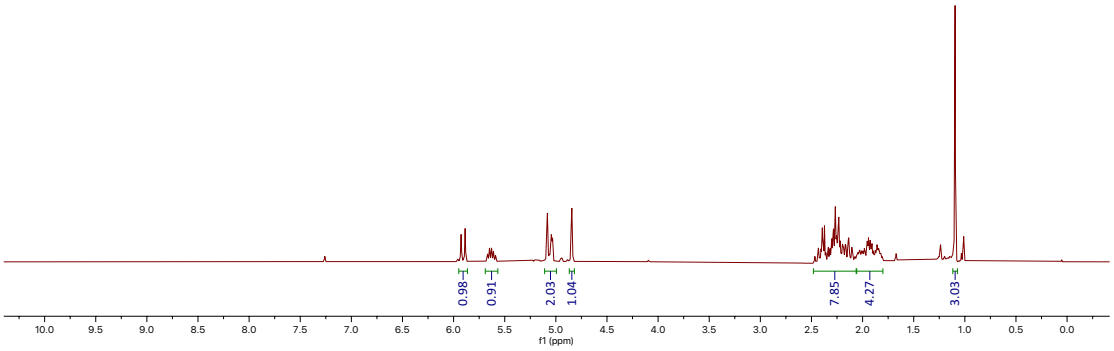
0.98
0.91
2.03
1.04
7.85
4.27
3.03
f1 (ppm)


220.2
175.1
142.4
136.5
128.1
116.3
78.4
53.3
35.4
34.4
33.8
31.4
26.2
24.8
22.0

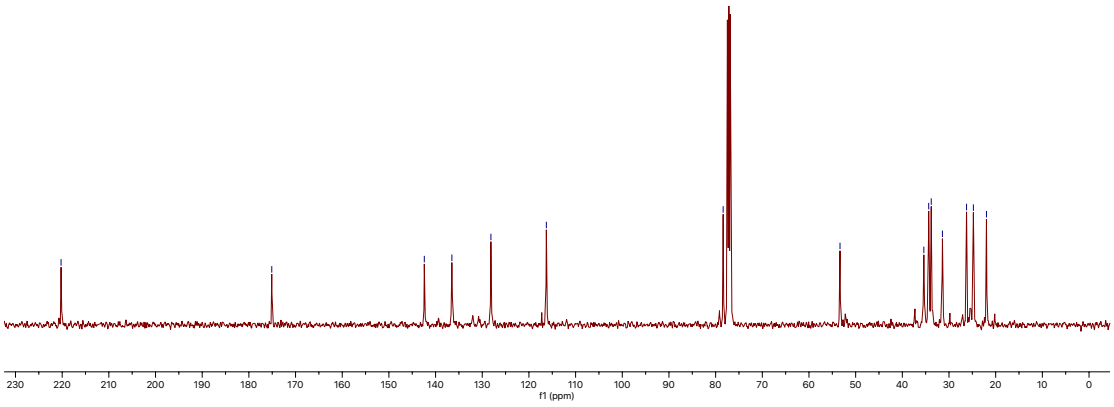
f1 (ppm)

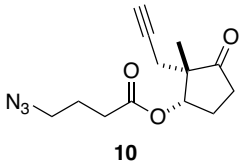
N3
O
O
O

10

1.00
1.93
3.82
2.10
1.08
1.15
2.91
3.09
f1 (ppm)

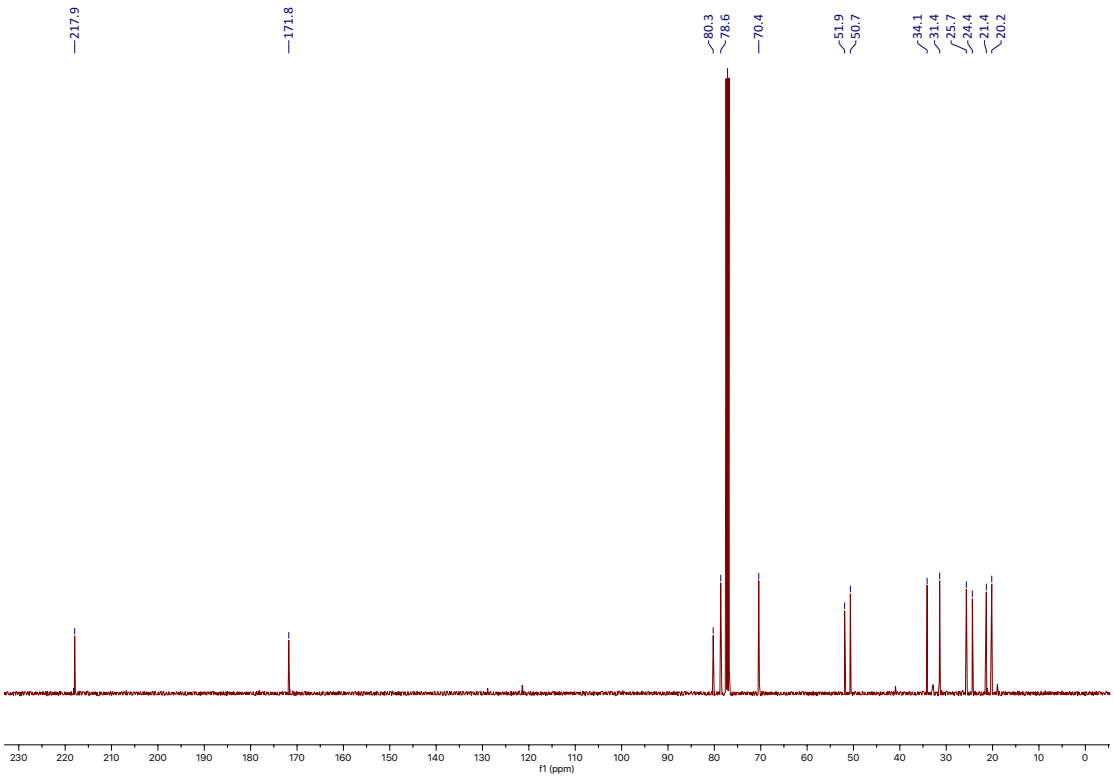
217.9
171.8
80.3
78.6
70.4
51.9
50.7
34.1
31.4
25.7
24.4
21.4
20.2
f1 (ppm)

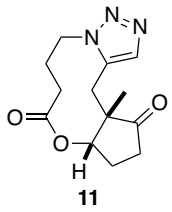

11

0.98
1.03
2.02
1.06
1.07
5.06
2.11
1.16
3.36
f1 (ppm)

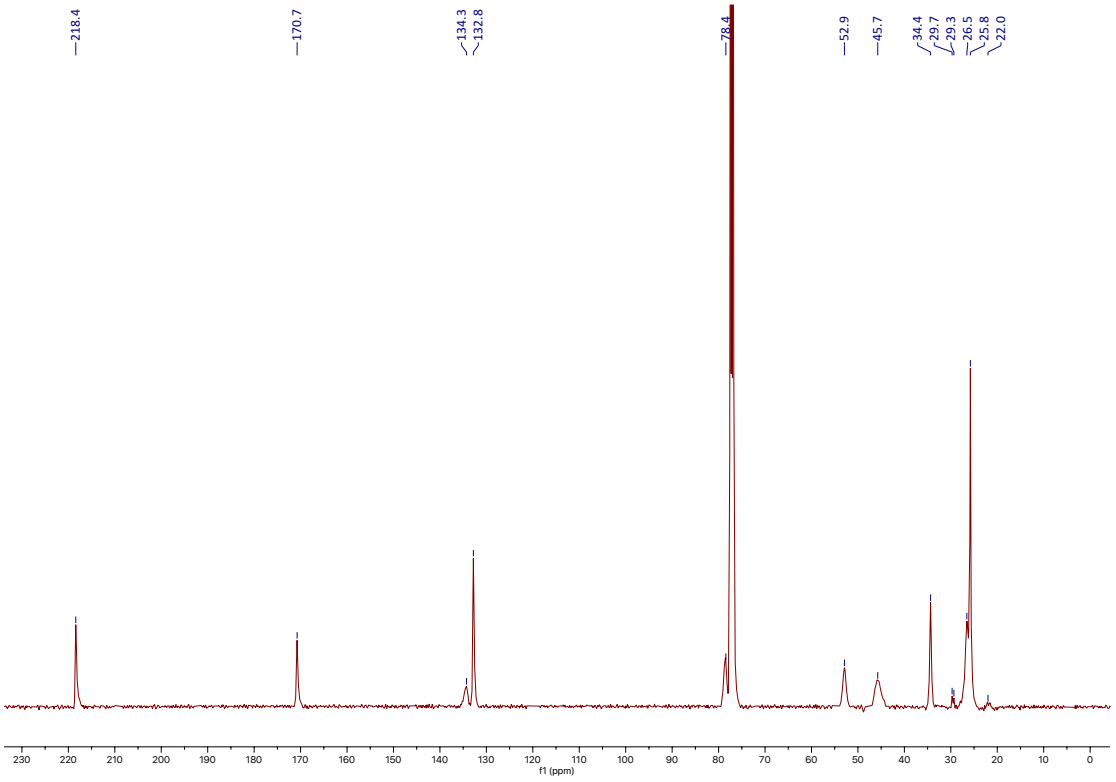
218.4
170.7
134.3
132.8
78.4
52.9
45.7
34.4
29.7
29.3
26.5
25.8
22.0
f1 (ppm)

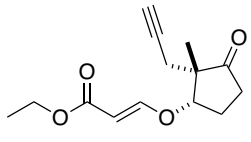

16

0.95
0.95
0.99
1.97
4.02
1.96
0.89
3.27
2.91
f1 (ppm)

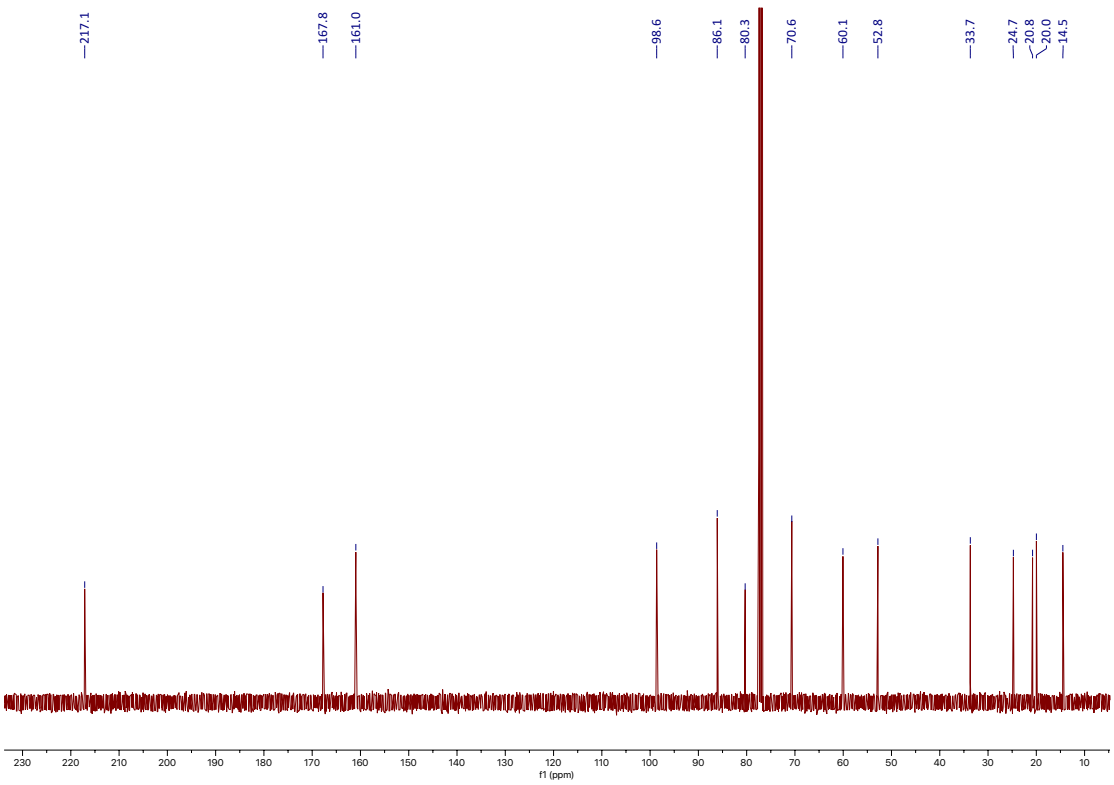
217.1
167.8
161.0
98.6
86.1
80.3
70.6
60.1
52.8
33.7
24.7
20.8
20.0
14.5
f1 (ppm)

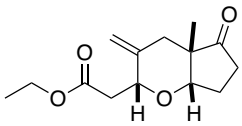

18

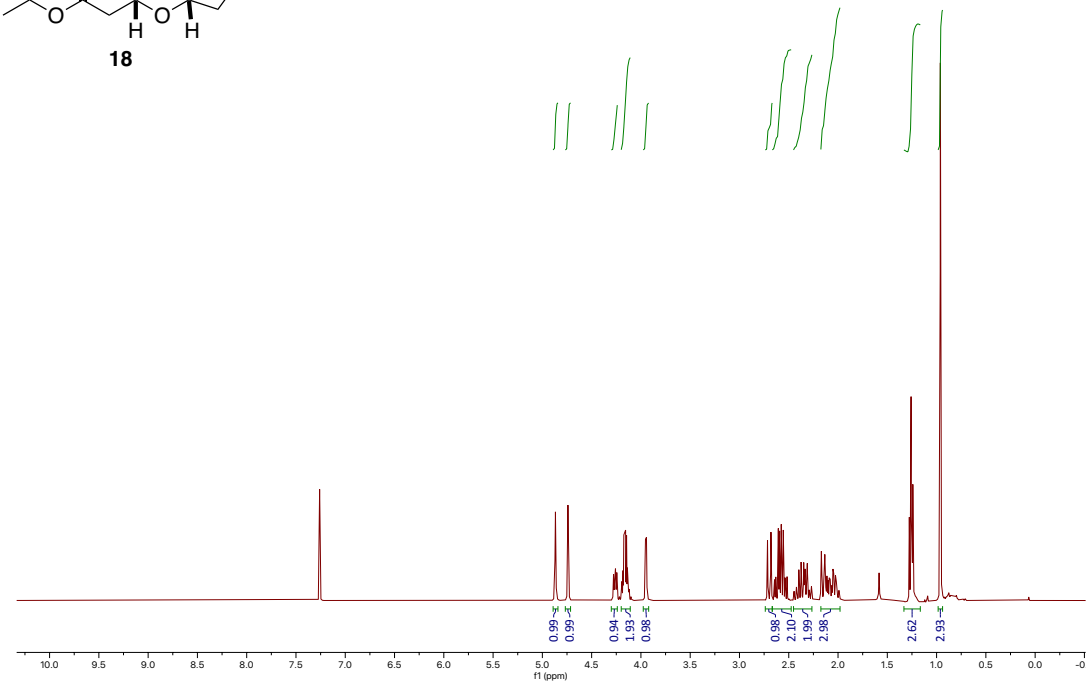
0.99
0.99
0.94
1.93
0.98
0.98
2.10
1.99
2.98
2.62
2.93
f1 (ppm)

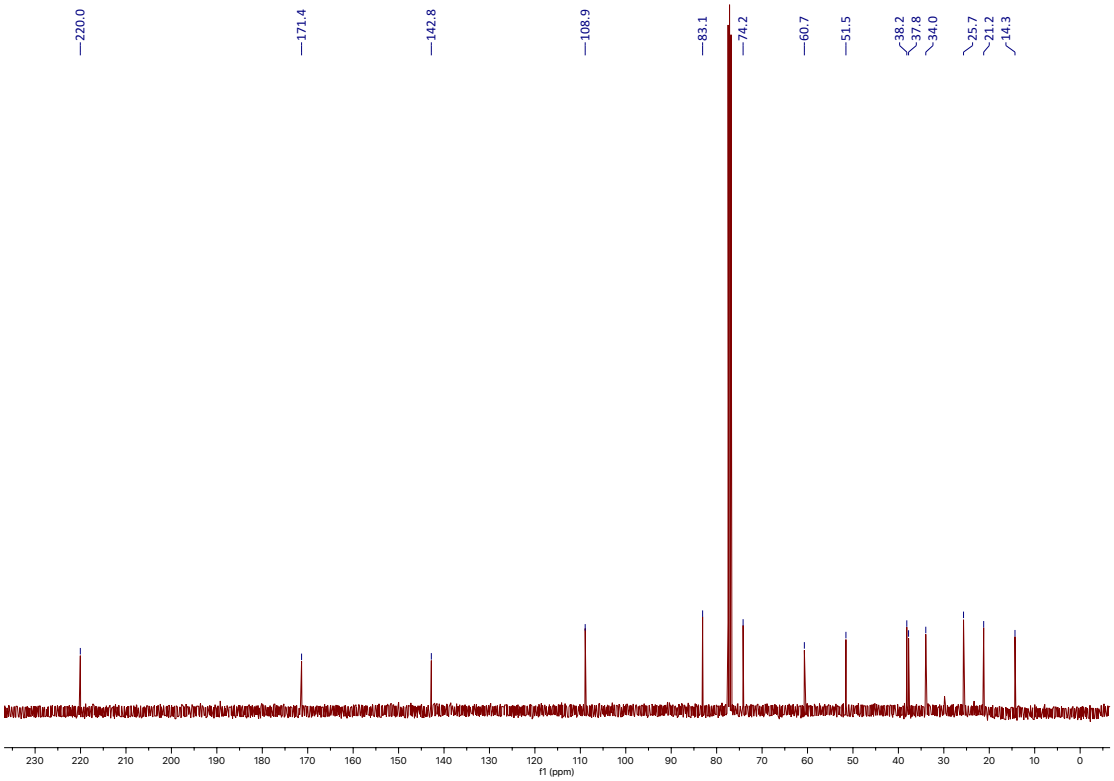
220.0
171.4
142.8
108.9
83.1
74.2
60.7
51.5
38.2
37.8
34.0
25.7
21.2
14.3
f1 (ppm)

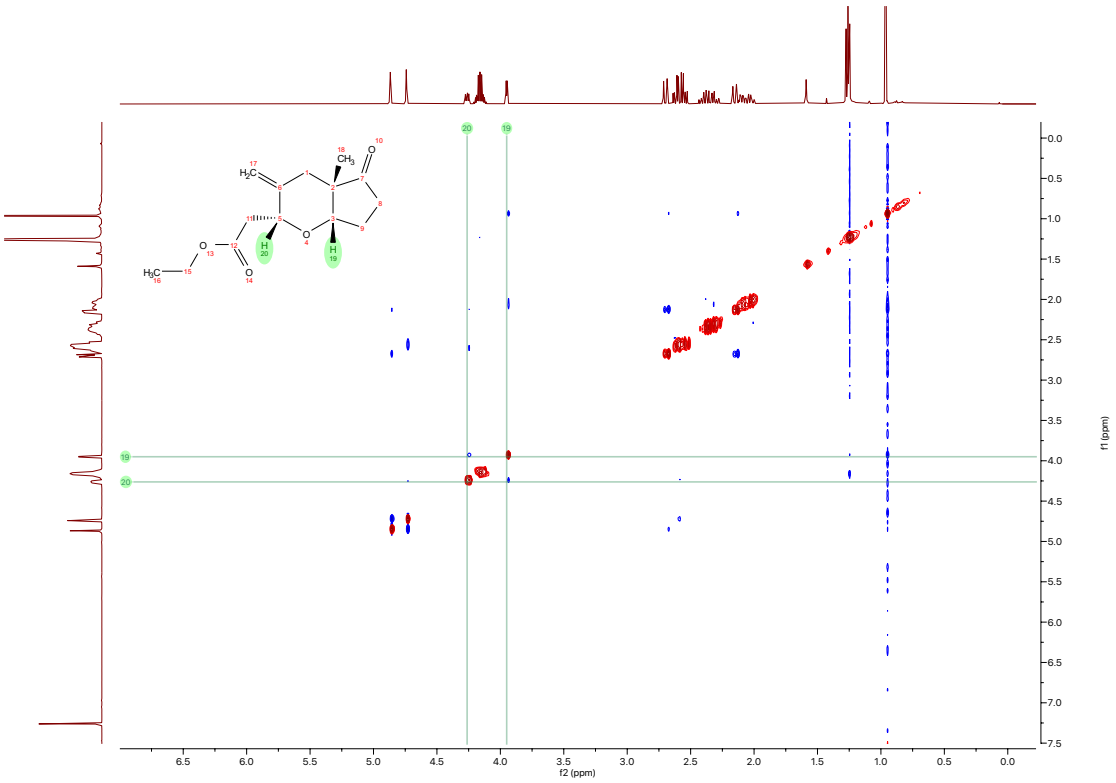
20
19
f2 (ppm)
f1 (ppm)

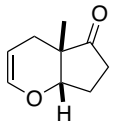

19

0.65
0.79
0.85
3.22
1.22
1.07
1.03
3.00
f1 (ppm)

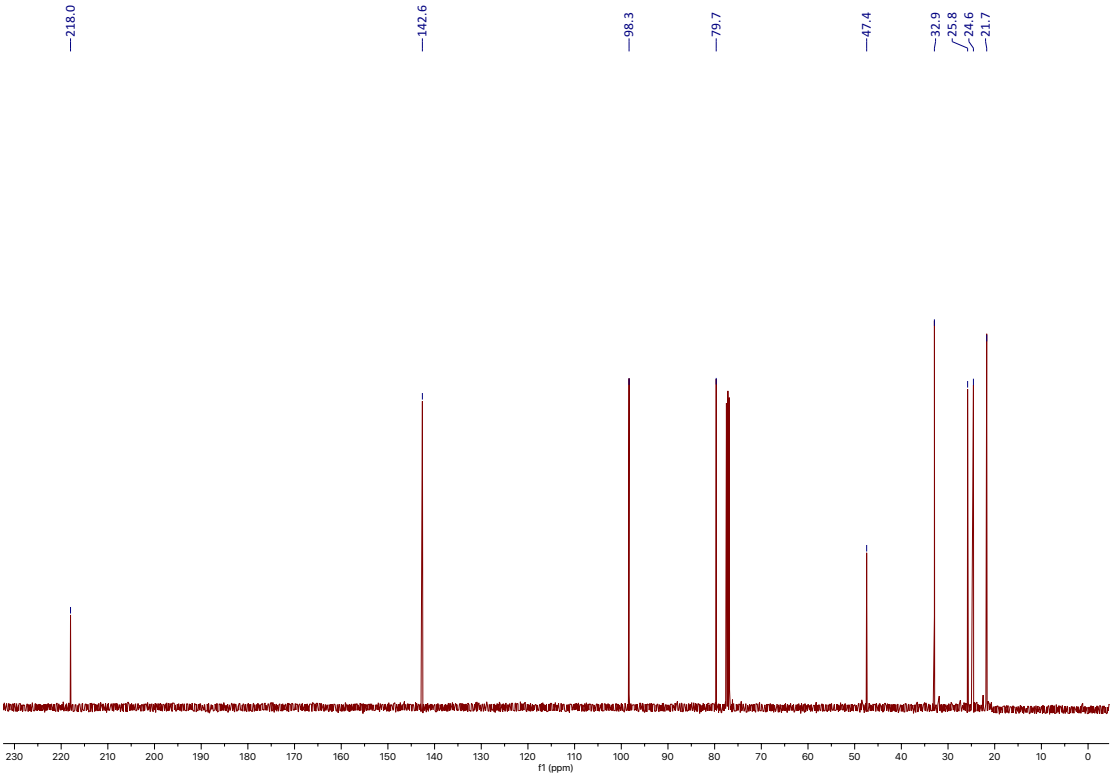
218.0
142.6
98.3
79.7
47.4
32.9
25.8
24.6
21.7
f1 (ppm)

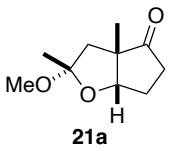
O
MeO
O
H

21a

0.98
3.00
1.08
1.17
2.16
2.13
3.17
3.27
10.0 9.5 9.0 8.5 8.0 7.5 7.0 6.5 6.0 5.5 5.0 4.5 4.0 3.5 3.0 2.5 2.0 1.5 1.0 0.5 0.0
f1 (ppm)

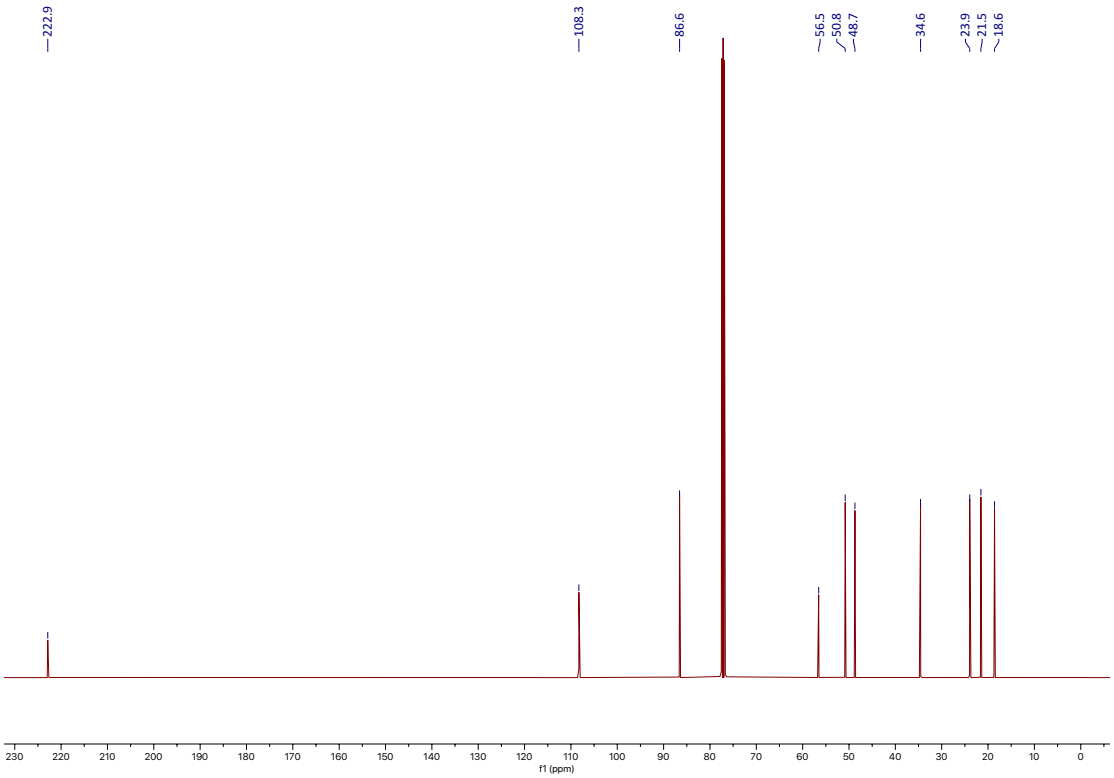
222.9
108.3
86.6
56.5
50.8
48.7
34.6
23.9
21.5
18.6
230 220 210 200 190 180 170 160 150 140 130 120 110 100 90 80 70 60 50 40 30 20 10 0
f1 (ppm)

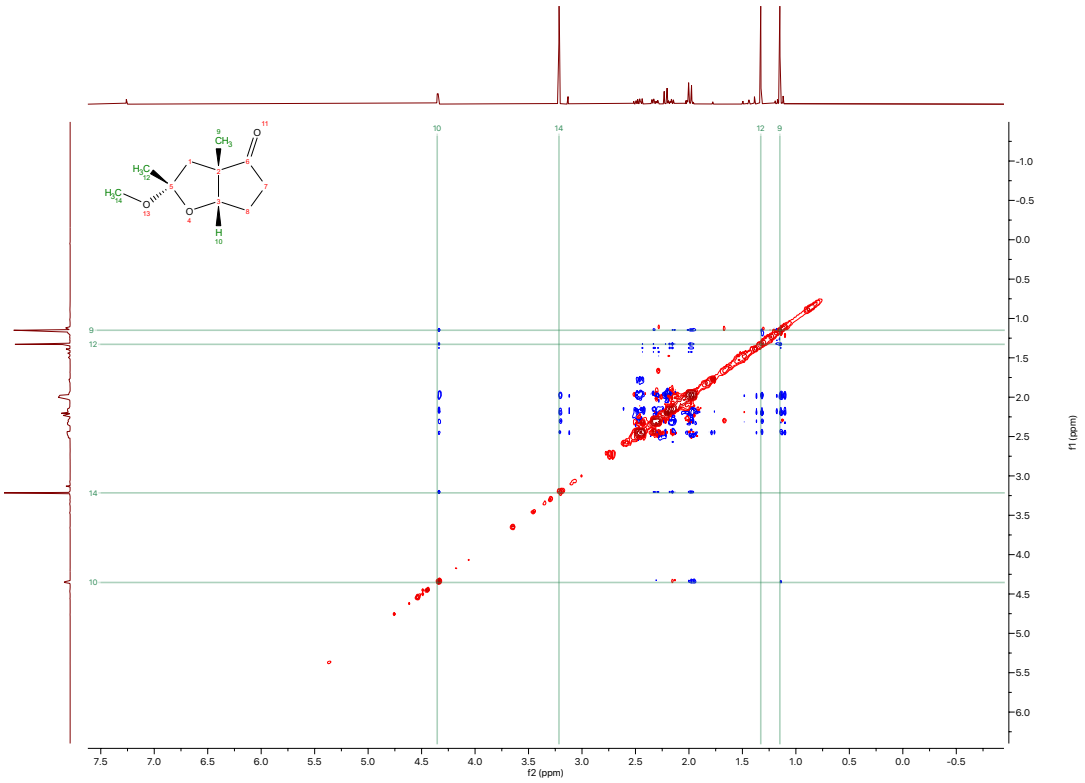
10
14
12
9
9
12
14
10
f2 (ppm)
f1 (ppm)

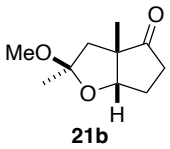
MeO
O
O
H

21b

1.00
3.08
2.07
1.06
2.14
1.01
3.15
3.16
f1 (ppm)

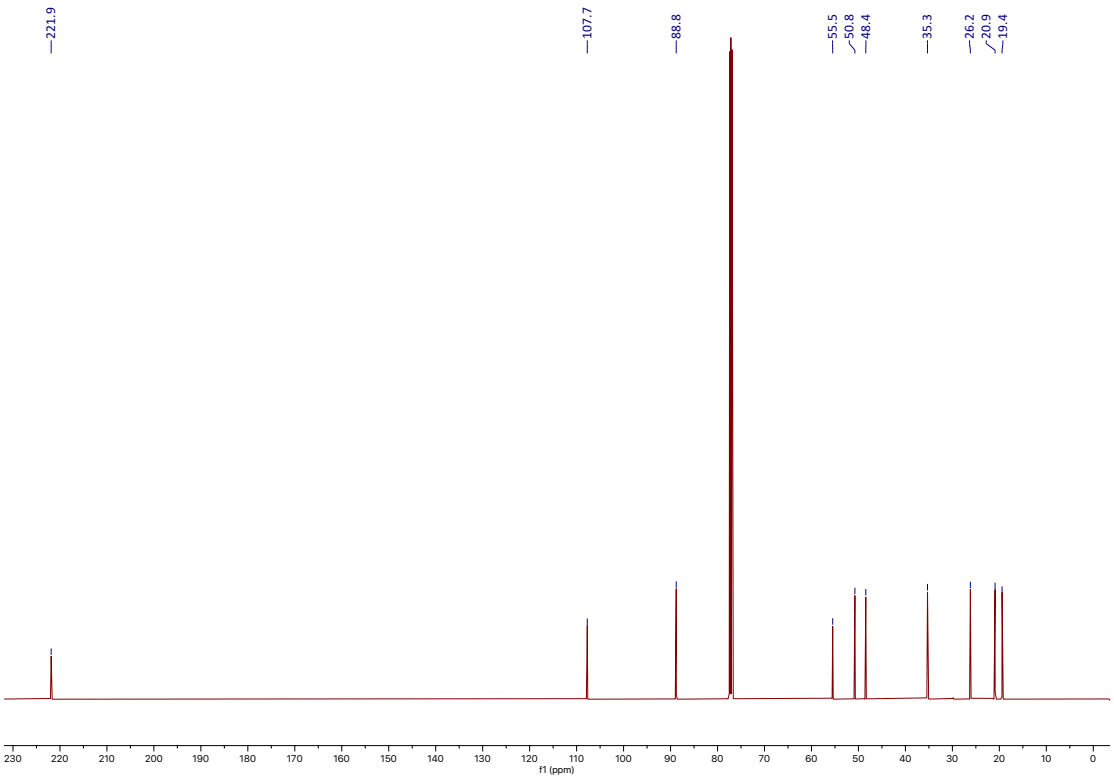
221.9
107.7
88.8
55.5
50.8
48.4
35.3
26.2
20.9
19.4
f1 (ppm)

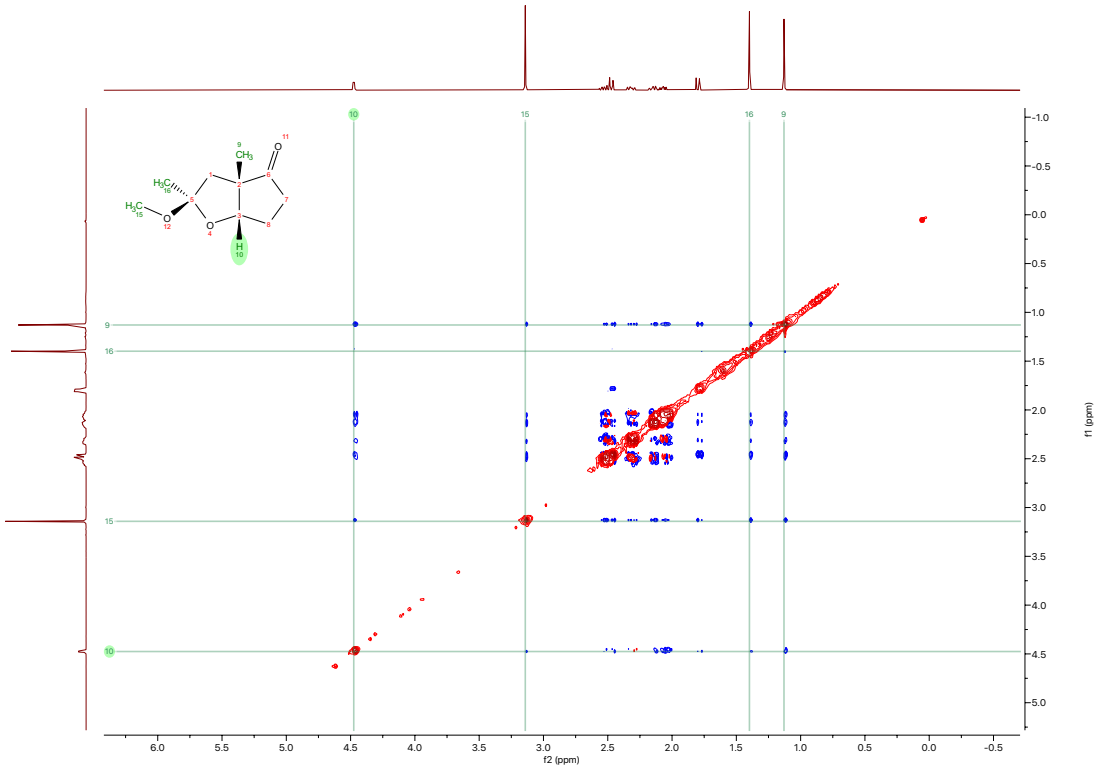
10
15
16
9
f2 (ppm)
f1 (ppm)

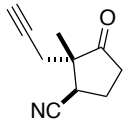
O
NC

anti-**23**

0.95
2.02
1.13
1.02
2.18
0.91
2.92
f1 (ppm)

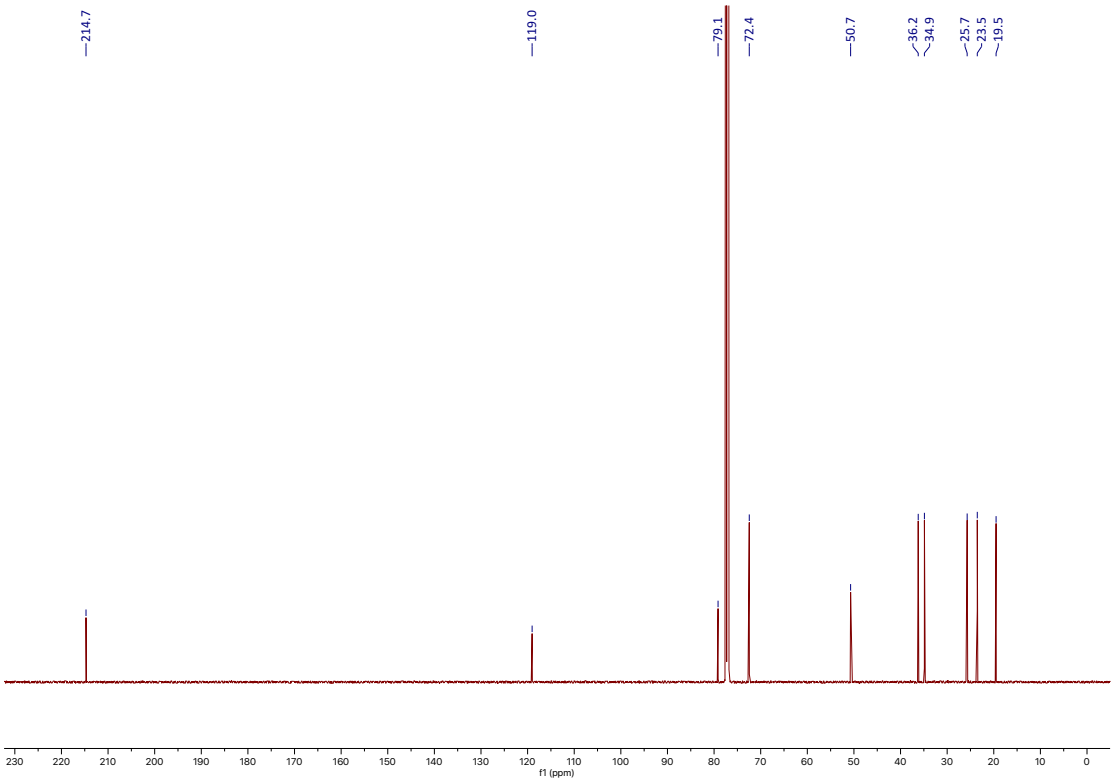
214.7
119.0
79.1
72.4
50.7
36.2
34.9
25.7
23.5
19.5
f1 (ppm)

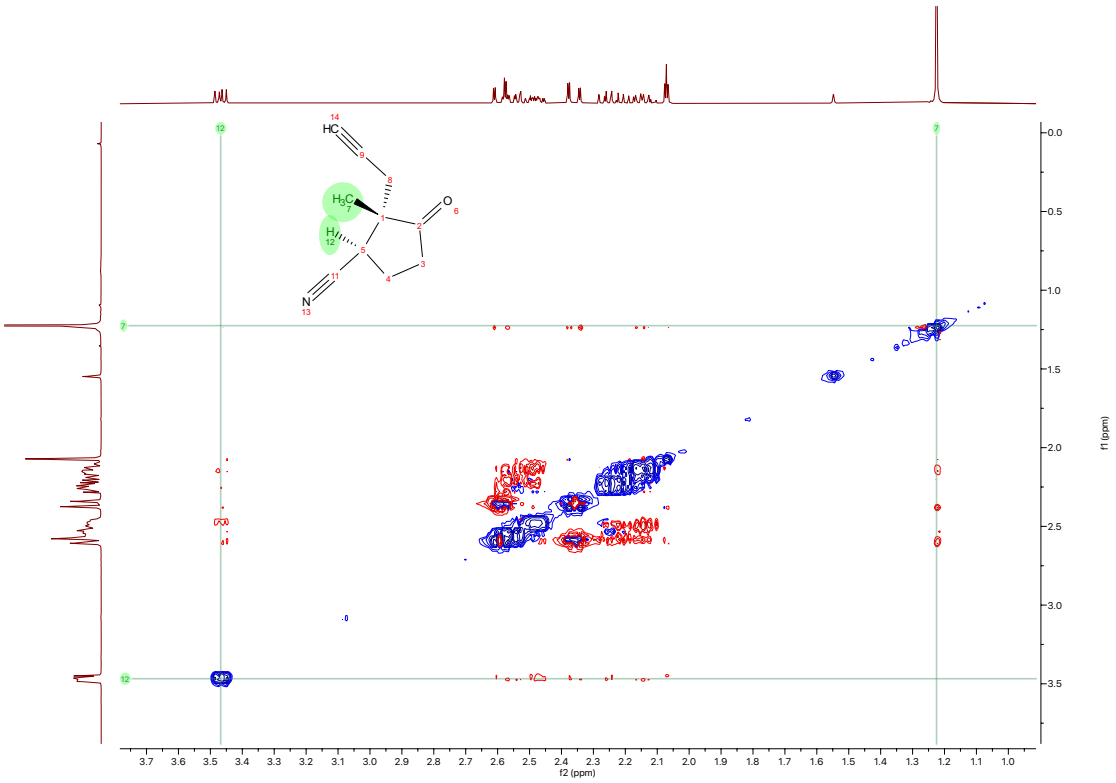
HC
14
9
8
H3C
7
1
2
O
6
H
12
5
3
4
11
N
13
12
7
7
12
0.0
0.5
1.0
1.5
2.0
2.5
3.0
3.5
f1 (ppm)
3.7 3.6 3.5 3.4 3.3 3.2 3.1 3.0 2.9 2.8 2.7 2.6 2.5 2.4 2.3 2.2 2.1 2.0 1.9 1.8 1.7 1.6 1.5 1.4 1.3 1.2 1.1 1.0
f2 (ppm)

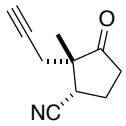
O
NC

syn-**23**

1.04
6.09
0.96
2.80
f1 (ppm)

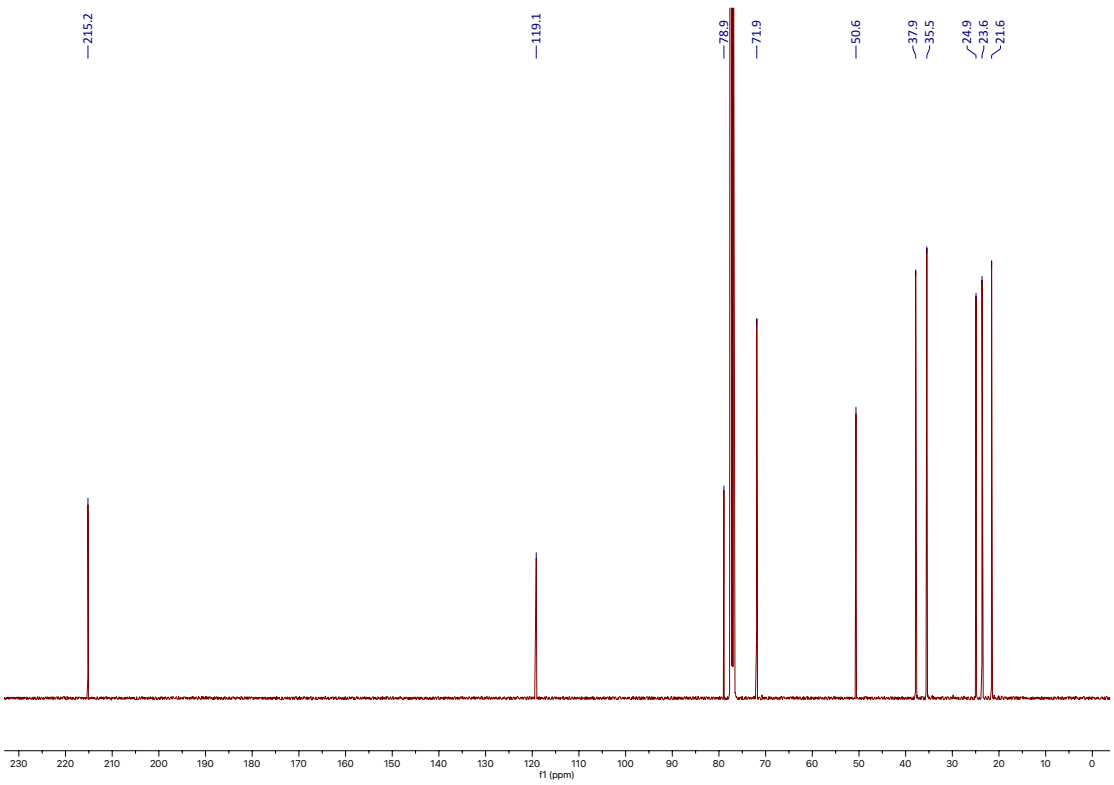
215.2
119.1
78.9
71.9
50.6
37.9
35.5
24.9
23.6
21.6
f1 (ppm)

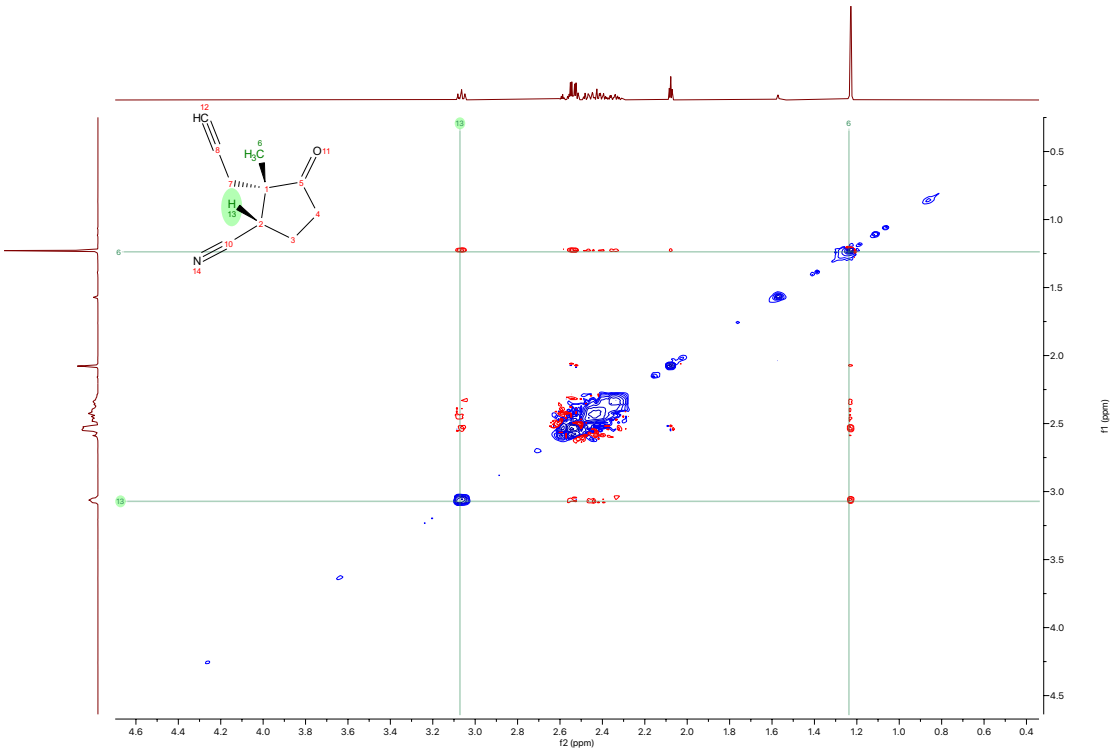
HC
12
8
H3C
6
O
11
7
1
5
4
H
13
2
3
10
N
14
13
6
6
13
0.5
1.0
1.5
2.0
2.5
3.0
3.5
4.0
4.5
f1 (ppm)
4.6
4.4
4.2
4.0
3.8
3.6
3.4
3.2
3.0
2.8
2.6
2.4
2.2
2.0
1.8
1.6
1.4
1.2
1.0
0.8
0.6
0.4
f2 (ppm)

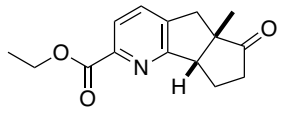
O
O
N
H
O
O

27

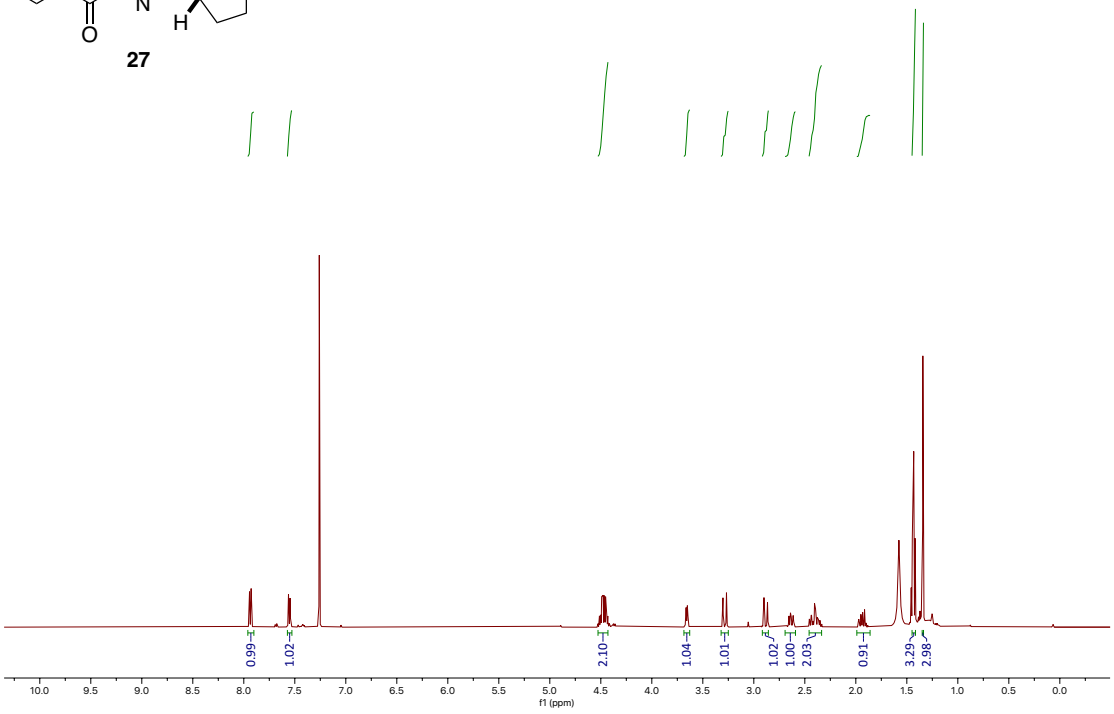
0.99
1.02
2.10
1.04
1.01
1.02
1.00
2.03
0.91
3.29
2.98
f1 (ppm)

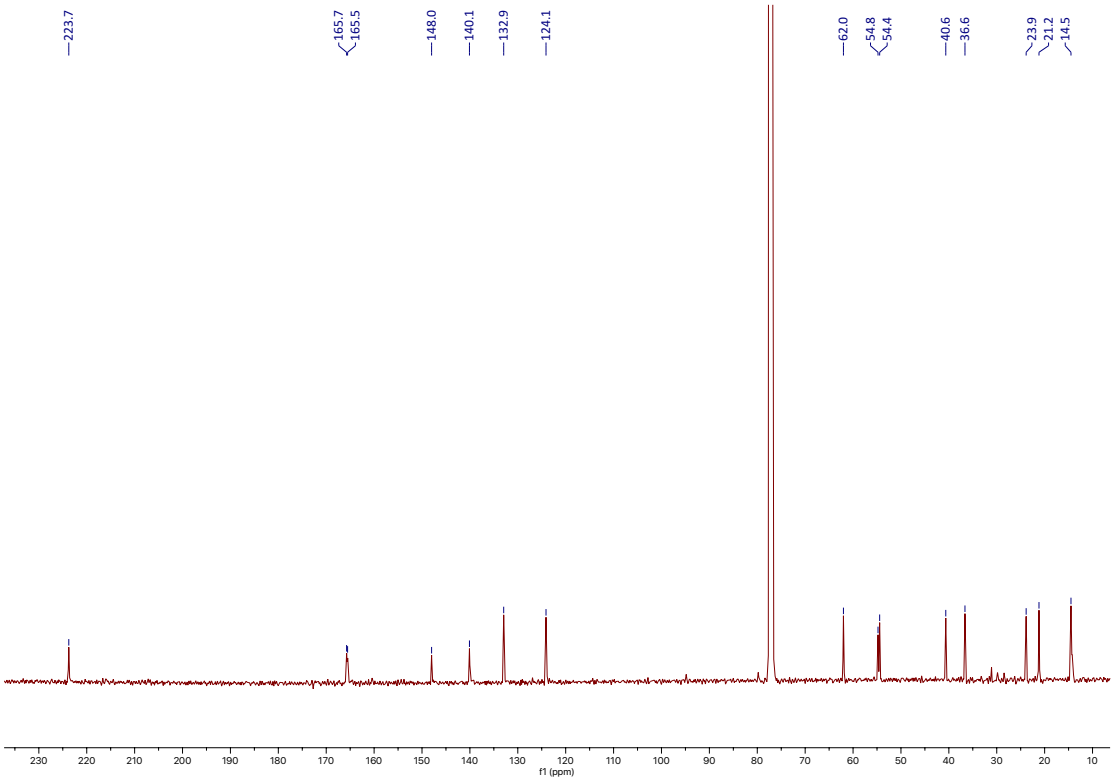
223.7
165.7
165.5
148.0
140.1
132.9
124.1
62.0
54.8
54.4
40.6
36.6
23.9
21.2
14.5
f1 (ppm)

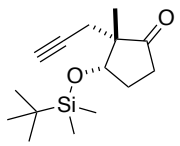
O
O
Si

syn-**28**

0.96
4.04
1.05
1.92
2.93
9.04
2.91
2.86
f1 (ppm)

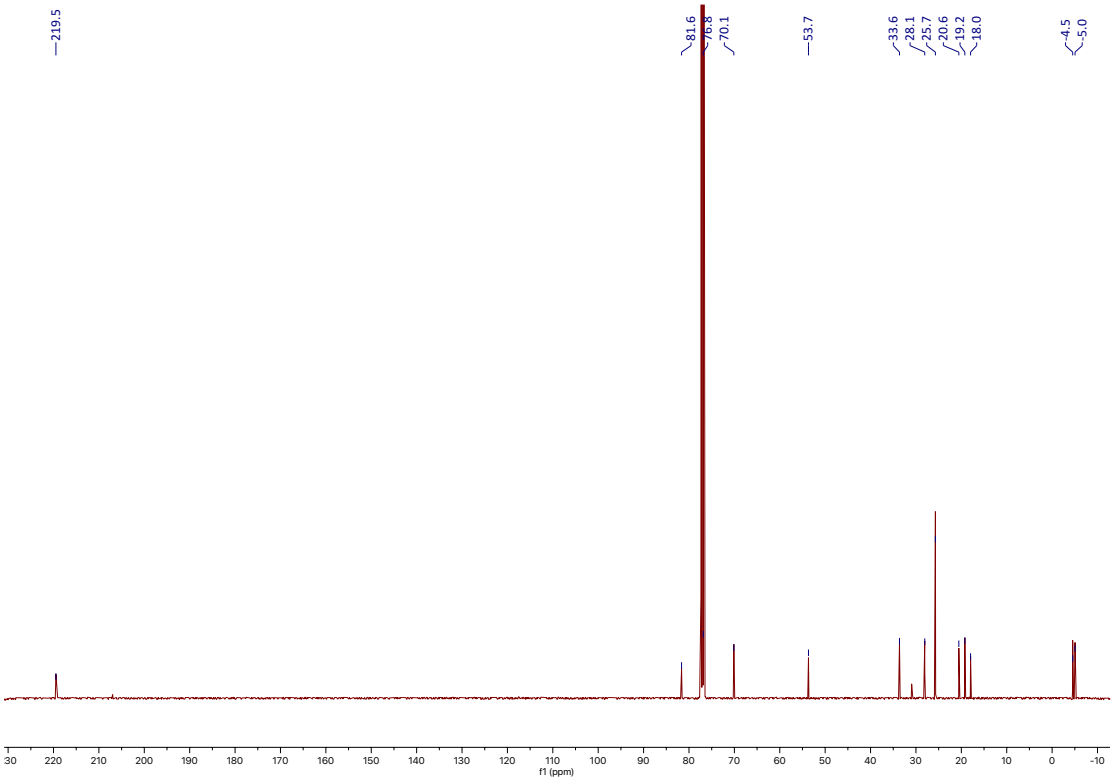
219.5
81.6
76.8
70.1
53.7
33.6
28.1
25.7
20.6
19.2
18.0
-4.5
-5.0
f1 (ppm)

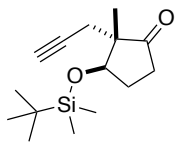
O
O
Si

anti-**28**

0.97
2.05
3.02
0.92
1.04
2.97
9.01
5.94
f1 (ppm)

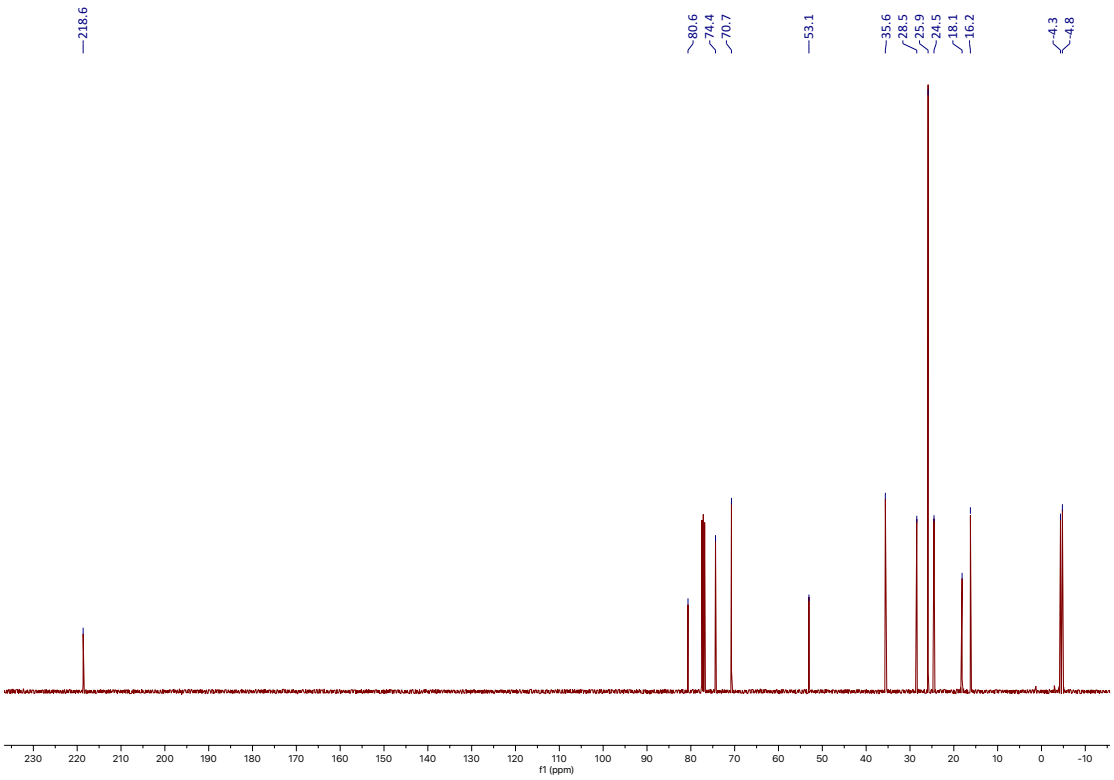
218.6
80.6
74.4
70.7
53.1
35.6
28.5
25.9
24.5
18.1
16.2
4.3
-4.8
f1 (ppm)

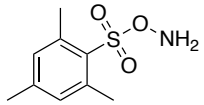

29

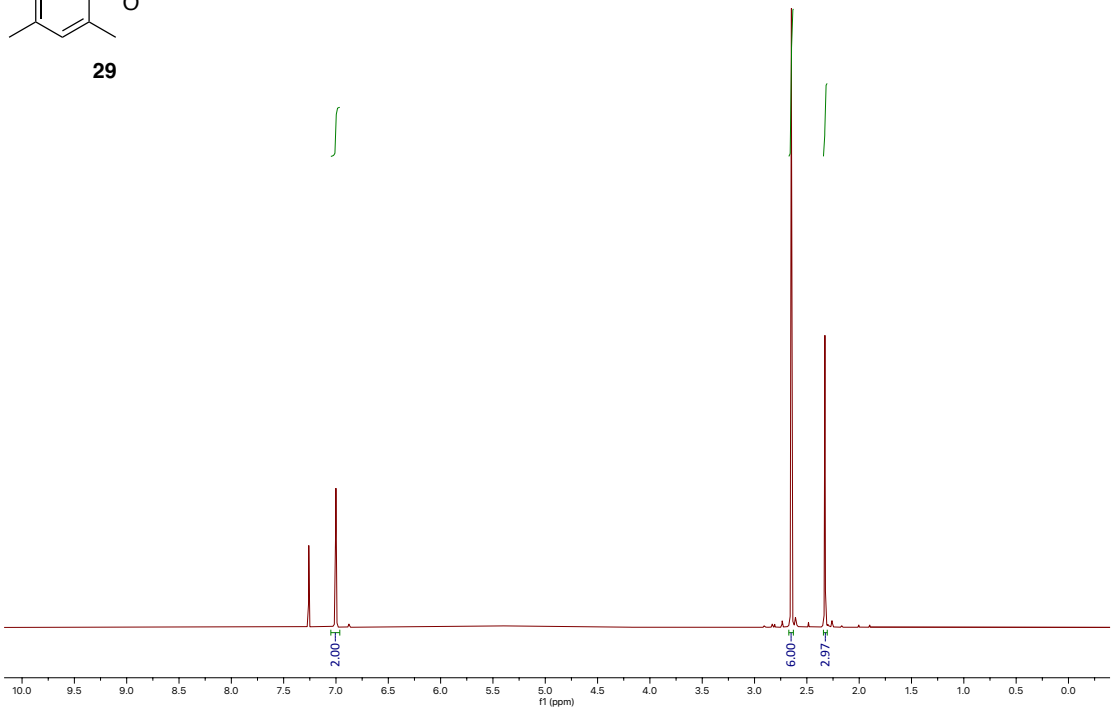

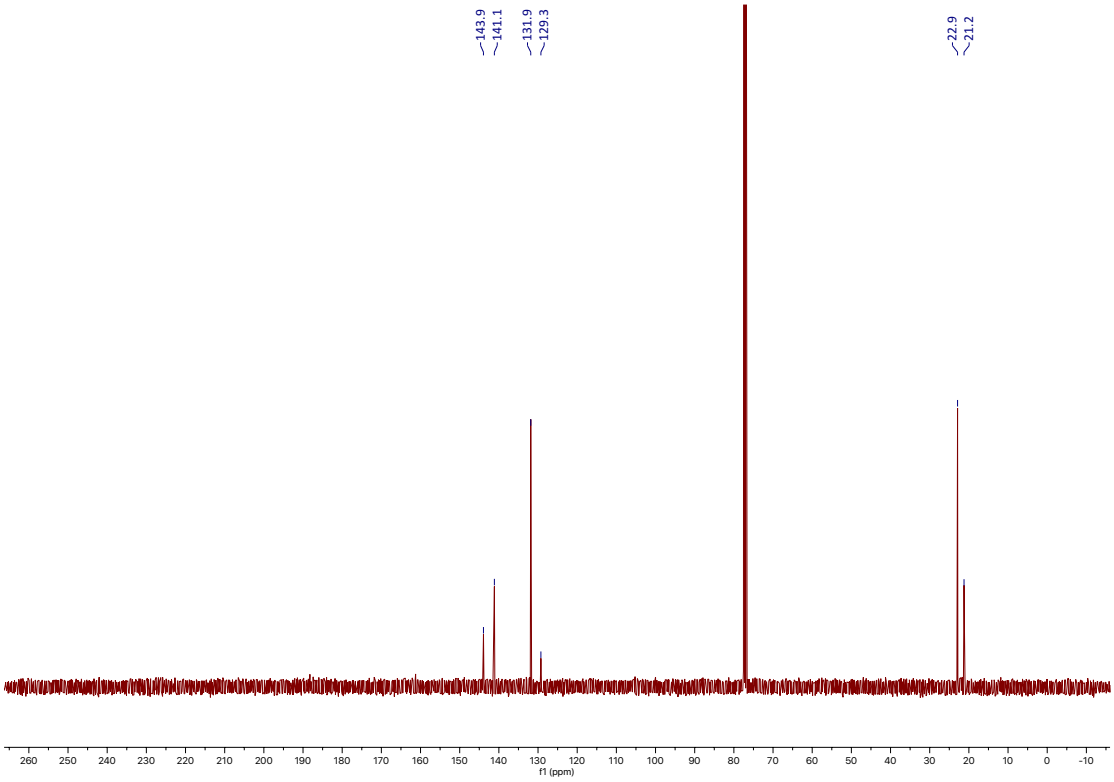

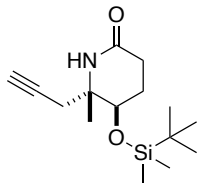
O
HN
O
Si

31

0.94
1.00
4.21
0.97
2.07
2.87
9.00
6.10
f1 (ppm)

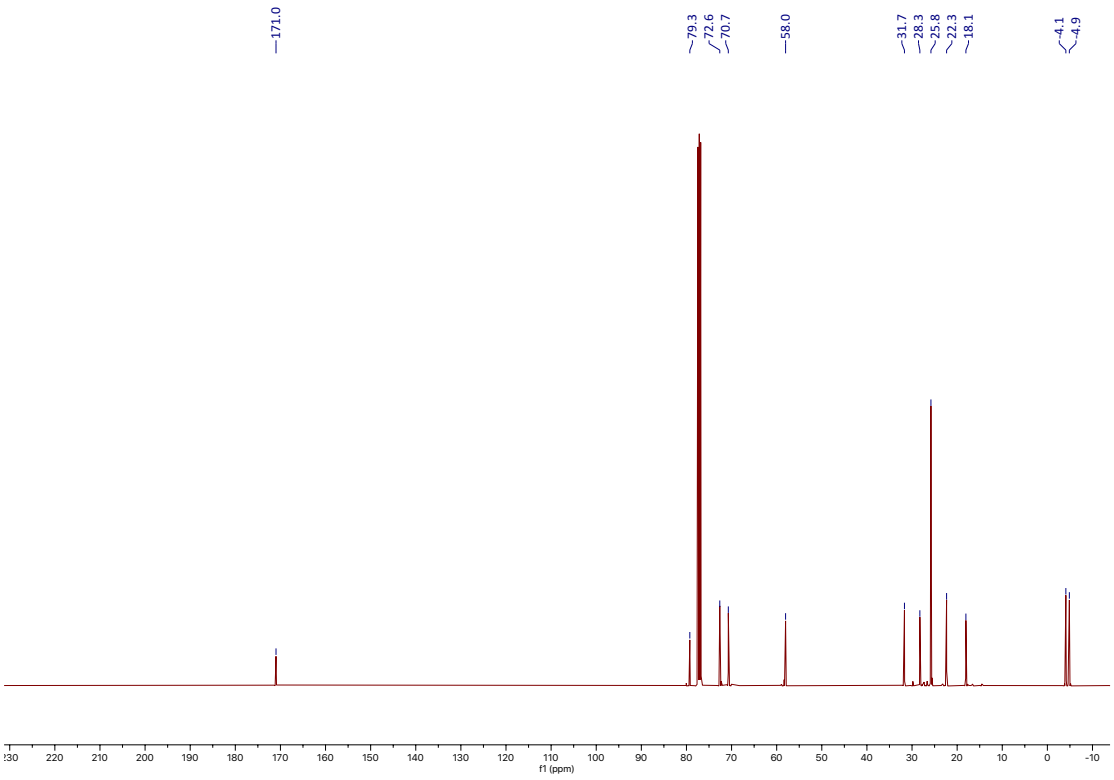
171.0
79.3
72.6
70.7
58.0
31.7
28.3
25.8
22.3
18.1
-4.1
-4.9
f1 (ppm)

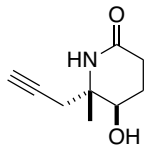
O
HN
OH

32

0.97
1.03
4.15
0.95
1.03
2.19
3.00
f1 (ppm)

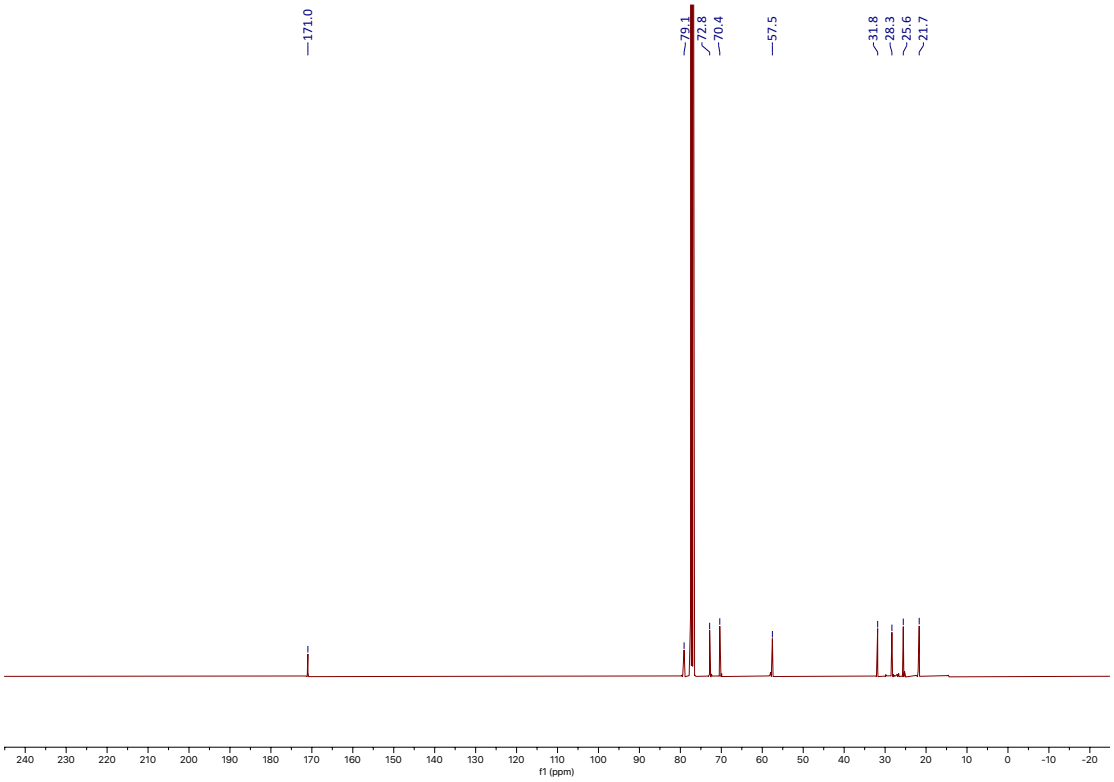
171.0
79.1
72.8
70.4
57.5
31.8
28.3
25.6
21.7
f1 (ppm)

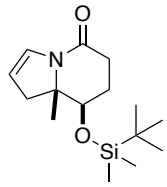

33

0.95
0.96
0.97
2.00
1.97
1.97
3.16
9.12
6.07
f1 (ppm)

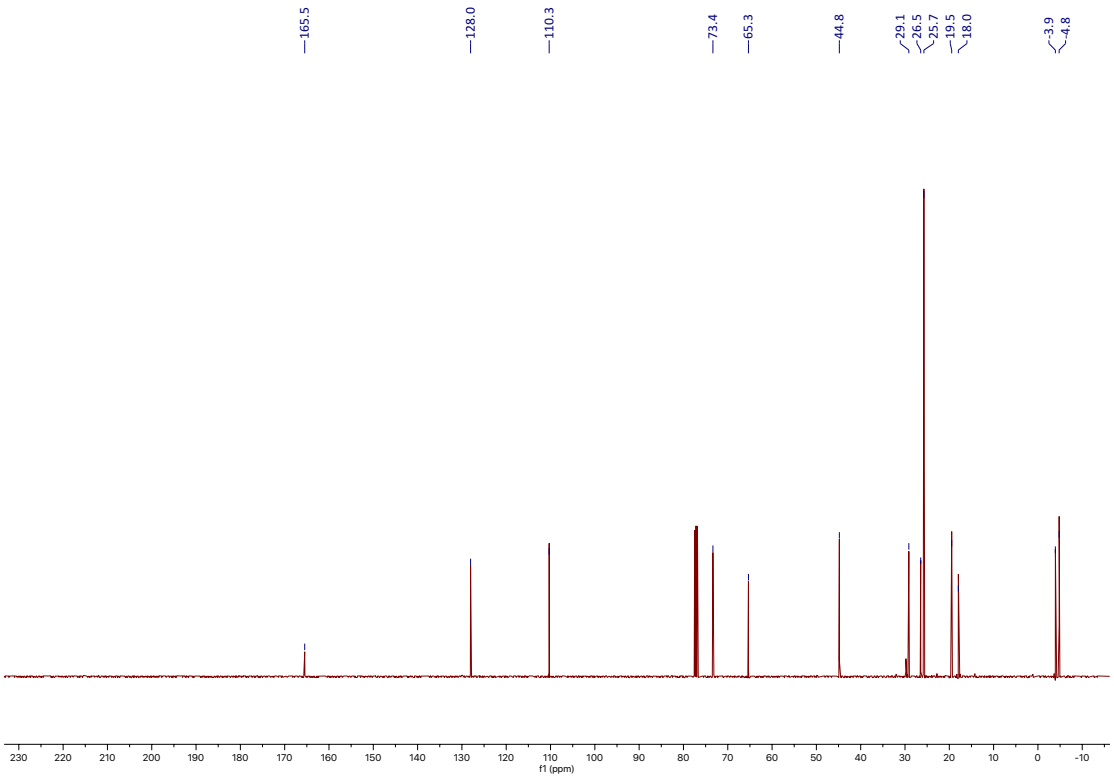
165.5
128.0
110.3
73.4
65.3
44.8
29.1
26.5
25.7
19.5
18.0
-3.9
-4.8
f1 (ppm)

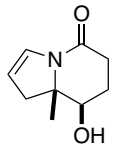
O
N
OH

34

0.97
0.98
1.01
1.03
1.06
2.02
2.16
3.03
10.0 9.5 9.0 8.5 8.0 7.5 7.0 6.5 6.0 5.5 5.0 4.5 4.0 3.5 3.0 2.5 2.0 1.5 1.0 0.5 0.0
f1 (ppm)

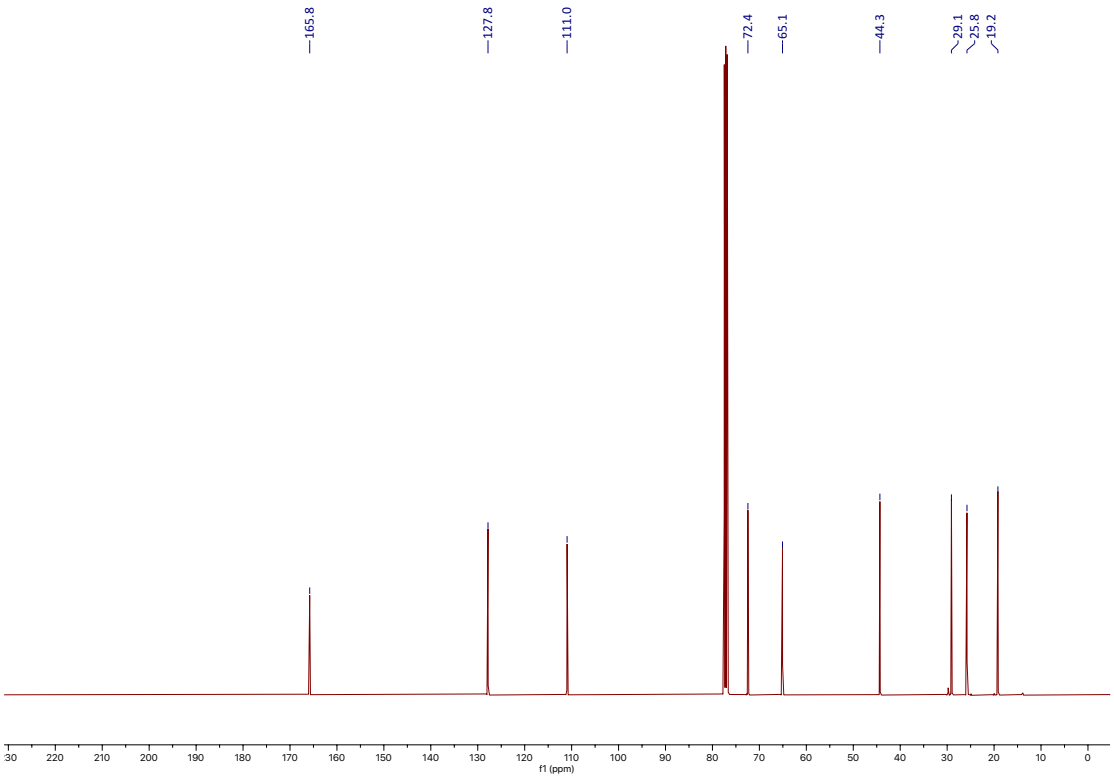
165.8
127.8
111.0
72.4
65.1
44.3
29.1
25.8
19.2
230 220 210 200 190 180 170 160 150 140 130 120 110 100 90 80 70 60 50 40 30 20 10 0
f1 (ppm)

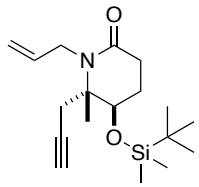

35

1.09
2.16
1.06
1.02
1.07
2.05
2.19
0.95
1.07
0.99
2.90
9.02
6.04
f1 (ppm)

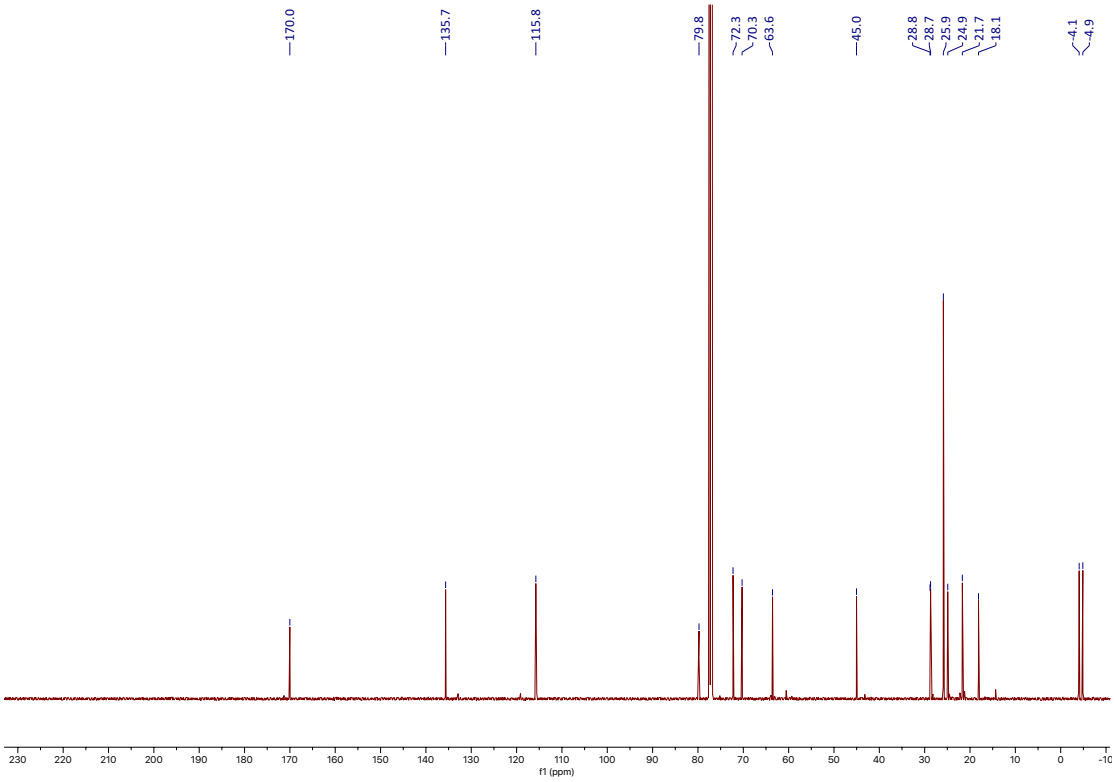
170.0
135.7
115.8
79.8
72.3
70.3
63.6
45.0
28.8
28.7
25.9
24.9
21.7
18.1
-4.1
-4.9
f1 (ppm)

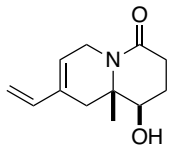
O
N
OH

36

1.06
0.90
1.00
0.97
1.01
0.96
1.04
1.97
1.12
1.03
2.03
3.00
10.0 9.5 9.0 8.5 8.0 7.5 7.0 6.5 6.0 5.5 5.0 4.5 4.0 3.5 3.0 2.5 2.0 1.5 1.0 0.5 0.0
f1 (ppm)

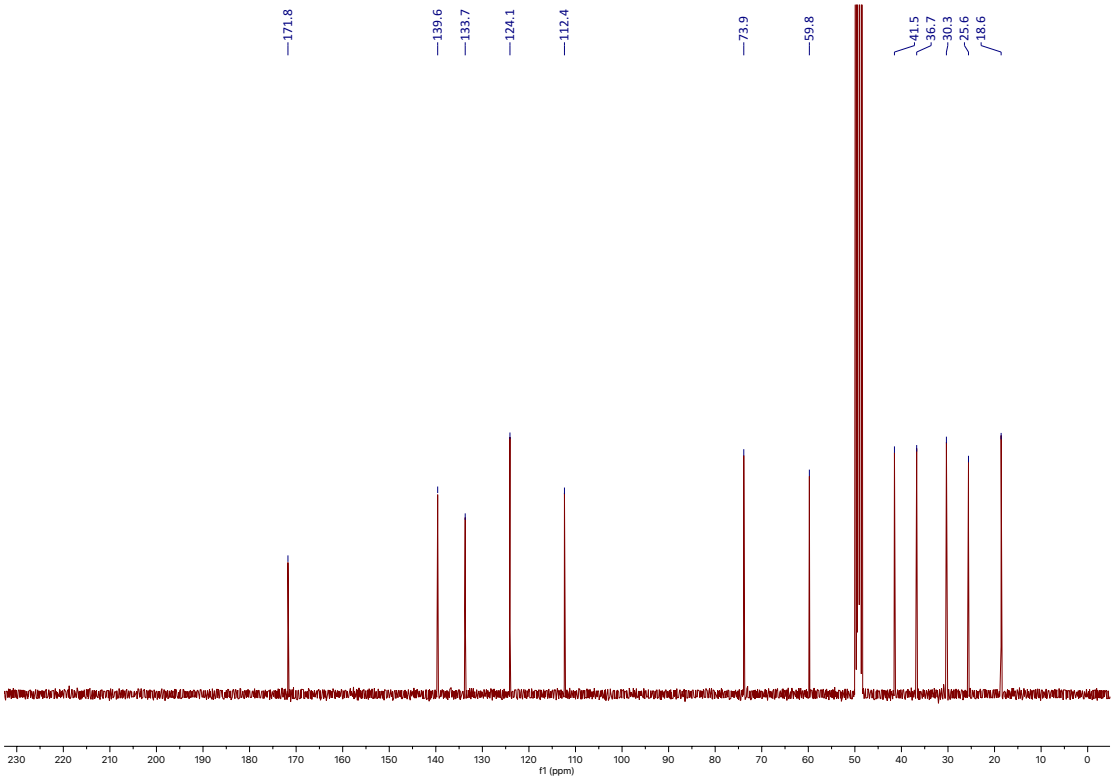
171.8
139.6
133.7
124.1
112.4
73.9
59.8
41.5
36.7
30.3
25.6
18.6
230 220 210 200 190 180 170 160 150 140 130 120 110 100 90 80 70 60 50 40 30 20 10 0
f1 (ppm)

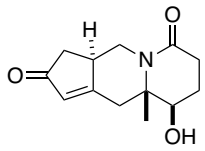
H
O
O
N
OH

37

0.89
1.02
1.03
0.94
1.06
5.04
0.90
2.02
2.94
f1 (ppm)

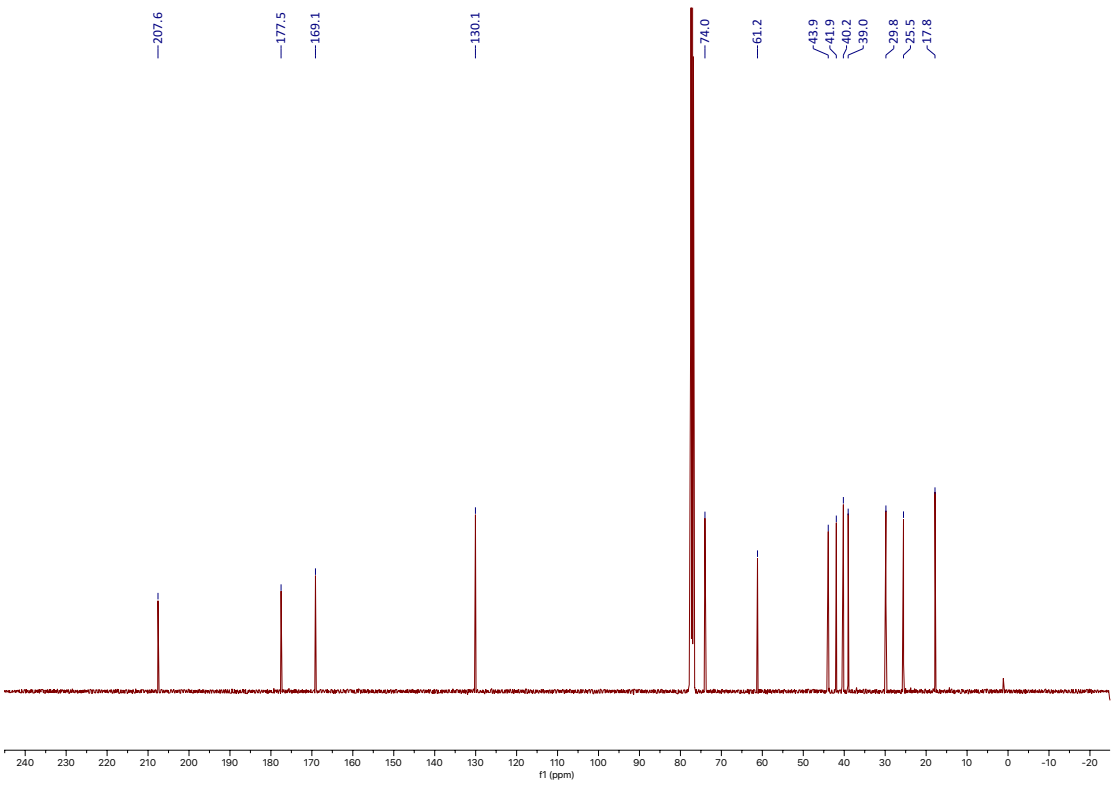
207.6
177.5
169.1
130.1
74.0
61.2
43.9
41.9
40.2
39.0
29.8
25.5
17.8
f1 (ppm)

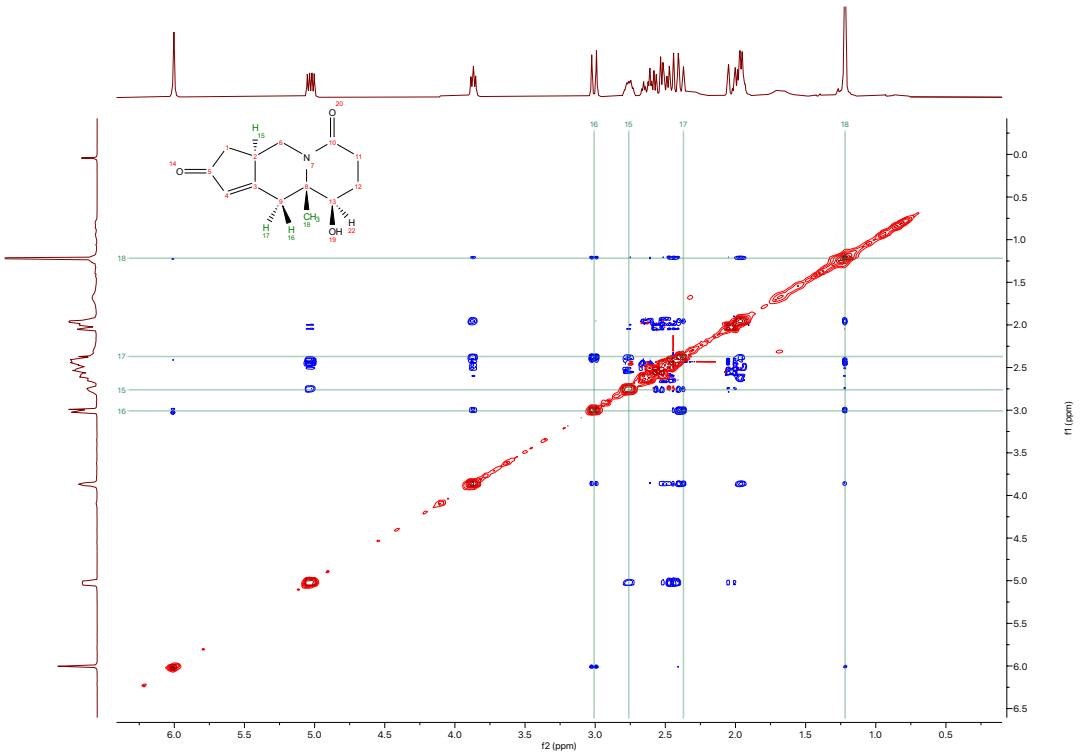
f2 (ppm)
f1 (ppm)

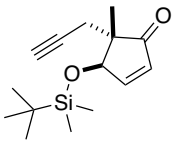

45

0.99
0.96
0.90
1.01
1.07
0.83
2.92
9.28
2.82
3.17
f1 (ppm)

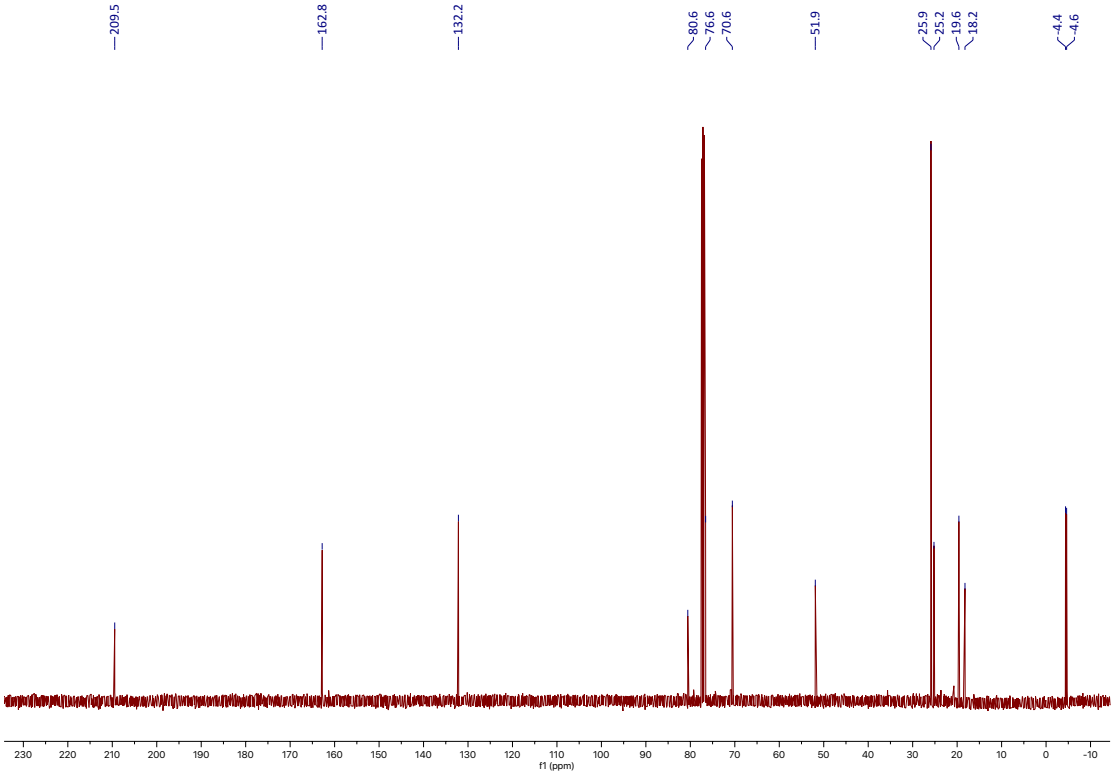
209.5
162.8
132.2
80.6
76.6
70.6
51.9
25.9
25.2
19.6
18.2
-4.4
-4.6
f1 (ppm)

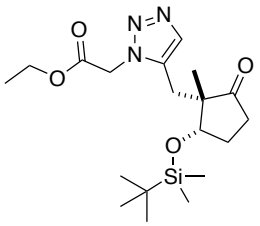

57

0.96
0.99
0.99
3.07
1.99
2.05
1.04
1.00
3.13
3.03
8.98
2.97
3.00
f1 (ppm)

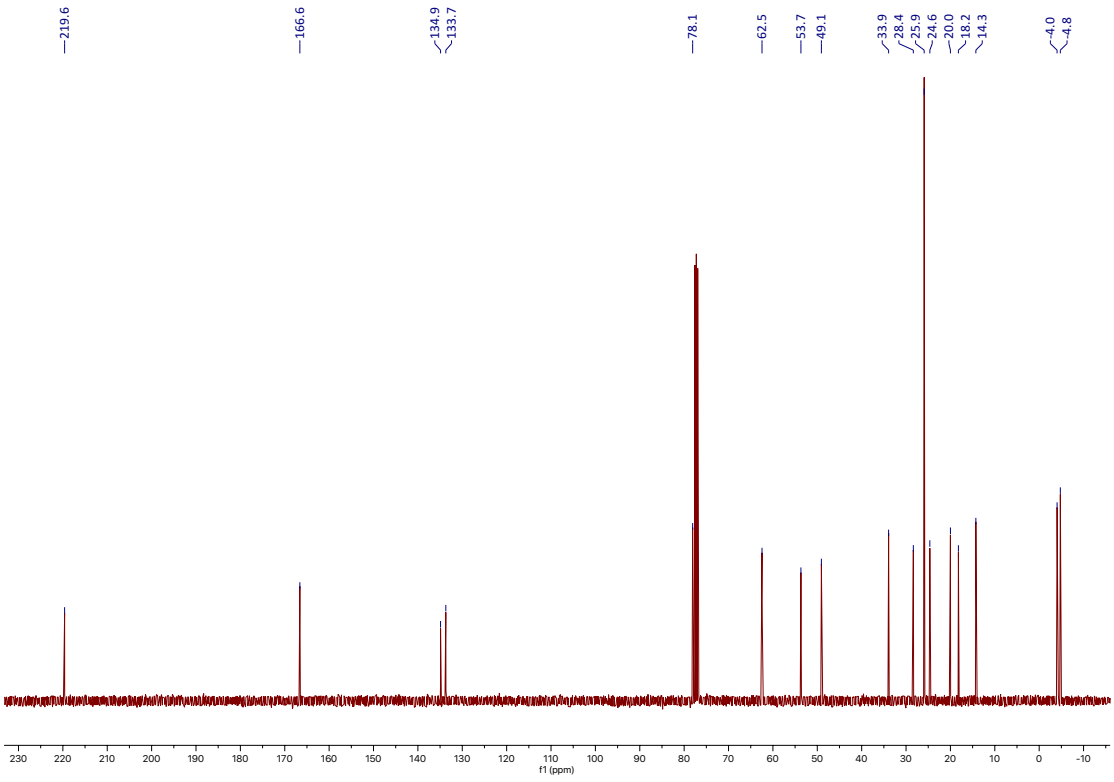
219.6
166.6
134.9
133.7
78.1
62.5
53.7
49.1
33.9
28.4
25.9
24.6
20.0
18.2
14.3
-4.0
-4.8
f1 (ppm)

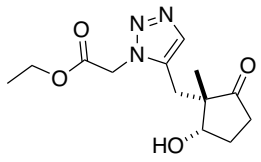
O
N
N
N
O
O
HO

58

1.01
1.06
1.05
1.96
1.00
1.04
1.04
2.23
1.36
1.02
3.06
2.80
f1 (ppm)

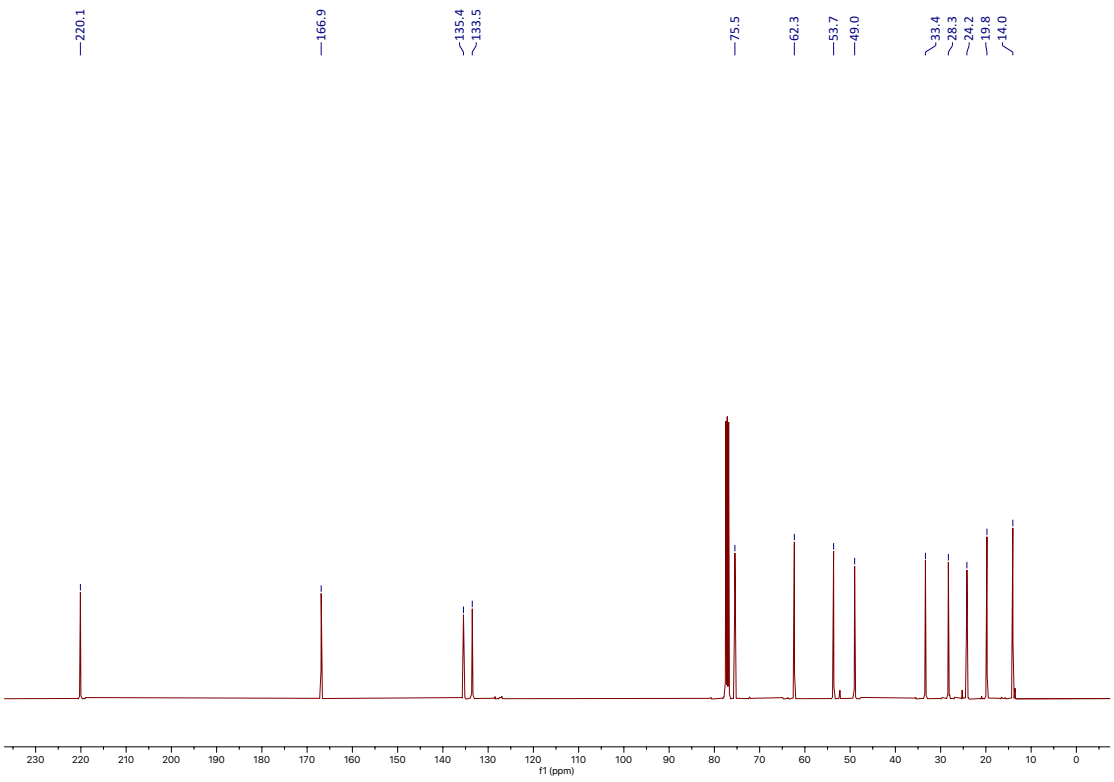
220.1
166.9
135.4
133.5
75.5
62.3
53.7
49.0
33.4
28.3
24.2
19.8
14.0
f1 (ppm)

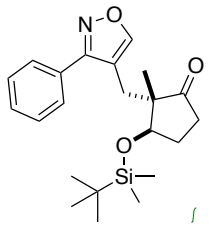

60

0.88
1.95
3.02
0.99
1.01
1.01
1.02
2.11
1.07
3.10
9.00
2.93
2.91
f1 (ppm)

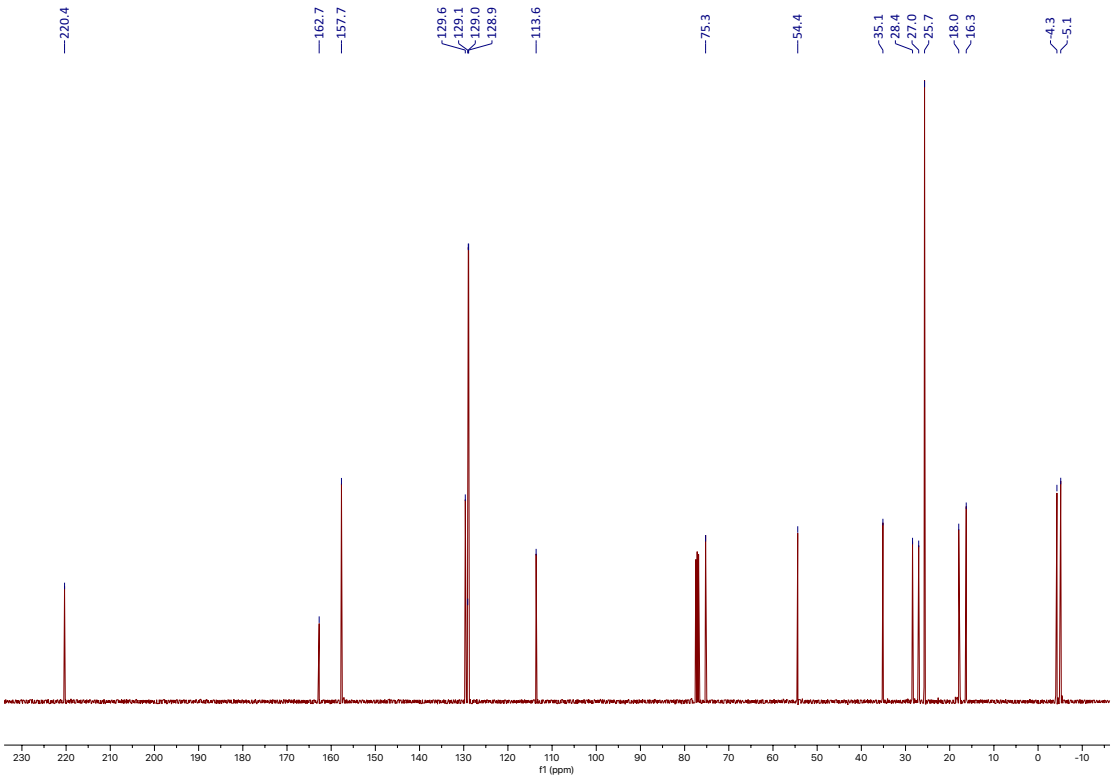
220.4
162.7
157.7
129.6
129.1
129.0
128.9
113.6
75.3
54.4
35.1
28.4
27.0
25.7
18.0
16.3
4.3
5.1
f1 (ppm)

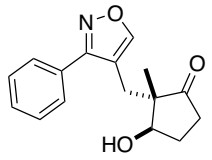
N
O
O
HO

61

0.91
2.03
3.04
0.99
1.03
1.01
1.04
1.04
1.11
1.15
0.70
2.94
f1 (ppm)

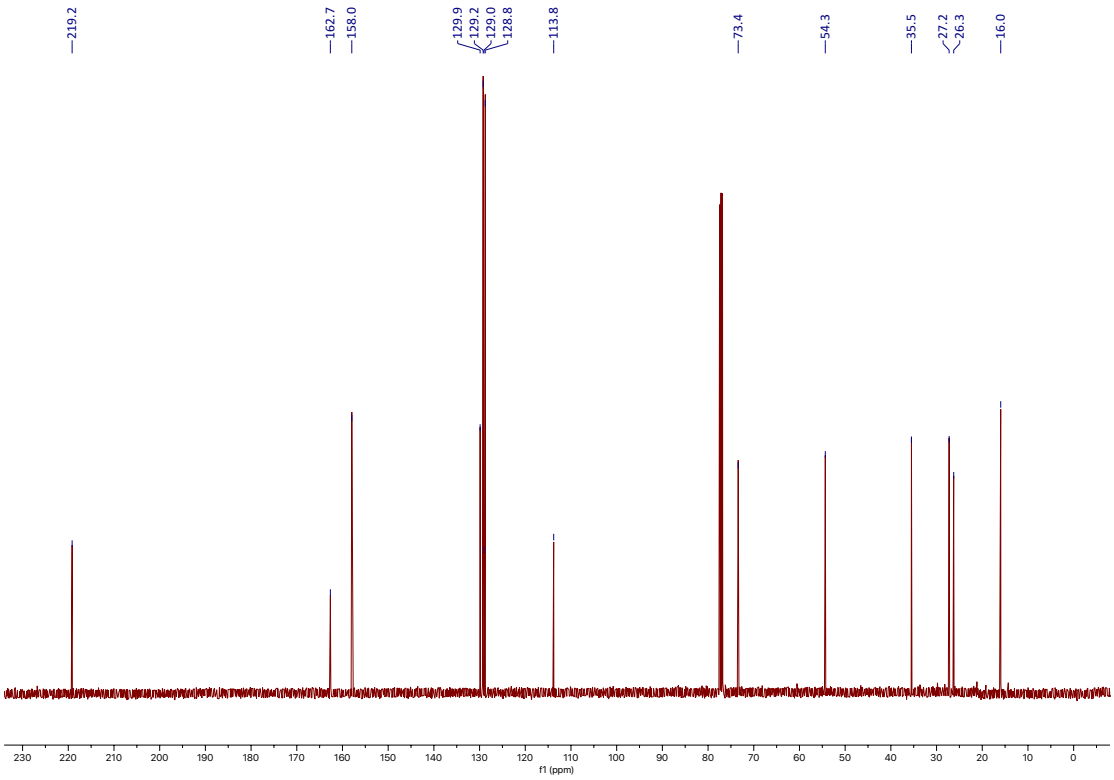
219.2
162.7
158.0
129.9
129.2
129.0
128.8
113.8
73.4
54.3
35.5
27.2
26.3
16.0
f1 (ppm)

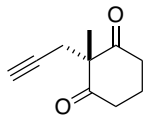

63

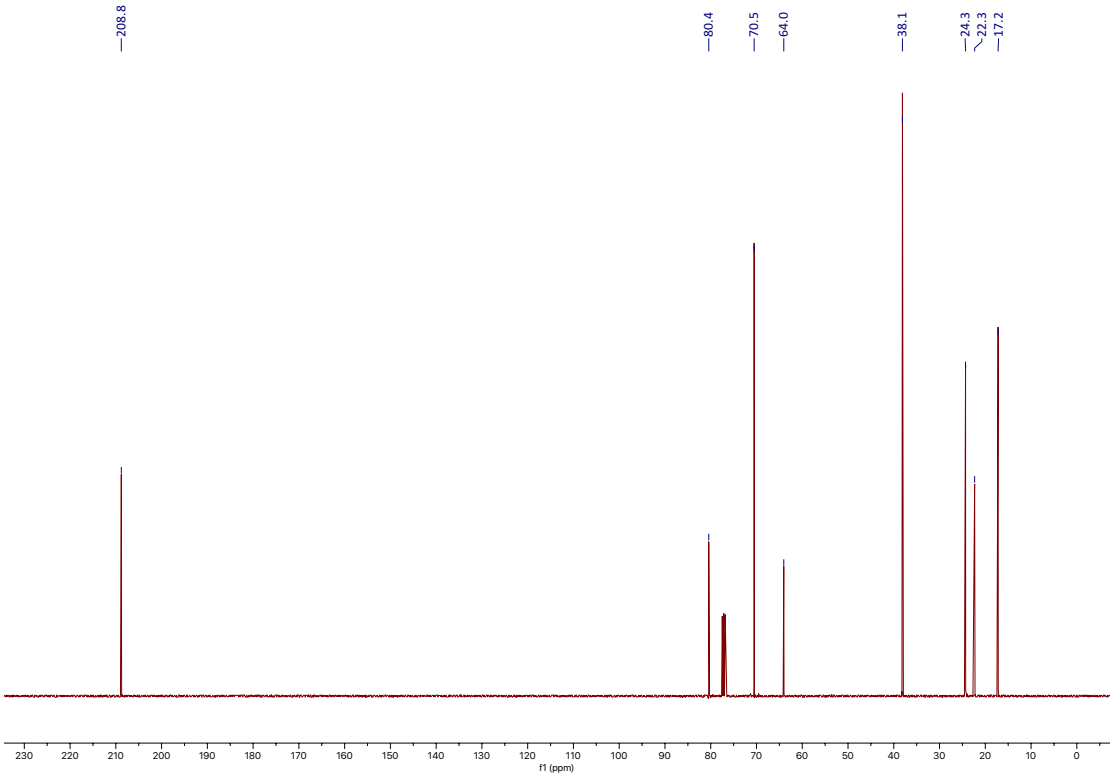

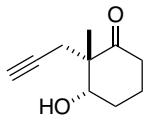
O
HO

syn-**64**

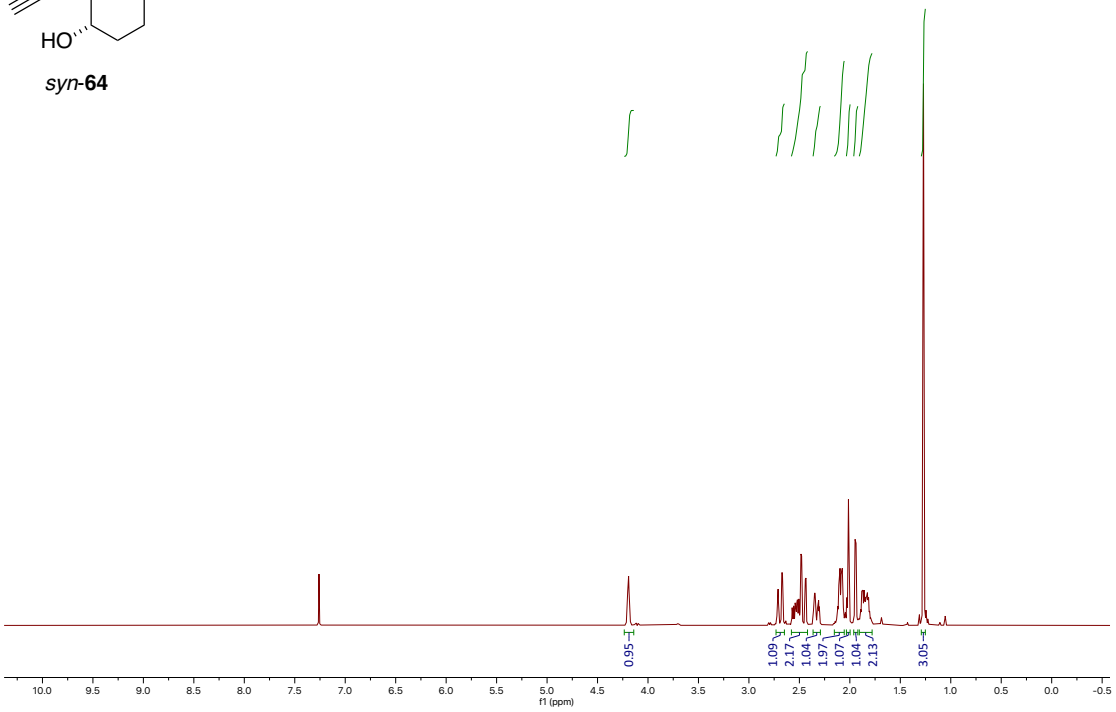
0.95
1.09
2.17
1.04
1.97
1.07
1.04
2.13
3.05
f1 (ppm)

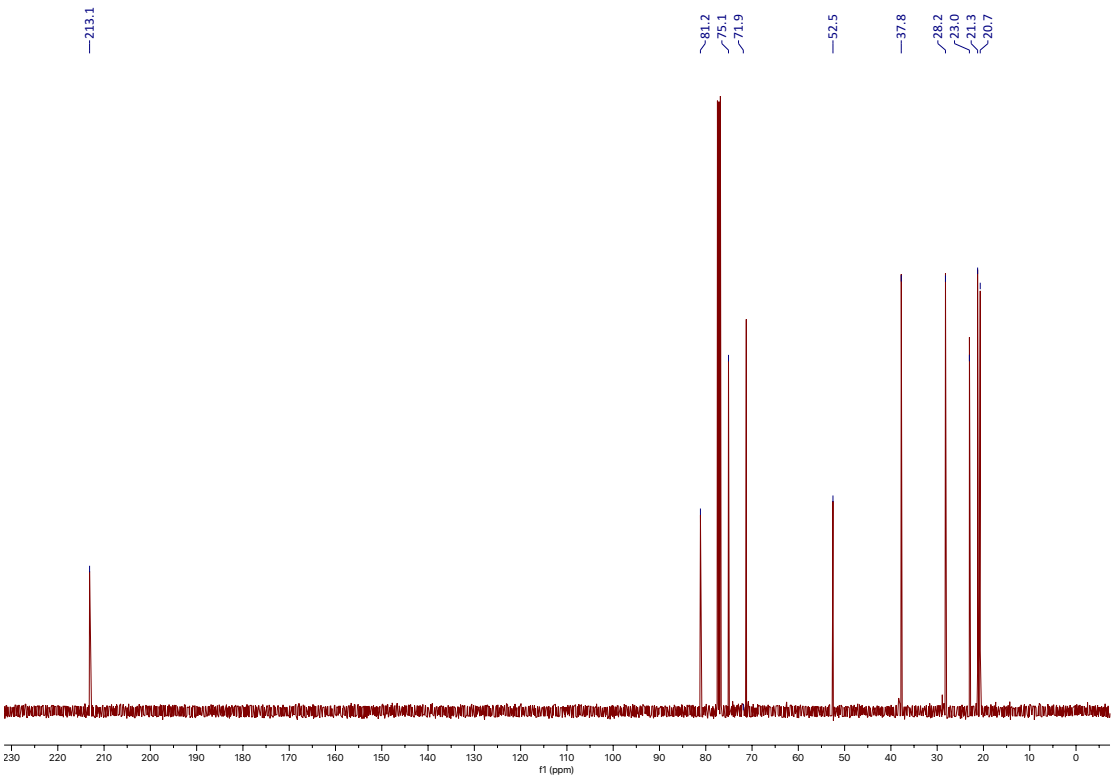
213.1
81.2
75.1
71.9
52.5
37.8
28.2
23.0
21.3
20.7
f1 (ppm)

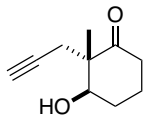
O
HO

anti-**64**

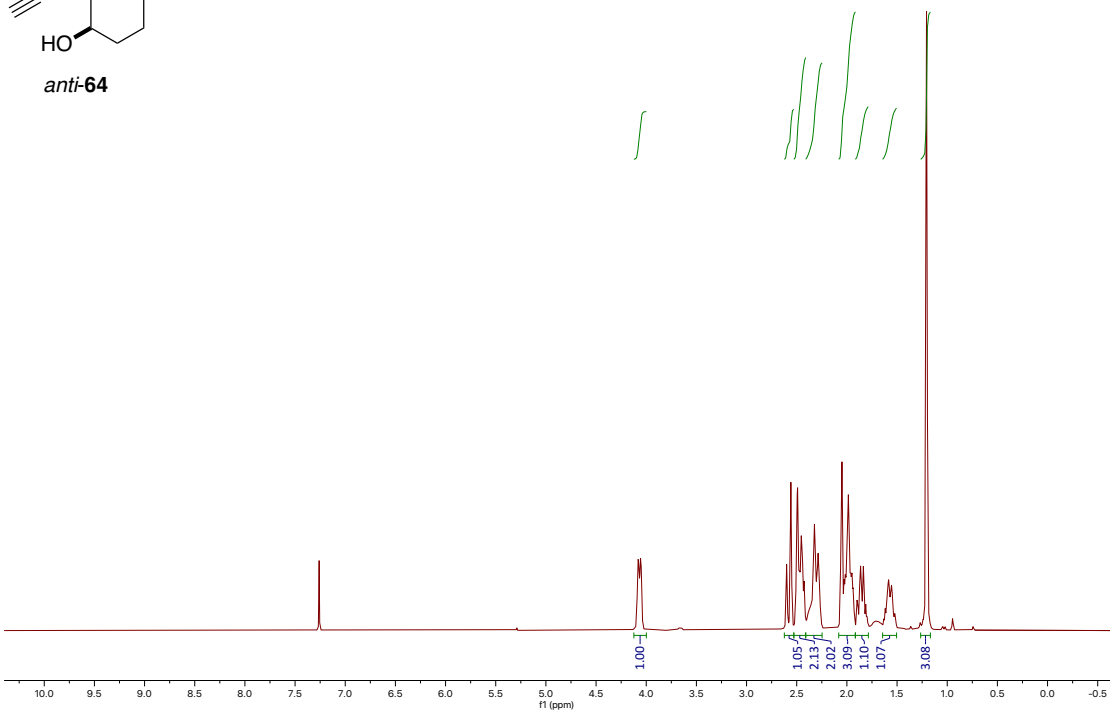
1.00
1.05
2.13
2.02
3.09
1.10
1.07
3.08
10.0 9.5 9.0 8.5 8.0 7.5 7.0 6.5 6.0 5.5 5.0 4.5 4.0 3.5 3.0 2.5 2.0 1.5 1.0 0.5 0.0 -0.5
f1 (ppm)

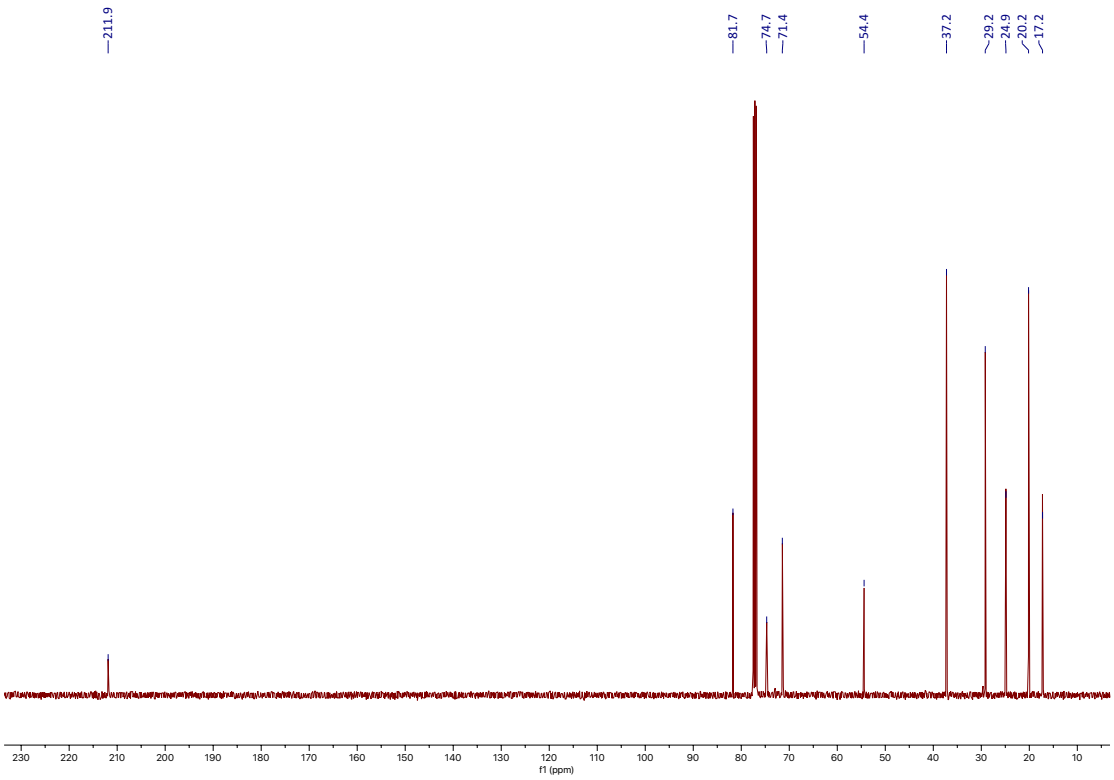
211.9
81.7
74.7
71.4
54.4
37.2
29.2
24.9
20.2
17.2
230 220 210 200 190 180 170 160 150 140 130 120 110 100 90 80 70 60 50 40 30 20 10
f1 (ppm)

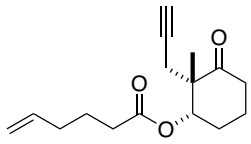

65

0.95
1.01
1.93
6.13
4.03
1.00
2.00
2.00
3.01
f1 (ppm)

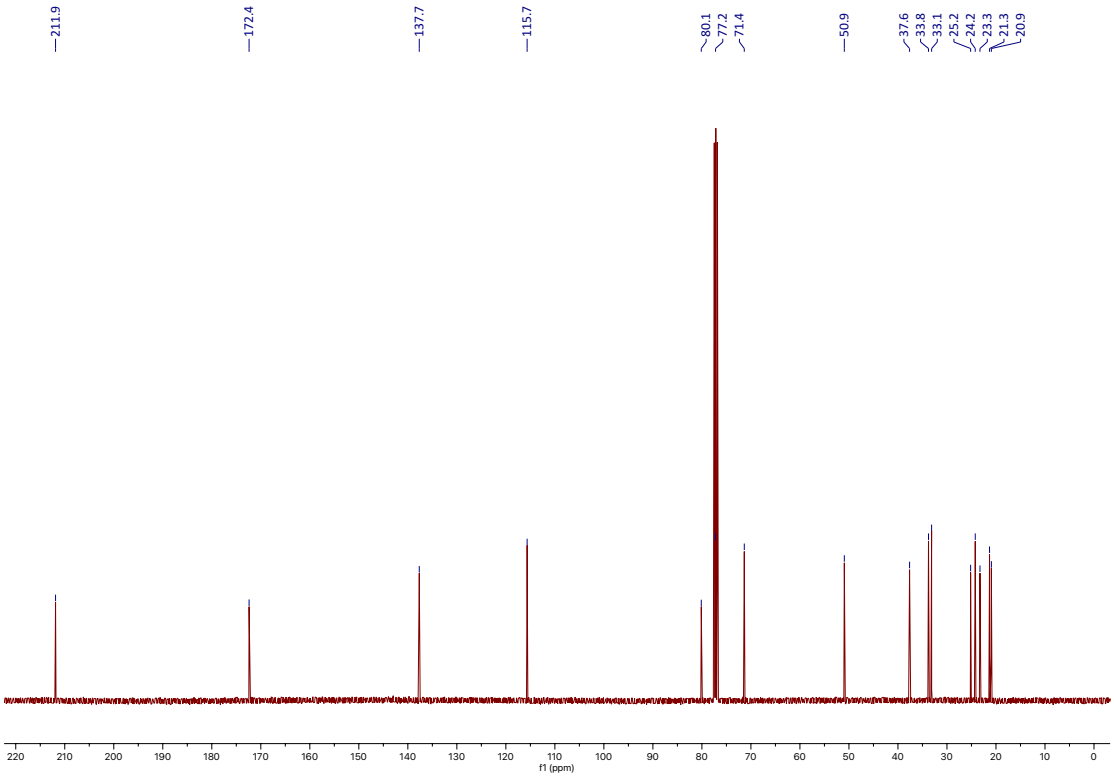
211.9
172.4
137.7
115.7
80.1
77.2
71.4
50.9
37.6
33.8
33.1
25.2
24.2
23.3
21.3
20.9
f1 (ppm)

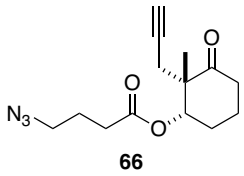
O
O
N3
O

66

0.97
1.93
6.00
2.09
0.99
3.90
3.01
f1 (ppm)

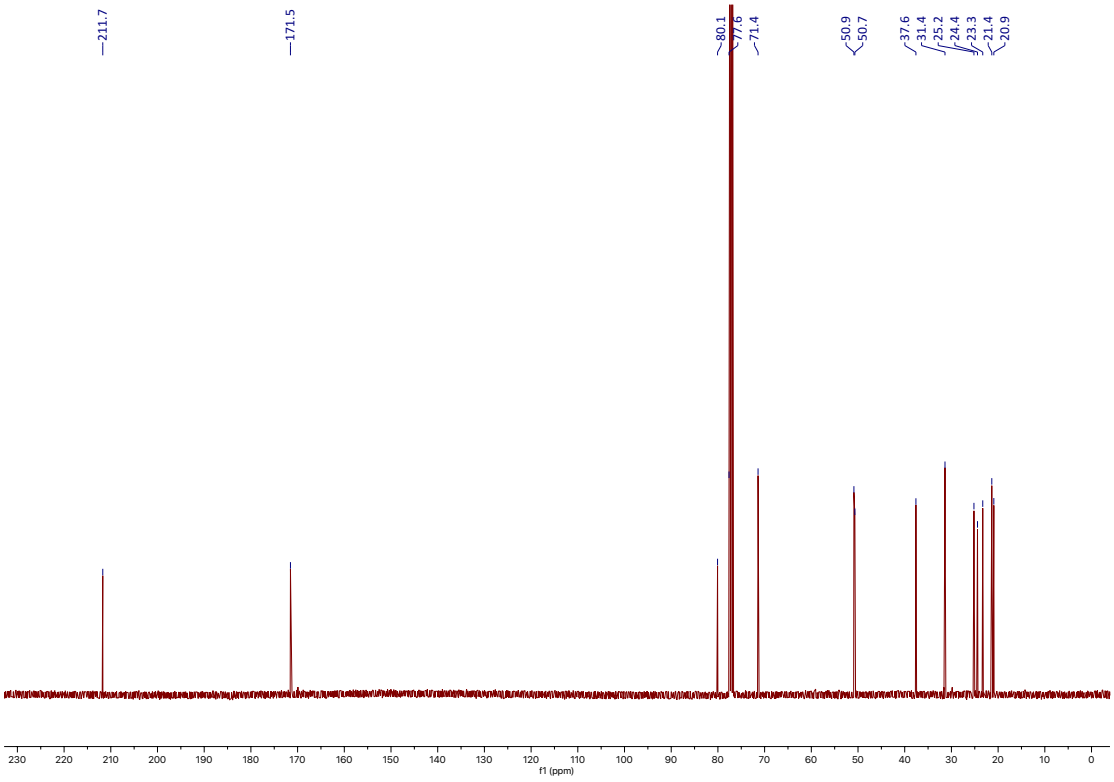
211.7
171.5
80.1
77.6
71.4
50.9
50.7
37.6
31.4
25.2
24.4
23.3
21.4
20.9
f1 (ppm)

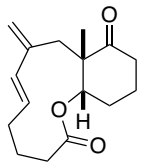

67

1.04
0.84
0.98
1.01
1.07
1.07
6.25
7.12
2.89
f1 (ppm)

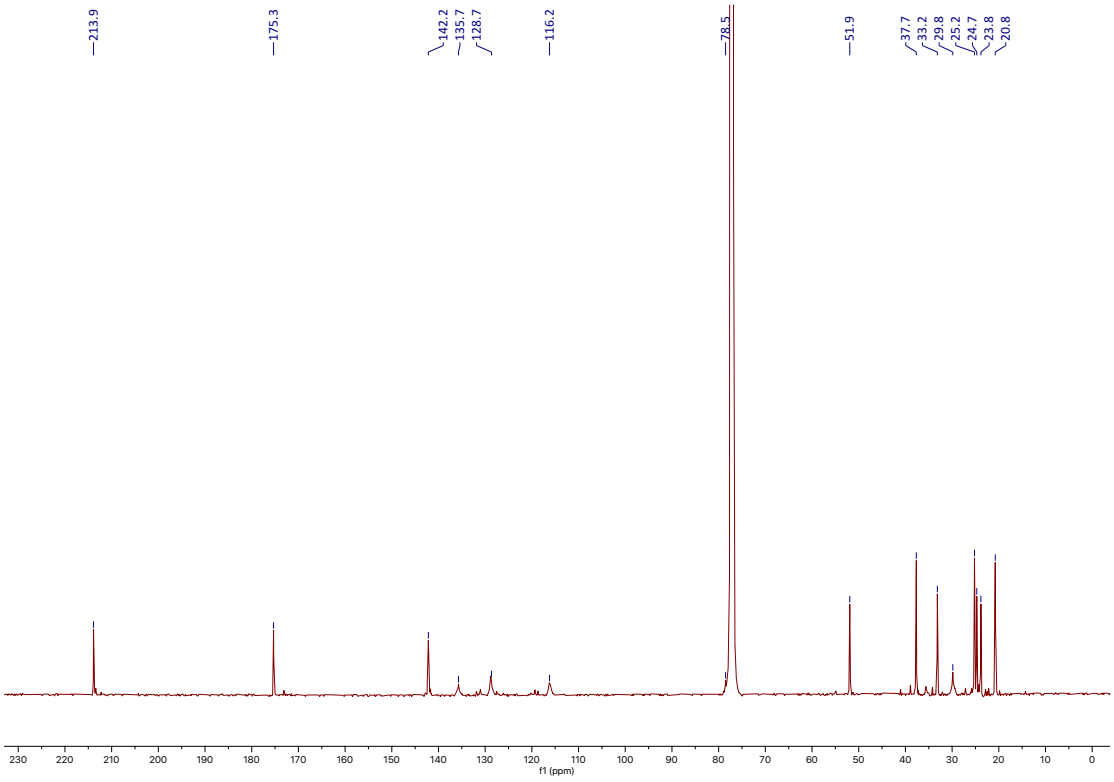
213.9
175.3
142.2
135.7
128.7
116.2
78.5
51.9
37.7
33.2
29.8
25.2
24.7
23.8
20.8
f1 (ppm)

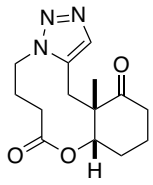

68

0.98
1.79
1.04
1.02
2.97
3.96
4.13
3.00
f1 (ppm)

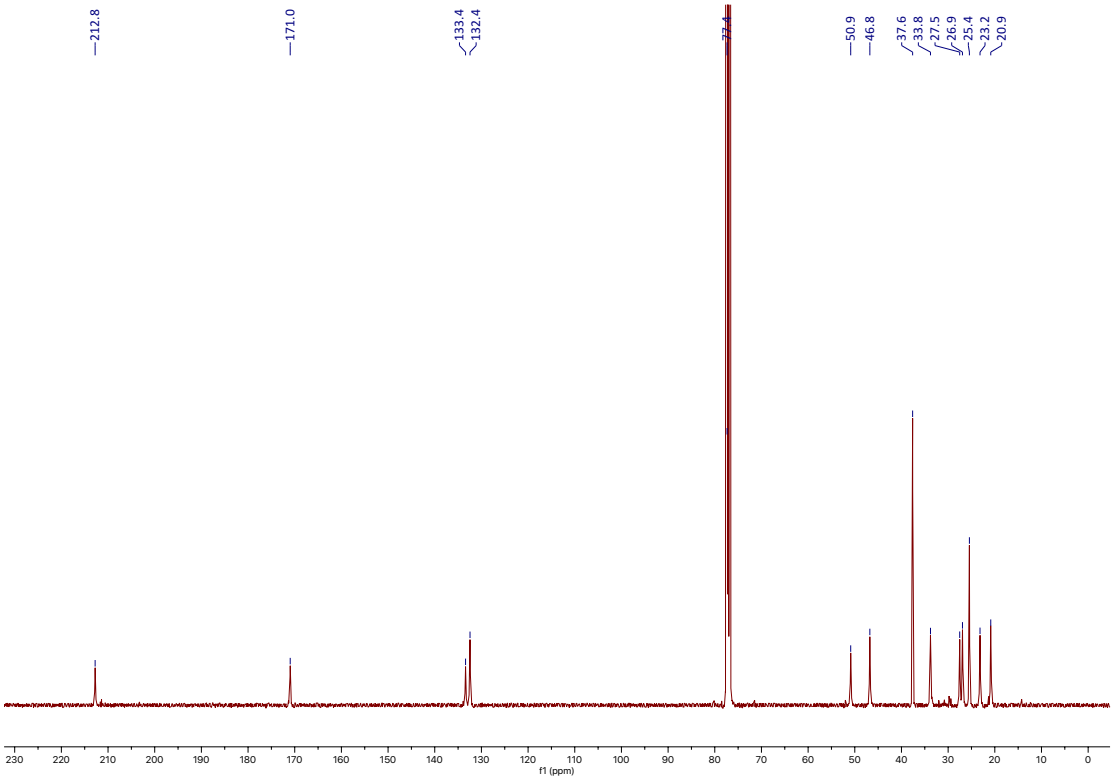
212.8
171.0
133.4
132.4
77.4
50.9
46.8
37.6
33.8
27.5
26.9
25.4
23.2
20.9
f1 (ppm)

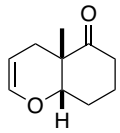
O
O
H

69

0.70
0.85
0.89
2.10
1.04
2.13
1.08
1.11
1.05
3.09
f1 (ppm)

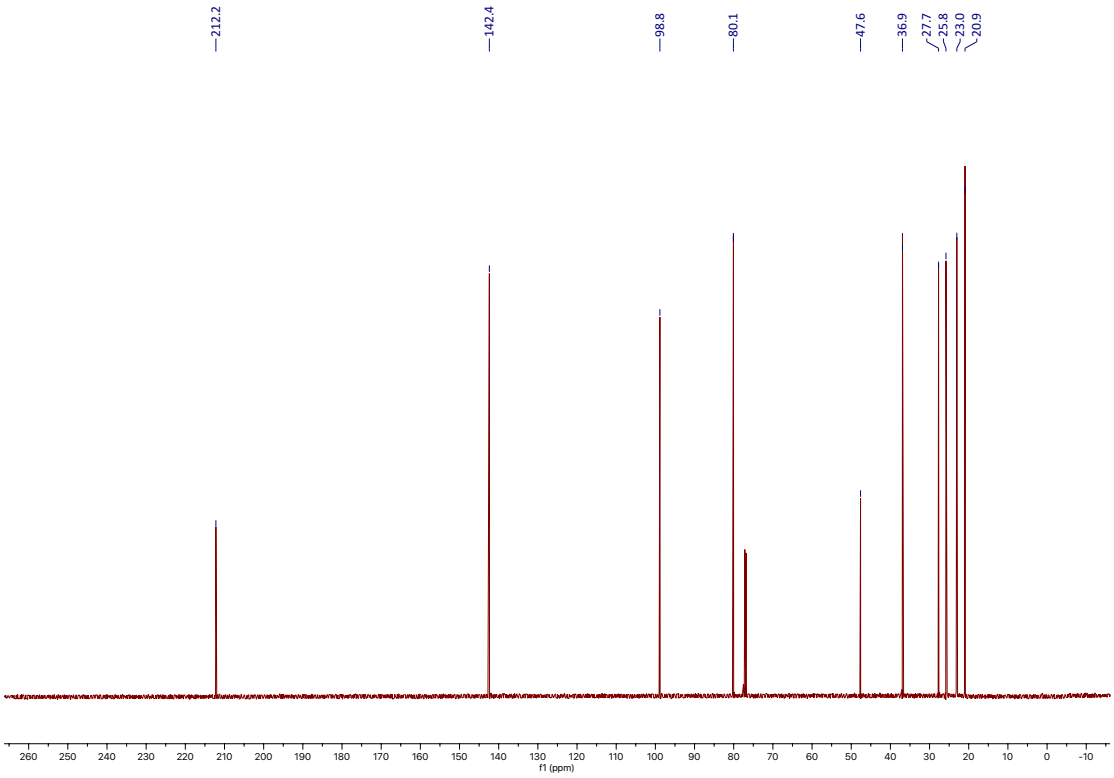
212.2
142.4
98.8
80.1
47.6
36.9
27.7
25.8
23.0
20.9
f1 (ppm)

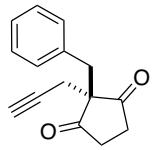
O
O

72

3.10
1.97
2.00
2.97
1.03
2.00
0.95
f1 (ppm)

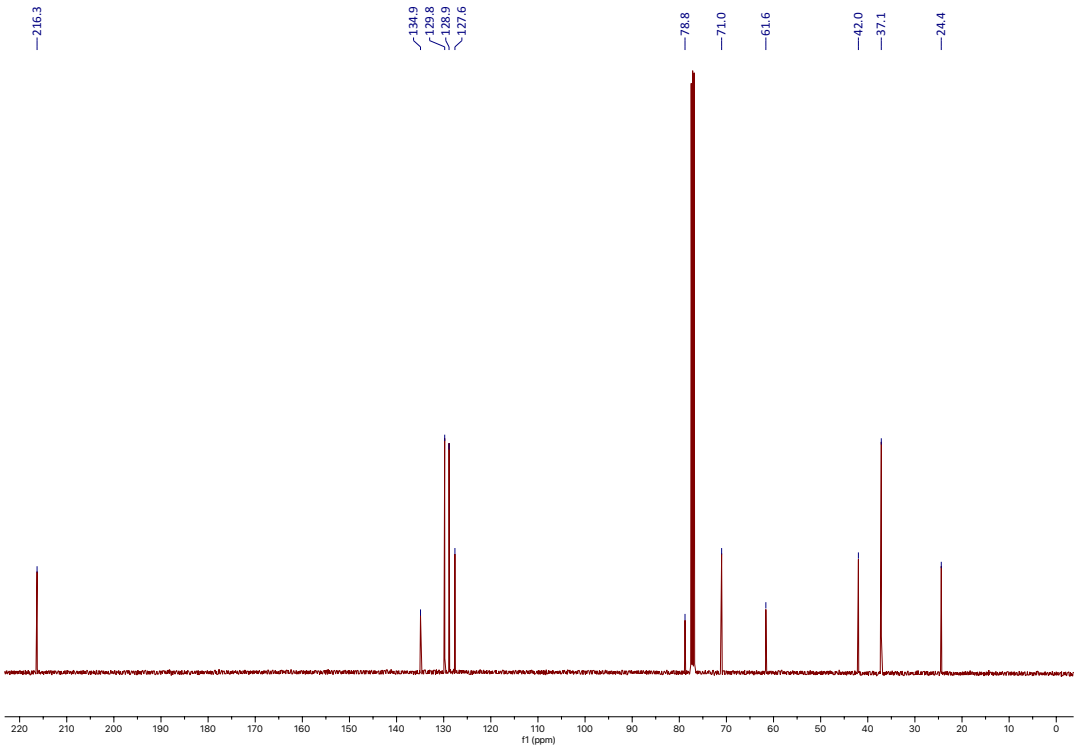
216.3
134.9
129.8
128.9
127.6
78.8
71.0
61.6
42.0
37.1
24.4
f1 (ppm)

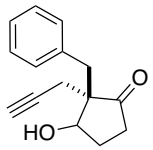
O
HO

73

6.25
1.21
0.98
1.47
2.74
5.34
0.82
0.99
f1 (ppm)

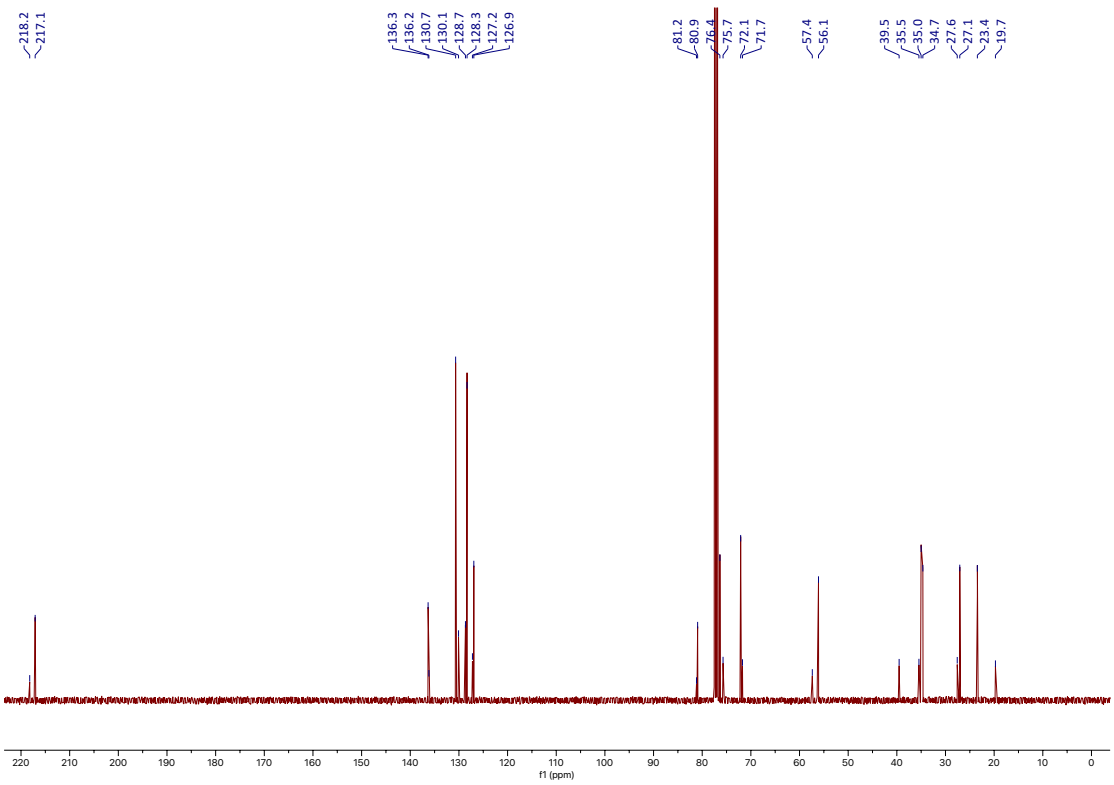
218.2
217.1
136.3
136.2
130.7
130.1
128.7
128.3
127.2
126.9
81.2
80.9
76.4
75.7
72.1
71.7
57.4
56.1
39.5
35.5
35.0
34.7
27.6
27.1
23.4
19.7
f1 (ppm)

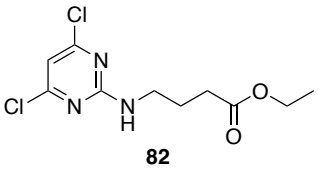
Cl
N
Cl
N
N
H
O
O

82

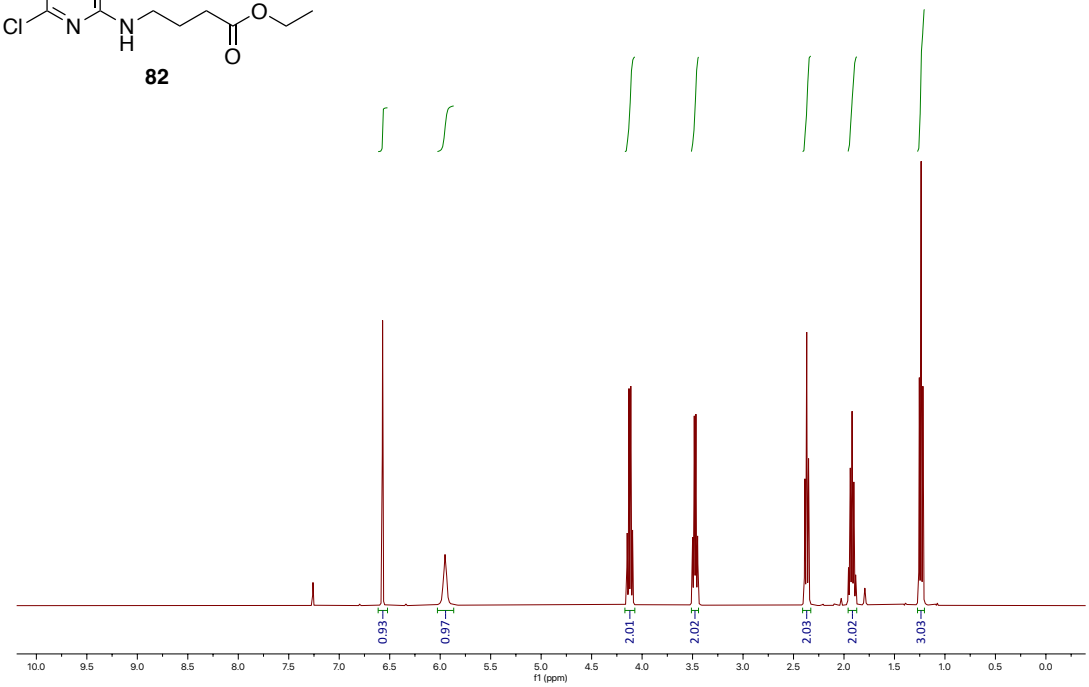
0.93
0.97
2.01
2.02
2.03
2.02
3.03
f1 (ppm)

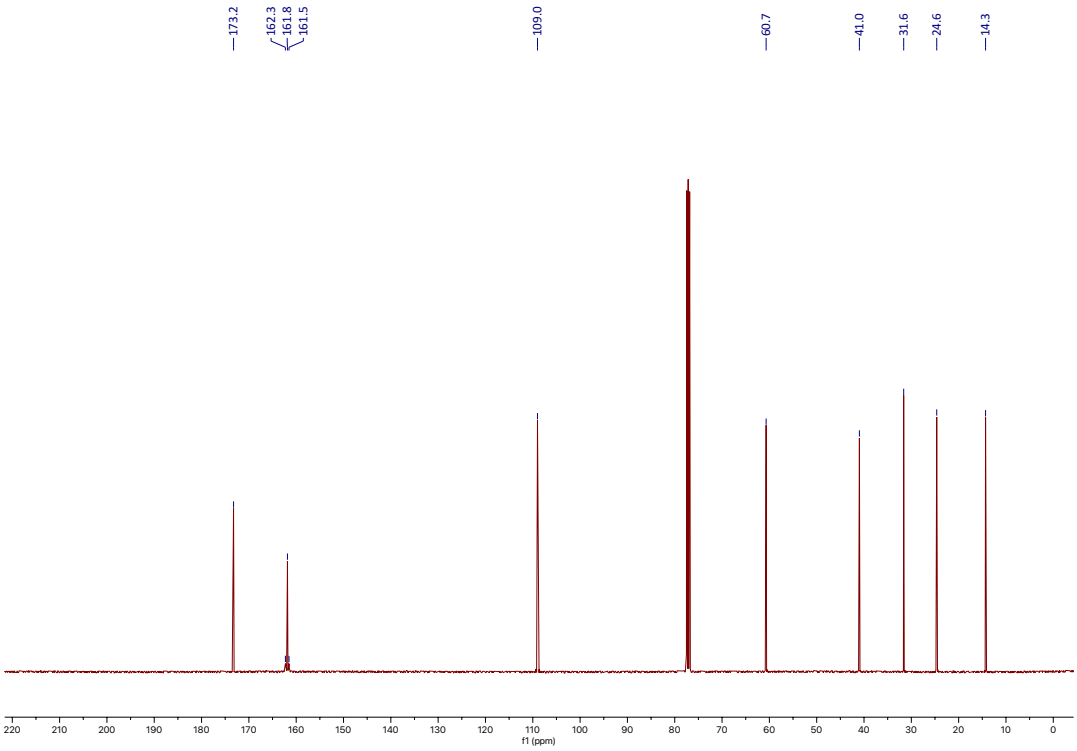
173.2
162.3
161.8
161.5
109.0
60.7
41.0
31.6
24.6
14.3
f1 (ppm)

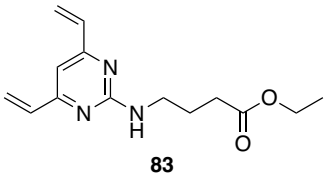

83

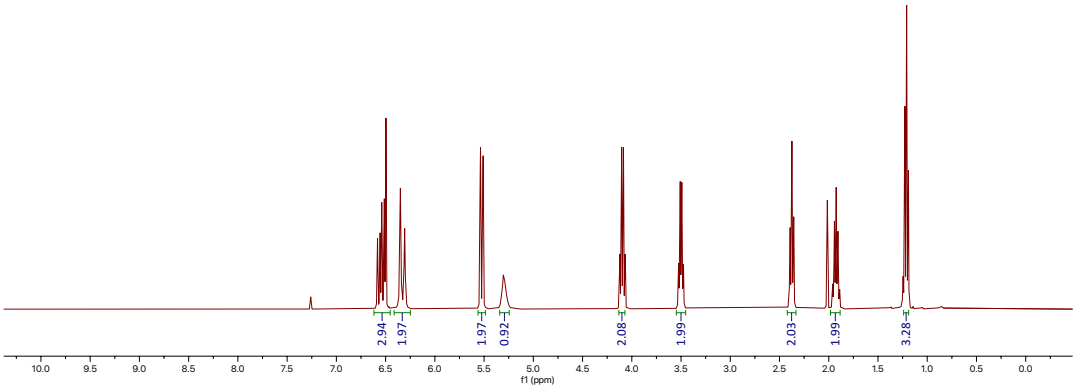
2.94
1.97
1.97
0.92
2.08
1.99
2.03
1.99
3.28
f1 (ppm)


173.5
163.7
162.7
136.0
121.4
105.7
60.4
40.7
31.8
25.2
14.3

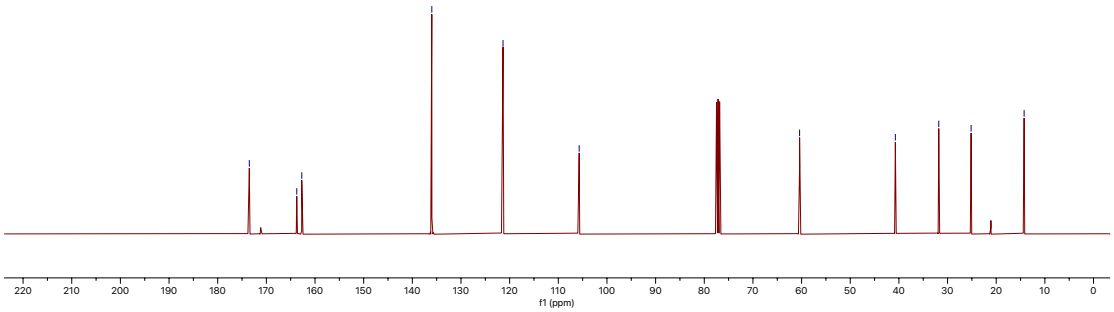
f1 (ppm)

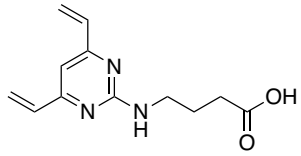
N
N
N
H
OH
O

80

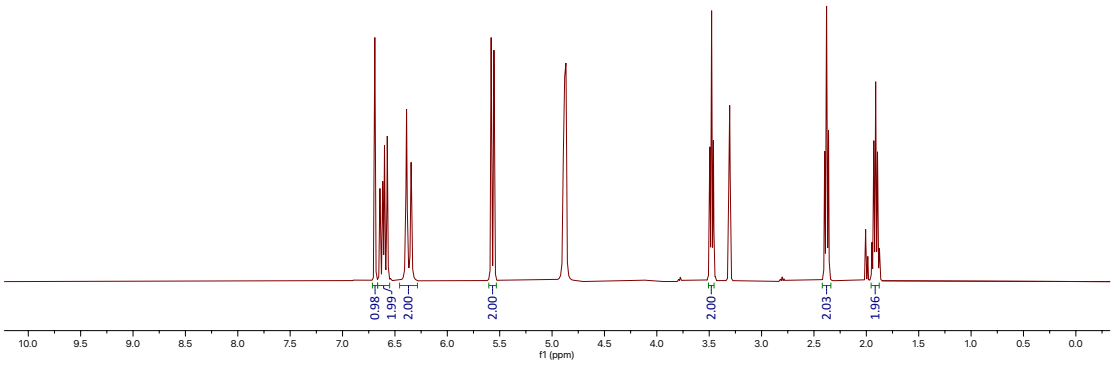
0.98
1.99
2.00
2.00
2.00
2.03
1.96
10.0 9.5 9.0 8.5 8.0 7.5 7.0 6.5 6.0 5.5 5.0 4.5 4.0 3.5 3.0 2.5 2.0 1.5 1.0 0.5 0.0
f1 (ppm)

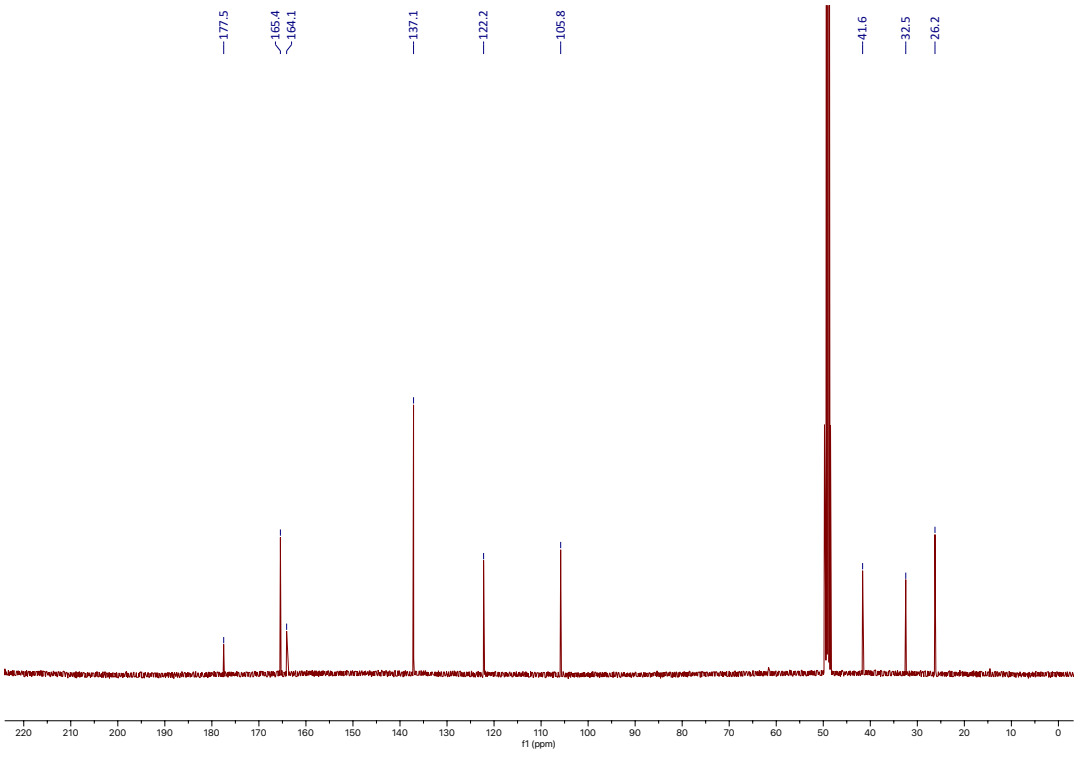
177.5
165.4
164.1
137.1
122.2
105.8
41.6
32.5
26.2
220 210 200 190 180 170 160 150 140 130 120 110 100 90 80 70 60 50 40 30 20 10 0
f1 (ppm)

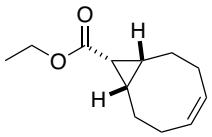
O
H
O
H

85

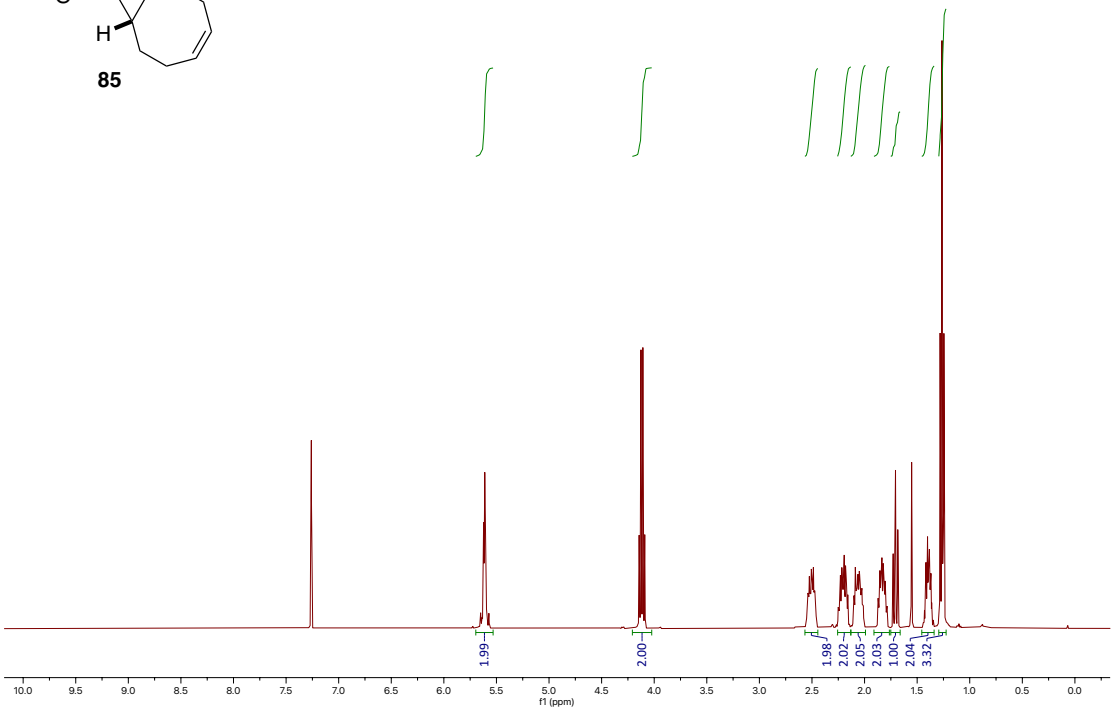
1.99
2.00
1.98
2.02
2.05
2.03
1.00
2.04
3.32
f1 (ppm)

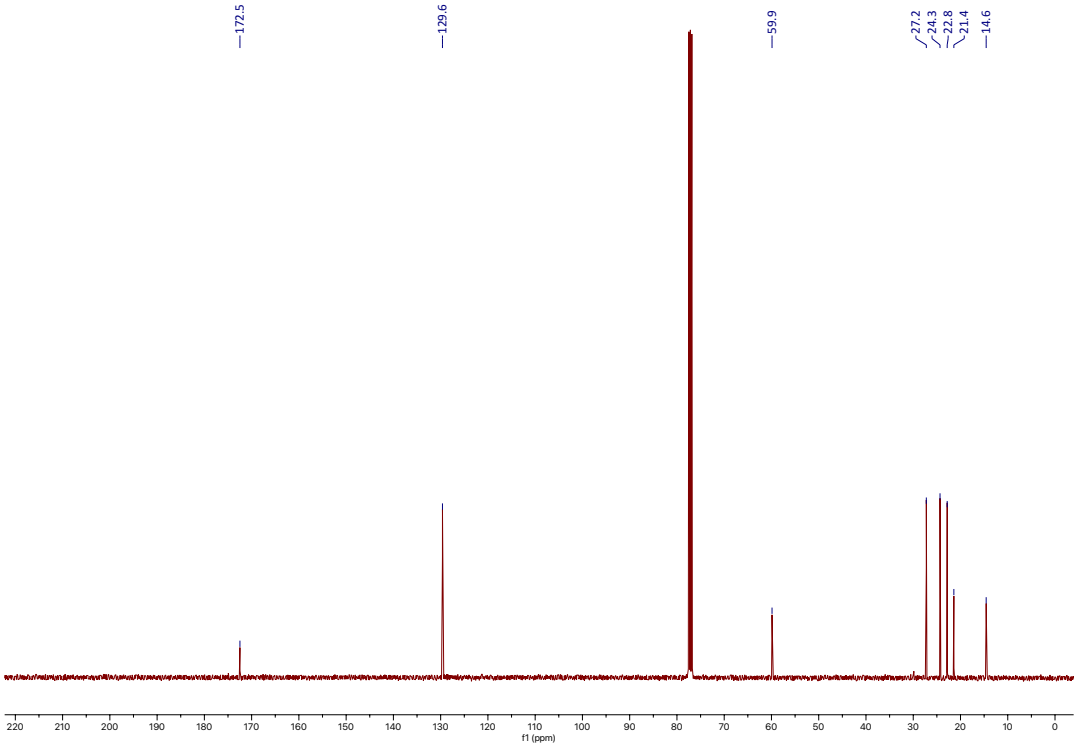
172.5
129.6
59.9
27.2
24.3
22.8
21.4
14.6
f1 (ppm)

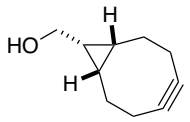
HO
H
H

86

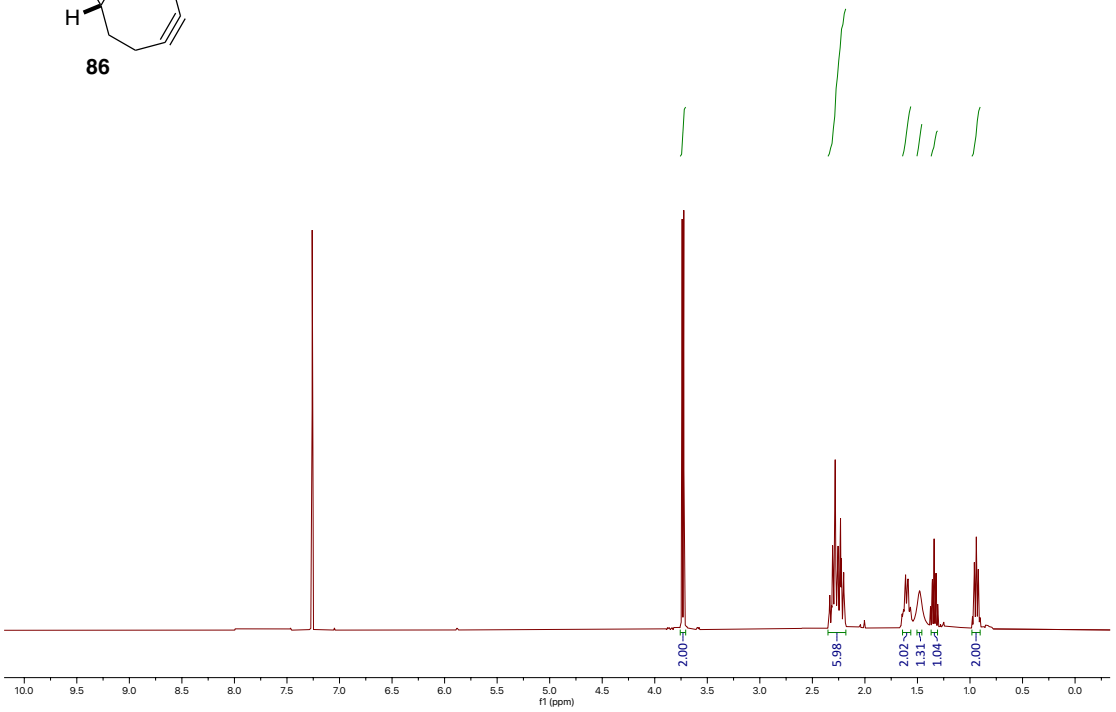
2.00
5.98
2.02
1.31
1.04
2.00
f1 (ppm)

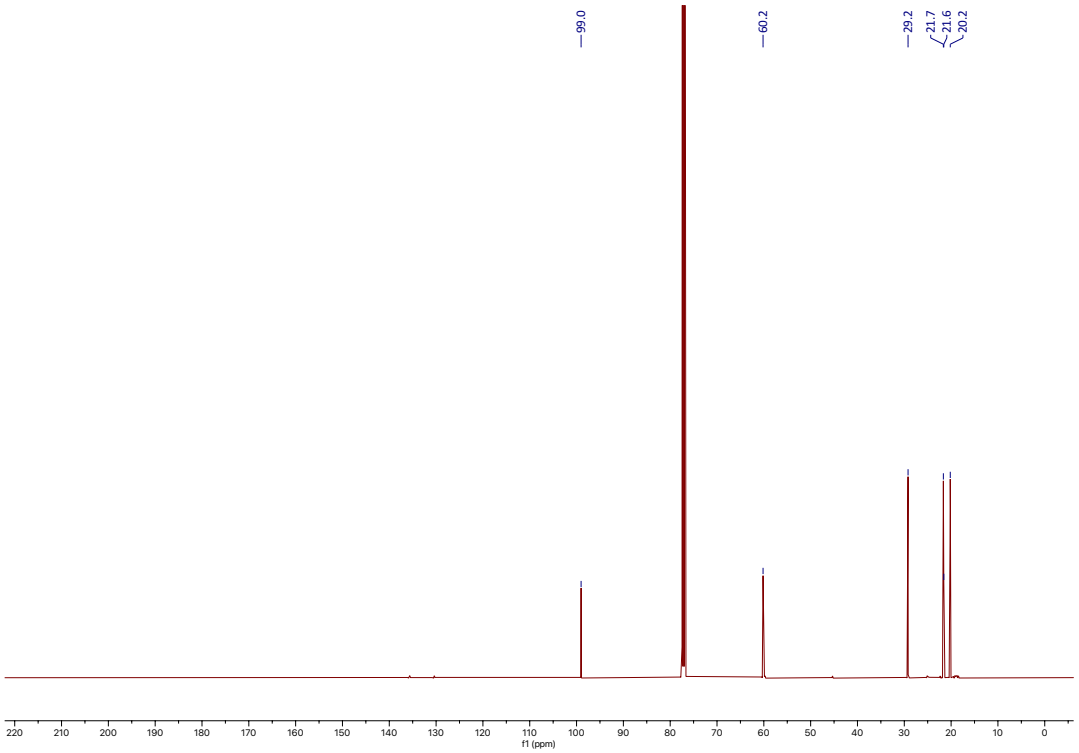
99.0
60.2
29.2
21.7
21.6
20.2
f1 (ppm)

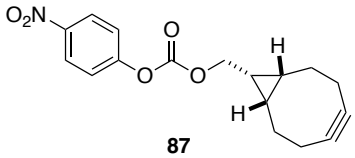
O2N
O
O
O
H
H

87

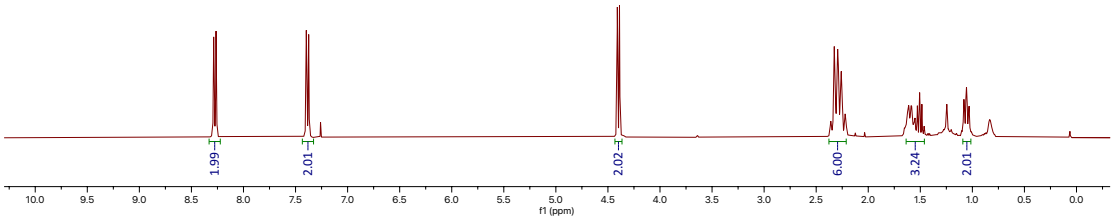
1.99
2.01
2.02
6.00
3.24
2.01
f1 (ppm)


155.7
152.7
145.5
125.4
121.9
98.8
68.1
29.2
21.5
20.6
17.4

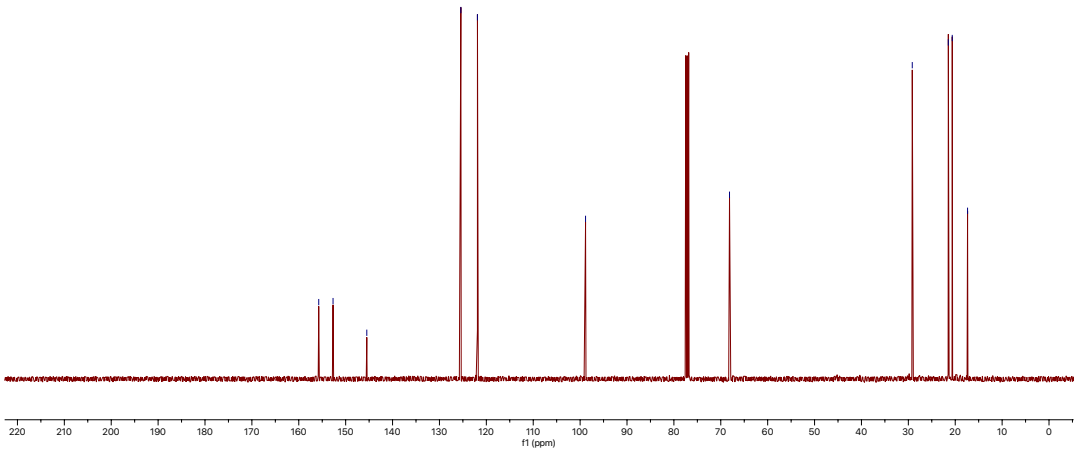
f1 (ppm)

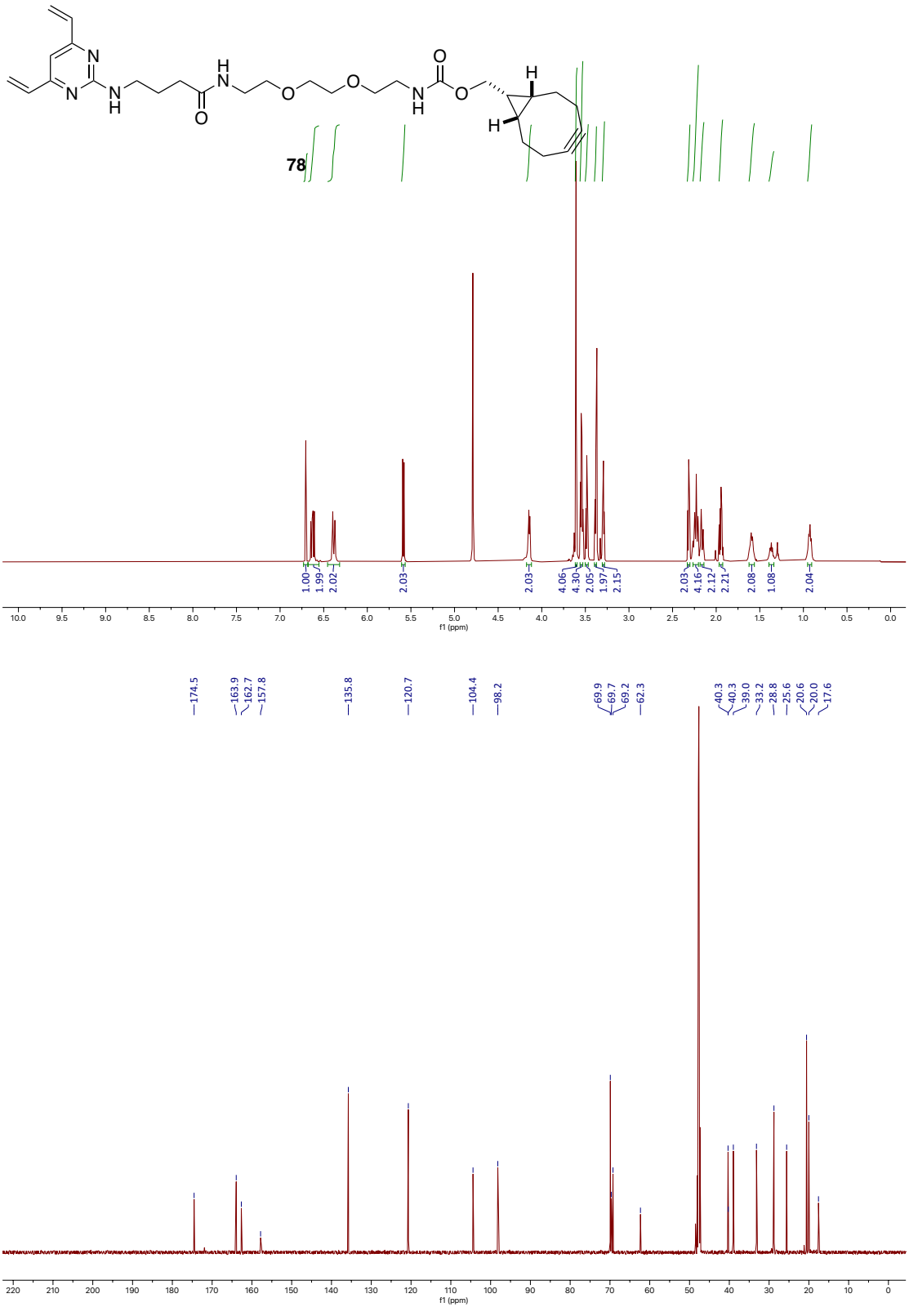
78
1.00
1.99
2.02
2.03
2.03
4.06
4.30
2.05
1.97
2.15
2.03
4.16
2.12
2.21
2.08
1.08
2.04
f1 (ppm)
174.5
163.9
162.7
157.8
135.8
120.7
104.4
98.2
69.9
69.7
69.2
62.3
40.3
40.3
39.0
33.2
28.8
25.6
20.6
20.0
17.6
f1 (ppm)

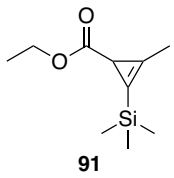
O
O
Si

91

1.99
3.01
0.94
3.08
9.02
f1 (ppm)

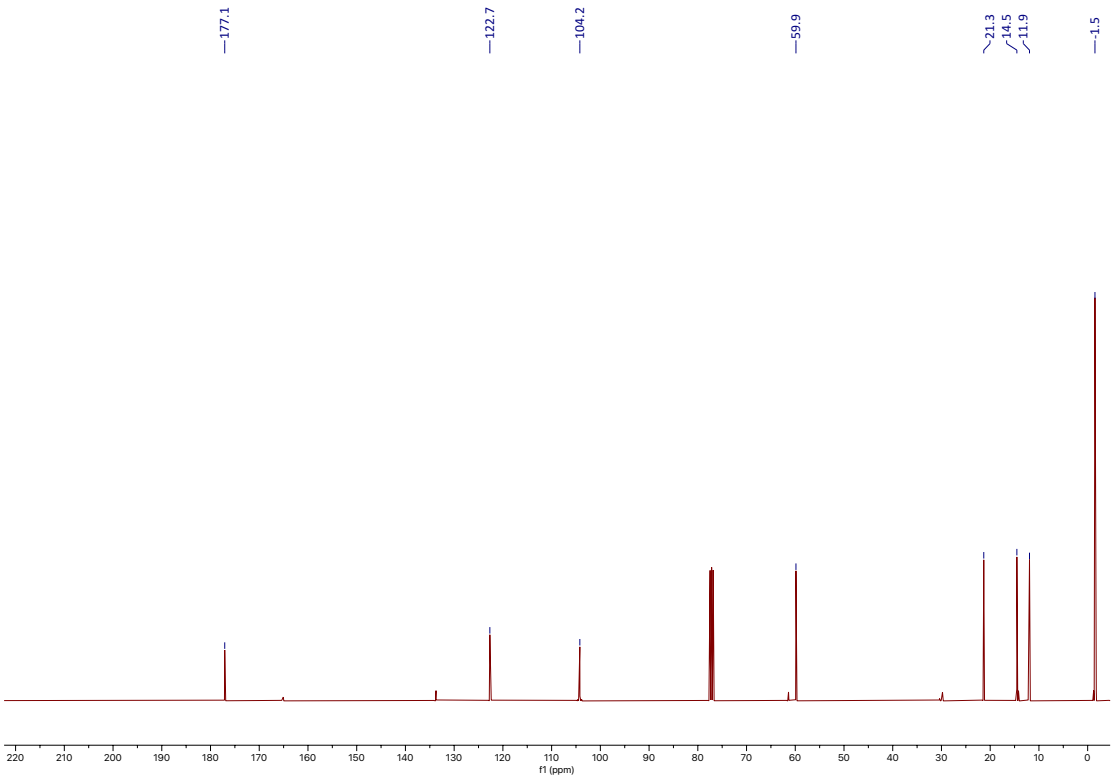
177.1
122.7
104.2
59.9
21.3
14.5
11.9
-1.5
f1 (ppm)

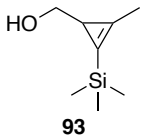

93

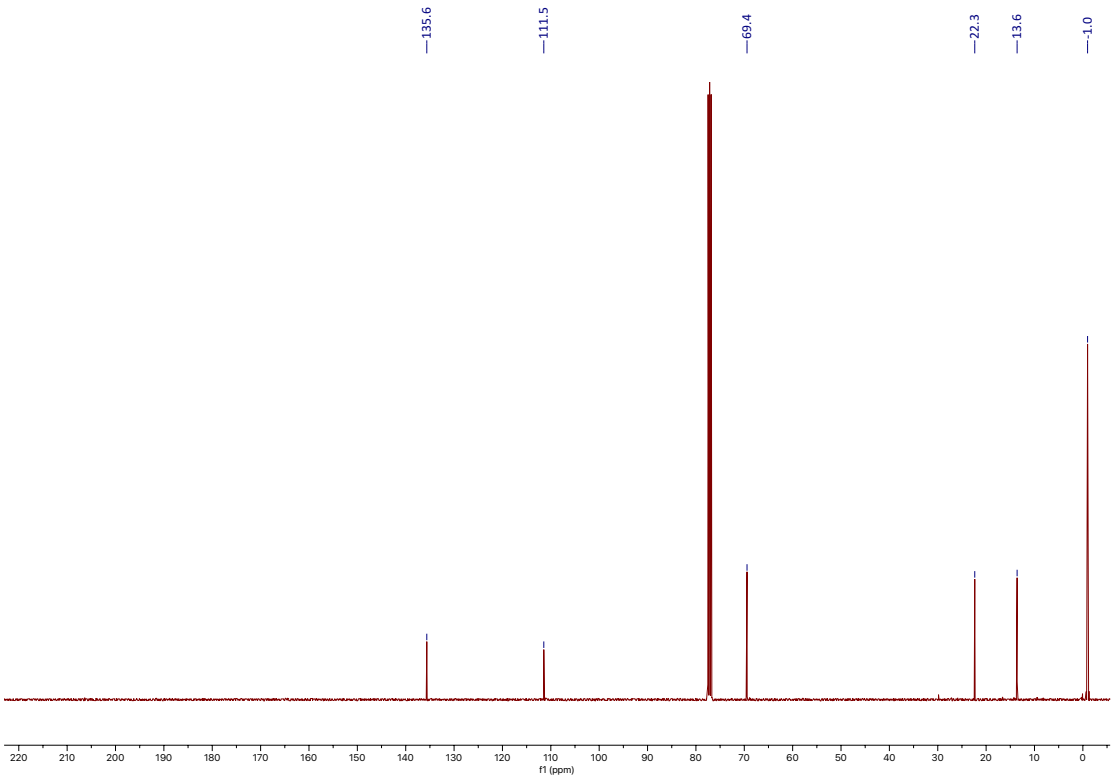

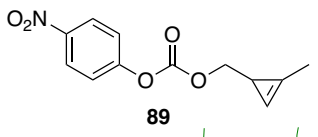

89

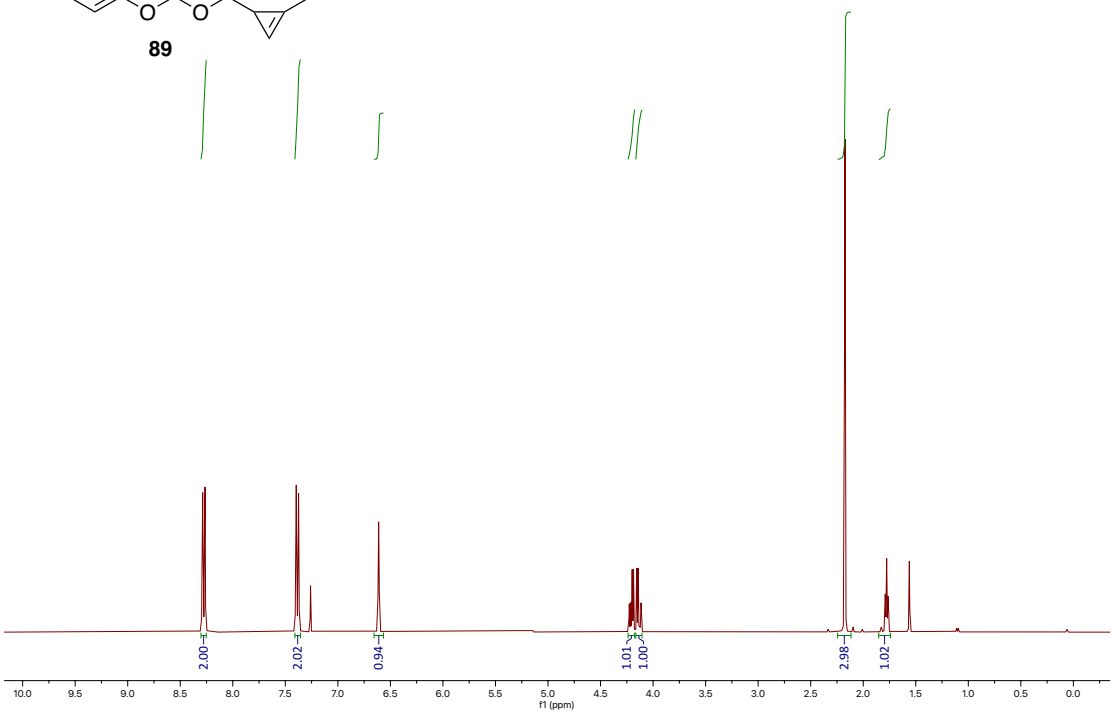
2.00
2.02
0.94
1.01
1.00
2.98
1.02
f1 (ppm)

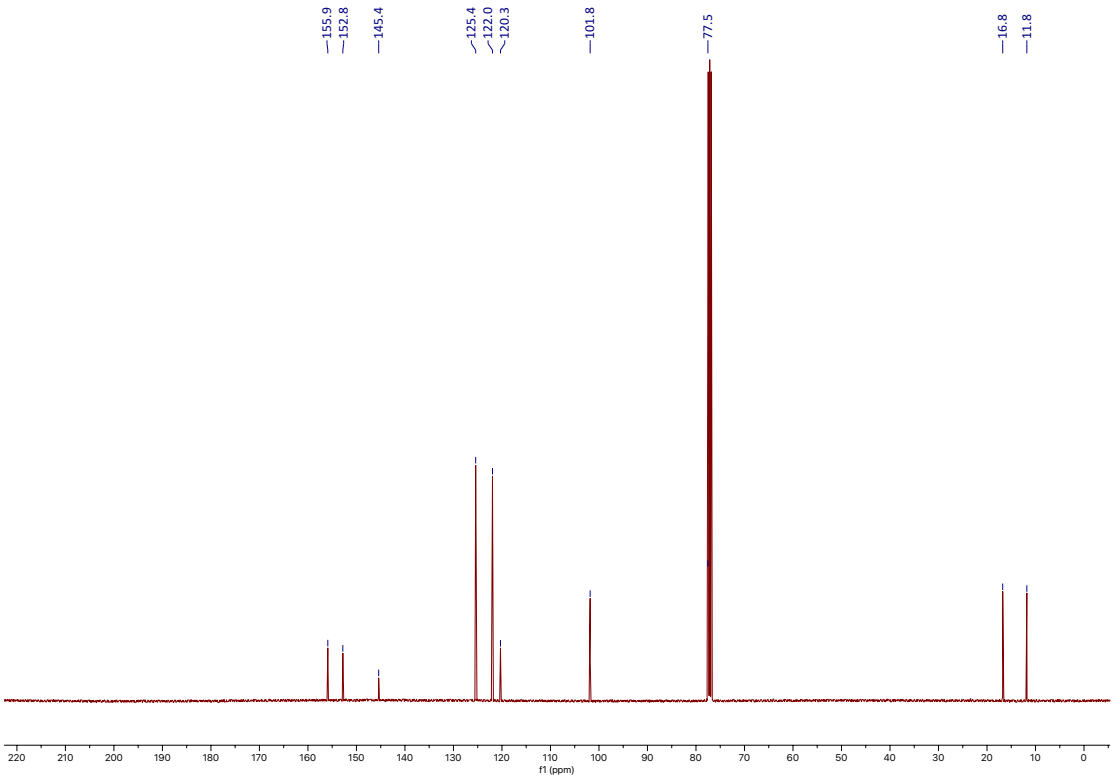
155.9
152.8
145.4
125.4
122.0
120.3
101.8
77.5
16.8
11.8
f1 (ppm)

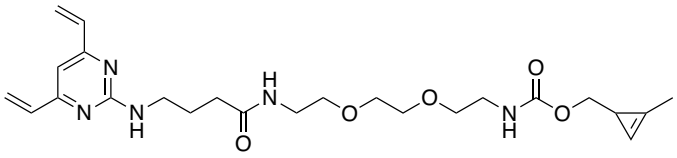

79

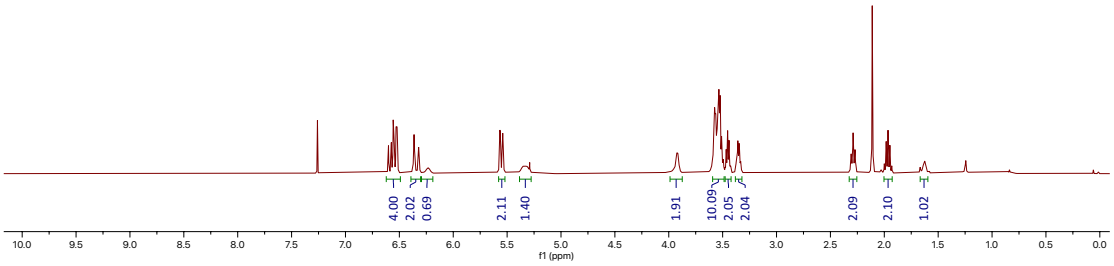
4.00
2.02
0.69
2.11
1.40
1.91
10.09
2.05
2.04
2.09
2.10
1.02
f1 (ppm)

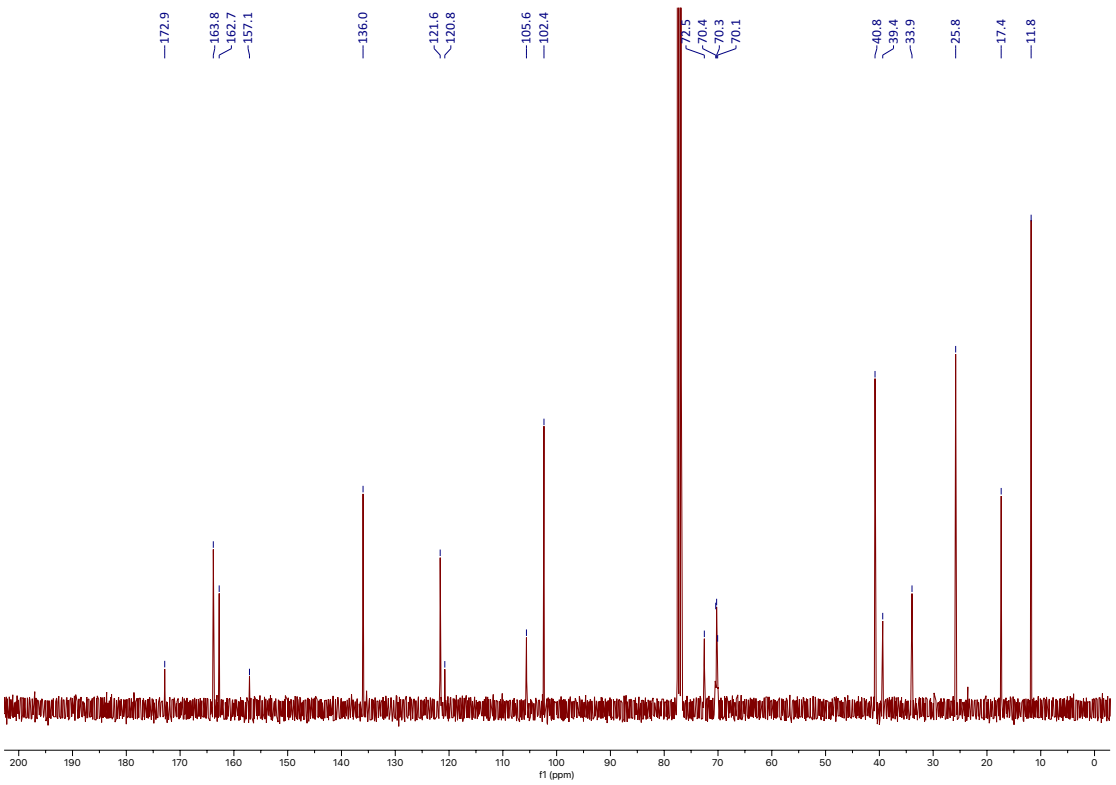
172.9
163.8
162.7
157.1
136.0
121.6
120.8
105.6
102.4
72.5
70.4
70.3
70.1
40.8
39.4
33.9
25.8
17.4
11.8
f1 (ppm)

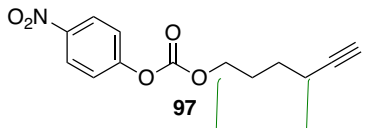
O_2N
O
O
O

97

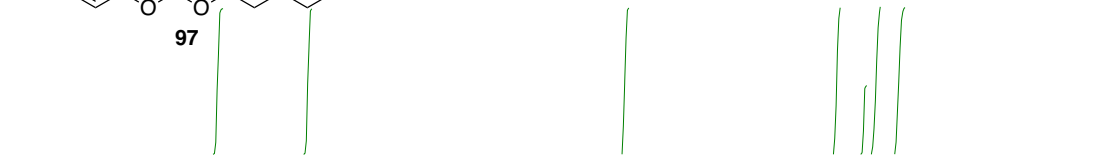

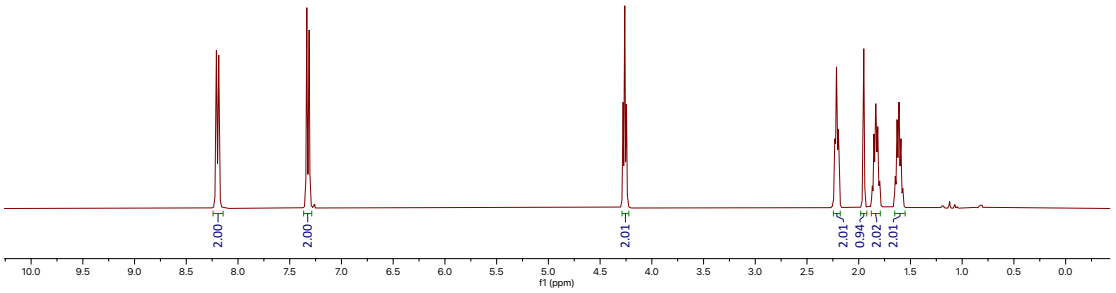
2.00
2.00
2.01
2.01
0.94
2.02
2.01
10.0 9.5 9.0 8.5 8.0 7.5 7.0 6.5 6.0 5.5 5.0 4.5 4.0 3.5 3.0 2.5 2.0 1.5 1.0 0.5 0.0
f1 (ppm)


155.5
152.4
145.3
125.2
121.7
83.5
69.0
68.9
27.4
24.5
17.9

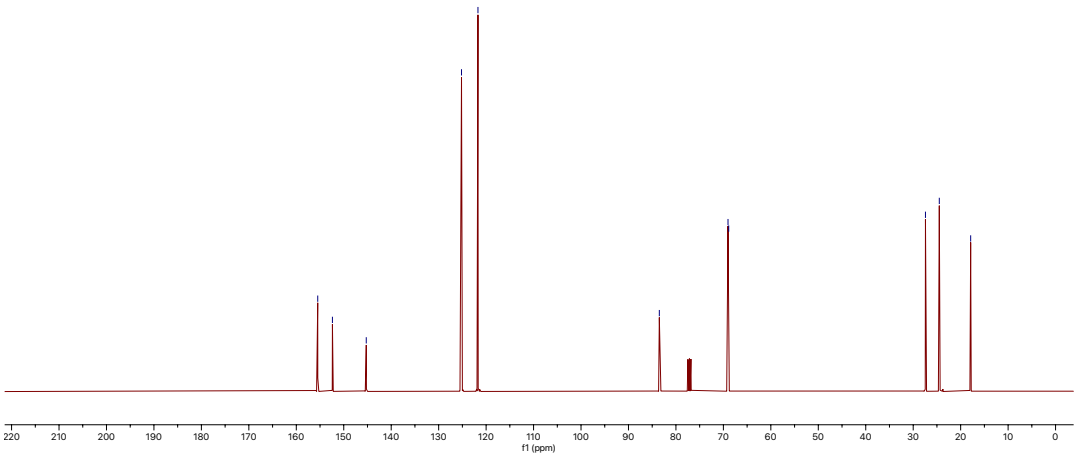
220 210 200 190 180 170 160 150 140 130 120 110 100 90 80 70 60 50 40 30 20 10 0
f1 (ppm)

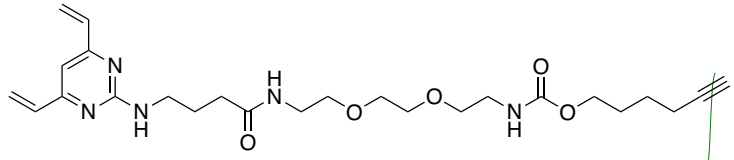

95

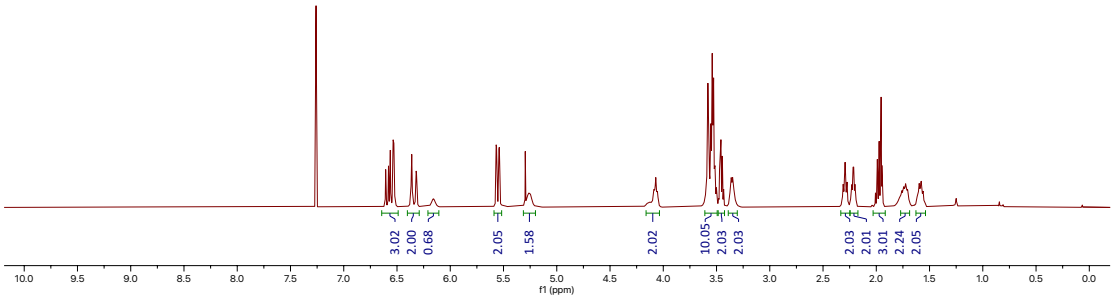
3.02
2.00
0.68
2.05
1.58
2.02
10.05
2.03
2.03
2.03
2.01
3.01
2.24
2.05
f1 (ppm)

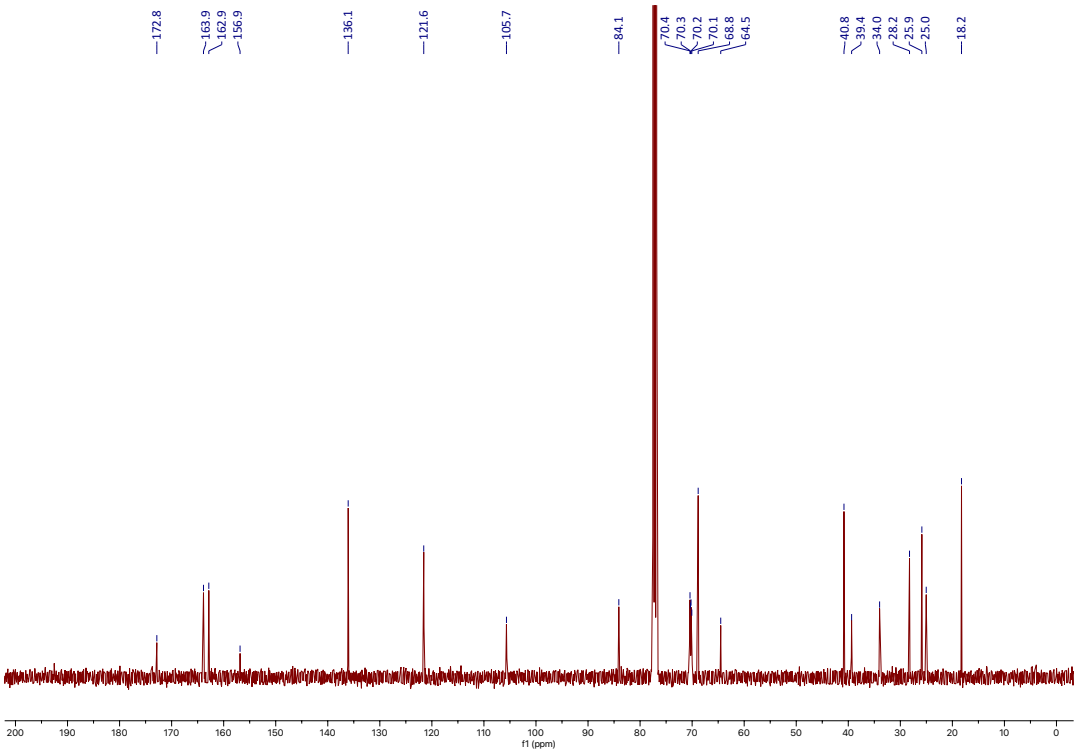
172.8
163.9
162.9
156.9
136.1
121.6
105.7
84.1
70.4
70.3
70.2
70.1
68.8
64.5
40.8
39.4
34.0
28.2
25.9
25.0
18.2
f1 (ppm)

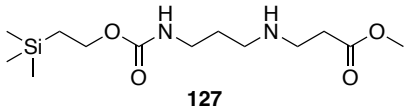

127

2.00
3.00
2.01
2.03
2.01
2.01
1.98
1.96
9.00
f1 (ppm)

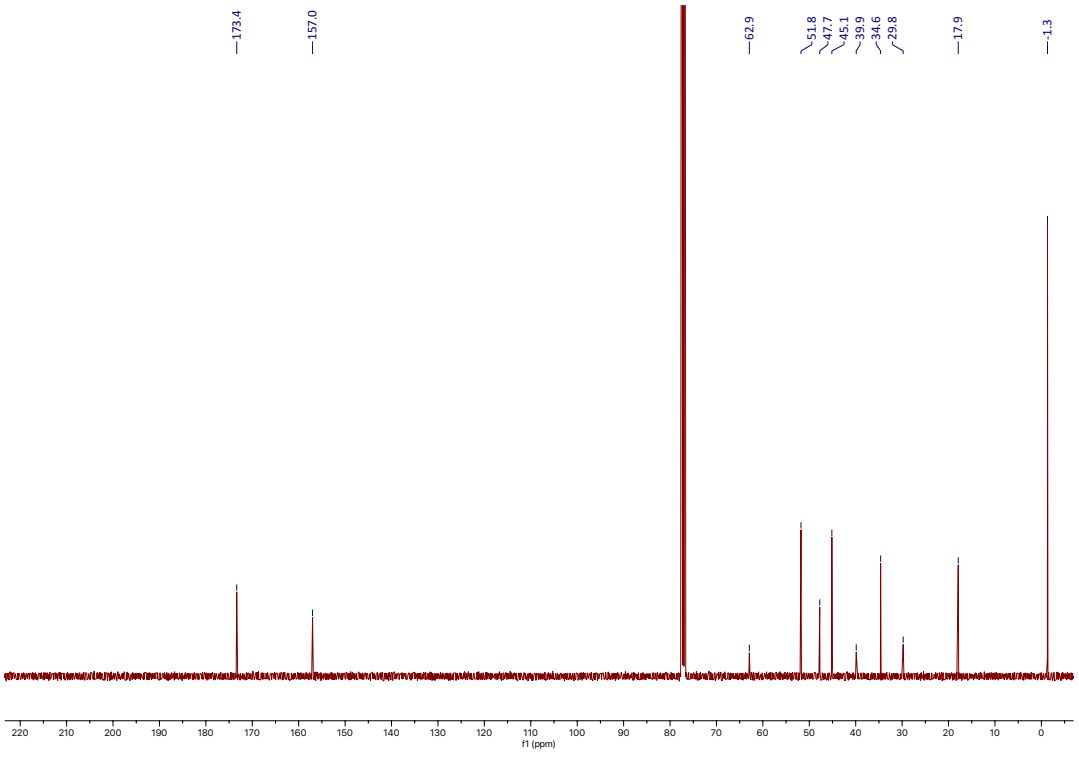
173.4
157.0
62.9
51.8
47.7
45.1
39.9
34.6
29.8
17.9
-1.3
f1 (ppm)

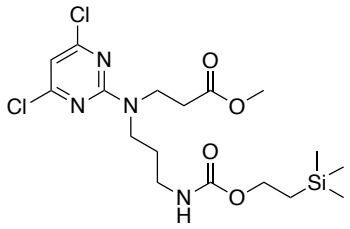

128

0.97
0.79
1.99
2.01
5.06
2.00
2.09
2.00
2.02
9.10
f1 (ppm)

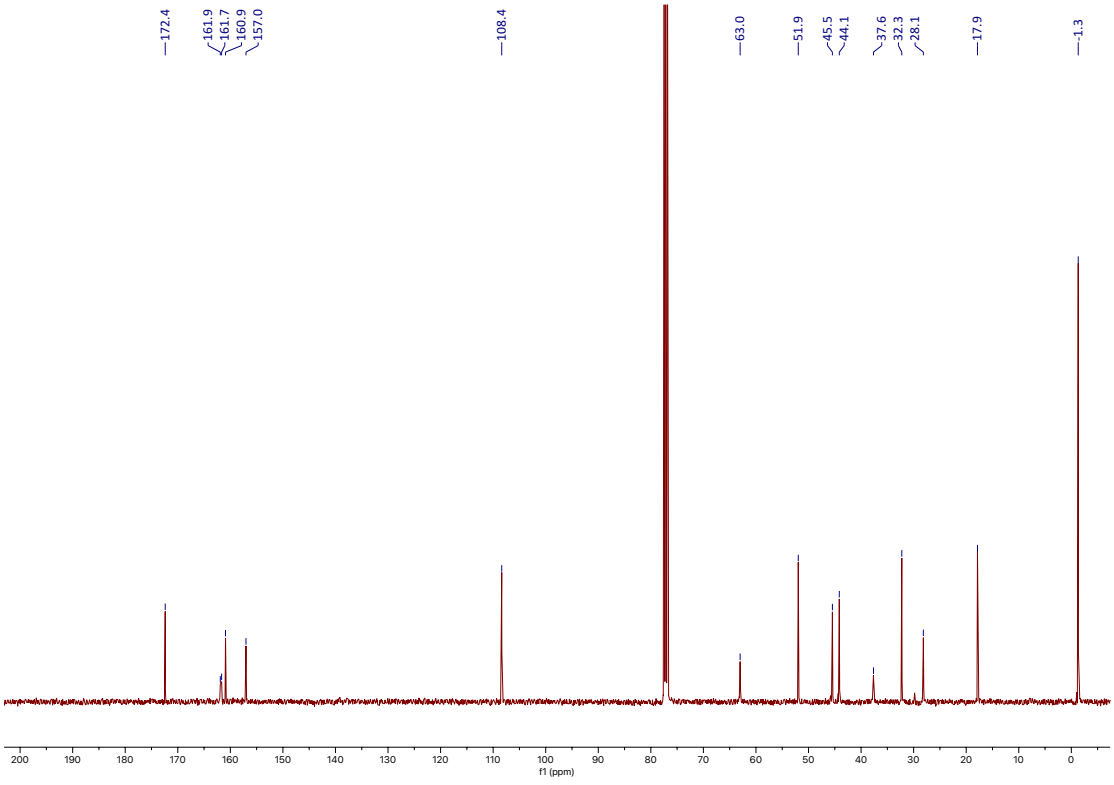
172.4
161.9
161.7
160.9
157.0
108.4
63.0
51.9
45.5
44.1
37.6
32.3
28.1
17.9
-1.3
f1 (ppm)

129

1.97
1.00
1.90
0.74
1.95
2.04
2.02
1.96
3.03
2.01
1.96
2.13
1.98
9.19
f1 (ppm)

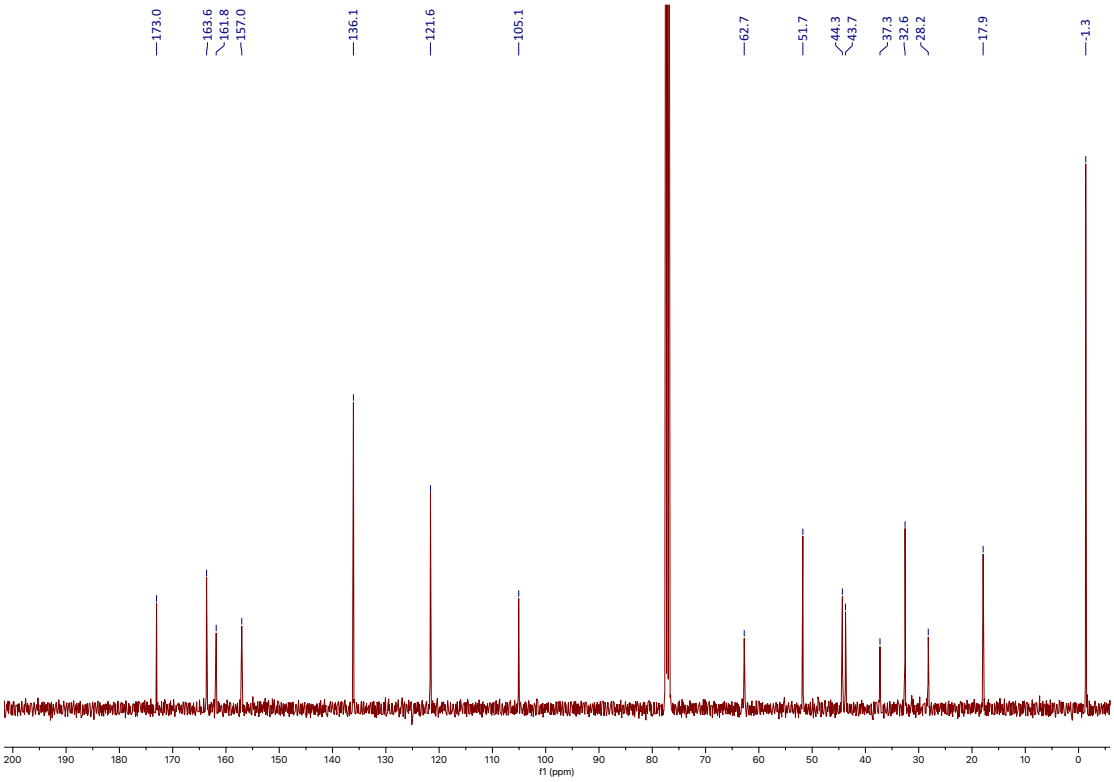
173.0
163.6
161.8
157.0
136.1
121.6
105.1
62.7
51.7
44.3
43.7
37.3
32.6
28.2
17.9
-1.3
f1 (ppm)

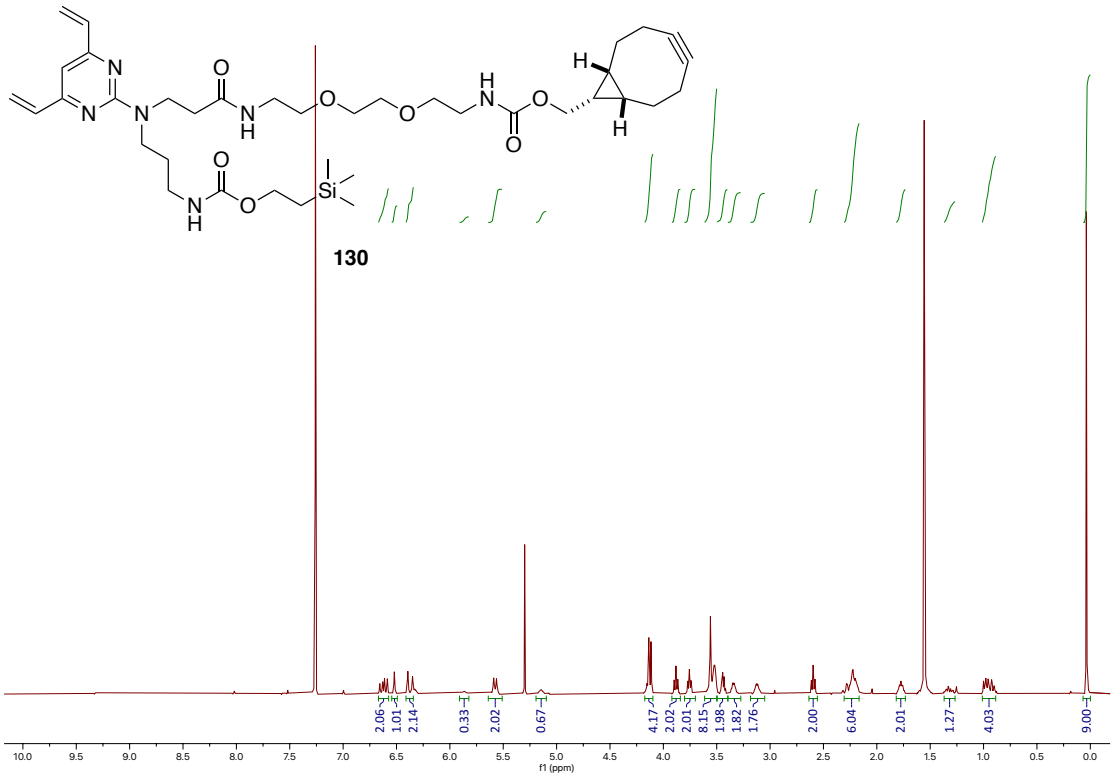
130
2.06
1.01
2.14
0.33
2.02
0.67
4.17
2.02
2.01
8.15
1.98
1.82
1.76
2.00
6.04
2.01
1.27
4.03
9.00
f1 (ppm)

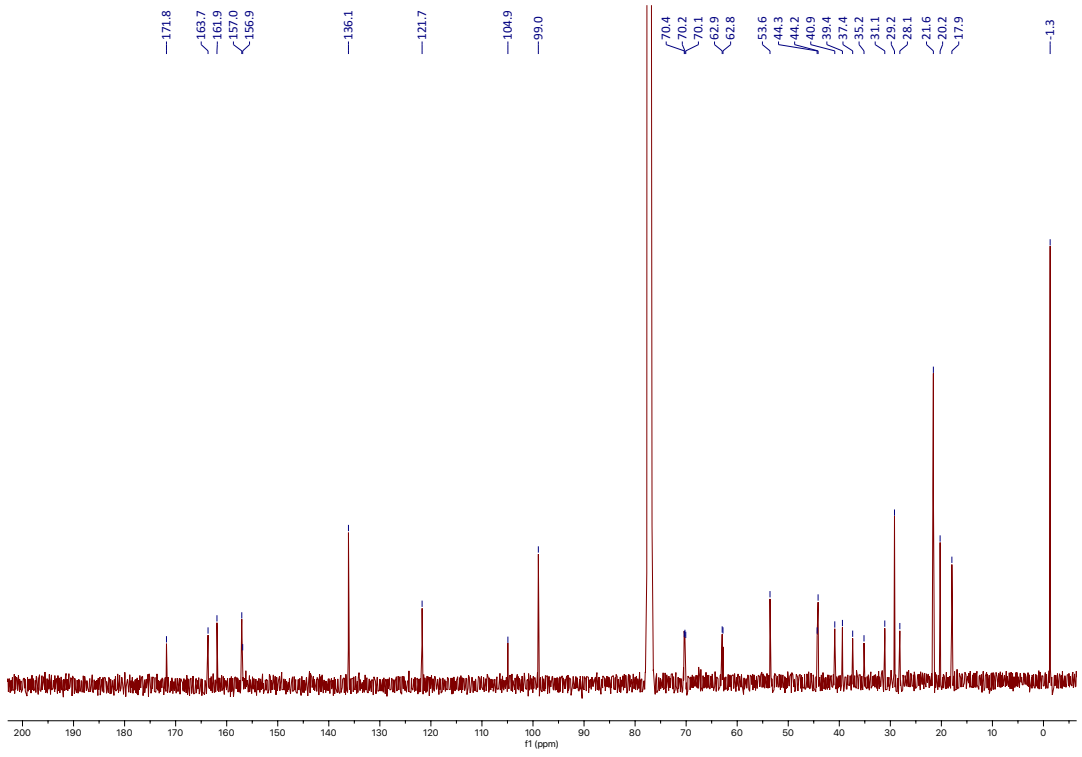
171.8
163.7
161.9
157.0
156.9
136.1
121.7
104.9
99.0
70.4
70.2
70.1
62.9
62.8
53.6
44.3
44.2
40.9
39.4
37.4
35.2
31.1
29.2
28.1
21.6
20.2
17.9
-1.3
f1 (ppm)

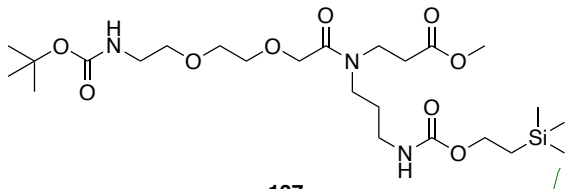

137

4.08
11.06
4.10
0.87
1.20
2.04
2.16
8.94
2.01
9.03
f1 (ppm)

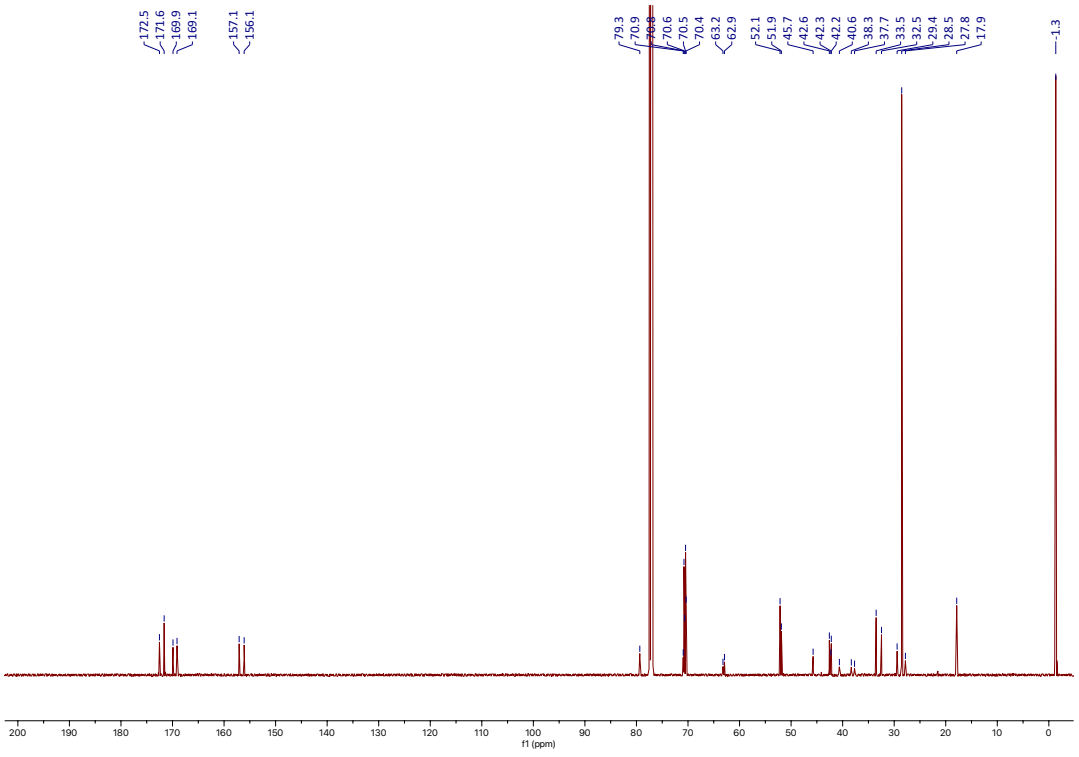
172.5
171.6
169.9
169.1
157.1
156.1
79.3
70.9
70.6
70.5
70.4
63.2
62.9
52.1
51.9
45.7
42.6
42.3
42.2
40.6
38.3
37.7
33.5
32.5
29.4
28.5
27.8
17.9
-1.3
f1 (ppm)

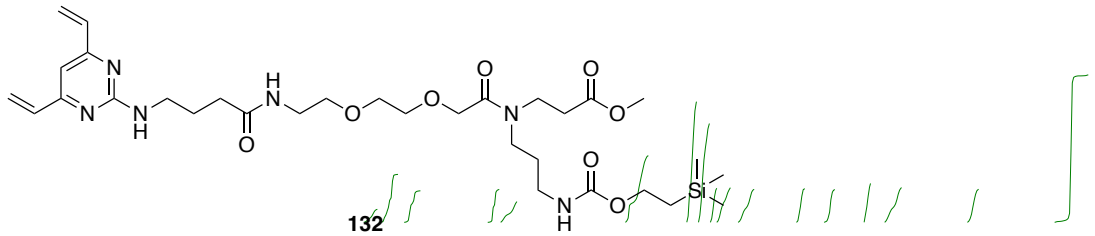

132

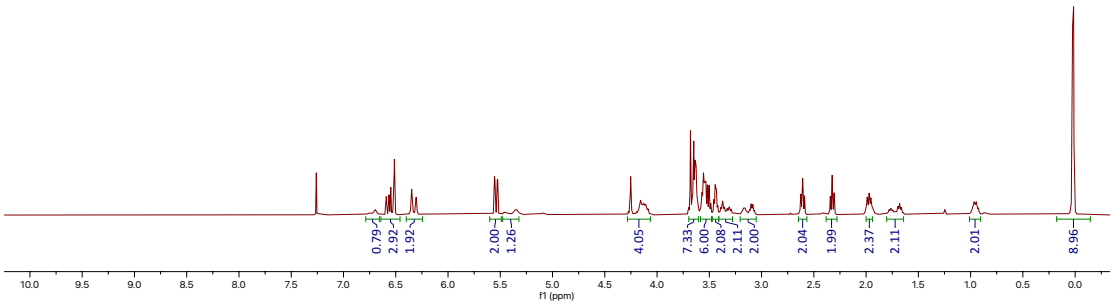
0.79
2.92
1.92
2.00
1.26
4.05
7.33
6.00
2.08
2.11
2.00
2.04
1.99
2.37
2.11
2.01
8.96
f1 (ppm)

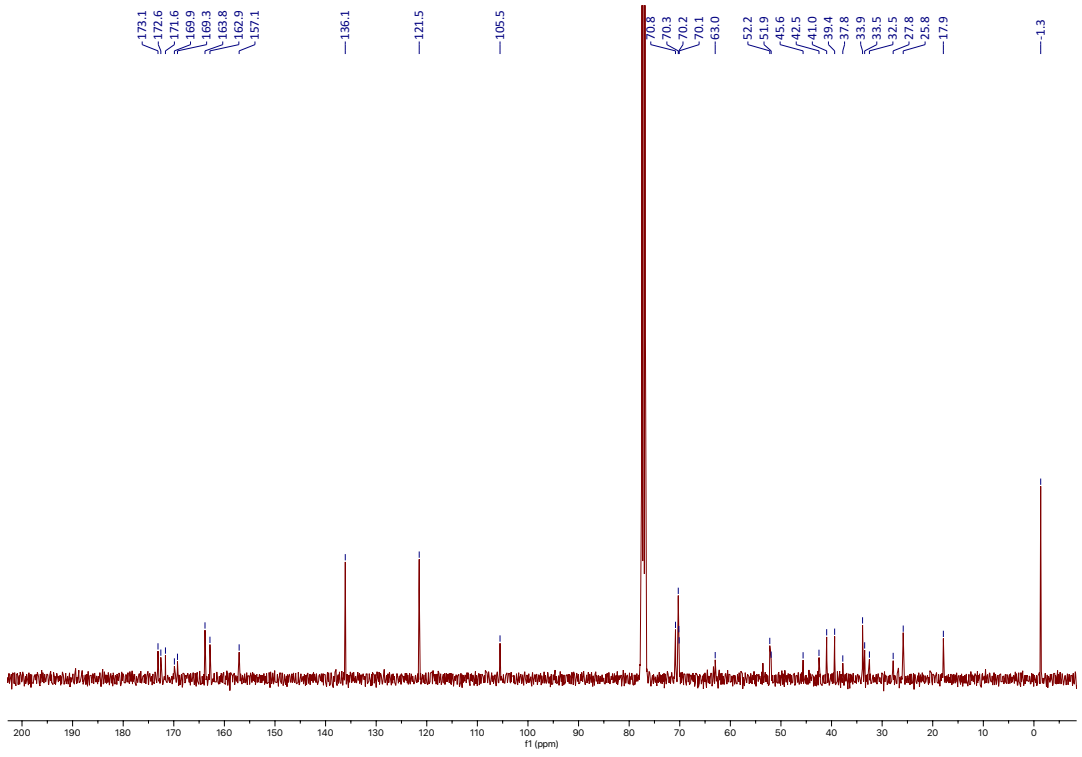
173.1
172.6
171.6
169.9
169.3
163.8
162.9
157.1
136.1
121.5
105.5
70.8
70.3
70.2
70.1
63.0
52.2
51.9
45.6
42.5
41.0
39.4
37.8
33.9
33.5
32.5
27.8
25.8
17.9
-1.3
f1 (ppm)

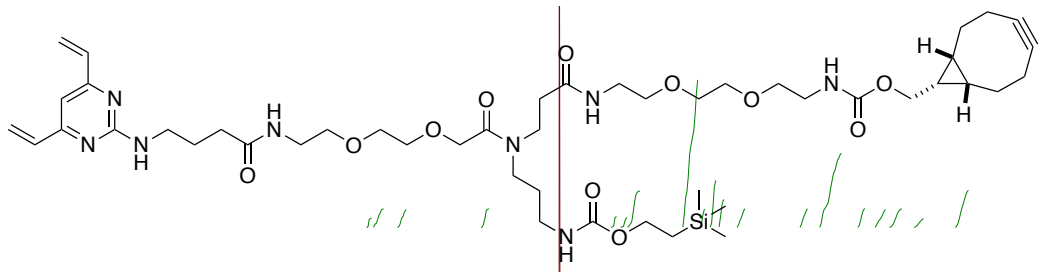

135

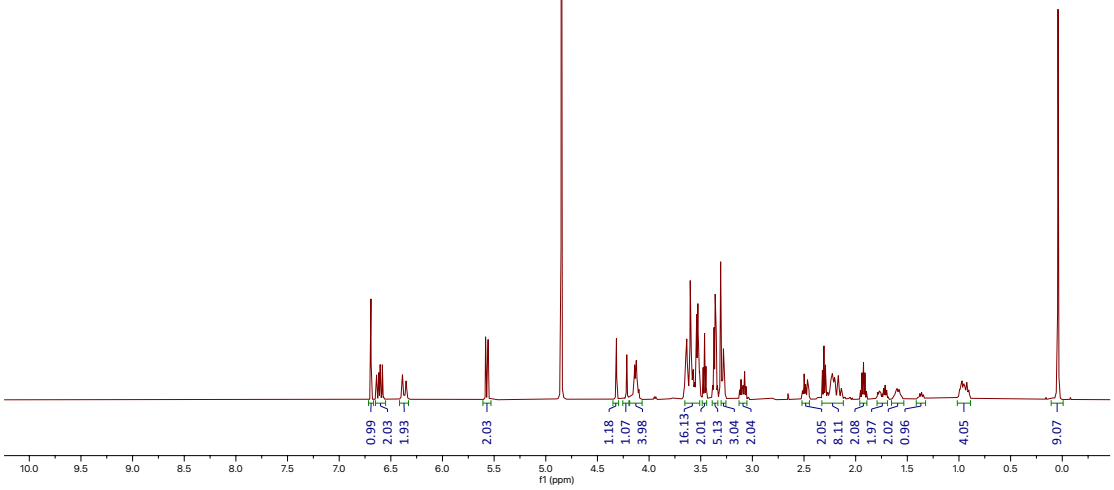
0.99
2.03
1.93
2.03
1.18
1.07
3.98
16.13
2.01
5.13
3.04
2.04
2.05
8.11
2.08
1.97
2.02
0.96
4.05
9.07
f1 (ppm)

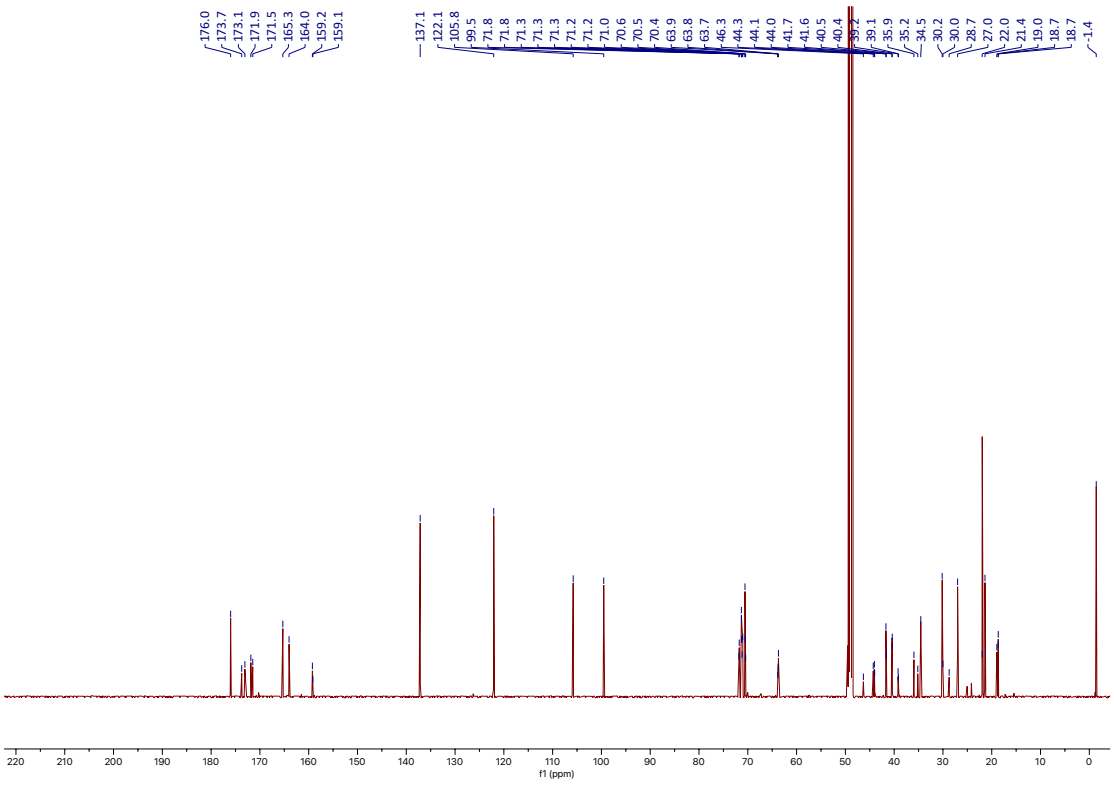
176.0
173.7
173.1
171.9
171.5
165.3
164.0
159.2
159.1
137.1
122.1
105.8
99.5
71.8
71.8
71.3
71.3
71.3
71.2
71.2
71.0
70.6
70.5
70.4
63.9
63.8
63.7
46.3
44.3
44.1
44.0
41.7
41.6
40.5
40.4
39.2
39.1
35.9
35.2
34.5
30.2
30.0
28.7
27.0
22.0
21.4
19.0
18.7
18.7
-1.4
f1 (ppm)

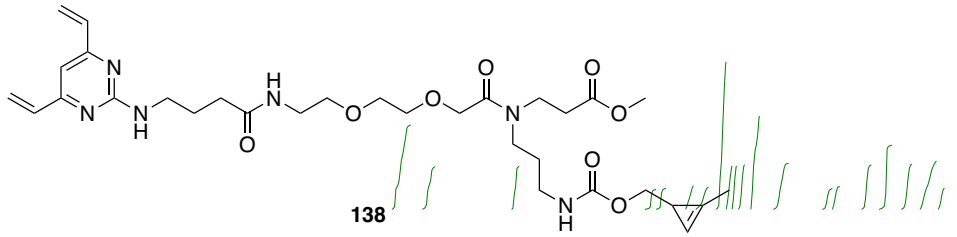

138

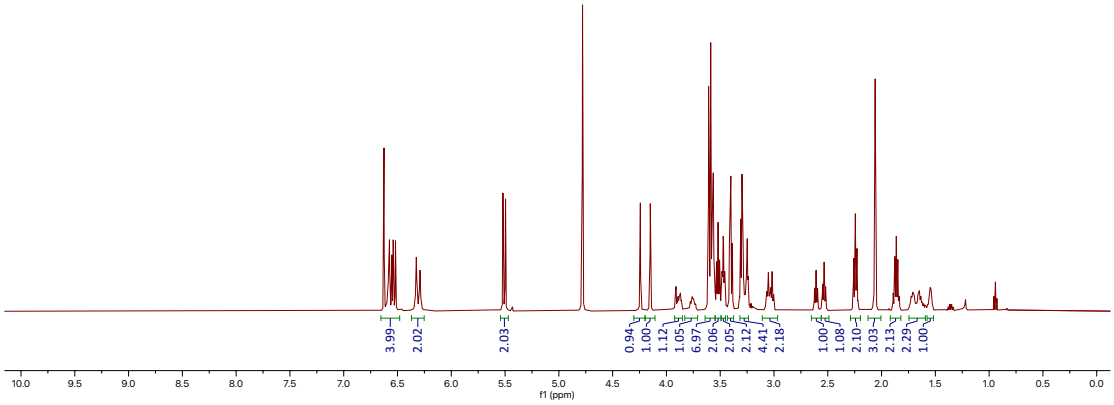
3.99
2.02
2.03
0.94
1.00
1.12
1.05
6.97
2.06
2.05
2.12
4.41
2.18
1.00
1.08
2.10
3.03
2.13
2.29
1.00
f1 (ppm)

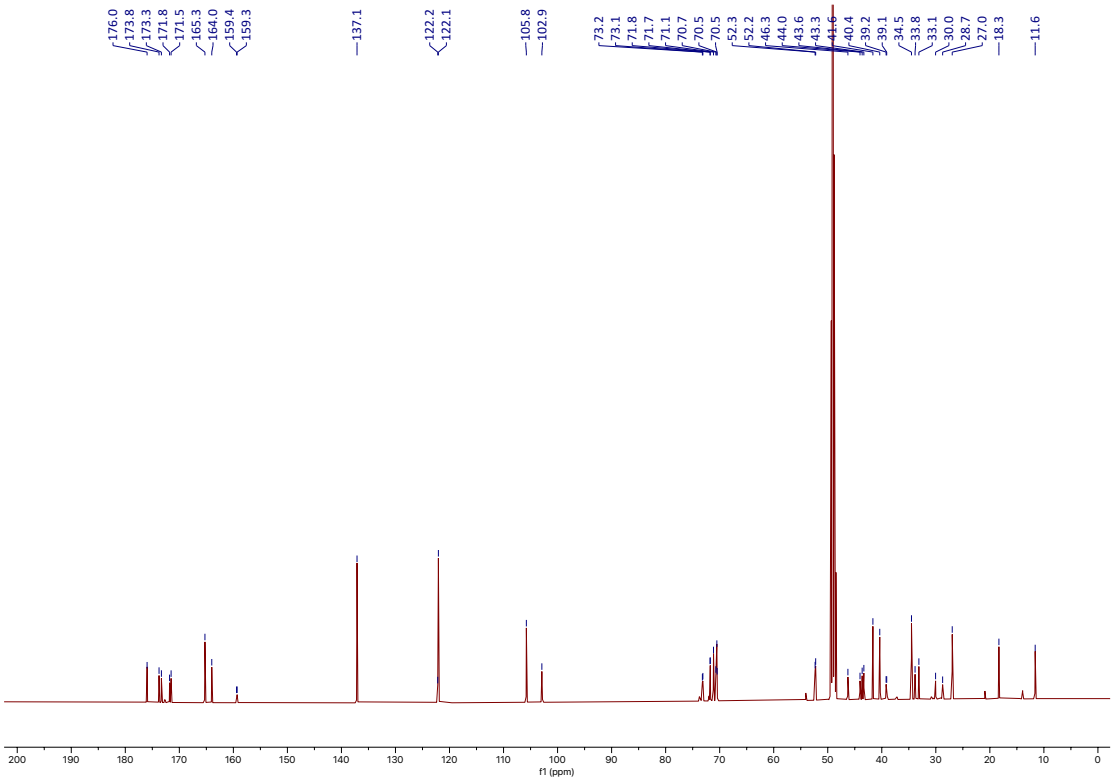
176.0
173.8
173.3
171.8
171.5
165.3
164.0
159.4
159.3
137.1
122.2
122.1
105.8
102.9
73.2
73.1
71.8
71.7
71.1
70.7
70.5
70.5
52.3
52.2
46.3
44.0
43.6
43.3
41.6
40.4
39.2
39.1
34.5
33.8
33.1
30.0
28.7
27.0
18.3
11.6
f1 (ppm)

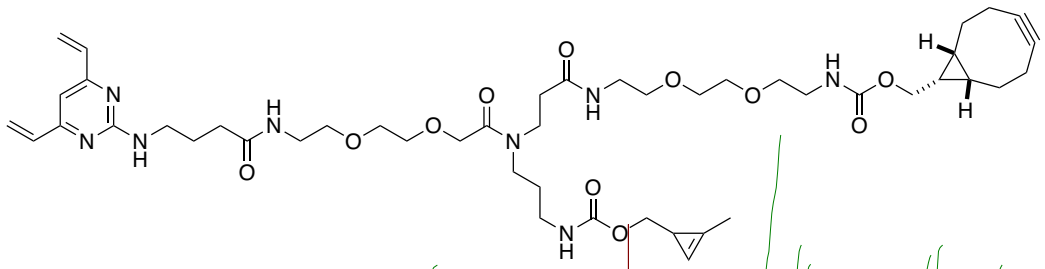

131

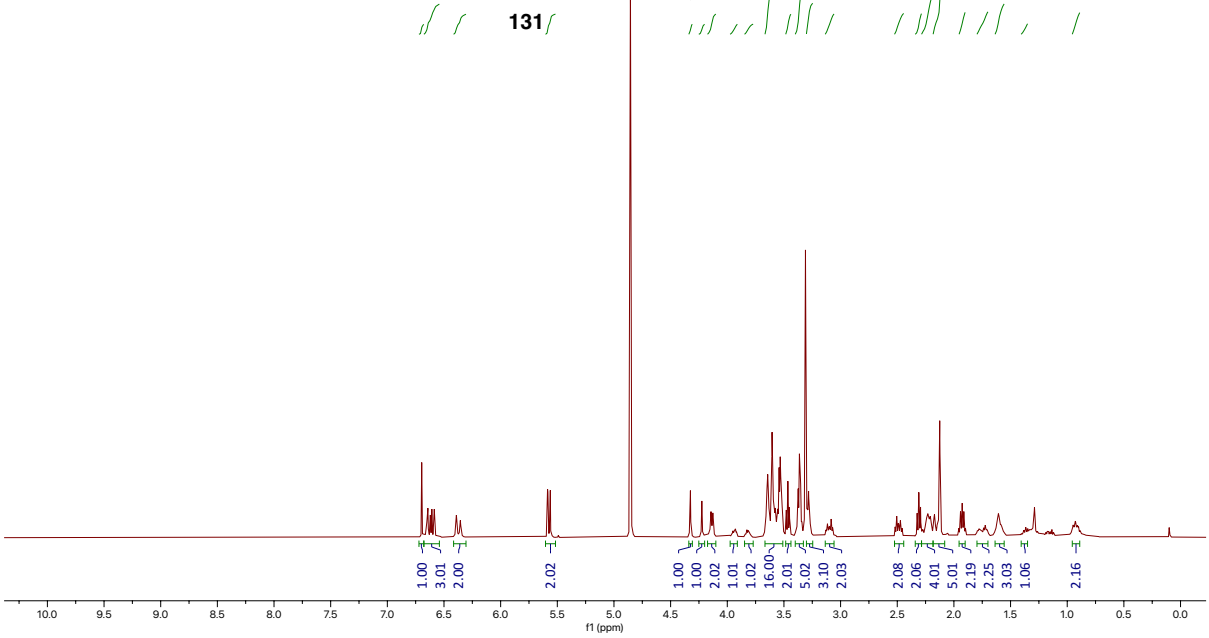
1.00
3.01
2.00
2.02
1.00
1.00
2.02
1.01
1.02
16.00
2.01
5.02
3.10
2.03
2.08
2.06
4.01
5.01
2.19
2.25
3.03
1.06
2.16
f1 (ppm)

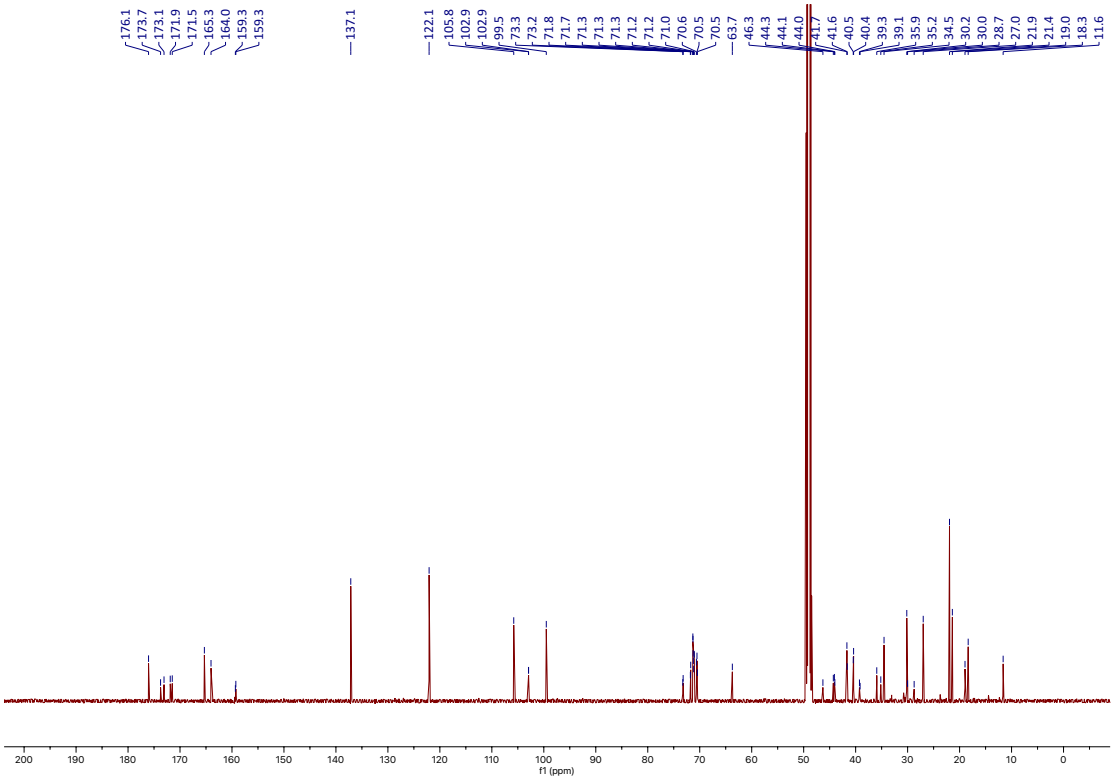
176.1
173.7
173.1
171.9
171.5
165.3
164.0
159.3
159.3
137.1
122.1
105.8
102.9
102.9
99.5
73.3
73.2
71.8
71.7
71.3
71.3
71.3
71.2
71.2
71.0
70.6
70.5
70.5
63.7
46.3
44.3
44.1
44.0
41.7
41.6
40.5
40.4
39.3
39.1
35.9
35.2
34.5
30.2
30.0
28.7
27.0
21.9
21.4
19.0
18.3
11.6
f1 (ppm)

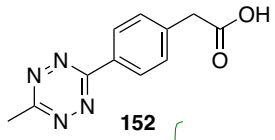
OH
O
N
N
N
N

152

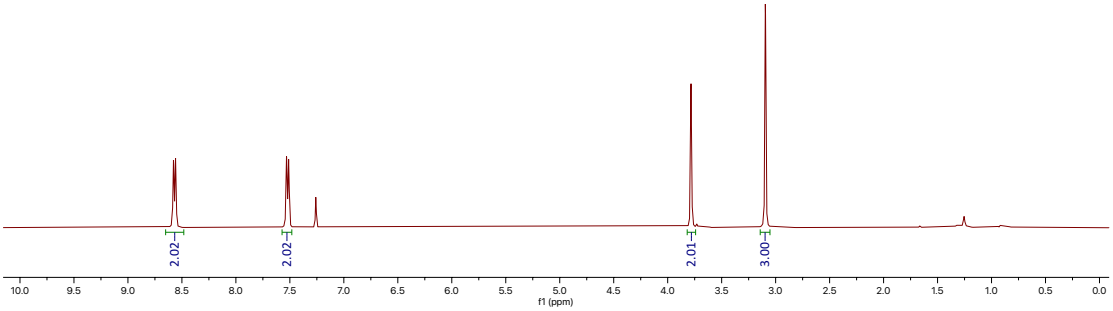
2.02
2.02
2.01
3.00
10.0 9.5 9.0 8.5 8.0 7.5 7.0 6.5 6.0 5.5 5.0 4.5 4.0 3.5 3.0 2.5 2.0 1.5 1.0 0.5 0.0
f1 (ppm)

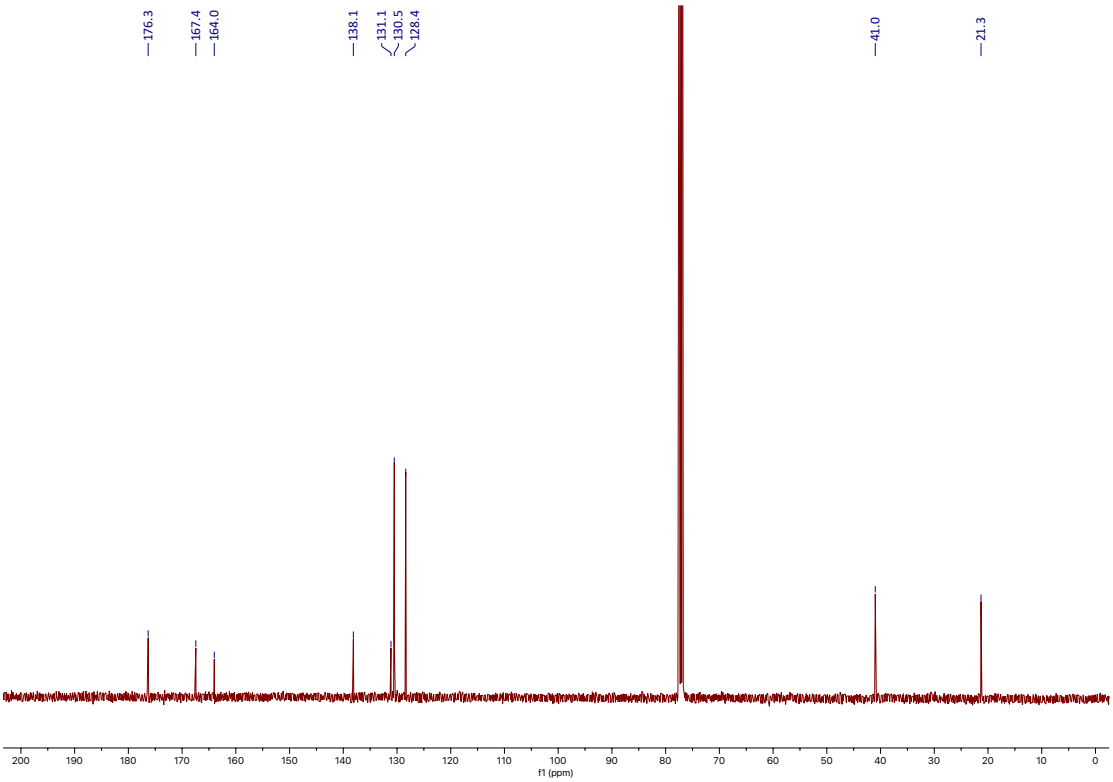
176.3
167.4
164.0
138.1
131.1
130.5
128.4
41.0
21.3
200 190 180 170 160 150 140 130 120 110 100 90 80 70 60 50 40 30 20 10 0
f1 (ppm)

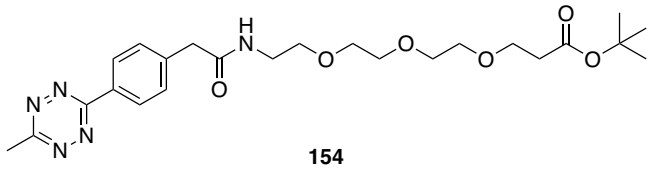

154

2.00
2.02
0.86
2.05
2.03
8.17
2.09
1.98
3.00
2.08
9.03
f1 (ppm)

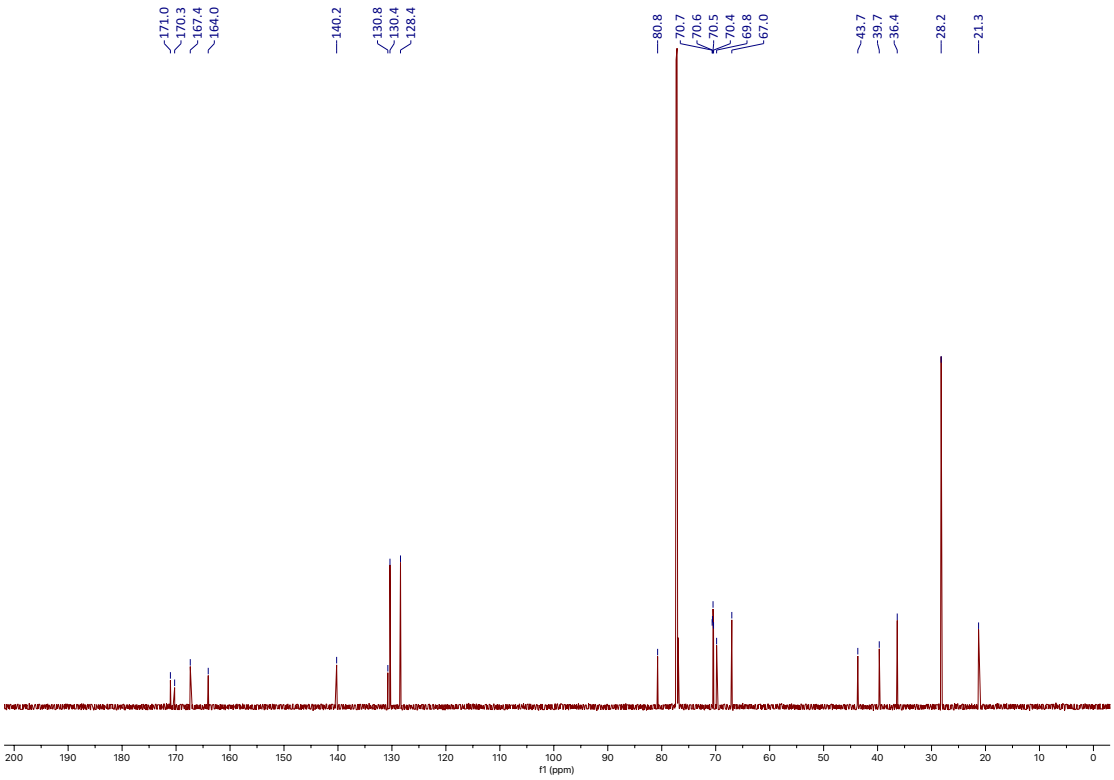
171.0
170.3
167.4
164.0
140.2
130.8
130.4
128.4
80.8
70.7
70.6
70.5
70.4
69.8
67.0
43.7
39.7
36.4
28.2
21.3
f1 (ppm)

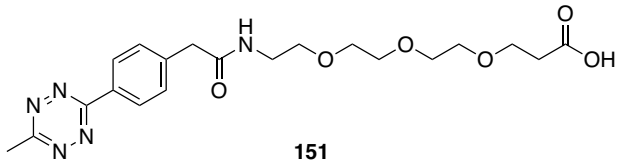
H
N
O
O
O
O
O
OH
N
N
N

151

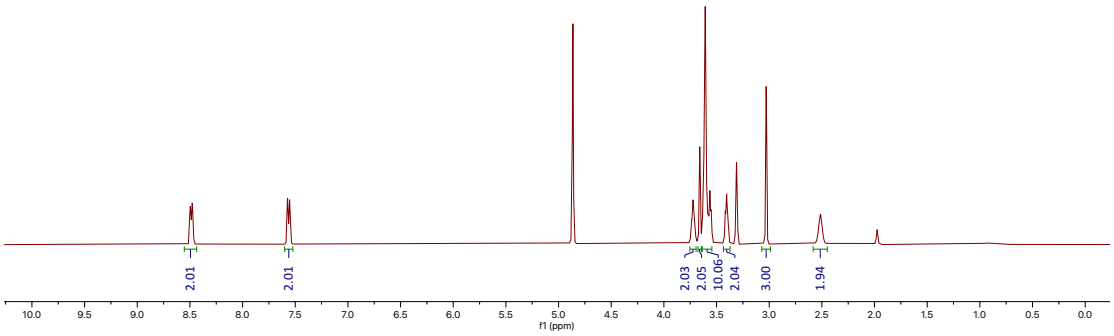
2.01
2.01
2.03
2.05
10.06
2.04
3.00
1.94
f1 (ppm)

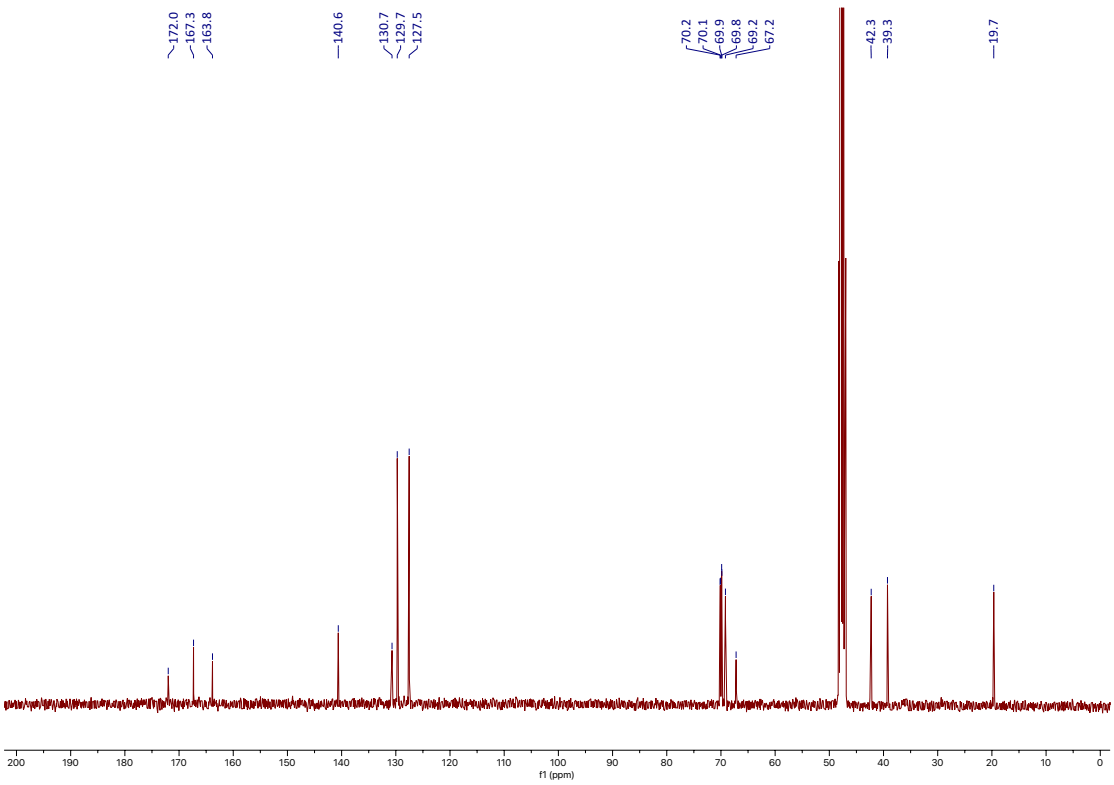
172.0
167.3
163.8
140.6
130.7
129.7
127.5
70.2
70.1
69.9
69.8
69.2
67.2
42.3
39.3
19.7
f1 (ppm)

9.3 Appendix 3: Selected Analytical HPLC Traces

Methyl 17-((4,6-divinylpyrimidin-2-yl)amino)-4-(3-((((2-methylcycloprop-2-en-1-yl)methoxy)carbonyl)amino)propyl)-5,14-dioxo-7,10-dioxa-4,13-diazaheptadecanoate (138)

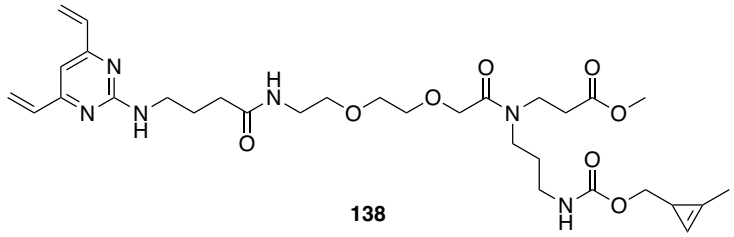

138

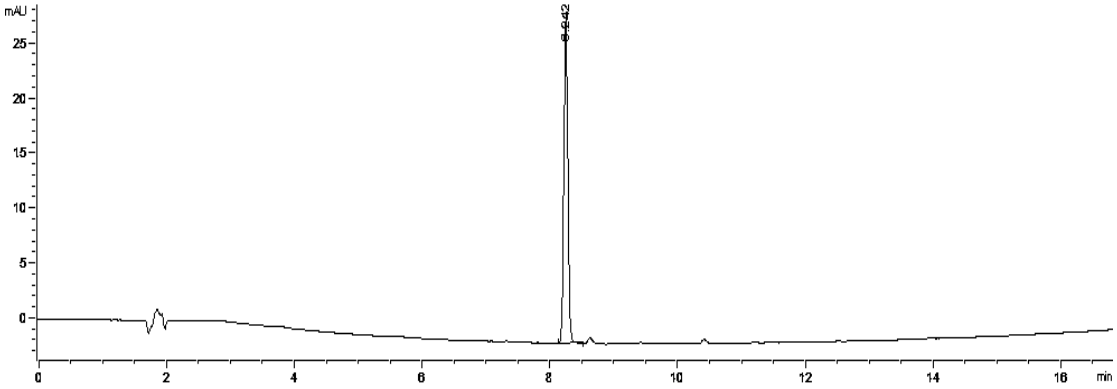

Bicyclo[6.1.0]non-4-yn-9-ylmethyl ((2-methylcycloprop-2-en-1-yl)methyl) (13-(2-(2-(2-(4-((4,6-divinylpyrimidin-2-yl)amino)butanamido)ethoxy)ethoxy)acetyl)-10-oxo-3,6-dioxa-9,13-diazahexadecane-1,16-diyl)dicarbamate (131)

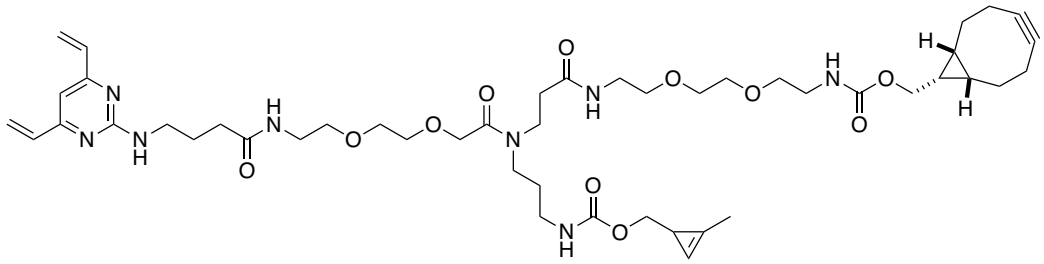

131

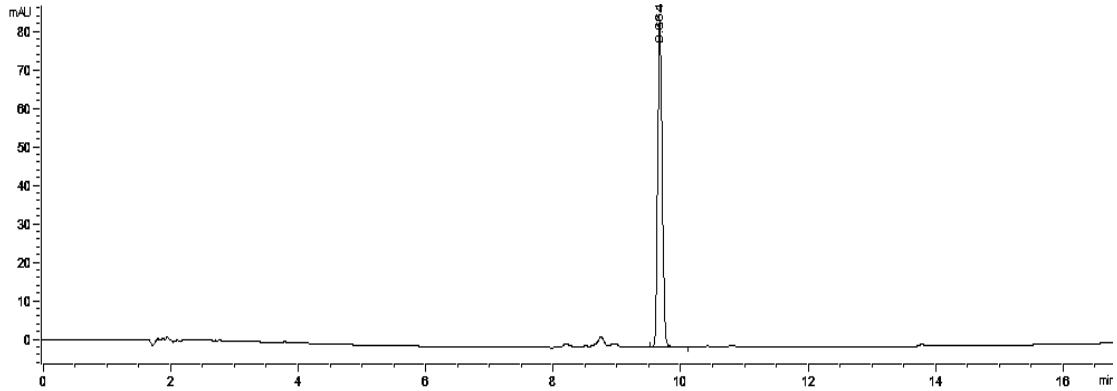

Crizotinib

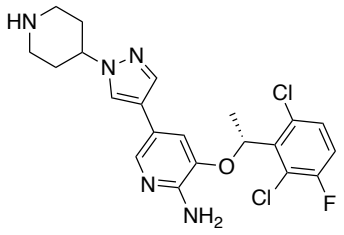

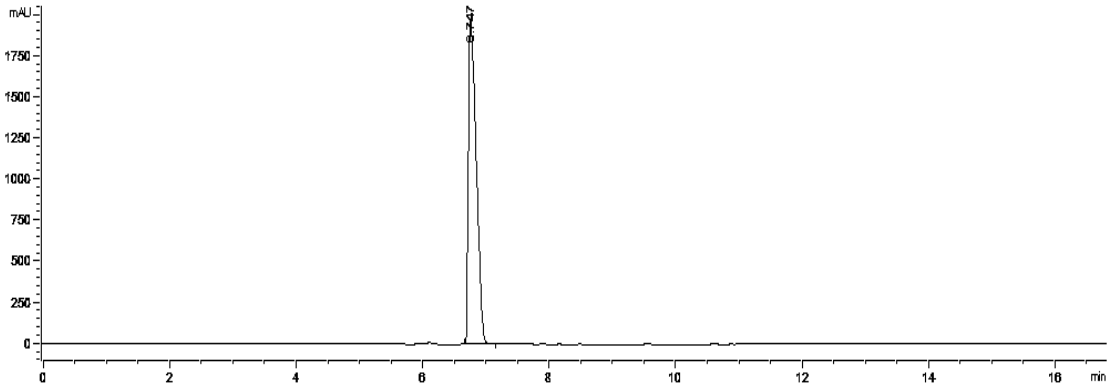

Alloc-Val-Ala-PAB-Crizotinib (149)

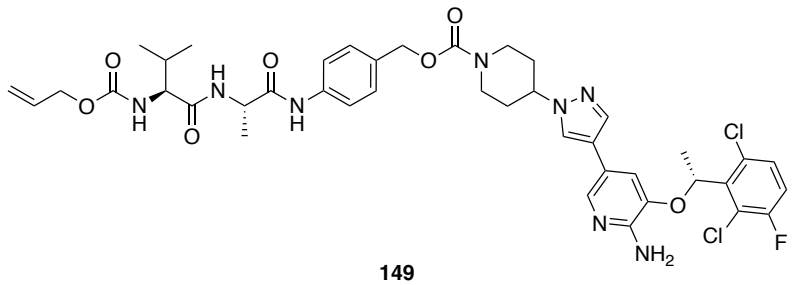

149

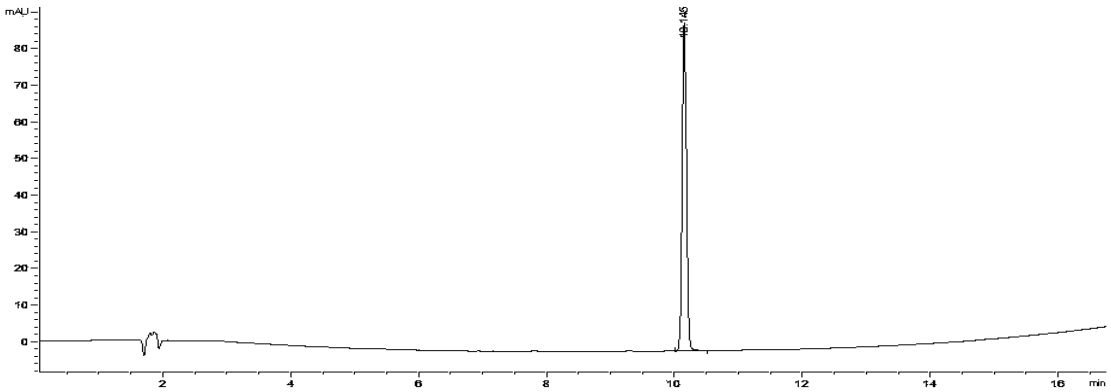

N_3-PEG$_4$-Val-Ala-PAB-Crizotinib (147)

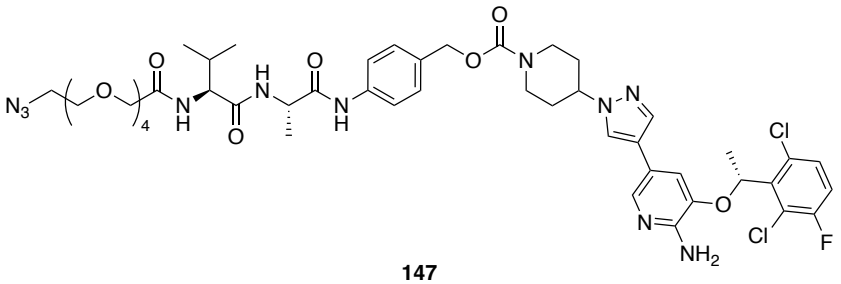

147

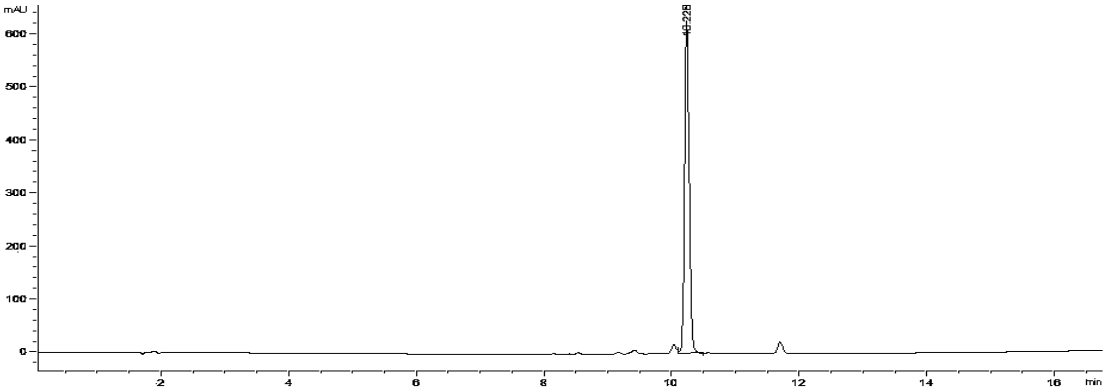

Doxorubicin

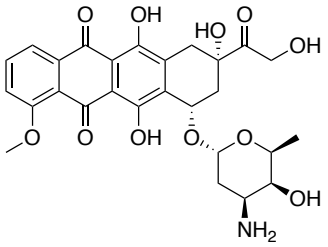

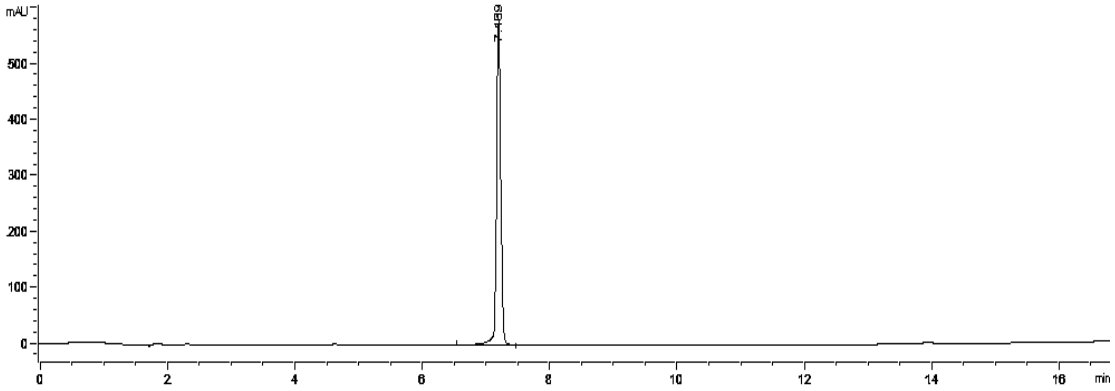

Alloc-Val-Ala-PAB-Doxorubicin (156)

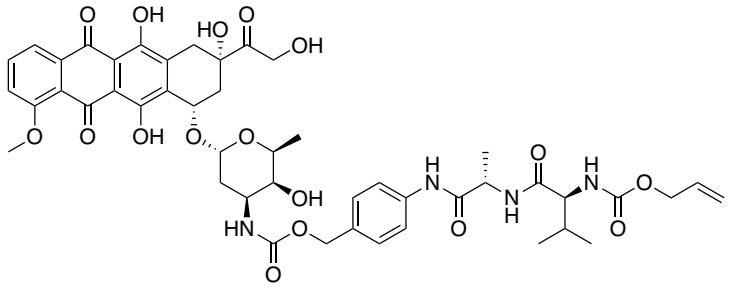

156

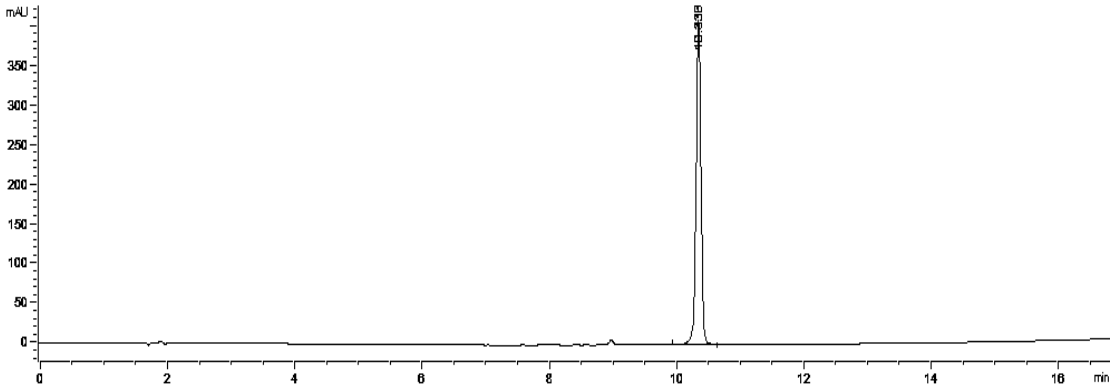

6-Methyl-Tetrazine-PEG$_3$-va-PAB-Doxorubicin (155)

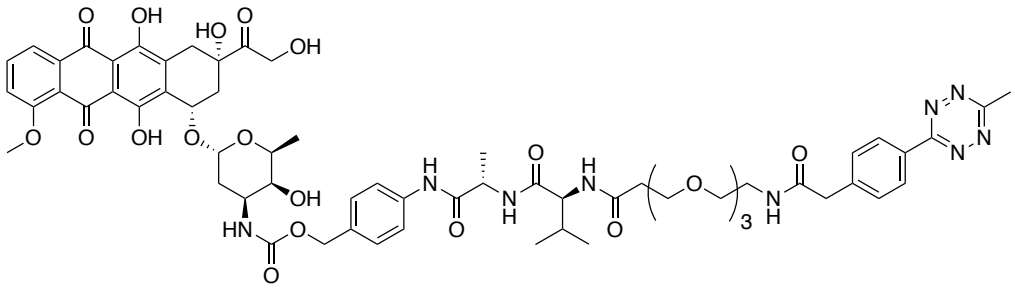

155

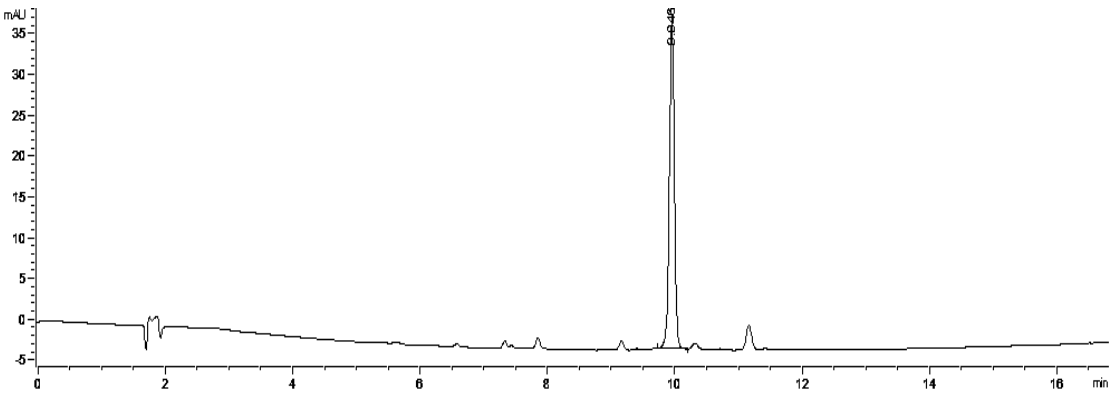

6-Methyltetrazine-PEG12-va-PAB-Doxorubicin (159)

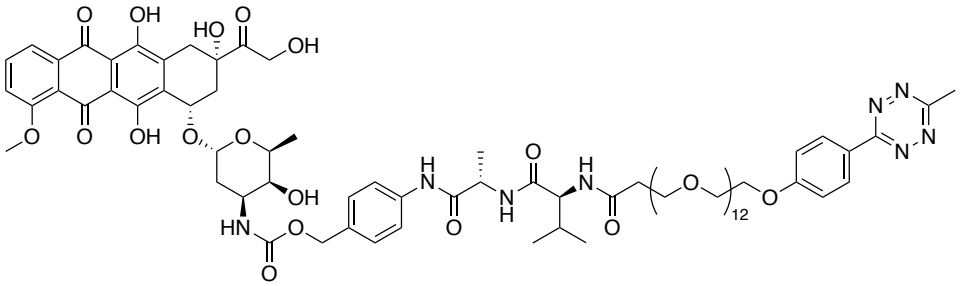

159

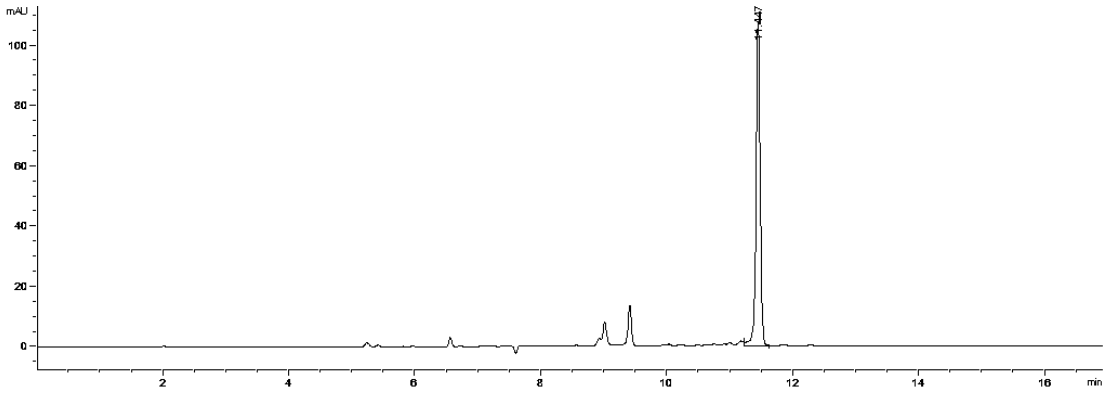

9.4 Appendix 4: Protein LCMS

Trastuzumab-BCN (**101**)

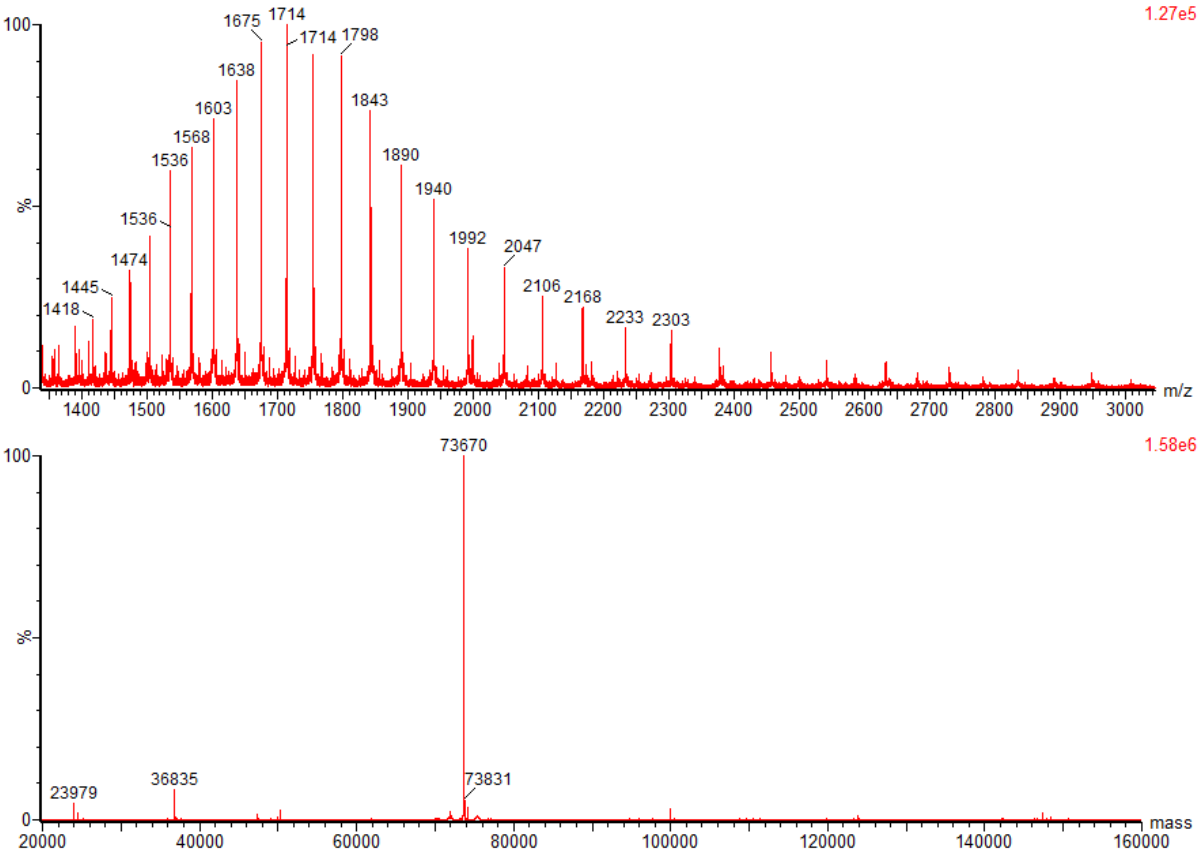

Trastuzumab-Cyp (**102**)

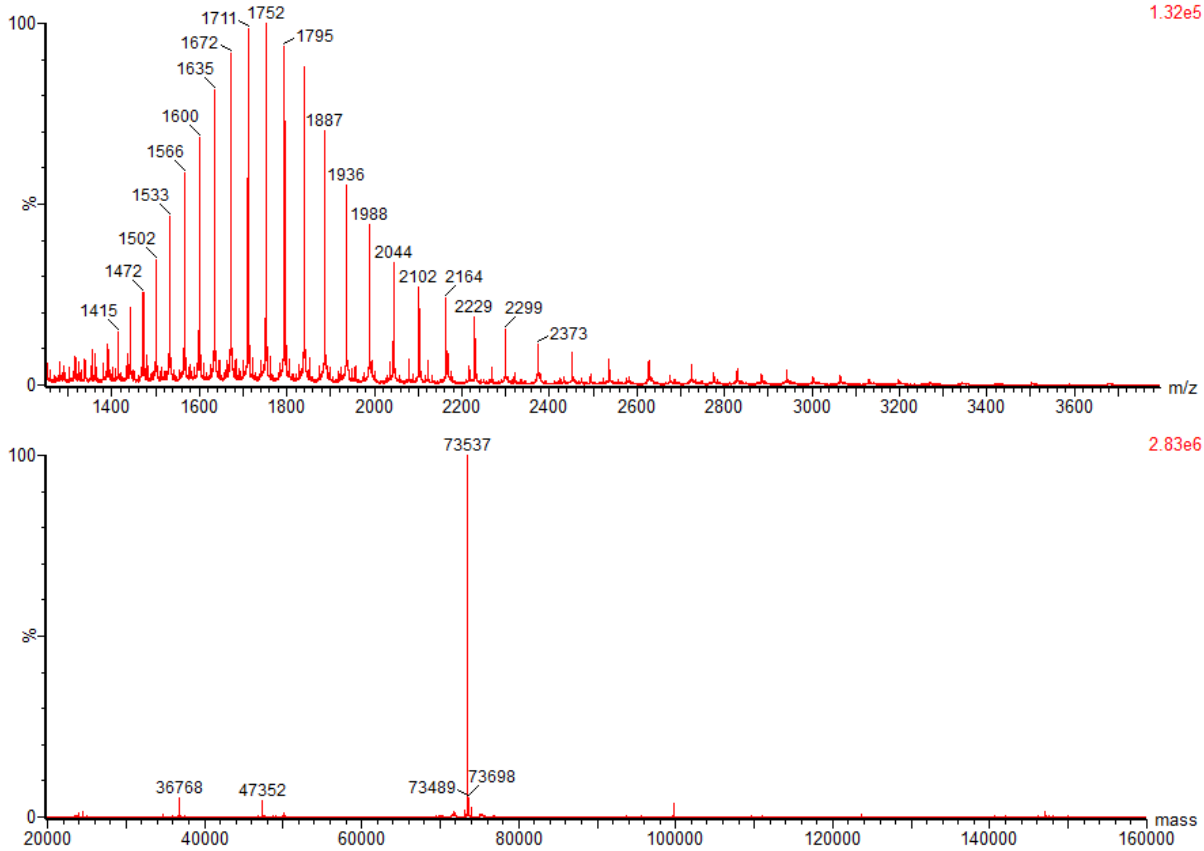

Trastuzumab-Alkyne (**103**)

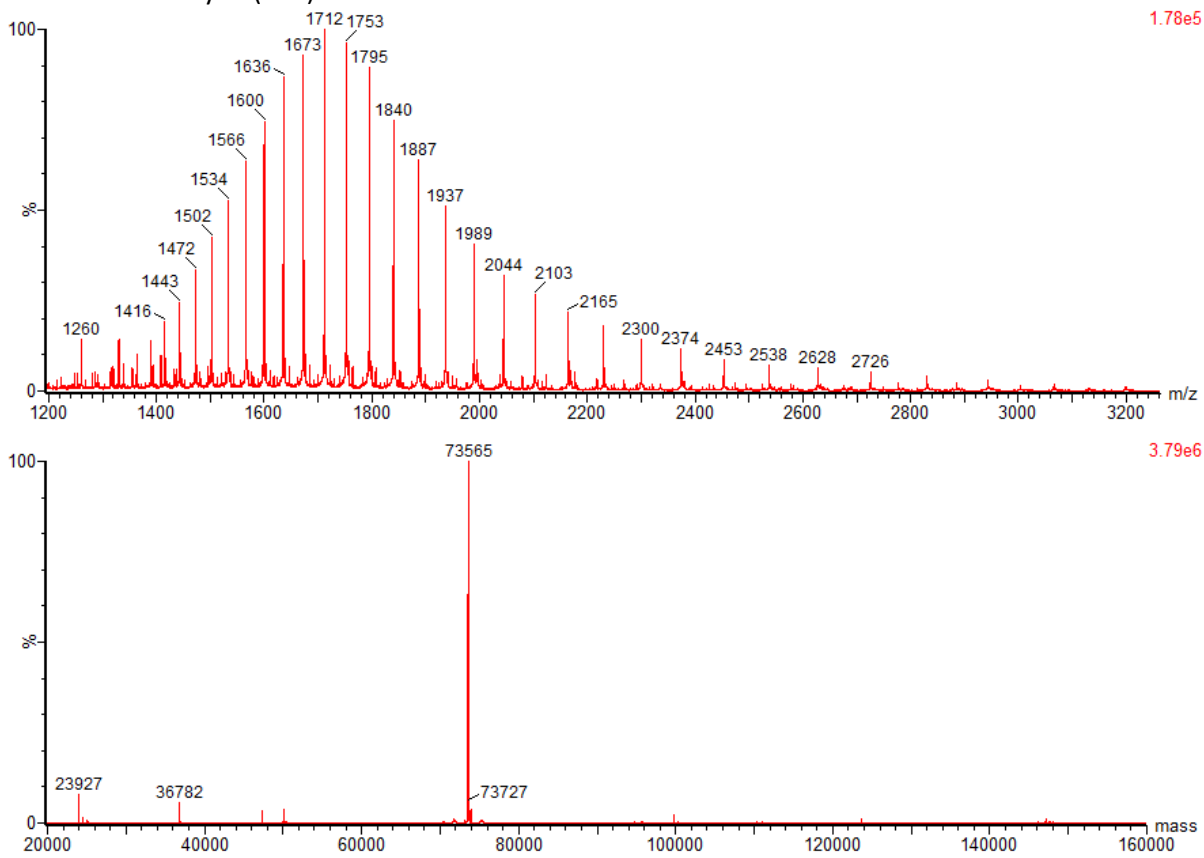

Trastuzumab-BCN-AF488 (**106**)

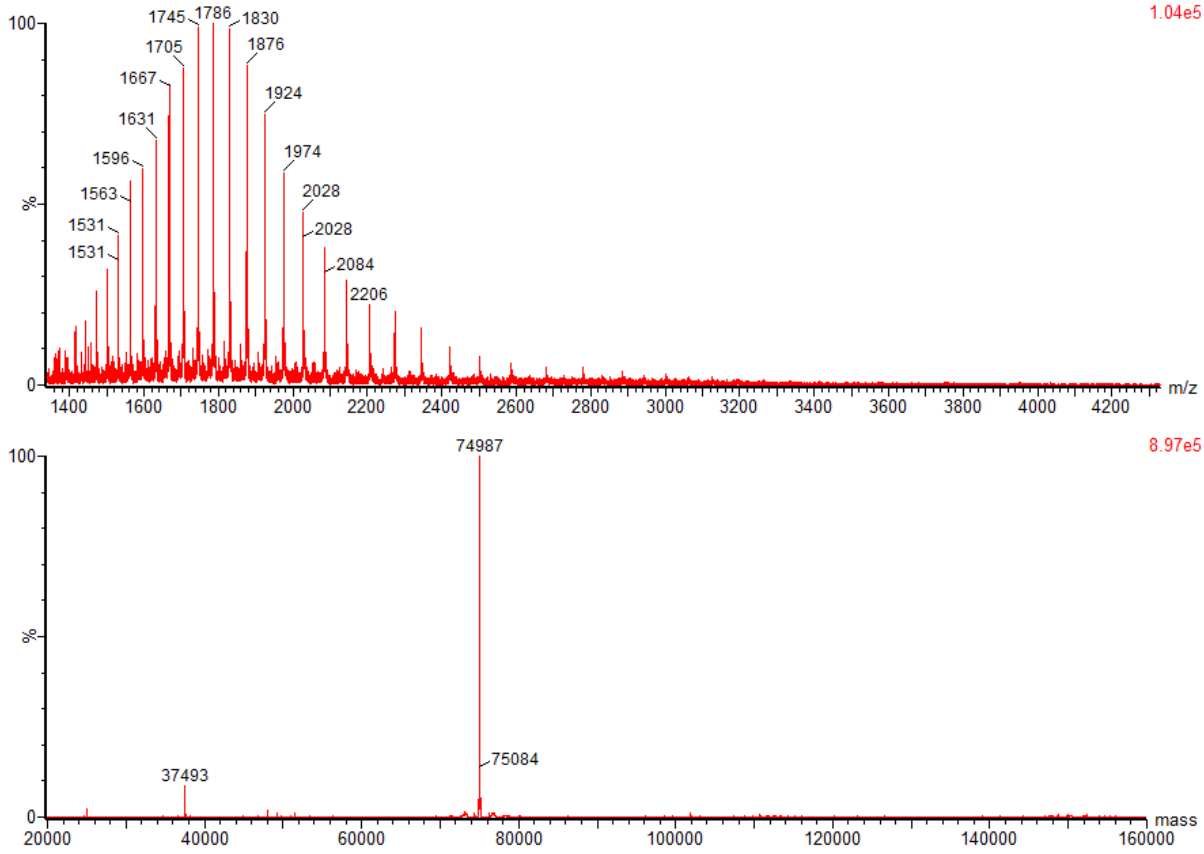

Trastuzumab-Cyp-AZDye 488 (**107**)

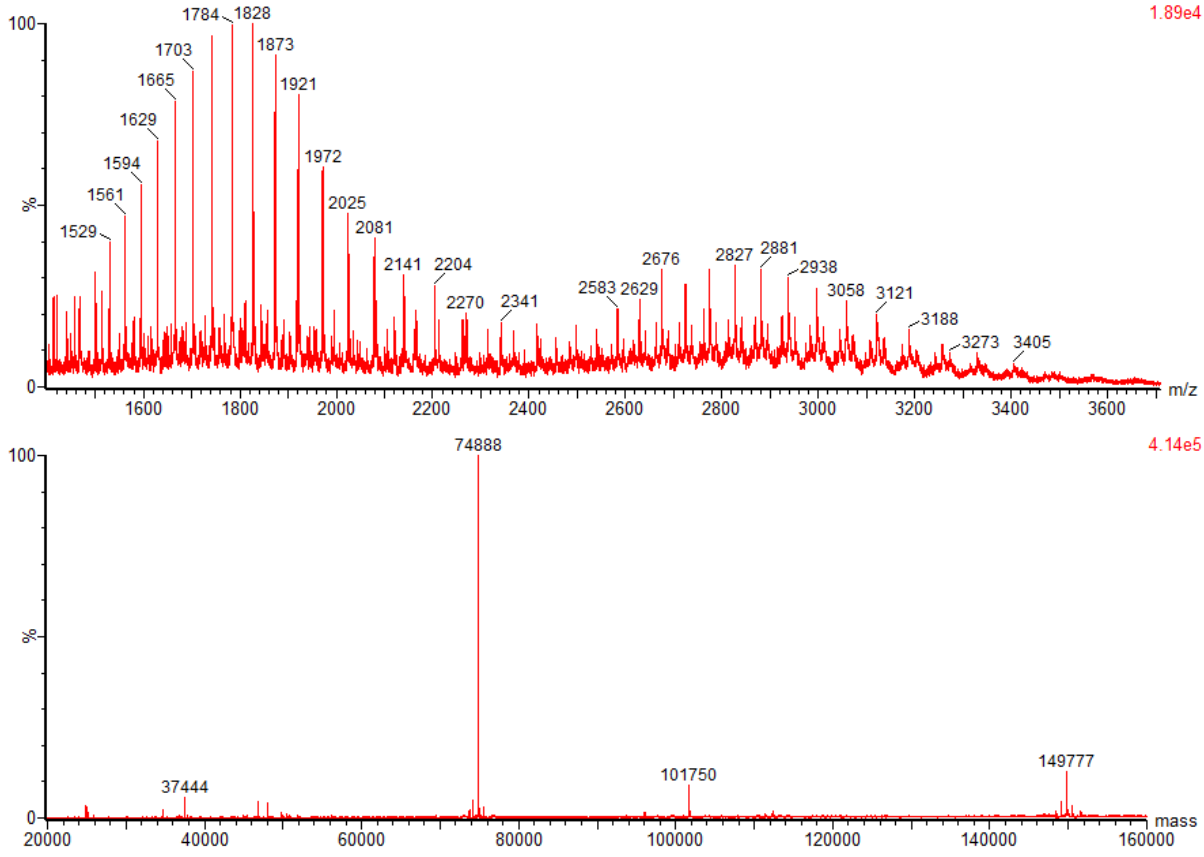

Trastuzumab-BCN-AZDye 488 (**108**)

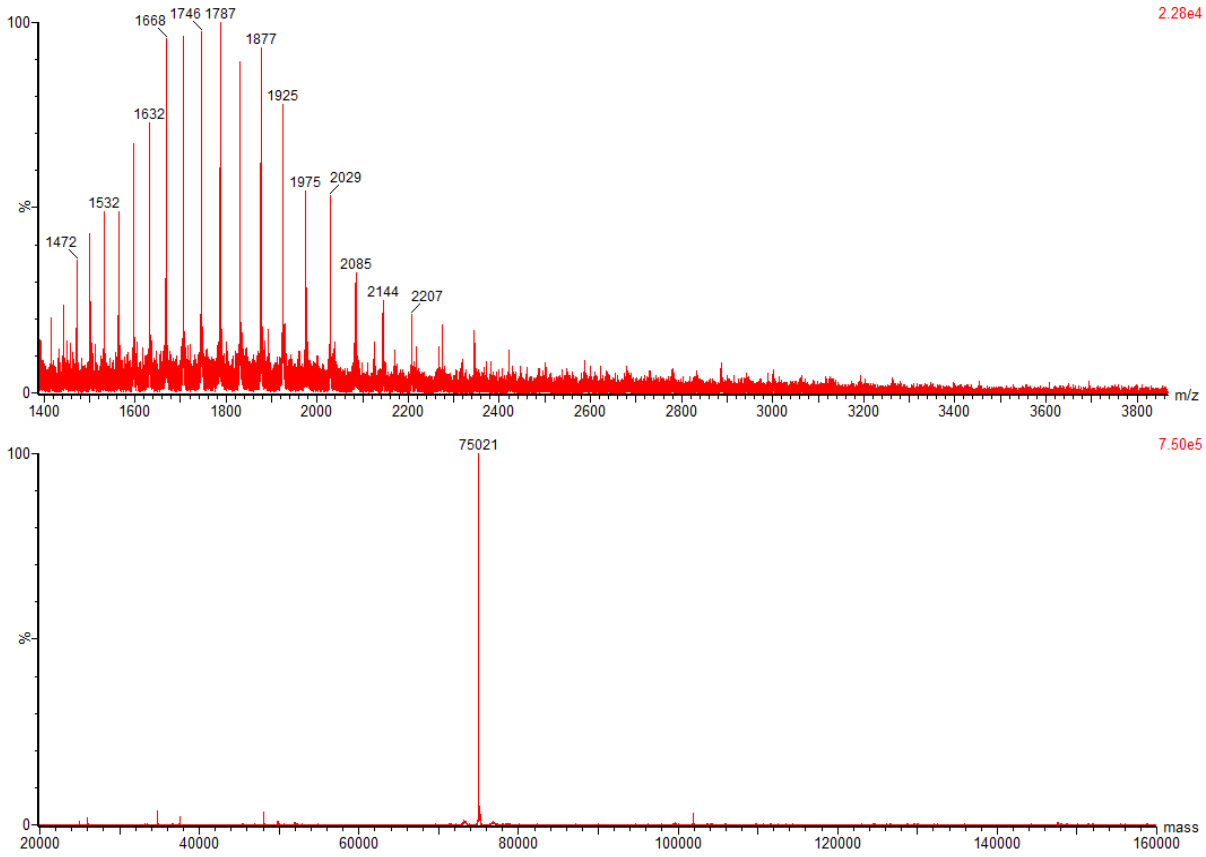

Trastuzumab-alkyne-AF488 (**109**)

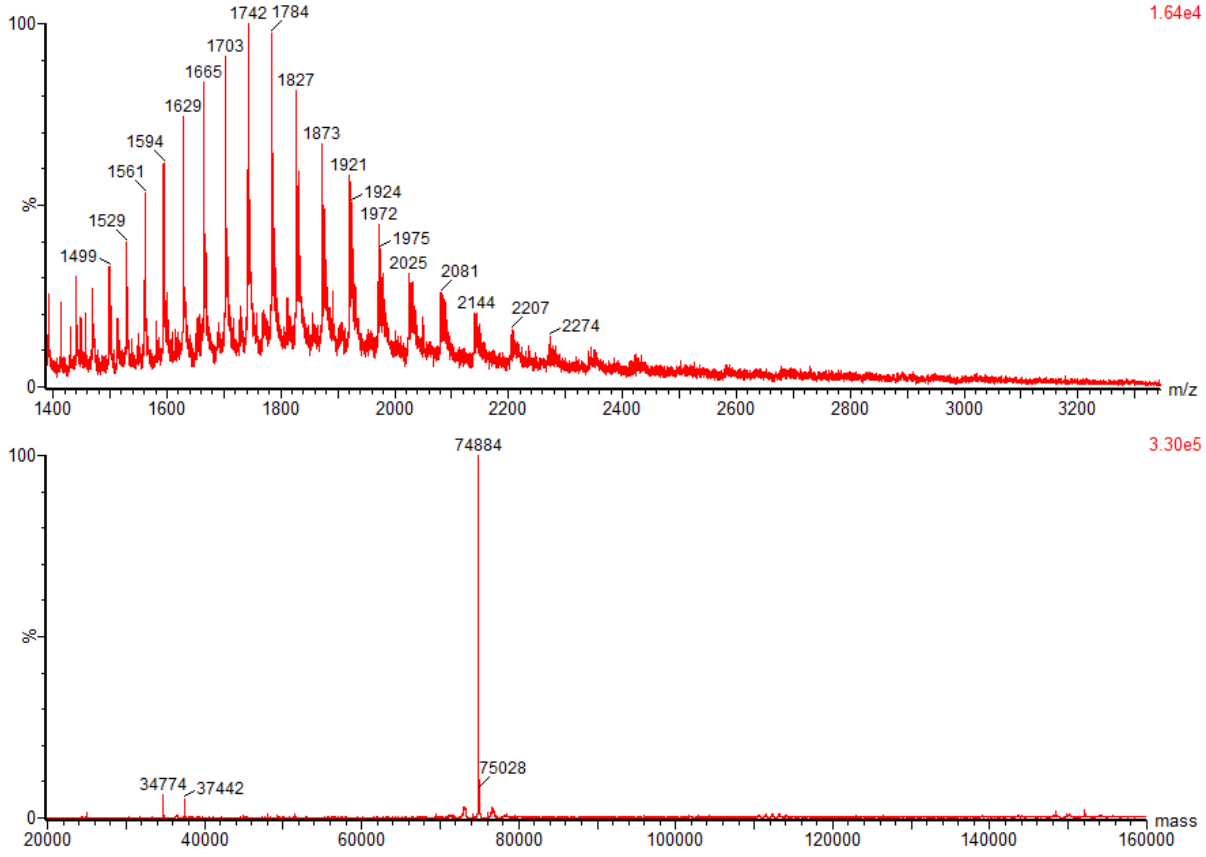

Trastuzumab-dfDVP (**139**)

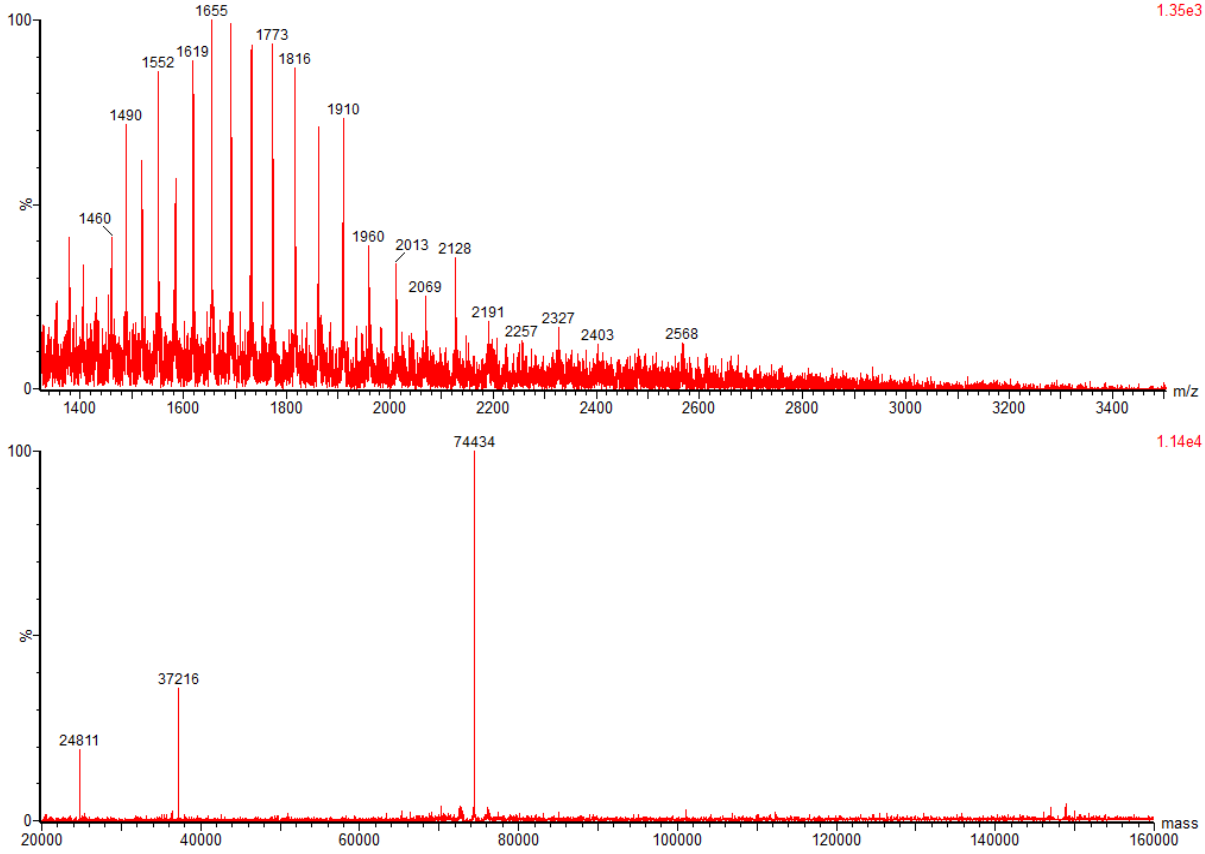

Trastuzumab-dfDVP-MMAE (**139**)

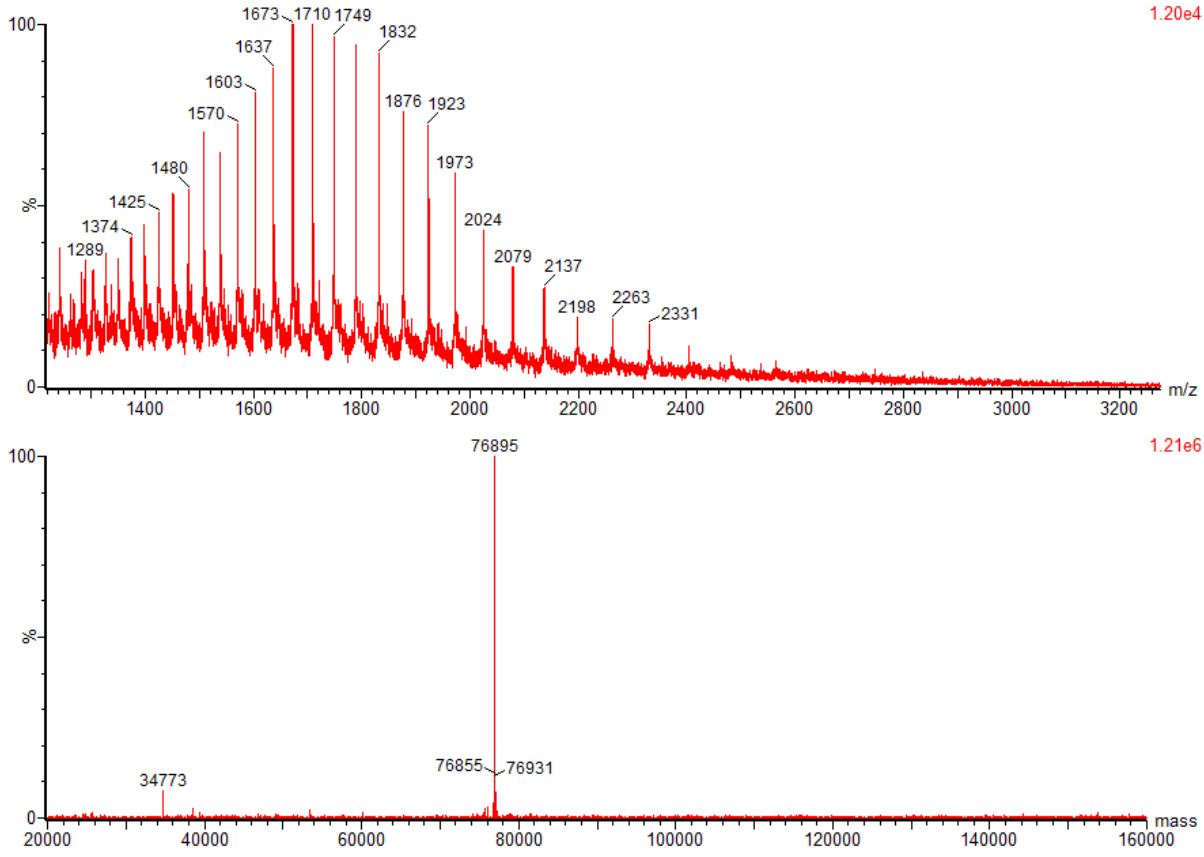

Trastuzumab-dfDVP-MMAE-AF488 (**142**)

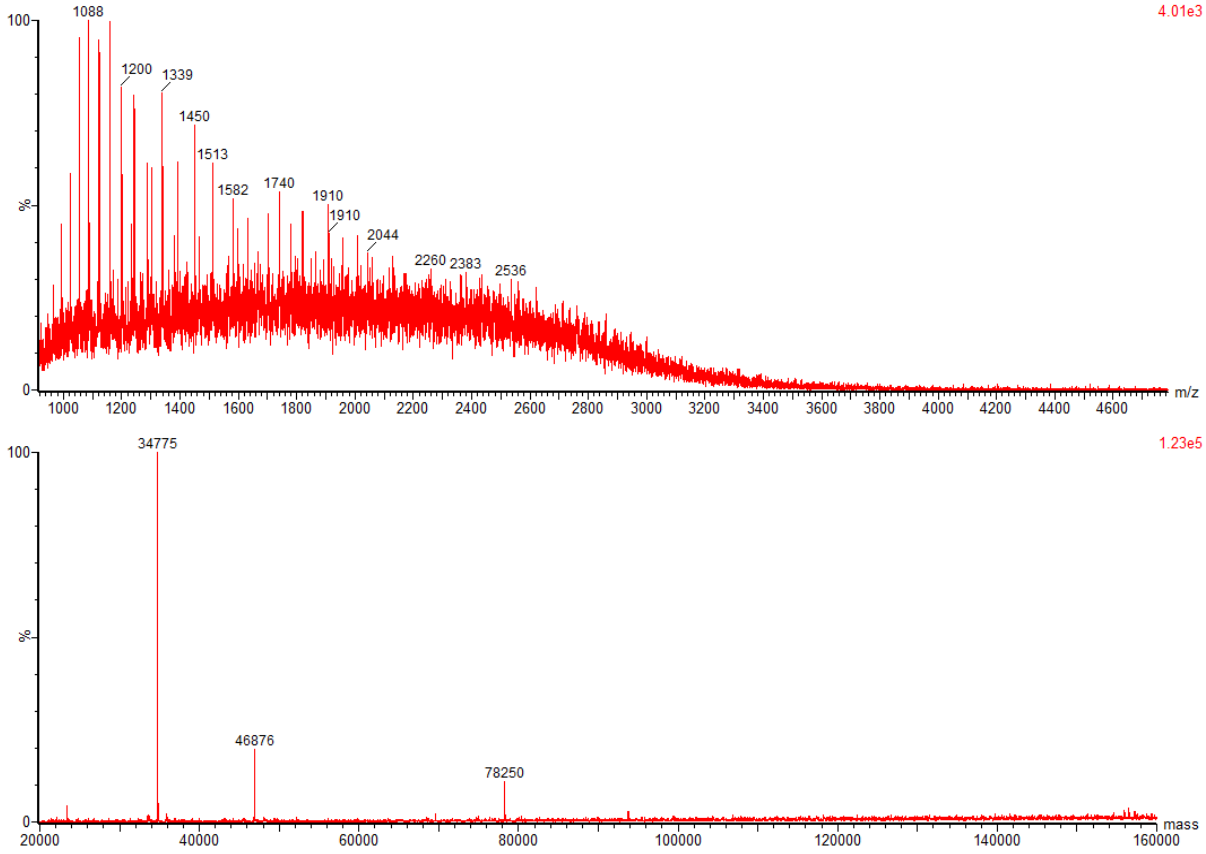

Trastuzumab-dfDVP-MMAE-TAMRA (**145**)

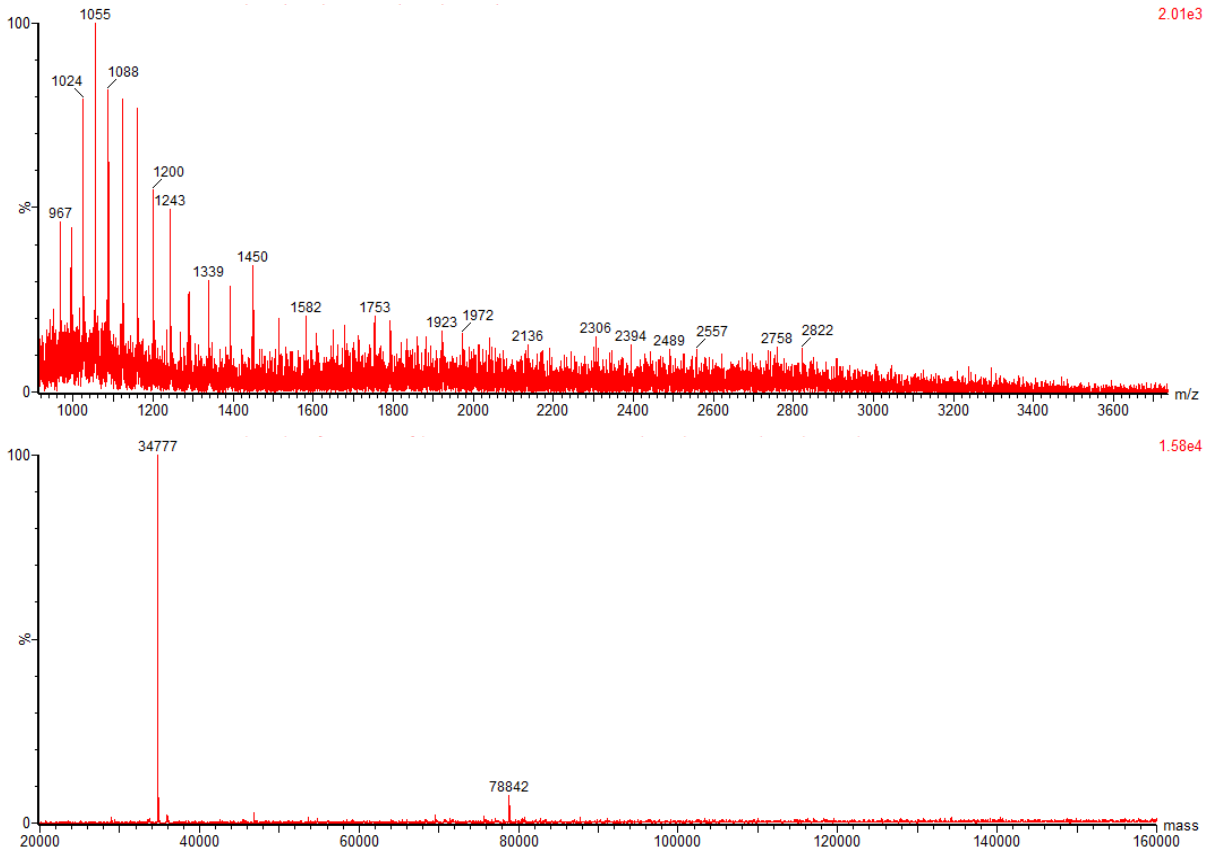

Trastuzumab-BCN-MMAE (**146**)

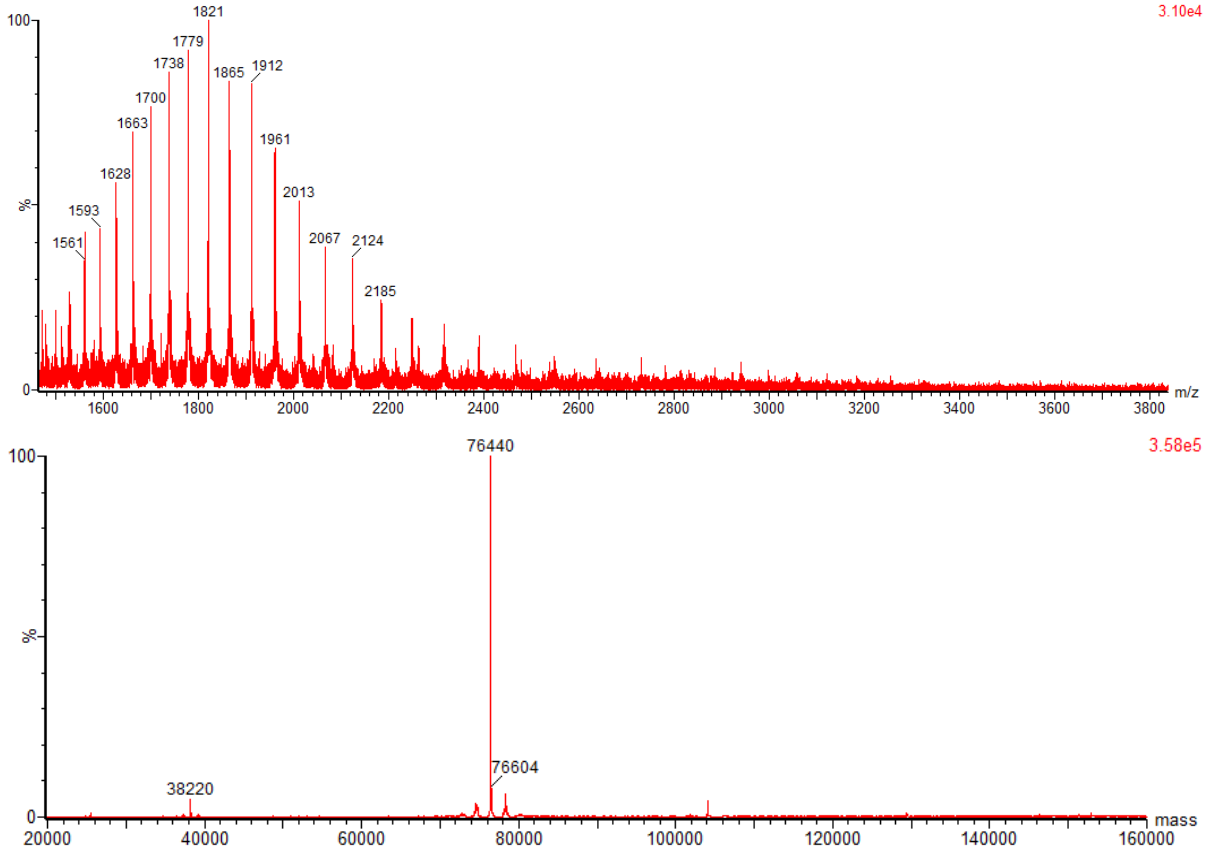

Trastuzumab-BCN-Criz (**150**)

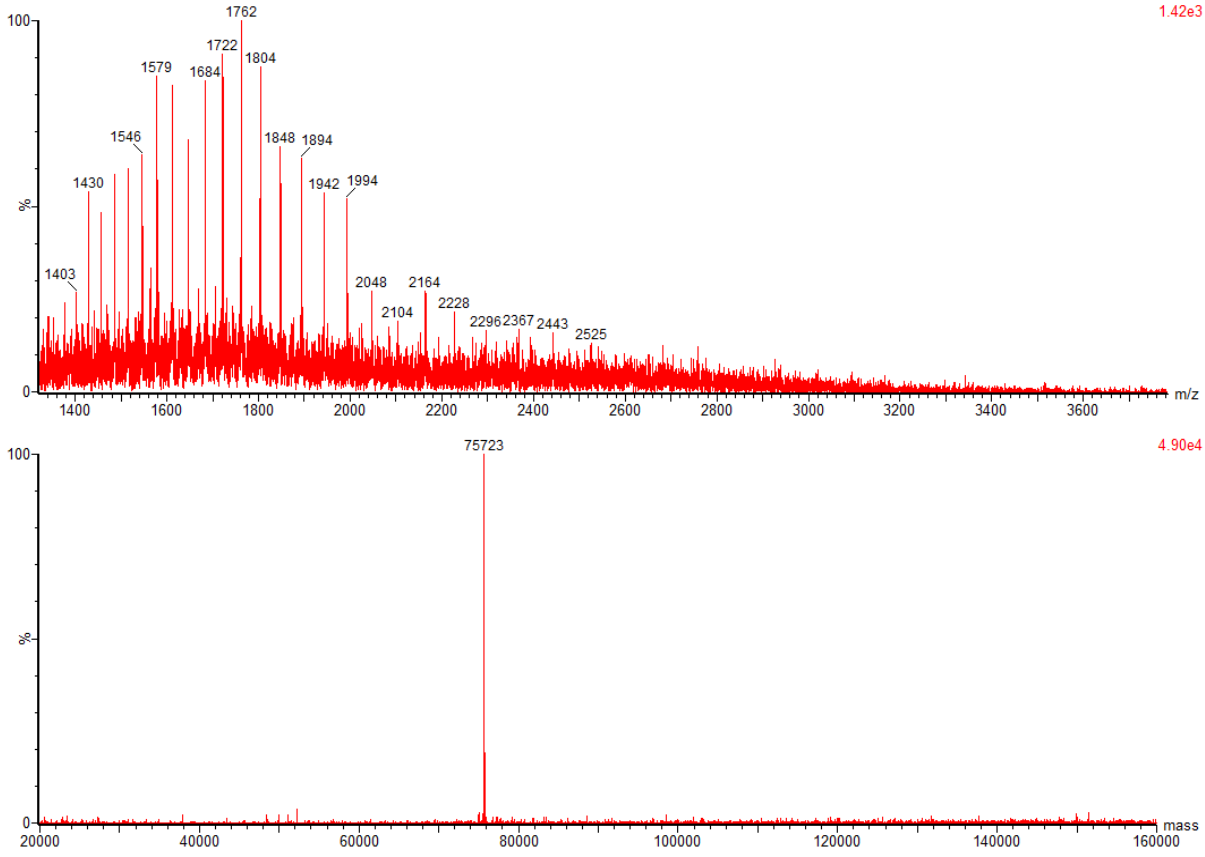

9.5 Appendix 5: Publications List

Site-selective modification strategies in antibody-drug conjugates, S. J. Walsh, J. D. Bargh, F. M. Dannheim, A. R. Hanby, H. Seki, A. J. Counsell, X. Ou, E. Fowler, N. Ashman, Y. Takada, A. Isidro-Llobet, J. S. Parker, J. S. Carroll, D. R. Spring, *Chem. Soc. Rev.* 2021, ***50***, 1305–1353.

An efficient, stereocontrolled and versatile synthetic route to bicyclic heteroaromatic privileged scaffolds, H. L. Stewart, A. R. Hanby, T. A. King, A. D. Bond, T. A. Moss, H. F. Sore, D. R. Spring, *Chem. Commun.* 2020, ***56***, 6818–6821.

Fsp^3-rich and diverse fragments inspired by natural products as a collection to enhance fragment-based drug discovery, A. R. Hanby, N. S. Troelsen, T. J. Osberger, S. L. Kidd, K. T. Mortensen, D. R. Spring, *Chem. Commun.* 2020, **56**, 2280-2283.